

# **TOPIC 1**

Seismic Behaviour  
Bridges' Dynamics



## LONGITUDINAL AND TRANSVERSE SEISMIC RETROFIT OF BRIDGES

Olga Markogiannaki<sup>1</sup>, Ioannis Tegos<sup>2</sup>, Spyridon Vasileiou<sup>3</sup>

<sup>1,2,3</sup> Aristotle University of Thessaloniki, Dept. of Civil Engineering, Greece  
e-mail: omarkogiannaki@civil.auth.gr , itegos@civil.auth.gr, spyridov@civil.auth.gr

**ABSTRACT:** The main goal of the present paper is to demonstrate an innovative method of indirect seismic retrofit of bridges for both horizontal seismic directions. Longitudinally a restraining system of struts-ties is applied, while transversely a ties-only. Time history analyses on R/C bridge case studies indicated remarkable improvement in the response for both seismic directions.

**KEY WORDS:** Concrete Bridge, Restrainer, Seismic Movements, Unbonded Tendon

### 1 INTRODUCTION

Bridge retrofit against seismic requirements is often identified as a strong necessity for existing bridges in seismic prone areas. Generally, retrofit solutions aim on complying with the safety inequality [1], Eq.(1), which requires structural capacity of bridge members to exceed load seismic demand at all times. Various retrofit methods have been developed [2], which can be summarized in two retrofit philosophies depending on the focus of each procedure on the first or second term of Eq.(1). The first retrofit philosophy which is the direct approach involves methods that are applied on the as-built bridge components with the objective to increase their capacity against the seismic loads. For instance, these methods include pier retrofit with steel or concrete jackets or FRP materials, [3]. The disadvantage of these methods is that they result in conservative solutions because they depend on the existing components capacity which is unreliable and difficult to determine.

$$Capacity \geq Demand \quad (1)$$

The second retrofit philosophy, the indirect approach, involves the addition of new members in the bridge structural system. The new bridge components are intended to reduce the seismic demand loads of the as-built bridge members at the level of their structural capacity and they are properly designed for contributing to the seismic resistance by receiving the seismic forces. Such common indirect approach retrofit methods include the use of bearings or energy dissipating devices, i.e. dampers, or restrainer cables[4]. A key point in the effectiveness of such methods is the timely activation of the mechanism

installed on the bridge; otherwise it is possible that the capacity of the existing components will be exceeded before the activation of the retrofit system. In case of continuous monolithic concrete bridges appropriate indirect retrofit methods are devices like dampers, whilst bearings and restrainer cables are more often used for simply supported bridges, [5],[6]. Herein, alternative retrofit systems are proposed, a longitudinal and a transverse restraining system for continuous concrete integral bridges and are presented as another reliable and effective retrofit indirect approach. The longitudinal retrofit system has been presented in previous research work [7],[8]. The transverse retrofit system consists of steel bars anchored at the bridge piers. Both systems are investigated for their effectiveness in upgrading the seismic performance multi-span concrete integral bridges from seismic level I to seismic level II.

## 2 DESCRIPTION OF THE RETROFIT SYSTEMS

### 2.1 Longitudinal seismic retrofit

The longitudinal seismic retrofit mechanism, the struts-ties system, has been investigated for its effectiveness and applicability in previous research work [7], [8]. It is presented schematically in *Fig. 1*.

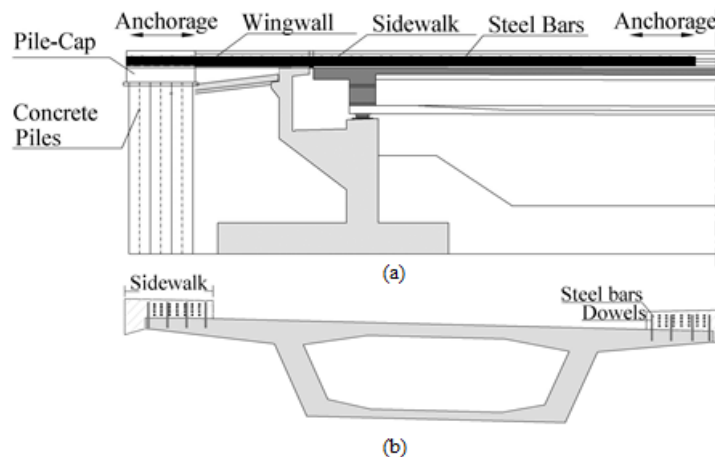


Figure 1. a) Indicative Longitudinal Elevation, c) Indicative Cross Section Detail

It involves the application of bundles of steel bars in the bridge superstructure. The steel bundles are installed in the sidewalks of the bridge longitudinally in the end spans and anchored in a structure of concrete walls at the end of the abutment wing walls. The method results in a number of four bundles, one at each wing wall. The bars are placed in plastic ducts in order to prevent bonding with the sidewalks' concrete. They are bonded only at their ends by their anchorage length. The steel bundles can receive both tension and compression loading since their installation in the sidewalks protects them from

buckling. As an indirect retrofit approach they restrain longitudinal bridge seismic movements and reduce seismic demand on piers. The restraining system is activated as a struts-ties system under in-service loading,[7], as well. The sidewalks are reconstructed at the positions where the steel bars are placed with high strength concrete and concrete dowels in a mesh. A reliable new structure behind the abutments is constructed for the safe anchorage of the steel bundles and the transfer of the seismic forces, since the existing abutments are not designed for receiving seismic forces. The new structure is a concrete pile-diaphragm at the end of the wing-walls which consists of three rectangular piles connected with a pile cap. The steel bars are anchored inside the pile cap.

## 2.2 Transverse seismic retrofit

Retrofit demands for the transverse earthquake direction in bridges that do not have wall type piers and that present substantial safety issues against earthquakes are difficult to be accommodated and can be distinguished to two parts; one is related to the piers and the other to piers' foundation. Regarding the piers a traditional approach for shear retrofit can be easily performed by the capabilities provided by the use of fiber reinforced polymers. When the piers present flexural deficiencies, the traditional approach of jacketing requires safe anchorages for the additional longitudinal reinforcement both at the top and bottom of piers which are difficult to be successful achieved. Therefore, it seems to be more preferable to select an indirect retrofit approach that aim on changing the second term of the safety inequality, which is interpreted as reducing the seismic demand on the piers. Consecutively, the invention of a restraining system of transverse seismic movements that differs from the longitudinal retrofit can be an acceptable solution. The proposed unconventional seismic retrofit consists of steel bars that are placed along the transverse direction of the bridge at the piers. In *Fig. 2* the proposed system of crosswise ties is presented. In detail, the upper end of the steel bars is anchored at the lower part of the deck close to the piers in steel plates of L-shapes that follow the inclination of the concrete box cross-section, whilst the lower is anchored at the opposite transverse side in the cap of a micro-pile structure next to the pile cap of the pile foundation and connected to it. The retrofit bars are anchored in the micro-pile cap with the adequate anchorage length. The steel bars are placed at appropriate distances, so as to avoid any disruptions with each other, in a length equal to the transverse dimension of the pile-cap.

The steel bars can receive only tension loading when the bridge is transversely excited since they are not protected for receiving compression loading. However, the activation of the retrofit system can be achieved for both transverse earthquake directions because the ties are placed crosswise, bars 1 and 2 in *Fig. 2*. In this manner they can contribute to bridge's seismic performance at all times, as a ties-only system which restrains the transverse

bridge movements and limits the pier seismic forces. The seismic forces transferred by their anchorages are received safely by the micro-pile series while the forces at the deck do not arise any response issues.

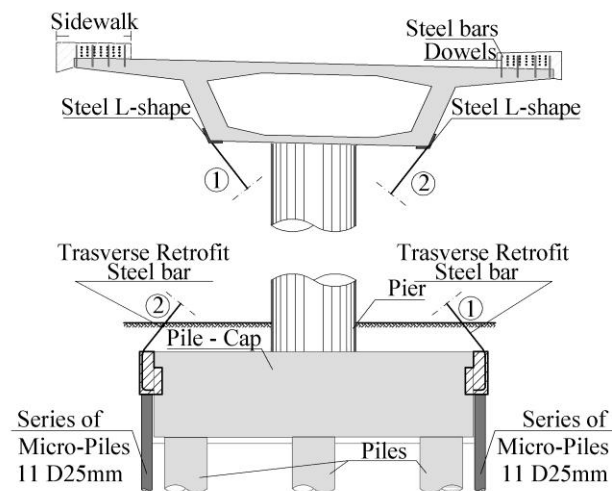


Figure 2. a) Indicative Longitudinal Elevation, c) Indicative Cross Section Detail

### 3 BRIDGE CASE STUDIES – 3D MODEL

The Benchmark Bridge that was studied is a monolithic three span prestressed R/C bridge. The end spans are 45.10m, the middle is 45.60m and the total length is 135,80m. The deck is a concrete box section, connected to the piers rigidly and is supported on the abutments by sliding bearings of low friction. The piers are circular and are founded on 3x3 pile groups. The bridge's abutments are seat-type and have transverse seismic links-stoppers. The bridge is founded on ground type B and the area is in seismic zone I, [9]. 3-D finite element bridge models were generated in the analysis software OpenSees, [10], accounting for soil-structure interaction. *Fig. 3* demonstrates the properties of one of the models including both the longitudinal and the transverse retrofit. Bridge members are modeled with frame elements with material nonlinearities. The section analysis for the assignment of concentrated plasticity (hinges) at the top and bottom of piers was performed with Bomber-Biaxial,[11], *Fig. 4a*. The foundation springs were provided by the geotechnical report. The passive resistance of the abutments due to embankment mobilization was simulated according to Shamsabadi guidelines [12],[13] and the HyperbolicGap compression material was used in OpenSees, as shown in *Fig. 4b*. The longitudinal and transverse retrofit systems were studied for various parameters in order to identify their efficiency in limiting seismic movements. The properties of the systems used for the study are presented in *Table 1*. Force-Displacement relationships are based on the bilinear steel material law and were

assigned to nonlinear springs of equivalent stiffnesses, *Fig. 4c*. For the transverse retrofit the tension-only system is simulated as a struts-ties system with half the stiffness of the real one. The minimum length of the longitudinal bars is determined based on the condition that the steel bars remain elastic under serviceability loading,[7]. The transverse springs correspond to the horizontal component of the ties stiffness. The seismic analyses were conducted using five artificial accelerograms complying with zones I and II spectra.

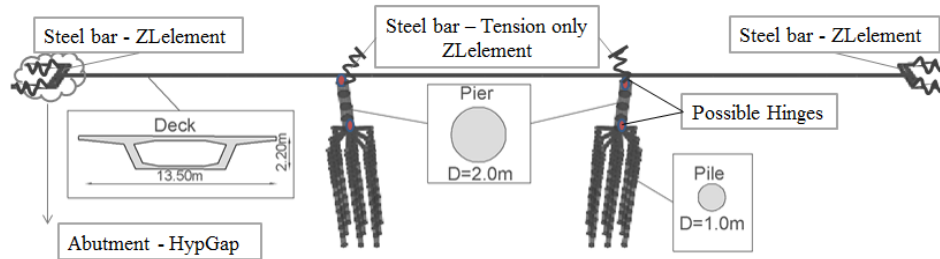


Figure 3. 3-D OpenSees Bridge Model

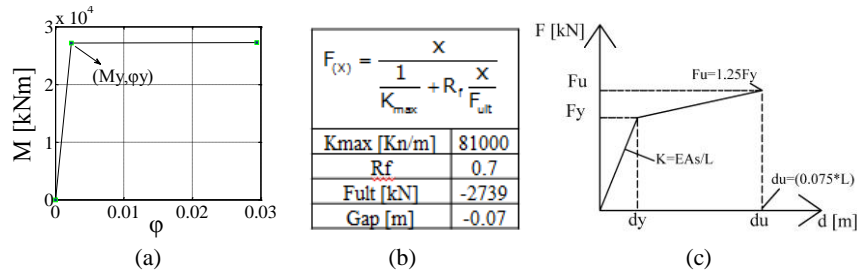


Figure 4. a) Moment - Curvature at Hinges, b) Abutment HypGap c) Steel bar ZElement

Table 1. System Properties

Longitudinal		Transverse	
Bar-Diameter [mm]	16	Bar-Diameter [mm]	14-20
E [GPa]	200	E [GPa]	200
L [m]	20-25	L[m]	11.65
Number of bars ( No. )/wing wall	21-42	Number of bars ( No. )/wing wall	28-110
$A_s$ [cm <sup>2</sup> ]	No. * $A_{bar}$	$A_s$ [cm <sup>2</sup> ]	No. * $A_{bar}$
$F_y$ [MPa]	435	$F_y$ [MPa]	435

#### 4 SEISMIC ANALYSIS AND RESULTS DISCUSSION

The parametric analyses were performed for the benchmark bridge and for a hybrid model of two spans. For the longitudinal response, a number of various steel bundle properties was studied for evaluating bridge responses. The data shown in the following figures includes the maximum values resulting from the application of the five accelerograms. *Fig. 5* presents the longitudinal

movement reduction with respect to the existing bridge without the retrofit system movement. The reductions are evident for all retrofit solutions; they are 48% for 42D16mm bars 20m long and are primarily dependent on the steel bundles cross-section. In addition, larger lengths result in a small reduction in the efficiency of the retrofit. An increase in length would be advantageous if the stresses on the steel bundles and the forces transferred to the structure at the abutments, respectively, had to be reduced. In Fig 6. the absolute value results of the bridge with and without the mechanism for the two spans indicate the efficiency of the retrofit system, as well. Both cases indicate that the initial bridges designed for seismic zone I can be upgraded to seismic zone II with the proposed retrofit solution for longitudinal earthquake direction.

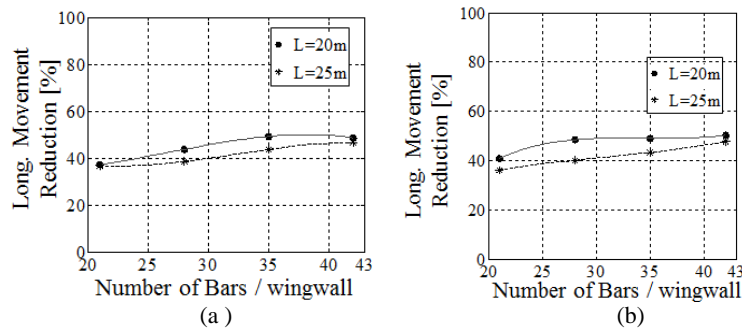


Figure 5. Long. Movement reduction 3-spans bridge a) seismic level I b) seismic level II

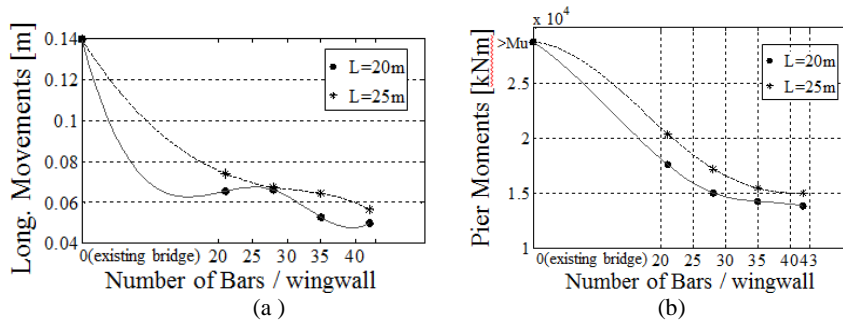


Figure 6. 2-spans bridge, 0.24g a) Long. Movement Reduction b) Pier Moment Reductions

The transverse retrofit analysis results are presented in Fig. 7, for both bridge case studies and for the two seismic levels. Fig. 7 a,c demonstrate the reductions with respect to the existing bridge without the retrofit system of the transverse seismic movements, i.e. 30% for the 55D20mm. Similar reductions are observed in Fig. 7 b,d to the pier seismic forces, as well. Although the use of larger cross sections results in higher reductions, the large forces transferred to the micro-piles anchorage, Table 2, indicates that it is preferable to use smaller cross sections and take advantage of the yielding of the steel bars when smaller reductions are required. It should be pointed out that the retrofit



solutions bring the maximum seismic demand of the piers to the level of their capacity for seismic intensity of 0.24g which introduces 50% higher than the original design acceleration of 0.16g.

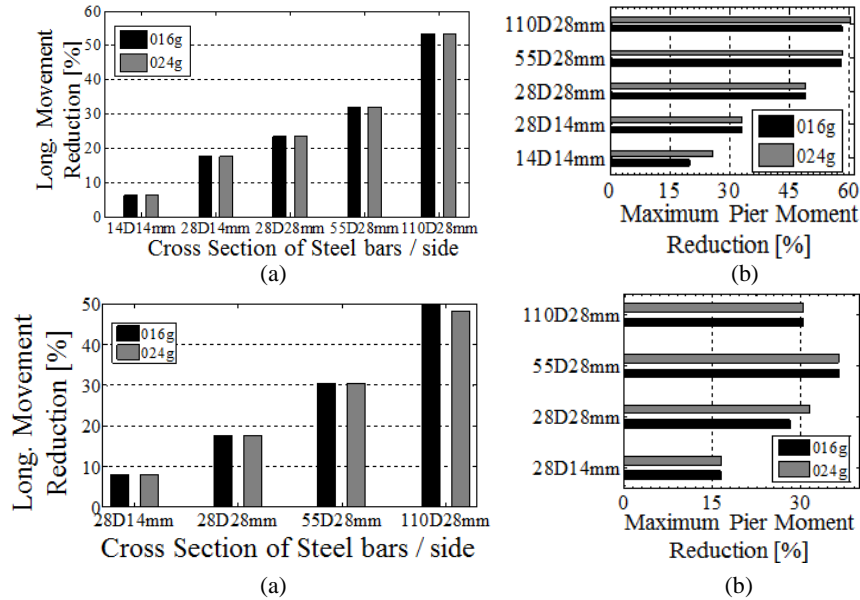


Figure 7. 3-spans bridge a) Transverse movement reduction ,b) Pier moment reductions  
2-spans bridge a) Transverse movement reduction ,b) Pier moment reductions

Table 2. Maximum Forces developed at the steel retrofit bars

3-SPANS 0.24g			2-SPANS 0.24g		
Cross-section	Force/side [kN]	Behavior	Cross-section	Force/side [kN]	Behavior
14D14mm	1294.96	>yielding	28Φ14	1661.623	<yielding
28D14mm	2274.36	>yielding	28Φ20	2953.739	<yielding
28D20mm	4211.58	>yielding	55Φ20	4833.167	< yielding
55D20mm	7228.19	< yielding	110Φ20	6870.445	< yielding
110D20mm	9774.37	< yielding			

## 5 CONCLUSIONS

The present paper is an attempt to seismically upgrade a bridge that presents deficiencies at both earthquake principal directions. For this purpose, two independent seismic movement restraining systems were used; one consisting of struts-ties for the longitudinal direction and the other consisting of ties-only for the transverse. The first achieved a decrease in the seismic demand of the piers by the transfer of part of the seismic forces to the abutments and the embankment, while the second reached the seismic demand decrease by transferring seismic forces to the existing foundation. On the light of the above the following are the main conclusions derived:

- The indirect accommodation of the increased seismic demand is in general the safest way to perform retrofit solutions. Therefore, regarding the longitudinal requirements, the surplus of the seismic actions was driven through the use of the appropriate restraining system to new structures behind the abutments and, similarly, for the transverse direction the surplus was driven to the retrofitted foundation.
- The high seismic demand in combination with the low available additional bearing capacity of the abutments required the introduction of a special structure capable of safely receiving high horizontal forces
- The transverse retrofit solution required the retrofit of the foundation for receiving the seismic forces, which was achieved by the use of series of micro-piles adjacent to the existing pile-cap.
- The coarsely evaluated retrofit solution applied in a concrete bridge can be characterized as safer and more economical than a conventional one which often is not even feasible.

## REFERENCES

- [1] CEN[Comité Européen de Normalisation], “Eurocode 2: Design of concrete structures - Part2: Concrete Bridges,” 2001.
- [2] Buckle, I, Friedland, I, Mander, J, Geoffrey, M, Nutt, R, Power, M, “Seismic Retrofitting Manual for Highway Structures: Part 1 – Bridges,” 2006.
- [3] Priestley, M. J. N, Seible, F, Calvi, GM, *Seismic Design and Retrofit of Bridges*. John Wiley & Sons, New York, USA, 1996.
- [4] Rustum, A, “Evaluating the Retrofit of Highway Bridges Using Fluid Viscous Dampers,” University of Waterloo, Ontario, Canada, 2012.
- [5] Kim, J-M, Feng, MQ, Shinozuka, M, “Energy Dissipating Restrainers for Highway Bridges,” *Soil Dynamics and Earthquake Engineering*, Vol. 19, No. 1, pp. 65–69, 2000.
- [6] Desroches, R, Pfeifer, T, Leon, RT, Lam, T, “Full-Scale Tests of Seismic Cable Restrainer Retrofits for Simply Supported Bridges,” *Journal of Bridge Engineering*, Vol. July, pp. 191–198, 2003.
- [7] Markogiannaki, O, Tegos, I, “Seismic retrofit of bridges through the external installation of a new type restraining system,” *15WCEE*, Lisbon, 2012.
- [8] Markogiannaki, O, Tegos, I, “Seismic reliability of a reinforced concrete retrofitted bridge,” *ICOSSAR*, 2013.
- [9] CEN[Comité Européen de Normalisation], “Eurocode 8: Design of structures for earthquake resistance — Part 1: General rules, seismic actions and rules for buildings,” 2003.
- [10] Constantinou, MC, Soong, TT, Dargush, GF, “Passive Energy Dissipation Systems For Structural Design and Retrofit,” 1998.
- [11] Papanikolaou, VK, “Analysis of arbitrary composite sections in biaxial bending and axial load,” *Computers & Structures*, Vol. 98–99, pp. 33–54, 2012.
- [12] Shamsabadi, A, Rollins, KM, Kapuskar, M, “Nonlinear Soil – Abutment – Bridge Structure Interaction for Seismic Performance-Based Design,” *Journal of Geotechnical and Geoenvironmental Engineering*, No. June, pp. 707–720, 2007.
- [13] Stewart, JP, Taciroglu, E, Wallace, JW, Lemnitzer, A, Hilson, C, Nojoudi, A, Keowan, S, Nigbor, R, Salamanca, A, “Nonlinear Load-Deflection Behavior of Abutment Backwalls with Varying Height and Soil Density,” 2011.

IBSBI 2014, October 16-18, 2014, Athens, Greece

## **A PROPOSAL FOR IMPROVING REGULARITY OF INTEGRAL CONCRETE BRIDGES**

Vasileios Pilitsis<sup>1</sup> and Ioannis Tegos<sup>2</sup>

<sup>1,2</sup> Aristotle University of Thessaloniki, Faculty Of Engineering, Dept. of Civil Engineering  
Greece

e-mail: vpilitsi@civil.auth.gr, itegos@civil.auth.gr

**ABSTRACT:** The uncertainty about the seismic behaviour and the financially burdensome “penalty” imposed by EC8-part2 in irregular bridges is the motivation to seek ways to improve regularity. In this study a way of improving regularity of bridges is suggested and applied alternatively in a long road bridge of Egnatia Motorway.

**KEY WORDS:** Regularity; Cross-section dividing; Pier; Stiffness.

### **1 INTRODUCTION**

The seismic response of a bridge depends mainly on its piers. In cases where piers are monolithically connected to the deck, the uniform distribution of the total stiffness is desired when possible. This leads to the favorable effect of the nearly simultaneous development of plastic hinges in predicted positions and therefore the improved exploitation of the piers' ductility. On the other hand, the geomorphology of the area the bridge is founded on, in most cases imposes a great variation in piers' height. Due to aesthetics, the choice of same geometry of section for all the piers has the effect of stiffness maldistribution in piers and consequently the non-uniform distribution of seismic shear force. The short piers receive the greatest amount of seismic shear force while the higher ones are partially inactive. In this case, when the higher piers have the minimum by the codes reinforce percentage, the plastic hinges of the stiffer piers form prematurely. These piers reach first the yielding limit state and this leads to unacceptably high ductility demands. On the other hand, the premature yielding of short piers leads to the dramatic weakening of the structure in terms of seismic shear force capacity which cannot be restored by the stiffness of the higher piers. EC8 - Part2 takes into account the above case by classifying the bearing-structure of bridges into regular and non-regular [1]. Cases like the above mentioned are classified into irregular bridges and are treated by proper provisions of EC8 - Part2. Irregular bridge structures are preferable to be avoided as Eurocode's 8 provisions lead to uneconomical solutions.

Worth mentioned is a case of irregular bridge in United States. This road

bridge of seven spans and rigid pier – deck connections failed during the Northridge earthquake in 1994 because of large shear force development in the shorter piers of the bridge. The bridge was reconstructed by dividing the deck into two statically independent parts each of which has piers of the same height. The same height of the piers was achieved by a forming properly the soil in the foot of each pier [3]. Purpose of the applied solution was the uniform distribution of stiffness and therefore of seismic shear force to piers. In this case the regularity of the bridge is derived from the division of the deck into two statically independent parts which cannot be generalized. On the other hand this causes problems regarding the bearing capacity of the bridge in gravity loads.

The present study suggests a proper pier's section forming of irregular bridges, due to great variation of piers' height, aiming to improve their seismic response. The proposed modification is applied in a road bridge of great length in Egnatia Motorway in Greece which was designed according to former codes [2], but according to EC8 - Part2 is characterized irregular. Finally comparative results are extracted and evaluated.

## 2 CODE PROVISIONS

Regarding the seismic design of bridges Eurocodes introduce the concept of regular seismic behaviour. According EC8 - Part2 the dimensionless quantity  $r_i$  for each one of the bridge's is defined by the following expression:

$$r_i = q \cdot \frac{M_{Ed,i}}{M_{Rd,i}} \quad (1)$$

where  $q$  is the behaviour of the bridge as calculated based on  $\eta_k$  and the minimum shear span ratio of the piers,  $M_{Ed,i}$  is the maximum design moment at the intended plastic hinge location of ductile member  $i$  as derived from the analysis for the seismic design situation and  $M_{Rd,i}$  the design flexural resistance of the same section with its actual reinforcement under the concurrent action of the non-seismic action effects in the seismic design. From the Eq.(1) derives the possible diminution of the  $r_i$  factor in cases  $M_{Rd}$  exceeds  $M_{Ed}$  due to the use of minimum reinforcement, which is not rare in bridge designing. In the case when in every pier the reinforcement ratio exceeds the minimum then  $r \approx q$  and this is a definite case of regular bridge. However, EC8 pushes the boundaries of regularity and uses as criterion for the classification of a bridge the quotient  $r_{max}/r_{min}$ , where  $r_{max}$  and  $r_{min}$  are respectively the maximum and the minimum  $r$  for all of the piers of the bridge. According to EC8, a bridge is considered to have regular seismic behaviour when the quotient  $r_{max}/r_{min}$  does not exceed the value of  $\rho_0$  which is defined in the National Annex. The suggested value for  $\rho_0$  is 2.0.

$$\rho = \frac{r_{\max}}{r_{\min}} \leq \rho_0 = 2 \quad (2)$$

When  $r_{\max}/r_{\min}$  is greater than 2.0, the bridge is considered to have irregular seismic behaviour. In this case during the consecutive forming of plastic hinges there is increased likelihood of unacceptably high ductility demands at least for the pier  $r_{\max}$ .

Regarding the design the bridge a priori is considered to be regular. Subsequently, after the calculation of flexural resistance of the piers, the definitive classification of the bridge takes. In the design of irregular bridges EC8 – Part2 imposes the “penalty” of a reduced value of q-factor according to the following expression:

$$q_r = q \cdot \frac{\rho_0}{\rho} \quad (3)$$

Instead of the aforementioned reduction of the value of q-factor, the bridge shall be designed based on results of non-linear analysis. Thereby, a better supervision can be acquired regarding the sequence of formation of plastic hinges and a possible change in the distribution of stiffness [1]. Either by the use of a reduced q-factor or the use of more complex non-linear methods of analysis the cost of the bridge is increased significantly.

### 3 APPLY OF THE MODIFICATION IN AN INTEGRAL BRIDGE OF GREAT LENGTH

#### 3.1 Purpose of the modification

The suggested modification, which is explained subsequently, was applied in a long integral road bridge of Egnatia Motorway in Greece and the analysis results were evaluated by being compared with the results of the analysis of the “reference” bridge, which has been designed according to the German DIN-1075 [2]. The “reference” bridge is suitable for this study because deviates from regularity due to its geometrical characteristics. For the study purposes the bridge was designed two times according to EC8 –Part2: a) as irregular, considering the section geometry of the piers as they were constructed according to DIN-1075 and b) with modified section geometry of the piers so that it corresponds to provisions about regularity. The above mentioned designs led to comparative results which have been used to evaluate the suggested modification.

#### 3.2 Description of the “reference” bridge

The bridge which is used as a “reference” case of study is the left part of a viaduct, part of Egnatia Motorway, connecting Arachthos with Peristeri in Greece. It has six spans (34m+4x43m+34m) and a total length of 240m (*Fig.1*).

The cross section of the deck is a box-girder and has a total width of 12.90m (Fig.2a). The deck is rigidly connected with the five piers and is seated on both of the abutments on sliding bearings. Abutments' bearings have a circular section with diameter equal to 600mm. There is also a shear key with a load capacity of 176ton. Piers have the section shown in Fig.2 and are founded on 3 x 3 pile groups which are connected to 7.90x8.70x2.20m pile caps. The diameter of the piles is 1.20m and their length is 12.0m for all the piers. The abutments have a height of 2.0m and 4.0m, are conventional seat-type abutments and are founded on a shallow foundation with dimensions of 5.50x13.20x1.20m and 6.00x13.20x1.20m respectively. The bridge is founded on ground similar to Eurocode's 8 ground type B and a design ground acceleration equal to 0.16g was used in the final design. The importance factor adopted was equal to 1.30 and the behaviour factors (q-factors) were equal to 3.50 for the longitudinal, 2.24 for the transverse, without taking into account the reduction due to irregularity, and 1.00 for the vertical direction of the bridge [4].

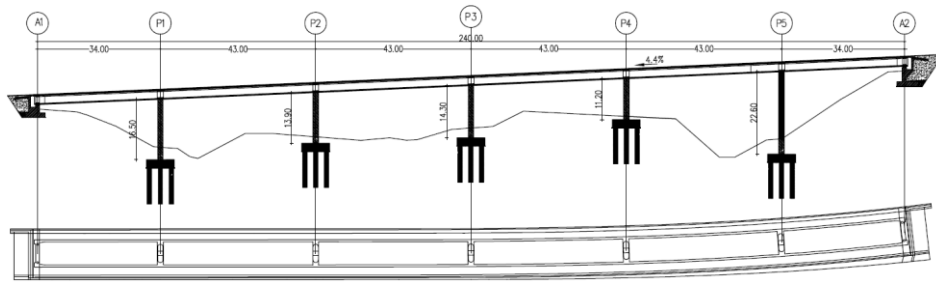


Figure 1. Longitudinal section plan view of the left part of the bridge

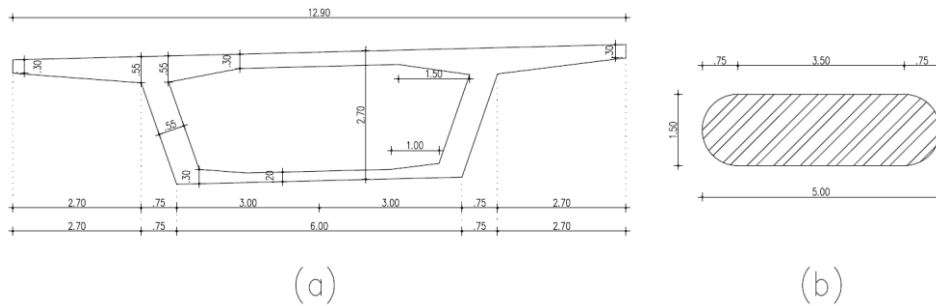


Figure 2. (a) Cross section of the deck at mid-span – (b) Cross section of the piers

### 3.3 Description of the proposed modification

From the Eq.(1) and Eq.(2) derives the deduction that regularity depends closely on the actual reinforcement of the piers. Specifically it can be said that the fewer the piers with the minimum by the codes reinforcement ratio of 1.0% are, as well as the closer the requisite reinforcement of these piers to the minimum ratio, the more the regularity of the bridge gets improved.

In the present study is attempted the diminution of the value of  $\rho$ -factor by minimizing the numerators in Eq.(1) and Eq.(2). This means that the diminution of the moment  $M_{Ed,i}$  in Eq.(1) is requisite to be reduced. This can be achieved by the drastic reduction of the effective section height of the pier which develops the largest percentage of seismic shear. Thus a dividing of its section into two, three or more segments of equal height can affect positively the  $\rho$ -factor. Regarding the transverse direction of the ‘reference’ bridge, in which the proposed modification cannot be applied for obvious reasons, the choice of this type of section (*Fig.2b*) for the piers in combination with the low value of shear span ratio for most of the piers are determinant and lead to a low value of  $q$ -factor. Therefore, it is estimated that a further reduction of the  $q$ -factor due to irregularity, is not expected to induce drastic alteration. In this contributes as well the favorable orientation of the piers’ sections which with a relatively low percentage of longitudinal reinforcement can receive seismic forces calculated with the minimum by the codes for integral bridges  $q=1.5$ .

Regarding the improvement of the longitudinal direction it is deemed necessary to modify the section of four of the bridge’s piers except of the end-pier which is the highest and hence it can be omitted from the calculation process of regularity. Specifically, the following modifications are required: a) in the most adverse of the piers, which is the shortest (P4), is demanded the dividing of its section into two segments (*Fig.3*) throughout its height (11.20m), b) in the other three piers (P1, P2 and P3) is also demanded the dividing of their sections into two segments, extending symmetrically to their mid-height for 11,20m. A solid section is used for the rest of their height.

Based on the above mentioned the resulting  $\rho$ -factors are  $\rho_x=2.0$  for the longitudinal and  $\rho_y=1.16$  for the transverse direction of the bridge. It is noted that the  $r$ -factors for the ‘reference’ bridge are  $\rho_x=2.85$  for the longitudinal and the same as above for the transverse direction of the bridge. Subsequently are sited the following observations:

1st: The suggested modification resulted in the drastic reduction of the total stiffness of the system, as the fundamental period  $T_x=1.74\text{sec}$  for the longitudinal direction of the regular bridge, which is designed with a behaviour factor  $q_x=3.50$ , versus  $T_x=1.06\text{sec}$  of the irregular bridge, which is designed with a reduced  $q$ -factor, led to additional reduction of the design seismic actions.

2nd: The reduced  $q$ -factor of the irregular bridge induced an increase in the

longitudinal reinforcement of the piers which led to an improved  $\rho$ -factor  $\rho_x=2.0$ . Regarding the re-calculation of the  $\rho$ -factor, it is supposed that if a bridge accrues irregular after the design with a reduced  $q$ -factor it is not required to reduce furthermore the  $q$ -factor.

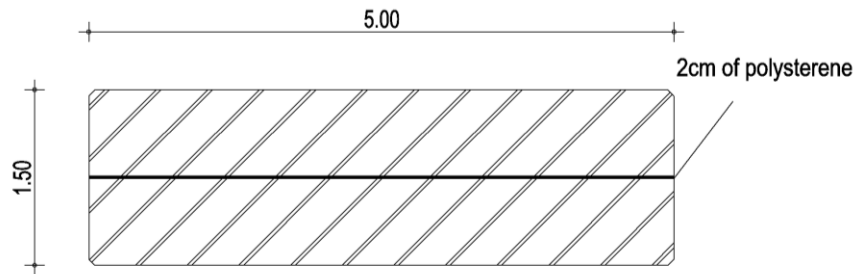


Figure 3. Modified section of the piers

#### 4 RESULTS

For the dynamic analysis was used S.A.P.2000 v.11.0.4 [5] and for the calculation of the flexural resistance, the yield curvature necessary for the calculation of the effective stiffness of the piers was used the program of the piers was used the program RCCOLA.NET v.0.972 [6].

Regarding the dynamic attributes, as above mentioned, is noticed a significant increase of the fundamental period of the structure for the longitudinal direction. More specifically, the “reference” bridge has a fundamental period  $T_x=1.06\text{sec}$  while the bridge with the modified piers has a fundamental period  $T_x=1.74\text{sec}$ . The observed increase is 64.2% while the reduction of the total seismic shear force in the longitudinal direction is 53.2%. In transverse direction, the fundamental period is unchanged, equal to  $T_y=0.67\text{sec}$ . The inelastic transaction ( $q \cdot d_E$ ) in the longitudinal direction for the “reference” bridge is equal to 9.6cm while for the modified system is equal to 11.0cm.

In Fig.4 is displayed the distribution of seismic shear force in the longitudinal direction for the “reference” bridge, considering the reduced behaviour factor  $q_{r,x}=2.46$  and for the modified one, considering  $q_x=3.50$ . It is obvious that in the modified bridge the distribution of shear force in the piers is uniform due to similar stiffness of the piers. In the “reference” bridge the ratio of the maximum and the minimum seismic shear force in piers P4 and P5 respectively is equal to  $V_{E,\max}/V_{E,\min}=7.9$  while in the modified system is equal to 1.9. It is noted that uniformity in shear distribution is desired.

Regarding the reinforcement ratio of the piers of the “reference” bridge, all the piers except of the pier P4 are reinforced with the minimum ratio of 1.00%. In pier P4 a reinforcement ratio of 1.70% is required. In piers P1, P2, P3 and P5



the required reinforcement ratio is clearly less than 1.00%. This is reflected in the  $r_i$  quantities which are clearly of lower value than the  $q$ -factor (Table 1 and Table 2). It is reminded that the lower the value of  $r_i$  of a ductile member  $i$ , the less the exploitation of its available ductility. In the modified bridge it is obvious that we have better exploitation of the available ductility of the piers. In this case the required reinforcement ratio is 1.00% for all of the piers.

The factor  $\rho = r_{max}/r_{min}$  for the “reference” bridge in the longitudinal direction is equal to  $2.85 > \rho_0 = 2$ . In this case a reduced behaviour factor  $q_r = 2.46$  instead of  $q = 3.50$  is considered. Contrariwise, in the modified bridge the  $\rho$ -factor is equal to  $\rho_x = 2.0$  and a behaviour factor of  $q = 3.50$  is acceptable. Regarding the transverse direction, as above mentioned, there is no change in results. In this case the  $\rho$ -factor is equal to  $\rho_y = 1.16$  due to the ignoring of the piers P1 and P5, which total seismic shear force does not exceed 20% of the total seismic shear.

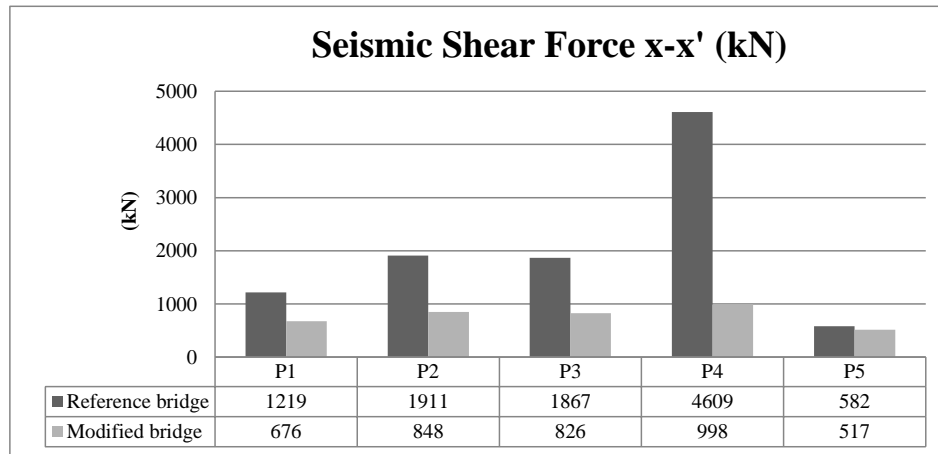


Figure 4. Comparison of seismic shear force in the longitudinal direction for the irregular bridge with reduced  $q$ -factor and the modified-regular bridge

Table 1. Summarized results of the “reference” bridge

	$V_{E,x}/V_{E,x,tot}$ (%)	$V_{E,y}/V_{E,y,tot}$ (%)	$M_{Ed,x}$ (kNm)	$M_{Ed,y}$ (kNm)	$M_{Rd,x}$ (kNm)	$M_{Rd,y}$ (kNm)	$r_x$	$r_y$
P1	12.80	11.60	24694.94	16470.17	27785.50	81652.30	3.11	0.61
P2	20.55	29.07	20324.88	36228.53	27969.40	82124.40	2.54	1.33
P3	20.19	23.31	9509.02	31835.58	28007.00	82220.80	1.19	1.17
P4	40.50	32.34	31296.73	35671.77	32360.00	93496.90	3.38	1.15
P5	5.96	3.68	14312.18	5898.65	28344.90	83085.60	1.77	0.21

Table 2. Summarized results of the modified bridge

	$V_{E,x}/V_{E,x,tot}$ (%)	$V_{E,y}/V_{E,y,tot}$ (%)	$M_{Ed,x}$ (kNm)	$M_{Ed,y}$ (kNm)	$M_{Rd,x}$ (kNm)	$M_{Rd,y}$ (kNm)	$r_x$	$r_y$
P1	17.48	11.29	5865.27	7119.43	7296.30	39455.30	2.81	0.54
P2	21.94	29.02	4857.45	16215.91	7367.50	39795.50	2.31	1.23
P3	21.38	24.34	3038.05	15236.32	7340.80	39688.10	1.45	1.16
P4	25.82	31.61	6088.45	17711.00	7364.50	39780.90	2.89	1.34
P5	13.38	3.73	16425.85	6304.13	28429.40	83301.20	2.02	0.23

## 5 CONCLUSIONS

In the present study is suggested a process of modification in piers of necessarily orthogonal section of irregular, according to EC8-Part2, integral bridges. The proposed modification process consists in the selective section dividing into segments of equal thickness of one or more piers of the bridge. Taking into account the results taken by the implementation of the proposal in a clearly irregular integral bridge of great length, the following conclusions are noted:

- The proposed method of modification is simple in understanding and application.
- Its association with economy is obvious as by applying this modification, the “penalty” of irregularity in the behaviour factor of the bridge system can be avoided. The effect on economy becomes more intense as the stiffness of the modified bridge is reduced and so do the design seismic forces.

## ACKNOWLEDGMENTS

The authors wish to express their gratitude to METE SYSM S.A. for providing the original study of the bridge for the purposes of the present study.

## REFERENCES

- [1] CEN [Comité Européen de Normalisation], *EN 1998-2: Eurocode 8: Design of Structures for Earthquake Resistance - Part 2: Bridges*, 2005.
- [2] Deutsches Institut Fur Normung E.V., *DIN 1075: Concrete Bridges; Dimensioning and Construction*, 1981.
- [3] Saïid Saïidi, M, Moore, TR, Itani, A, “Seismic performance of reinforced concrete bridges with unconventional configurations”, *ACI Structural Journal*, American Concrete Institute, title no. 98-S69, 2001
- [4] Pilitsis, V, Tegos, I, “Employment of abutments and approach embankments for seismic protection of bridges”, *Proc. Intl. Van Earthquake Symposium*, Van, Turkey, 2013.
- [5] Computers and Structures Inc., *S.A.P. 2000 Nonlinear ver.11.0.4*, 2007
- [6] Kappos, AJ, Panagopoulos, G, *RCCOLA.NET ver.0.972*, 2011

## **VULNERABILITY FUNCTIONS TO ESTIMATE THE SEISMIC DAMAGE RESPONSE FOR THE KRYSTALLOPIGI BRIDGE OF EGNATIA MOTORWAY, NORTHERN GREECE**

Asterios Liolios<sup>1</sup>, Panagiotis Panetsos<sup>2</sup>, Angelos Liolios<sup>1</sup>,  
George Hatzigeorgiou<sup>3</sup> and Dimitrios Kalkinis<sup>4</sup>

<sup>1</sup> Democritus University of Thrace, Dept. Civil Engineering, Xanthi, Greece,

<sup>2</sup> Structures Inspection & Maintenance, EGNATIA ODOS A.E., Thessaloniki – Themi, Greece,

<sup>3</sup> Democritus University of Thrace, Dept. Environmental Engineering, Xanthi, Greece,

<sup>4</sup> Aristotle University of Thessaloniki, Dept. Civil Engineering, Thessaloniki, Greece,  
e-mails: <sup>1</sup> liolios@civil.duth.gr, <sup>2</sup> ppane@egnatia.gr, <sup>4</sup> dkalkinis@hotmail.com

**ABSTRACT:** Vulnerability functions represent a critically important step in seismic damage estimation process. A simplified analytical methodology, combining the nonlinear static pushover procedure and the capacity spectrum method, is applied for establishing fragility curves for an existing reinforced concrete bridge with seismic stoppers in the Krystallopigi – Psilorahi section of Egnatia Motorway, in the county of Epirus, northern Greece.

**KEY WORDS:** Assessing structural vulnerability, Bridges fragility curves.

### **1 INTRODUCTION**

A key element in formulating mitigation and disaster planning strategies is the estimation of the urban seismic risk in Earthquake Engineering [1]. In this respect, development of vulnerability relationships for both, the existing and under design Civil Engineering structures, represents a critically important step in damage estimation process. Scope of the vulnerability analysis is the creation of the so-called fragility curves [1-4, 9-11], through which the probability that a specific damage level will be exceeded for a given intensity of a seismic event may be quickly estimated, supporting significantly the decision-making procedures.

So, fragility curves for Civil Engineering Structures, such as buildings and especially bridges, are a useful tool for the assessment of the damage they may sustain for a certain level of earthquake shaking. In combination with seismic hazard analysis at the bridge sites, they can lead to a reliable assessment of the seismic risk of highways. Furthermore, they can even be used by the authorities in charge to prioritize the on site aftershock inspections, in order to check the structural integrity of the bridges subjected to a severe seismic event.

Several methodologies dealing with the assessment of fragility curves for bridges can be found in recent literature, based on either empirical or analytical procedures [2-3,9-11]. Also, methodologies originally proposed for buildings can sometimes be extended for use in the case of bridges [2-4,14].

In the present article, a simplified analytical methodology for the evaluation of vulnerability curves for bridges having deck on precast beams, seating through elastomeric bearings on the piers and with seismic stoppers is presented. The methodology combines the nonlinear static pushover procedure and the capacity spectrum method [1-3,9-11], and in connection to the details of [5,16] is applied for establishing fragility curves for an existing reinforced concrete bridge crossing a steep slope in the Kristallopigi – Psilorahi section of Egnatia Motorway, in the county of Epirus, Northern Greece.

## 2 METHODS FOR ASSESSING STRUCTURAL VULNERABILITY

The vulnerability functions, required for the fragility curves, are expressed [2-4, 9-11] in terms of a Lognormal cumulative probability function in the form of next eq. (1):

$$P_f(DP \geq DP_i | S) = \Phi \left[ \frac{1}{\beta_{tot}} \cdot \ln \left( \frac{S}{S_{mi}} \right) \right] \quad (1)$$

Here  $P_f(\cdot)$  is the probability of the damage parameter  $DP$  being at, or exceeding, the value  $DP_i$  for the  $i$ -th damage state for a given seismic intensity level defined by the earthquake parameter  $S$  (here the Peak Ground Acceleration-PGA or Spectral Displacement- $S_d$ ),  $\Phi$  is the standard cumulative probability function,  $S_{mi}$  is the median threshold value of the earthquake parameter  $S$  required to cause the  $i$ -th damage state, and  $\beta_{tot}$  is the total lognormal standard deviation. Thus, the description of the fragility curve involves the two parameters,  $S_{mi}$  and  $\beta_{tot}$ , which must be determined.

Now we consider briefly the problem of computing the vulnerability functions (1) for reinforced concrete bridges with seismic stoppers. This case is a contact mechanics problem, where pounding of adjacent beams can take place. Pounding belongs to the so-called Dynamic Inequality Problems of Mechanics, for which a strict mathematical treatment can be obtained by using the variational or hemivariational inequality concept. As well known, the latter one has been introduced in Mechanics by P.D. Panagiotopoulos [4]. As their numerical treatment is concerned, many significant contributions are already available, see e.g. [4,6]. So, for the case of two interacting structures (A) and (B), following e.g. the procedure of [7], the problem is first formulated as an inequality one by using concepts of Non-Convex Analysis. Next, double discretization, in space by the Finite Element Method and in time by a direct-time integration scheme (e.g. the central difference method), and optimization

methods are used. Thus, by piecewise linearization of the interface unilateral contact laws, at each time-step a nonconvex linear complementarity problem of the following matrix form with reduced number of unknowns is finally solved:

$$v \geq 0, \quad A v + a \leq 0, \quad v^T \cdot (A v + a) = 0. \quad (2)$$

So, the nonlinear Response Time-History (RTH) for a given seismic ground excitation can be computed.

The present study focuses on the simplified practical fragility analysis of bridges, that involve impacts due to the seismic stoppers designed to effectively withstand earthquake loads and reduce the size of the piers. For such a practical simplified analysis, these systems are represented by single and multi degree of freedom models with piecewise linear elastic stiffness elements that often involve strong inelastic behavior in parts of the system. So, the previous general approach for pounding of adjacent structures is simplified by considering the simple bridge with seismic stoppers shown in Figure 1a. The bridge deck is connected to the piers by elastomeric bearings and seismic stoppers are added on the pier caps that have a small gap with the deck structure so that the elastomeric bearings are free to move under ambient or traffic loads, while they impact on the stoppers only under moderate or strong earthquake loads. Activation of the stoppers due to impact results in sudden increase of the stiffness of the structure.

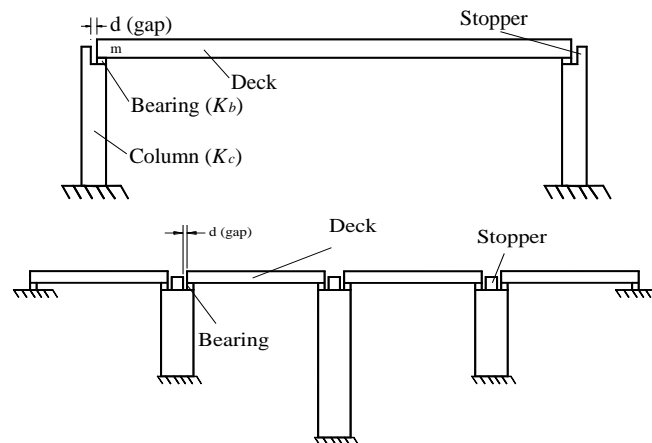


Figure 1. Schematic diagram of (a) single span bridge and (b) multi span bridge.

Further, assuming a heavy undeformed deck of mass  $M$  and representing the stiffness of the piers and the elastomeric bearing by massless linear or inelastic springs, one can construct [8] a single degree of freedom (SDOF) simplified model of the bridge as shown in Figure 2a. For the case of stopper activation but no pier yielding, the springs are linear and the simplified system in Figure

2a behaves as a SDOF piecewise linear elastic system. For the case of elastoplastic spring representing the inelastic behavior of the deck, the system in Figure 2a behaves as a SDOF piecewise linear inelastic system with gap elements.

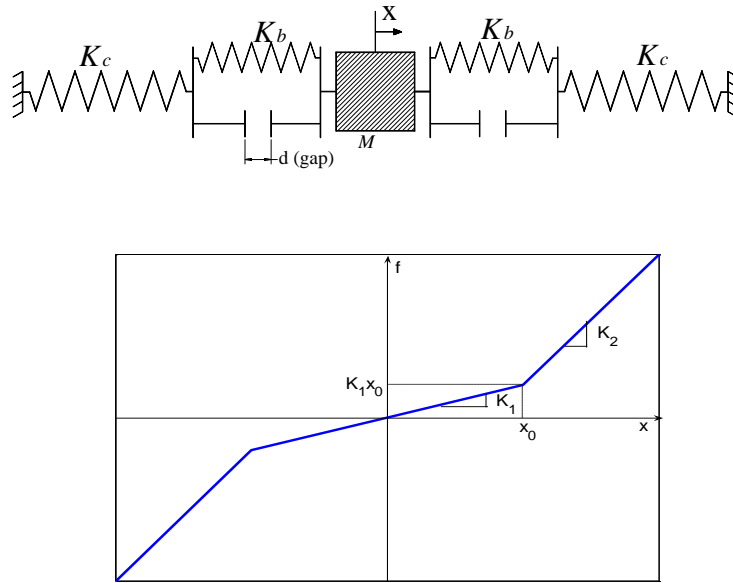


Figure 2. (a) Simplified SDOF system with bilinear stiffness and (b) elastic force-displacement relationship.

Consider in Figure 2a the SDOF model of the structure, shown in Figure 1a, with mass  $M$ , column stiffness  $K_c$ , bearing stiffness  $K_b$  and base excitation  $\ddot{z}(t)$ , assumed same at both left and right supports. The equation of motion for the model is given by:

$$M\ddot{x} + C\dot{x} + f(x) = -M\ddot{z} \quad (3)$$

where the term  $C\dot{x}$  accounts for the overall viscous damping on the system.

The bilinear restore force due to the gap  $d$  is given by:

$$f(x) = \begin{cases} K_1 \cdot x & -x_0 \leq x \leq x_0 \\ K_1 \cdot x_0 + K_2(x - x_0) & x > x_0 \\ -K_1 \cdot x_0 + K_2(x + x_0) & x < -x_0 \end{cases} \quad (4)$$

where  $K_1 = 2K_c / (1 + \kappa)$ ,  $K_2 = K_1 / (1 + \kappa / 2)$ ,  $x_0 = d(1 + \kappa) / \kappa$ ,  $\kappa = K_c / K_b$ .

If the input ground acceleration  $\ddot{z}(t)$  is given, and under given initial conditions, the response history  $x(t)$  can be computed as in [7,8] on the basis of (3) and (4).

From the previous analysis is obvious that the damage level depends on the input seismic excitation, i.e. the seismic ground acceleration. As well known from Structural Dynamics and Earthquake Engineering [1], because this input is not known for future earthquakes, the spectral approach is used according to various aseismic building codes, e.g. the Greek Aseismic Code EAK2000 [12]. So here, instead of a non-linear dynamic analysis, which is time consuming [1], the approach of [4,14, 16] is followed.

According to equation (1), the description of the fragility curve involves only two parameters,  $S_{mi}$  and  $\beta_{tot}$ . The first parameter  $S_{mi}$  is estimated on the basis of the capacity spectrum method [1, 16], wherein the demand spectrum is plotted for a range of values of the earthquake parameter  $S$  (in spectral acceleration vs. spectral displacement format) and it is superimposed on the same plot with the capacity curve of the bridge. The second parameter of Eq. (1) is the total lognormal standard deviation  $\beta_{tot}$ , which takes into account the uncertainties in seismic input motion (demand), in the response and resistance of the bridge (capacity), and in the definition of damage states. This parameter ( $\beta_{tot}$ ) can be estimated by a statistical combination of the individual uncertainties (in demand, capacity, and damage state definition) assuming these are statistically independent. For more details of the proposed methodology see [17].

### **3 THE CASE OF AN EGNATIA MOTORWAY BRIDGE WITH SEISMIC STOPPERS**

The bridge considered herein is the G2 valley-bridge near Kristallopigi, Epirus, built on the west sector of the Egnatia Motorway, in northern Greece. The 100m long bridge is carrying the right branch of the motorway over a steep mountain slope near Kristallopigi.

The bridge consists of three equal spans, each constructed using six 33m long prestressed – precast concrete beams that rest on two piers and two abutments via elastomeric bearings, as shown in Photos 1,2.



Photos 1,2. The G2/Kristallopigi bridge on Egnatia Motorway.

The reinforced concrete piers are twin square columns, 20m high, framed by an orthogonal beam that supports the precast beams through 6 type NB4 rectangular elastomeric bearings with dimensions 600x700x255 (135) in (mm).

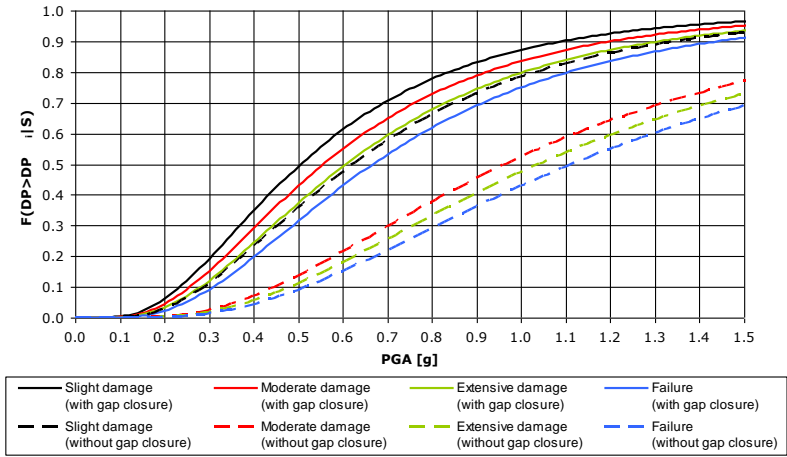
A 25cm thick in situ reinforced concrete slab, on the top of the beams, continues over the piers. It is acting as a diaphragm along the total length of the bridge, which is separated by the abutment ballast walls through elastometallic anchored joints, by gaps of 20 cm. Stoppers on the pier's beams were designed to be distant from the superstructure such as to be activated after the exceeding of the maximum spectral displacement.

Due to limited space here, details for the geometric and elastic characteristics of the bridge elements are given in [17], where also the computation steps for obtaining the fragility curves are given in details. Finally, Fig. 3 shows the fragility curves, which were computed assuming a lognormal cumulative probability distribution for the damage ratio as a function of peak ground acceleration PGA.

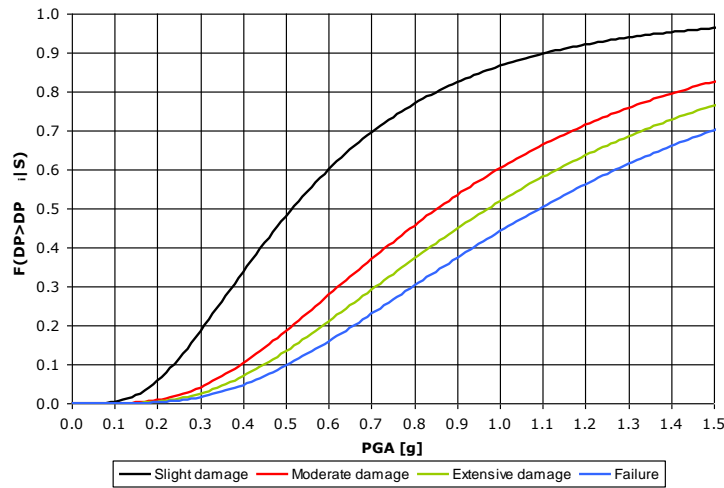
#### 4 CONCLUSIONS

A simplified methodology has been presented for the calculation of the vulnerability curves of bridges in the presence of seismic stoppers. This methodology is based on a modal pushover nonlinear static analysis and on a capacity demand spectrum approach, instead of a time consuming non-linear dynamic based vulnerability analysis. Using the aforementioned approach, fragility curves were developed for the G2 Kristallopigi valley bridge, which is situated in the Egnatia Motorway, Epirus section, northern Greece.





(a) Longitudinal direction



(b) Transverse direction

Figure 3. Fragility curves of the G2 Kristallopigi bridge

**ACKNOWLEDGEMENTS**

The first two co-authors of this paper have participated in the Research Project ASPROGE (ASeismic PROtection of BRidges), funded by the General Secretariat of Research and Technology of Greece and by EGNATIA ODOS S.A., Thessaloniki, Greece.

## REFERENCES

- [1] Chopra, A.K. (2007). "Dynamics of Structures. Theory and Applications to Earthquake Engineering." *Pearson Prentice Hall*, New Jersey
- [2] Elnashai A., Rossetto T. (2003). "Derivation of Vulnerability Functions for European Type RC Structures Based on Observational Data". *Engng Structures*, 25, 1241-1263
- [3] Shinozuka, M., Feng, M.Q., Lee, J., and Naganuma, T. (2000). "Statistical Analysis of Fragility Curves". *Journal of Engineering Mechanics*, 126, No. 12, 1224-1231
- [4] Panagiotopoulos, P.D. (1993). "Hemivariational Inequalities and Applications in Mechanics and Engineering". *Springer Verlag*, Berlin.
- [5] Makarios Tr., Lekidis V., Kappos A., Karakostas Chr. and Moschonas J. (2007). "Development of seismic vulnerability curves for a bridge with elastomeric bearings". In: Papadrakakis E. et al (Eds.), *Proceedings of the COMPDYN 2007, ECCOMAS*, Rethymno, Crete, Greece.
- [6] Panagiotopoulos, P.D., Glocker, Ch. (2000). "Inequality constraints with elastic impacts in deformable bodies. The convex case". *Arch. Appl. Mech.* 70, 349-365.
- [7] Liolios, A.A. (1989). "A linear complementarity approach to the nonconvex dynamic problem of unilateral contact with friction between adjacent structures." *Z. Angew. Math. Mech. (ZAMM)*, 69, T 420-422.
- [8] Perros K., Papadimitriou C., Karamanos S. and Panetsos P. (2007). "Response and Reliability of Nonlinear Systems with Impacts Subjected to Transient Excitations". In: Papadrakakis E. et al (Eds.), *Proceedings of the COMPDYN 2007, ECCOMAS*, Rethymno, Crete, Greece.
- [9] Hwang H.H.M and Jaw J.W. (1990). "Probabilistic damage analysis of structures." *J. struct. Enging. ASCE*, 116(7), 1992-2007.
- [10] Shinozuka M., Hwang H. and Reich M. (1984). "Reliability assessment of reinforced concrete containment structures." *Nuc. Enging. Des.*, 80, 247-267.
- [11] Park Y-J., Ang A.H-S.: Mechanistic Seismic Damage Model for Reinforced Concrete. *Journal of Structural Engineering (ASCE)*, 111, 740-757 (1985).
- [12] EAK2000: Greek Aseismic Code. (2000). *Ministry of Public Works and Environment, OASP (Organization of Seismic Protection)*, Athens,
- [13] SAP2000 (2005). "Linear and Non linear Static and Dynamic Analysis and Design of Three-Dimensional Structures". *Computers and Structures Inc.*, Berkeley, California
- [14] ASPROGE (2007). "Research Project for the ASeismic PROtection of Bridges. Egnatia Odos S.A", Thessaloniki, Greece.
- [15] Liolios, A., Panetsos, P. & Makarios, T. (2007). "Seismic fragility functions for a bridge of Egnatia motorway in northern Greece". *Proceedings of the 6th German-Greek-Polish Symposium "Recent Advances in Mechanics"*, Alexandroupolis, Greece, Sept. 17-21, 2007.
- [16] Moschonas, I.F., Kappos, A.J., Panetsos, P., Papadopoulos, V., Makarios, T., Thanopoulos, P. (2009). "Seismic fragility curves for greek bridges: Methodology and case studies". *Bulletin of Earthquake Engineering*, 7(2), pp. 439-468.
- [17] Panetsos, P. & Liolios, A. (2010). "Seismic vulnerability functions for a bridge case of Egnatia motorway". In: Kappos, A.J. (editor), *"Aseismic design and constructions in EGNATIA ODOS, the highway connecting Epirus through Macedonia to Thrace and eastern border of Greece"*, Hellenic Society for Earthquake Engineering, Thessaloniki, 2010.

IBSBI 2014, October 16-18, 2014, Athens, Greece

## **“DE BOSSET” MONUMENTAL STONE BRIDGE IN CEPHALONIA: STRENGTHENING MEASURES AND SEISMIC RESPONSE UNDER THE EARTHQUAKES OF 26/01/2014 AND 03/02/2014**

Emmanouil Rovithis<sup>1</sup>, Kyriazis Pitolakis<sup>2</sup>, Themistoklis Vlachoulis<sup>3</sup>,  
Ioanna Karani<sup>3</sup>, Efi Chorafa<sup>3</sup> and Eleni Zarogiani<sup>3</sup>

<sup>1</sup>Earthquake Planning and Protection Organization EPPO-ITSAK, Greece

<sup>2</sup>Aristotle University of Thessaloniki, Dept. of Civil Engineering, Greece

<sup>3</sup>Directorate for the Restoration of Byzantine and Post-byzantine Monuments, Greek Ministry of  
Culture, Greece

e-mail: rovithis@itsak.gr, kpitolak@civil.auth.gr, thvlachoulis@culture.gr, ikarani@culture.gr,  
efi.chorafa@yahoo.gr, ezaro22@yahoo.com

**ABSTRACT:** The historic stone masonry “De Bosset” bridge in Argostoli sustained the recent Cephalonia earthquake sequence of 26/01/2014 and 03/02/2014 mainshocks with no damages or visible defects. The above seismic performance of the bridge is analyzed in conjunction with the favorable effect of rehabilitation measures deployed prior to the two earthquakes.

**KEY WORDS:** Cephalonia earthquakes; finite-element analysis; micropiles; stone masonry bridges;

### **1 INTRODUCTION**

The assessment of interventions effect on the seismic response of old stone masonry bridges requires careful consideration of a large number of parameters such as foundation soil conditions, complex geometry, inhomogeneity of construction materials, deterioration of structural strength due to past loading, identification of failure modes and knowledge of the existing vulnerability level of the structure ([1], [2], [3]). Along these lines, in-situ inspection, field measurements and, most importantly, real earthquake recordings following an earthquake event compose a particularly valuable piece of information when dealing with the behavior of such complex structural systems under seismic loading [4].

In January 26, 2014 and February 3, 2014 two strong earthquakes of magnitude M6.1 and M6.0, respectively, stroke the Cephalonia Island inducing severe geotechnical failures and major damages on structures and lifelines due to the particularly high ground accelerations that were recorded close to the peninsula of Paliki and the nearby regions. The latter was verified from the

ground motions recorded by the permanent accelerometric stations installed on island of Cephalonia by EPPO-ITSAK as part of the Greek National Accelerometric Network and complemented by temporal accelerometric stations deployed after the first earthquake of 26/01/2014 ([5], [6]).

Despite the high acceleration levels induced by the above earthquake sequence, the historic multi-span stone masonry “De Bosset” bridge, connecting the city of Argostoli with the opposite shoreline (Drapano) at the southern side of Argostoli bay, experienced no damages or visible defects indicating a particularly good seismic performance. Prior to the two earthquakes, extensive rehabilitation works were undertaken at the bridge site under the auspices of the Directorate for the Restoration of Byzantine and Post-byzantine Monuments of the Greek Ministry of Culture, by combining foundation soil improvement and structural strengthening measures proposed in the study of Pitilakis et al. [7].

As a follow up on the earlier study reported by the authors in reference [8], this paper gives a detailed description of the interventions scheme and the architectural restoration. Specific emphasis is placed on technical solutions applied on-site to overcome practical difficulties that emerged during the construction phase. The particularly good seismic performance of the bridge following the two earthquakes is investigated by implementing ground motions recorded by a nearby accelerometric station. For this reason, the three-dimensional finite-element model of the bridge employed for the design of the intervention scheme [8] is reanalyzed herein under the recorded ground motions to conclude on the effectiveness of the strengthening measures.

## **2 PRE-REHABILITATION STATE OF THE BRIDGE**

The “De Bosset” bridge of 750m length (*Fig. 1a*) and varying height between 2 to 4m was first constructed in 1830 comprising of successive stone arches founded on stiff block-type abutments. The destructive  $M_s = 7.2$  earthquake of 1953 [9] induced severe damages to the bridge such as differential settlement, extensive longitudinal cracks and local out-of-plane collapse of the arch walls and the filling material (*Fig. 1b*) resembling the characteristic failure mechanism of old stone masonry bridges [10]. Major parts of the bridge were reconstructed during the period of 1960–1970 with reinforced concrete leading to structural materials inhomogeneity, poor connection between old and new structural system and substantial modification of the original bridge stiffness. It is noted that the authentic dry stone material was preserved only in the first two arches.

### **2.1 Observations based on field and laboratory tests**

A large experimental campaign was performed on 2005 as part of a project for the seismic assessment and restoration of the “De Bosset” bridge undertaken by the Laboratory of Soil Mechanics, Foundations & Geotechnical Earthquake

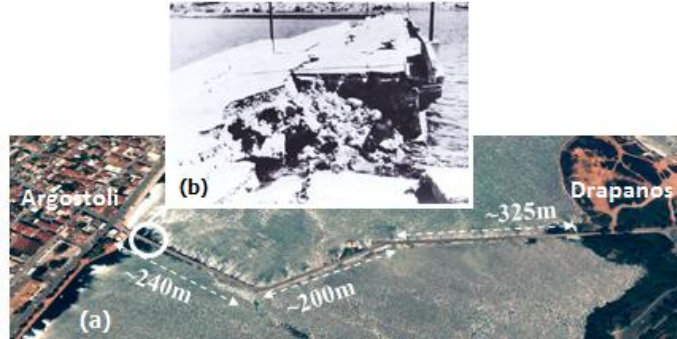


Figure 1. (a) Google earth image of the 750m long “De Bosset” bridge connecting Argostoli to the opposite shoreline (Drapanos) (b) Out-of-plane collapse at a bridge section close to Argostoli after the 1953 earthquake ( $M_s=7.2$ ).

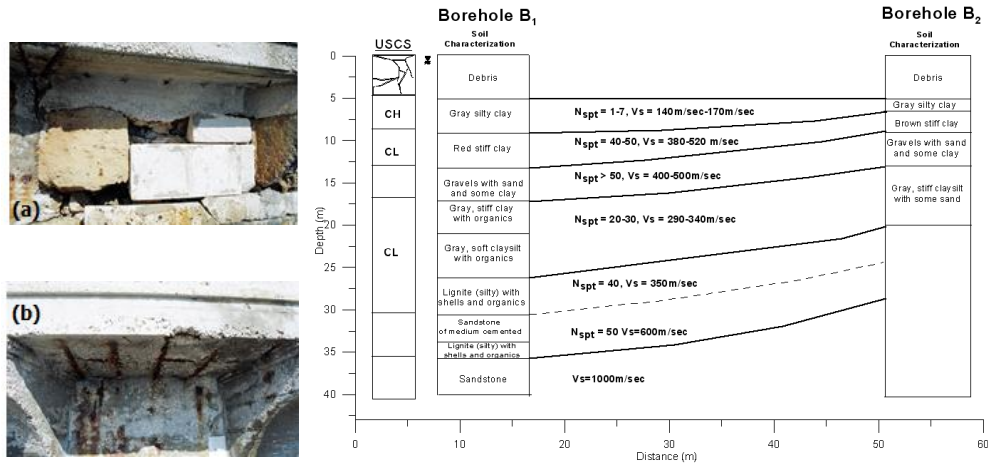


Figure 2. (a-b) Pre-rehabilitation state of the bridge: Major defects on stone and concrete sections of the bridge (c) 2D geotechnical cross-section and foundation soil characterization at the bridge site based on field surveys and laboratory tests.

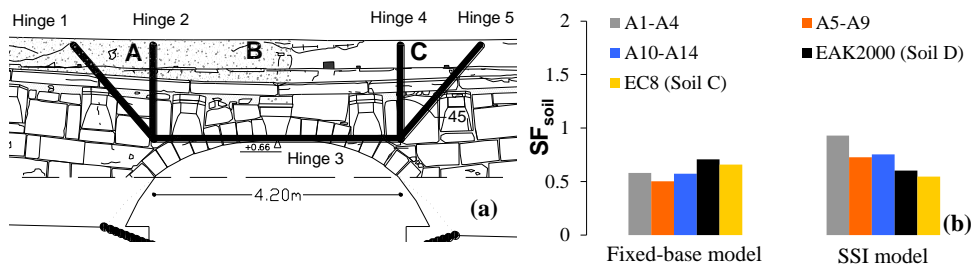


Figure 3. (a) Fracture line pattern employed for the assessment of the bridge structural stability against transverse loading following Erdogmus and Boothby [12] (b) Safety factor against bearing capacity of the foundation soil under different loading considerations for both fixed- and flexible-base bridge abutments

Engineering of the Aristotle University of Thessaloniki under the auspices of the Directorate for the Restoration of Byzantine and Post-byzantine Monuments of the Greek Ministry of Culture [7]. A wide set of in-situ inspections and laboratory tests on structural specimens, geophysical and geotechnical field surveys and sampling boreholes were performed to obtain a detailed knowledge on the existing pathology of the bridge and the natural, mechanical and dynamic properties of both the structure and the foundation soil. In terms of structural stability, extensive cracks in the tensile zones were observed, especially under the arches. The original stone masonry materials were highly deteriorated by deep corrosion, loss of mass and poor condition of joint mortars whereas significant loss of strength, delamination and detachment of covering was observed for the concrete sections [11]. With reference to foundation soil conditions, the geotechnical investigations revealed a particularly deformable foundation soil reflected in the presence of a soft surficial silty-clayey layer of 5m thickness with  $N_{SPT}$  blows count lower than 10 and shear wave propagation velocity between 140 and 170m/sec (*Fig. 2c*).

## **2.2 Structural transverse strength and bearing capacity of the foundation soil**

Transverse structural stability of the bridge was assessed by means of the fracture line method [12] assuming a failure pattern (*Fig. 3a*) similar to the one observed after the 1953 earthquake (*Fig. 1b*). A mean value of acceleration at the foundation level of the bridge was estimated at 0.6g based on a series of soil response analyses implementing twenty five real earthquake events recorded by an accelerometric station at a close distance (approximately 500m) from the bridge ( $3.7 < M_s < 5.2$ ,  $0.02g < pga < 0.2g$ ) and scaled to 0.36g at bedrock level as specified in EAK2000 seismic code for the particular seismic zone [8]. The tensile strength of stone masonry was estimated from laboratory tests and design norms [13]. The corresponding safety factor was computed at 0.7 denoting a critical zone of structural instability in agreement with the observed pathology of the bridge.

With reference to bearing capacity of the foundation soil, a stress-based analysis of a detailed 3D FE bridge model was performed by implementing mean values for the materials elastic properties from laboratory tests [11]. Soil-bridge interaction was introduced through spring supports at the abutments base computed from pertinent analytical formulas for surface footings [14]. It is worth noting that the comparison of natural modes between fixed- and flexible-base models revealed a remarkable effect of soil-structure interaction by increasing the fundamental natural period of the bridge from 0.03sec under fixed-base conditions to 0.6sec for the SSI case. Mean acceleration response spectra obtained from soil response analysis (A1-A4, A5-A9 and A10-A14, [8]) and code-defined elastic spectra (EAK2000, EC8) were specified at the base

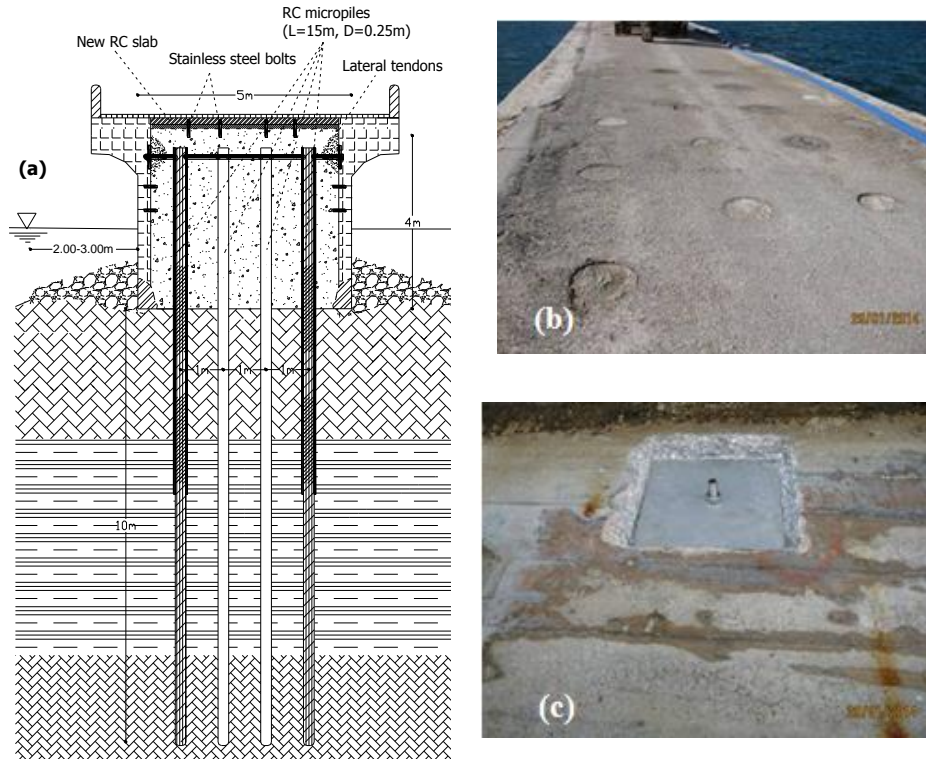


Figure 4. (a) Typical cross-section of the bridge in the transverse direction showing the proposed intervention measures (b) Group of micropiles embedded from the bridge deck (c) Steel plate embedded in the façades of the bridge anchoring the lateral tendons.



Figure 5. (a) Filling material of the bridge revealed during restoration works (b) Steel tubes embedded consecutively to restrain debris fall inside the borehole during drilling

nodes as seismic loading. Numerical results were reviewed in terms of a mean vertical stress developed under the abutment and compared with the bearing capacity of the foundation soil under seismic loading based on the acquired

geotechnical data. The corresponding safety factors are plotted in *Fig.3b* for both fixed- and flexible-base (SSI) conditions. Each bar in the graph refers to a different loading scenario. Evidently, low safety factors below unity indicate another critical zone of structural instability that should have contributed to the observed deformation of the bridge.

### 3 DESIGN AND APPLICATION OF THE REHABILITATION SCHEME

Based on the identified zones of inadequate strength, rehabilitation measures were designed (*Fig.4a*) following a set of basic principles:

- Replacement of the concrete facades of the bridge and construction of new ones with stone elements compatible to the authentic material.
- Increase of the transverse strength of the bridge by means of (a) highly-resistant mortar at the interface of the new stone masonry elements and (b) closely spaced stainless steel lateral tendons to upgrade the monolithic behavior of the structure under lateral loading.
- Improvement of the foundation soil by a group of slender piles (micropiles – *Fig.4b*) designed as (a) a complementary transfer mechanism of the vertical bridge loads and (b) a soil improvement technique to increase the bearing capacity of the foundation soil.

Upon implementing the elastic spectrum of EAK2000 for the particular seismic zone (i.e.  $a_g=0.36g$ ), a group of 22 micropiles (S/D=8, L/D= 60) was proposed for each one of the fifteen bridge abutments. In this manner, the safety factor against bearing capacity of the foundation soil increased up to 50% with respect to the pre-rehabilitation case.

#### 3.1 Construction issues and technical solutions

During on-site restoration works, it was revealed that the concrete parts of the bridge were constructed by two parallel unconnected reinforced concrete walls of 40cm width each. The filling material between the two spandrel walls was composed of soil, sparse steel bars and debris (*Fig. 5a*) making drilling of micropiles particularly difficult. Due to the above unfavourable conditions, a set of corrective actions with respect to original design were considered necessary:

- Conservation of the limestone facades and repair of the concrete ones with corrosion resistant mortars. A thin (6cm) stone layer was attached to the concrete facades as part of the bridge morphological restoration.
- In stone facades, the stainless steel lateral tendons were anchored to newly-constructed stone walls in the inner part of the facades (*Fig.4c*).
- Use of 7 steel tubes of 30cm diameter and 1,5m length placed consecutively to prevent debris fall inside the borehole during drilling. Deployment of piles reinforcement and protection for sea currents were obtained by means of a permanent PVC tube introduced within the steel ones (*Fig.5b*).



#### 4 SEISMIC RESPONSE OF THE REHABILITATED BRIDGE TO CEPHALONIA EARTHQUAKES

The rehabilitated bridge was inspected in-situ by ITSAK and AUTH-LSDGEE reconnaissance teams after the two major Cephalonia earthquakes. No damages or visible defects were observed indicating a good seismic performance of the bridge (Fig.6a). On the contrary, the adjacent quay walls suffered a permanent horizontal displacement of 20cm and a vertical settlement of the backfill at 20cm approximately (Fig.6b).

Towards identification of the rehabilitation measures effectiveness, the 3D FE model of the bridge was reanalysed considering the response spectrum imposed by each earthquake at the foundation level of the structure (Fig.6c). The latter was obtained from soil response analyses by utilizing the recordings (NS component) from the nearby accelerometric station ARG2 of ITSAK ([5], [6]). In the same graph, EAK2000 (considered as the design loading of the rehabilitation measures) and EC8 elastic spectra are also plotted. The favourable effect of the interventions stems from the corresponding safety factors against bearing capacity of the foundation soil having values larger than 1 (Fig. 6d).

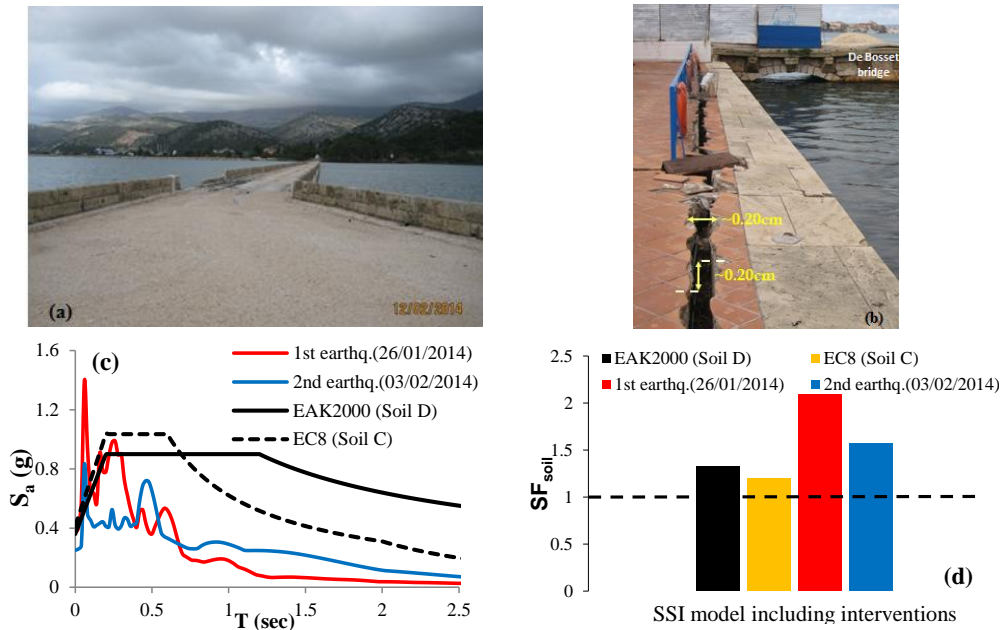


Figure 6. (a) Rehabilitated bridge with no damages recorded after the two major earthquakes of 01/26/2014 and 02/03/2014 (b) Permanent lateral displacement of the quay wall and settlement of the backfill adjacent to the De Bosset bridge after the second earthquake of 03/02/2014 (both pictures taken on 12/02/2014) (c) Response spectra of the two earthquake motions computed at the foundation level of the bridge (d) Safety factor against foundation soil bearing capacity of the rehabilitated bridge considering the seismic loading induced by the two earthquakes

## 5 CONCLUSIONS

The seismic response of the historic stone masonry “De Bosset” bridge to the recent strong earthquakes that stroke Cephalonia Island on 26/01/2014 and 03/02/2014 was examined, towards a first-level interpretation of the very good seismic performance of the bridge. In this regard, the beneficial contribution of intervention measures combining foundation soil improvement and structural strengthening of the bridge deployed prior to the above earthquake sequence is demonstrated.

## REFERENCES

- [1] Page, J, “Repair and strengthening of masonry arches”, *Proc. IABSE Symposium on Structural Preservation of the Architectural Heritage*, Rome, 1993.
- [2] Proske, D, and Van Gelder, P, *Safety of Historical Stone Arch Bridges*, Springer Publications, 2009.
- [3] Asteris, PG, Chronopoulos, MP, Chrysostomou, CZ, Varum, H, Plevris, V, Kyriakides, N, and Silva, V, “Seismic vulnerability assessment of historical masonry structural systems”, *Engineering Structures*, Vol. 62-63, pp. 118-134, 2014.
- [4] Krstevska, LS, Kustura, M, and Tashkov, LA, “Experimental in-situ testing of reconstructed old bridge in Mostar”, *Proc. 14<sup>th</sup> World Conference on Earthquake Engineering*, Beijing, 2008.
- [5] EPPO-ITSAK, “The earthquake of 26/01/2014 (M6.1) in Cephalonia (Greece): Strong ground motion, soil behaviour and response of structures”, Preliminary report, 2014 (available online at <http://www.itsak.gr/en/news/news/70>)
- [6] EPPO-ITSAK, “Strong ground motion of the February 3, 2014 (M6.0) Cephalonia earthquake: Effects on soil and built environment in combination with the January 26, 2014 (M6.1) event” Final report, 2014 (available online at <http://www.itsak.gr/en/news/news/79>)
- [7] Ptilakis K. et al. “Rehabilitation and Reinforcement Study of DeBosset bridge at Argostoli, Cephalonia” Final Report submitted to Directorate for the Restoration of Byzantine and Post-byzantine Monuments, Greek Ministry of Culture, 240p, 2006.
- [8] Rovithis, Emm, and Ptilakis, K, “Seismic performance and rehabilitation of old stone bridges in earthquake-prone areas: the case of Debosset bridge in Greece”, *Proc. 1<sup>st</sup> Intl. Conference on Bridges “Innovations on Bridges and Soil-Bridge Interaction”*, pp. 311-318, Athens, 2011.
- [9] Papazachos, B, and Papazachou C, *Earthquakes of Greece*, Ziti publications, Thessaloniki, 1997.
- [10] Griffith, M, Magenes, G, Melis, G, and Picchi, L, “Evaluation of out-of-plane stability of unreinforced masonry walls subjected to seismic excitation”, *Journal of Earthquake Engineering*, Vol. 7, Special Issue 1, pp. 141-169, 2003.
- [11] Papayianni, I, Pacht, V, and Alexiou, A, “Study of the constructing materials, techniques and pathology symptoms of the stone bridge DeBosset in Kefalonia”, *Proc. 5<sup>th</sup> International Conference on Arch Bridges*, pp. 147-154, Madeira, 2007.
- [12] Erdogmus, E, and Boothby, T, “Strength of spandrel walls in masonry arch bridges”, *Journal of Transportation Research Board*, Vol. 1892, pp. 47-55, 2004.
- [13] OPCM 3274. Ordinanza del Presidente del Consiglio dei Ministri n. 3274 del 20 Marzo 2003: Primi elementi in materia di criteri generali per la classificazione sismica del territorio nazionale e di normative tecniche per le costruzioni in zona sismica, 2005 (ANNEX 11.D).
- [14] Gazetas, G, “Formulas and charts for impedance functions of surface and embedded foundation”, *Journal of Geotechnical Engineering*, ASCE, Vol. 177, pp. 1363-1381, 1991.

## **A PROPOSAL FOR THE USE OF A NEW TYPE OF PIER CONNECTIONS WITH DECK AND PILE CAP WITH IN-SERVICE AND SEISMIC ADVANTAGES**

Ioannis Tegos<sup>1</sup>, Vasileios Pilitsis<sup>2</sup> and Theodoros Chrysanidis<sup>3</sup>

<sup>1,2,3</sup> Aristotle University of Thessaloniki, Faculty Of Engineering, Dept. of Civil Engineering  
Greece

e-mail: itegos@civil.auth.gr, vpilitsi@civil.auth.gr, theodoros\_gr@yahoo.com

**ABSTRACT:** The present work examines the possibility of using appropriate connections between piers, deck and their pile-caps. This type of connection contributes in moment and shear force developing but with no rigid connection between piers and deck or pile-caps. With this adjustment a degradation of piers' resistance in seismic transaction of the deck is achieved and thus an increase in fundamental period and a reduction in seismic forces, as in the case of elastomeric bearings. The proposal is applied in a long road bridge of Egnatia Motorway.

**KEY WORDS:** Monolithical; Pier; Connection; Unbonded; Seismic isolation.

### **1 INTRODUCTION**

Several ways of transfer seismic inertial forces to the abutments and the approach embankments, which are usually seismically isolated, have been proposed aiming to relief the main seismic resisting components of the bridge sub-structure, namely piers. As substitutes of isolation systems, different kinds of concrete components (stoppers) have been proposed and among other, components through which a part of seismic inertial forces are directly transferred to the abutments and their approach embankments [1], [2].

A new technique for precast concrete bridges is the use of rocking as seismic isolation (Fig.1). Pure precast elements are connected though unbonded post-tensioning techniques; the inelastic demand is accommodated within the connection where a "controlled rocking" motion occurs with opening and closing of existing gap [3], [4], [5].

In this study instead of using elastomeric bearings for increasing the fundamental period of a structure, an innovative technique is applied, based on the appropriate connection of piers with the deck and their pile caps, by which it is possible to develop large seismic displacements and thus a greater fundamental period in monolithic bridges. The proposed type of connection is applied as an alternative design in a large road bridge of Egnatia Motorway.

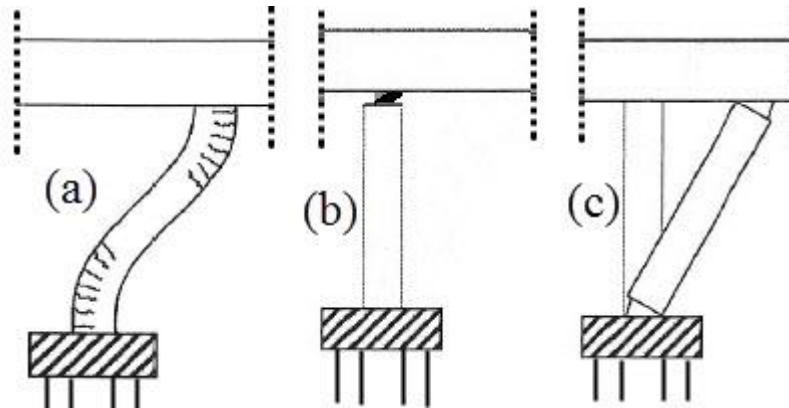


Figure 1. (a) Conventional ductile response, (b) Conventional seismic isolation response, (c) Unconventional rocking response

## 2 DESCRIPTION OF THE PROPOSED TYPE OF CONNECTION

A delineation of the title of this study is as follows: an innovative way of connecting the piers' web with the underlying pile cap the overlying deck of the bridge is proposed, which aims at the improvement of the response, comparatively with the corresponding monolithic connection, regarding the in-service and seismic requirements while reducing the cost. The innovation consists in the way of anchoring the longitudinal reinforcement in the underlying pile-cap and the overlying deck of the bridge (Fig.2). According to Fig.2, longitudinal reinforcement is lapped with awaiting rebars which are not anchored to the pile-cap with the usual way, but in a specific way that a portion of reinforcement, which is nearest to the web of the pier, is not integrated into the surrounding concrete. Similarly the outbound awaiting rebars from the head of the pier are not anchored to their full length into the deck, but the lower portion is not integrated in the concrete either. The construction joint in the footing of the pier is below the upper surface of the pile-cap by 15cm, while the upper construction joint, at the heading of the pier enters at 15cm in the deck. These measures aim to prevent drifts at the interface of construction joints. The measures taken in order to prevent full fixity of the longitudinal reinforcement in the areas of anchorages, lead to the partial release regarding the rotations of the end-part sections of the piers. Via these rotations the stiffness of the piers can be dramatically degraded for the benefit of in-service requirements which are associated with alleviating the stresses arising from the constraints caused by the expansion and contraction of the deck. By the system's generated high degree of flexibility is also achieved a satisfactory degradation of seismic inertial forces because that leads to the significant increase of the fundamental period. It should be noted that the above mentioned are achieved without the

construction and maintenance costs that would require a conventional case of elastomeric bearings.

For evaluating the stiffness of piers with the proposed type of connection, the example of a simple system is presented (Fig.3, Fig.4), which illustrates a simple beam, fixed at both ends, with length of 2.00m, cross section dimensions 20cm x 20cm. Research' s parameters were the percentage and the unbonded length of longitudinal reinforcement to anchor positions.

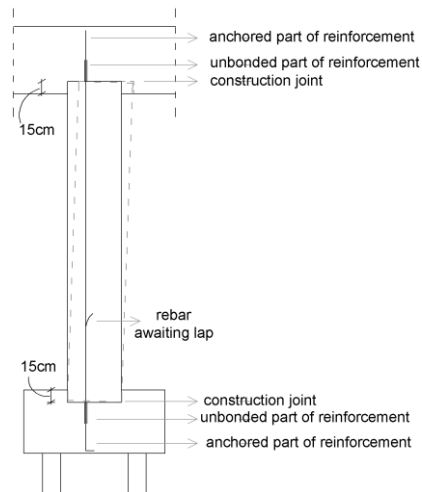


Figure 2. Anchorage conditions of typical reinforcement

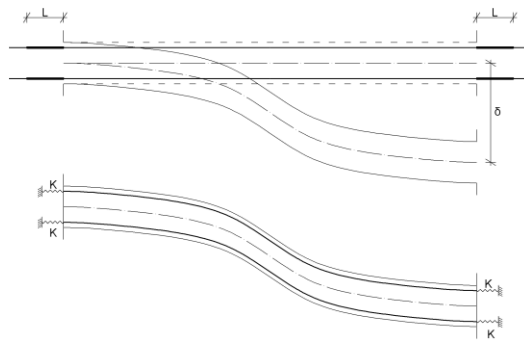


Figure 3. Example of a simple system

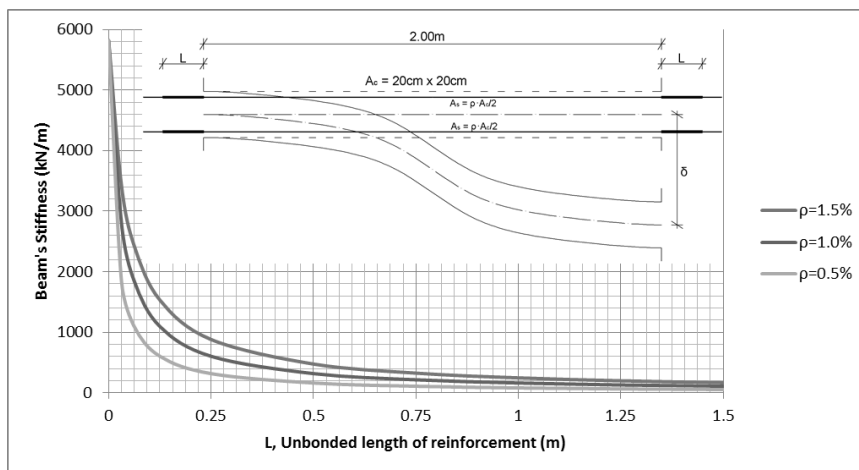


Figure 4. Stiffness – unbonded length of rebars relation investigation in simple beam

### 3 CASE STUDY

#### 3.1 Description of the “reference” bridge

The proposed type of connection was applied as an alternative design in a large road bridge of Egnatia Motorway. The following figures illustrate the geometry data of the bridge (Fig.5, Fig.6). The bridge was designed based on earlier Greek codes, for ground similar to type B of EC8 and design ground acceleration of 0.16g. A behaviour factor equal to  $q_x=3.50$  was taken into account for the longitudinal direction of the bridge while a  $q_y=2.24$  for the transverse direction. Regarding the longitudinal reinforcement of piers, pier P1 has  $\rho_l=1.26\%$ , pier P2 has 1.44%, pier P3 and P5 have 1.00% and pier P4 has 2.04%.

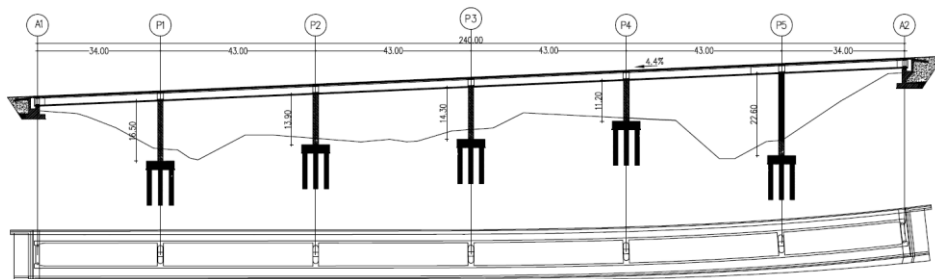


Figure 5. Longitudinal section plan view of the left part of the bridge

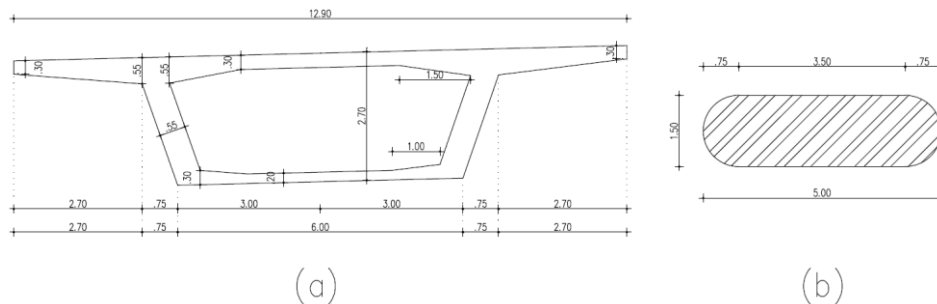


Figure 6. (a) Cross section of the deck at mid-span – (b) Cross section of the piers

#### 3.2 Description of modelling of the proposed type of connection

The program CSI S.A.P.2000 v.11.0.4 [6] was used for the analyses. The elastic response spectrum of EC8 for soil type B and design ground acceleration 0.16g was used for dynamic spectrum analysis. For confirmation of the results it was also conducted and a nonlinear time-history analysis, using an artificial accelerogram (Fig.9) generated using the program SeismoSoft SeismoArtif [7], consistent with the elastic spectrum of EC8 calculated by Halldorsson & Papageorgiou method [8] and adjusted by correction in frequency domain. The

modeling of the connection of pier with the deck and the pile cap is illustrated in (Fig.7, Fig.8).

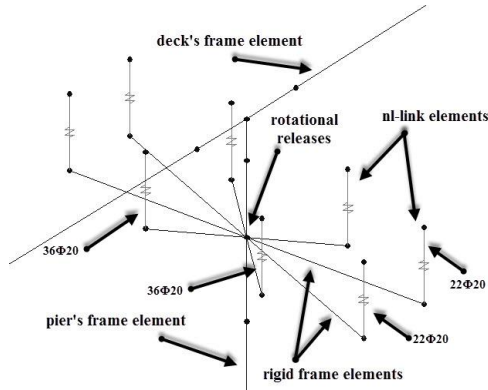


Figure 7. Modelling of the connection of pier with deck

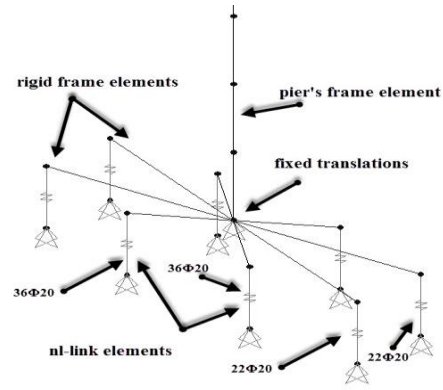


Figure 8. Modelling of the connection of pier with pile cap

It is worth mentioned that in Fig.7 the upper nodes of the link elements, by which longitudinal reinforcement is simulated, are grouped in a constraint of equal translations and rotations with the node of the deck over the pier. Link elements' stiffness is calculated by the Eq.1:

$$K = \frac{E \cdot A}{l} \quad (1)$$

Where:

E is the modulus of elasticity of reinforcement steel

A is the area of longitudinal reinforcement corresponding to each link element

l is the unbonded length of longitudinal reinforcement on anchor positions

In the present study the unbonded length of longitudinal reinforcement was chosen to be 1.00m for both the heading and the footing of all the bridge's piers. The examined longitudinal reinforcement ratio for all of the piers was  $\rho_l=1.0\%$ , namely 232Ø20 arranged in the perimeter of the cross-section in two layers. In the nonlinear time history analysis was used Newmark method as time integration method, law Takeda hysteresis model of S.A.P.2000 was used for the nllink elements and the stress at yield and failure and the corresponding deformations were defined according to EC2 for steel type B500C [9].

#### 4 RESULTS

Initially, a dynamic spectral analysis was conducted. Regarding the dynamic characteristics of the bridge as designed and constructed, the fundamental

period in longitudinal and transverse direction are close to the constant spectral acceleration branch. It should be noted that in the original design, for the determination of the seismic forces, effective stiffness was chosen common for all the piers and equal to the geometrical stiffness, while for the determination of the displacements was chosen equal to 40% of the stiffness of the uncracked section. For reasons of comparison between the two solutions, it was decided to consider effective stiffness of the piers of similar values and not as defined in Eurocodes [10]. The results are cited in the next table.

*Table 1.* Dynamic characteristics and results of dynamic spectrum analysis

	$T_x$ (sec)	$T_y$ (sec)	$d_{E,x}$ (cm)	max $d_{E,y}$ (cm)	$V_{E,x}$ (kN)	$V_{E,y}$ (kN)
Reference bridge	0.65	0.42	7.2	4.2	34253	39007
Redesigned bridge	1.26	0.55	10.9	5.2	17789	33468

As seen in Table 1, a significant increase in the fundamental period is observed in the proposed case, which leads to a significant drop of the seismic shear force of the piers and also to an increase of seismic displacements. Particularly, an increase in fundamental period regarding the longitudinal direction by 94% and the transverse direction by 31% was observed. This resulted in the increase of displacements by 51% in the longitudinal and 24% in the transverse direction. Thus, total seismic shear force was decreased in the redesigned bridge by 93% for the longitudinal and 14% for the transverse direction.

Regarding stresses on the unbonded parts of the longitudinal reinforcement in the footing and heading of the piers, for full elastic behavior of steel, they accrued twice as high as design yield strength. More specifically, rebar in the footing of the shortest pier (P4) for earthquake action in the transverse direction outputted a stress equal to 892MPa. This result indicated that the system's behaviour is not elastic in the design situation and for this reason it was decided to perform a nonlinear time-history analysis with an indicative time history as mentioned in the previous paragraph (Fig.9).

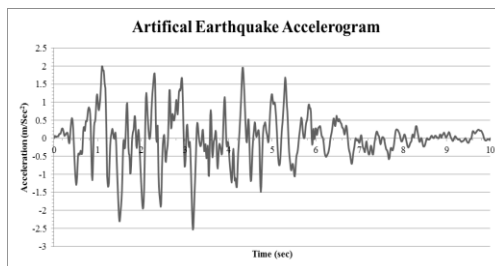


*Figure 9.* Artificial earthquake accelerogram

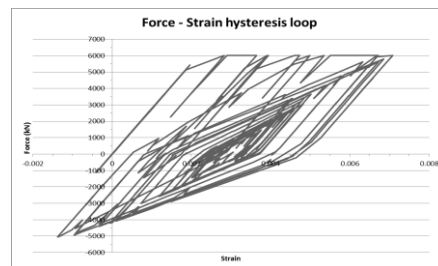


*Figure 10.* Force-Strain hysteresis loop of nllink57



The results showed that the maximum deformation of the reinforcement was 0.71% (Fig.10) which is about three times larger than the design yield strain but is much smaller than the design strain at maximum load (6.75%) as defined in EC2-Part1 for steel type B500C [9]. The results of the nonlinear time-history analysis are listed in the table below (Table 2).

Table 2. Results of nonlinear time-history analysis

	max $d_{Ex}$ (cm)	max $d_{Ey}$ (cm)	max $\epsilon_s$ (‰)	max total $V_{E,x}$ (kN)	Max total $V_{E,x}$ (kN)
Redesigned bridge (non-linear analysis)	9.65	6.16	7.1	16380	39110

A coarse investigation showed that with proper segmentation of the web of the shortest piers [11], namely P2 and P4, can result to a further augmentation of fundamental period in the longitudinal direction and thus a further reduction to seismic inertial forces (Fig.11).

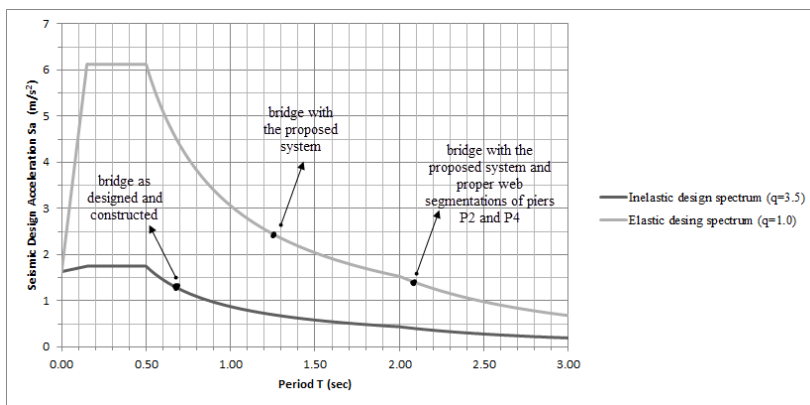


Figure 11. Impact on fundamental period in longitudinal direction

Finally, regarding the serviceability limit state, it was checked considering an equivalent thermal contraction of the deck corresponding to a temperature difference of 50 °C on the safe side. The maximum in-service stress was occurred on the pier M1, near the end-part of the deck, and had a value of 248MPa, which is an acceptable value.

## 5 CONCLUSIONS

In the present study an innovative technique for degrading stresses of piers due to seismic inertial forces. This is achieved by the use of appropriate connections between piers, deck and their pile caps. By the suggested type of connection, the increase of fundamental period of the structure is achieved and this leads to the degradation of seismic inertial forces. The main conclusions of the research

are listed below:

1. With appropriate adaptations, such as minimization of the longitudinal reinforcement and proper segmentation of the piers' web, it is possible to achieve significant downgrade of seismic inertial forces similar to that achieved by the use of elastomeric bearings.
2. In long monolithic bridges in which the in-service problems, due to expansion-contraction of the deck, are accentuated, the proposed system provides the ability of "painless" absorption of changes in length and neutralization of stresses due to thermal actions, creep and shrinkage.
3. The cost effectiveness of the proposed system is due to the drastic reduction in maintenance costs, owing to the absence of elastomeric bearings, and saving in concrete and steel of the piers' webs and their foundations.

It is believed that with further researching of the involved parameters and with the implementation of the proposed system in more cases, more details will accrue and a further documentation will be produced.

## ACKNOWLEDGMENTS

The authors wish to express their gratitude to METE SYSM S.A. for providing the original study of the bridge for the purposes of the present study.

## REFERENCES

- [1] Tegou, S, Mitoulis, S, Tegos, I, "An Unconventional Earthquake Resistant abutment with Transversely Directed R/C Walls", *Engineering Structures*, Elsevier, title no. 32(11), 3801-3816, 2010
- [2] Pilitsis, V, Skordeli, M, Tegos, I, "A Suggestion for Adjustment of the Load-Bearing Structure of Bridges with Antiseismic, Economic and Aesthetic Benefits", *Proc. FIB Symposium 2013*, Tel-Aviv, Israel, 2013.
- [3] Priestley, M J N, "The PRESSS Program – Current Status and Proposed Plans for Phase III", *PCI Journal*, title no. 41(2), 22-40, 1996
- [4] Priestley, M J N, Sritharan, S, Conley, J R, Pampanin, S, "Preliminary Results and Conclusions from the PRESSS Five-story Precast Concrete Test-building", *PCI Journal*, title no. 44(6), 42-67, 1999
- [5] Palermo, A, Pampanin, S, Calvi, G M, "Use of "Controlled Rocking" in Seismic Design of Bridges", *Proc. 13<sup>th</sup> World Conference on Earthquake Engineering*, Vancouver, Canada, 2004.
- [6] Computers and Structures Inc., *S.A.P. 2000 Nonlinear ver.11.0.4*, 2007
- [7] Seismosoft, *SeismoArtif ver.1.0.0*, 2012
- [8] Halldorsson, B, Papageorgiou, A S, "Calibration of the specific barrier model to earthquake of different tectonic regions," *Bulletin of the Seismological Society of America*, title no. 95(4), 1276-1300, 2005.
- [9] CEN [Comité Européen de Normalisation], *EN 1992-1: Eurocode 2: Design of Concrete Structures - Part 1-1: General Rules and Rules for Buildings*, 2004.
- [10] CEN [Comité Européen de Normalisation], *EN 1998-2: Eurocode 8: Design of Structures for Earthquake Resistance - Part 2: Bridges*, 2005.
- [11] Pilitsis, V, Tegos, I, "A Suggestion for Improving the Regular Seismic Behaviour of Integral Concrete Bridges", *Proc. of 2<sup>nd</sup> Intl. Conference on Bridges IBSBI 2014*, Athens, 2014.

IBSBI 2014, October 16-18, 2014, Athens, Greece

## **A PROPOSAL FOR THE IMPROVEMENT OF THE EARTHQUAKE RESISTANCE OF MULTI-SPAN PRECAST I-BEAM BRIDGES**

Ioannis A. Tegos<sup>1</sup>, Sevasti D. Tegou<sup>2</sup>

<sup>1,2</sup> Aristotle University of Thessaloniki, Dept. of Civil Engineering, Greece  
e-mail: itegos@civil.auth.gr, stegou@civil.auth.gr

**ABSTRACT:** This study presents an innovative earthquake resistant abutment which behave as seismic stopper. This stopper is activated when the bridge moves toward the embankment and has the ability to resist loading due to the longitudinal earthquake. The reduction in the stiffness of the piers is a desirable result which, on one hand, leads to the reduction of the bridge seismic loading and on the other hand, offers the opportunity to develop the code's provisions about the use of active seismic stoppers at the head of the piers. The flexibility of the bridge system due to the reduction of the dimensions of the piers' cross-section also serves the contraction and expansion of the bridge deck due to the serviceability requirements.

**KEY WORDS:** Bridge; Abutment; Stopper; Ductility; Serviceability

### **1 INTRODUCTION**

Precast construction constitutes one of the most common bridge construction types. Many partly or completely precast bridge structural systems have been built in the past 50 years [1]. The usual structural scheme adopted for multi-span bridges has been the span by span simply supported bridges with R/C precast beams or steel beams. These bridges have been widely used from the sixties until nowadays. In such structural systems, the bridge deck is composed of several inverted T – or I- shaped beams positioned at a specific distance. After erection of the beam, a deck slab is cast on site, while expansion joints are applied on the bridge supports. Precast beams are usually supported on piers through elastomeric bearings, which results in increasing the natural period of the system and consequently, in reducing earthquake induced forces significantly. In many countries, this bridge type is accepted as a good alternative solution to cast in-situ bridges, as it is preferable for rapid construction.

In high seismicity regions, precast I-beam bridges with tall piers that are connected to the deck through elastomeric bearings usually develop large displacements. As a result, a critical part of these bridge systems is the

sensitivity to seismic displacements [2]. Energy dissipation devices are usually used to limit seismic displacements [3], while alternative methods that lead to a reliable and cost effective design have been proposed in recent studies [4] [5].

An alternative design methodology which is suggested by the current Design Codes, [6] is based on the use of seismic stoppers at the head of the piers in the longitudinal direction of the bridge. These seismic stoppers are usually provided with an adequate gap in order to allow the free expansion and contraction of the deck due to serviceability requirements (creep, shrinkage and thermal effects) and are activated only during the longitudinal earthquake. The aforementioned alternative design method aims at the cost effectiveness of the bridge through the increase of the value of the behavior factor. As it is known the behavior factor is used by Eurocode [6] for design purposes to reduce the forces obtained from a linear analysis, in order to account for the non-linear response of a structure, associated with the material, the structural system and the design procedures. The behavior factor is taken equal to one for accounting only for elastic response, while it is greater than one for accounting for non-linear response. In general, the best compromise between cost effectiveness and seismic safety is achieved more easily, not only in bridges but also in buildings, through the ability of the structures to dissipate a considerable amount of energy, namely ductility, rather than through their elastic response. Specifically, according to the Code provisions [6], precast I – beam bridges are considered as structures with limited ductile behavior and analyzed for values of behavior factors less or equal to 1.5. It is known that despite the fact that seismic actions are effectively reduced due to the presence of elastomeric bearings, which increase the flexibility of the system, the aforementioned design leads to a conservative dimensioning of piers, foundations and bearings, especially in high seismicity regions. However, the aforementioned alternative Code suggestion is considered as insecure and tends to be ignored. The insecurity is due to the difficulty in reaching a compromise between the proposed methodology and serviceability requirements of the bridge. The existence of the gaps causes the non-simultaneous activation of the stoppers during earthquake, which leads, either to a possible failure of inadequate designed stoppers or to disproportional stopper dimensions, if a capacity design procedure is used for ensuring the hierarchy of strengths of the various structural components.

The investigation on the improvement of the earthquake resistance and cost effectiveness of precast I –beam bridges with tall piers constitutes a quite interesting subject. An effort on this direction has been presented in a previous study [7]. In this study the investigation is extended in order to include methods for further reduction of the seismic displacements of precast bridges with tall piers. The use of an external stopper located at the bridge abutment is presented and is, in preliminary stage, analytically investigated the activation way of this system.

## 2 DESCRIPTION OF THE PROPOSED METHODOLOGY

A methodology for the improvement of the seismic efficiency of flexible multi-span precast I – beam bridges with tall piers is presented in this study. The proposed methodology includes two stages.

In the first stage, precast I-beam bridges are converted to ductile systems. The proposed methodology is based on the provisions of Eurocode 8-Part 2 [6] referring to the use of seismic stoppers in the longitudinal direction of the bridge. The applicability of this part of the proposed methodology was analytically investigated in a previous study [7]. According to the proposed method, seismic stoppers are used to transmit the longitudinal design seismic action to two or three contiguous piers, preferably the tallest ones, provided that serviceability requirements are preserved. The difference between this methodology and the Code's suggestion is that, the seismic stoppers are continuously activated and restrain the movements of the deck. The aforementioned seismic stoppers are combined with the application of elastomeric bearings which allow the free rotation of the supported nodes. The transverse movement of the deck is also restrained through seismic stoppers. The in-service movements of the bridge deck due to creep, shrinkage and thermal effects are properly accommodated for by the flexibility of the piers. The in-service loading of the piers is also adequately controlled through their reinforcements [8].

Fig. 1 illustrates two cases with respectively active and inactive longitudinal seismic stoppers. It should be noted that, in both cases the stoppers shall be designed with an excess strength of 40%. The possible seismic design of precast I –beam bridges for a value of the behavior factor greater than one, as well as the consequent reduction of seismic design actions leads to smaller pier cross-section requirements. The usual seismic design of these bridge systems for a value of the behavior factor equal to one requires huge pier cross-sections. In these cases, the use of hollow circular or hollow rectangular cross-sections is desirable. This is due to the fact that heat diffusion has a negative influence on the concrete strength for solid piers' cross- sections with a diameter greater than 2.5m. After thorough study of the proposed methodology, the consequences of the reduction of pier cross-sections were thoroughly checked. It was found that smaller piers cross-sections are positive for construction purposes and negative as far as the occurrence of second order effects is concerned.

The second stage of the proposed methodology includes the construction of an external stopper, Fig. 2, aiming at the further reduction of the bridge deck seismic movements. The aforementioned stopper is activated when the bridge moves toward the embankment and has the ability to resist loading due to the longitudinal earthquake. The proposed method is based on the extension of the deck's slab and the transfer of the end expansion joint over the abutment's web. A contraction joint separates the beam that is rigidly connected to the backwall

from the extrusion at the end of the extension of the deck's slab. An expansion joint also separates the bridge system from the embankment.

The reduction in the stiffness of the piers is a desirable result which, on one hand, leads to the increase of the bridge fundamental period and to the reduction of the seismic loading and on the other hand, offers the opportunity to develop the code's provisions presented in the previous paragraphs about the use of active seismic stoppers at the head of the piers. The flexibility of the bridge system due to the reduction of the dimensions of the piers' cross-section also serves the contraction and expansion of the bridge deck due to the serviceability requirements.

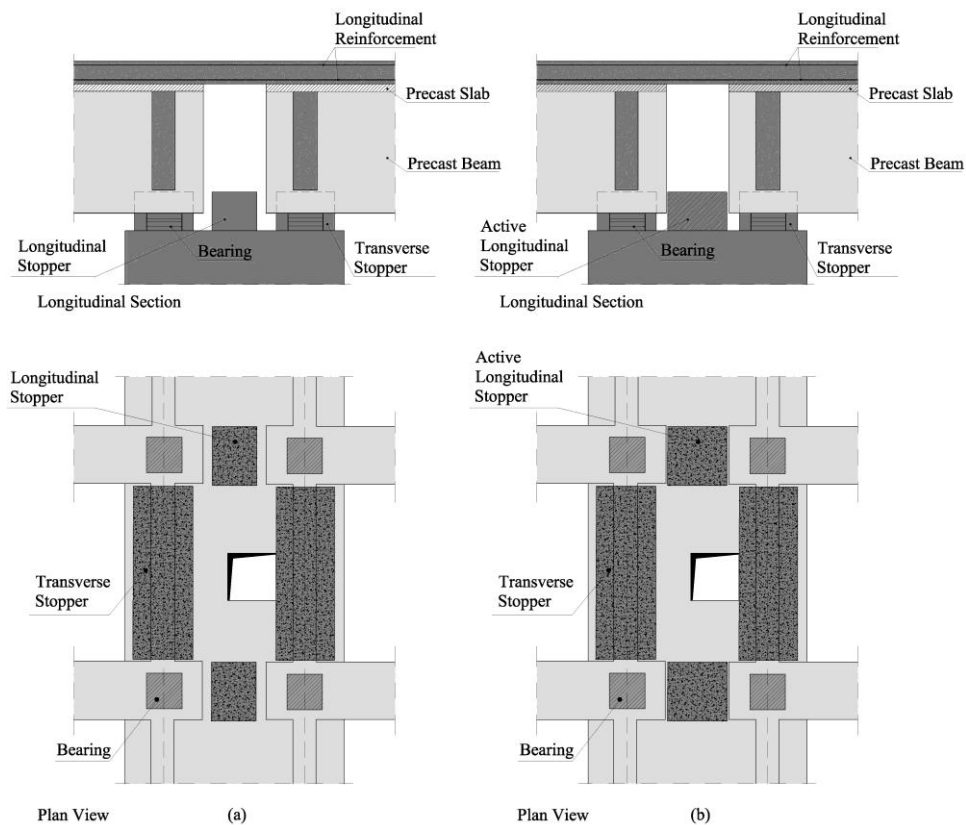


Figure 1. Longitudinal section and plan view of a pier's head with (a) inactive and (b) active longitudinal seismic stoppers

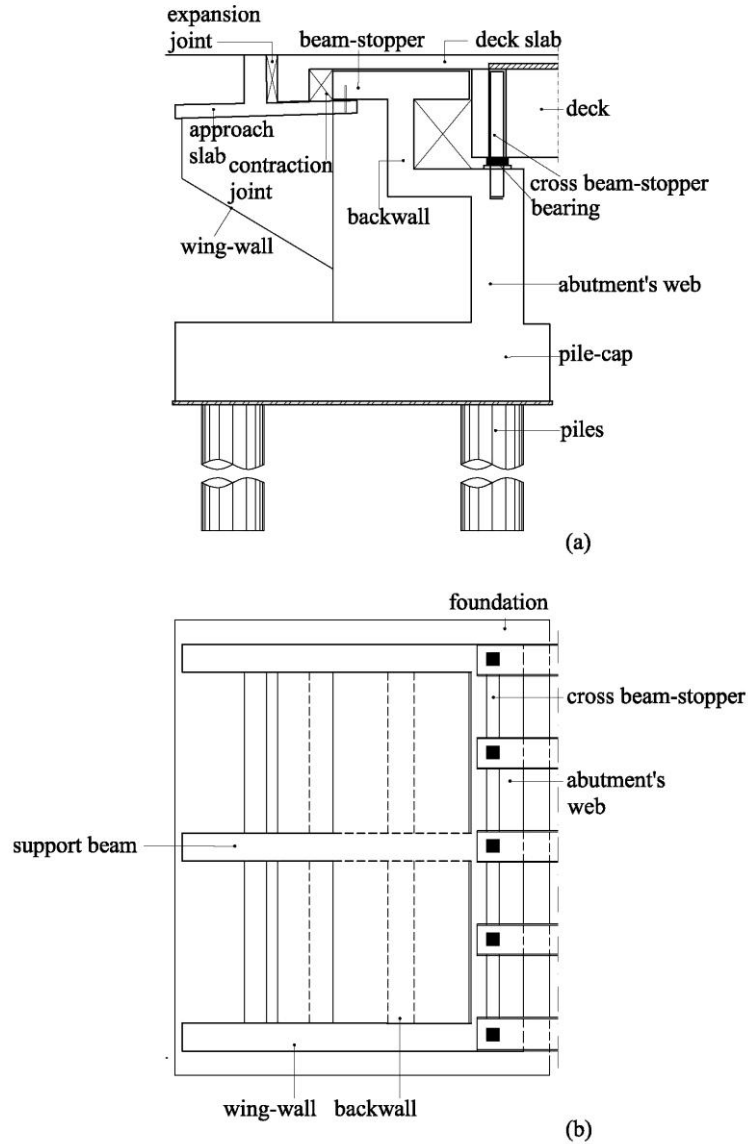


Figure 2. (a) Longitudinal section and (b) plan view of the proposed external stopper

### 3 PRELIMINARY INVESTIGATION ON THE APPLICABILITY OF THE PROPOSED METHODOLOGY

A precast I-beam bridge is used for the investigation on the applicability of the proposed methodology, aiming at the improvement of the seismic resistance of this type of bridges. This bridge is located at Asprovalta territory of Egnatia

Odos Motorway and is given in Fig. 3(a). This “reference” bridge has four spans and a total length equal to 137.6m. The deck, Fig. 3(b), consists of five simply supported precast and prestressed I-beams, precast deck slabs and a cast in-situ part of the slab. The deck is supported on both abutments and on the piers through low damping rubber bearings. The piers of the “reference” bridge, Fig. 3(c), are hollow rectangular sections with external dimensions 3.1x5.1m and a web thickness equal to 0.45m. The bridge is founded on a ground type B according to the Greek seismic design code [9]. The design ground acceleration was equal to 0.16g. The importance factor adopted was equal to  $\gamma_I=1.3$ , while the behavior factors were equal to 1.0 for the three directions.

In the first stage of the investigation, this bridge is converted to a ductile bridge system according to the method proposed in the first part of the previous section. The properties of this ductile bridge alteration are the same with the initial one apart from the cross-section of the piers (circular cross-sections), Fig. 3(d). This bridge has also active longitudinal seismic stoppers at the head of piers P1 and P2 (as illustrated at Fig. 1(b)).

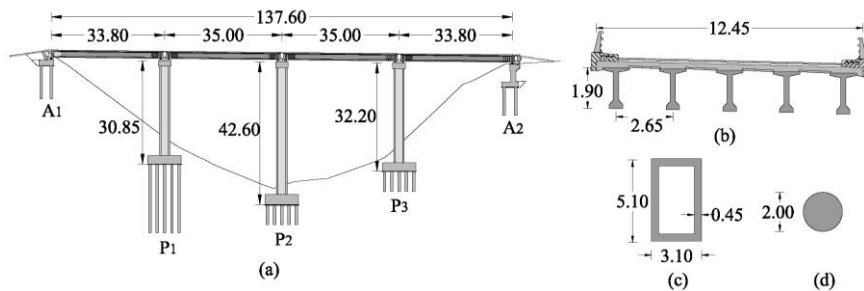


Figure 3. (a) Longitudinal section of the “reference” bridge, (b) Cross – section of the deck, (c) Cross – section of the piers of the “reference” bridge and (d) Cross-section of the piers of the ductile alteration of the “reference” bridge

A fundamental mode-based pushover analysis was performed, for the preliminary assessment of the inelastic response of the ductile bridge. The natural periods  $T_n$  were calculated for linearly elastic vibration of the bridge. The number of modes that were considered was quite high in order to capture all modes whose masses contribute to at least 90% of the total mass of the bridge according to the Codes’ criterion [6]. The first mode shape is dominated by longitudinal deck motion and the corresponding mass ratio is 91.6%, while the second mode shape is dominated by transverse deck motion with corresponding mass ratio 80.9%.

The pushover curve calculated by applying the modal load pattern of the first mode in the longitudinal direction of the bridge is shown in Fig. 4. The vertical axis of the diagram corresponds to the ratio of the base shear of the bridge  $V$  to the total bridge weight while the horizontal one to the longitudinal displacement



of the bridge. The monitoring point was selected as the deck displacement at the location of the middle pier P2 of the bridge, which practically coincided with the centre of mass of the structure (which is the recommended location in Eurocode 8). The sequence of plastic hinge formation (along with the normalized force ( $V/W$ )–displacement curves), was also derived for the longitudinal direction of the bridge.

It can be deduced that for the design PGA of 0.053g the response of the bridge is inelastic while the maximum base shear is noticed for a design ground acceleration equal to 0.059g. However, a remarkable result is the large displacements in which the yielding of the critical sections of the bridge piers is observed due to the flexibility of the piers (height and cross-section). The large longitudinal displacements contributes to the early failure of the tallest bridge pier, namely pier P2, due to buckling. This failure is observed for deck displacement equal to 0.61m. As a result bridge ductility is reduced due to the early failure of the piers. For this reason the activation of the proposed seismic stopper located at the bridge abutments is necessary, in order for the longitudinal movements of the bridge to be reduced. In this case, the seismic loading is transmitted through the stopper to the wing-walls and consequently to the rest members of the abutment, which activate the passive earth pressures of the approach embankment. The width of the end joint is mainly determined according to the serviceability requirements of the bridge (creep, shrinkage and thermal effects). Finally, it is noted that, the relative axial force of the piers is about 0.15. This value can be increased to 0.30 through the further reduction in the dimensions of the piers' cross-section. However in this case is recommended the construction of extrusions at the head of the piers for the secureness of the safe support of the bridge deck.

Transverse earthquake, which is not as critical as the longitudinal one, is more easily to be treated through the construction of cross beams, Fig. 2, rigidly connected to the abutment web. Bridge piers are also provided with similar cross beams.

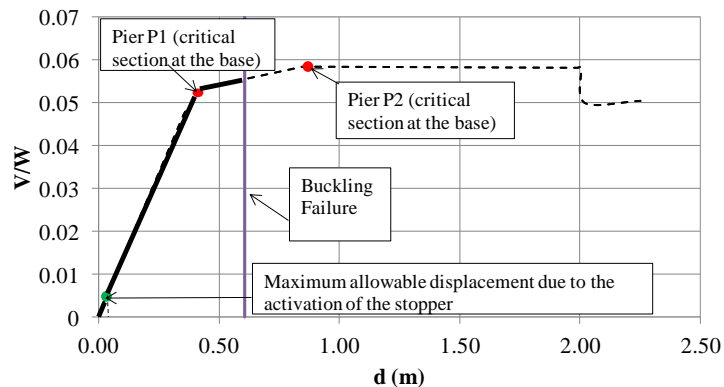


Figure 4. Base shear versus deck displacement at central pier location (P2)

#### 4 CONCLUSIONS

This study presents an innovative proposal for the improvement of the earthquake resistance of precast I-beam bridges. The drastically reduction on the required volume of the bearings and the seismic activation of the bridge abutments constitute the innovation of the study. A real precast I-beam bridge of Egnatia Odos Motorway in Greece was used as the reference case for the preliminary investigation on the applicability of the proposal. The main conclusions of the investigation are summarized to the following:

- The volume of the elastomeric bearings as well as the required width of the end expansion joints are significantly reduced and consequently, the maintenance cost of the bridge is lower than the corresponding one of the initial, conventionally constructed bridge.
- The reduction in the diameter of the piers cross-section improves the aesthetic view of the bridge and contributes to the increase of the flexibility of the system. A desirable advantage derived from the increased bridge flexibility is the possibility of the application of active seismic stoppers to more than two bridge piers.
- Both proposed systems can be constructed without any significant constructability issues, while, from the economic point of view, they have minor cost considering their effectiveness on the longitudinal earthquake, which is generally more difficult to be treated than the transverse.

#### ACKNOWLEDGMENTS

The authors would like to thank Egnatia Odos S.A. for the kind decision to provide the study of the bridge for the purposes of the investigation.

#### REFERENCES

- [1] CEB-FIB, *Precast concrete bridges State-of-the-art report*, bulletin 29, fib Task Group 6.4, Switzerland, 2004.
- [2] Priestley M, Seible F. and Calvi G., *Seismic Design and Retrofit of Bridges*, John Wiley and Sons, Inc., New York, 1996.
- [3] Ruangrassamee A, Kawashima K, “Control of nonlinear bridge response with pounding effect by variable dampers”, *Engineering Structures*, Vol. 25, Issue 5, pp. 593–606, 2003.
- [4] Tegou SD, Mitoulis SA and Tegos IA, “An unconventional earthquake resistant abutment with transversely directed R/C walls”, *Engineering Structures*, Vol. 32, Issue 11, pp.3801-16, 2010.
- [5] Mitoulis SA and Tegos IA, “Restrain of a seismically isolated bridge by external stoppers”, *Bulletin of Earthquake Engineering*, Vol. 8, Issue 4, pp. 973-93, 2010.
- [6] CEN, *Eurocode 8: Design of structures for earthquake resistance, Part 2: Bridges*, 2003.
- [7] Tegou, SD, Tegos, IA, “A proposal for cost-effective design of precast I-beam bridges”, *International Conference IBSBI 2011- Innovations on Bridges and Soil- Bridge Interaction*, 13-15 October 2011, Athens, Greece, 2011.
- [8] CEN, *Eurocode 2: Design of concrete structures - Part 1: General rules and rules for buildings*; 2004.
- [9] Ministry of public works of Greece, *Greek seismic code-EAK2000*, (In Greek), Athens, 2000.

## THE USE OF UNBONDED TENDONS ON BRIDGES IN SEISMIC REGIONS

Olga Markogiannaki<sup>1</sup>, Ioannis Tegos<sup>2</sup>, Spyridon Vasileiou<sup>3</sup>

<sup>1,2,3</sup> Aristotle University of Thessaloniki, Dept. of Civil Engineering, Greece  
e-mail: omarkogiannaki@civil.auth.gr, itegos@civil.auth.gr, spyridov@civil.auth.gr

**ABSTRACT:** In the present paper, an alternative and innovative use of prestressed unbonded tendons is proposed and investigated analytically. The tendons are activated by the seismic excitation and limit the longitudinal bridge movements while complying with in-service requirements. The prestress design of the unbonded tendons aims on keeping them under tension at all times.

**KEY WORDS:** Concrete Bridge, Restrainer, Unbonded Tendon, Seismic movements

### 1 INTRODUCTION

Prestressing in bridges is used mostly for providing necessary resistance to the superstructure's vertical loading and to ensure that concrete stays within its tensile and compressive capacity under the range of the loading applied, [1]. The process involves applying forces to the concrete structure by stressing tendons relative to the concrete member. The term prestress is used globally to name all the permanent effects of the prestressing process, which comprise of internal forces in the sections and deformations of the structure, [2]. It can be applied by tendons (wires, strands, bars) that are of high strength steel. They can be either internal or external,[3], to the concrete member and can be bonded or unbonded to the structure's concrete. External prestressing can be a rational strategy for strengthening existing bridge superstructures against increased traffic loading demands, as well,[4].

Various research efforts have been conducted for utilizing prestressing for upgrading bridge's seismic response. Increasing resistance against seismic demand focuses mainly on the piers and can take several forms, such as enhancing pier's flexural resistance with prestressed tendons and rebars [5],[6], introducing prestressed confinement systems for piers, i.e. prestressed FRP strips [7] or prestressing pile and pier caps[8]. Some researchers have investigated the use of unbonded prestressing tendons for limiting the horizontal displacements but their applications are limited to beams in building frame and wall systems [9],[10].

The key objective of the present paper is to propose an innovative use of

unbonded prestressing tendons for upgrading bridges seismic response by restraining longitudinal seismic movements of bridges. The seismic upgrade does not focus on the strengthening of a specific bridge member but on the improvement of bridge's seismic behaviour. The proposed method is based on other restraining systems that have been proposed by the authors for limiting longitudinal bridge movements that use steel bars ,[11], [12] and FRP strips applied longitudinally in the bridge superstructure receiving tension and compression loading. The system can be applied in common monolithic bridges, mainly, and the expected tendons response that reduces their longitudinal movements can be characterized similar to that of seismic links,[13], and dampers which dissipate seismic energy in seismically isolated bridges,[14]. The study presented herein includes an analytical investigation on the efficiency of the restraining system of unbonded tendons.

## **2 DESCRIPTION OF THE UNBONDED TENDONS SYSTEM**

The system proposed in the present study is a restraining system of seismic movements in bridges. The traditional seismic links – stoppers, which can be applied as restraining systems,[13], are parts of the piers and they can resist earthquake movements when the superstructure, which represents the mass of the bridge system, pounds on them. In this manner, they activate the primary bridge components receiving seismic forces, the piers. As an alternative solution, for the longitudinal earthquake direction, unbonded prestressed tendons can be used similarly to the traditional seismic links. The prestress is determined close to 50% of the yielding stress, so that the tendons will be in tension at all times under earthquake excitations. In this manner, it is possible to respond appropriately to the requirements of a struts-ties system by increasing and decreasing stresses according to the changing earthquake directions.

The prestressed unbonded tendons antiseismic system is shown in *Fig. 1*. The unbonded tendons are placed longitudinally in the bridge superstructure. Specifically, the tendons are placed in the bridge sidewalks at the outer spans and are anchored at the abutments' wing walls. The number of the tendons can vary from one to multiple depending on the size of the bridge that is applied on. Since tendons are applied at each wing wall, every tendon selection results in four identical selections that are placed to the wing walls. Typical anchorages for tendons are performed at their both ends one inside the outer bridge span and one at the abutments. The proposed restraining system is an evolution of the struts-ties system that has been proposed by the authors, which uses common steel bars placed in the superstructure instead of tendons. Although the steels bars are a reliable solution, as well, at the positions of the outer expansion joints they require special care for buckling protection in order to respond as a struts-ties system. Therefore, it was considered that the reception of the compression

loading could be transferred to pretensioned unbonded tendons that could produce “struts” results by decreasing their initial tensile stress.

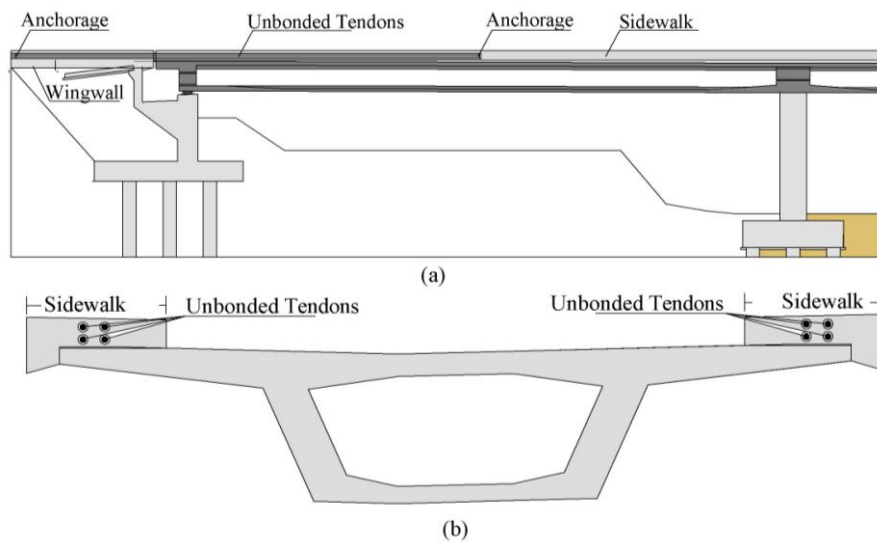


Figure 1. a) Indicative Longitudinal Elevation of the system, c) Indicative Deck Cross Section

The advantages acquired by the tendons solution bring forward issues like the abutments' stability, as the pretension induces forces at the abutments that shall be received by them. These forces have negative effects on their stability. For this reason the tendons' size shall be selected accordingly. Besides, whatever mechanism is used for transferring part of the seismic forces to the abutments and embankments, it is always required that the mechanism receives a reasonable part of the forces so that the conventionally contributing to the seismic resistance components, the piers, continue to receive a large portion of the seismic demand. The forces from the tendons are transferred to the wing walls, firstly, which, consequently, shall transfer the forces to the abutment foundation safely. At this point, it shall be noted that the anchorage and transfer of forces at the bridge deck shall be considered as it is for the abutments. An investigation on the issue has shown that the positions of the spans where the dead load moments become zero are more suitable for anchoring the tendons.

It is remarkable that the pretension stresses act as serviceability loads in the entire lifetime of a bridge and increase or decrease during its service under expansion or contraction constraints, accordingly. Specifically, they decrease when the superstructure expands and increase when it is contracted. In seismic events the increase and decrease in forces is more intense. The in-service change of stresses around the initial prestress at 50% of the yielding stress is possible to be limited by the selection of large lengths, which can receive the excessive tension part. The size of the excessive tension depends on the length

of the bridge. Therefore, the issue is limited for short-span bridges and is more evident for larger bridge lengths where the use of long tendons is unavoidable. The activation of the restraining system by the design earthquake requires an assumption of the size of the maximum stress developed which, in general, is expected to become higher than the 50% of the yielding stress, since the contraction and expansion deformations that affect the initial prestress have asymmetrical influence on the tendons' stress. Specifically, the contraction effects are larger due to the influence of creep and shrinkage. The asymmetric behavior based on the uncertainties of the phenomenon can be neglected since it does not lead to inactivation of the mechanism but to a minor introduction to the post-elastic behavior of the tendons. An advantage of tendons is that they have an acceptably low level of susceptibility to stress corrosion which results in long lifetime of the proposed restraining system.

The restraining mechanism can have several applications. Except the use in common monolithic bridges, it is possible to be used in bridges with high piers, where the P-Delta effect is a critical factor for the safety of the bridge system. Instead of the conventional use of dampers, the restraining system of tendons can be used. In addition, in case of railway bridges, the presence of such a mechanism can be a feasible solution for braking forces demands.

### **3 R/C CONTINUOUS CONCRETE BRIDGE – 3D MODEL**

The Benchmark Bridge that was studied for its response when designed with the restraining system is a monolithic three span prestressed R/C bridge. The end spans are 45.10m, the middle span is 45.60m and the total length is 135,80m. The deck is a concrete box cross section, connected to the piers rigidly and is supported on the abutments by sliding bearings with low friction. The piers are circular and are founded on 3x3 pile groups. The bridge's abutments are conventional seat-type abutments that provide the appropriate clearance, [13], between the deck and the back-wall. There are capacity design transverse seismic links-stoppers installed on the abutments. The bridge is founded on ground type B and the design ground acceleration in the area is 0.16g, [15]. 3-D finite element bridge models were generated in the analysis software OpenSees, [16], accounting for soil-structure interaction. *Fig. 2* demonstrates the properties of one of the models including both the longitudinal and the transverse retrofit. Bridge members are modeled with frame elements with material nonlinearities. The section analysis for the assignment of concentrated plasticity (hinges) at the top and bottom of piers was performed with Bomber-Biaxial [17], *Fig. 3a*. The foundation springs were provided by the geotechnical report. The passive resistance of the abutments due to embankment mobilization was simulated according to Shamsabadi guidelines [12],[13] and the HyperbolicGap compression material was used in OpenSees, as shown in *Fig. 3b*. The prestressed tendon system was studied for various parameters in order to

identify its efficiency in limiting seismic movements. The properties of the tendons used for the investigation are presented in *Table 1*. The 7T15 cross section corresponds to a tendon cross section of 7 strands of 15mm diameter. Force-Displacement relationship used was based on the bilinear high strength steel material law, *Fig. 3c*. The seismic analyses were conducted using five artificial accelerograms complying with zones I and II spectra.

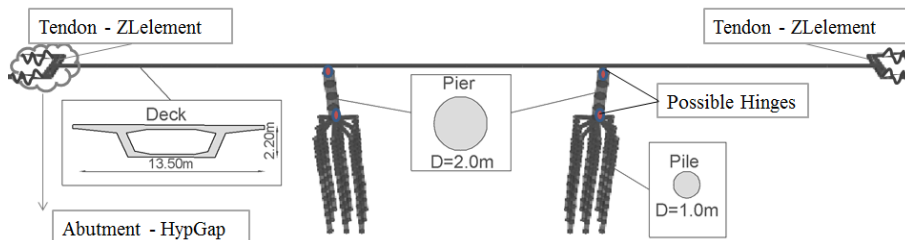


Figure 2. 3-D OpenSees Bridge Model

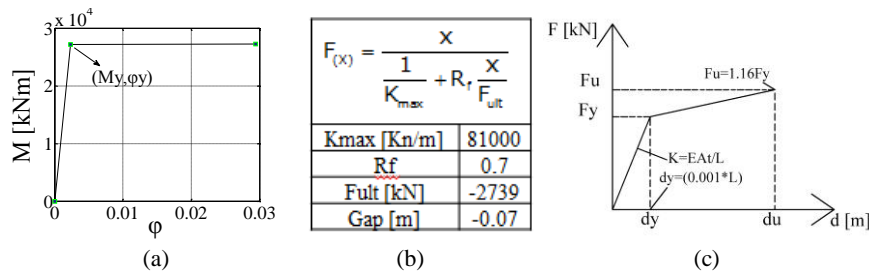


Figure 3. a) Moment - Curvature at Hinges, b) Abutment HypGap c) Tendon ZLElement

Table 1. Tendon properties in parametric analysis

No. Parameter	Tendons Cross Section	Length [m]
1	1x 7T15	20
2	2x 7T15	20
3	2x 7T15	25
4	2x 7T15	30
5	3x 7T15	20
6	3x 7T15	25
7	3x 7T15	30

#### 4 PARAMETRIC STUDY AND RESULTS DISCUSSION

The restraining system was applied in the benchmark bridge to investigate the seismic response of the new structural system. Two different types of parametric analyses were performed. The first includes the observation of the bridge responses for various tendon cross sections but with a specific amount of longitudinal reinforcement arrangement in the piers, (ratio of 1.75%). The second parametric analyses aimed on achieving acceptable design solutions (various reinforcement ratios), for seismic zone II, for the piers depending on

the number of tendons used mild or strong selection of the size of the restraining system. The data shown in the following figures includes the maximum values resulting from the application of the five accelerograms. *Table 2* includes the values obtained by seismic analysis for a benchmark bridge without the restraining mechanism.

*Table 2. Benchmark Bridge - Seismic demand (0.16g and 0.24g)*

	Long. Movement [m]	Pier Moment [kNm]
0.16g	0.087074	25277.89
0.24g	0.130611	>Mu =27530

Regarding the first parametric analysis *Fig. 4 a,b* demonstrate the results regarding the reductions achieved with respect to the benchmark bridge for various cross sections and tendon lengths, while *Fig. 4c* shows the reductions achieved in pier moments. In all diagrams x axis represents the different sets of parameters as defined in *Table 1*. The three figures indicate the high efficiency of the system with reductions arriving to over 30%. The restraining system achieves the transfer of part of the seismic demand to the abutments that are activated in the seismic response. An indicator of the contribution of the abutments and piers in the seismic resistance is the observation of the ratio of the abutment and pier shear forces to the total base shear of the structural system, *Fig. 5*. A lower contribution of the piers when large tendon cross sections are used, “strong restraining system” indicates that the abutment stability issues may arise and that the actual pier capability in the seismic resistance is not used.

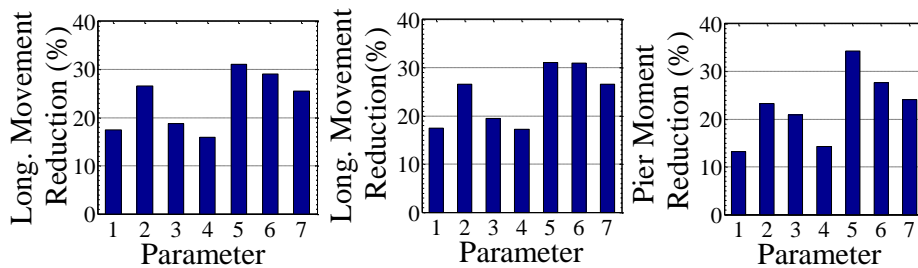


*Figure 4.* a) Long Movement Reduction (%), 0.16g, b) Long Movement Reduction (%), 0.24g c) Pier Moment Reduction (%), 0.24g

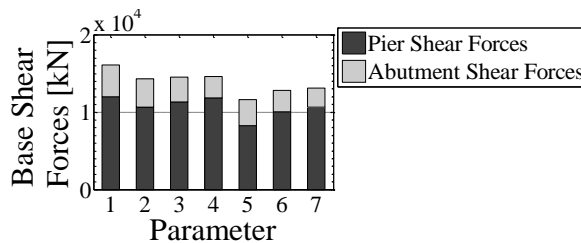


*Figure 5.* Base shear Forces 024g



On the light of the above a parametric analysis was performed in order to arrive to acceptable design solutions with higher pier reinforcement ratios and lower tendon cross sections, as shown in *Table 3*. It is remarkable that even the use of one or two tendons of 7T15mm can be used when the reinforcement ratio is increased to 3.25% or 2.45% respectively.

*Table 3. Acceptable Pier Reinforcement ration for Seismic Zone II (0.24g)*

No. Parameter	Tendons Cross Section	Length [m]	Required pier reinforcement ratio $\rho$ [%]
1	1x 7T15	20	3.25
2	2x 7T15	20	2.45
3	2x 7T15	25	2.85
4	2x 7T15	30	3.20
5	3x 7T15	20	1.5
6	3x 7T15	25	1.75
7	3x 7T15	30	1.75

## 5 CONCLUSIONS

The key objective of the present study was to propose a system for limiting longitudinal movements by using prestressed unbonded tendons responding in a way similar to that of dampers of a seismic isolation system. There were two applications of the system, one mild and one strong on a bridge in a seismic prone area. The main conclusions derived were the following:

- The efficiency in reducing longitudinal movements, the long lifetime of the tendons and the simplicity of the proposed system contribute to the high reliability of the proposed system.
- The restraining system is applicable in the longitudinal direction. However, the transverse has the advantage of the capability of using wall cross section of the piers towards this direction that can accommodate easily seismic demands.
- The use of the proposed system is considered unsuitable for precast concrete bridges which in general are seismically isolated. In these cases the reduction of the seismic movements has negative effects on the bridge response.
- The capability of transferring part of the seismic forces to the abutments and the embankments shall be used judiciously, so that the piers are relieved but the abutments are not extensively loaded. Therefore mild selections of unbonded tendons are found to be more preferable.

The application of the restraining system on other bridge types is expected to provide safer results regarding the economy and efficiency of the system.

## ACKNOWLEDGMENTS

The authors would like to acknowledge the assistance of METESYSM Company and EGNATIA ODOS A.E, since they provided all the necessary data and drawings for the investigated reference bridge.

## REFERENCES

- [1] Hewson, N, *Prestressed Concrete Bridges*. Thomas Telford Publishing, London, UK, 2003.
- [2] CEN[Comité Européen de Normalisation], “Eurocode 2: Design of concrete structures - Part 1: General rules and rules for buildings,” Vol. 1, No. November, 2002.
- [3] Burdet, O, Badoux, M, “Comparison of Internal and External Prestressing for Typical Highway Bridges Highway bridge models,” *16th Congress of IABSE*, Lucerne, 2000.
- [4] Park, YH, Park, C, Park, YG, “The Behavior of an In-Service Plate Girder Bridge Strengthened with External Prestressing Tendons,” *Engineering Structures*, Vol. 27, No. 3, pp. 379–386, 2005.
- [5] Davis, PM, Janes, TM, Eberhard, MO, Stanton, JF, “Unbonded Pre-Tensioned Columns for Bridges in Seismic Regions,” 2012.
- [6] Dawood, HM, ElGawady, M, “Performance-based seismic design of unbonded precast post-tensioned concrete filled GFRP tube piers,” *Composites Part B: Engineering*, Vol. 44, No. 1, pp. 357–367, 2013.
- [7] Zhou, C, Lu, X, Li, H, Tian, T, “Experimental Study on Seismic Behavior of Circular RC Columns Strengthened with Pre-stressed FRP Strips,” *Earthquake Engineering and Engineering Vibration*, Vol. 12, No. 4, pp. 625–642, 2013.
- [8] Buckle, I, Friedland, I, Mander, J, Geoffrey, M, Nutt, R, Power, M, “Seismic Retrofitting Manual for Highway Structures : Part 1 – Bridges,” 2006.
- [9] Walsh, KQ, Kurama, YC, “Behavior and Design of Unbonded Post-Tensioning Strand / Anchorage Systems for Seismic Applications,” 2009.
- [10] Weldon, BD, “Behavior, Design, and Analysis of Unbonded Post-Tensioned Precast Concrete Coupling Beams,” University of Notre Dame, Indiana, USA, 2010.
- [11] Markogiannaki, O, Tegos, I, “Seismic reliability of a reinforced concrete retrofitted bridge,” *ICOSSAR*, 2013.
- [12] Markogiannaki, O, Tegos, I, “A smart and costless solution for upgrading the seismic resistance of bridges Description of the proposed struts-ties system,” *IABSE Conference*, Sharm el Sheikh, Egypt, 2012.
- [13] CEN[Comité Européen de Normalisation], *Eurocode 8 — Design of Structures for Earthquake Resistance — Part 2: Bridges*, Vol. 3. 2005, pp. 1–152.
- [14] Rustum, A, “Evaluating the Retrofit of Highway Bridges Using Fluid Viscous Dampers,” University of Waterloo, Ontario, Canada, 2012.
- [15] CEN[Comité Européen de Normalisation], “Eurocode 8 : Design of structures for earthquake resistance — Part 1: General rules, seismic actions and rules for buildings,” 2003.
- [16] Constantinou, MC, Soong, TT, Dargush, GF, “Passive Energy Dissipation Systems For Structural Design and Retrofit,” 1998.
- [17] Papanikolaou, VK, “Analysis of arbitrary composite sections in biaxial bending and axial load,” *Computers & Structures*, Vol. 98–99, pp. 33–54, 2012.
- [18] Shamsabadi, A, Rollins, KM, Kapuskar, M, “Nonlinear Soil – Abutment – Bridge Structure Interaction for Seismic Performance-Based Design,” *Journal of Geotechnical and Geoenvironmental Engineering*, No. June, pp. 707–720, 2007.
- [19] Stewart, JP, Taciroglu, E, Wallace, JW, Lemnitzer, A, Hilson, C, Nojumi, A, Keowan, S, Nigbor, R, Salamanca, A, “Nonlinear Load-Deflection Behavior of Abutment Backwalls with Varying Height and Soil Density,” 2011.
- [20] Markogiannaki, O, Tegos, I, “Seismic retrofit of bridges through the external installation of a new type restraining system,” *15WCEE*, Lisbon, 2012.

## THE DYNAMICS OF A VERTICALLY RESTRAINED ROCKING BRIDGE

Nicos Makris<sup>1</sup> and Michalis F. Vassiliou<sup>2</sup>

<sup>1</sup>Dept. of Civil Engineering, Division of Structures, University of Patras, GR-26500, Greece  
<sup>2</sup>Institute of Structural Engineering (IBK), ETH Zürich, Switzerland, Formerly: PhD Student,  
Dept. of Civil Engineering, University of Patras, Greece  
e-mail: nmakris@upatras.gr, mfvassiliou@gmail.com

**ABSTRACT:** This paper investigates the rocking response and stability analysis of an array of slender columns capped with a rigid beam which are vertically restrained. This simplified system describes models a rocking bridge. The nonlinear equation of motion is formulated in which the stiffness and the prestressing force of the tendons are treated separately. In this way, the post-uplift stiffness of the vertically restrained rocking bridge can be anywhere from negative to positive depending on the axial stiffness of the vertical tendons. The paper shows that the tendons are effective in suppressing the response of rocking bridges with small columns subjected to long period excitations. As the size of the columns, the frequency of the excitation or the weight of the cap-beam increases, the vertical tendons become immaterial.

**KEY WORDS:** Rocking, uplifting, negative stiffness, earthquake engineering

### 1 THE DYNAMICS OF THE VERTICALLY RESTRAINED ROCKING FRAME

The main motivation for this study is to establish the dynamics of the vertically restrained rocking frame which emerges as a most promising alternative design concept for tall bridges [1]. Our analysis goes beyond the one bay configuration introduced in [1], which essentially represents the transverse motion of the bridge system as shown in Figure 1 (top left) and examines the planar rocking response of an array of  $N$  identical vertically restrained columns capped with a rigid beam that is clamped with the vertical restrainers. This configuration, shown in Figure 1, idealizes the longitudinal motion of a multi-span bridge.

When the elasticity,  $EA$ , of the restrainer is small compared to the weight of the rocking columns,  $m_c g$ , upon uplifting the lateral stiffness of the systems remains negative as in the free rocking case. As the elasticity,  $EA$ , of the restrainer increases, the lateral stiffness of the rocking frame increases gradually from negative to positive as shown in Figure 1 (bottom-left).

Assuming that the rocking column will not topple, it will recenter, impact will happen at the new pivot point and subsequently it will rock with opposite

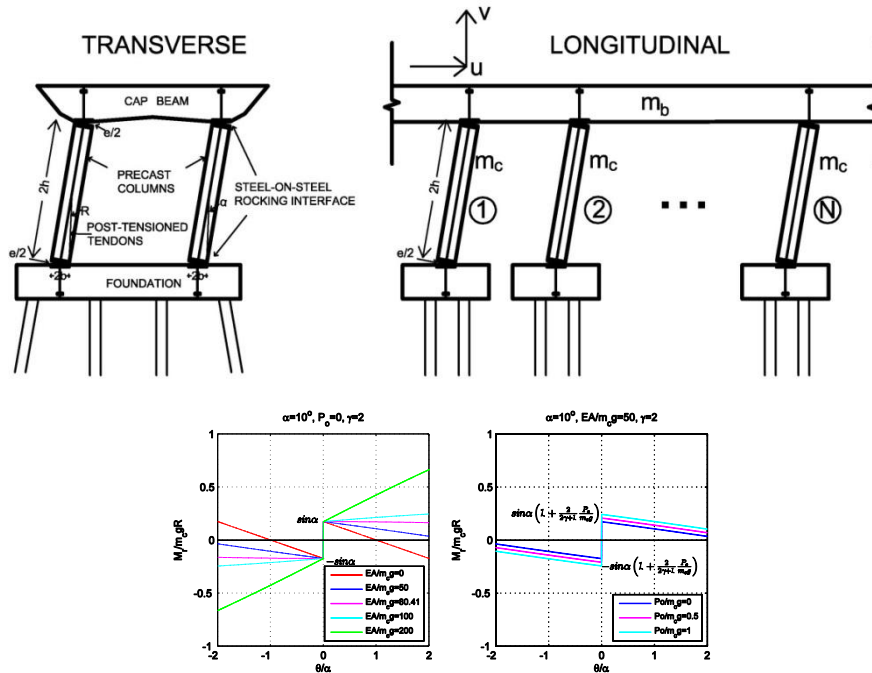


Figure 1. Transverse (top left) and longitudinal (top right) sections of the vertically restrained rocking frame together with the moment-rotation diagrams for various values of the dimensionless stiffness of the tendon  $EA/m_c g$  (bottom-left) and the dimensionless prestressing force  $P_o/m_c g$  (bottom right.)

rotations. During rocking, the dependent variables  $u(t)$  and  $v(t)$  of the center of mass of the cap-beam with mass  $m_b$  are given for  $\theta(t) < 0$  and  $\theta(t) > 0$  by the following expressions:

$$\ddot{\theta}(t) = -\frac{1+2\gamma}{1+3\gamma} p^2 \left[ \sin(\alpha \operatorname{sgn} \theta - \theta) + \frac{\ddot{u}_g}{g} \cos(\alpha \operatorname{sgn} \theta - \theta) \right] - \frac{2}{1+3\gamma} p^2 \sin \alpha \sin \theta \left[ \underbrace{\frac{EA}{m_c g} \tan \alpha}_{\text{elasticity}} + \underbrace{\frac{P_o}{m_c g} \frac{1}{\sqrt{2-2\cos \theta}}}}_{\text{prestressing}} \right] \quad (1)$$

Where  $p = \sqrt{3g/4R}$  and  $\gamma = m_b/Nm_c$ .

The first bracket in equation (1) describes the dynamics of the free standing rocking frame [2,3] whereas the second bracket describes the contribution of the

vertical tendons. The only damping in the system comes from energy loss during impact. The ratio of the kinetic energy of the rocking frame after and before impact [2] is:

$$r = \frac{\dot{\theta}_2^2}{\dot{\theta}_1^2} = \left( \frac{1 - \frac{3}{2} \sin^2 \alpha + 3\gamma \cos 2\alpha}{1 + 3\gamma} \right)^2 \quad (2)$$

## 2 COMMENTS ON THE EFFECT OF THE RESTRAINING TENDONS AND THE MASS OF THE CAP BEAM

The mathematical structure of equation (1) offers some valuable information regarding the effectiveness of the vertical restrainers in association with the size of the columns and the weight of the cap-beam. The term associated with the first bracket of equation (1) expresses the dynamics of the free-standing rocking frame ([2], [3]). The quantity  $\hat{p} = \sqrt{\frac{1+2\gamma}{1+3\gamma}} p$  is the frequency parameter of the

free-standing rocking frame showing that its dynamic response is identical to the rocking response of a single free-standing column with the same slenderness; yet with larger size – that is a more stable configuration.

The term associated with the second bracket of equation (1) expresses the contribution of the vertical restrainers. As the size of the columns increases (smaller  $p$ ), the effectiveness of the vertical restrainers is suppressed with  $p^2$ ; while the effectiveness of the restrainers further reduces as the weight of the cap-beam increases (large  $\gamma$ ). Simply stated, the combination of a heavy deck atop tall columns enhances the seismic stability of the free-standing rocking frame while it reduces the effectiveness of the vertical restrainers.

On the other hand, at the limiting case of a massless rigid cap-beam ( $\gamma=0$ ), equation (1) indicates that the vertically restrained rocking frame experiences an apparent restraining stiffness that is 4 times larger and an apparent prestressing force that is 2 times larger than the corresponding values of the solitary rocking column that is vertically restrained with the same tendon (same  $\frac{EA}{m_c g}$  and same  $\frac{P_o}{m_c g}$ , [4]).

## 3 FROM NEGATIVE TO POSITIVE STIFFNESS

In the vertically restrained rocking frame, the negative stiffness originates from the fact that as the rotation increases the restoring weight vectors of the columns and the cap-beam approach the pivot point; whereas, the positive stiffness originates from the presence of the vertical elastic restrainers which offer an increasing restoring moment.

Without loss of generality we concentrate in the case of positive rotations ( $\theta(t) > 0$ ). Equation (1) indicates that the rotation-dependent restoring moment is

$$M(\theta) = m_c g R \left[ \sin(\alpha - \theta) + \frac{2}{1 + 2\gamma} \sin \alpha \sin \theta \left( \tan \alpha \frac{EA}{m_c g} + \frac{1}{\sqrt{2}\sqrt{1 - \cos \theta}} \frac{P_o}{m_c g} \right) \right] \quad (3)$$

Figure 1 (bottom) plots the expression given by equation (3) for various values of the dimensionless elastic force  $\frac{EA}{m_c g}$  for a column with slenderness  $\alpha = 10^\circ$ . Linearization of (3) gives:

$$\frac{M(\theta)}{m g R} = \sin \alpha \left[ 1 + \frac{2}{2\gamma + 1} \frac{P}{m g} + \theta \left( \frac{2}{2\gamma + 1} \tan \alpha \frac{EA}{m g} - \cot \alpha \right) \right] \quad (4)$$

The factor of the rotation  $\theta$  in equation (4) is the stiffness of the system upon uplifting; and therefore, the condition for the linearized system to exhibit a positive stiffness is

$$\frac{EA}{m_c g} > \left( \frac{1}{2} + \gamma \right) \frac{1}{\tan^2 \alpha} \quad (5)$$

For instance, when  $\alpha = 10^\circ$ , according to expression (5) a vertically restrained rocking frame exhibits a positive stiffness if  $\frac{EA}{m_c g} > 48.25$  for  $\gamma = 1$  and  $\frac{EA}{m_c g} > 80.41$  for  $\gamma = 2$ . When inequality (5) becomes an equality the vertically restrained rocking column exhibits a rigid-plastic behavior without enclosing any area.

#### 4 ACCELERATION NEEDED TO INITIATE UPLIFT

The minimum uplifting acceleration of the vertically restrained rocking frame is

$$\ddot{u}_g^{up} = g \tan \alpha \left( 1 + \frac{2}{2\gamma + 1} \frac{P_o}{m_c g} \right) \quad (6)$$

Equation (6) indicates that as the ratio of the weight of the deck to the weight of the columns increases (larger  $\gamma = \frac{m_b}{N m_c}$ ), the effect of the prestressing force,  $P_o$ , reduces and the uplift acceleration tends to that of the free-standing rocking frame, that is  $g \tan \alpha$  [2,3].

#### 5 ROCKING SPECTRA: SELF SIMILAR RESPONSE

The pulse excitation shown as an insert in the subplots of Figure 2 is the well known symmetric Ricker wavelet given by

$$\psi(t) = a_p \left(1 - \frac{2\pi^2 t^2}{T_p^2}\right) e^{-\frac{1}{2} \frac{2\pi^2 t^2}{T_p^2}} \quad (7)$$

The first two terms in the right-hand-side of equation (1) express the response of the free standing rocking frame which is fully described by five independent dimensionless variables [2],  $\Pi_\theta = \theta$ ,  $\Pi_\omega = \omega_p/p$ ,  $\Pi_\alpha = \tan\alpha$ ,  $\Pi_\gamma = \gamma = m_b/Nm_c$ ,  $\Pi_g = a_p/g$  where  $a_p$  and  $\omega_p = 2\pi/T_p$  is the acceleration amplitude and the cyclic frequency of the excitation pulse.

The contributions of the elasticity,  $E$  and the prestressing force of the tendon,  $P_o$ , are entering into equation (1) in a dimensionless form,  $\Pi_E = EA/m_c g$  and  $\Pi_P = P_o/m_c g$ .

With the seven dimensionless  $\Pi$ -terms established, the dynamic response of the vertically restrained rocking frame can be expressed as

$$\theta(t) = \varphi\left(\frac{\omega}{p}, \tan\alpha, \gamma, \frac{a}{g}, \frac{EA}{m g}, \frac{P}{m g}\right) \quad (8)$$

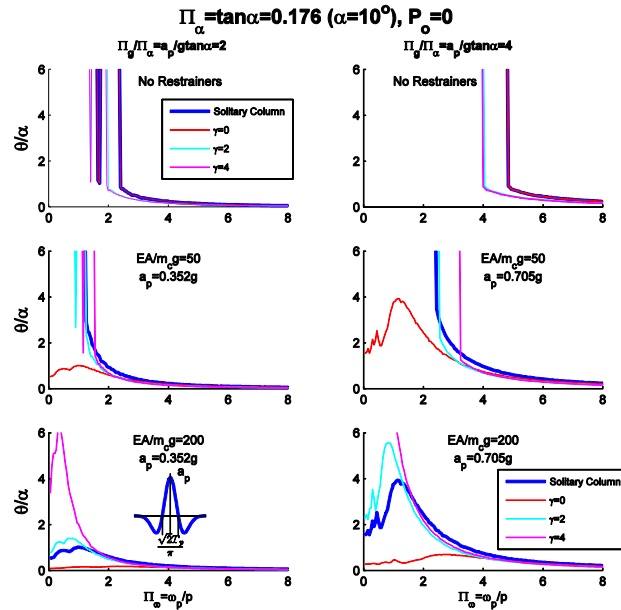


Figure 2. Rocking Spectra for different values of the dimensionless products  $\Pi_g = a_p/g$ ,  $\Pi_E = EA/m_c g$  and  $\Pi_\gamma = \gamma$  when a vertically restrained rocking frame with columns having slenderness  $\alpha = 10^\circ$  ( $\Pi_\alpha = \tan\alpha = 0.176$ ) is subjected to a symmetric Ricker wavelet. In tall rocking frames (large values of  $\omega_p/p$ ) the effect of the vertical restrainers is marginal.

## 6 THE CONTINGENCY OF RESONANCE

Equation (4) indicates that the linearized rotational stiffness of the vertically

restrained rocking column is given by

$$K_r = m_c g R \sin \alpha \left( \frac{2}{2\gamma + 1} \tan \alpha \frac{EA}{m_c g} - \frac{1}{\tan \alpha} \right) \quad (9)$$

When  $\frac{EA}{m_c g}$  is sufficiently large and satisfies inequality (5),  $K_r$  is positive and upon uplifting ( $\theta \neq 0$ ) the rotational frequency of the vertically restrained rocking frame (see equation (20)) is (for  $\sin \alpha \approx \tan \alpha$ )

$$\omega_r = \sqrt{\frac{1+2\gamma}{1+3\gamma}} p \sqrt{\frac{2}{2\gamma+1} \tan^2 \alpha \frac{EA}{m_c g} - 1} \quad (10)$$

At resonance,  $\omega_p = \omega_r$  and this happens when

$$\frac{\omega_p}{p} = \sqrt{\frac{1+2\gamma}{1+3\gamma}} \sqrt{\frac{2}{2\gamma+1} \tan^2 \alpha \frac{EA}{m_c g} - 1} \quad (11)$$

Figure 2 shows rocking spectra of a vertically restrained rocking frame for two levels of the ground excitation ( $\Pi_g/\Pi_\alpha=2$  and 4) and three different values of the elasticity of the tendon (free-standing= $EA/m_c g=0$ , 50 and 200) as the weight of the cap-beam (deck) increases ( $\gamma=0, 2$  and 4). The ground excitation is the symmetric Ricker pulse expressed by equation (7). Clearly, as the weight of the cap-beam increases (larger  $\gamma$ ), for a given value of the elasticity of the restrainers, the lateral stiffness of the rocking frame decreases (see eq. 4).

Figure 3 shows rocking spectra of a vertically restrained frame with slenderness  $\alpha=10^\circ$  and  $\gamma=4$  for different values of the dimensionless products  $\Pi_g$ ,  $\Pi_E$  and  $\Pi_p$  when subjected to a symmetric Ricker pulse. All plots show that at small values of  $\omega_p/p$  (rocking frames with short columns or long duration pulses), the vertically restrained frames exhibit large rotations-overturning; whereas, when the stiffness is positive, they exhibit the expected amplification in the neighborhood of resonance. On the other hand, as  $\omega_p/p$  increases (larger columns or shorter duration pulses) the response from all configurations reduces to a single curve showing that the effect of the vertical restrainers becomes marginal compared to the seismic resistance that originates from the mobilization of the rotational inertia of the columns.

At this point it is worth translating the dimensionless products of Figure 3 to physical quantities of typical bridges. First we consider 9.6m tall piers with width  $2b=1.6$  m ( $R=4.87$ ,  $p=1.23$  rad/s and  $\tan \alpha=1.6/9.6=0.166$ ). These are typical dimensions of bridge piers of highway overpasses and other smaller bridges in Europe and the USA. Let us assume that this rocking frame with  $p=1.23$  rad/s,  $\tan \alpha=0.166$  and  $\gamma=4$  is excited by the Ricker pulse that approximates the strong 1992 Erzincan Turkey record ( $a_p=0.35g$ ,  $T_p=1.44$  sec). This gives  $\Pi_\omega = \omega_p/p = 2\pi/pT_p = 3.54$ . Figure 3 (left) that is for  $a_p=0.352g$ , shows that at  $\omega_p/p=3.54$  the effects of the restrainers is marginal and that the free-



standing rocking frame experiences approximately the same uplift as the vertically restrained rocking frame with  $EA=200m_c g$ . Figure 3(center) indicates that when the acceleration amplitude of the 1.44s long Ricker pulse is increased to  $a_p=0.53g$  (that is a most strong excitation) the free- standing rocking frame is at the verge of overturning; however, its stability is appreciably enhanced even

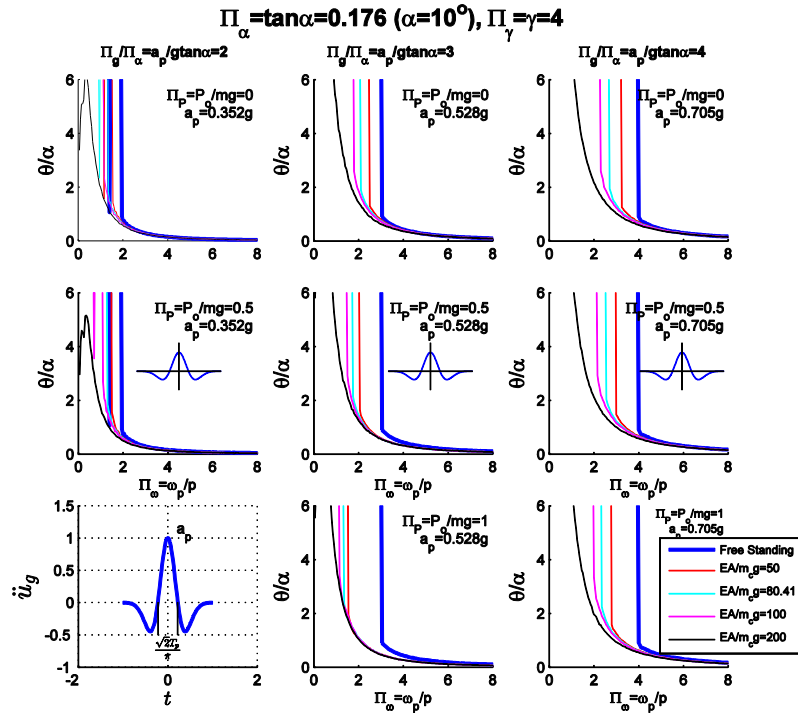


Figure 3. Rocking spectra for different values of the dimensionless products.  $\Pi_g = a_p/g$ ,  $\Pi_E = EA/m_c g$  and  $\Pi_p = P_o/m_c g$  when the vertically restrained rocking frame with column slenderness  $\alpha=10^\circ$  ( $\Pi_\alpha = \tan\alpha = 0.176$ ) and  $\Pi_\gamma = \gamma = 4$  is subjected to a symmetric Ricker wavelet. For values of  $\Pi_\omega = \omega_p/p > 4$ , the response of the free standing rocking frame is essentially identical to the response of the restrained frame showing that for tall rocking frames the effect of the vertical restrainers is marginal.

with the use of relative flexible restrainers (say  $EA=50m_c g$ ) which maintains a negative lateral stiffness

We now consider a 24m tall bridge pier with  $2b=4.0m$  ( $R=12.17m$ ,  $p=0.778rad/s$  and  $\tan\alpha=4/24=0.166$ ). Such tall piers are common in valley bridges. Let us again assume that this rocking frame with  $p=0.778rad/s$ ,  $\tan\alpha=0.166$  and  $\gamma=4$  is excited by a Ricker pulse with  $a_p=0.35g$  and  $T_p=1.44s$ . This gives  $\Pi_\omega = \omega_p/p = 2\pi/pT_p = 5.61$ . For such value of  $\omega_p/p$ , the free standing rocking frame with  $(24m) \times (4m)$  piers survives the 1.44s long acceleration pulse even when its acceleration amplitude is as high as  $a_p=0.705g$  as shown in Figure 3 (right). The main conclusion that emerges from Figure 3 is that as the size of

the columns (or the frequency of the excitation) increases, the effect of the vertical restrainers becomes immaterial given that most of the seismic resistance originates from the mobilization of the rotational inertia of the columns.

## 7 CONCLUSIONS

This paper investigates the rocking response and stability analysis of an array of slender columns capped with a rigid beam which are vertically restrained with elastic prestressed tendons that pass through the center lines of the columns. While the lateral stiffness of a free standing rocking frame is negative, the lateral stiffness of a vertically restrained rocking frame can be anywhere from negative to positive depending on the axial stiffness of the restraining tendons.

The paper shows that the restraining tendons are effective in suppressing the response of rocking frames with small columns when subjected to long period excitations. As the size of the columns, the frequency of the excitation or the weight of the cap beam increases, the vertical restraining tendons become immaterial given that most of the seismic resistance of tall rocking frames originates primarily from the mobilization of the rotational inertia of their columns.

The paper shows that for up to medium-size rocking frames, where the concept of vertical restrainers may be attractive there is engineering merit for the vertical tendons to be flexible enough so that the overall lateral stiffness of the rocking frame remains negative. In this way, the pivot points are not overloaded with high compressive forces; while at the same time the rocking structure enjoys ample seismic stability by avoiding resonance.

## ACKNOWLEDGEMENT

This work was funded by the research project “Seismo-Rock Bridge” with grant No 2295 which is implemented under the “ARISTEIA” action of the “OPERATIONAL PROGRAMME EDUCATION AND LIFELONG LEARNING” and is co-funded by the European Social Fund (ESF) and Greek National Resources.

## REFERENCES

- [1] Mander, J. B., & Cheng, C. T. (1997). Seismic resistance of bridge piers based on damage avoidance design. *Technical Report NCEER, 97*.
- [2] Makris, N. and Vassiliou, M. F. (2013), Planar rocking response and stability analysis of an array of free-standing columns capped with a freely supported rigid beam. *Earthquake Engng. Struct. Dyn.*, 42: 431–449
- [3] Makris, N., & Vassiliou, M. F. (2014). Are some top-heavy structures more stable? *Journal of Structural Engineering ASCE* (in press)
- [4] Vassiliou MF (2010), «Analytical investigation of the dynamic response of a pair of columns capped with a rigid beam and of the effect of seismic isolation on rocking structures», Doctoral Dissertation, Department of Civil Engineering, University of Patras, Greece (in Greek)

# THE USE OF PIERS OF HIGH FLEXIBILITY FOR THE DEGRADATION OF SEISMIC INERTIAL FORCES ON INTEGRAL BRIDGES

Ioannis Tegos<sup>1</sup> and Vasileios Pilitsis<sup>2</sup>

<sup>1,2</sup> Aristotle University of Thessaloniki, Faculty Of Engineering, Dept. of Civil Engineering  
Greece

e-mail: itegos@civil.auth.gr, vpilitsi@civil.auth.gr

**ABSTRACT:** This study is about finding ways equivalent to seismic isolation in monolithic bridges. For this purpose, the possibility of achieving that by drastically degrading piers' stiffness is examined. The obtained results from the application of the proposal in a long road bridge of Egnatia Motorway vindicated the expectations of the authors.

**KEY WORDS:** Flexible; Pier; Circular cross-section; Stiffness.

## 1 INTRODUCTION

The issue of pier flexibility is related to two basic requirements in bridge designing. The first one associates with serviceability since pier flexibility allows system's adaption to expansion-contraction of the deck due to thermal actions, creep and shrinkage. Treatment of these deformations is possible without the use of expansion joints and bearings, which treat the above mentioned condition but create other problems. Thus, today's trend in bridge designing is the riddance of these devices.

Flexibility is related also to seismic resistance of structures, since it affects the value of fundamental period by which the magnitude of horizontal seismic actions depends. In this approach, piers' flexibility acts in an analogous manner with seismic isolation as the value of the fundamental period of the structure gets a greater value and the seismic inertial loads of the bridge degrade.

In literature there are papers, relevant with the exploitation of flexibility, which refer to the appropriate division of the cross-sections of piers and abutments in order the system to gain in-service and seismic advantages [1]. In the same way of dividing cross-section of the piers, bridges that are irregular according to EC8-Part 2 [2] is possible to improve their seismic response and avoid the "penalty" of reducing the value of the behaviour factor [3].

In the present study is suggested a new type of cross-section for the piers which has the advantage of flexibility and consists of a symmetrically arranged, statically independent, individual circular cross-sections situated in contact with

each other. The reasonably emerging doubt about the aesthetics and the durability of the proposed choice is insubstantial according to authors' opinion.

## 2 COMPLIANCE CRITERIA

The compliance criteria that govern the choices of the designer of any structure are the seven well known which relate to safety, serviceability, economy, aesthetics, integration in physical environment, durability and constructability. In this case flexibility affects all of these criteria, but especially is related to safety, in terms of seismic safety, serviceability and constructability.

Flexibility also affects other critical issues. For example, the dividing of a pier's section for gaining in flexibility, so that the moment of inertia to be reduced in the desired level, affects both the area of the cross-section and its dimensions, that is the diameter of the circle surrounding the section. Subsequently, the area of the cross-section affects the normalized axial force of the pier while the surrounding region of the cross-section affects the aesthetics of the pier.

In this study two cases of segmentation of piers' cross-section are examined. The first one consists of circular cross-sections, equal in diameter, such as the section of *Fig.1a*, and the second one consists of unequal circular sections, as there is a large circular section in the center of the cross-section, surrounded by twelve smaller ones, situated in contact with each other and with the large one (*Fig.1b*).

Apart from the above mentioned effects on the aesthetics and normalized axial force, there is the issue of regularity in bridges as defined in EC8 - Part2. It is interesting to investigate the effect of the piers' cross-section division on regularity, which in the case of not fulfilling the code provisions leads to the dramatic increase of horizontal seismic design actions.

Two additional problems arising from the fragmentation of the cross-section are buckling and P- $\delta$  effects, which are more intense in the case of the unequal sections of *Fig.1b*. Regarding the issue of buckling, it is possible to seek out a criterion which relates the Euler buckling load to the upper bound of the normalized axial force due to ductility demands. Therefore, applying this rationale and taking into account a value of  $\eta_k=0.30$  for the normalized axial force, in the case of the longitudinal direction of the reference bridge of this study:

$$P_{cr} = \frac{\pi^2 \cdot E \cdot I}{L_{eq}^2} \Rightarrow \frac{P}{\frac{\pi \cdot d^2}{4} \cdot f_{ck}} \leq \frac{4 \cdot \pi \cdot E_c \cdot I}{L_{eq}^2 \cdot d^2 \cdot f_{ck}} \Rightarrow \quad (1)$$

$$d \leq \sqrt{\frac{4 \cdot \pi \cdot E_c \cdot I}{0.25 \cdot L_{P5}^2 \cdot \eta_k \cdot f_{ck}}} = 1.05m$$

In the transverse direction the problem becomes worse, as the effective length must be taken equal to the total height of the pier and hence the resulting minimum acceptable value of diameter for the cross-section is two times greater than the previous one:

$$d \leq \sqrt{\frac{4 \cdot \pi \cdot E \cdot I}{L_{P5}^2 \cdot \eta_k \cdot f_{ck}}} = 0.53\text{m} \quad (2)$$

Regarding the above mentioned, from the two proposed cross-section types, the first one is more appropriate when there are issues with expansion-contraction of the deck in combination with low-height piers in end-positions, so that the effects of expansion-contraction of the deck on serviceability to be drastically reduced due to the adaptability of this type of cross-section. In the case of intense problems in regularity, the use of cross-section of (Fig.1b) is more appropriate, since it gives the possibility, in the case of low-height piers, of reducing the diameter of the inner circular section without downgrading the aesthetics of the bridge. Regarding aesthetics, Fig.4 is provided for comparing the two proposed cross-section types.

Regarding the constructability, the following advantages are mentioned: (a) In the case of the cross-section of equal diameters (Fig.1a), the piers can be constructed much easier in contrast to the case of the conventional hollow piers which are also disadvantaged in the case of earthquake. Indeed, it is possible to use a cardboard disposable formwork like the ones used in building constructions, provided that the construction along height will be scattered. (b) The same thing applies in the case of the cross-section of (Fig.1b), whereas the large circular central section can be constructed by using a simplified metallic sliding formwork. Geometric and mechanical properties of the cross-sections of the reference pier and the proposed alternatives are presented in following table (Table 1).

Table 1. Properties of the cross-sections of the reference piers and the two proposed alternatives

	Area (m <sup>2</sup> )	I <sub>x</sub> (m <sup>4</sup> )	I <sub>y</sub> (m <sup>4</sup> )
Reference bridge	7.017	1.2329	12.9885
Case A	5.498	0.3436	0.3436
Case B	4.367	0.3585	0.3585

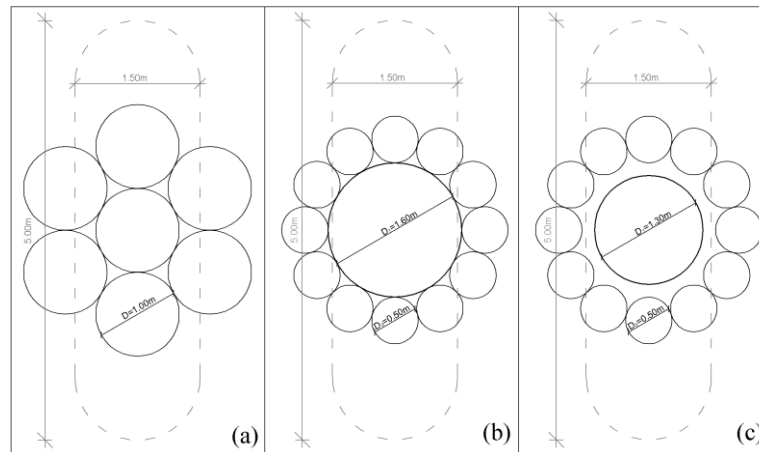


Figure 1. (a) Cross-section of piers of Case A – (b) Cross-section of piers of Case B and P1, P2, P3 and P5 of case C – (c) Cross-section of pier P4 of Case C in contrast with the cross-section of the reference pier

### 3 CASE STUDY

The proposed solution is applied as seismic isolation in a road bridge of great length of Egnatia Motorway, with particularly unfavorable characteristics regarding regularity and serviceability as well, since its great length imposes major in-service moments and shear forces on the piers.

The bridge which is used as a “reference” case of study is the left part of a viaduct, part of Egnatia Motorway, connecting Arachthos with Peristeri in Greece. It has six spans (34m + 4x43m + 34m) and a total length of 240m (Fig.2). The cross section of the deck is a box-girder and has a total width of 12.90m (Fig.3a). The deck is rigidly connected with the five piers and is seated on both of the abutments on sliding bearings. Abutments’ bearings have a circular section with diameter equal to 600mm. There is also a shear key with a load capacity of 176ton. Piers have the section shown in (Fig.3b) and are founded on 3x3 pile groups which are connected to 7.90x8.70x2.20m pile caps. The diameter of the piles is 1.20m and their length is 12.0m for all the piers. The abutments have a height of 2.0m and 4.0m, are conventional seat-type abutments and are founded on a shallow foundation with dimensions of 5.50 x 13.20x1.20m and 6.00x13.20x1.20m respectively. The bridge is founded on ground similar to Eurocode’s 8 ground type B and a design ground acceleration equal to 0.16g was used in the final design. The importance factor adopted was equal to 1.30 and the behaviour factors (q-factors) were equal to 3.50 for the longitudinal, 2.24 for the transverse, without taking into account the diminution due to irregularity, and 1.00 for the vertical direction of the bridge [4].

In the present study the bridge's piers are redesigned according to EC8. In particular, apart from the different design spectra of the code, a different behaviour factor of the transverse direction ( $q_y=3.02$ ) and different effective stiffness for the piers was taken into account, according to Annex C of EC8 - Part2 [2].

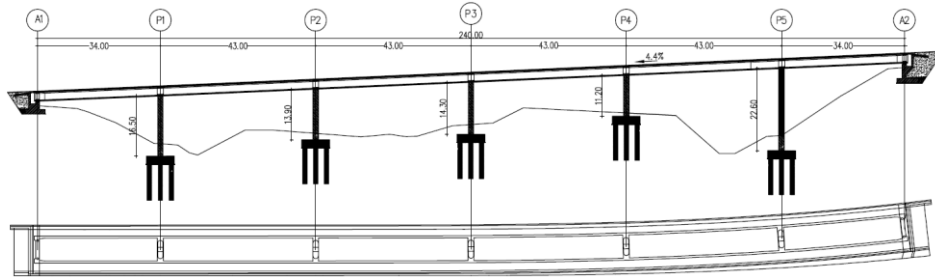


Figure 2. Longitudinal section plan view of the left part of the bridge

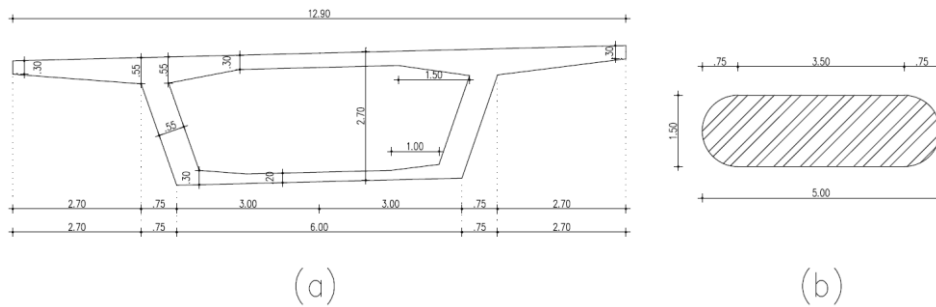


Figure 3. (a) Cross section of the deck at mid-span – (b) Cross section of the piers of “reference” bridge

Based on the aforementioned “reference bridge”, three additional analysis were conducted: (a) One using the cross-section type of (Fig.1a) for all of the bridge's piers (Case A), (b) One using the cross-section type of (Fig.1b) for all of the bridge's piers (Case B), (c) and one using the cross-section type of (Fig.1b) for all of the bridge's piers except of pier P4 in which the central circular section of the cross-section had a diameter of 1.30m (Case C), aiming to improve the distribution of horizontal seismic shear force among the piers and thus to improve regularity of the bridge.

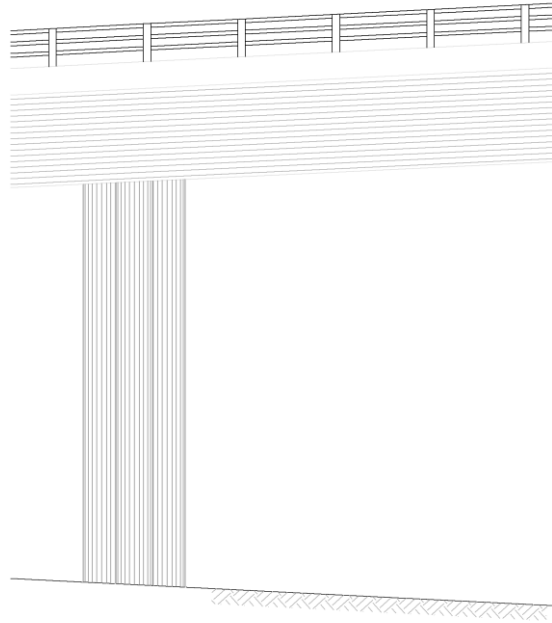


Figure 4. Aesthetics in Case A

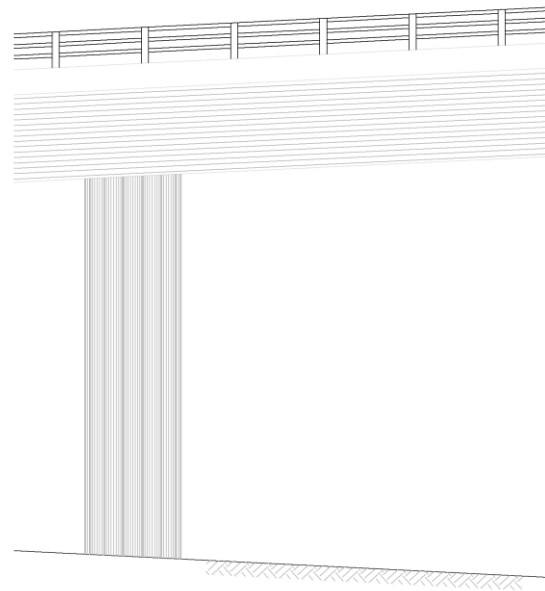


Figure 5. Aesthetics in Cases B and C



#### 4 ANALYSIS RESULTS

The program used for the analysis was S.A.P.2000 v.11.0.4 [5]. The analysis results are summarized in the following tables.

What can be said is that in all cases we have a reduction of the required longitudinal reinforcement and concrete, except of “case C” in which a slight increase of required longitudinal reinforcement is observed relatively to the case of piers with the original cross-section. The degradation of piers’ stiffness led to this result, since it led to an increase in fundamental period of the structure, thus to an increase in the design seismic displacements and to a significant reduction in horizontal seismic actions (Table 2).

Regularity is significantly improved in the proposed solutions, as the value of  $\rho$ -factor in all cases is less than 2.00. In the case of “reference bridge” the  $\rho$ -factor for the longitudinal direction has a value of 2.85, and so the bridge is considered to be irregular and a final behaviour factor with value of  $q_x=2.46$  instead of 3.50, which is the value for the considered geometry of the cross-section (Table 3). In all the rest cases, both in longitudinal and transverse direction a behaviour factor with value of 3.50 was used.

Table 2. Summarized results of “reference” bridge and three alternative cases

	$T_x$ (sec)	$T_y$ (sec)	$d_{Ed,x}$ (cm)	$\max d_{Ed,y}$ (cm)	$\rho_x$	$\rho_y$
Reference Bridge	1.06	0.68	8.0	5.2	2.85	1.16
Case A	1.85	1.51	14.6	15.0	1.41	1.23
Case B	1.64	1.46	13.0	14.7	1.48	1.26
Case C	1.89	1.59	14.8	15.4	1.16	1.23

Table 3. Changes in quantities in contrast with the “reference” bridge

	Change in concrete (%)	Change in longitudinal reinforcement (%)
Case A	-21.7	-17.2
Case B	-37.8	-30.1
Case C	-39.5	-36.5

#### 5 CONCLUSIONS

Based on the comparative evaluation of the results of four analyses of the case study, namely (a) the bridge as constructed, (b) considering a cross-section with seven – in contact – circular sections with diameter of 1.00 each (Fig.1a), (c) considering a cross-section as shown in (Fig.1b), (d) considering a cross-section as shown in (Fig.1b) but with variable diameter of the inner circular section among piers in order to improve the regularity of the bridge, the following

conclusions can be posed:

1. The suggestion at this stage is processed coarsely and is only appropriate for cast-in-situ bridges of relatively low height.
2. Aesthetics, judged as objectively as possible, not only was not damaged but may be considered as improved.
3. Constructability of the suggested piers is much easier compared to the conventional case of hollow circular cross-sections.
4. The proposed modification's behaves in an analogous manner with a seismic isolation system and additionally has the advantage of homogeneity with the protected deck of the bridge. Hence, it has the same lifetime and requires no maintenance.
5. Although deck has the greatest share in the total cost of the bridge, economy of the suggestion, both in terms of short and long-term, regarding piers and its foundations, is quite important.

## ACKNOWLEDGMENTS

The authors wish to express their gratitude to METE SYSM S.A. for providing the original study of the bridge for the purposes of the present study.

## REFERENCES

- [1] Tegou, S, Mitoulis, S, Tegos, I, "An unconventional earthquake resistant abutment with transversely directed R/C walls", *Engineering Structures*, Elsevier, title no. 32(11), 3801-3816, 2010
- [2] CEN [Comité Européen de Normalisation], *EN 1998-2: Eurocode 8: Design of Structures for Earthquake Resistance - Part 2: Bridges*, 2005.
- [3] Pilitsis, V, Tegos, I, "A Suggestion for Improving the Regular Seismic Behaviour of Integral Concrete Bridges", *Proc. of 2<sup>nd</sup> Intl. Conference on Bridges IBSBI 2014*, Athens, 2014.
- [4] Pilitsis, V, Tegos, I, "Employment of abutments and approach embankments for seismic protection of bridges", *Proc. Intl. Van Earthquake Symposium*, Van, Turkey, 2013.
- [5] Computers and Structures Inc., *S.A.P. 2000 Nonlinear ver.11.0.4*, 2007

## **TOPIC 2**

Maintenance

Monitoring

Stone Bridges



## **ENVIRONMENTAL EFFECTS ON BRIDGES**

### **Statistical durability study based on existing inspection data**

Filippos Alogdianakis<sup>1</sup>, Ioannis Balafas<sup>2</sup> and Dimos C. Charmpis<sup>3</sup>

<sup>1,2,3</sup> University of Cyprus, Dept. of Civil and Environmental Engineering, Nicosia, Cyprus  
e-mail: alogdianakis.filippos@ucy.ac.cy, ibalafas@ucy.ac.cy, charmpis@ucy.ac.cy

**ABSTRACT:** Published bridge inspection data are analysed to assess the durability of bridge components (deck, superstructure and substructure) with respect to time from construction. The data are also used to estimate the resistance of common construction types/materials (steel, reinforced/prestressed concrete) to various deterioration factors (water, sea/deicing salt, etc.).

**KEY WORDS:** Bridge; Corrosion; Deterioration; Durability; Environment.

## **1 INTRODUCTION**

The durability of existing bridge stocks is one of the biggest problems governments around the globe have to face. Vast budgets are spent annually to keep bridges in serviceable condition. Bridge durability depends on the type of structure, the material as well as the environmental exposure. This study identifies the conditions, under which bridges deteriorate rapidly. For this purpose, inspection data from the USA bridge stock are used, in which recordings for more than half a million bridges are included. The results of this work may help authorities to optimally allocate funding for bridge construction and maintenance.

## **2 BRIDGE INSPECTION DATABASE**

USA's Federal Highway Administration, in order to assist the maintenance and rehabilitation of the built infrastructure, preserves an up to date inventory of bridges, tunnels and culverts. This inventory is known as NBI (National Bridge Inventory) and contains a vast amount of information in coded form (116 items) concerning: location, structural condition, age, materials, traffic etc. [1]. To keep the inventory up to date, biennial inspections are conducted from specially qualified personnel, whose responsibility is to evaluate the condition of different structural parts of each bridge. Condition ratings use a scale 0-9 (Table 1); 9 for excellent and 0 for failed condition, respectively. From these ratings the evaluated infrastructure is prioritized for further inspection, repair work or replacement.

The database refers to data from 608,533 structures; 470,417 of these met

certain requirements to be included in the processed sample. In particular, 131,980 non-bridge elements (e.g. culverts) were excluded from the analysis. Also, 545 bridges built before 1900 and 2685 bridges last inspected before 2000 were also excluded. The database includes data from prestressed concrete bridges built before 1950, most of which are rebuilt. To avoid misleading interpretation of results, those bridges were excepted (332 bridges). Finally, taking into account limitations posed by NBI standards on bridge length, a number of bridges were excluded, in order to obtain certain uniformity of the processed data, in regards to inspection standards.

The bridge parts which are rated include the: substructure (i.e. columns), superstructure (i.e. beams) and deck. Structural deficiency is defined in this work as a condition rating of either superstructure, substructure or deck evaluation of 5 or less.

*Table 1. Condition scale used to assess bridges in USA [1]*

Rating	Description
9	<b>EXCELLENT CONDITION</b>
8	<b>VERY GOOD CONDITION</b> - no problems noted.
7	<b>GOOD CONDITION</b> - some minor problems.
6	<b>SATISFACTORY CONDITION</b> - structural elements show some minor deterioration.
5	<b>FAIR CONDITION</b> - all primary structural elements are sound but may have minor section loss, cracking, spalling or scour.
4	<b>POOR CONDITION</b> - advanced section loss, deterioration, spalling or scour.
3	<b>SERIOUS CONDITION</b> - loss of section, deterioration, spalling or scour have seriously affected primary structural components. Local failures are possible. Fatigue cracks in steel or shear cracks in concrete may be present.
2	<b>CRITICAL CONDITION</b> - advanced deterioration of primary structural elements. Fatigue cracks in steel or shear cracks in concrete may be present or scour may have removed substructure support. Unless closely monitored, it may be necessary to close the bridge until corrective action is taken.
1	<b>'IMMINENT' FAILURE CONDITION</b> - major deterioration or section loss present in critical structural components or obvious vertical or horizontal movement affecting structure stability. Bridge is closed to traffic but corrective action may put back in light service.
0	<b>FAILED CONDITION</b> - out of service - beyond corrective action.

### 3 THE EFFECT OF DISTANCE FROM SEA COAST

This section examines the influence of sea salt on bridge deterioration. Near the coastline the environmental conditions are normally more aggressive in comparison to inland due to the sea salt existence, which enhances the atmosphere's chloride concentration. The NBI database is used to evaluate the effect of the distance from the sea coastline on bridge durability.

To study this effect, the state of Florida was chosen, so that uniformity could be achieved on repair policies [2]. Florida also has a great coastline length and a large sample of bridges, which increased the probability of locating bridges near the coast. Additionally, the area's low earthquake hazard and the non-deicing policy within the coastline region provided a good analysis sample.

The bridge coordinates, which are included in the NBI database, can be used to locate the bridges. Fig. 1 shows the coastline of east USA and Fig. 2 highlights the bridge locations at a certain part of the state of Florida.

Coastline coordinates were obtained from the National Geophysical Data Centre. Equal coastline distance polylines were drawn at various inland distances forming bridge-area-zones near the coastline (see example of Fig. 3 from other area). The bridges in each area were captured and their conditions were determined and compared to bridges located to other formed areas.

Florida's climate can be categorized mostly as humid subtropical and tropical in regions located south from Lake Okeechobee. The geographical terrain has low rises and the existence of high intensity winds can lead to greater transfer distances of airborne chlorides.

Fig. 4 gives condition probabilities on built-only bridges (i.e. excluding rebuilt bridges) at zones up to 10km from the coastline for substructures, superstructures and decks. The 'appraisal' line refers to minimum rating between substructure and superstructure. The analysis was performed on the entire Florida's coastline, along which 3934 bridges are located (3251 built-only and 683 rebuilt) within 10km from the coastline.

The results of Fig. 4 and others show that the coastline affects bridge durability at distances up to 3km. Bridge condition probabilities remain practically flat at coastline distances  $>3\text{km}$ ; the probability of structurally deficient bridges within 3km from the coastline is significantly higher. In other studies, the coastline-affected zone is reported to be around 1-2 km wide [3-5].



Figure 1. Map of USA with areas under study

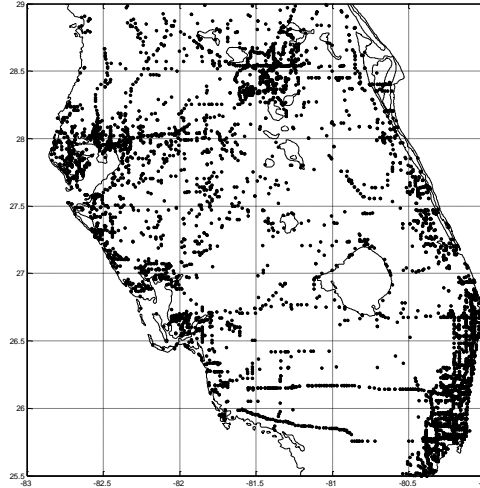


Figure 2. Bridge locations at a certain part of the state of Florida (see also Fig. 1)

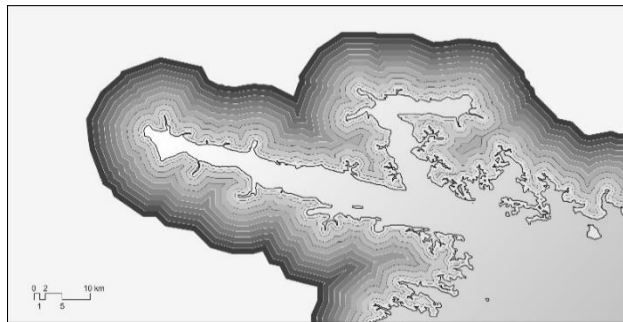


Figure 3. Formed zones near and parallel to North Carolina's coastline (see also Fig. 1)

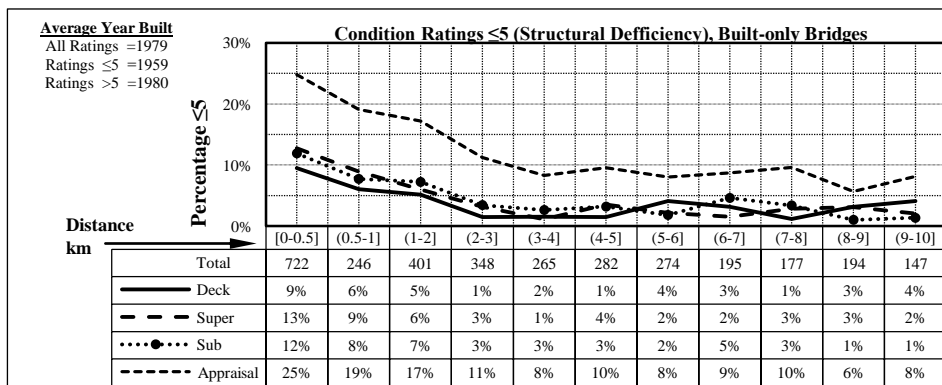


Figure 4. Condition probabilities for bridges in Florida at various distances from the coastline



#### 4 THE EFFECT OF WATER AND DEICING SALTS

To evaluate bridge durability under other environmental conditions, four different environments are examined:

- ‘water’: bridges with water underneath;
- ‘deicing’: bridges exposed to deicing salts;
- ‘deicing & water’: bridges with water underneath and exposed to deicing salts;
- ‘normal’: bridges without water underneath and deicing salts.

Note that bridges located near the sea coastline are excluded from this analysis.

Fig. 5 shows corrosion probabilities (condition  $\leq 5$ ) for bridge substructures. The presence of water increases corrosion probabilities to more than double in comparison to bridges located in ‘normal’ environments. Corrosion probabilities for bridges exposed to deicing salts for the first 20 years are similar to ‘normal’, but for older bridges the corrosion probabilities are increased to values between ‘normal’ and ‘water’ environments. This is attributed to the time needed for chlorides to diffuse through the concrete cover and initiate corrosion.

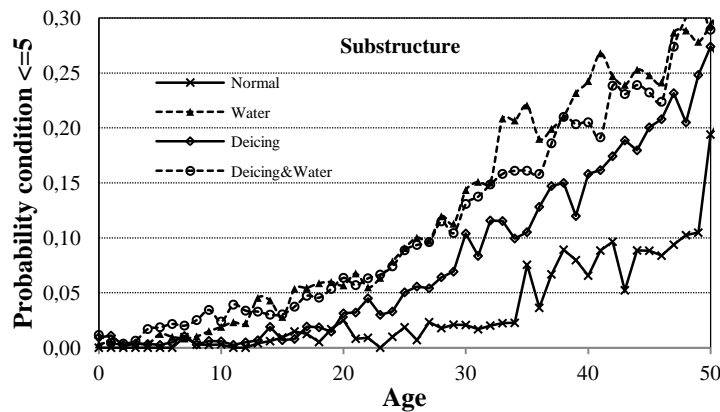


Figure 5. Condition probabilities with age for bridge substructures

The evolution of corrosion probabilities with age for bridge decks (Fig. 6) shows that deicing salts fuel corrosion, while water presence does not seem to affect corrosion. This is an expected outcome, because water runs underneath the bridge, hence it is not in direct contact with the bridge deck. However, water increases the environmental humidity. This enhances chloride convection and reduces the time-to-corrosion-initiation. This effect is evident in Fig. 6 in the rise of the ‘deicing & water’ condition probability curve at young ages in comparison to the ‘deicing’ curve.

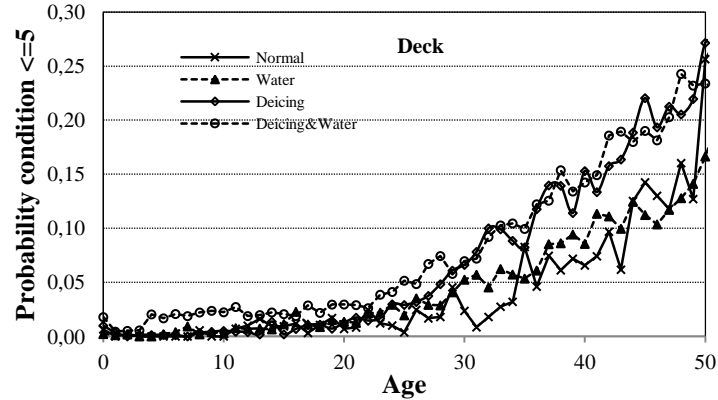


Figure 6. Condition probabilities with age for bridge decks

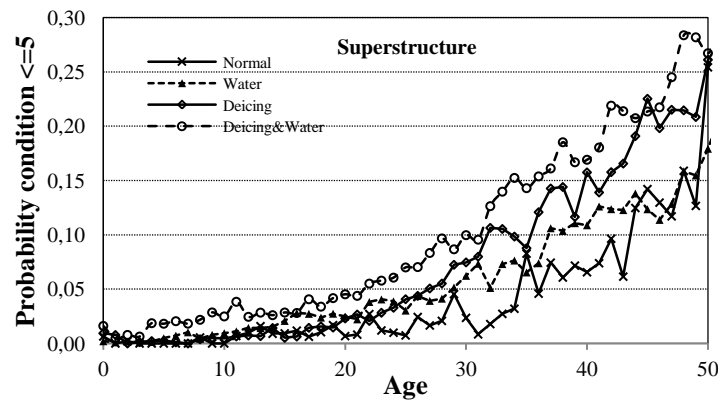


Figure 7. Condition probabilities with age for bridge superstructures

The above is more pronounced in superstructures shown in Fig. 7. It can be observed that, up to the bridge age of 20 years, the environments that contain water possess higher threats for corrosion. At later age, corrosion initiates and the curve of bridges exposed to chlorides without water rises to give similar corrosion probabilities to those with water present.

## 5 THE EFFECT OF STRUCTURAL MATERIAL

The corrosion resistance of bridges made of steel and reinforced/prestressed concrete and exposed to various environments are examined in this section. The results in Figs. 8, 9 and 10 show that steel structures are prone to corrosion at humid environments. At the same time, they give similar corrosion probabilities as reinforced/prestressed concrete bridges at low humidity conditions. Fig. 8 shows such conditions when deicing salts are used. All lines follow a similar

corrosion probability path with age. Similar results are found at low humidity environments and warm environments, hence without deicing salt used.

An early jump is observed on steel structure's corrosion propagation curve at humid locations exposed to chlorides (Fig. 10). This is not seen at similar environments not exposed to chlorides (Fig. 9). Chloride exposure causes rapid corrosion initiation at early ages and, in humid locations exposed to chlorides, building a steel bridge should be considered with caution.

Reinforced and prestressed concrete bridges appear to be similarly influenced irrespective of the environmental conditions. In humid environments, such bridges exhibit lower deterioration rates than steel bridges.

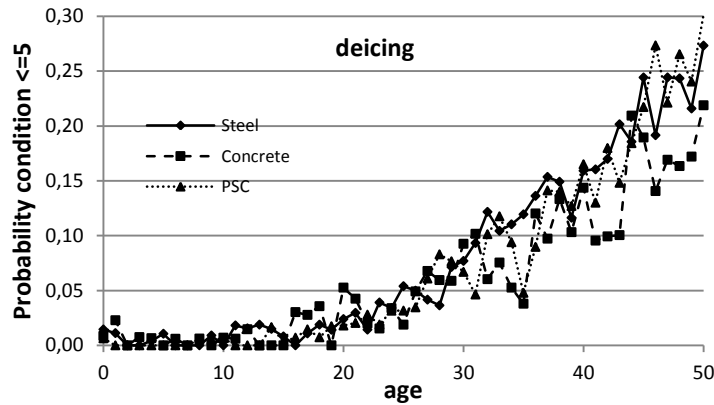


Figure 8. Condition probabilities for steel, reinforced and prestressed concrete bridges exposed to deicing salts at low humidity environments

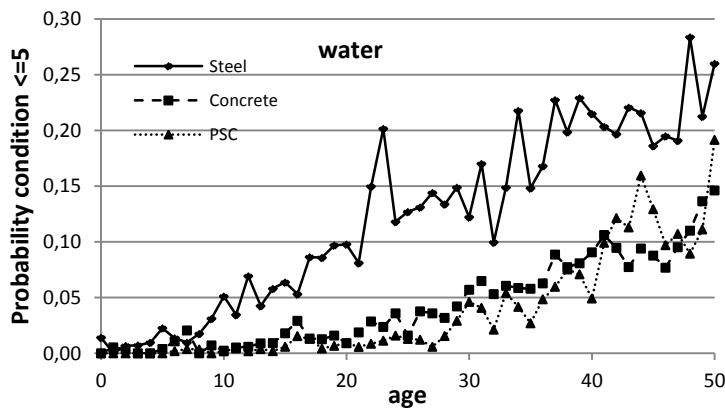


Figure 9. Condition probabilities for steel, reinforced and prestressed concrete bridges located at humid environments

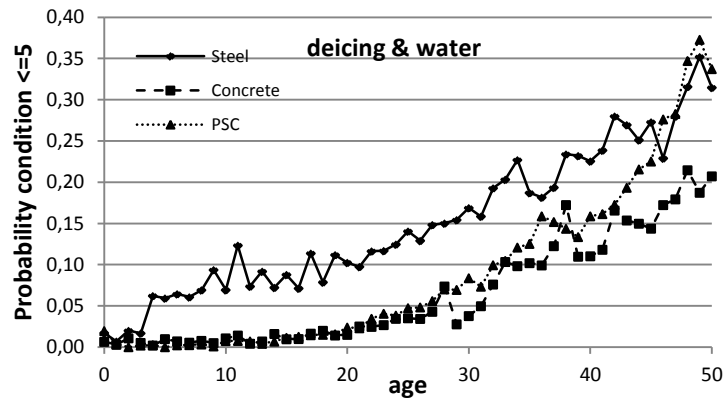


Figure 10. Condition probabilities for steel, reinforced and prestressed concrete bridges located at humid environments exposed to chlorides

## 6 CONCLUSIONS

Data from bridge inspections are used to study the durability of bridges under various environmental conditions and materials. The results show that durability is threatened for:

- bridges located within the first 3km from the sea coastline;
- substructures at humid locations, because they are often in direct contact with water;
- decks and superstructures exposed to deicing salts;
- steel structures at humid locations, especially when exposed to chlorides.

Finally, reinforced and prestressed bridges gave similar corrosion probabilities at all environmental exposures.

## REFERENCES

- [1] Federal Highway Administration (FHWA), *Recording and coding guide for the structure inventory and appraisal of the nation's bridges*, Report No. FHWA-PD-96-001, U.S. Department of Transportation, Washington D.C., 1995.
- [2] Dunker, KF, Rabbat, BG, "Assessing infrastructure deficiencies: the case of highway bridges", *ASCE Journal of Infrastructure Systems*, Vol 1, No. 2, pp. 100-119, 1995.
- [3] Meira, GR, Padaratz, IJ, Alonso, C, Andrade, C, "Effect of distance from sea on chloride aggressiveness in concrete structures in brazilian coastal site", *Materiales de Construccion*, Vol. 53, No. 271-272, pp. 179-188, 2003.
- [4] Meira, GR, Andrade, C, Padaratz, IJ, Alonso, C, Borba Jr, JC, "Chloride penetration into concrete structures in the marine atmosphere zone – Relationship between deposition of chlorides on the wet candle and chloride accumulated into concrete", *Cement & Concrete Composites*, Vol. 29, pp. 667-676, 2007.
- [5] Pontes, RB, Monteiro, ECB, de Oliveira, RA, de Paiva, SC, "Chloride ion propagation in onshore zone of Recife-PE", *Concrete repair, Rehabilitation and Retrofitting II*, Alexander et al. (eds), Taylor & Francis Group, London, pp. 449-454, 2009.

# EVALUATION OF THE REMAINING STRENGTH OF RION-ANTIRION CABLE-STAYED BRIDGE USING THE MULTISCALING FRACTURE MECHANICS APPROACH

Dimitrios Zacharopoulos, Thomas Panagiotopoulos

Democritus University of Thace, Dept. of Civil Engineering, Greece  
e-mail: dzachar@civil.duth.gr, thomas.a.panagiotopoulos@gmail.com

**ABSTRACT:** Innately fatigue failure is a typical problem between two different scales because fatigue crack growth increases from microscale to macroscale. Classical continuum mechanics is inadequate to deal with such a problem, since it disqualifies the effect of the scale, making the assumption that the material is continuous and homogeneous, something that is not applicable in microscale due to the discontinuity and inhomogeneity of materials. In this paper an effort is made to fill the gap between microscale and macroscale in the process of continuous fatigue of suspension and cable-stayed bridges cables. This problem is solved according to the application of the mesoscopic fracture mechanics theories. To illustrate the proposed approach the Charilaos Trikoupi Bridge (Rion-Antirion Bridge) has been chosen to perform the numerical computations. From the numerical computations it can be concluded that the size of the initial crack is the primary factor for the life expectancy of steel wires. Consequently the life expectancy of the suspension and cable-stayed bridges cables depends on the size of the initial crack too.

**KEY WORDS:** Cable stayed bridge; Mesoscopic fracture mechanics; Micro / Macro dual scale crack; Multiscale; Fatigue life; Damage evolution.

## 1 INTRODUCTION

The reduction of the life expectancy of steel wires depends on many factors as cracking due to mechanical stress, corrosion, hydrogen embrittlement, fatigue. These factors endanger strength and wire ductility. Therefore the accurate estimate of life expectancy due to steel wire fatigue is necessary for the safety of the bridge [1]. The life expectancy of steel wires is estimated from statistic research using fatigue results [2].

Nevertheless, the fatigue problem has not a complete solution and is still in the process of research despite that it is an old problem. In conclusion, the fatigue process is divided into two stages, the first stage is fatigue crack initiation

and the second stage is the fatigue crack propagation. The aforementioned derive from different theories and are dealt individually [3],[4].

In recent years a theory called multiscale crack models theory [5], has been formulated. To describe a crack from microscale to macroscale, a dual scale crack has been proposed, using the factor of stress intensity or strain energy density. In this paper a multiscale crack model is used that takes into account the different scales. The results of this research will be able develop control processes for the betterment of the Rion - Antirion Bridge safety.

## 2 GENERAL

### 2.1 Physical model

The multiscale crack model is based on the assumption of the appearance of restraining zone stress, as shown in *Fig.1*. In *Fig.1(a)* a plate under uniaxial tension without damage is shown. It is supposed that exists one crack in the center of the plate as shown in *Fig.1(b)* and the stresses will appear in the edge of the crack that are indicated as  $\sigma_0$ . If the ratio of restraining stress to applied stress,  $\sigma_0/\sigma_\infty=1$ , then  $\sigma_0 = \sigma_\infty$  the cases a and b are the equivalents. If  $\sigma_0=0$ , then the cases b and c (*Fig.1(c)*) are identical.

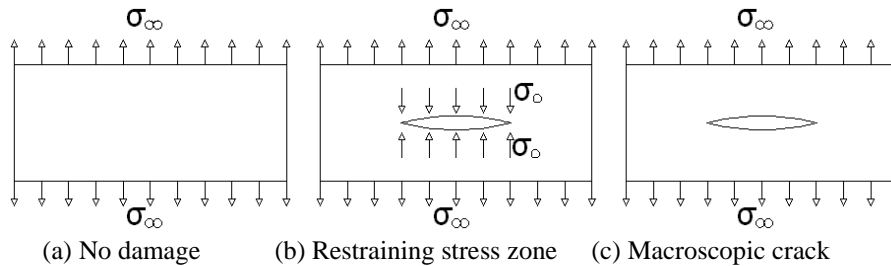


Figure 1. Crack micro to macro scale

According to the multiscale crack model, the restraining zone stress can define the fatigue process with a continuous way. This way the fatigue process is analyzed in an integrated theory and the separation of the fatigue process into two stages is not needed [6]. The macro/micro dual scale energy density factor range  $\Delta_{micro}^{macro}$  in a fatigue process for the dual scale edge crack model can be written as:

$$\Delta_{micro}^{macro} = \frac{2(1-2\nu_{micro})(1-2\nu_{macro})^2 \sigma_a \sigma_m \mu^* (1-\sigma^*) \sqrt{d^*} \sqrt{\frac{d_0}{r}}}{\mu_{macro}} \quad (1)$$

where :

$$\mu^* = \frac{\mu_{micro}}{\mu_{macro}}, \quad \sigma^* = \frac{\sigma_0}{\sigma_\infty}, \quad d^* = \frac{d}{d_0} \quad (2)$$

$$\sigma_a = \frac{\sigma_{\max} - \sigma_{\min}}{2}, \quad \sigma_a = \frac{\sigma_{\max} + \sigma_{\min}}{2} \quad (3)$$

The  $\nu_{micro}$  and  $\nu_{macro}$  are the microscopic and macroscopic Poisson's ratio respectively,  $\sigma_{\max}$  and  $\sigma_{\min}$  are the maximum and minimum stress respectively,  $\mu_{micro}$  and  $\mu_{macro}$  are the microscopic and macroscopic shear module respectively and  $\sigma_0$  and  $\sigma_\infty$  are the restraining stress and applied stress respectively. Also,  $d_0$  is the crystalline grain size and  $r$  is related to the crack segment length at each time.

## 2.2 Fatigue crack growth

The crack growth ratio  $da/dN$  from microscale to macroscale in cables  $\Delta S_{micro}^{macro}$  depends on the dual scale energy density factor. According to the dual scale crack model the crack growth ratio can be expressed as:

$$\frac{da}{dN} = C_0 (\Delta S_{micro}^{macro})^n \quad (4)$$

where :  $C_0$  and  $n$  are material fatigue parameters

For the high strength steel wire Eq.(4) is simplified to

$$\frac{da}{dN} = C_0 (\Delta S_{micro}^{macro}) \quad (5)$$

Inserting Eq(5) into Eq(1) yields:

$$\frac{da}{dN} = C_0 \frac{2(1-2\nu_{micro})(1-2\nu_{macro})^2 a \sigma_a \sigma_m \mu^* (1-\sigma^*) \sqrt{d^*} \sqrt{\frac{d_0}{r}}}{\mu_{macro}} \quad (6)$$

By defining a parameter C as

$$C = C_0 \frac{2(1-2\nu_{micro})(1-2\nu_{macro})^2}{\mu_{macro}} \quad (7)$$

Eq.(6) then becomes

$$\frac{da}{dN} = Ca \sigma_a \sigma_m \mu^* (1-\sigma^*) \sqrt{d^*} \sqrt{\frac{d_0}{r}} \quad (8)$$

By the numerical integral operation from Eq.(8)

$$\Delta \alpha_i = Ca_{i-1} \sigma_a \sigma_m \mu_{(a_{i-1})}^* (1-\sigma_{(a_{i-1})}^*)^2 \sqrt{d_{(a_{i-1})}^*} \sqrt{\frac{d_0}{r}} \Delta N \quad (9)$$

$$\text{and } \alpha_i = a_{i-1} + \Delta \alpha_i \quad (10)$$

### 3 THE RION – ANTIRION BRIDGE

#### 3.1 Geometrical and technical data



Photo 1. Rion - Antirion bridge

The Charilaos Trikoupis Bridge (Rion - Antirion Bridge), is the world's longest multi-span cable-stayed bridge that is 2252 m long. It crosses the Gulf of Corinth near Patras, linking the town of Rio on the Peloponnese to Antirion on mainland Greece by road. The bridge deck is suspended with 368 cables from 4 pylons. According to the aforementioned there are 46 pairs of cables which are fixed to every pylon bilaterally [7]. The 4 pylons divide the bridge into 5 spans with the following: 286m-560m-560m-560m-286m the geometry of which is shown in Fig.2 [8].

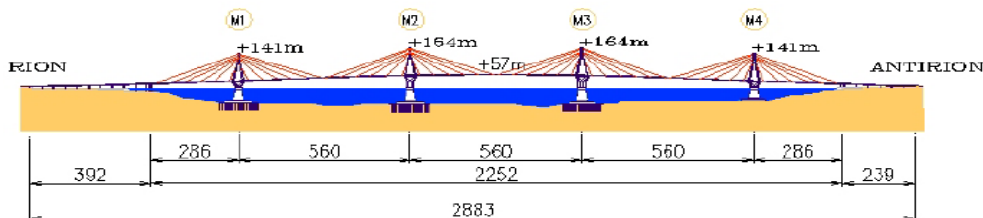


Figure 2. Rion - Antirion length

Every cable constitutes of 43 – 73 clones wrapped in PVC. The classification of the number of clones in every cable is done so that the mean stress is equal in every cable. Every clone has diameter 15.7 mm and consists of 7 parallel wires. The effective area of every clone is 150 mm<sup>2</sup> and the ultimate tension stress strength of the wires is 1770 MPa [9].

#### 3.2 Loads

The loads for which the bridge is calculated are:

- Dead Loads
- Live Loads (according to EC-1)



### 3.3 Modeling of bridge

The modeling of the bridge is accomplished with the use of software that specializes in linear elastic analysis with the finite element method. The model was designed on the basis of the geometry, the mechanical parameters of the materials and the static function of each element and is constituted of:

- **Beam elements:** Linear elements with 6 degrees of freedom (d.o.f) per joint.
- **Pylon elements:** Linear elements with 6 d.o.f per joint.
- **Cable elements:** Linear elements with compression release.
- **Brace elements:** Linear elements with 3 d.o.f per joint.
- **Plate elements:** Shell finite elements with 5 d.o.f per joint

## 4 RESULTS

### 4.1 Stress analysis in steel wires

- Cable force due to dead loads:  $N_g=6732\text{kN}$
- Cable force due to live loads:  $N_q=1641\text{kN}$

However, the stress distribution in the cable section is not uniform in fact. This indicates that the stress value of each wire in the same cable must be different. In addition, the cable forces would vary with time due to the tightening and loosening effects caused by many reasons. According to the aforementioned two parameters A and B are inserted in Eq.(3) which yields:

$$\text{Case I: } \sigma_a = \frac{A\sigma_{\max} - \sigma_{\min}}{2}, \sigma_m = \frac{A\sigma_{\max} + \sigma_{\min}}{2} \quad (11)$$

$$\text{Case II: } \sigma_a = \frac{\sigma_{\max} - B\sigma_{\min}}{2}, \sigma_m = \frac{\sigma_{\max} + B\sigma_{\min}}{2} \quad (12)$$

The factors A and B take into consideration the tightening and loosening factors of only the live loads or only the dead loads accordingly.

### 4.2 Determination of microscopic and macroscopic material parameters

Table 1. Mechanical parameters of steel wire

Elastic modulus	Shear modulus	Poisson's ratio	Ult. strength	Ultimate strain
$E_{\text{macro}}$ (GPa)	$\mu_{\text{macro}}$ (GPa)	$\nu_{\text{macro}}$	$\sigma_{\text{ult}}$ (MPa)	$\epsilon_{\text{uk}}$
210	80.8	0.3	1770	$\geq 20\%$

The material parameters depend of the scale. The macroscopic parameters are

presented to the *Table 1*. For the microscopic parameters assume that:

$$v_{micro} = 0.4, d_0 / r = 1.0, d_0 = 10^{-3} mm$$

Also, for the material fatigue parameter  $C_0$  we assume that:

$$C_0 = 3.5 \times 10^{-4} \frac{mm^2}{N}$$

### 4.3 Modes of crack growth

With the fatigue crack growth, the crack depth gradually increases from microscale to macroscale. The three basic ratios  $d^*$ ,  $\mu^*$  and  $\sigma^*$  are inserted into determination of crack growth when the crack is  $\alpha < 1$  mm. Intended three different Modes (Mode A – Mode B – Mode C), depended on the ratios  $d^*$ ,  $\mu^*$  and  $\sigma^*$ . The variation of  $d^*$ ,  $\mu^*$  and  $\sigma^*$  according to three modes is shown in *Fig.3, 4* and *5*.

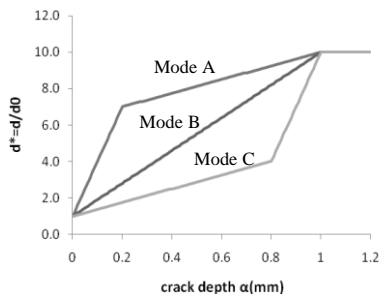


Figure 3. Change of length  $d^*$  ratio with crack depth

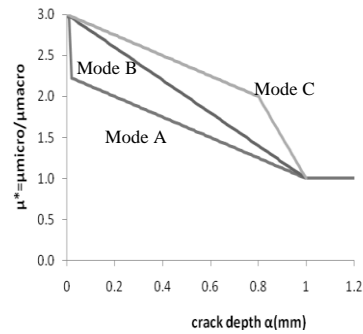


Figure 4. Change of modulus  $\mu^*$

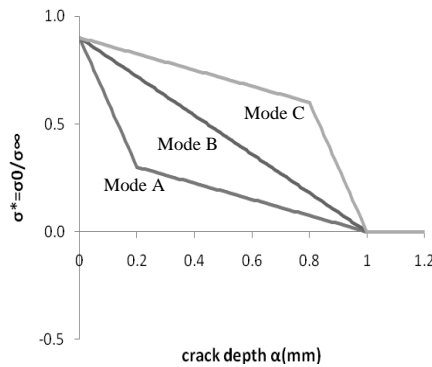


Figure 5. Change of stress  $\sigma^*$  ratio with crack depth

### 4.4 Influence of initial crack size

This section focuses on the effect of the initial crack size to the crack depth according to the cyclic number  $N$ .

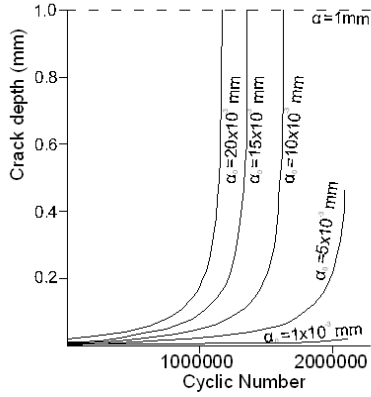


Figure 6. Case I (A=1.0) & Case II (B=1.0)

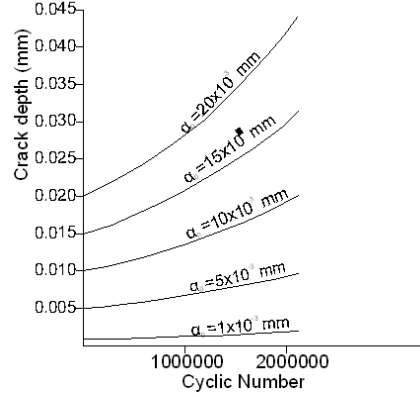


Figure 7. Case I (A=0.85)

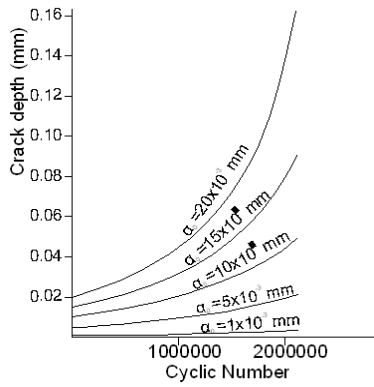


Figure 8. Case I (A=0.9)

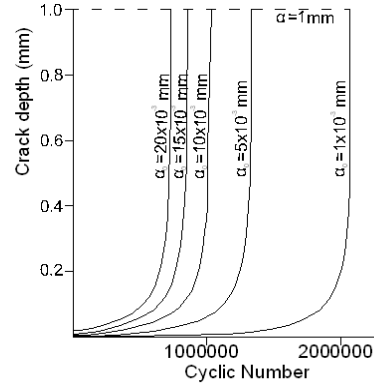


Figure 9. Case I (A=1.1)

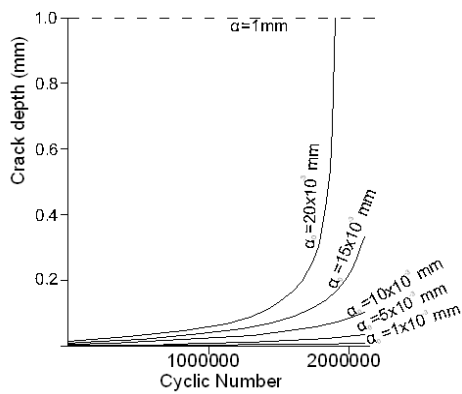


Figure 10. Case II (B=1.1)

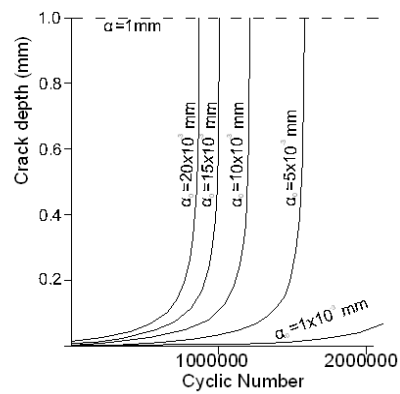


Figure 11. Case II (B=0.9)

## 5 CONCLUSIONS

The problem of fatigue is of vital importance for the life expectancy of a bridge, especially for a cable-stayed bridge. According to the mesoscopic fracture mechanics, in paper for this particular bridge the following results have emerged:

- The extent of the initial crack is of immense importance for the life expectancy of the bridge.
- In normal stress ( $A=1$ ) for Case I the examined cable fails in less than two million circles of load if the first crack exceeds  $\alpha_0 \geq 10 \times 10^{-3}$  mm. In Case I if the value of coefficient is  $A > 1.1$  the wire fails in less than two million circles if the first crack exceeds  $\alpha_0 \geq 5 \times 10^{-3}$  mm. This means that the tightening factor has negative effect, conversely the loosening factor  $A < 1.0$  has positive effect as even for  $A=0.85$  and initial crack  $\alpha_0 = 20 \times 10^{-3}$  mm the wires exceed two million circles.
- In Case II for the value of coefficient  $B=0.9$  the wire fails in less than two million circles for initial crack  $\alpha_0 \geq 5 \times 10^{-3}$  mm, whereas for  $B=1.1$  the wire fails in less than two million circles for initial crack  $\alpha_0 \geq 15 \times 10^{-3}$  mm. This means that the loosening factor has negative effect in Case II and that the tightening factor has positive effect.

According to this research the control of the cable wires initial cracks is considered as a critical factor in order to predict the number of circles, as an approach for the estimation of the life expectancy of a wire as well as its replacement.

## REFERENCES

- [1] Li, C, Tang, X, Xiang, G, “*Fatigue crack growth of cable steel wires in a suspension bridge : Multiscale and mesoscopic fracture mechanics*”, Theoretical and Applied Fracture Mechanics, Vol. 53, pp. 113-126, 2010.
- [2] Wang, S, Dang, Z, “*Research on Heavy – Load High Fatigue Stress Amplitude Cable and Anchorage of Cable - Stayed Bridge*”, Bridge Construction in Chinese, pp. 14-16, 2002.
- [3] Miner, M, “*Cumulative Damage in Fatigue*”, Journal of Applied Mechanics Vol.12, pp. A159-A164, 1945.
- [4] Paris, P, “*The Growth of Cracks Due to Variations in Load*”, Ph.D. Dissertation, Department of Mechanics, Lehigh University, 1962.
- [5] Sih, X, Tang, X, “*Simultaneous Occurrence of Double Micro / Macro Stress Singularities for Multiscale Crack Model*”, Theoretical and Applied Fracture Mechanics, Vol. 46, pp. 87-104, 2006.
- [6] Sih, X, Tang, X, “*Form – Invariant Representation of Fatigue Crack Growth Rate Enabling Linearization of Multiscale Data*”, Theoretical and Applied Fracture Mechanics, Vol. 47, pp. 1-14, 2007.
- [7] Combault, J, Morand, P, Pecuer, A, “*Structural Response of the Rion – Antirion Bridge*”, 12WCEE 2000, pp. 1-8, 2004
- [8] Marchetti, M, Boudon, R, Monnerie, J, Bouve, P, Dupuis, D, Dadoun, F, Baechler, G, Olsfors, J, “*Adjustment of the Rion – Antirion Cable – Stayed Bridge: An Innovative Multidisciplinary Response to a Construction Challenge*”, International Symposium of Engineering Surveys for Construction Works and Structural Engineering, Vol. 1, Nottingham, 2004.
- [9] Papanikolas, P, Liolios, A, “*The Stay – Cable System of Rion – Antirion Bridge*”, National Conference of Steel Structures, Vol. 5, pp. 196 – 206, Xanthi, 2005

## **IDENTIFICATION OF SOIL-STRUCTURE INTERACTION EFFECTS BASED ON GEODETIC MONITORING OF A RAILWAY BRIDGE**

Panos Psimoulis<sup>1</sup>, Stathis Stiros<sup>2</sup> and Fanis Moschas<sup>2</sup>

<sup>1</sup> Nottingham Geospatial Institute, Dept. of Civil Engineering, University of Nottingham, UK

<sup>2</sup> Geodesy and Geodetic Application Lab., Dept. of Civil Engineering, University of Patras,  
Greece

e-mail: panagiotis.psimoulis@nottingham.ac.uk, stiros@upatras.gr, fmoschas@upatras.gr

**ABSTRACT:** The monitoring of bridges using geodetic methodologies permits the direct measurement of displacements and potential identification of effects of soil-structure interaction. In this study the response of the historical Gorgopotamos railway (Central Greece) has been measured using a Robotic Total Station (RTS) during the passage of trains on different times of the year and under various soil conditions. The measurements revealed that the initial impact response of the deck to the train loading presents differences which seem to correlate with the differences in the moisture content of the bridge foundation ground.

**KEY WORDS:** RTS, Geodetic Monitoring, Railway Bridge, Deflection

### **1 INTRODUCTION**

The response of structures to dynamic loads is to a certain degree influenced by the interaction between structure, soil and foundations in general. Although the soil-structure interaction is always present to some degree, it is generally assumed that the motion at the structure does not influence the motion of the foundation [1]. However, when the soil-structure interaction becomes significant, this assumption is not true due to the feedback from the structure to the foundation and the surrounding soil medium [2]. Thus, the soil-structure interaction influences the motion of the structure due to the soil motion, which is expressed through the displacement of the structure and its modal frequencies [3].

Furthermore, there is a large interest in monitoring of structures response based on the modern geodetic techniques, GPS and Robotic Total Station (RTS). Many studies have been made, which proved that GPS and RTS can be sensitive and accurate enough for the monitoring of rigid structures with modal frequencies larger than 2-3Hz [4,5].

In this paper, we present an extraordinary case of historical railway bridge in

which we measured the response of the bridge when trains were passing in different environmental conditions using a RTS. The RTS technique was selected due to its high accuracy (of 1mm level) for modal frequencies up to 5-6Hz. The aim of the study is to detect the influence of the soil-structure interaction on the response of the bridge and how this is expressed on the bridge displacement, through the RTS recordings.

Finally, from this study was revealed that when the soil of the bridge foundation, corresponding to marls, was saturated, the passage of heavy trains was causing an atypical displacement of larger amplitude than the one caused under usual conditions of unsaturated soil. In this study a preliminary analysis of the RTS displacement time series and their correlation with the soil condition are presented.

## **2 THE GORGOPOTAMOS RAILWAY BRIDGE**

The Gorgopotamos Railway Bridge is located about 150km northwest of Athens, in central Greece, and was constructed in 1905. The bridge was destroyed and rebuilt twice during Second World War (Fig.1). The first destruction was in 1942 and after its reconstruction in 1943, it was destroyed again in 1944. The bridge was reconstructed again in 1948 and since then is still in use.

The bridge has total length of 211m and 32m maximum height. It is curved in plan, consisting of seven sub-linear spans of approximate length of ~30m, which are supported by six pylons. The bridge is a composite structure with a truss deck, two steel pylons ( $M_1$ ,  $M_2$ ) and four masonry pylons ( $M_3$ - $M_6$ ); see Figure 1.

The foundations of the bridge are on marls causing a long-term (static) instability, and for this reason drainage works had been made in the near past. The instability of the bridge seemed to affect the passage of the train, which are usually forced to reduce speed.

## **3 RTS – PRINCIPLES AND METHODOLOGY**

RTS is the evolution of the common total station. The instrument emits a ray which is reflected on a reflector fixed on the specific point is received back and analysed, and the instantaneous 3-D polar coordinates of the reflector are computed in a pre-defined coordinate system. RTS is also equipped with a servo-mechanism and an automatic target recognition device, permitting to lock on a specific target, follow its movement and record its coordinates with a rate higher than 5-6 Hz.

Basic requirements for accurate measurements are the visibility of the reflector, the absence of perturbations of the atmosphere along the raypath and the use of a high-quality prismatic reflector. Further details about the instrument and the RTS monitoring are described in [6].

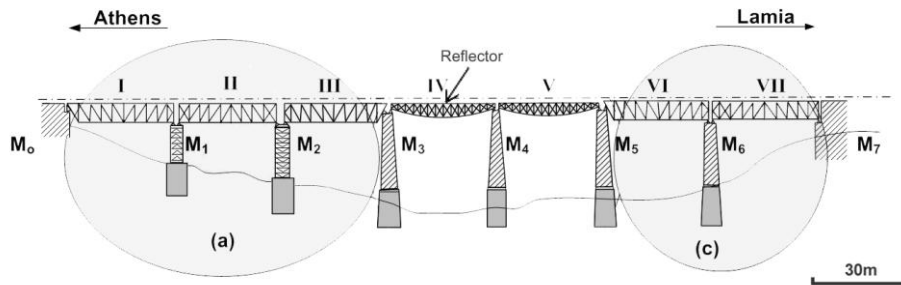


Figure 1. The Gorgopotamos Railway Bridge with area a and c indicating the destroyed parts of the Bridge in 1942 and 1944, respectively. Also the reflector position discussed in this article is indicated.

#### 4 METHODOLOGY

The aim of this study was to estimate the deflection of the bridge caused by passing trains, of similar type and size, and try to detect potential influence of the soil condition to the bridge response. For this reason we focused on excitation on the excitation of the bridge of similar passing trains for two different times in the same year.

We focused on the midspan of an opening, where the maximum displacement of the bridge was expected and corresponding to the most saturated soil of the bridge foundation. The measurements were made before, during and after the passing trains. The measurement noise (uncertainty) was estimated based on the measurements of the intervals before and after the train passage, corresponding to intervals of no bridge excitation. Measurements during passing trains, corresponding to the train excitation intervals, were compared with the measurement noise, and if the signal of the excitation interval was larger than the noise, measurements corresponded to real displacements.

Finally, based on a simple low-frequency filter (e.g. moving average) we separated the semi-static (low-frequency) from the dynamic (high-frequency) displacement of the structure and we estimated the corresponding amplitude.

#### 5 FIELD MEASUREMENTS

Our study was focused on measurements of the displacements of point at the midspan between pylons  $M_3$ - $M_4$ , through which the Gorgopotamos river is passing, causing the saturation of the foundation soil. This point was marked by a high-accuracy prismatic AGA-type reflector, fixed on the metallic bridge handrail. A Leica TCA 1201 RTS was set on stable ground at a distance of circa

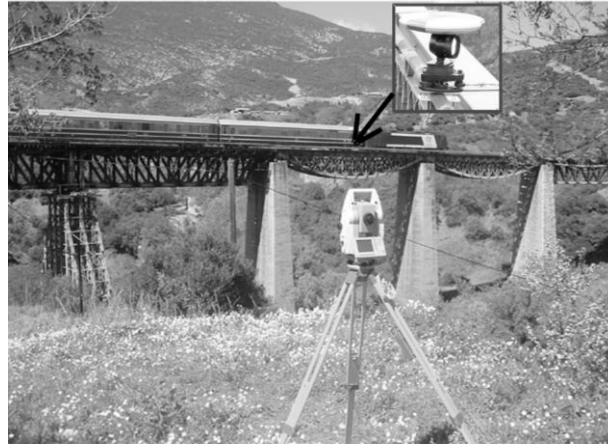


*Figure 2.* The Gorgopotamos Railway Bridge and in the foreground the RTS used for the measurements focusing on reflector. An inset shows the prismatic reflector and on top of it the antenna of a GPS, used as a chronograph.

150m from the reflectors, at a point permitting unobstructed view of the reflectors (Fig.2). Details on the use and the limitations of this instrument, and the solutions adopted to obtain high-accuracy data, useful for structural analysis are described in [6] and [7].

Measurements during the passage of several trains were made. In this study we focus on the recordings of two passing train cases: i) a 8-wagon freight train on 12.04.06 (case 1) and ii) a 7-wagon freight train on 12.07.06 (case 2). Thus, we compared the response of the bridge in the passage of two similar trains, in April and July, where the soil conditions were different; in April the marls are saturated, while in July they are practically dry.

## 6 DATA ANALYSIS

Using a common linear transformation [6,7,8] the recorded coordinates relative to a rather arbitrary system were transformed into coordinate system consistent with the one of the bridge, where the y-axis is tangent to the railway at the observation point and x-axis normal to it. Then the mean value of the recordings from the intervals before and after the passing train was subtracted from each instantaneous coordinate. Thus three time series describing the apparent displacements along the longitudinal, lateral and vertical were obtained.

The time interval of the passing train was defined by combining the records of the chronographer, the GPS records and the RTS records. It was identified the time the train entered and left the bridge (solid lines 1 and 4, Fig.3) and the time interval the train was passing in front of the target (dotted lines 2 and 3, Fig.3).



The measurement noise was estimated based on the data from the intervals before and after the passing train corresponding to no excitation interval. The data formed zones of amplitude  $\pm 1\text{mm}$  expressing the noise level of measurements. This amplitude was smaller than that defined from experiments,  $\pm 2\text{mm}$  [7], which, was however adopted as a pessimistic estimate.

In general, the time series of the longitudinal and lateral axes appear lower signal than the noise level, and hence expressed only measurement noise, while the signal of the vertical axis reached the amplitude of  $6\text{mm}$  and hence they reflected real displacement of the bridge due to the train excitation.

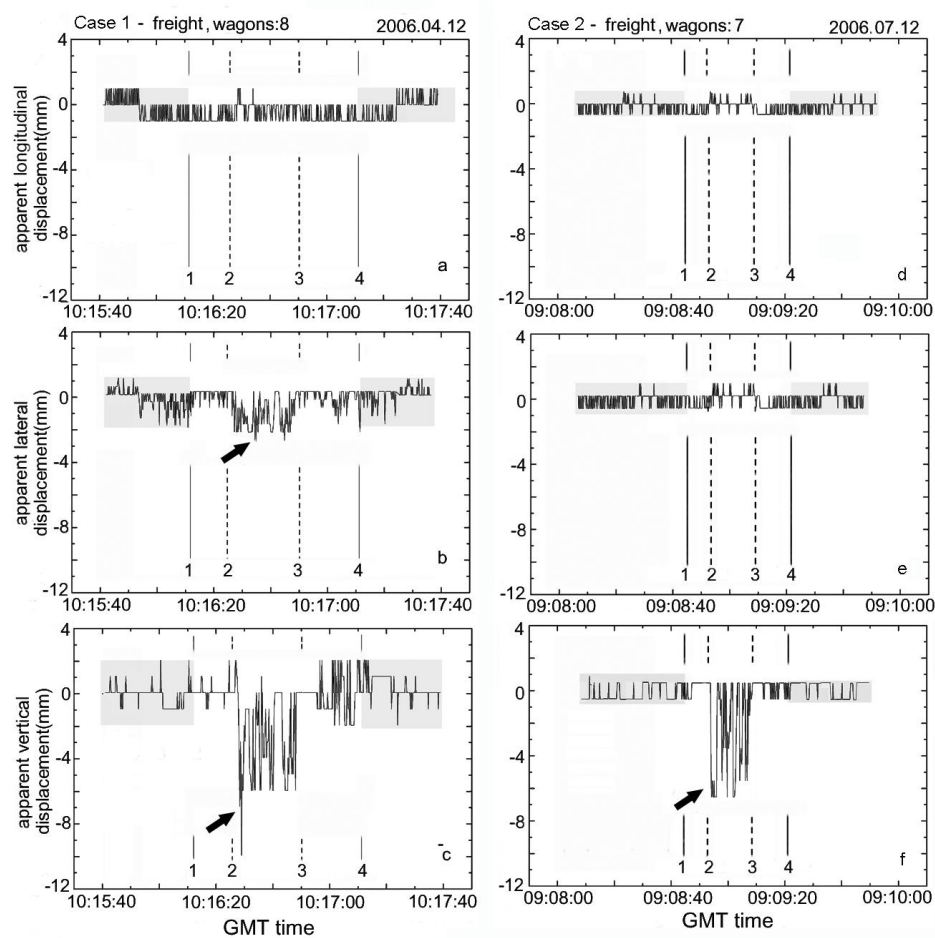


Figure 3. The RTS displacement time series of the three components (longitudinal, lateral, vertical) for the two examined cases. The signal of the lateral (a,d) and longitudinal (b,e) components are close to the noise level, while the vertical component (c,f) is above the noise level expressing displacement. The train lines 1 and 4 indicate the entrance and exit of the train from the bridge and 2 and 3 the passage in front of the target.

Finally, the moving average filter was used for the separation of the semi-static and the dynamic displacement of the two vertical displacement time series. For these time series we used moving average filter of step 21 and overlap 20 [10] and the derived low-frequency (semi-static) time series was subtracted by the initial one, resulting finally to the high-frequency time series (dynamic; Fig. 4).

## 7 ANALYSIS OF DEFLECTIONS

From the derived semi-static and dynamic displacement time series of the vertical components of the two examined cases (Fig. 4), it was estimated the mean semi-static and dynamic displacement. The semi-static displacement has similar trapezoid pattern for both cases of amplitude  $\pm 3.5$  and 4mm, while the dynamic displacement express an oscillation of amplitude  $\pm 3$ -4mm. The latter agrees with the typical deformation of railway bridge during the train passage [10]. However, for the case 1 (April) is observed an additional pulse response in the beginning of the excitation, when the first wagon is entering the surveyed opening, reaching the amplitude of 10mm, double the amplitude of the dynamic displacement. This pulse response is not observed in the case 2 (July). Furthermore, increased lateral displacement in the case 1 is also observed. Thus, it is evident of atypical response of the bridge in the case 1 (April) and indicates that the response of the bridge is less rigid and typical in April than July. The latter can be attributed mainly to the differentiation of the structure response due to the saturation of the marls during April.

## 8 CONCLUSIONS

The output of this study is that the RTS monitoring was not only efficient for the monitoring of the historical Gorgopotamos railway bridge, but even for the identification of the soil-structure interaction. Based on RTS records and simple analysis techniques was possible the identification of the different behavior of the bridge for the two time periods in the year.

It was shown that for the similar excitation (size and train type), the bridge appeared an atypical response (initial extreme pulse response) and lower rigidity (larger lateral displacement) during April (case 1), relatively to July (case 2). The main difference between the two examined periods is the soil condition, as during April the marls are expected to be saturated, which seems to weaken the bridge response.

Thus, the current study shows that the geodetic techniques are reliable and accurate not only for the monitoring of the bridge response but even for the identification of potential effect of soil-structure interaction.

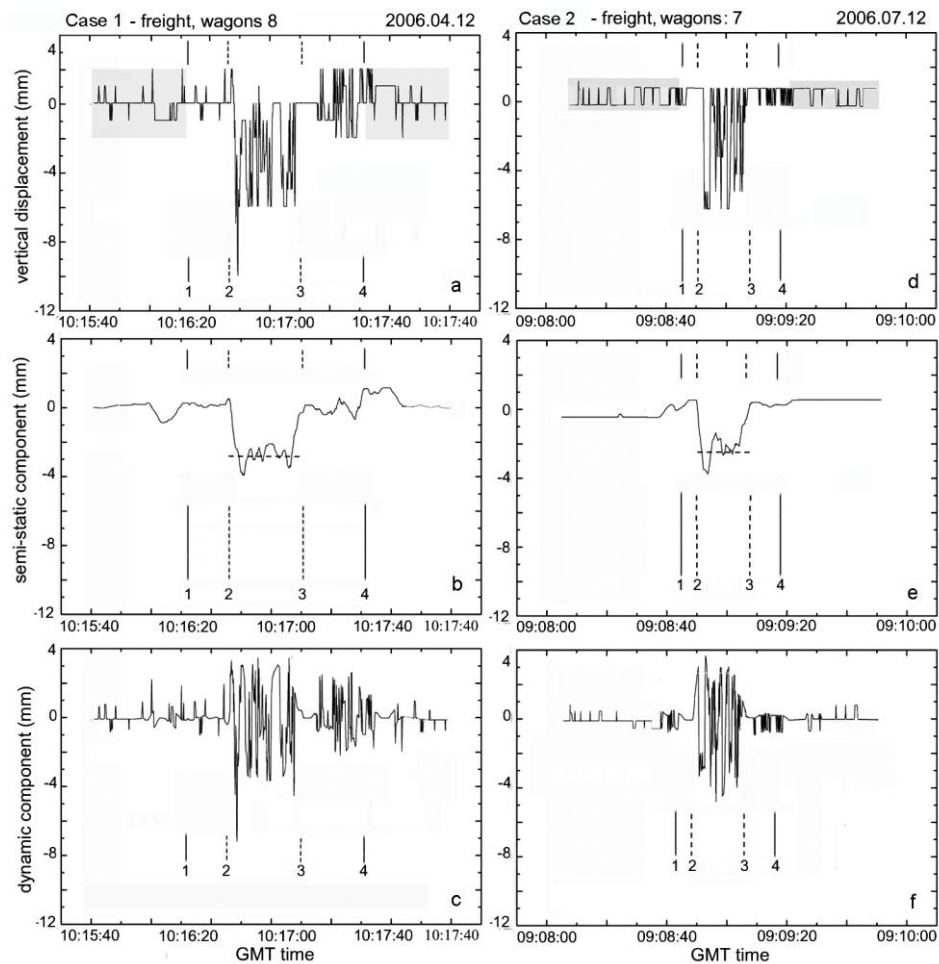


*Figure 4.* The decomposition of the apparent vertical displacement (a,d) into low-frequency (b,e) and high-frequency (c,f) components, expressing the semi-static and dynamic displacement of the two cases, respectively. The dynamic displacement of case 1 appears a pulse response in the beginning of the oscillation, which makes the response atypical.

## ACKNOWLEDGMENTS

We are indebted to OSE SA, the Greek Railroad Company and especially to Mrs D. Spyropoulou, Mr. K. Tzanakakis and Mr. S. Kariotis for granting permission to study the Gorgopotamos Railway Bridge and for field support. Elina Kokkinou made a preliminary analysis of the geodetic data and with Spyros Rezos, they participated in the field survey.

**REFERENCES**

- [1] Safak, E., "On identification of soil-structure interaction from recorded motions of buildings", *Earthquake Engineering*, 1885-1890, 1992
- [2] Safak, E., "Detection and identification of soil-structure interaction in building from vibration recordings", *Journal of Structural Engineering*, Vol. 121, No. 5, 899-906, 2001
- [3] Mylonakis, G., Gazetas, G., "Seismic soil-structure interaction: beneficial or detrimental?", *Journal of Earthquake Engineering*, Vol. 4, No. 3, 277-301, 2000.
- [4] Moschas, F., Psimoulis, P., Stiros, S., "GPS/RTS data fusion to overcome signal deficiencies in certain bridge dynamic monitoring projects", *Smart Systems and Structures*, 12 (3-4), 251-269, 2013
- [5] Moschas, F., Stiros, S., «Measurement of the dynamic displacements and of the modal frequencies of a short-span pedestrian bridge using GPS and an accelerometer». *Engineering Structures*, Vol. 33, 10-17, 2011
- [6] Psimoulis, P. and Stiros, S., «Measurement of deflections and of oscillation frequencies of engineering structures using Robotic Theodolites (RTS)», *Engineering Structures*, Vol. 29, No. 12, 3312-3324, 2007
- [7] Psimoulis, P., Stiros, S., "Measuring deflections of a short-span railway bridge using a Robotic Total Station", *ASCE Journal of Bridge Engineering*, Vol. 18, No. 2, 182-185, 2013
- [8] Psimoulis, P.A. and Stiros, S., «Experimental assessment of the accuracy of GPS and RTS for the determination of the parameters of oscillation of major structures», *Computer-Aided Civil and Infrastructure Engineering*, Vol. 23, No. 5, 389-403, 2008
- [9] Psimoulis, P.A. and Stiros, S., «A supervised learning computer-based algorithm to derive the amplitude of oscillations of structures using noisy GPS and Robotic Theodolite (RTS) records», *Computer and Structures*, Vol. 92-93, 337-348, 2008
- [10] Xia, H., and Zhang, N., «Dynamic analysis of railway bridge under high-speed trains», *Computers and Structures*, Vol. 83, 1891-1901, 2005

IBSBI 2014, October 16-18, 2014, Athens, Greece

# **DESIGN AND IMPLEMENTATION OF A MULTI-SENSOR MONITORING SYSTEM FOR STRUCTURAL INTEGRITY ASSESSMENT**

## **The Case of Attiki Odos, Pallini Cable-Stayed Bridge**

Vassilis Gikas<sup>1</sup>, Phaedon Karydakis<sup>2</sup>, George Piniotis<sup>3</sup>,  
Thanassis Mpimis<sup>4</sup>, Fanis Papadimitriou<sup>5</sup> and Alexandros Panagakis<sup>6</sup>

<sup>1,3,4</sup> National Technical University of Athens, School of Rural and Surveying Engineering, Greece

<sup>2</sup> National Technical University of Athens, School of Civil Engineering, Greece

<sup>5,6</sup> Attikes Diadromes SA, Attica Tollway Operations Authority, Greece

e-mail: piniotis@survey.ntua.gr, vgikas@central.ntua.gr, phsolkar@central.ntua.gr,

ampimis@central.ntua.gr, FPAPADIM@attikesdiadromes.gr,

APANAGAK@attikesdiadromes.gr

**ABSTRACT:** This article presents the design and implementation of a multi-sensor geodetic monitoring system used to record the response and evaluate the structural integrity of a small-sized, cable-stayed bridge for a number of static & dynamic load scenarios and ambient vibration tests. Preliminary data analysis revealed the main dynamic characteristics of the bridge, whereas in this paper emphasis is given in the dynamic behavior of stay cables.

**KEY WORDS:** Bridge load testing; vibration monitoring; OMA; microwave interferometry; digital image correlation.

## **1 INTRODUCTION**

Static and dynamic load tests have traditionally been used in order to verify the actual structural behavior of bridges compared with those predicted by analytical models. Also, structural performance examination of bridges includes ambient vibration tests, which are used to provide critical information about the behavior of a bridge due to operational conditions that relate mainly to vehicular traffic and variations in environmental parameters such as wind load and temperature [1, 2].

In this regard, this article presents the design, deployment and implementation of a multi-sensor system that was realized to perform a series of non-destructive tests of a single-span, cable-stayed bridge. As a whole, the goals and objectives of this work is twofold. Firstly, to perform a structural integrity verification study of the test bridge. This goal aims to obtain a better understanding of the bridge response to static and dynamic loads and to produce a “foot-print” of the current condition of the structure that can be used for future

condition assessment in relation to its present status. Secondly, to generate a library of “reference datasets” for use in research related to Structural Health Monitoring (SHM) of bridges. Specifically, it is envisioned that the quality, the volume, the spatial distribution and the great variety of data collected would allow research to be undertaken in many areas, including the assessment of the potential of individual sensors for SHM, optimal sensor placement studies, data fusion techniques for bridge monitoring as well as damage detection modeling [3]. In order to accommodate the second objective, provision was taken so that: (a) a great number of heterogeneous multi-sensor systems was used, (b) a complete as possible coverage of all structural elements (i.e. deck, cables and pylons) was attained during field campaigns and, (c) various Non-Destructive Testing (NDT) scenarios were implemented.

## **2 TESTING SCENARIOS AND MONITORING METHODS**

### **2.1 Static and Dynamic Tests**

In this study two types of deformation monitoring scenarios are considered. Static load tests aim to verify the structural integrity of the bridge in relation to the assumptions made at a design stage. Such tests are associated with the analysis of the geometry and the materials of the structure, and conclude to an assessment and (potentially) calibration of the Finite Element Model (FEM) of the structure. In this study, in order to realize the static tests a three-axle truck, weighting 300 kN (total mass of 30 metric tons) was used. Subsequently, for a number of predefined truck locations, the deck settlements, the cable vibrations and the pylon movements were measured, analyzed and compared with the corresponding values of the FEM analyses.

Dynamic tests are carried out to perform a modal analysis to identify the main dynamic properties of the bridge by applying well established output-only modal identification methods [4]. In this study, dynamic tests involve the same truck used for static testing being driven in the centre of the deck at constant speed (10 km/h, 20 km/h and 40 km/h). Also, testing involved truck runs at constant speed with a road bump of 30 mm as well as emergency brake tests. These tests, in addition to information on the natural frequencies and damping ratios of the bridge, they provide a picture of the variation in the dynamic amplification factor. Moreover, they are used in order to assist in the excitation of cables in order to compute their dynamic properties. Also, in this study a number of ambient vibration tests of variable time length for the three structural elements (deck, pylons and cables) of the bridge were undertaken.

### **2.2 Monitoring Methods and Systems**

As already stated, in order to generate a pool of “benchmark” bridge monitoring datasets a variety of heterogeneous sensor systems was employed. These systems feature different operating principles, produce observables of various

types, whereas, each system has its own advantages and limitations. However, in order to facilitate comparisons between sensors and for research concerning sensor fusion, particular attention was paid so that all monitoring systems were synchronized using the GPS PPS time stamp. Specifically, six types of sensors used for data collection as follows:

- *Precise Leveling (PL)*: A precise level (Leica DNA03;  $\pm 0.3$  mm/km @  $1\sigma$ ) was used to measure the vertical deflections of the deck along three lines (road axis and sidewalks) during the static load tests.
- *Digital Inclometers (DIN)*: Digital inclination sensors (Leica Nivel 220) were placed at five locations along one of the sidewalks of the deck to measure the deflection of vertical in two perpendicular directions. These sensors were located at points of expected maximum change in deck curvature. The measurements produced will be processed to produce deck settlements that, ultimately, shall allow comparisons with precise leveling.
- *Ground-Based Microwave Interferometry (GBMI)*: The GBMI technique was used to monitor deck settlements and in-plane cable vibrations during the static, dynamic and ambient vibration tests. The operating principle of the method relies on the computation of scattering object displacements using the phase information obtained by a microwave radar sensor from repeated electromagnetic pulse transmissions [5]. In this study, the IDS IBIS-S system used consisting of the radar module, a control PC and a power supply unit. The system operates at a maximum frequency 200 Hz and provides displacement accuracy better than 0.1 mm.
- *Digital Image Correlation (DIC)*: Video-based measurements were used to compute point displacements in two directions [6]. The iMETRUM Video Gauge system used to produce 2D vertical displacements for a number of specifically designed (ring type and tape) targets placed on the bridge deck, the pylon and the cables. Original displacements were computed on the video frames with an accuracy of at least 0.1 pixels, whereas actual displacements are obtained after a scale factor and relevant corrections have been applied.
- *Accelerometers (ACC)*: Two types of accelerometers (high sensitivity piezobeam and integrated K-BEAM) were used to record the deck and cable response of the bridge [7, 8, 9]. These units were operated by personnel of the System Dynamics Laboratory of the University of Thessaly in the frame of collaboration with the project participants from the National University of Athens.
- *Integrated GNSS / Inertial system (GNSS/INS)*: A high accuracy integrated GNSS/INS system was fixed on the truck vehicle to record continuously its position and kinematics. This information is valuable for bridge-vehicle interaction studies planned for the future as well as for documentation purposes of the tests.

In addition to the monitoring systems used in this study, environmental parameters were digitally recorded, whereas field operations were video recorded for documentation purposes.

### 3 BRIDGE DESCRIPTION AND SENSOR DISTRIBUTION

#### 3.1 The Bridge

The bridge under test is a roadway, single-span, cable-stayed bridge that overpasses “Attiki Odos” tollway which connects the metropolis of Athens to its international airport. The bridge has a suspended span 58.3 m long, variable width between 13.4 m and 18.5 m and pylon height 18.5 m. It consists of steel-composite deck with girder and floor beams with concrete slab of variable thickness 0.20 m to 0.40 m. The bridge features two  $\Lambda$ -shaped pylons, in which their stretched and distressed legs are made of prestressed concrete and of steel respectively (*Fig. 1*). The two pylons are connected near the top. The deck is suspended by three cables from each of the two pylons.

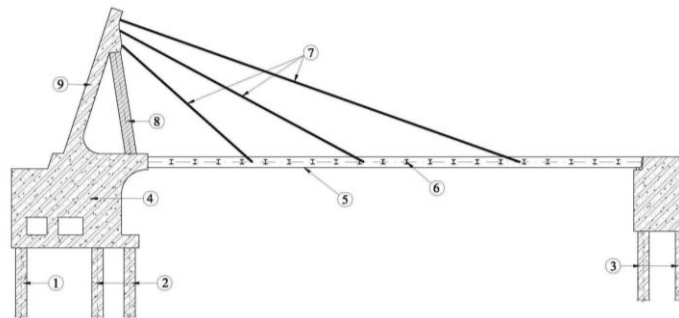


*Figure 1.* Structural elements of Pallini cable-stayed bridge (Attikes Diadromes SA)

#### 3.2 Monitoring Setup

*Fig. 2* shows the distribution of all monitoring sensors used as well as the targets and other observation points considered during the field trials. Specifically, one GBMI unit and two DIC cameras were used at a time. Therefore, most of the tests were repeated in order to collect observations from all station points shown in *Fig. 2*. Also, this plot shows the six truck vehicle locations considered during the static tests. Specifically, in order to maximize the effect of truck loading on the structure the vehicle was placed asymmetrically, by the sidewalk curbs, at the cross sections passing the six cable anchor points. *Table 1* provides a classification of the systems used to monitor the bridge elements (deck, pylon and cables) in relation to the test types (static, dynamic and ambient) adopted. Particularly, for the static tests that required several hours to complete is critical that variations in environmental



conditions are as small as possible. Therefore, all tests were performed night time.

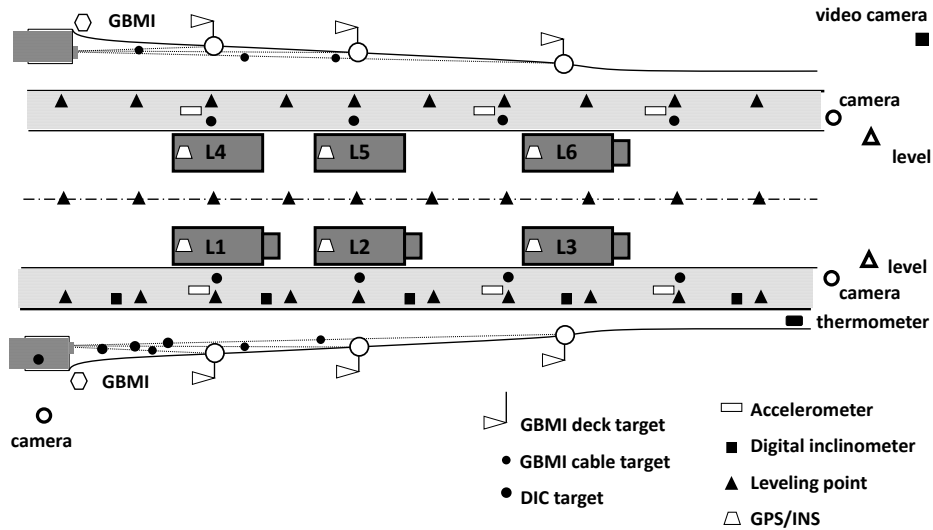


Figure 2. Monitoring systems and sensor distribution

Table 1. Use of monitoring systems for the three test types; PL: Precise Levelling, DIN: Digital Inclinometers, GBMI: Ground-Based Radar Interferometry, ACC: ACCelerometers, DIC: Digital Image Correlation, T: Temperature

element →	DECK					CABLES			PYLON	TRUCK	OTHER		
	PL	DIN	GBMI	ACC	DIC	GBMI	ACC	DIC	GBMI	DIC	GPS/INS	T	VIDEO
STATIC	x	x	x		x	x		x	x	x	x	x	x
DYNAMIC			x	x	x	x	x	x	x	x	x	x	x
AMBIENT			x	x	x	x	x	x	x			x	x

#### 4 BRIDGE DECK AND CABLE RESPONSE – FIRST RESULTS

At the time of writing this paper (July 2014) fieldwork has been completed, whereas data analysis is confined in selected sensor datasets, including some preliminary modal analyses tests. These analyses aim to assist in the design of various FEM sensitivity tests to study the structural integrity of the bridge. In this paper only some preliminary results obtained for the deck and cables response using the GBMI system for the static and dynamic tests will be discussed.

Firstly, the modal identification of the bridge deck using the displacements determined from Digital Image Correlation (DIC) ambient measurements revealed the first bending mode at 1.22 Hz, the first torsional mode at 2.13 Hz and the second bending mode at 2.71 Hz. This task was achieved using the

Frequency Domain Decomposition (FDD), which is a well known output-only modal identification method. Also, preliminary analysis of the available data indicated higher modes, not reported here as further investigation is still required.

*Fig.3* shows the GBMI derived displacements as follows: (a) the deck settlements obtained by the anchor point of the long cable and, (b) the cable movements obtained perpendicular to the cable axis at a distance about 1/3 of the cable length measured from its top anchor point. As expected, deck settlements are becoming more significant for the truck locations which are closer to the target points observed. Notably, the minimum and maximum values are obtained for load scenarios L0 and L3 respectively.

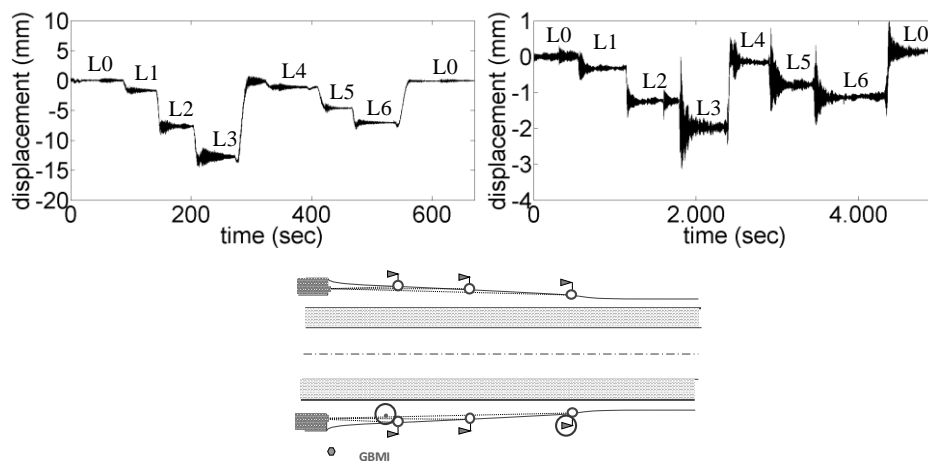


*Figure 3.* GBMI derived displacements at deck and long cable

*Fig. 4* shows the PSD plot obtained from the radar subset that contains the displacements occurred for the long cable, for the case of an empty bridge (L0). The first three peaks at 1.24, 2.16 and 2.76 Hz (marked with squares) are the cable's response to the bridge deck's stimulation, since they have been identified as deck modes. The plot also exhibits two dominant peaks at 2.86 and 3.14 Hz ((marked with circles). The latter peak appears to be the first modal frequency of the cable (local mode), whereas the first peak is attributed to the deck-cables interaction (global mode). Notably, this peak value (2.86 Hz) is evident (marked with circle) in the PSD plot of the radar data acquired from the long cable for the case of an empty bridge (L0) (*Fig. 5*).

Finally, *Fig. 4* exhibits the peaks at 6.24, 9.38, 12.52, 15.7, 18.46 and 21.38 Hz (marked with triangles) that appear to be the next six modal frequencies of the cable. It is worth mentioning that the values of all the aforementioned

frequencies are very close to the integer multiples of the fundamental cable frequency (3.14 Hz), which implies that the dynamics of the stay-cable can be described by the taut string model.

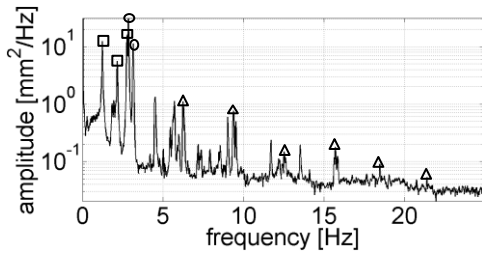


Figure 4. PSD of the long cable radar data for the L0 bridge loading scenario (log scale)

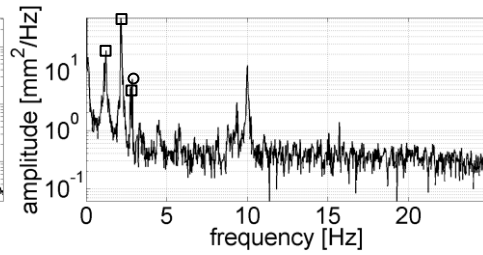


Figure 5. PSD of the deck target radar data for the L0 bridge loading scenario (log scale)

The global and local character of the frequency values 2.86 Hz and 3.14 Hz respectively are also verified in Fig. 6, which depicts the Short Time Fourier Transform (STFT) plot of the long cable radar data derived for all bridge test loading scenarios. From this plot it is evident that every time the truck brakes to reach the predetermined location of each loading scenario (L1, ..., L6), the frequency at 2.86 Hz is uniformly stimulated for all scenarios (circle marks in Fig.6). On the contrary, the level of stimulation of the frequency value 3.14 Hz is strongly depended on the truck position along the bridge deck, exhibiting its greatest value for the truck position that is closest to the long cable.

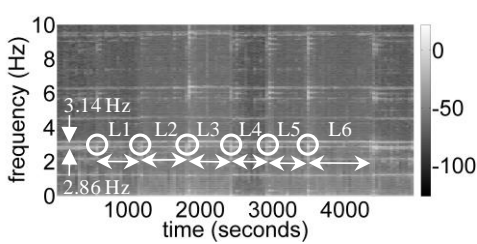


Figure 6. Short Time Fourier Transform (STFT) plot of the long cable radar data for all the bridge loading scenarios time period

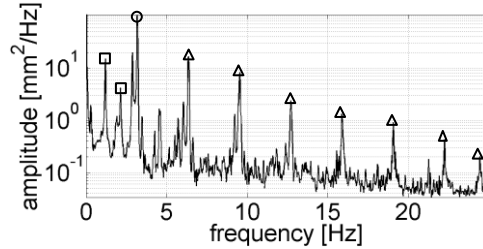


Figure 7. PSD of the long cable radar data for the L3 bridge loading scenario (log scale)

Fig. 7 shows the PSD plot obtained from the radar displacements measured on the long cable for the time span of the truck vehicle standing next to that cable (L3). As expected, the dominant peak in this plot is 3.18 Hz (marked with circle), which corresponds to the first modal frequency of the cable (3.14Hz) that exhibits a shift as a result of the cable stretching due to truck loading.

Moreover, the peaks at 6.36, 9.54, 12.72, 15.88, 19.08, 22.24 and 24.46 Hz (marked with triangles) refer to the next seven modal frequencies of the cable.

As part of an undergoing study, the evaluation of tension forces of stay-cables and their changes (using their modal frequencies in the application of the taut string model) for the unloaded and loaded bridge would yield critical information regarding the structural integrity of the bridge. At a next stage, the findings discussed in this paper will be further evaluated and used to assist in the assessment of the bridge condition and to the updating of FE models.

## 5 REMARKS AND FUTURE WORK

This paper presented the design and implementation of a multi-sensor monitoring system used to record the response of a small size, cable-stayed bridge for a complete set of static and dynamic load scenarios and ambient vibration tests. Currently, the structural integrity of the bridge is being investigated through a number of sensitivity tests on selected parts of the monitoring data. As following steps, it is planned to undertake a thorough evaluation of the performance of the various sensors involved in the tests through independent checks. Such cross-comparisons would allow a comprehensive characterization of their potential under real operating conditions that, by extension, would contribute in optimal sensor placement studies and sensor fusion techniques.

## REFERENCES

- [1] Batel, M, "Operational Modal Analysis-Another Way of Doing Modal Testing," Sound and Vibration, August, 2002.
- [2] Gikas, V, Karydakis, P, Mpimis, A, Piniotis, G, Rodopoulos, J, "Structural Integrity Verification of a Cable-stayed Footbridge Based on Conventional and Non-Conventional Geodetic Data", *2<sup>nd</sup> Joint Int. Symp.on Deformation Measurements*, Nottingham, Sept. 9-10, 2013.
- [3] Papadimitriou, C, Fritzen, C-P, Kraemer, P and Ntotsios, E, "Fatigue Predictions in Entire Body of Metallic Structures from a Limited Number of Vibration Sensors Using Kalman Filtering", *Structural Control and Health Monitoring*, 2010.
- [4] Cunha, A, Caetano, E, Magalhaes, F and Moutinho, C, "From input-output to output only modal identification of civil engineering structures," SAMCO final report, 2006.
- [5] Gikas, V, "Ambient Vibration Monitoring of Slender Structures by Microwave Interferometer Remote Sensing", *Journal of Applied Geodesy*, Vol. 6, No. 3-4, pp. 167-176, 2012.
- [6] McCormick, N, Lord, J, "Digital image correlation for structural measurements", *Proc. of the Institution of Civil Engineers, Civil Engineering 165*, Issue CE4, pp. 185-190, 2012.
- [7] Moschas, F, Stiros, S, "Measurement of the Dynamic Displacements and of the Modal Frequencies of A Short-Span Pedestrian Bridge Using GPS and an Accelerometer", *Engineering Structures*, Vol. 33, No. 1, 2011.
- [8] Kaloop, M, R, Li, H, "Tower Bridge Movement Analysis with GPS and Accelerometer Techniques: Case Study Yonghe Tower Bridge", *Information Technology Journal*, Vol. 8, No. 8, pp. 1213-1220, 2009.
- [9] Kaloop, M, R, Sayed, M, A, Kim, D, Kim, E, "Movement Identification Model of Port Container Based on Structural Health Monitoring System", *Structural Engineering and Mechanics*, Vol. 50, No. 1, pp. 105-119, 2014.

## **STRENGTHENING AND MAINTENANCE MEASURES OF A BAILEY-TYPE ROAD BRIDGE**

Vasileios D. Papavasileiou<sup>1</sup> and Ioannis G. Raftoyiannis<sup>2</sup>

<sup>1,2</sup>Laboratory of Steel Structures, Department of Civil Engineering  
National Technical University of Athens  
e-mail: vasiliospapavasiliou@yahoo.com, rafto@central.ntua.gr

**ABSTRACT:** In this paper, a survey based on experimental data accompanied by a detailed study on the assessment of the carrying capacity of an old Bailey-type steel truss road-bridge that is still in service is presented. This task is achieved through field measurements under static and dynamic loads as well as experimental results based on the properties of the steel material. An analytical model has been employed to assess the carrying capacity of the bridge under seismic loads and wind loads according to the provisions of current regulations. Based on the experimental and analytical results presented herein, strengthening and maintenance measures have been proposed in order to ensure strength and carrying capacity of the bridge under the current requirements. Also, an estimation of the remaining life of the bridge against fatigue is presented taking into account the proposed strengthening measures.

**KEYWORDS:** Bridge dynamics, maintenance, strengthening measures

### **1 INTRODUCTION**

Designed and developed during the 2<sup>nd</sup> W.War, the Bailey-type steel truss bridge played a leading role in as much the various geomorphology fields of battle as in the reconstruction of the Hellenic road network thereafter.

For the re-establishment of the road network in the region of Thermon-Aetoloakarnania in 1954 after the destruction with explosives of the arched stone Bania bridge in 1944, a new simply supported single-span steel truss bridge of Bailey-type has been constructed with the method of promotion with span length 54,87m.

During the 70's, the increase of traffic loads in the Western sector of National Road Network and the periodical redirection of traffic circulation on the particular road axis (Antirion – Bania bridge – Agrinion – Epirus) in order to cover transport and travel needs has led the local authorities to build an intermediate pier-support in order to strengthen the structure.

The challenge of the present evaluation resulted after the obvious surface deteriorations of the bridge due to corrosion of the steel elements of the bridge

as well as the deck. The problems which resulted at the phase of in-situ inspection are lack of constructional and maintenance data regarding the intermediate pier-support.



*Photo 1.* The Bania bridge up to 1986



*Photo 2.* The Bania bridge in its present form

The measured dimensions of cross-sections of the truss members were certified by a similar study [1]. The particular structures have been designed to accommodate passage of military vehicles for temporary use under controlled conditions. The extensive and non-verified use of such bridges due to the passage of heavy vehicles increases the danger of failure due to fatigue.

## **2 BRIDGE DESCRIPTION**

The steel truss bridge of Bailey-type was named after the team head British engineer Sir Donald Bailey. It constitutes from elements assembled with bolts and can cover either single or multiple spans.

Each frame has length of 3,048m with cross-section as shown in Fig. 1 and it has four holes at its edges where connection with neighboring frames is done

with bolts. The Bania bridge in Thermon - Aetoloakarnania is characterized as a triple-double truss-frame since it is constituted from two complex truss beams with three lines of frames at width and two lines at height each (Fig. 2). The total span length is 54,87m covered by 108 such frames.

In order to support the deck and to distribute the traffic loads to the main truss beams, cross girders made from IPN profile have been used as shown in Fig. 3.

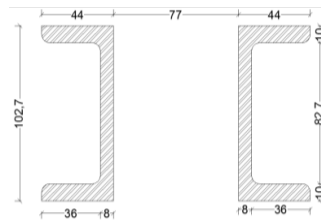


Figure 1. Top and bottom cross section in mm

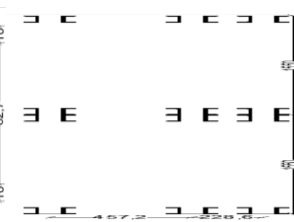


Figure 2. Cross section of the main beam in mm

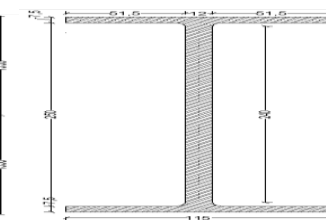


Figure 3. Cross girder cross section in mm

The transfer of loads from the deck to the main beams is through the cross girders. The deck is wooden with galvanized sheets of thickness 5mm. The weight per frame is 5.880kgr, which results to a total weight of the bridge  $18 \times 5.880 \text{ kgr} = 105840 \text{ kgr}$  or 1058,4 kN, and total mass of  $107,8 \text{ kNsec}^2\text{m}^{-1}$  considered in the dynamic analysis. The inertia properties of the main truss beams resulting from EC-3 is  $I_{\text{eff}} = 0,08895 \text{ m}^4$  according to eq(1).

$$I_{\text{eff}} = 0.5 \cdot A_f \cdot h_0^2 \quad (1)$$

where  $A_f$  is the area of cross-section of each flange and it is  $0,31 \text{ m}^2$ , while when calculated theoretically and with the use of software it is  $I_{\text{eff}} = 0,0833\text{m}^4$ . In the analysis the most unfavorable value  $I_{\text{eff}}=0,0833\text{m}^4$  has been used.

### 3 STRUCTURAL STEEL PROPERTIES

Specimens have not been taken for this particular study due to practical and economical reasons since valuable results on the material with the same year of production and similar use before placement in local Pakistan are reported in a similar work [1]. The steel quality BS 968 is met in various forms at this time period of production in combination with the development of metal industry and it is used in the frames and the cross girders while for the rest elements it is used steel BS 15 [2].

Table 1. Properties for structural steel BS 968

Property	Material	Units	Value
E: elasticity modulus	Steel BS 968	GPa	206,8
$f_y$ : yield stress	Steel BS 968	MPa	344
$f_u$ : failure stress	Steel BS 968	MPa	540

The steel used in this bridge has presented deterioration and damage in various members as well as extensive corrosion.



Photo 3. Corrosion of steel



Photo 4. Keystone damage

#### 4 IN-SITU MEASUREMENTS AND QUALITY CONTROL

The maximum deflection of a simply supported beam under uniform load is given by:

$$w_{\max} = \frac{5}{384} \cdot \frac{p \cdot \ell^4}{EI} \quad (2)$$

where  $\ell$  is the length of the beam = 54,864 m

$p$  is the uniform load = 1058,4kN/54,864m = 19,29 kN/m

$EI$ : is the bending stiffness = 206,8 GPa \* 0,0833m<sup>4</sup>.

and hence

$$w_{\max} = \frac{5}{384} \cdot \frac{19,29 \cdot 54,864^4}{206,8 \cdot 0,0833} = 0,132\text{m} = 132\text{mm} \quad (3)$$

On site measurements of the maximum deflection due to bending with the use of geodetic instruments resulted 34mm. This means that, after erection of the intermediate support, the bridge has been elevated and then was left to rest on the bearing, so that the initial deflection was decreased by 98mm. Taking into account the effect of initial slippage  $e_o$ .

$$e_o = \frac{0,5 \cdot L \cdot \delta_o}{h \cdot \cos \alpha} \quad (4)$$

it has been calculated that the maximum bending deflection was finally decreased by  $w_M + e_o = 123$  mm.



Photo 5. Intermediate support detail



Considering the simply supported beam as a single degree-of-freedom oscillator the first (fundamental) eigenfrequency results from eq (5)

$$f_1 = \frac{1}{2\pi} \left(\frac{\pi}{L}\right)^2 \sqrt{\frac{EI}{m}} \quad (5)$$

where  $m = (1058,4 \text{ kN} / 9,81 \text{ m/sec}^2) / 54,864 \text{ m} = 1,967 \text{ kNm}^{-2} \text{sec}^2$ . The computed value is  $f_1 = 1,545 \text{ sec}^{-1}$ .

It was not possible to setup instrumented dynamic measurements on site. For this reason and in order to validate the reliability of the model in which beam elements have been used, instrumented measurements have been performed on a similar simply supported bridge with length 18,29 m regarding free oscillation as well as the Frequency Response Function. From these measurements, a time history response has been obtained which was then applied on the FE model via the Sap2000 FE software. The correlation of the results of the real structure and the FE model was excellent.

## 5 NUMERICAL RESULTS

In order to validate the analytical results, a numerical model has been developed in which the same loading was applied so that the improved behavior of the bridge after placement of the intermediate support can be evaluated. Besides the classical static and dynamic analyses, resulting the basic load combinations ULS and SLS, analyses with one moving load of class group 12 passing through both models as well as three moving loads of class group 12 according to the current code provisions have been performed [3,4].



Photo 6. The triple-double Bania bridge

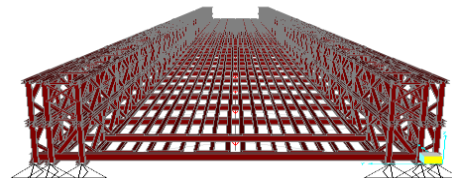


Photo 7. Finite element model of the bridge

Numerical analyses have also been performed in two bridge models, one simply supported and a second with two spans. Imperfections or damages in the analysis of the single span bridge were not taken into account since the main goal was not to evaluate the structural behavior of the bridge before 1986 for which no information was available. All structural damages were assumed to occur after the placement of the intermediate support. Extensive corrosion of the structure is obvious in all members and its extent is not possible to be assessed by visual inspection. In the evaluation of the results, the effect of the corrosion was based on reliable experimental measurements [5].

From the analyses of the two models, the fundamental eigenfrequency and eigenvector are determined, i.e.,  $T_1 = 0,664 \text{ sec}$  ( $f_1 = 1,51 \text{ sec}^{-1}$ ) for the case of single span simply supported bridge with theoretical value  $0,647 \text{ sec}$  (2,5% error) while for the two span bridge with intermediate support it is  $T_1=0,248 \text{ sec}$ .

The fundamental eigenshapes resulted from the analysis of the two models are shown in Figs 4 and 5, respectively.

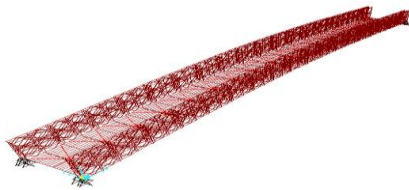


Figure 4. Fundamental eigenshape of 1-span

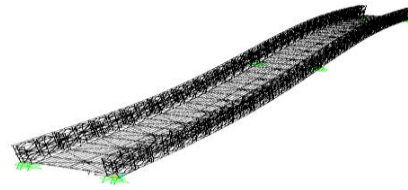


Figure 5. Fundamental eigenshape of 2-span

The effectiveness of intermediate support placement becomes more clear by observing the following diagrams.



Figure 6. Dynamic response for 1 vehicle pass



Figure 7. Dynamic response for 3 vehicles pass

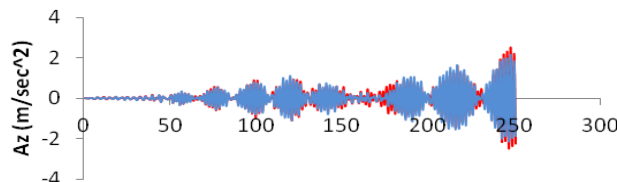


Figure 8. Acceleration diagram for 3 vehicles pass

From the load combinations including the effect of wind loading, it resulted no high stress values capable to cause failure or serviceability issues.

For the control of strength against fatigue in this particular type of structure, the main points of interest [6] are the connection points of the vertical stands to the bottom flange of the frames as well as the holes to which the horizontal stiffening members are connected. The evaluation of fatigue strength for this particular bridge is imperative since the policy of equitable use refers to short time operation and under continuous supervision [7].

The fatigue detail for the vertical stands and for the holes to which the horizontal stiffening members are connected is determined to be 100.

The number of vehicles that are passing annually through the particular bridge classifies the structure into traffic category 4 that is  $0,05 \cdot 10^6$ , while the life duration from the erection time is 60 years. The check against fatigue is done according to the criteria given by eqs (6) and (7) and it resulted that for equitable use as well as overloading conditions, the bridge does not suffer any problems due to fatigue

$$\gamma_{Ff} \cdot \Delta\sigma_{E_2} \leq \frac{\Delta\sigma_c}{\gamma_{Mf}} = \frac{90}{1,15} = 78,26 \quad \text{where } \gamma_{Ff}=1,0 \text{ and } \gamma_{Mf}=1,15 \quad (6)$$

$$\gamma_{Ff} \cdot \Delta\tau_{E_2} \leq \frac{\Delta\tau_c}{\gamma_{Mf}} = \frac{75}{1,15} = 65,22 \quad \text{where } \gamma_{Ff}=1,0 \text{ and } \gamma_{Mf}=1,15 \quad (7)$$

$$\Delta\sigma_{E_2} = \lambda \cdot \varphi_1 \cdot \Delta\sigma_p \quad \text{where } \varphi_1=1 \text{ (dynamic factor for road bridges)} \quad (8)$$

$$\Delta\tau_{E_2} = \lambda \cdot \varphi_2 \cdot \Delta\tau_p \quad \text{where } \varphi_2=1 \text{ (dynamic factor for road bridges)} \quad (9)$$

## 6 MODELING CONSIDERATIONS

However, the ideal conditions described in the finite element model and the current regulation are not possible to take into account all the imperfections and structural damages that may influence the operation of the bridge structure. This requires also experimental verification for numerous cases checked against normal use. Evaluating the full structure including the foundation and abutments as well as the superstructure, damages were detected at the bearing positions of the bridge since it rests on stone abutments where a concrete plate has been placed to facilitate the support of the bridge. In both abutments, damage has been detected in the keystone of the arches most likely due to heavy vehicles, which when entering and leaving the bridge cause impact phenomena. During the inspection, it was detected that a small number of frames has suffered damages due to the collision of vehicles on the vertical stands as well as buckling.

A full row of bolts is missing at the connection of to the first line of frames. The cross-girders fasteners are relaxed because of cyclic loading. Oxidation of the bridge structure is extensive and deep in all structural elements. During the effort of surface scratching with a metal brush it was not possible to detect clean steel. Because the big height of the frame and the connection detail between secondary beams and the deck, the vertical stiffeners have not been inspected in detail but only visually with the aid of photographs. Also, the intermediate support bearings do not fully conform to the instructions of the manufacturer handbook [3] since the item required to achieve pinned support conditions is missing. All the above findings render enough difficulty to create a reliable model.

## **7 CONCLUSIONS – STRENGTHENING MEASURES**

Summarizing the above, one concludes that the intermediate support affects positively the development of dynamic phenomena as well as the fatigue strength of the members. An increase of the bearing capacity of the structure is also achieved according to the manufacturer handbook by transforming the single span bridge to a two-span continuous bridge after placement of the intermediate support. The vertical displacements and accelerations at L/4 are decreased in all load cases. The danger of fatigue failure has been completely eliminated based on the numerical results. However, the existing cracks at welded connections should be under constant monitoring. Given that the structure cannot be strengthened with the addition of new frames, it is alternatively proposed to maintain the existing frame. At first, the keystones of the abutment arches must be restored with repair mortars to maintain their form as well as their historical character. Replacement or full repair of damaged existing frames or structural members must follow. The whole deck must be temporarily removed in order to replace damaged horizontal stiffeners. The steel member surfaces must be cleaned with sandblast and anti-corrosion paint. All damaged connections must be restored. A final step is to build bumpers just before the entry at both sides of the bridge in order to decrease vehicle speeding that influences the dynamic behavior of institution. Other solutions such as the placement of tuned mass dampers or a steel-concrete composite deck were excluded as non-favorable alternatives.

## **REFERENCES**

- [1] Associated Consulting Engineers L.T.D, Evaluation of a Bailey Bridge at Arduun (Kunar River), Lahore, Pakistan, 1990
- [2] Bates W. (1991) Historical Structural Steelwork Handbook, London, BCSA
- [3] Department of the Army (DOA) (1986), Bailey Bridges FM5-277, Washington D.C
- [4] EN 1993-2, EUROCODE 3: Design of Steel Structures, Part 2. Steel Bridges (2004)
- [5] Chen Y.Y, Corrosion resistance and mechanical properties of low-alloy steels under atmospheric conditions, Corrosion Science 47 (2005) 1001–1021
- [6] Greenaway L.R., (1968) Fatigue Risk in Bailey Bridges, Technical Memorandum, Ministry of Transport, London
- [7] FHWA, (2013), Manual for Repair and Retrofit of Fatigue Cracks in Steel Bridges Publication No. FHWA-IF-13-020

IBSBI 2014, October 16-18, 2014, Athens, Greece

# THE EFFECT OF STEREOTOMY ON THE SHAPE OF THE THRUST-LINE AND THE MINIMUM THICKNESS OF MASONRY ARCHES

Nicos Makris and Haris Alexakis

University of Patras, Dept. of Civil Engineering, Greece  
e-mail: nmakris@upatras.gr, alexakis@upatras.gr

**ABSTRACT:** More than a century ago Milankovitch presented for the first time the correct and complete solution for the theoretical minimum thickness,  $t$ , of a semicircular masonry arch with radius,  $R$  ( $t/R=0.1075$ ). This paper uses a variational formulation approach and shows that this solution is not unique and that it depends on the stereotomy exercised.

**KEY WORDS:** Catenary curve; Limit analysis; Lines of resistance; Stone arches; Variational formulation

## 1 INTRODUCTION

Robert Hooke [1] was apparently the first to propose a rational rule for sizing masonry arches by describing the analogy in the load-path between a “hanging chain”, which forms a catenary in tension under its own weight and a masonry arch which stands under compression. This analogy conceived by Hooke is expressed in the literature “As hangs the flexible line, so but inverted will stand the rigid arch” ([2-4]). The problem of determining the minimum thickness of masonry arches has challenged the engineering community since the early eighteenth century (Couplet [5]), was tackled with remarkable ingenuity by Monasterio in the early nineteenth century ([6,7]), was addressed rigorously in the early twenty century in the nearly unknown work by Milankovitch [8,9] and remains worth discussing until today (Heyman [10]).

This paper shows that Milankovitch’s [8,9] solution for the minimum thickness of a semicircular arch  $t/R=0.1075$  is not unique and that it depends on the stereotomy exercised and the associated coordinate system adopted. The adoption of vertical cuts, first introduced by Lamé and Clapeyron [11] (see also Timoshenko [12]) and an associated cartesian coordinate system yields a slightly higher value for the minimum thickness ( $t/R=0.1095$ ) than the one computed by Milankovitch. Furthermore, the paper shows that Heyman’s [13] widely accepted solution ( $t/R=0.106$ ) remains unconservative regardless the stereotomy exercised on the arch—even if one assumes vertical joints (Heyman [10]).

## 2 PHYSICALLY ADMISSIBLE THRUST-LINES OF AN ARCHED MONOLITH WITH ZERO TENSILE STRENGTH

The remarkable directness of Hooke's [1] "hanging chain" as a design tool for sizing stable masonry arches is probably the reason that even in the recent literature it is widely believed that the catenary (the alysoid) is a physically admissible thrust-line of the masonry arch. The thrust-line (or the *line of resistance*, Moseley [14], or the *druckkurve*, Milankovitch [8,9]) is defined as the geometrical locus of the application points of the resultant thrust-force that develops at any cross section of the arch. Given that the calculation of the minimum thickness of the masonry arch derives from the limiting arch that is thick enough so that it can just accommodate a physically admissible thrust-line, the identification of physical admissible thrust-lines is central in this study. *Fig. 1* (left) plots two different minimum thrust-lines within a monolithic elliptical arch with  $b/a=0.75$  and  $t/a=0.15$  ( $a$  and  $b$  are the semispan and the height of the arch respectively). They have been constructed with a custom-made computer code which repeats the force equilibrium as point  $O$  runs from the crown to the springing. These two physically admissible thrust-lines are not distinguishable in the scale of the arch; yet, if one zooms in the neighbourhood isolated with the dashed parallelogram, the two thrust-lines are clearly different as shown in *Fig. 1* (right). Both minimum thrust-lines are equally correct and the fact that they lie within the physical boundaries of the arch ensures that the arch is stable (see also Alexakis and Makris [16]).

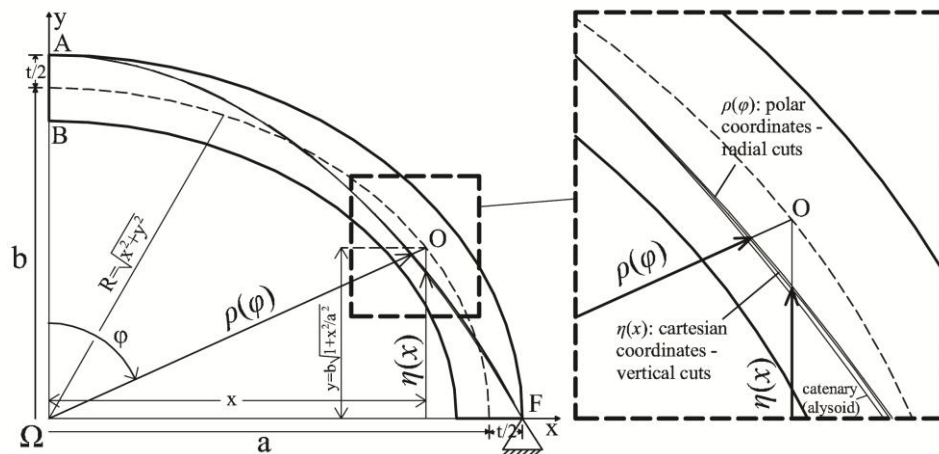


*Figure 1.* Monolithic elliptical arch with the two different physically admissible minimum thrust-lines (left),  $b/a=0.75$  and  $t/a=0.15$  ( $a$ =semispan and  $b$ =height). The two physically admissible thrust-lines ( $\rho(\varphi)$  obtained with successive radial cuts and  $\eta(x)$  obtained with successive vertical cuts) are distinguishable in the enlarged parallelogram (right). The catenary (alysoid) that passes by points A and F is not a physically admissible thrust-line.

In structural engineering the derivation of multiple solutions from equilibrium analysis is not common. The “counterintuitive” result of having two different yet neighboring theoretically correct answers for the thrust-line depending on the coordinate system adopted, derives from the request to express the load path in a two-dimensional structure with finite thickness,  $t$ , with the thrust-line—that is a concept inherent to a one-dimensional structure (the “hanging chain”). Interestingly, the inverted “hanging chain” (catenary) that passes from the extreme points A and F of the extrados of the arch shown in *Fig. 1* offers a third line that is different from the two minimum thrust-lines—the one computed by taking radial cuts after adopting a polar coordinate system and the other computed with vertical cuts after adopting a cartesian coordinate system.

The idea of analyzing the stability of masonry arches by taking vertical cuts rather than radial cuts goes back to the seminal work of Lamé and Clapeyron [11], who showed that for symmetrical arches of any shape, the calculation of the position of the intrados hinge can be greatly simplified if instead of radial cross-sections, vertical cross-sections are contemplated ([12]).

### 3 MINIMUM THICKNESS OF A SEMICIRCULAR MONOLITH WITH ZERO TENSILE AND INFINITE COMPRESSION STRENGTH

#### 3.1 Polar coordinate system—Solution with a variational formulation

Milankovitch [8,9] computed the correct value of the minimum thickness of the arched monolith,  $t/R=0.10748$  by deriving the closed-form expression of the minimum thrust-line in association with the information that when the circular monolith assumes its minimum thickness, the minimum thrust-line also touches the intrados of the arch.

When the thickness of the arch is sufficiently reduced and the minimum thrust-line touches the intrados, the arch reaches a limit-equilibrium state by developing a five-hinge symmetric mechanism (Couplet [5]). Accordingly, points A, K, and F shown in *Fig. 2* (left) are imminent hinges of the arch at its limit equilibrium state. When assuming a rupture along the radial direction (that is consistent with the polar coordinate system adopted by Milankovitch [8,9]) moment equilibrium of half the arch and of the top hinged portion of the arch ABK about hinge K gives (Makris and Alexakis [17,18], Alexakis [19])

$$\left[2\frac{t}{R}\left(\frac{t^2}{R^2}+12\right)-3\pi\left(\frac{t^2}{R^2}-4\right)\right]\cos\phi_r=3\pi\left(\frac{t}{R}+2\right)^2+6\left(\frac{t^2}{R^2}-4\right)\phi_r\sin\phi_r \quad (1)$$

where  $\phi_r$  is the rupture angle (see *Fig. 2* left). Adopting as a reference level the horizontal axis  $x$  ( $y=0$ ), the potential energy of the semicircular arch is

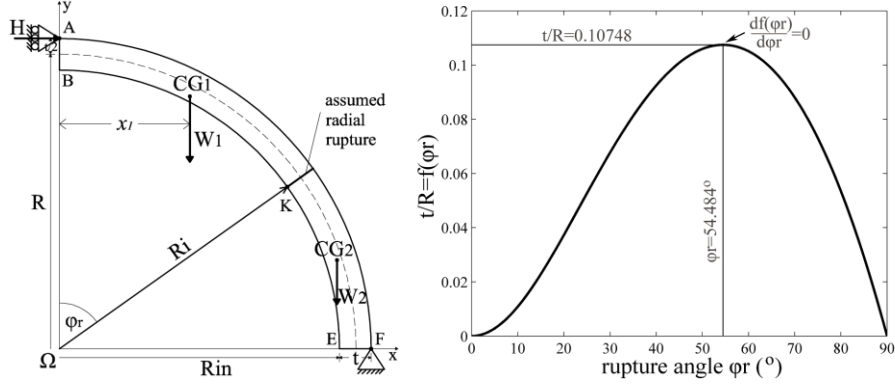


Figure 2. Left: Formation of a hinge mechanism by assuming that the rupture at the intrados hinge, K, happens along the radial direction. Right: Admissible values of  $t/R$  for a given rupture angle  $\phi_r$  as they result from moment equilibrium of the hinged mechanism shown in Fig. 2 left. The principle of stationary potential energy ( $\delta V(\phi_r)=0$ ) indicates that the hinged semicircular arch with a radial rupture is in equilibrium when  $df(\phi_r)/d\phi_r=0$ . This happens when  $\phi_r=54.484^\circ$  and the corresponding minimum thickness is  $t/R=0.10748$ .

$$V = W \cdot y_o = R^3 \frac{t}{R} \left(1 + \frac{1}{12} \frac{t^2}{R^2}\right) \quad (2)$$

where  $W=(\pi/2)tR$  is the weight and  $y_o=R(12+(t/R)^2)/6\pi$  is the vertical coordinate of the center of gravity of half the arch. When a radial rupture has been assumed the two unknowns  $t/R$  and  $\phi_r$  are related via moment equilibrium with a relation  $t/R=f(\phi_r)$ , which represents the accepted root of Eq. (1) ([17-19]). Accordingly, the potential energy of the circular arch given by Eq. (2) can be expressed as a function of  $\phi_r$

$$V(\phi_r) = R^3 f(\phi_r) \cdot \left(1 + \frac{1}{12} f(\phi_r)^2\right) \quad (3)$$

The structural system shown in Fig. 2 (left) is a typical case where the only forces (weights) acting in the system are conservative and where the work of all forces is accounted by the potential energy  $V(\phi_r)$  given by Eq. (3). According to the principle of stationary potential energy, the geometrically admissible hinged mechanism shown in Fig. 2 (left) is in an equilibrium state if and only if the total potential energy is stationary, i.e.

$$\delta V(\phi_r) = \frac{dV(\phi_r)}{d\phi_r} \delta\phi_r = 0 \quad (4)$$

Substitution of Eq. (3) into Eq. (4) gives



$$\frac{df(\phi_r)}{d\phi_r} \left[ 1 + \frac{1}{4} f(\phi_r)^2 \right] = 0 \quad (5)$$

The quantity in brackets in Eq. (5) is always positive; therefore, Eq. (5) is satisfied when  $df(\phi_r)/d\phi_r=0$ . The result of Eq. (5) shows that the symmetric hinged arch is in an equilibrium state ( $\delta V(\phi_r)=0$ ) if and only if

$$\frac{df(\phi_r)}{d\phi_r} = \frac{d(t/R)}{d\phi_r} = 0 \quad (6)$$

The solution of Eq. (6) offers the unknown location of the rupture angle  $\phi_r=54.484^\circ$  which is precisely the value computed by Milankovitch [8,9]. Substitution of the value of the rupture angle  $\phi_r=54.484^\circ$  (that is for a rupture assumed along the radial direction) into the acceptable root of the moment equilibrium of Eq. (1) one obtains the minimum thickness value  $t/R=0.10748$ . *Fig. 2* (right) shows that the maximum of equation  $df(\phi_r)/d\phi_r=0$  happens at  $\phi_r=54.484^\circ$  and that the maximum value of the thickness is  $t/R=0.10748$ .

Heyman's [13] "work-balance" concept was implemented by Ochsendorf [15] who developed a trial-and-error procedure by selecting successive values of the rupture angle  $\phi_r$  together with the corresponding values of  $t/R$  until the "work-balance" equation is satisfied. Ochsendorf [15] assumed that the rupture of the arch at the intrados hinge is along the radial direction and his trial-and-error procedure converged to the correct value of the rupture angle  $\phi_r=54.5^\circ$  and minimum thickness  $t/R=0.1075$  initially discovered by Milankovitch [8,9].

### 3.2 Cartesian coordinate system - Solution with a variational formulation

In this section we consider again that the circular arch has reached its limit equilibrium state by developing a five-hinge symmetric mechanism. Accordingly, points A, K, and F shown in *Fig. 3* (left) are imminent hinges of the arch at its limit equilibrium state. We now assume that the rupture happens along the vertical direction that is consistent with a cartesian coordinate system. For a vertical rupture the weight  $W_1$  of the hinged portion of the semicircular arch ABK and the abscissa  $x_1$  of their center of gravity are

$$W_1 = R^2 \frac{1}{2} \left[ \frac{x_r}{R} \left( \sqrt{c_1^2 - \frac{x_r^2}{R^2}} - \sqrt{c_2^2 - \frac{x_r^2}{R^2}} \right) + c_1^2 \arcsin\left(\frac{x_r}{Rc_1}\right) - c_2^2 \arcsin\left(\frac{x_r}{Rc_2}\right) \right] \quad (7)$$

$$x_1 = R \frac{2 \frac{t}{R} \left( 1 + \frac{1}{12} \frac{t^2}{R^2} \right) - \frac{2}{3} \left[ \left( c_1^2 - \frac{x_r^2}{R^2} \right)^{3/2} - \left( c_2^2 - \frac{x_r^2}{R^2} \right)^{3/2} \right]}{\frac{x_r}{R} \left( \sqrt{c_1^2 - \frac{x_r^2}{R^2}} - \sqrt{c_2^2 - \frac{x_r^2}{R^2}} \right) + c_1^2 \arcsin\left(\frac{x_r}{Rc_1}\right) - c_2^2 \arcsin\left(\frac{x_r}{Rc_2}\right)} \quad (8)$$

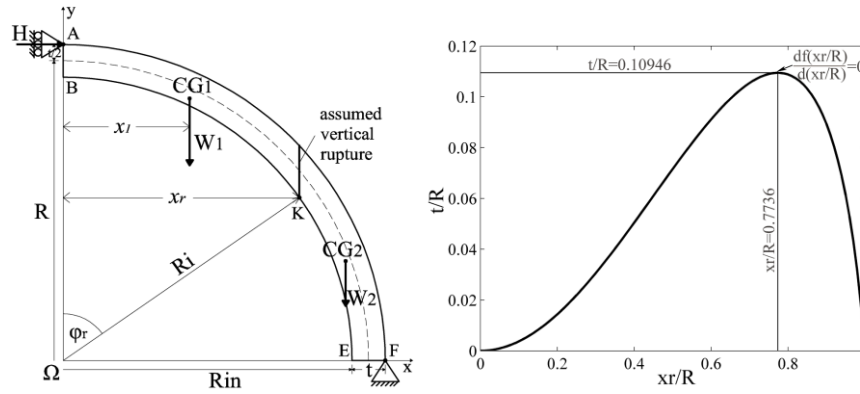


Figure 3. Left: Formation of a hinge mechanism by assuming that the rupture at the intrados hinge K happens along the vertical direction. Right: Admissible values of  $t/R$  for a given rupture location  $x_r/R$  as they result from moment equilibrium of the hinged mechanism shown in Fig. 3 left. The principle of stationary potential energy ( $\delta V(x_r/R)=0$ ) indicates that the hinged semicircular arch with a vertical rupture is in equilibrium when  $df(x_r/R)/d(x_r/R)=0$ . This happens when  $x_r=0.7736R$  and the corresponding minimum thickness is  $t/R=0.10946$ .

In Eqs. (7) and (8),  $x_r=Rc_2\sin(\varphi_r)$  is the unknown abscissa of the rupture of the arch; while,  $c_1$  and  $c_2$  are the dimensionless quantities

$$c_1 = 1 + \frac{1}{2} \frac{t}{R}, \quad c_2 = 1 - \frac{1}{2} \frac{t}{R} \quad (9)$$

With reference to Fig. 3 (left), moment equilibrium of the top portion of the arch ABK about hinge K gives

$$H\left(R + \frac{t}{2} - y_{in}(x_r)\right) = W_1(x_r - x_1) \quad (10)$$

while moment equilibrium of the entire half arch about hinge F gives the expression of the horizontal thrust-force at the crown  $H$

$$\frac{H}{W} = 1 - \frac{1}{\pi} \frac{4 + \frac{1}{3} \frac{t^2}{R^2}}{2 + \frac{t}{R}} \quad (11)$$

The calculus that follows is identical to the calculus that has been presented in the case of a polar coordinate system (Eqs. (2) to (5)); therefore, the symmetric hinged arch with a vertical rupture at point K is in an equilibrium state ( $\delta V(x_r/R)=0$ ) if and only if

$$\frac{df(\frac{x_r}{R})}{d\frac{x_r}{R}} = \frac{d(\frac{t}{R})}{d\frac{x_r}{R}} = 0 \quad (12)$$

Numerical processing of the graph appearing in *Fig. 3* (right) shows that the maximum of the graph  $df(x_r/R)/d(x_r/R)$  happens at  $x_r=0.7736R$  which corresponds to a rupture angle  $\varphi_r=B\Omega K=54.923^\circ$  and a minimum thickness value  $t/R=0.10946$ . Heyman [13] incorrectly assumed that the line of action of the resultant thrust-force is tangent to the intrados of the arch—therefore tangent to the minimum thrust-line at point K; and this was the origin of the slight error in the calculation of his minimum thickness,  $t/R=0.106$ ; rather than the correct value  $t/R=0.1075$  ([10,16-20]). Furthermore, Heyman's [13] solution remains unconservative regardless the stereotomy exercised on the arch—even if one assumes vertical joints (Heyman [10]).

The results for the minimum allowable thickness and the rupture location of a semicircular monolith with zero tensile strength subjected to its own weight is summarized in Table 1 together with the list of past publications which derived the correct results with various approaches.

*Table 1.* Minimum allowable thickness and rupture locations of a semicircular monolith with zero tensile strength

Radial cuts – Polar Coordinate System		Vertical cuts – Cartesian Coordinate System	
Rupture angle $\varphi_r=B\Omega K=54.484^\circ$	Minimum thickness $t/R=0.10748$	Rupture angle $\varphi_r=B\Omega K=54.923^\circ$	Minimum thickness $t/R=0.10946$
M. Milankovitch [8,9]: Geometric Solution J. Ochsendorf [15]: Trial-and-error solution of the “work balance” equation This work: Principle of Stat. Potential Energy		This work: Principle of Stationary Potential Energy	

#### 4 CONCLUSIONS

This paper revisits the limit equilibrium analysis of a semicircular monolith with zero tensile strength and radius  $R$ . When the monolith assumes its minimum thickness  $t$ , a symmetric five hinge mechanism is imminent and at this state any physically admissible thrust-line shall pass by the extrados springing points and be tangent to the extrados at the center of the crown of the arch. The paper shows that Milankovitch's [8,9] solution,  $t/R=0.1075$ , is not unique and that it depends on the stereotomy exercised and the associated coordinate system. The adoption of a cartesian coordinate system yields a neighboring thrust-line and a different, slightly higher value for the minimum thickness ( $t/R=0.1095$ ). This result has been obtained in this paper with a variational formulation which emerges as a powerful analysis tool that is liberated from the concept of the thrust-line ([16-20]).

## ACKNOWLEDGMENTS

Financial support for this study has been provided by the project “SeismoRockBridge” No 2295 which is implemented under the "ARISTEIA" Action of the "OPERATIONAL PROGRAMME EDUCATION AND LIFELONG LEARNING" and is co-funded by the European Social Fund (ESF) and Greek National Resources.

## REFERENCES

- [1] Hooke, R, *A description of helioscopes, and some other instruments*, London, 1675.
- [2] Heyman, J, *Structural Analysis: A Historical Approach*, Cambridge University Press, Cambridge, 1998.
- [3] O’Dwyer, D, “Funicular analysis of masonry vaults”, *Comp. Struct.*, Vol. 73, pp.187-197, 1999.
- [4] Block, P, DeJong, M, Ochsendorf, “As Hangs the Flexible Line: Equilibrium of Masonry Arches”, *Nexus Netw. J.*, Vol. 8, pp. 13-24, 2006.
- [5] Couplet, P, *De la poussée des voûtes*, Histoire de l’Académie Royale des Sciences, pp. 79-117, 117-141. Académie royale des sciences, Paris, 1729, 1730.
- [6] Foce, F, “On the safety of the masonry arch. Different formulations from the history of structural mechanics”, *Essays in the history of theory of structures*, (ed. S. Huerta), pp. 117-142, Instituto Juan de Herrera, Madrid, 2005.
- [7] Albuérne, A, Huerta, S, “Coulomb’s theory of arches in Spain ca. 1800: the manuscript of Joaquín Monasterio”, *Proc. 6th int conf. on Arch Bridges (ARCH’10)* (ed. B. Chen & J. Wei), pp. 354-362, College of Civil Engineering, Fuzhou University, Fuzhou, China, 2010.
- [8] Milankovitch, M, *Beitrag zur Theorie der Druckkurven*, Dissertation zur Erlangung der Doktorwürde, K.K. technische Hochschule, Vienna, 1904.
- [9] Milankovitch, M, “Theorie der Druckkurven”, *Zeitschrift für Mathematik und Physik*, Vol. 55, pp. 1-27, 1907.
- [10] Heyman, J, “La Coupe des Pierres”, *Proc. 3rd int. cong. on Construction History*, Vol. 2, pp. 807-812, Neunplus1, Berlin, 2009.
- [11] Lamé, MG, Clapeyron E, “Mémoire sur la stabilité des voûtes”, *Annales des mines*, Vol. 8, pp. 789-836, 1823.
- [12] Timoshenko, SP, *History of Strength of Materials*, McGraw-Hill Book Company, Inc., New York, 1953.
- [13] Heyman, J, “The safety of masonry arches”, *Int. J. Mech. Sci.* Vol. 11, 363-385, 1969.
- [14] Moseley, H, *The mechanical principles of engineering and architecture*, London, 1843.
- [15] Ochsendorf, J, *Collapse of masonry structures*. PhD thesis, Department of Engineering, University of Cambridge, Cambridge, U.K, 2002.
- [16] Alexakis, H, Makris, N, “Minimum thickness of elliptical masonry arches”, *Acta Mechanica*, Vol. 224, pp. 2977-2991, 2013.
- [17] Makris, N, Alexakis, H, *From Hooke’s “Hanging Chain” and Milankovitch’s “Druckkurven” to a variational formulation: The adventure of the thrust-line of masonry arches*, Report series in EEAM 2012-02, Sept. 2012, University of Patras, Greece, 2012.
- [18] Makris, N, Alexakis, H, “The effect of stereotomy on the shape of the thrust-line and the minimum thickness of semicircular masonry arches” *Arch Appl Mech*, Vol. 83, pp. 1511-1533, 2013.
- [19] Alexakis, H, *Limit state analysis and earthquake resistance of masonry arches*, PhD thesis (in Greek), Febr. 2013, Department of Civil Engineering, University of Patras, Greece, 2013.
- [20] Alexakis, H, Makris, N, “Limit equilibrium analysis and the minimum thickness of circular masonry arches to withstand lateral inertial loading” *Arch Appl Mech*, Vol. 84, 757-772, 2014.

## **TOPIC 3**

Design Methods

Stability



## **APPRAISAL OF SIMPLIFIED METHODS FOR THE ANALYSIS OF BOX-GIRDER BRIDGES**

Leonidas Stavridis<sup>1</sup>, Konstantinos Spiliopoulos<sup>1</sup>, Antonia Afantenou<sup>1</sup>,  
Ioannis Kapogiannis<sup>1</sup>

<sup>1</sup>National Technical University of Athens, Dept. of Civil Engineering, Greece  
e-mail: stavrel@central.ntua.gr, kvspilio@central.ntua.gr, tonia1810@hotmail.com,  
john\_kapogiannis@hotmail.com

**ABSTRACT:** This paper has two goals. Firstly to present a simplified method of evaluation of the additional longitudinal stresses that develop under the torsional response both for rectilinear and curved bridges and secondly to perform a comparison with the results deduced from a finite element simulating the real three dimensional structure. It is proved that the simplified method provides a safe estimation of the response and may be used for preliminary design purposes.

**KEY WORDS:** Box-girder; Torsion; Simplified method; Finite element.

### **1 INTRODUCTION**

Box girders constitute generally a good choice for the superstructure of bridges and in most of the cases represent the best solution at all, thanks to their inherent capacity to overtake in the most efficient way the eventually occurring torsional response. This response in the case of rectilinear girders is due to the eccentric position of traffic loading, whereas in the case of curved bridges in plan is already permanently present due to the girder self-weight alone, apart from any eccentricity of the incoming live loads.

Although under a given torsional moment diagram in a girder no longitudinal stresses are developed according to the classical technical theory of torsion, the existing overall girder deformability as a thin walled section leads generally to such stresses. These stresses are of rather negligible intensity according to the theory of “warping torsion” if the deformability of the cross section profile is prevented by some inserted transversal diaphragms along the girder, but in their absence – as it is constructionally always preferred – the existing deformability of the cross section leads to substantial longitudinal stresses in addition to the shear stresses developed according to the classical Bredt theory of torsion. It is obvious that the above longitudinal stresses have to be superposed with those due to the longitudinal bending moments of the girder.

To account for this effect formulas have been suggested on the basis of simulating the cross section profile as a folded plate ([1]-[3]). The present work examines the accuracy of this approximation using a closer to reality simulation with the aid of 3D finite elements. Both rectilinear and curved girders are examined. The comparison shows that the formulas provide conservative results, are on the safe side and may be used for preliminary design purposes.

## 1. RECTILINEAR GIRDERS

### 1.1 General loading case

In the typical box section of Fig. 1, an eccentric layout of the traffic load is shown.

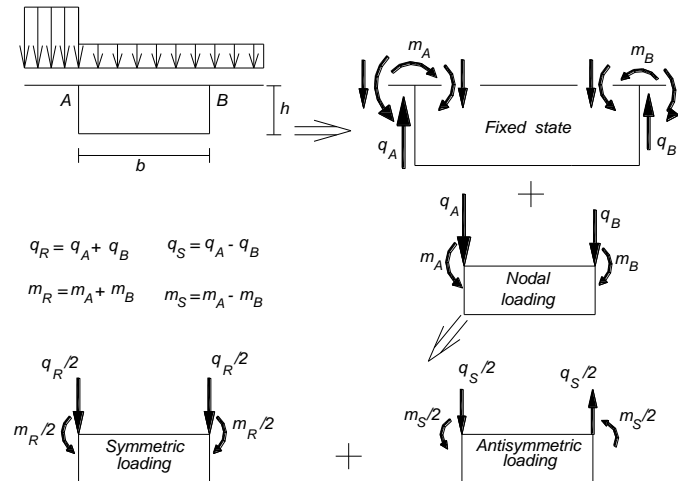


Figure 1. Resolution of eccentric load actions

It may be considered that the state of stress of the girder results from the superposition of the fixed state (I) containing the loads with the appropriate nodal actions and of the state (II) containing only these opposite nodal actions  $q_A$  and  $m_A$ , together with  $q_B$  and  $m_B$ .

The fixed state (I) is a trivial one and can be determined directly, so that the state (II) is considered only. This state - provided the section is symmetric- may be always split in a symmetric and an anti-symmetric part.

As the symmetric loading does not present any other peculiarity, the whole problem is essentially shifted to the anti-symmetric loading part. This one acts as a distributed torsional load  $m_D = (q_S/2) \cdot b + m_S$ .

In the present work only an anti-symmetric edge line load  $q_S$  will be considered. In this case  $m_A = m_B = m_S = m_R = 0$ .



### 1.2 Response due to the deformability of the profile section

The imposed torsional loading causes deformation of the closed section, resulting to longitudinal bending of the section walls, which is coupled with the resulting transverse bending of the section profile itself ([1]). It is pointed out that this response comes additionally to the initially existing Bredt shear flow in the section walls.

In order to investigate the influence of the deformability of the section on the response, the equilibrium of a cut-out girder strip of unit length is at first considered with the antisymmetric loads  $q_s/2$  acting at the section edges  $A$  and  $B$  (Fig. 2). It is clear that the segment is in equilibrium under the above external forces and the differential shear flow  $\Delta v$ , which is obtained as the resultant of the occurring Bredt shear flows on the two faces of the strip considered.

Given that the torsional moment along the beam is  $M_T$ , the shear flow is  $v = \frac{M_T}{2F_k}$ . From the strip equilibrium it turns out:  $\Delta v = \frac{q_s b_0}{4F_k}$

According to the section dimensions appearing in Fig. 1 it is:  $F_k = hb$ .

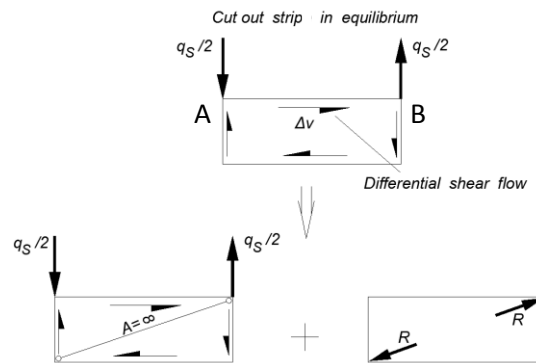


Figure 2. Static analysis of the deformable cross section under load

Obviously, the examined strip tends to deform under the forces  $q_s/2$  and  $\Delta v$ . This deformation consists essentially in a change of length of its diagonals and induces an additional state-of-stress for each section wall. So it is considered appropriate to insert a hinged strut of an infinite axial stiffness along the diagonal (Fig. 2). It is clear that this diagonal element develops a tensile axial force  $R$  (kN/m) distributed along the length of the girder. Applying now the opposite of the acting forces  $R$  on the respective longitudinal edges of the girder in the absence of the diagonal strut, it is obvious that the superposition of the thus resulting state-of-stress with the one of the blocked strip, will give the final response (Fig. 2).

To examine this last ‘diagonal loading’ it is at first considered that the forces  $R$  act on a girder having hinged connections at the section edges instead of

monolithic ones (Fig. 3). The forces  $R$  may be resolved equivalently at each edge into the two concurring walls, therefore each one of them can be considered as a longitudinal beam loaded by the corresponding component, developing bending moments  $M_0$  and corresponding normal stresses  $\sigma$ , according to the classical theory of bending. However the resulting strains  $\sigma/E$  at the common edges of the walls with the slabs are not equal -as they should be - and for this reason some distributed longitudinal forces have to be additionally introduced along the edges of each wall, in order to establish the strain compatibility at each edge. It is clear that in this way the initially determined normal stresses  $\sigma$  will be changed.

By following the above analysis, the determination of the longitudinal axial stresses is possible. For example, if we concentrate on the left web of the hinged box section, they can be determined through the classical bending formula on the basis of the moment  $M_0$ . It is proved [1] that the moment of inertia  $I^*$  used is slightly larger than the normal value  $I_w$  for the web by a factor  $k^w$  and the new 'neutral axis' lies at a distance  $y_0$  from the top fiber, which is somewhat less than its 'normal value', i.e. the half of the web height.

The moment  $M_0$  results from the loading of the left web with the respective component  $R_w$  of the 'diagonal force'  $R$ . It is found that:  $R_w = R \cdot h / s$ , where  $s$  is the length of the diagonals. Thus it is:

$$\sigma_o = -\frac{M_0}{I^*} y_0, \sigma_u = \frac{M_0}{I^*} (h - y_0) \quad (1)$$

where  $I^* = I_w k^w$

Furthermore it is found:  $k^w = \frac{1}{2} \frac{(\alpha_0 + 2)^2 - 1}{3 + \alpha_0}, y_0 = \frac{1}{2} h$

with  $\alpha_0 = \frac{t_0 b}{t_w h}$ , where  $t_0, t_w$  represent the thickness of both the flanges and of both the webs respectively.

The longitudinal web-beam obeys the following typical differential equation

$$EI^* \frac{d^4 w}{dx^4} = R_w \quad (2)$$

where  $R_w$  and  $I^*$  represent the initial distributed web loading and the equivalent moment of inertia respectively, as explained above. It is noted that  $w$  represents the in-plane deflection of the web and it is due merely to the assumed deformability of the section.

One may now account for the monolithic connection of the section walls.

The bending deformation of the hinged section profile, under the action of diagonal forces  $R$ , has as a consequence the increase of its diagonal length by  $d$  (Fig. 3). However, this change cannot be realised without any resistance, given that the transverse stiffness  $C$  of the closed monolithic section profile is automatically mobilised. This stiffness is expressed through the relation  $r = dC$ ,

as that diagonal pair of forces  $r$  required to produce the deformation  $d$  ( $C$  may be evaluated as the required diagonal force to cause a unit elongation of the closed frame diagonal).

Then the tendency of the hinged section profile to be deformed by  $d$ , is counteracted by the resistance  $r$  of the monolithic closed frame and in this way the web is subjected, apart to its ‘initial’ loading  $R_w$  also to the loading of the component  $r_w$  of the force  $r$ , obviously with the opposite sense. In the same way as before:  $r_w = r \cdot (h / s)$ .

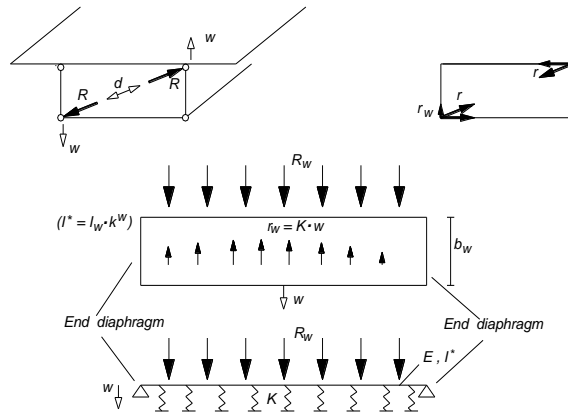


Figure 3. Equivalent beam on elastic foundation

Taking into account that the bending deformation  $w$  of the web may be expressed through the diagonal deformation  $d$  by the relation  $d = wD$ , where:

$$D = \frac{4h}{s} = \frac{4h}{\sqrt{h^2 + b^2}} \tag{3}$$

it is found that the component  $r_w = wDC(h / s)$ . Using  $K = DC(h / s)$  one may write down the differential equation for the web beam restored to the rigid section profile, and

$$EI^* \frac{d^4 w}{dx^4} = (R_w - r_w) = R_w - wK \tag{4}$$

taking finally the form:

$$EI^* \frac{d^4 w}{dx^4} + Kw = R_w \tag{5}$$

This equation is recognized as the typical equation of a beam on elastic foundation with modulus of subgrade reaction  $K$ . Indeed, the web is carried by the elastic support offered by the profile resistance when undergoing diagonal deformation.

## 2 CURVED GIRDERS

The box girder is particularly suitable for bridges curved in plan. These bridges have a permanent torsional response caused even by non-eccentric loads, as e.g. the self-weight of the girder.

### 2.1 Determination of bending and torsional response

The girder is assumed to have a constant radius of curvature equal to  $R$ . The loading consists of a vertical distributed load  $q$  passing through the shear centre of the cross-section. It is reminded here that exactly as in the case of grids, any part of the beam must satisfy three conditions of equilibrium, namely with respect to vertical forces, as well as with respect to the projections of moment vectors on two arbitrary horizontal axes.

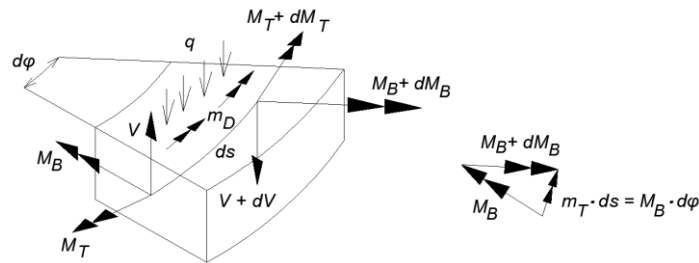


Figure 4. Equilibrium of a curved box girder segment

The equilibrium equations of an elementary segment of length  $ds$  forming an angle  $d\varphi$  ( $1/R = d\varphi/ds$ ), may be written in the form:

$$\frac{d^2 M_B}{ds^2} = - \left( q - \frac{1}{R} \frac{dM_T}{ds} \right) \quad (6)$$

$$\frac{dM_T}{ds} = - \left( \frac{M_B}{R} + m_D \right) \quad (7)$$

If the arc span length  $L$  is much smaller than the radius of curvature  $R$ , (i.e.  $L/R < 0.3$ ) it may be concluded that the term  $-(1/R) \cdot (dM_T/ds)$  on the right side of equation (6) is much smaller than  $q$ .

Thus, the first equation results to:  $\frac{d^2 M_B}{ds^2} = -q$

i.e. resembling the equilibrium relation of a rectilinear beam between bending moment and load. This means that, under the above conditions, the bending moments of the curved girder may be approximated by the bending moments of a straight beam of span  $L$  equal to the arch length of the girder. This equivalence is illustrated in the Fig.5.

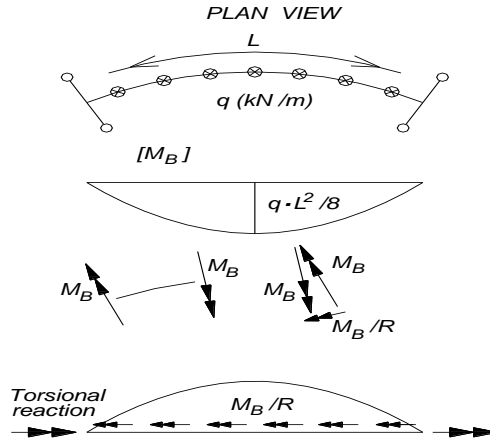


Figure 5. Static analysis of a curved beam in plan

### 2.2 The response of the cross sectional walls

The torsional response of the girder implies, beyond the Bredt peripheral flow, an additional response for the box section walls. This response results from the way the gravity loads are introduced to the girder.

First it should be noted that the acting compressive forces  $D$  and tensile forces  $Z$  in the curved top and bottom flanges respectively, cause distributed deviation forces  $q$ .

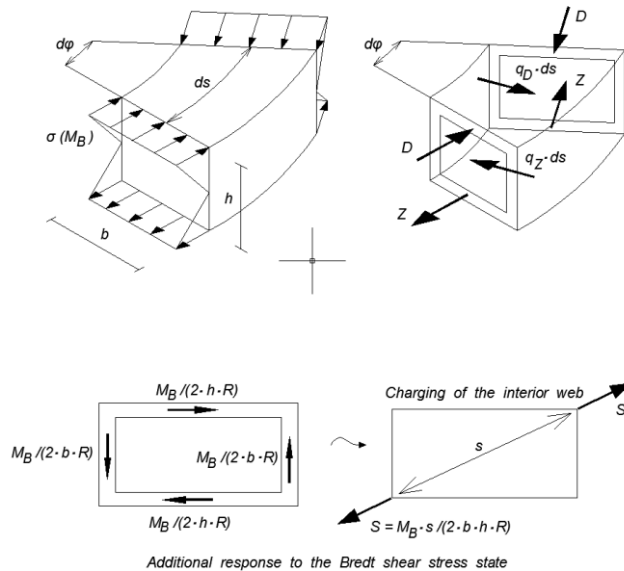


Figure 6. Static analysis of the deformable cross section of the curved girder under load

It is clear from Fig.5, that the transversely distributed equal and opposite forces  $q_D$  and  $q_Z$ , which the top and bottom slab is obliged to take up respectively, create a torsional load per unit of curved length, being nothing else than the one resulted from the vectorial variation of bending moments, as it was examined in the previous section. It is [2]:

$$q_D = \frac{D}{R} = \frac{M_B}{hR}, \quad q_Z = \frac{Z}{R} = \frac{M_B}{hR} \text{ and given that } D=Z \text{ we have } q_D h = \frac{M_B}{R}$$

Thus, it can be seen that, even without the action of an externally applied torsional moment  $m_D$ , merely the existence of bending along a curved axis implies the imposition of a distributed torsional load ( $M_B/R$ ), according to equation (7): The cut out strip of unit length, receiving the forces  $q_D$  and  $q_Z$  at its top and bottom side respectively, is in equilibrium with the developed Bredt shear flow at both its faces (Fig. 5). The resultant of these two flows is the so-called *differential shear*. According to Bredt's formula it is:

$$\frac{dv}{ds} = \frac{dM_T}{ds} \frac{1}{2bh} = - \frac{M_B}{2bhR} \quad (8)$$

Thus the strip being in equilibrium as a plane structure, under the loads  $q_D$ ,  $q_Z$  and  $dv$ , gives rise to the self-equilibrated diagonal loading of the profile

$$S = \frac{M_B}{2R} \sqrt{\frac{1}{b^2} + \frac{1}{h^2}} \quad (9)$$

as shown in the figure, which causes longitudinal bending of the walls as well as transverse bending of the section profile, as it has been examined in detail for the rectilinear girder.

Although the analogy is not quite accurate, for the preliminary design needs and for ratios  $L/R < 0.3$ , it may be considered that the left web wall takes the downward parabolically distributed along the length of the girder according to the Fig. 5 load  $S_w = M_B / (2 \cdot R \cdot b)$ , acting, as in the case of rectilinear beam, like a beam resting on an elastic foundation with a 'subgrade modulus'  $K$ , as examined previously.

### 3 NUMERICAL EXAMPLES

The above theory was tested on two simply supported box girder bridges, a straight one and a curved one. Both the bridges of a 40m span were designed to have a cross section with  $b=6.2\text{m}$  and  $h=2.5\text{m}$ , top and bottom slab of thickness of 0.25m and a web thickness of 0.5m.

#### 3.1 Straight bridge

The straight box-girder bridge was subjected to a couple of anti-symmetric line loads extending over 8m symmetrically about the mid-point of the bridge. 4466 shell elements were used to discretise the girder. The results of the FE program

[4] (Fig.7) showed a value of approximately 345 KN/m<sup>2</sup> at the top and bottom of the element located at the middle of the bridge. The beam on elastic foundation having inertia and spring data according to section 1.2, was loaded by a uniform load spanning 8 m, over the centre, and provided a respective value of 465 KN/m<sup>2</sup>, meaning a difference of roughly 35 %, showing that the theory is quite conservative and on the safe side.

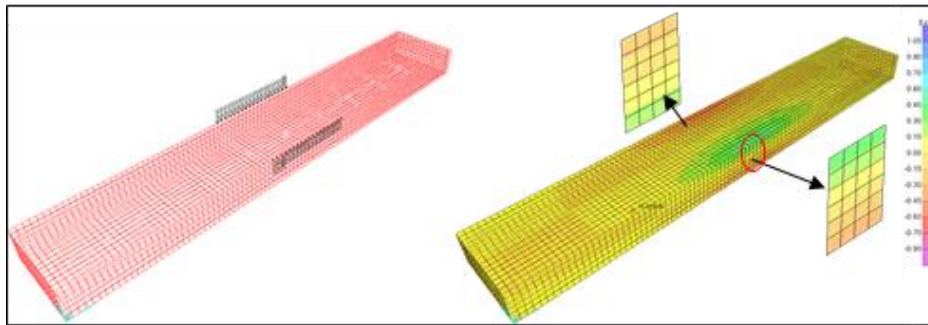


Figure 7. 3D FE results and distribution of stresses along the middle section

### 3.2 Curved Bridge

The discretization of the bridge with 4466 shell elements may be seen in Fig. 8.

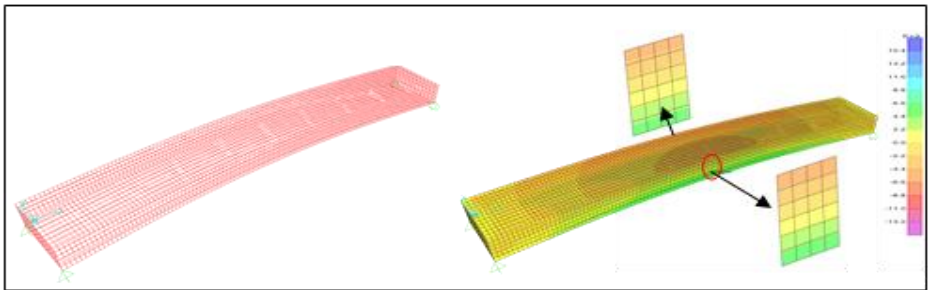


Figure 8. 3D FE results and distribution of stresses along the middle section

SAP2000 Results				Theory Results			
-5937		-6560		-6521		-7545	
outer	[Diagram of a rectangular cross-section with thick top and bottom flanges]		inner	outer	[Diagram of a rectangular cross-section with thick top and bottom flanges]		inner
+5990		+6615		+6521		+7545	

Figure 9. Comparison of analytical and numerical results

The bridge is subjected to its own weight. According to the analysis exposed in section 2.2 a curved beam on elastic foundation having inertia and spring data the same as for the straight bridge was considered, which was loaded by a parabolic continuous loading over the whole length of the beam. This beam provided results which were superposed with those due to pure bending. The comparison with the results of the FE program [4] may be followed in Fig. 9. One may see that the theory results are on the safe side with a maximum discrepancy of approximately 15%.

#### **4 CONCLUSIONS**

The deformability of the box section of a bridge girder under a torsional response leads to non-negligible longitudinal stresses which can't be predicted according to the classical theory of torsion (Bredt). However, following the deformability of the folded plate system it is possible to derive the above stresses using a methodology reducing the whole problem to the response of a beam on elastic foundation both for the rectangular and the curved girder. Comparison with FE results shows that this methodology leads to results lying on the safe side making it suitable for preliminary design purposes.

#### **REFERENCES**

- [1] Schlaich J., Scheef H, *Concrete Box-Girder Bridges*, Zurich: IABSE Structural Engineering Documents, 1982.
- [2] Menn, C. *Prestressed Concrete Bridges*, Birkhäuser Verlag, Basel 1996.
- [3] Stavridis, L.T., *Structural systems: behaviour and design*, Thomas Telford, 2010.
- [4] SAP 2000, User's manual, 2012.



## INVESTIGATION ON STABILITY PROBLEMS OF PIERS WITH PRACTICALLY INFINITE BENDING STIFFNESS

Elisabeth Karatzas Roussou<sup>1</sup>, Velvet Karatzas<sup>2</sup>, George Karydis<sup>3</sup>,  
Theodore Konstantakopoulos<sup>4</sup>

<sup>1</sup> Karatzas Consultant Engineers, Greece

<sup>2,3</sup> Karydis and Associates, Greece

<sup>4</sup> Konstantakopoulos Consultant Engineers, Greece

e-mail: ikara@tee.gr, velvet@karatzas.gr, info@karydis.gr, theokons@teemail.gr

**ABSTRACT:** Structural failure is governed by excessive deflection. The same is true for foundation failure. Therefore, it is evident that determining the deflection that occurs under certain loadings proves to be a handy tool in the assessment of the structure's behavior. In this paper, the calculation method is shown of the  $P_{limit\ load}$  that a structure can undertake, taking into consideration its actual deformations, boundary conditions of the restraint supports (foundations), and the construction imperfections using spring rotational constants. Note that the  $P_{limit\ load}$  is less than the  $P_{critical\ joint\ load}$  due to the existence of second order theory moments. The method presented defines the actual resistance for a structure with compression members whose slenderness is  $(\lambda) \leq 25$ , commonly found in seismic regions i.e. strong piers and their respective foundations.

**KEYWORDS:**  $P_{critical\ joint\ load}$ ;  $P_{limit\ load}$ ; deflection angles; boundary limits.

### 1 INTRODUCTION

During design, while dimensioning a compression member engineers usually check the member against Euler's critical load. This criterion always holds true when the slenderness ratio of the compression member is small ( $\lambda < 25$ ) and its bending stiffness ( $EI$ ) is infinite, i.e. large shear walls. Unfortunately, this check does not ensure that the structure is failure-proof. Hence, it was proposed to introduce an additional check that of the  $P_{critical\ joint\ load}$ . However, the  $P_{critical\ joint\ load}$  is a stability check directly related to the overall structural shape/form of the structural system. It does not ensure though, that the individual structural members and/or their restraints have the required resistance capacity in case a boundary limit is reached. In fact, individual structural members of a structural system may fail under certain loading less than the  $P_{critical\ joint\ load}$ . Hence, it is of interest to determine the member's and/or its restraint resistance capacity. In

other words, the aim of this paper is to determine the actual limit load in relation to deflection.

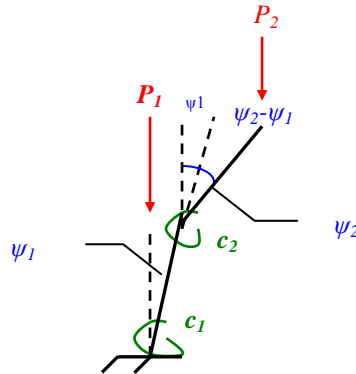


Figure 1. Two member structural model.

## 2 STRUCTURAL ANALYSIS

Considering Fig. 1 above, the following equations are derived:

$$(P_1 + P_2 + \dots P_n) \cdot h_1 \cdot \sin(\psi_1) + c_2 \cdot (\psi_2 - \psi_1) = c_1 \cdot \psi_1 \tag{1}$$

$$(P_2 + \dots P_n) \cdot h_2 \sin(\psi_2) + c_3 \cdot (\psi_3 - \psi_2) = c_2 \cdot (\psi_2 - \psi_1) \tag{2}$$

Where  $P$ =load,  $h$ = height,  $\psi$ =deflection angle, and  $c$ =spring rotational constant. Thus, for  $n$  number of members:

$$(P_{n-1} + P_n) \cdot h_{n-1} \cdot \sin(\psi_{n-1}) + c_n \cdot (\psi_n - \psi_{n-1}) = c_{n-1} \cdot (\psi_{n-1} - \psi_{n-2}) \tag{3}$$

Solving further, the following equation is derived:

$$P_n \cdot h_n \sin(\psi_n) = c_n \cdot (\psi_n - \psi_{n-1}) \tag{4}$$

due to very small rotational angles, the following is true

$$\left[ (P_1 + P_2 + \dots P_n) \cdot h_1 - c_2 - c_1 \right] \cdot \psi_1 + c_2 \cdot \psi_2 = 0 \tag{5}$$

$$c_2 \cdot \psi_1 + \psi_2 \left[ (P_2 + \dots P_n) \cdot h_2 - c_3 - c_2 \right] = -c_3 \cdot \psi_3 \tag{6}$$

$$(P_{n-1} + P_n) \cdot h_{n-1} \cdot \psi_{n-1} + c_n \cdot (\psi_n - \psi_{n-1}) = c_{n-1} \cdot (\psi_{n-1} - \psi_{n-2}) \tag{7}$$

---


$$c_n \cdot \psi_{n-1} + \psi_n \cdot (P_n \cdot h_n - c_n) = 0: \tag{8}$$

From this homogeneous system of equations when the matrix denominator is equal to zero ( $N=0$ ), one can determine  $P_{critical\ joint\ load}$ . Next, from equations 4, 5, 6... one can determine the rotational angle ratio i.e.  $\psi_1/\psi_2, \dots, \psi_{n-1}/\psi_n$ . In other words, one may compute the minimum failure load and its possible respective structure's deformation mechanism figure. From these calculations one obtains the minimum deflection angle ratio for a  $P_{critical\ joint\ load}$ , but not the actual absolute value of each deflection angle. Thus, it is classified as an eigenvalue problem. However, there cases, where it is of importance to estimate the limit range of the magnitude of the deflection angles, in order to assess the structural safety limit and/or their possible failure mechanism. These are the cases where one needs to know the actual limit load.

Hence, rearranging the initial equations it is obtained that:

$$c_2 \cdot \psi_2 = [c_1 + c_2 - (P_1 + P_2 + \dots P_n) \cdot h_1] \cdot \psi_1 \tag{9}$$

$$c_3 \cdot \psi_3 = [c_1 + c_2 - (P_2 + \dots P_n) \cdot h_2] \cdot \psi_2 - c_2 \cdot \psi_1 \tag{10}$$

.....

$$c_n \cdot \psi_n = [c_n + c_{n-1} - (P_{n-1} + P_n) \cdot h_{n-1}] \cdot \psi_{n-1} - c_{n-1} \cdot \psi_{n-2} \tag{11}$$

$$(c_n - P_n \cdot h_n) \cdot \psi_n = c_n \cdot \psi_{n-1} \tag{12}$$

Since the original equations contain circular functions (sine and cosine), they are generally solved by iteration. Thus, the actual magnitude/size of the angles is estimated theoretically like this: from equation (9) for an initial estimation value of  $\psi_1^0$ , angle  $\psi_2^0$  is computed. Then, using equation (10)  $\psi_3^0$  is computed. Similarly,  $\psi_4^0$  is found using equation (11). This procedure is repeated until the two values for the angle  $\psi_n^0$  obtained from either side of the equation are almost the same. In the case that the two values are not acceptably close, the procedure is carried out again until the outcomes match. This procedure may also be carried out with a simple PC program or spreadsheet. The questions that rise are how does one estimate the initial value  $\psi_1^0$  to begin the iteration procedure and what is an acceptable deflection interval  $\Delta(\psi_1^0 - \psi_1^1)$  for two consecutive values. That is problem that the designer has to assess each time.

### 3 ESTIMATION OF THE DEFLECTION ANGLES RANGE FOR A CERTAIN STRUCTURAL LOADING

The system of equations (5) ...(8), has more than just one apparent solution ( $\psi_{1,n}=0$ ) that defines the eigenvalues of the system. But, only the critical eigenvalues are of interest to the designer. From the boundary conditions of the

structure, i.e. allowable soil stress, one estimates the magnitude of the deflection angles for that particular loading condition. Thus, based on the structural loads, the bending moments acting upon the foundation of the structure are obtained. Then, from the known geotechnical relationships, one determines the allowable soil stress for the maximum allowable moment. The difference between these two moments  $\Delta M = M_{\text{max allowable}} - M_{\text{actual}}$  results in a range of additional moments (second order theory) and within this range lies an interval with the respective deflection angles. Therefore, two possible variable values for the deflection angles may be obtained. In the example presented below, a method for solving this type of problem is shown.

### a. Discussion on equation (13)

The calculation of  $P_{\text{limit load}}$  is achieved using the following equations that have been derived from rearranging the previous equations. Therefore,

$$\psi_2 = \left(1 + \frac{c_1}{c_2} - \frac{P_1 + P_2 + \dots + P_n}{c_2} \cdot h_1\right) \cdot \psi_1 \quad (13)$$

$$\psi_3 = \left(1 + \frac{c_2}{c_3} - \frac{P_2 + \dots + P_n}{c_3} \cdot h_2\right) \cdot \psi_2 - \frac{c_2}{c_3} \cdot \psi_1 \quad (14)$$

Therefore, for  $n$  number of members:

$$\psi_n = \left(1 + \frac{c_{n-1}}{c_n} - \frac{P_n + P_{n-1}}{c_n} h_{n-1}\right) \cdot \psi_{n-1} - \frac{c_{n-1}}{c_n} \cdot \psi_{n-2} \quad (15)$$

$$\psi_{n-1} = \left(1 - \frac{P_n}{c_n} \cdot h_n\right) \cdot \psi_n \quad (16)$$

### b. Investigation of equation (13)

Equation (13) offers significant information for the assessment of structural behavior. Rewriting equation (13):

$$\frac{\psi_2}{\psi_1} = 1 + \frac{c_1}{c_2} - \frac{P_1 + P_2 + \dots + P_n}{c_2} \cdot h_1 \quad (17)$$

It is found that, the ratio of the deflection angles  $\psi_2/\psi_1$  depends upon the constant number 1, the ratio of spring rotational constants  $c_1/c_2$ , and the ratio of the total axial loads times the height of the first structural member with the respective spring constant  $c_2$  regardless the number of structural members (or storeys). Hence, during the design process it is quite easy to assess a future behavior, since it is quite easy to determine  $c_1$ ,  $c_2$ ,  $h_1$ ,  $P_1$ , ...,  $P_n$ . From these values, one may compute the deflection angle ratio  $\psi_1$ ,  $\psi_2$  that prevails in the structural failure assessment.

It is also found that when the rotational spring constant ratio is  $c_1/c_2 \leq 1$  that means  $c_2 > c_1$  then, a smaller deflection angle ratio results and hence, the convergence of the values for the homogeneous system  $\psi_1, \psi_2, \dots, \psi_n$  is achieved at a safer and faster rate.

**4 EXAMPLE**

In the 7<sup>th</sup> Annual Congress of Geotechnics 2010 that took place in Volos, Greece, a paper with the title “*Experimental Validation of Bridge Pier Seismic Design Employing Soil Ductility*” [2] was presented. The paper shows the behavior and the points of failure of the two piers with respect to their foundations as tested in different experiments that took place in the National Technical University of Athens (see Fig. 2 below). Now, an effort is made to explain why the pier in the first case and the foundation on the other case failed the way they did using the term  $P_{limit\ load}$  discussed in this paper. This case study is used as an example along with the book called “*Statik and Stabilitat der Baukonstruktionen*” [3] as reference.

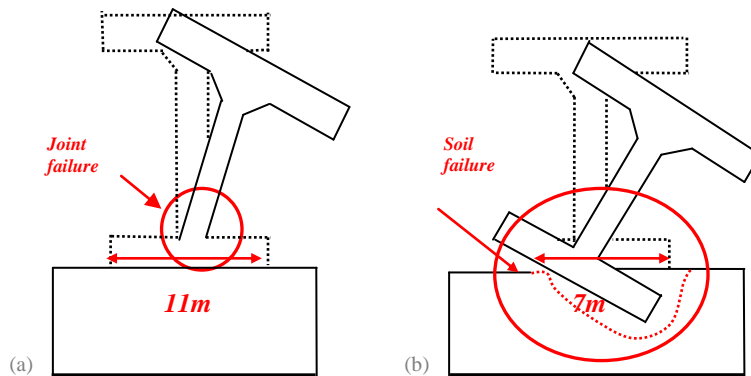


Figure 2. Piers and their foundations with their points of failure.

Assume that the pier and its respective foundation act as a two member model, where the foundation is member 1 and the pier is member 2. Also, consider as a given that the superstructure’s loads are 12000 kN and the pier’s loads are 2200 kN. First the spring rotational constants are found as:

$$c_1 = 9.29 \cdot 10^{12} Ncm/1 \quad \text{for the 11m foundation (large)}$$

$$c_1 = 2.095 \cdot 10^{12} Ncm/1 \quad \text{for the 7m foundation (small)}$$

$$c_2 = 1.0125 \cdot 10^{12} Ncm/1 \quad \text{for the pier}$$

Next, the respective  $P_{critical\ joint\ load}$  are determined using equations (5) and (6). Due to space limitations, the actual computations will be omitted and will be shown during the presentation. Thus, it is found that equations (5) and (6) become:

$$\begin{aligned} [(0,183 \cdot P + P) \cdot 0,25 \cdot h - 0,11 \cdot c - c] \cdot \psi_1 + 0,11 \cdot c \cdot \psi_2 &= 0 \\ 0,11 \cdot c \cdot \psi_1 + \psi_2 [(P) \cdot h - 0,11 \cdot c] &= 0 \end{aligned}$$

And the following 2<sup>nd</sup> order equations result:

$$0.296 \cdot h^2 \cdot P^2 - 0.142 \cdot h \cdot P + 0.11 \cdot c^2 = 0 \text{ for the large foundation and}$$

$$0.296 \cdot h^2 \cdot P^2 - 1.548 \cdot h \cdot P + 0.48 \cdot c^2 = 0 \text{ for the small foundation.}$$

Hence, for the large foundation:

$$P_{critical\ joint\ load} = 770,000 \text{ kN}, \psi_1 = 0.09945\psi_2 \text{ and } \psi_2 = 10.0548\psi_1$$

Similarly, for the small foundation:

$$P_{critical\ joint\ load} = 570,000 \text{ kN}, \psi_1 = 0.227\psi_2 \text{ and } \psi_2 = 4.403\psi_1$$

Next, the designer must check if the natural frequencies of the structure are close to the resonance frequency that produces additional dynamic loading. Applying the natural frequency equation shown below, the following results are obtained:

$$\omega = \sqrt{\frac{g}{h}} \cdot \sqrt{\frac{P_{critical\ joint\ load}}{P}} \cdot \sqrt{1 - \frac{P}{P_{critical\ joint\ load}}}$$

$\omega = 6.06 \text{ sec}^{-1}$  for the large foundation and  $\omega = 4.95 \text{ sec}^{-1}$  for the small foundation. Thus, for a dynamic loading with a frequency greater than  $\Omega = \sqrt{2} \times 6.06 = 8.54 \text{ sec}^{-1}$  and  $\Omega = \sqrt{2} \times 4.95 = 7.00 \text{ sec}^{-1}$  respectively, the structure is not be affected by dynamic loading due to resonance. Only static loads act upon the structure. Moreover, the response of the structure to dynamic loading results in oscillations with an amplitude,  $s_{dynamic}$ , that are lesser in comparison to the amplified oscillations due static loading ( $s_{dynamic} < s_{static}$ ).

### **Evaluation of the deflection angle interval under a certain loading: Large foundation**

The largest deflection  $\psi_1$  of the system occurs when the axial force resultant will cause the soil stresses greater than the allowable ones. From boundary limits such as the allowable soil stresses one may estimate the possible size of the deflection angles for that particular structural loading. Assume an allowable soil stress of  $250 \text{ kN/m}^2$ . Since the resultant lies beyond the internal core of the foundation, but within the external core then solving further for the eccentricity

$e$ , results in:  $e^* = a/2 - e = 11/2 - 3.44 = 2.07$  m therefore, the allowable moment capacity for this foundation for that given soil stress is:  $M = (12000 + 2200) \cdot 2.07 = 29394$  mkN. The respective deflection angle  $\alpha_\infty$  for circular section foundations is obtained from following equation found in DIN 4019 Part 2 where  $e \leq r/3$  and solving results in  $\alpha_\infty = 0.004627$ .

This is the maximum allowable system deflection for loads found using first order theory (a non-deflective system). However, due to second order theory (deflective system) the iteration should be confined to an interval between zero and maximum allowable deflection, otherwise surcharge pressure prevails and failure occurs. If one now wishes to narrow down this interval to shorten the iteration process, then the deflection angle that develops due to the actual must be evaluated. Assume axial loading with an eccentricity: i.e. 1.83 metres. This means that the axial loading lies near of edge of the internal core of the section and as such, a moment  $M$  equal to 26023mkN is produced. It follows that,  $\Delta\psi_1 = 0.004627 - 0.00028 = 0.004347$ .

In other words, the deflection angle interval ranges from 0 to 0.004347 and with the iteration method, after 12 loops it is obtained that:  $\psi_1=0.00002$  and  $\psi_2=0.00020342$ . The additional second order theory moments are:  $M_1 = c_1\psi_1 = 1858$  mkN,  $M_2=2060$  mkN and  $\psi_1/\psi_2 = 10.1711$ . Thus, the total moments are:  $\Sigma M_1=26023+1858=27881$  mkN < 2994mkN. Note, that they are less than the allowable moment found earlier and hence, there is no failure of the foundation as verified by the experiment. On the other hand, for the pier the actual moment was found to be 20818 mkN. The sum of the moments is 22878mKN > 20818 mkN. Thus, the pier fails due to a surcharge of second order theory moments.

### Small foundation

Acting accordingly, for comparison reasons assume the same type of loading on the structure and soil stress with a small foundation, inducing an eccentric axial loading then,  $e = a/6 = 7/6 = 1.1667 < 1.83m < 2.3334$  m. These axial loads are found within the external section's core and so the force resultant lies at a distance of 1.67m from the edge of the section. The moment produced is the same as before (26023mkN). The soil stress was found to be  $810\text{kN/m}^2 > 250 \Rightarrow$  unacceptable. Therefore, the foundation fails as verified by the experiment, despite the fact that the deflection angles may be quite small. The pier suffers from no damage whatsoever.

## 5 CONCLUSIONS

It is concluded that special consideration must be given during the design of a structure to the evaluation of the deflection ratio. This paper investigates a

method for solving second order theory stability problems with the help of spring rotational constants, for loads smaller than  $P_{critical\ joint\ load}$ , that due to the existence of second order deflections structural failure may result. This method deals with actual loads that define the true load limits of a structure with compression members whose slenderness ratio ( $\lambda \leq 25$ ), i.e. large shear walls, commonly found in seismic regions due to regulations' requirements.

From the investigation of equation (13) it is deduced that, in seismic regions where large axial accelerations may occur, i.e. significant fluctuations of axial loads, structures fail at a greater extend. That is because as observed from equation (13) a reduction in the axial loading results in an increase of the  $\psi_2/\psi_1$  ratio in relation to the increased lateral loading. Hence, it goes without say that the  $\psi_2/\psi_1$  ratio is the principle factor for evaluating structural failures.

A case study was used to present the application of this proposed methodology for dealing with stability problems. The experimental outcomes obtained from the National Technical University of Athens were verified by the analysis presented in this paper. Namely, in the case of a large foundation, the pier failed at the base due to a large second order moment that created a respective large deflection, although  $P_{critical\ joint\ load}$  was not reached. There was no failure of the soil (only small stresses developed). On the contrary, for the case with the small foundation, the soil crushed due to the formation of large stresses, while smaller moments formed at the base of the foundation and yet again,  $P_{critical\ joint\ load}$  was not reached.

## REFERENCES

- [1] Velvet Karatzas, Elisabeth Karatzas, "Instability Problems-Investigation of  $P_{critical\ joint\ load}$  under moment loads", Washington, 3rd international fib 2010.
- [2] Drosos, Georgarakos, Anastasopoulos, and Gazetas, "Experimental Validation of Bridge Pier Seismic Design Employing Soil Ductility", 7th Annual Congress of Geotechnics, Volos-Greece, October 2010.
- [3] Petersen, "Statik und Stabilität der Baukonstruktionen", Vieweg, pp. 910- 912, 1982.
- [4] Elisabeth Karatzas, Velvet Karatzas, George Karydis "Investigation of structures whose slenderness ratio is  $\lambda \leq 25$  and is based on  $P_{crit.joint}$  and the eigenvalue ratio", STESSA (2012), Chile
- [5] 7th Annual Congress of Geotechnics, (2010), Drosos, Georgarakos, Anastasopoulos, and Gazetas, "Experimental Validation of Bridge Pier Seismic Design Employing Soil Ductility", Volos, Greece.



## **INCLINED BRIDGE UNDER FREE MOVING LOAD** **A special problem**

Tassos Avraam<sup>1</sup> and George T. Michaltsos<sup>2</sup>

<sup>1,2</sup> National Technical University of Athens, Dept. of Civil Engineering, Greece  
e-mail: avraamt@central.ntua.gr, michalts@central.ntua.gr

**ABSTRACT:** This paper deals with the linear dynamic response of an inclined bridge subjected to a load of constant magnitude, which moves under the action of its weight, while the bridge rises up. This analysis focuses attention on the effect of the bridge's angular speed on its behavior under the action of a single load (one-axis load) or a real vehicle model (two-axis load).

**KEYWORDS:** Inclined bridges; Moving loads.

### **1 INTRODUCTION**

The determination of the dynamic effect of moving loads on elastic structures and, particularly, on bridges is a very complicated problem.

The problem of the dynamic response of bridges under the action of moving loads is reviewed in detail by Timoshenko [1] and later by Kolousek [2]. One should also mention the excellent monograph on this subject by Fryba [3] and also his studies on the effect of the constant speed and damping on the response of a beam [4, 5]. Many investigators studied a lot of parameters usually neglected but affecting, some times significantly, the dynamic behavior of a bridge. Although the influence of a variable speed is studied in detail [6], and also the influence of the inclined of a beam [7, 8], the combination of both parameters that appear in a declining bridge is an interesting case.

There is a lot of papers dealing mainly with reconstruction [9], monitoring [10], or design of bascule (inclined) bridges [11], and also the behavior of the deck pavement under different conditions [12, 13], while only a little of these papers study the dynamic behavior under seismic forces (as for example [14]).

The present paper examines the influence of the angular speed of an inclined bridge subjected to the action of a load or of a vehicle moving on the bridge under the action of its weight. The current operation codes are very strict. Thus, such a scenario is an unrealistic one. Nevertheless, there are some cases of accidents occurring due to violation of the codes or human negligence.

**2 MATHEMATICAL FORMULATION**

We consider the declined bridge, of figure 1, having a prismatic cross-section with constant mass per unit length  $m$ , flexural rigidity  $EI$  and damping coefficient  $c$ . At the instant  $t=0$ , there is a load (or a vehicle)  $F$  (of mass  $M$ ) at the edge  $B$  of the left beam (fig. 1). The bridge can go up, with angular speed  $\varphi_0$ . At time  $t$ , the bridge will rotate by angle:

$$\varphi = \varphi_0 t \tag{1.a}$$

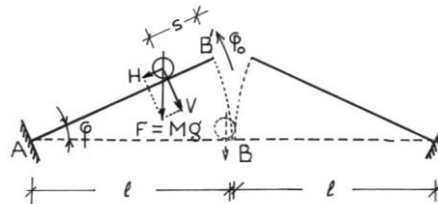


Figure 1. Sketch of a inclined bridge

Therefore, the load or the vehicle will start moving towards the left end of the bridge with acceleration, speed and travelled distance given by:

$$\left. \begin{aligned} \gamma = \frac{H}{M} = \frac{F \cdot \sin \varphi}{F/g} = g \cdot \sin \varphi_0 t, \quad v = \int_0^t g \cdot \sin \varphi_0 t \, dt = \frac{g}{\varphi_0} (1 - \cos \varphi_0 t), \\ s = \int_0^t \frac{g}{\varphi_0} (1 - \cos \varphi_0 t) \, dt = \frac{g}{\varphi_0} t - \frac{g}{\varphi_0^2} \sin \varphi_0 t \end{aligned} \right\} \tag{1.b,c,d}$$

If the load  $F$  travels the distance  $(l-s_0)$  in time  $t_0$  (where  $s_0$  is the distance of the initial position of load  $F$  from the end  $B$ ) will be:

$$\frac{g}{\varphi_0} t_0 - \frac{g}{\varphi_0^2} \sin \varphi_0 t_0 = l - s_0 \tag{1.e}$$

Through the solution of the above equation, one can determine the needed time passage  $t_0$ . The needed time for the complete pull up of the bridge is:

$$t_d = \pi / 2\varphi_0 \tag{1.f}$$

**2.1 The concentrated load**

The simplest and more usual case is the one of a moving load  $F$  without consideration of inertia forces (like mass, or centripetal and Coriolis forces, the influence of which has been already studied in [15, 16]). This leads to:

$$EIw''''(x, t) + cw(x, t) + m\ddot{w}(x, t) = F \cdot \cos \varphi_0 t \cdot \delta(x - l + s) \tag{2.a}$$

where  $\delta(x - a)$  is the Dirac delta function.

A series solution of equation (2.a) in terms can be sought in the form:

$$w(x, t) = \sum_n w_n(x, t) = \sum_n X_n(x) T_n(t) \tag{2.b}$$

where  $X_n(x)$  is the shape functions of a cantilever beam, given by many technical books as for example by [17], and  $T_n(t)$  are time functions under determination. Introducing (2.b) into (2.a), we get:

$$EI \sum_n X_n'''' T_n + c \sum_n X_n \dot{T}_n + m \sum_n X_n \ddot{T}_n = F \cdot \cos \varphi_o t \cdot \delta(x - \ell + s)$$

and because  $X_n$  satisfies the equation of the free motion, the above becomes:

$$\sum_n X_n \ddot{T}_n + \frac{c}{m} \sum_n X_n \dot{T}_n + \sum_n \omega_n^2 X_n T_n = F \cdot \cos \varphi_o t \cdot \delta(x - \ell + s) \tag{2.c}$$

Multiplying the latter by  $X_\rho$ , integrating over the domain and considering the orthogonality condition, the differential equation of the  $\rho^{\text{th}}$  mode of the generalized deflection can be written as:

$$\ddot{T}_\rho + \frac{c}{m} \dot{T}_\rho + \omega_\rho^2 T_\rho = M \cdot g \cdot \cos \varphi_o t \cdot X_\rho(\ell - s) / m \int_0^\ell X_\rho^2 dx, \text{ and } : s = \frac{g}{\varphi_o} t - \frac{g}{\varphi_o^2} \sin \varphi_o t \tag{2.d}$$

where  $\omega_\rho$  is the  $\rho^{\text{th}}$  eigenfrequency of the freely vibrating cantilever. The solution of the above is given by the Duhamel's integral:

$$T_\rho(t) = e^{-\beta t} (A_\rho \sin \bar{\omega}_\rho t + B_\rho \cos \bar{\omega}_\rho t) + \frac{M \cdot g}{\Gamma_\rho} \int_0^t e^{-\beta(t-\tau)} \cos \varphi_o t \cdot X_\rho \left( \ell - \frac{g}{\varphi_o} \tau + \frac{g}{\varphi_o^2} \sin \varphi_o \tau \right) \cdot \sin \bar{\omega}_\rho (t - \tau) d\tau \tag{2.e}$$

where :  $\Gamma_\rho = 1 / m \bar{\omega}_\rho \int_0^\ell X_\rho^2 dx, \quad \beta = \frac{c}{2m}, \quad \bar{\omega}_\rho = \sqrt{\omega_\rho^2 - \beta^2}$

In order to compute the integral of eq (2e), we express  $\sin \varphi_o t$  with a series

$$\sin \varphi_o t = \sum_n (-1)^n \frac{(\varphi_o t)^{2n+1}}{(2n+1)!}. \text{ Neglecting the higher order terms, eq(2e) becomes:}$$

$$T_\rho(t) = e^{-\beta t} (A_\rho \sin \bar{\omega}_\rho t + B_\rho \cos \bar{\omega}_\rho t) + \frac{M \cdot g}{\Gamma_\rho} \int_0^t e^{-\beta(t-\tau)} \cos \varphi_o t \cdot X_\rho \left( \ell - \frac{g \varphi_o \tau^3}{6} \right) \cdot \sin \bar{\omega}_\rho (t - \tau) d\tau$$

The above integral can be found using the Euler's gamma integrals, namely using the integrals of the inverse error functions (Gaussian Integrals). There are also different simplest methods, but with the same accuracy, for the determination of the above integral. The simplest of them is the simulation of

the terms that compose the shape function, with simple algebraic and logarithmic functions that one can easily integrate.

Finally, the factors  $A_p$  and  $B_p$  are determined by the initial conditions:

$$\left. \begin{aligned} w(x,0) &= \frac{F \ell^3}{3EI} \left( \frac{3x^2}{2\ell^2} - \frac{x^3}{2\ell^3} \right) \\ \dot{w}(x,0) &= 0 \end{aligned} \right\} \quad (2.f)$$

because at the starting of the rotation there is the load  $F$  in  $B$  (see fig. 1).

**2.2 The real vehicle**

Let us consider now the biaxial vehicle of figure 2, having wheelbase equal to  $2d$  and distance of its gravity center  $S$  from the bridge's surface equal to  $h$ . We assume that at  $t=0$ , the front axis of the vehicle is located on point  $B$  and that for a bridge at rest ( $\varphi=0$ ), the load  $F=Mg$  is divided equally between the two axes of the vehicle.

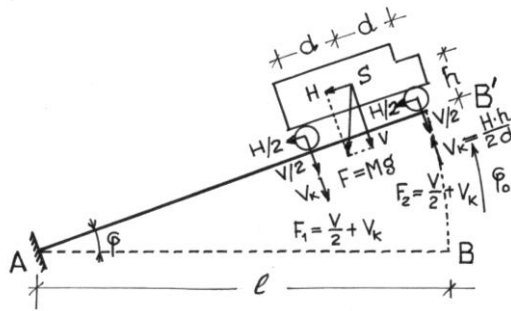


Figure 2. The real vehicle

Hence the forces  $F_1$  and  $F_2$  can be expressed as:

$$\left. \begin{aligned} F_1 &= \frac{M \cdot g}{2} \cdot \cos \varphi_0 t + \frac{M \cdot g \cdot h}{2d} \cdot \sin \varphi_0 t, & F_2 &= \frac{M \cdot g}{2} \cdot \cos \varphi_0 t - \frac{M \cdot g \cdot h}{2d} \cdot \sin \varphi_0 t \end{aligned} \right\} \quad (3.a)$$

The back wheel, will arrive first on A at time  $t_1$ , while the front wheel arrive on A at time  $t_2$  given by the solution of the equations:

$$\left. \begin{aligned} \frac{g}{\varphi_0} t_1 - \frac{g}{\varphi_0^2} \cdot \sin \varphi_0 t_1 &= \ell - 2 \cdot d, & \frac{g}{\varphi_0} t_2 - \frac{g}{\varphi_0^2} \cdot \sin \varphi_0 t_2 &= \ell \end{aligned} \right\} \quad (3.b,c)$$

The corresponding to (2.a) equation, for the vehicle of fig. 2 will be:

$$\left. \begin{aligned} EI w''''(x, t) + c \dot{w}(x, t) + m \ddot{w}(x, t) &= \frac{M \cdot g}{2} \cdot \left( \cos \varphi_0 t - \frac{h}{d} \sin \varphi_0 t \right) \cdot \delta(x - \ell + s) \\ &+ \frac{M \cdot g}{2} \cdot \left( \cos \varphi_0 t + \frac{h}{d} \sin \varphi_0 t \right) \cdot \delta(x - \ell + s + 2d) \end{aligned} \right\} \quad (4.a)$$

A solution is sought with the form of equation (2.b). Following a similar procedure like the one of §2.1, we conclude to the following equation:

$$\left. \begin{aligned} \ddot{T}_\rho + 2\beta\dot{T}_\rho + \omega_\rho^2 T_\rho &= \frac{Mg}{2m \int_0^\ell X_\rho^2 dx} \left( \cos \varphi_o t - \frac{h}{d} \sin \varphi_o t \right) \cdot X_\rho \left( \ell - \frac{g}{\varphi_o} t + \frac{g}{\varphi_o^2} \sin \varphi_o t \right) \\ &+ \frac{Mg}{2m \int_0^\ell X_\rho^2 dx} \left( \cos \varphi_o t + \frac{h}{d} \sin \varphi_o t \right) \cdot X_\rho \left( \ell - 2d - \frac{g}{\varphi_o} t + \frac{g}{\varphi_o^2} \sin \varphi_o t \right) \end{aligned} \right\} (4.b)$$

The solution of the above equation is given by the Duhamel's integral:

$$\left. \begin{aligned} T_\rho(t) &= e^{-\beta t} (A_\rho \sin \bar{\omega}_\rho t + B_\rho \cos \bar{\omega}_\rho t) + \\ &+ \frac{Mg}{2\Gamma_\rho} \int_0^t e^{-\beta(t-\tau)} \left( \cos \varphi_o \tau - \frac{h}{d} \sin \varphi_o \tau \right) \cdot X_\rho \left( \ell - \frac{g}{\varphi_o} \tau + \frac{g}{\varphi_o^2} \sin \varphi_o \tau \right) \sin \bar{\omega}_\rho (t - \tau) d\tau \\ &+ \frac{Mg}{2\Gamma_\rho} \int_0^t e^{-\beta(t-\tau)} \left( \cos \varphi_o \tau + \frac{h}{d} \sin \varphi_o \tau \right) \cdot X_\rho \left( \ell - 2d - \frac{g}{\varphi_o} \tau + \frac{g}{\varphi_o^2} \sin \varphi_o \tau \right) \sin \bar{\omega}_\rho (t - \tau) d\tau \end{aligned} \right\} (4.c)$$

where  $\Gamma_\rho$ ,  $\bar{\omega}_\rho$ ,  $\beta$  are given by eq (2.e). The above integrals can be determined as in §2.1.

Finally the coefficients  $A_\rho$  and  $B_\rho$  are determined by the initial conditions:

$$\left. \begin{aligned} w_{o1}(x,0) &= \frac{F_1}{2} \cdot \frac{(\ell - 2d)^3}{3EI} \left[ \frac{3x^2}{2(\ell - 2d)^2} + \frac{x^3}{2(\ell - 2d)^3} \right] + \frac{F_2}{2} \cdot \frac{\ell^3}{3EI} \left[ \frac{3x^2}{2\ell^2} + \frac{x^3}{2\ell^3} \right] \\ \text{for } 0 \leq x \leq \ell - 2d \\ w_{12}(x,0) &= w_{o1}(\ell - 2d, 0) + 2d \cdot w'_{o1}(\ell - 2d, 0) + \frac{F_2}{2} \cdot \frac{\ell^3}{3EI} \left[ \frac{3x^2}{2\ell^2} + \frac{x^3}{2\ell^3} \right] \\ \text{for } \ell - 2d \leq x \leq \ell \quad \dot{w}(x,0) &= 0 \end{aligned} \right\} (4.d)$$

### 3 NUMERICAL RESULTS AND DISCUSSION

We consider the bridge of figure 1, with:  $\ell=30m$ ,  $I=0.04m^4$ ,  $m=400 \text{ kg/m}$ ,  $c=1500 \text{ Nsec/m}$ . We will study the behavior of the bridge for the following three angular speeds:  $\varphi_o = 0.06, 0.08, \text{ and } 0.10 \text{ rad/sec}$ . As for the loads, we will study firstly the case of a concentrated load  $F=200 \text{ kN}$  and after the case of a biaxial vehicle having wheelbase  $2d=6m$ ,  $h=1.5m$  and  $F=200 \text{ kN}$ , and of a biaxial vehicle with wheelbase  $2d=3m$ ,  $h=1.5m$  and  $F=40kN$ .

### 3.1 The concentrated load

The time passages of the load  $F$  for each one angular speed are determined from equation (1.e) with  $s_0=0$ , as follows: For:  $\varphi_0=0.06$  rad/sec,  $t_0=6.712$  sec, for:  $\varphi_0=0.08$  rad/sec,  $t_0=6.106$  sec and for  $\varphi_0=0.10$  rad/sec,  $t_0=5.675$  sec

Applying the formulae of §2.1, we obtain the diagrams of fig.3, which show the vibrations of the bridge from  $t=0$  to  $t=\pi/2\varphi_0$ , when the bridge becomes vertical. For  $t > t_0$  the bridge vibrates freely.

### 3.2 The real vehicle

We will study the behavior of a bridge, under the action of a real vehicle, comparing simultaneously the bridge's behavior with the one under the action of a concentrated load of equal magnitude. We note that from now on we will continue keeping only the angular speed  $\varphi_0=0.06$  rad/sec, because, according to the previous paragraphs, this speed produces the worse dynamic behavior.

For a vehicle of weight  $F=200$  kN,  $2d=6.0$ m and  $h=1.5$ m we obtain the following diagrams of figure 4.

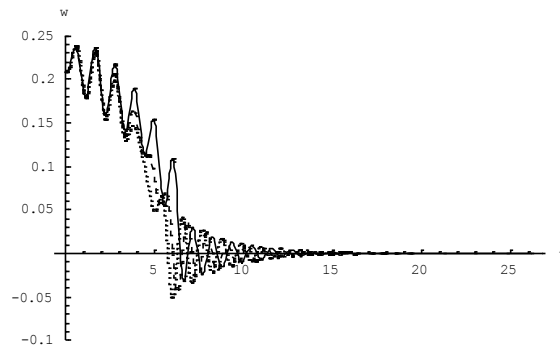


Figure 3. —  $\varphi_0=0.06$ , - - -  $\varphi_0=0.08$ , . . .  $\varphi_0=0.10$  rad/sec

For a vehicle of weight  $F=40$  kN,  $2d=3.0$ m and  $h=1.5$ m we obtain the following diagrams of figure 5.

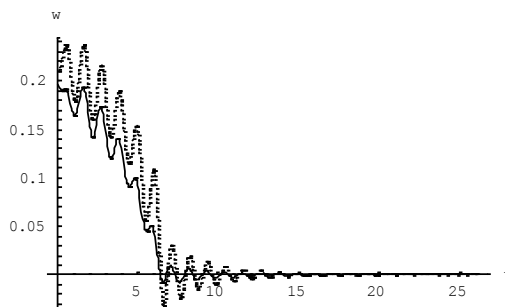


Figure 4. — the real vehicle, . . . the concentrated load

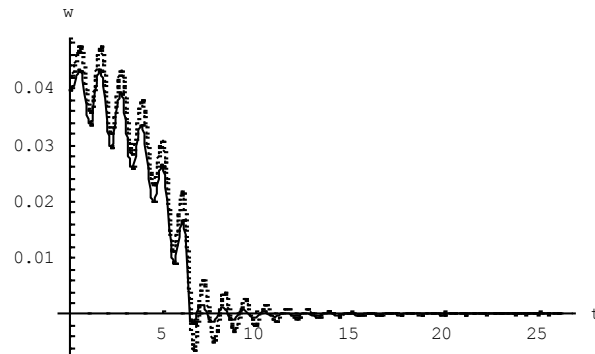


Figure 5. — the real vehicle, - - - the concentrated load

#### 4 CONCLUSIONS

From the results of the model considered herein, one may draw the following conclusions:

1. At the beginning of the bridge pull up, the dynamic deflections are, for any angular speed, practically equal, while after some instants, the lower angular speeds produce bigger deflections.
2. For small wheelbases (with  $2d < \ell/10$ ), the results are similar to the ones produced by a concentrated load with equal magnitude. This fact is also pointed out in [16, 21].
3. The dynamic deflections for concentrated loads or vehicles with small wheelbase are  $\sim 19\%$  greater than the static ones, but this difference becomes small or negligible for big wheelbases (with  $2d > \ell/5$ ).
4. After the load's exit, the bridge vibrates freely. This last motion ends before the complete pull up of the bridge.
5. The real vehicle model is of course more accurate than the one of the concentrated load.

#### REFERENCES

- [1] Timoshenko S.P., *History of the Strength of Materials*, (N.York:D.van Nostrand Co. 1953)
- [2] Kolousek V., *Dynamics of Civil Engineering Structures*. Part I – General Problems, second edition; Part II – Continuous beams and Frame Systems, second edition, Part III – Selected topics, (in Czech), *Prague: SNTL*. (1956, 1967, 1961).
- [3] Fryba L., *Vibration of Solids and Structures under Moving Loads*, (Research Institute of Transport, Prague, 1972)
- [4] Fryba L., Non stationary response of a beam to a moving random force, *J. of Sound and Vibration* 46, 323-338, (1976)
- [5] Fryba L., Estimation of fatigue life of railway bridges under traffic loads, *J. of Sound and Vibration* 70, 527-541, (1980).
- [6] Michaltsos G.T., Dynamic behavior of a single-span beam subjected to loads moving with variable speeds, *J. of Sound and Vibration*, 258(2), 359-372, (2002).

- [7] Wu J.J., Dynamic analysis of an inclined beam due to moving loads, *J. of Sound and Vibration*, 288, 107-133, (2005).
- [8] Mamandi A., Kargarnovin M.H., Younesian D., Non-linear dynamics of an inclined beam subjected to a moving load, *Nonlinear Dynamics*, 60, 277-293, (2010).
- [9] Kaderbek, S.-L.C., Quattrochi, J., Benitez, L., Haas, M., Sutfin, D., Congress street bascule bridge reconstruction, *Structures Congress 2012 – Proceedings of the 2012 Structures Congress*, 769-777, (2012).
- [10] Yarnold M.T., Moon F.L., Aktan A.E., Glisis B., Structural monitoring of the Tacony-Palmyra Bridge using video and sensor integration for enhanced data interpretation, *Proceedings of the sixth International Conference on Bridge Maintenance, Safety and Management*, 2168-2172, (2012).
- [11] Barpi F., Deakin M.A.B., The Belidor bascule bridge design, *Int. Journal for the History of Engineering and Technology*, 82(2), 159-175, (2012).
- [12] Liu Y., Yu X., Qian Z., Numerical study of dynamic response of steel deck pavement on the bascule bridge, *Advanced Materials Research*, N.148-149, 1246-1249, (2011).
- [13] Zhang Y., Jiang L., Zhang Z., Temperature control of Haihe Bascule Bridge based on thermo-mechanical modeling of concrete, *J. of Southeast University (Natural Science Edition)*, 40 (SUPPL. 2), 224-228, (2010).
- [14] Teo Y., Fawcett B., Moffat B., Perkins B., Schettler J., Ying S., Seattle's bridge seismic retrofit program: Ballard bridge case study, *TCLÉE 2009, Lifeline Earthquake Engineering in an Multihazard Environment* (357), p.4, (2009).
- [15] Michaltsos G.T., Sophianopoulos D., Kounadis A.N, The effect of a moving mass and other parameters on the dynamic response of a simply supported beam, *J. of Sound and Vibration*, 191, 357-362, .. (1996).
- [16] Michaltsos G.T., The influence of centripetal and Coriolis forces on the dynamic response of light bridges under moving vehicles, *J. of Sound and Vibration*, 247(2), 261-277, (2001).
- [17] Michaltsos G.T., Raftoyiannis I.G., *Bridges' Dynamics*, Bentham e-books, eISBN: 978-1-60805-220-2, (2011).



## **PRACTICAL METHOD FOR COMPLETED DEAD LOAD STATE DETERMINATION IN CABLE-STAYED BRIDGES WITH EARTH ANCHORS**

Bin Sun<sup>1</sup>, Rucheng Xiao<sup>1</sup>, Dongli Zhuang<sup>2</sup>, Shuaihua Yuan<sup>3</sup>, Erle Xue<sup>1</sup>

<sup>1</sup> Tongji University, Department of Bridge Engineering, China

<sup>2</sup> Tongji Architectural Design (Group) Co., Ltd., China

<sup>3</sup> Hunan University of Science and Technology, Dept. of Road & Bridge Engineering, China  
e-mail: sunbin@tongji.edu.cn, xiaorc@tongji.edu.cn, donlea\_zhuang@163.com, ysh74@163.com, erlexue@163.com

**ABSTRACT:** A practical method was proposed for the reasonable completed dead load state determination in cable-stayed bridges with earth anchors. Three cable-stayed bridge models were designed with the main spans of 1400 m. The reasonable completed dead load states of the three models were determined and compared.

**KEY WORDS:** cable-stayed bridge; practical method; reasonable completed dead load state

### **1 INTRODUCTION**

Recently, preliminary studies about partially earth-anchored cable-stayed bridges have been carried out<sup>[1,2]</sup>. The results turn out that the bridge type is feasible in the point view of both design and construction methods. Compared with fully self-anchored cable-stayed bridges, it has lower compression forces in the girder, improved stability and increased structural rigidity<sup>[3,4]</sup>. Relatively speaking, the cable-stayed-suspension bridge has a long history. It dates back to John A. Roebling's conception in the late 19th century and was improved by F. Dischinger in the 1930s<sup>[1]</sup>. This type of bridge combines the advantages of cable-stayed bridges and suspension bridges effectively by reducing the compressive forces in the girder and shortening the cantilever length during the construction.

Nowadays, there have been many researches about the methods for reasonable completed dead load state determination in self-anchored cable-stayed bridges<sup>[5,6]</sup>. The principle, scope and effect of each method differ from the others. However, none of them pays attention to partially earth-anchored cable-stayed bridges. Also, the study on the cable-stayed suspension bridge is not mature enough, which is generally analyzed by dividing the bridge into two independent structures, a cable-stayed one and a

suspension one. In the analysis of the two types of bridges, more and more results show that it is necessary to develop computer programs while using catenary cable element to model the main cables and stay cables. Hence, we can see that there is a lack of a mature and convenient method for the reasonable completed dead load state determination in cable-stayed bridges with earth anchors. With regard to it, this paper summarizes a practical method for the completed dead load state determination in cable-stayed bridges with earth anchors, emphasizing on the effect of the earth-anchored structures and the interaction between the two parts of cable-stayed and suspension structures.

## **2 PRACTICAL METHOD FOR COMPLETED DEAD LOAD STATE DETERMINATION IN PARTIALLY EARTH-ANCHORED CABLE-STAYED BRIDGES**

In order to reduce the bending moments of structural components in partially earth-anchored cable-stayed bridges, making them to be in an axial stress state as close as possible to take full advantage of the material strength, this paper summarizes a practical and convenient structural analysis process for the design of partially earth-anchored cable-stayed bridges. The proposed process is based on the engineering experience, combined with the rigidly supported continuous beam method, the feasible zone method and the optimization of ANSYS, an all-purpose FEM program.

(1) Initial estimation of cable forces in the mid span: Using rigidly supported continuous beam method, restrain the vertical displacement of the cable anchorage points along the girder and then calculate the constraint forces  $R$ . The vertical component of cable forces are set to be  $R$ .

(2) Adjustment of cable tension forces in the mid span: For long span cable-stayed bridges, as the influence of the vertical curve, the magnitude of bending moments in the girder caused with the horizontal component of the cable force cannot be ignored. Therefore, cable forces obtained in step (1) should be modified. The solution adopted in this paper is based on the assumption that the total moment produced with cable forces at the intersection point of the girder and pylons is equal to that generated with  $R$  in step (1).

(3) Determination of cable tension forces in side spans: Considering the moment equilibrium of the pylons, the cable tension forces in side spans are calculated according to the principle that stay cable forces at the same anchored point have an equal horizontal component in the mid span and side spans. Therefore, the self-anchored stay cable forces  $\{T_b^s\}$  and the earth-anchored stay cable forces  $\{T_b^e\}$  are achieved.

(4) Determination of weight hammers in side spans: Considering the moment equilibrium in the side span girder, the weight of the side span can be produced from  $\{T_b^s\}$ . By deducting the actual weight of the segments, the weight hammers  $\{G_b^s\}$  of the segments are obtained.

(5) Optimization of self-anchored cable forces: By using the APDL programming in ANSYS, the moments  $M_i$ ,  $M_j$  at both ends of the main beam elements are extracted, and the bending energy  $U$  are calculated with formula (1). At last, based on the first order optimization method offered in ANSYS, all the self-anchored cable forces  $\{T_z\}$  and  $\{T_b^s\}$  are optimized in order to make the bending energy  $U$  minimum.

$$U = \Sigma[L(M_i^2 + M_j^2) / (4EI)] \quad (1)$$

(6) Optimization of earth-anchored cable forces in side spans: The calculation in step (3) maintains the moment equilibrium of the pylons. In fact, under the service load, such as live load, pylons bend a lot to the main span. Therefore, under the dead load, pylons can be intentionally designed to bend to the side span, which makes the moments of both sides of the pylons to be equal under load combinations. That is the basic idea of structural optimization based on the feasible zone method. In self-anchored cable-stayed bridges, the bending moment of pylons can be optimized by adjusting the backstay cable forces. However, as to partially earth-anchored cable-stayed bridges proposed in the paper, it can be achieved by optimizing the earth-anchored cable forces: By calculating the deviations  $\delta M_i$  and  $\delta M_j$  between the bending moments at both ends of the main beam elements and the midline of the feasible zone, the first order optimization method are used to optimize earth-anchored stay cable forces in the side span. In the process,  $\{T_b^e\}$  are set as the optimization variables, and the total deviation calculated with formula (2) are set as the optimization target.

$$\Delta = \Sigma\{L[(\delta M_i)^2 + (\delta M_j)^2] / (EI)\} \quad (2)$$

(7) Adjust the areas of the cross-sections of the cables based on the combinations of the dead load and the service loads.

Generally, satisfying completed dead load state can be achieved through two or three trials.

### 3 PRACTICAL METHOD FOR COMPLETED DEAD LOAD STATE DETERMINATION IN CABLE-STAYED-SUSPENSION BRIDGES

Cable-stayed-suspension bridges consist of cable-stayed parts and suspension parts. The process of completed dead load state determination of this bridge type can be divided into four steps as follows:

(1) In the similar ways for the partially earth-anchored cable-stayed bridges mentioned above, the reasonable forces of both stay cables and hangers in the bridge type can be figured out.

(2) Under the reasonable forces of stay cables, the pylons have been in a

bending state. Therefore, the vertical component of the main cable force acting at the top of the pylons may cause additional moments in the pylons. Because the vertical component of the main cable force only relates to the total weight of the suspension structure in the main span and the inclination of the main cable at the top of the pylons, the moments of pylons can only be optimized by adjusting forces of stay cables. The cable forces in the side span are set as optimization variables with initial values as zero.  $\Delta$  in formula (2) is set as optimization target. At the same time, the weight hammers in the side span is adjusted according to the cable forces.

(3) Main cable forces and shapes are calculated. The problem in this step is that the positions of both ends of the main cables and the sag in the midpoint are artificially designated, while the coordinates of other points are still to be determined. The shapes of main cables in suspension bridges may use parabola approximately. However, it will cause large deviation if parabola is used in cable-stayed-suspension bridges because there are comparatively large areas without hangers. Based on the principle that the horizontal forces are equal along the main cable, the horizontal forces and shapes can be obtained via an inside and another outside iteration. By adjusting the magnitude of horizontal forces, the result of the inside iteration is that the lowest point of the main cable converges to the designed elevation, while the outside iteration seeks for the equilibrium position through free displacements of main cable nodes.

(4) The main cable shapes in side spans are calculated. Under the dead load, the horizontal component of the main cable force in the two side spans equals to that in the main span. Therefore, only the main cable shapes in the two side spans needs to be determined. After solving the main cable shapes in the main span, by removing the excessive horizontal constraints of main cables at the top of pylons, the real main cable shapes in side spans are obtained through free displacements of the main cable nodes.

At the end, ideal stress state of each element in cable-stayed-suspension bridges under the dead load has been obtained. Meanwhile, this method can also be applied in normal suspension bridges.

#### **4 TRIAL DESIGN OF CABLE-STAYED BRIDGE WITH EARTH ANCHORS AND COMPLETED DEAD LOAD STATE DETERMINATION AND COMPARISON**

Based on the same technical standard, load cases and material types, two experimental cable-stayed bridges with the same main span of 1400m with earth anchors were designed. The reasonable completed dead load states of the two bridges were determined using the method proposed in this paper. A fully self-anchored cable-stayed bridge was also designed and calculated for a comparison.

#### 4.1 Trial design of partially earth-anchored cable-stayed bridge

In order to reduce the size of anchors, the length of the main girder in the main span corresponding to the earth-anchored stay cables in side spans is only 400m, and the remaining 1000m span girder is self-anchored (Figure 1). The width and height of the streamlined girder are 41m and 4.5m, respectively. The full height of the “A” shaped tower is 357m, in which 287m is above the girder. 152 pairs of cables are installed, where 13 pairs of them are earth-anchored in each side span. The types of them are 187-313  $\Phi$ 7mm steel wires.

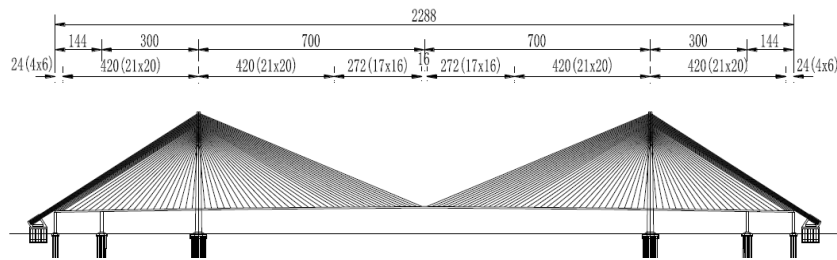


Figure 1. 1400m partially earth-anchored cable-stayed bridge (unit: m)

#### 4.2 Trial design of cable-stayed-suspension bridge

The bridge has a span combination of  $452+1400+452=2304$  m as shown in Figure 2. The middle part with a length of 416m is supposed to the main cables, and the other parts are cable-stayed. The structure of the girder is the same as the partially earth-anchored cable-stayed bridge, while the shape of pylons changes from “A” to “H”. At the same time, the full height of pylons reduces a lot to 306m, in which 236m is above the girder. The cable system consists of the stay cables, main cables and hangers. 104 pairs of stay cables are installed. The area of each stay cable is  $0.4 \text{ m}^2$  and two 85  $\Phi$ 7mm hangers are adopted in each hang point. Four crossing hangers are installed at both ends of the suspension part.

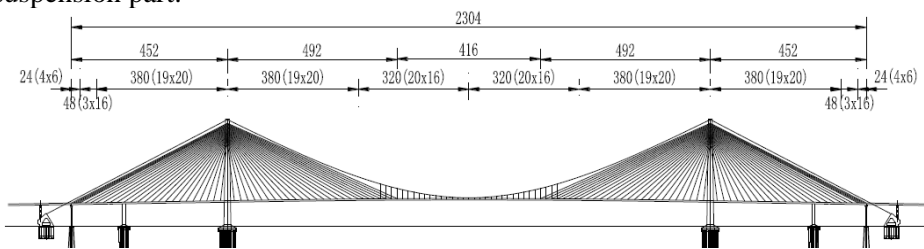


Figure 2. 1400m cable-stayed-suspension bridge (unit: m)

#### 4.3 Trial design of fully self-anchored cable-stayed bridge

The fully self-anchored cable-stayed bridge has a span combination of  $636+1400+636=2672$ m as shown in Figure 3. The pylon is the same as that in the partially earth-anchored cable-stayed bridge, so is the appearance of the

girder. However, the cross-sectional properties of the girder become larger. Types of stay cables have also been adjusted.

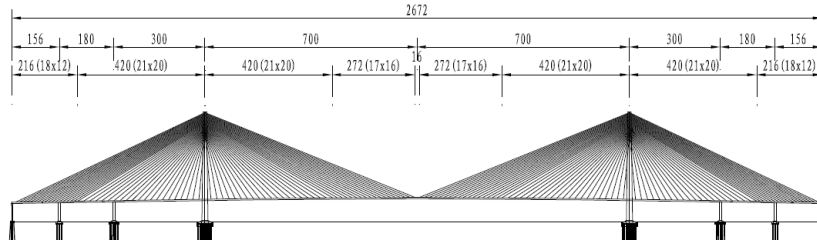


Figure 3. 1400m fully self-anchored cable-stayed bridge (Unit: m)

#### 4.4 Completed dead load state determination and comparison

Finite element models of the structures mentioned above are established in ANSYS. Each stay cable is divided into 8 pieces of bar elements in order to simulate the sag effect of cables. With the method proposed in this paper, the reasonable dead load states of three bridges are obtained. The structural responses are shown in Figure 4-6, which show that:

(1) Bending moments of the girder in the three bridges are all near zero and jaggedly distributed, with small absolute values. The local moment peaks exist only near the pylons and auxiliary piers in side spans. (Figure 4)

(2) The shapes and values of stress in the upper and lower edge of the girder are similar in the three bridges. The maximum stresses are 90-100MPa. (Figure 6)

The results show that the optimization method works well for the completed dead load state of all cable-stayed bridges. Furthermore, when comparing the three bridges, obvious differences can be found:

(1) The comparison of axial forces is shown in Figure 5. It indicates that the compressive parts of both the partially earth-anchored cable-stayed bridge and the cable-stayed-suspension bridge are the same, which is approximately an upward translation of the pressure line in the fully self-anchored cable-stayed bridge. The earth-anchored girder in the partially earth-anchored cable-stayed bridge is in tension. However, the axial force in the girder of the suspension part of the cable-stayed-suspension bridge is rather small, which improves the structural stability and saves materials a lot. It could also be seen from the comparison of cross-sectional areas of the girder. The results show that consumption of the girder decreases about 25.1%, which reduces the cable forces and the amount of cable material consumption further.

(2) The girder of the partially earth-anchored cable-stayed bridge is in compression and tension at the same time, which could take full advantages of steel whose tensile strength and compressive strength are the same. However, since the horizontal inclination of stay cables in the mid span is small, tension stresses in the girder accumulate rapidly. If the length of earth-anchored girder

is increased, the tensile stresses in the girder will become a control factor in the design.

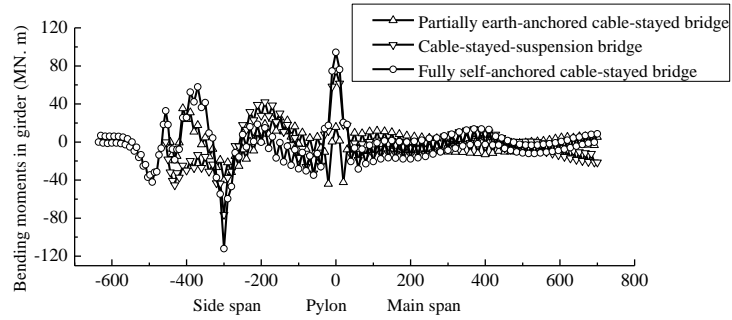


Figure 4. Comparison of bending moments in girder

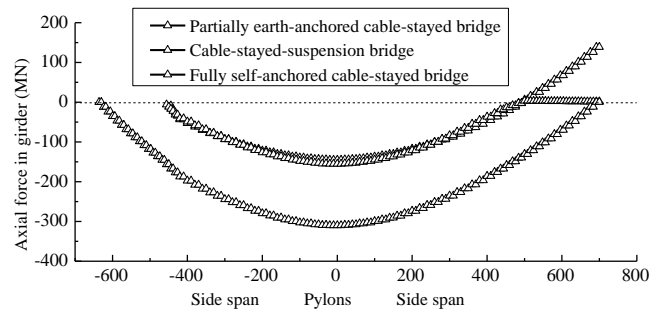


Figure 5. Comparison of axial forces in girder

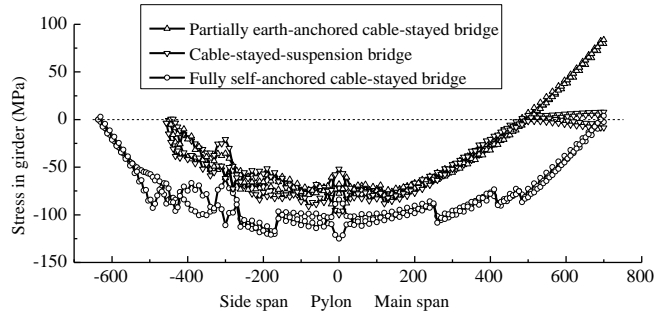


Figure 6. Comparison of stress in girder

(3) Compressive forces in the girder near pylons in the cable-stayed-suspension bridge are small, and it will not cause tension forces in the girder of the suspension part in the mid span at the same time. Therefore, it is the best structure for stresses in the girder.

(4) The calculation results also indicate that forces in the anchorage are smaller in the partially earth-anchored cable-stayed bridge compared with that in the cable-stayed-suspension bridge. The horizontal and vertical forces

decrease about 34.8% and 22.0%, respectively. Therefore, the amount of anchorage could be reduced more than 20% at least.

## 5 CONCLUSIONS

A practical method was proposed for the reasonable completed dead load state determination in cable-stayed bridges with earth anchors. The method was based on the rigidly supported continuous beam method and the feasible zone method, emphasizing on the mutual effect between the self-anchored structural parts and the earth-anchored ones. The method has been applied into three trial designs successfully. Conclusions based on the research are as follows:

(1) The applications in the trial designs show that the method achieves fast and works well. Meanwhile, cable-stayed bridges with earth anchors could be changed into fully self-anchored cable-stayed bridges and suspension bridges through the variation of structural parameters. Therefore, the method in the paper could be extended to all cable supported bridges.

(2) In the reasonable completed dead load state, compressive forces in the girder of cable-stayed bridges with earth anchors decrease more than 25% compared with that of fully self-anchored cable-stayed bridges. Therefore, it can save materials and increase the stability of the structure. Furthermore, partially earth-anchored structure is an effective approach to extend the span of cable-stayed bridges.

(3) Compared with the cable-stayed-suspension bridge, the tensile stress in the girder in main span of partially earth-anchored cable-stayed bridges may control the design, but the anchorage scale can be reduced more than 20%.

## ACKNOWLEDGMENTS

The authors appreciate the financial support from the National Basic Research Program of China (973 Program) (Project No. 2013CB036303) and the National Natural Science Foundation of China (Project No. 51008223 and 51078197). The opinions and statements do not necessarily represent those of the sponsors.

## REFERENCES

- [1] Gimsing N J. *Cable supported bridges - concept and design*. 3rd Edition. John Wiley & Sons Ltd, 2012.
- [2] Sun B, Cheng J, Xiao R C. "Preliminary design and parametric study of a 1400m partially earth-anchored cable-stayed bridge". *Science in China Series E: Technological Sciences*, Vol. 53, No. 2, pp. 502-511.
- [3] Nagai M, Fujino Y, Yamaguchi H, et al. "Feasibility of a 1400 m span steel cable-stayed bridge". *Bridge Engineering*, Vol. 9, No. 5, pp. 444-452.
- [4] Won J H, Park S J, Yoon J H, et al. "Structural effects of partially earth-anchored cable system on medium-span cable-stayed Bridges". *Steel Structures*, 2008, No. 8, pp. 225-236.
- [5] Chen W F, Duan L. *Bridge Engineering: Construction and Maintenance*. CRC Press. 2003.
- [6] Janjic D, Pircher M, Pircher H. "Optimization of cable tensioning in cable-stayed bridges". *Journal of Bridge Engineering*, 2003, 8 (3): 131-137.



## **CONVENTIONAL AND ALTERNATIVE DESIGN OF HIGHWAY BRIDGE IN EGNATIA MOTORWAY INCLUDING MANY INNOVATIVE SOLUTIONS**

Dimitrios Anastasopoulos<sup>1</sup>, Zacharoula Kopelia<sup>2</sup>, Vasileios Pilitsis<sup>3</sup>  
and Ioannis Tegos<sup>4</sup>

<sup>1,2,3,4</sup>Aristotle University of Thessaloniki, Dept. of Civil Engineering, Greece  
e-mail: dhmrhsana@hotmail.com, kopelza@gmail.com, vpilitsi@civil.auth.gr,  
itegos@civil.auth.gr

**ABSTRACT:** One of the largest highway bridges of the Egnatia Motorway was studied according to the Eurocodes, firstly as it was constructed and secondly with the implementation of many innovations. These innovations are referred to the following: a) the construction method b) the aesthetical improvement c) the designing and dimensioning of the infrastructure d) the activation of the abutments in seismic actions e) the resistance of the abutments and f) the saving of time and construction materials. The results of these two different construction methods are compared and many interesting conclusions occurred.

**KEY WORDS:** Innovations, cast in situ bridge, construction method, innovative abutments

### **1 INTRODUCTION**

At times the developing field of bridge construction embodies various innovations which are relative to the seismic safety, the serviceability, the economy, the aesthetics, the construction method and the durability over time. It is well-known that for many decades the dissected statically determined systems (Gerber system) dominated in conventional cast-in-situ bridge construction methods. Simultaneously, precast methods dominated in construction of higher-position cases. The threat of undesirable constrains and the inhibited great height of the cast-in-situ structure led to unavoidable implementations which, however, harmed the system's durability. For those reasons, the modern bridge construction methods return to the primarily monolithic solutions.

Regarding the seismic safety, a great amount of seismic isolation devices were appeared during the last years. Seismic isolation could be applied in two different ways: whether utilizing the elastomeric bearings as a medium to diminishing seismic actions, or using the damping devices in order to restrain seismic displacements. However, the previous two isolation options have both the same disadvantage. The existing components of the seismic devices create

heterogeneity in relation to protected infrastructure. This heterogeneity results to a significant differentiation between those devices' and infrastructure's lifetime. As a consequence, the necessity to maintain the whole structure burdens the estimated long-term cost of the project.

The construction method consists of a very important feature in building a highway bridge. The various data of the problem give the opportunity to improvise construction resolutions that could be adjusted to requirements of the structure and have less effects regarding the construction result. According to the construction method utilized, there are five different types of bridges might be occurred as shown below:

- a) The precast prestressed I-beam deck
- b) The conventional cast in situ bridge construction with stable scaffoldings
- c) Cast in situ utilizing movable scaffoldings normally supported to piers.
- d) Balanced cantilever bridge construction, which either utilizes scaffolding or precast deck segments
- e) The progressive span by span incrementally launched bridge construction

Undoubtedly, the current construction procedure for cast-in-situ bridges longer than two spans needs to be improved.

The present case of study attempts to evaluate a lot of innovative solutions regarding to the construction method, the seismic resistance of the infrastructure and the economical and aesthetical aspect of the structure.

## **2 APPLIED INNOVATIVE OPTIONS**

In general the described innovative options of the alternative solution are the following:

- a) Segmental construction method. The reasons imposed a cast-in-situ bridge to be constructed in segments are well-known. The segmental construction method is considered to be known as well. In this paper a completely different construction method than the conventional is proposed. In the new method the construction begins with the concrete casting of two 12m cantilevers, with variable section, from both sides of each pier. At the ends of the cantilevers reinforcement bars are placed at the perimeter of the section to ensure the proper connection with the middle sections. Straight tendons are used for the reinforcement of the cantilevers. The tendons are placed at the upper flange of the section and their prestressing force is the required one for the ultimate limit state (15Ø0,6'' straight tendons). Afterwards the rest segments of the spans are casted and point weights are placed at the ends of the cantilevers to avoid undesirable bending.

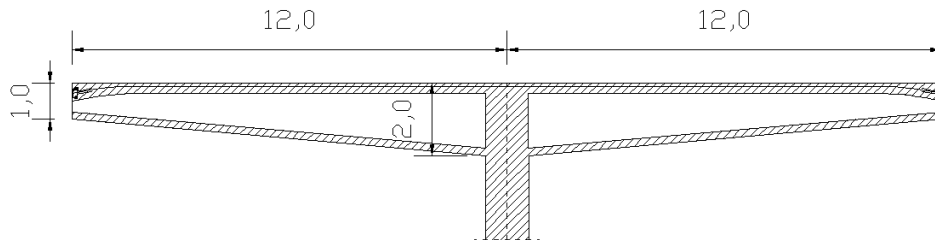


Figure 1. Longitudinal section of the pier and its cantilevers

b) the middle segments of the spans are casted after the cantilevers and for their reinforcement are used conventional steel bars to deliver the positive bending moments (125Ø25 steel bars are required for the middle of the span)

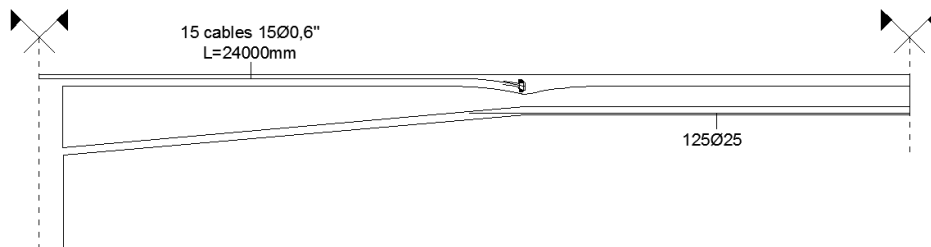


Figure 2. Longitudinal section of the cantilever - innovative reinforcement of the flanges

c) aesthetical requirements and the uniform management of the construction procedure impose the embedding of the deck at the abutments [1]. A new type of abutment is proposed with the ability to deliver bending moments [2].

d) the transfer of a part of seismic actions at the longitudinal direction to the abutment and to the embankment is succeeded with a mechanism of wall-web [3],[4]. This wall-web is rigidly connected with the end parts of the deck and the sliding bearings of the abutment are placed on the footing of the wall of the abutment, which is in a specific gap. The width of the gap depends on the total length of the bridge and is relevant to the expansion-contraction of the deck due to thermal actions and creep-shrinkage [5]. During an earthquake at the longitudinal direction the seismic movement of the deck is transmitted to the wall-web whose movement is limited due to the existence of the gap. As a result of that a great amount of seismic action is transmitted to the pile cap from the wall-web.

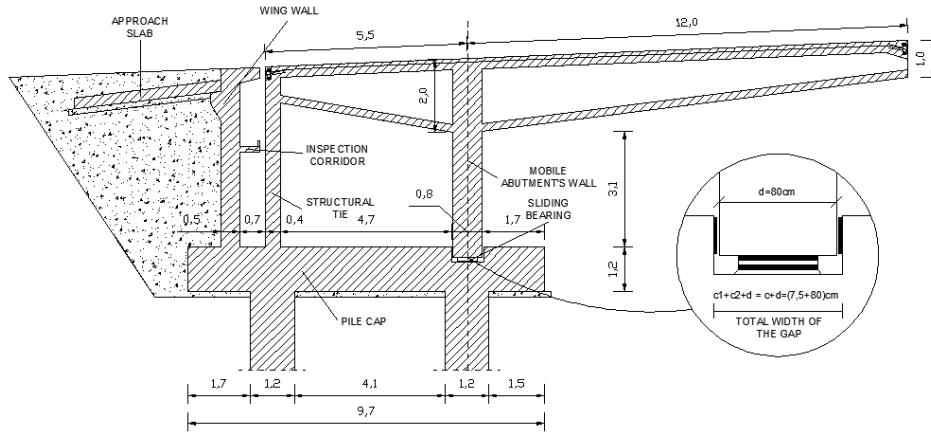


Figure 3. Longitudinal section of the proposed abutment

### 3 COMPARISON OF RESULTS

This paper examined the existing bridge positioned between Araithos – Peristeri locations at Egnatia Motorway. This bridge consists of two separate branches (one in each direction), and serves the transition between towns of Ioannina - Metsovo. However, in this paper, only the left branch of the bridge has been examined [Fig.11]. The structural system of the bridge is a 3D frame, which consists of the deck of the bridge, the abutments, the piers and foundation. The existing bridge is a continuous frame with six spans and a total theoretical length of 240,0m ( $2 \cdot 34 + 4 \cdot 43 = 240$ m). The length of the bridge is referred as theoretical because the deck in plan is not straight in all sectors but has a variable steering angle. The body has a longitudinal slope of 4.4% while the slope of the cross sections ranges from 2.5% to 7%. The cross section of the body is a box-girder with a fixed height of 2.70m. The deck of the bridge is based on five intermediate points on the piers with monolithic connection, while on the edges, on the abutments by elastomeric bearings. The cross section of the piers is solid with dimensions 5.00 x 1.50m.

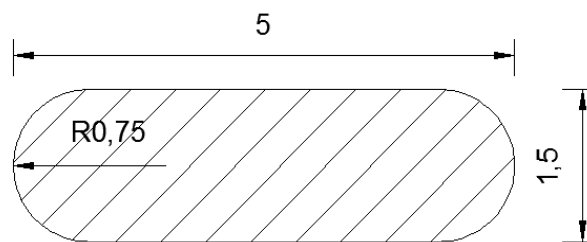


Figure 4. Cross section of the piers

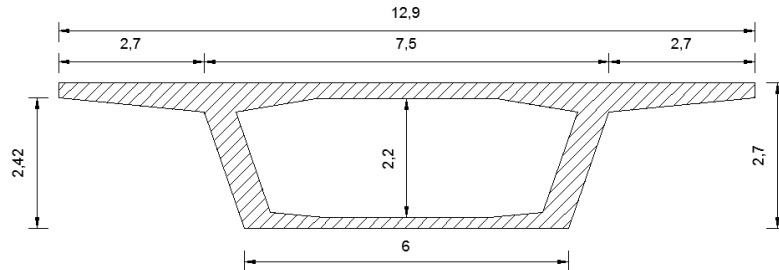


Figure 5. Cross section of the conventional deck

For aesthetical and economical reasons, at the proposed innovative bridge a variable-height section has been selected for the deck. As a result of that, longitudinal, ordinary steel bars are used for the reinforcement of the bottom flange, at the middle of the spans. This is considered to be accepted by the applied codes (Eurocodes) and also constitutes another innovation. The slope of the bottom flange of the cantilevers is constant (8,33%) and is extended across their length (12m).

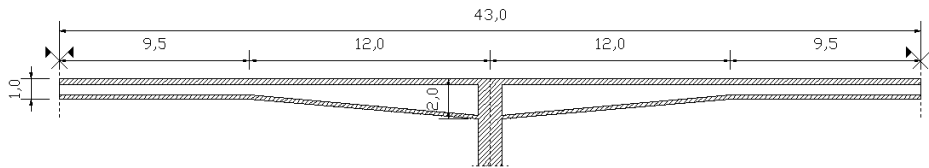


Figure 6. Longitudinal section of the pier and its cantilevers with the middle segments finished

The requirements of aesthetics led to the embedding of the end-parts of the deck on the abutments. Because of that, a new type of abutment has been introduced. This abutment is able to deliver significant bending moments. The cross section of the deck is a voided slab with reduced cross sectional height from 2m above the piers to 1m at the mid-span.

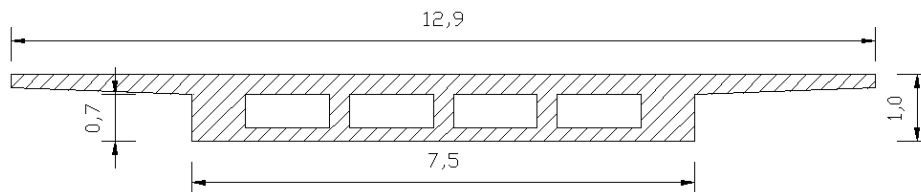


Figure 7. Cross section of the proposed deck in the middle of the span

The bearings are placed on the footing of the wall-web of the abutment in order to delivered seismic actions from the wall-web in case of a longitudinal earthquake.

The cross section of the wall-web of the abutments is 4,5x0,8m. The choice of these dimensions occurred by the requirement of an optimal distribution of the seismic force between the wall-webs and the piers of the bridge.

The cross section of the piers is 4,2x1,2m. These dimensions occurred by the analysis as the optimal for the new bridge because of the uses of the wall-webs. As a result of that, the bridge has a regular behavior in contrast to the constructed one. Moreover the new piers are more economical because of their smaller cross section.

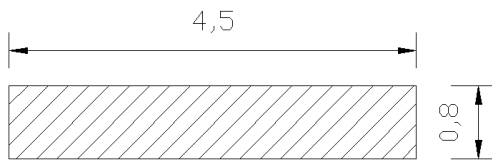


Figure 8. Cross section of the wall-web

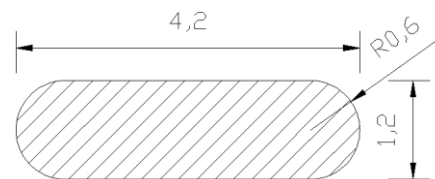


Figure 9. Cross section of the new pier

In both cases, the new European Codes (Eurocodes) have been applied. [6], [7], [8], [9], [10]. Two types of analyses were performed, for static and dynamic loads [11], [12]. The results from the two analyses are very interesting.

As a result of these innovations the new bridge:

- a) is 15% lighter (69,43MN the new one, 81,75MN the old one)
- b) the number of the tendons through a cross section is 15 while at the constructed bridge there was 20. (Same tendons' area in both cases)
- c) the total length of the tendons is less because they are used to deliver only the negative moments and they are straight. (Curved in the constructed one, delivering both negative and positive moments)

#### 4 CONCLUSION

Comparing the results of the two cases, we conclude to the following:

- a) The proposed construction method is more economical [13] and the extra cost that is required for the abutments is over covered by the more economical deck and piers.
- b) The proposed construction method has not only more aesthetical result but also is faster and simpler than the conventional one.
- c) The transfer of part of the seismic actions to the abutments takes advantage of parts of the bridge that were not used to deliver any forces [14].

The implementation of the innovations that this paper proposes in other bridges of different kinds and sizes would give credence to their feasibility.

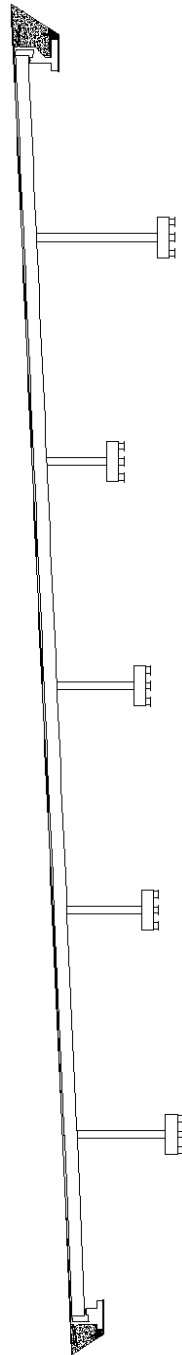


Figure 11. Longitudinal section of the conventional bridge

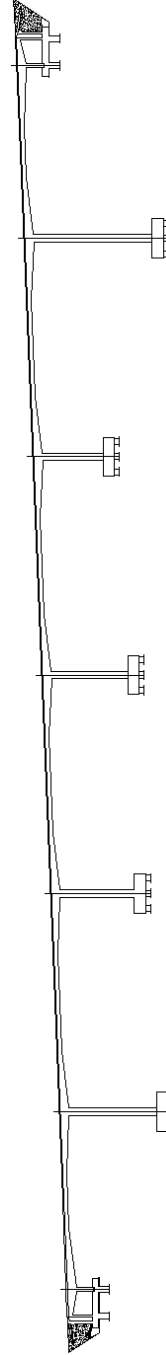


Figure 12 . Longitudinal section of the innovative bridge

## ACKNOWLEDGEMENT

The authors wish to express their gratitude to METE SYSM S.A. for providing the original study of the bridge for the purposes of the present study.

## REFERENCES

- [1] Mitoulis S. A., Tegos I. A. (2010), An unconventional restraining system for seismically isolated bridges. *Eng Struct* 32(4):1100-1112
- [2] Fib Bulletin 61 (2011), Design examples for strut-and-tie models. *fédération internationale du Béton (fib)*, Lausanne, Switzerland
- [3] Mikami T., Unjoh S., Kondoh M. (2003), The effect of abutments as displacement limiting measure on seismic performance of bridges. [www.pwri.go.jp/eng/ujnr/tc/g/pdf/19/4-1mikami.pdf](http://www.pwri.go.jp/eng/ujnr/tc/g/pdf/19/4-1mikami.pdf)
- [4] Mitoulis S., Tegos I. (2010), An Unconventional Restraining System for Limiting the Seismic Movements of Isolated Bridges. *Engineering Structures* Vol. 32, pp. 1100-1112, Elsevier Ltd.
- [5] Pilitsis V. Tegos I. A. (2013), Employment of abutments and approach embankments for seismic protection of bridges. 2013 International Van earthquake symposium, Turkey
- [6] CEN [Comite Européen de Normalisation] (2003), EN 1991-1-5: Eurocode 1: Actions on Structures – Part 1-1: General Actions – Thermal Actions.
- [7] CEN [Comite Européen de Normalisation] (2004), EN 1992-1-1: Eurocode 2: Design of Concrete Structures – Part 1-1: General Rules and Rules for Buildings.
- [8] CEN [Comite Européen de Normalisation] (2004), EN 1992-2: Eurocode 2: Design of Concrete Structures – Part 2: Concrete Bridges – Design and detailing rules
- [9] CEN [Comite Européen de Normalisation] (2005), EN 1998-1: Eurocode 8: Design of Structures for Earthquake Resistance – Part 1: General Rules, Seismic Actions and Rules for Buildings.
- [10] CEN [Comite Européen de Normalisation] (2005), EN 1998-2: Eurocode 8: Design of Structures for Earthquake Resistance – Part 2: Bridges.
- [11] Chopra K. A. (1995), *Dynamics of Structures: Theory and Applications to Earthquake Engineering*. Pearson Education Inc., New Jersey, USA
- [12] SAP2000 (2007), *Integrated finite element analysis and design of structures, nonlinear version 11.0.3*. Computers and Structures Inc., Berkeley
- [13] Tegos A.I., Stylianidis K., Tsitotas A.M., Mitoulis S. (2007), Seismic Resistance and Cost-effectiveness of Multispan Bridges. IABSE Symposium Report, IABSE Symposium, Weimar 2007, pp.9-16(8) Publisher: International Association for Bridge and Structural Engineering
- [14] Tegos A.I., Sextos A., Mitoulis S.A., Tsitotas M.(2005), Contribution to the improvement of seismic performance of integral bridges. 4<sup>th</sup> European Workshop on the Seismic Behavior of Irregular and Complex Structures.



## **THE DESIGN OF A NETWORK ARCH BRIDGE CROSSING OVER ARACHTHOS RIVER IN ARTA, GREECE.**

Dimitris Mouroukis<sup>1</sup>, Panagiotis Veros<sup>2</sup>, Kostantinos Lontos<sup>3</sup>

<sup>1,2</sup> Structural Engineers BEng,Msc. Lontos and Associates, Athens, Greece

<sup>3</sup> Managing Director, Lontos and Associates, Athens, Greece  
e-mail: info@lontos.gr

**ABSTRACT:** This paper describes the structural design of a network Arch bridge located in Arta over Arachthos River. A network arch is defined as an arch bridge with inclined hangers where some hangers cross other hangers at least twice. The development of the road Network and the peripheral road in the Area of Arta-Greece set the opportunity to design an innovative road Arch bridge that is intended to be a landmark for the city and to contribute to the quality of a new leisure area.

**KEY WORDS:** Bridge; Network Arch; Hanger



*Figure 1.* Architectural visualization of the Bridge.

### **1 INTRODUCTION**

Optimal hanger arrangement in arch bridges not only lead to minimum values of the axial forces and force variations in the hangers and minimum values of bending moment and moment variation in the arch, but also it allows to use

small cross sections and low weight with aesthetical and structural advantages.

In literature there are more bridges with fan and vertical hangers arrangement than network arch bridges; fan arrangement is generally chosen for aesthetical reasons even if other solutions show better structural behavior. Some network arch solutions with aesthetical advantages and very good structural behaviour have been designed by Tveit (1987, 2001). Brunn and Schanack (2003) proposed a new hanger arrangement for railway bridges with concrete decks. In our design we adopted these methods and we optimized the angle of hangers by solving multiple models.

The bridge is 160m long with spans 20m-120m-20m. The Central span is a network Arch Bridge.(Fig 2.). The central span crosses the river Arachthos which has constant flow during the winter and the summer.

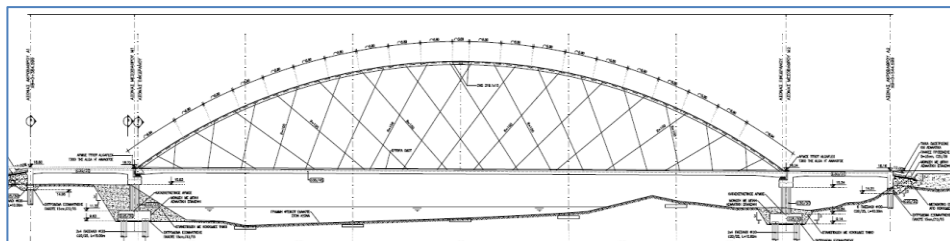
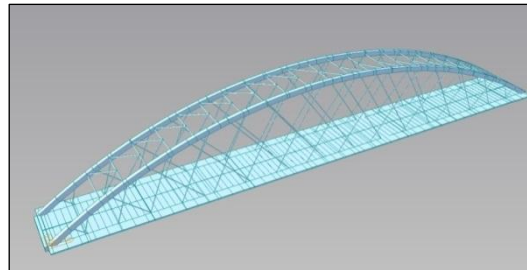


Figure 2. Structural Model using MIDAS Civil.

## 2 DESIGN

### 2.1 Hanger Arrangement and Arch.

Since bending moments in arches depend on the configuration of the line of thrust and they ought to be reduced in arch bridges, it is necessary to align the line of thrust with the center line of the arches. To have the best distribution of efforts, the upper hanger nodes should be placed equidistantly (shown with the distance  $d$  on the figure 3) and the hangers should cross the arch with the same angle (represented by  $\alpha$ ). This angle is actually the angle between the hanger and the line starting in the middle of two hangers to the center line of the arch (the dotted line in Fig.3).

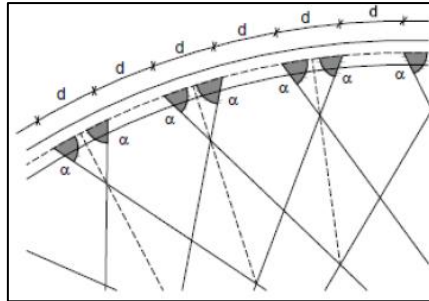


Figure 3. The hangers cross symmetrically the radii with same angle.

Following the above literature recommendations Arta bridge has 18.0m rise of the arch keeping a value close to optimal 15% of the span as Tveit advised. Larger arch rises decrease internal forces but respecting aesthetics it should not exceed 17% of the span. Also by making test with the hanger inclination and by literature it was decided to be  $35^{\circ}$ . Also by increasing the number of hangers the bridge behavior doesn't significantly change. There were used 30 rods hangers in each side with 100mm diameter and structural steel material S460 ML. The upper hanger connections are spaced 4.10m along the arch length.

The arches have a constant box cross section with external dimensions of  $H/W = 0.71 \text{ m} / 0.55 \text{ m}$ . (Fig 4.). The webs and flanges consist of 50 mm thick steel plates, respectively, and are made of structural steel S 350 ML. The cross section has a parallelogram shape with the web plates parallel to the arch planes; the flanges are horizontal. The arches are laterally supported by a wind bracing formed by rhombuses made of circular hollow steel sections (S 235) with an external diameter of 219.1 mm and a thickness of 10 mm.

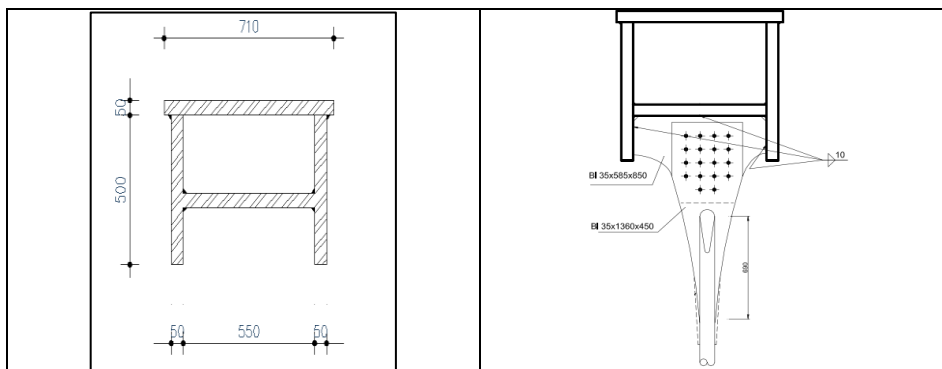


Figure 4. Arch cross section and connection with Rod member.

Each set of hangers is shifted half the diameter of the hangers out of the arch plane. This allows them to cross without deflections. The eccentricity causes torsional moments in the arch profiles, which are partially taken by the wind

bracing. The direction of the eccentricity changes from each hanger connection to the next, so the torsional moments counteract each other. In the bridge that we designed no relaxation occurred in the hangers.

## 2.2 Deck Cross section.

The tie of the bridge consists of a solid concrete slab spanning 10.65m between the hangers. The prestressing in longitudinal direction mainly counteracts thrust of the arches. The depth of the slab is 0.7m in middle span and 1.0m at supports.

When the distance between the arches is less than 18 m, the deck should be made of concrete and prestressed. This gives a slender structure, less noise and saves materials.(Fig 5.)

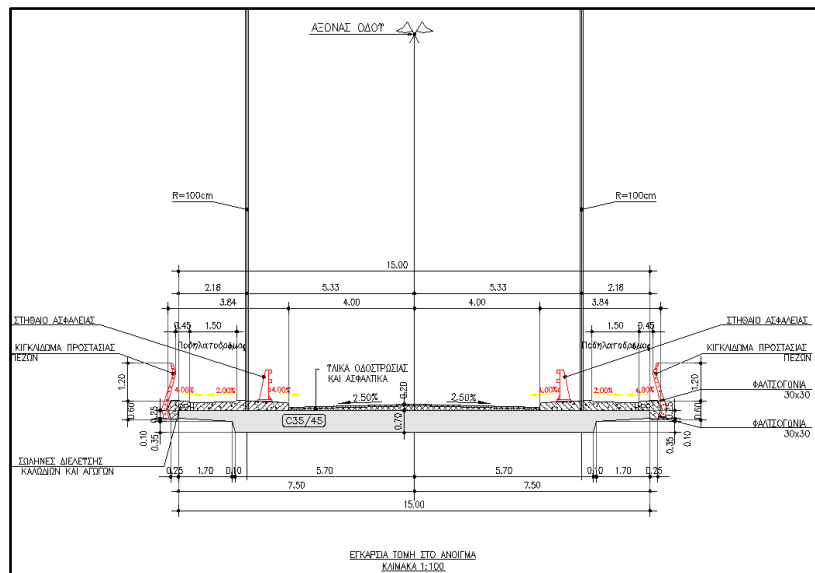


Figure 5. Cross section of the Deck.

Certainly, the increased dead load increases the bending moment. But the higher effective depth and the increased lever arm of the tendon counteracts the negative effect of the higher dead load. Therefore the required additional depth will be moderate and the compression reinforcement can be made redundant.

Approximate calculations showed that a thickness of about 70 cm at the slab's mid-span would be enough to eliminate compression reinforcement. Besides, a thicker tie improves the torsional rigidity and stiffness of the deck.

A thinner deck could be achieved by applying transverse prestressing in the length of the bridge. Although this could be the optimal solution it would lead to increased cost and design time.

The deck is made of C35/45-XC3 concrete (according to EN 1992-1-1 and EN 206-1 and is longitudinally prestressed by twelve 22-strand prestressing tendons.

The Design of the bridge adopted the Eurocode2-2 for the deck design. Midas Civil has compliance with the new codes and that was of great help. (Fig. 6.)

Figure 6. Midas Civil and Eurocodes Design.

### 3 FEM-CALCULATION

#### 3.1 General.

For the FEM-calculations a single structural analysis software package was used. Most of the investigations were performed with MIDAS CIVIL-KOREA. Several models were created in order to perform the necessary check. (ULS, SLS, Dynamic, Buckling, etc).

Mainly two models were created. One by simulating the deck as beam elements, and one by using plate elements.

For the model with plate elements their nodes were aligned to the bottom plane of the tie. In that way it was possible to shape the bridge deck like the real cross-sections by applying different thickness to the plane elements. The cantilevers were connected by couplings to the nodes of the bridge deck elements providing fixed connection to the rigid body at the reference nodes. (Fig. 7)

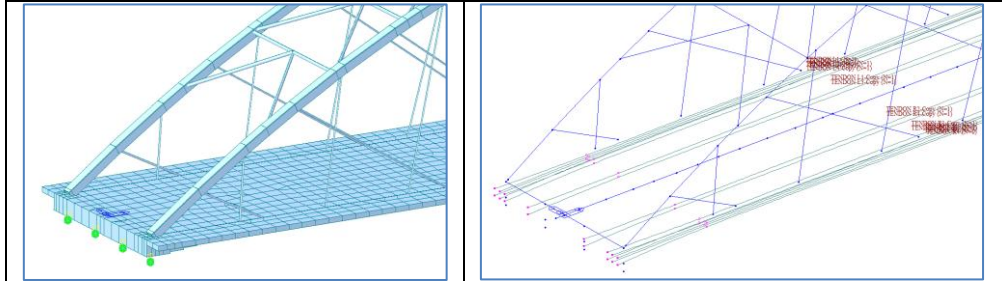


Figure 7. 3D plate elements model and beam element with prestressing tendons.

The arches were modeled using beam elements with a length of about 0.5 meters. The truss members of the wind bracing were also beam elements with truss properties. They originate mainly in the torsional moments in the arch due to the eccentric connection of the hangers and can be ignored for the assessment.

The hangers were modeled using cable elements that only sustain tension in case of non-linear analysis. This has to be considered when calculating influence lines. Since analysis is carried out in linear fashion, hangers will take compression forces, instead of relax. This leads to increased internal forces and is therefore on the safe side. The cable elements were connected eccentrically to the arch. At their intersections the horizontal deflection perpendicular to the arch plane was coupled. In that way it was possible to calculate deflections and mode shapes of the hanger web.

### 3.2 Buckling analysis of the Arch.

The arches receive mainly axial compression forces and are therefore in danger of collapse due to buckling. Additionally, there are in-plane bending moments  $M_y$  due to the hanger forces and out-of-plane bending moments  $M_z$  and torsional moments  $M_t$  due to horizontal forces (like wind) on hangers and arches. Additionally the eccentricity of the hanger connections causes torsional bending. The arches were verified using second order analysis to prove the buckling resistance.

For this purpose it is required to apply the initial bow imperfection specified in EN 1993-1-1: 5.3.2 on the arch. The relevant buckling curve is the first mode shape for each axis of the arch profile.

The mode shapes were determined by the dynamic analysis of MIDAS CIVIL(Fig 8.)

The stability verification of the arch is performed according to the following steps:

Step 1: Determining decisive buckling mode

Step 2: Calculating imperfections

Step 3: Implementing imperfections in the MIDAS model

Step 4: Running a geometrically nonlinear analysis

Step 5: Verification of the results

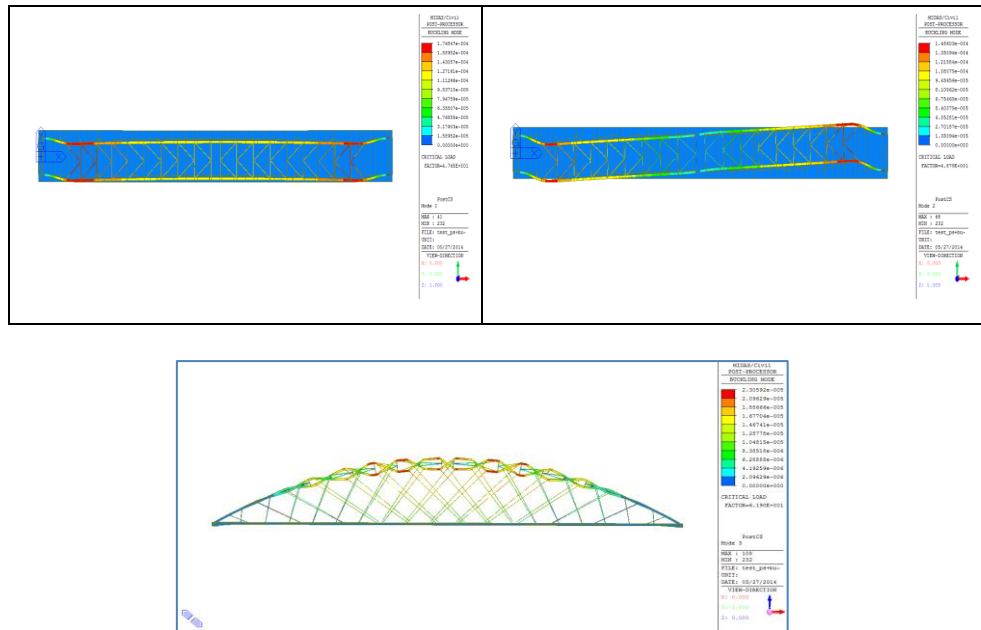


Figure 8. First three Buckling mode shapes.

#### 4 FATIGUE INVESTIGATION.

Bridges are subjected to dynamic loading, which makes the consideration of the fatigue behavior necessary. This is especially important for hangers and hanger connections, since they receive larger force variations than other bridge members. Subjected also to horizontal loading, hangers and their connections are therefore significantly prone to fatigue failure. In our bridge two fatigue assessments were made.

- Fatigue assessment based on nominal stress ranges.
- Fatigue assessment based on geometric stress ranges.

The second method of assessment is necessary because the hanger connection details are more complex than the test specimen with which the detail categories and fatigue strength curves, such as in the Eurocode 3, were created. If the geometry and the loading differ significantly from the listed detail categories, the nominal stress is not meaningful, and its application would lead to wrong results. Therefore, local stress concentrations at geometric discontinuities were investigated.

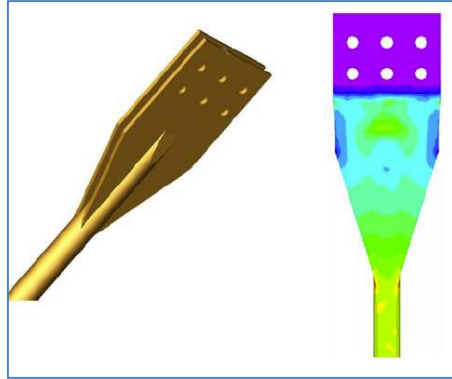


Figure 9. Fatigue assessment based on geometric stress ranges.

## 5 CONCLUSION

In this work the design of Arachthos bridge in Arta-Greece was discussed. The reduction of cost, resulting from the use of network arch bridges is of great interest. The structural members of network arches are mainly subjected to axial forces. Generally, structures with this characteristic are considered as efficient.

The arch root calls for special attention while designing it. The stress range due to live load is likely to exceed the allowed limits, because of the skew weld between the arch and the end plate which takes nominal stresses and shear stresses from the large axial force in the arch. One possible solution to improve this detail is enlarging the flanges of the arch profile and transferring the forces partially to the horizontal plate above the bearings. The minimum distance of the prestressing strand anchorages and the end cross girder require an enlargement of the concrete tie at the arch root.

Also care must be taken in the buckling calculation analysis and the fatigue of the steel components of the bridge.

## REFERENCES

- [1] Tveit P. Consideration for design of network arches. *J Struct Eng* 1987;10: 2198-207.
- [2] Tveit P. The network arch\_An extended manuscript from 21 lectures in 12Countries. Grimstad (Norway): Internet Edition; 2001.
- [3] Tveit P. The network arch. Bits of manuscript in September 2008 after lectures in 50 Countries. Internet Edition. 2008. <http://pchome.grm.hia.no/~ptveit/>.
- [4] Brunn B, Schanack F. Calculation of a double track railway network arch bridge applying the European standards. Technische Universität Dresden; 2003.
- [5] De Zotti A, Pellegrino C, Modena C. A parametric study of the hanger arrangement in arch bridges. In: 5th international conference on arch bridges. ARCH '07. 2007.



## **ROCKING AND OVERTURNING PROBLEMS IN BRIDGES**

George T. Michaltsos<sup>1</sup> and Ioannis G. Raftoyiannis<sup>2</sup>

<sup>1,2</sup>Department of Civil Engineering, National Technical University of Athens  
e-mail: michalts@central.ntua.gr, rafto@central.ntua.gr

**ABSTRACT:** This work presents a theoretical approach for dealing with the rocking and overturning problems in bridges subjected to near-source or long-distance earthquake actions. A simple mathematical model is developed for studying these phenomena in bridges as well as the conditions under which they may occur. Safety indicators for rocking and overturning of bridges subjected to earthquake actions are derived and presented in graphical form and useful conclusions are drawn.

**KEYWORDS:** Rocking, Overturning, Bridge dynamics, Earthquake actions

### **1 INTRODUCTION**

Rocking and overturning are very interesting problems in the study of a bridge behavior under earthquake actions. The ground motions may be due to a near-source earthquake, the epicenter of which is located at a distance shorter than 70 km, or by a distant one with epicenter at a distance longer than 70 km [1,2]. The near-source earthquake has usually the character of a shock, while the distant one has the character of a normal dynamic excitation. In addition, the so-called "focal depth" is a significant factor for the dynamic behavior of a structural system [3]. The ratio of the focal depth to the distance of a structure from the epicenter affects the structural behavior in a special manner. From the last strong earthquakes in California and worldwide, it was pointed out that some bridges experienced overturning at their supports, while others have been cracked and serious damages occurred near their supports [4,5,6,7]. The aforementioned destructions and damages were caused by the phenomena of overturning and rocking.

The rocking phenomenon takes place when the vertical forces, caused by the vertical component of an earthquake excitation, are greater than (at least) one of the bridge's reactions. The overturning phenomenon occurs when the overturning moment of the whole bridge is higher than the corresponding stabilizing moment of the bridge [8]. In the earthquake of March 27, 1964, in the Gulf of Alaska, the steel trusses of the Copper River and Northwestern Railroad Bridge near Round Island were shifted from one-third to two-thirds of

a meter. Figure 1(a) shows one of the displaced trusses, which pounded against an adjacent steel girder span. The girder span was moved to the right, its concrete pedestal was rotated, and the girder span almost fell into the river. Note the shortening indicated by buckling of the guardrail.

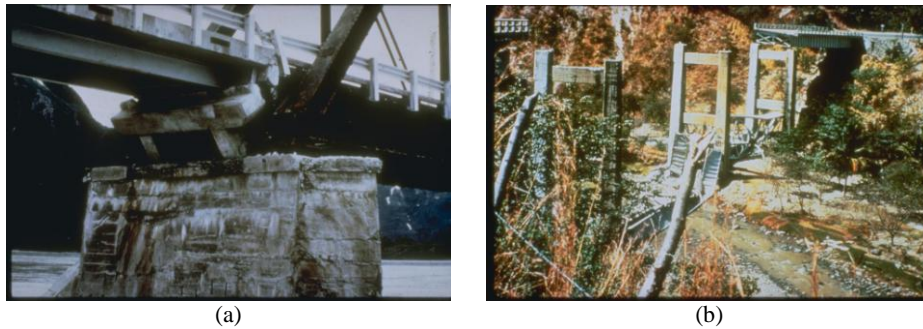


Figure 1. (a) Support damage due to rocking, (b) Overturning of three spans

In the earthquake of February 4, 1976, in Guatemala, three central spans of the Agua Caliente Bridge collapsed on the road to the Atlantic Ocean. Both ground shaking and ground failure contributed to this collapse (see Fig. 1(b)). The above characteristic cases [10], a few among many similar events worldwide, show that the rocking and overturning phenomena are commonly met in bridges subjected to actions of near-source and long-distance earthquakes.

The present work deals with the above phenomena by considering a simple bridge model whose supports can move differently and that is subjected to the action of a shallow, middle depth or deep focus earthquake. The equations of motion of the bridge are derived using the influence functions and employing modal superposition analysis [11]. Next, the conditions for rocking and overturning are presented and safety indicators for each one of the aforementioned cases are derived. Illustrative examples are presented for various earthquake and bridge parameters and useful conclusions are drawn regarding the influence of these parameters on the safety indicators.

## 2 BASIC CONSIDERATIONS

Let us consider the bridge B shown in Fig. 2, that is subjected to an earthquake with focus A and epicenter A'. The horizontal distance between the bridge and the epicenter is L and the focal depth is H. The ground motion can be due to a near-source earthquake (for  $L \leq 70\text{km}$ ) or by a distant one (for  $L > 70\text{km}$ ). An earthquake has either the character of a shock, or the character of a normal dynamic excitation. For the first case, the time function of the ground motion can be approximated by the following expression [12]

$$f_o(t) = k e^{-\beta t} \sin \Omega_0 t \quad (1)$$

while for the case of a distant earthquake, it can be used [13]

$$f_o(t) = kt e^{-\beta t} \sin \Omega_0 t \tag{2}$$

where  $k$  is a constant that depends on the soil characteristics,  $\beta$  is the damping ratio and  $\Omega_0$  is the frequency of the ground motions.

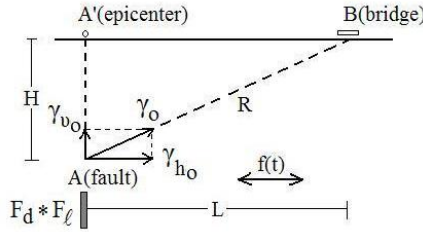


Figure 2. Earthquake's focus A, epicenter A' and bridge B locations

### 2.1 The equations of motion for the bridge model

The equations of lateral-torsional motion of a bridge, as shown in Fig. 3(a), whose supports can move differently (according to the ground motions  $f_1(t)$  for the support at the left, and  $f_2(t)$  for the support at the right) are:

$$\left. \begin{aligned} EI_y w_0'''' - c_z \dot{w}_0 + m \ddot{w}_0 &= -m[g_1(x) \ddot{f}_{v1} + g_2(x) \ddot{f}_{v2}] - c_z [g_1(x) \dot{f}_{v1} + g_2(x) \dot{f}_{v2}] \\ EI_z v_0'''' - EI_z z_M \theta'''' + c_y \dot{v}_0 + m \ddot{v}_0 &= -m[g_1(x) \ddot{f}_{h1} + g_2(x) \ddot{f}_{h2}] - c_y [g_1(x) \dot{f}_{h1} + g_2(x) \dot{f}_{h2}] \\ EC_s \theta'''' - EI_z z_M v_0'''' + c_y \dot{\theta} - GJ_d \theta'' - \Theta_x \ddot{\theta} &= 0 \end{aligned} \right\} \tag{3}$$

where,  $EI_y$ ,  $EI_z$ ,  $GJ_d$  and  $EC_s$  are the bending, torsional and warping rigidity of the bridge cross section, respectively,  $m$  is the mass per unit length and  $\Theta_x$  is the rotational inertia of the bridge,  $c_y$  and  $c_z$  are the damping coefficients corresponding to linear viscous damping,  $z_M$  is the distance between the center of gravity and the shear center,  $g_1(x)$  and  $g_2(x)$  are the influence functions and  $f_1(t)$  and  $f_2(t)$  the time functions for the motions of the supports.

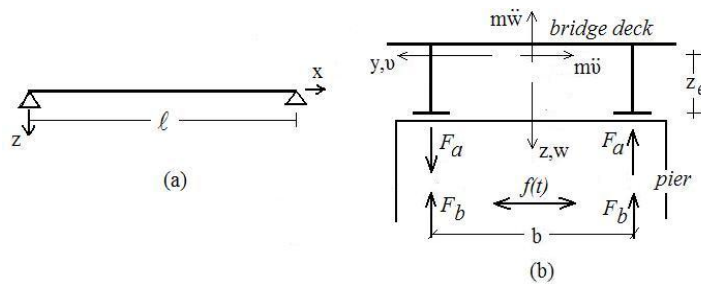


Figure 3. (a) Single-span bridge model, and (b) detail at the support

Since the first of eqs(3) is independent of the other two, we are searching for a solution in the form of separate variables where  $W_n(x)$ ,  $V_n(x)$  and  $\Phi_n(x)$  are the shape functions of the bridge deck, corresponding to displacements  $w_0$ ,  $v_0$  and rotation  $\theta$ , while  $P_n(t)$  and  $T_n(t)$  are the time functions to be determined.

Introducing the expressions for  $w_0$ ,  $v_0$  and  $\theta$  into eqs(3) and solving the resulting differential system after employing the orthogonality conditions for the bridge deck, we obtain the expressions for the time functions  $P_n(t)$  and  $T_n(t)$ . Assuming that the length of the bridge  $\ell$  is small compared to the epicentral distance  $L$ , both supports are subjected to the same ground motion, and hence, the resulting solution for the equations of motion is:

$$\left. \begin{aligned} g_1(x) &= g_2(x) = 1 \\ P_n(t) &= -\frac{\int_0^\ell W_n(x) dx}{\bar{\omega}_{zn} m \int_0^\ell W_n^2(x) dx} \int_0^t e^{-\beta_z(t-\tau)} [\ddot{f}_v(\tau) + 2\beta_z \dot{f}_v(\tau)] \sin \bar{\omega}_{zn}(t-\tau) d\tau \\ T_n(t) &= -\frac{\int_0^\ell V_n(x) dx}{\bar{\omega}_{\theta n} [m \int_0^\ell V_n^2(x) dx + \Theta_x \int_0^\ell \Phi_n^2(x) dx]} \int_0^t e^{-\beta_y(t-\tau)} [\ddot{f}_h(\tau) + 2\beta_y \dot{f}_h(\tau)] \sin \bar{\omega}_{\theta n}(t-\tau) d\tau \\ w(x,t) &= f_v(t) + \sum_n W_n(x) P_n(t) \\ v(x,t) &= f_h(t) + \sum_n V_n(x) T_n(t) \end{aligned} \right\} \quad (4)$$

### 3 THE ROCKING PHENOMENON

Let us consider the bridge shown in Fig. 3(a) with a cross-section as shown in Fig. 3(b). The reactions developing due to the inertia forces  $m\ddot{w}(x)$  and  $m\ddot{v}(x)$  for a non-loaded bridge are  $V_1$  and  $H_1$  for the left support and  $V_2$  and  $H_2$  for the right support. In the case of a long-span bridge, where each support is subjected to different ground motion, it is  $V_1 \neq V_2$  and  $H_1 \neq H_2$ . In the present analysis, where bridges with relatively short spans are considered, we assume that both supports are subjected to the same ground motion and thus,  $V_1 = V_2 = V$  and  $H_1 = H_2 = H$ . The produced overturning forces  $F_a$  are:

$$F_a = \frac{1}{b} (H z_e + V \frac{b}{2}) \quad (5)$$

where,  $z_e$  is the distance between the center of gravity of the cross-section and the supports, and  $b$  is the horizontal distance between the supports (see Fig. 3b). On the other hand, taking into account that the bridge is supported by two bearings on each pylon, the vertical reactions are:

$$F_b = \frac{m g \ell}{4} \quad (6)$$

Thus, the condition expressing safety of the bridge against rocking is  $F_a \leq F_b$ , and using eqs(3), the safety condition against rocking is given by the following inequality:

$$\frac{z_e}{b\ell} \int_0^\ell m x [\ddot{f}_h(t) + \sum_n V_n(x) \ddot{T}_n(t)] dx + \frac{1}{2\ell} \int_0^\ell m x [\ddot{f}_v(t) + \sum_n W_n(x) \ddot{P}_n(t)] dx \leq \frac{m g \ell}{4}$$

or, in a more concise form:

$$A = \frac{4}{g \ell^2} \left[ \frac{z_e}{b} \int_0^\ell x [\ddot{f}_h(t) + \sum_n V_n(x) \ddot{T}_n(t)] dx + \frac{1}{2} \int_0^\ell x [\ddot{f}_v(t) + \sum_n W_n(x) \ddot{P}_n(t)] dx \right] \leq 1 \quad (7)$$

where  $A$  is the safety indicator against rocking, reciprocal of the corresponding safety factor.

#### 4 THE OVERTURNING PHENOMENON

The condition expressing safety against overturning of the bridge can be readily derived in a similar manner. Considering the entire length of the bridge, the overturning moment must be less or equal to the stabilizing moment, i.e. the following condition must be satisfied

$$z_e \int_0^\ell m \dot{v}(x,t) dx + \frac{b}{2} \int_0^\ell m \ddot{w}(x,t) dx \leq m g \ell \frac{b}{2}$$

Using eqs(3), the safety condition against overturning is given by the following inequality:

$$z_e \int_0^\ell m [\ddot{f}_h(t) + \sum_n V_n(x) \ddot{T}_n(t)] dx + \frac{b}{2} \int_0^\ell m [\ddot{f}_v(t) + \sum_n W_n(x) \ddot{P}_n(t)] dx \leq \frac{m g \ell b}{2} \quad (8)$$

or, in amore concise form

$$B = \frac{1}{g \ell b} \left[ 2z_e \int_0^\ell [\ddot{f}_h(t) + \sum_n V_n(x) \ddot{T}_n(t)] dx + b \int_0^\ell [\ddot{f}_v(t) + \sum_n W_n(x) \ddot{P}_n(t)] dx \right] \leq 1 \quad (9)$$

where  $B$  is the safety indicator against overturning.

#### 5 NUMERICAL RESULTS AND DISCUSSION

Let us consider a simply supported bridge with length  $\ell = 70\text{m}$  and doubly symmetric cross-section ( $z_M = 0$ ), as shown in Fig. 4. The bridge is made from structural steel (isotropic and homogeneous material) with modulus of elasticity  $E = 2,1 \times 10^8 \text{kN/m}^2$ , shear modulus  $G = 0,8 \times 10^8 \text{kN/m}^2$ , moments of inertia  $I_y = 0,80 \text{m}^4$  and  $I_z = 8,50 \text{m}^4$ , torsional constant  $J = 0,50 \text{m}^4$ , warping constant  $C_s = 0,04 \text{m}^6$ , mass per unit length  $m = 800 \text{ kg/m}$  and rotational inertia  $\Theta_x = 2500 \text{kgm}^2$ . Since the cross-section is doubly symmetric, the bending and torsional problems are uncoupled. The modal functions for a simply supported beam, that can be readily obtained, are:  $W_n(x) = V_n(x) = n\pi x/\ell$ .

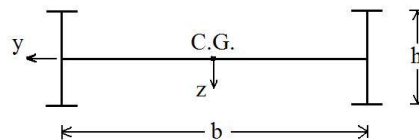


Figure 4. Cross-sectional geometry of a simply supported bridge

In the present study, we consider a shallow depth earthquake of  $H = 1\text{km}$ , a middle depth of  $H = 30\text{km}$ , and a deep focus earthquake of  $H = 70\text{km}$ .

Two cases of soil properties are considered: granite soil with characteristics  $V=5,5$  m/s,  $\zeta_1=0,001$ ,  $\zeta_2=0,05$  and  $\zeta_3=0,004$ , and schist soil with characteristics  $V=2,5$  m/s,  $\zeta_1=0,05$ ,  $\zeta_2=0,08$  and  $\zeta_3=0,015$ .

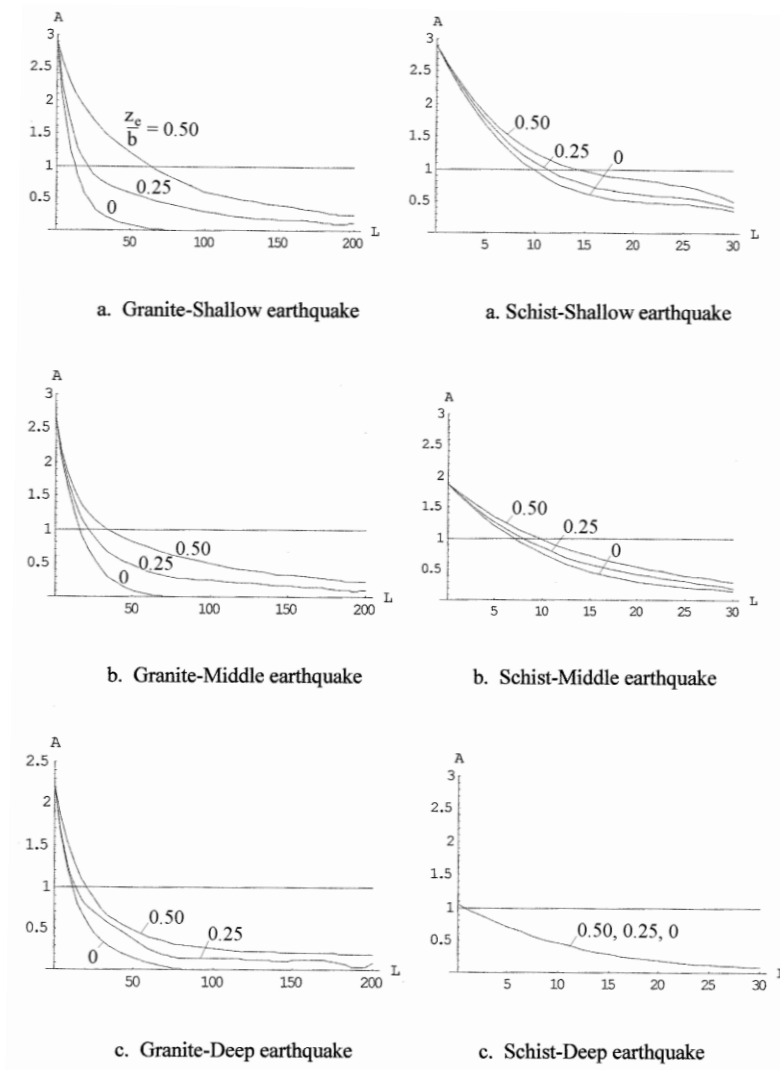


Figure 5. Variation of the safety indicator  $A$  against rocking for granite and schist soils for: (a) shallow depth earthquake, (b) middle depth earthquake, and (c) deep focus earthquake

The influence of the vertical distance  $z_e$  between the center of gravity and the supports of the bridge on the safety against rocking and overturning is studied for the values  $z_e = 0, 0,25$  and  $0,50$ .

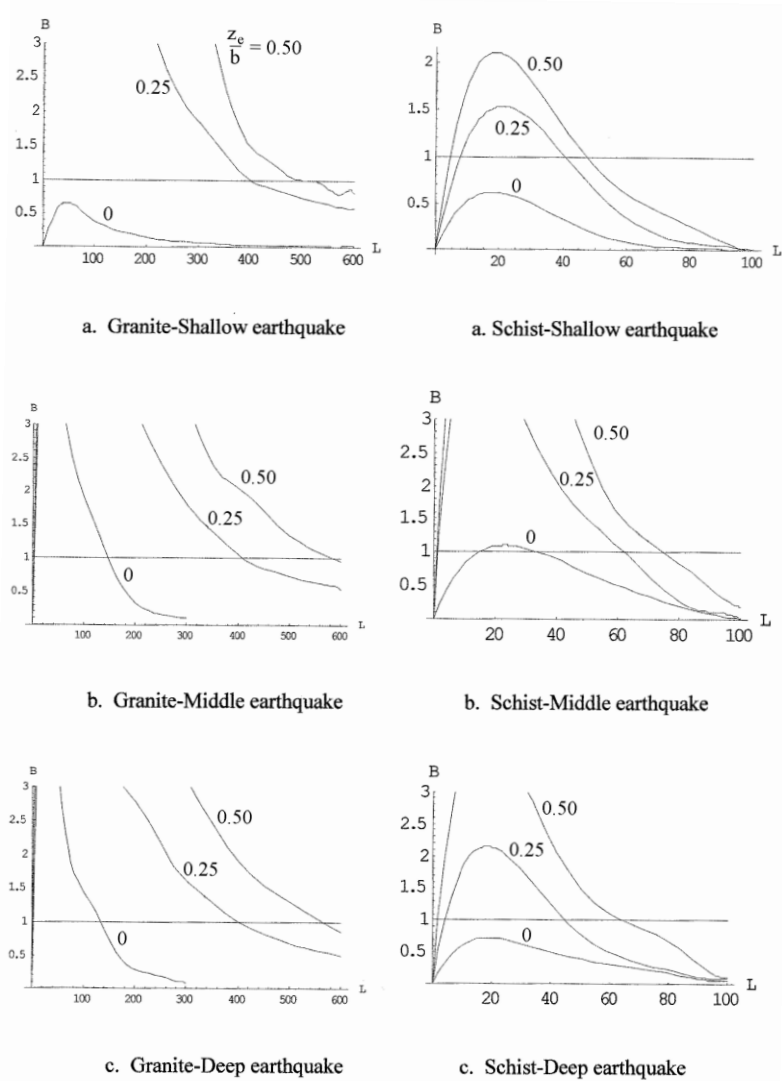


Figure 6. Variation of the safety indicator  $B$  against overturning for granite and schist soils for: (a) shallow depth earthquake, (b) middle depth earthquake, and (c) deep focus earthquake

## 6 CONCLUSIONS

From the examined case studies, one can draw the following conclusions:

1. The influence of the ratio  $z_e/b$  that depends on the bridge's characteristics is particularly significant for rocking and overturning. It is prudent that this

ratio must be smaller than the values 0,2 to 0,3 for the protection against rocking, while for safety against overturning the ratio has to be kept smaller than 0,4.

2. For structures laid or erected near an active tectonic fault with ratio  $H/L < 1$ , one must pay great attention to the design of the bridge and study the influence of each one of its characteristics on the rocking and, especially, on the overturning phenomena, in order to avoid disastrous and costly consequences.
3. Bridges built near a shallow fault must be protected against shifting by special construction measures that will be able to undertake the developed horizontal forces.
4. A shallow earthquake with epicentral distance about 80km, a middle depth earthquake with distance 40km and a deep earthquake with distance 20km transmitting in granite soil can produce damages in bridges due to rocking. The corresponding distances for schist soil are 25km, 10km and ~0km.
5. An earthquake in granite soil is more dangerous for overturning of bridges for epicentral distances up to 350km and practical values of the eccentricity ratio  $z_e/b$  (~0,25) regardless of the focal depth, while for an earthquake in schist soil and the same eccentricity ratio severe danger of overturning exists for epicentral distances of 45km (shallow), 60km (middle depth) and 40km (deep focus).

## REFERENCES

- [1] Price TE, Eberhard MO. Effects of spatially varying ground motions on short bridges. J Struct Eng, ASCE 1998;124(8): 948-955.
- [2] Zerva A. Spatial variability of seismic motions recorded over extended ground surface areas. In: Kausel E, Manolis G, editors. Wave motion in earthquake engineering, MIT Press, Cambridge, Mass. 1999.
- [3] Harichandran RS, Wang W. Response of indeterminate two-span beam to spatially varying seismic excitation. Earthquake Eng & Struct Dynamics, 1990;19: 173-187.
- [4] Betti R, Abdel-Ghaffar AM, Niazy AS. Kinematic soil-structure interaction for long-span cable-supported bridges. Earthquake Eng & Struct Dynamics, 1993;22: 415-430.
- [5] Monti G, Nuti C, Pinto P. Nonlinear response of bridges under multisupport excitation. J Struct Eng, ASCE, 1996;122(10): 1147-1158.
- [6] Nikolaou A, Mylonakis G, Gazetas G, Tazoh T. Kinematic pile bending during earthquakes: Analysis and measurements. Geotechnique, London, 2001;51(5): 425-440.
- [7] Zerva A. Response of multi-span beams to spatially incoherent seismic ground motions. Earthquake Eng & Struct Dynamics, 1990;19: 819-832.
- [8] ENV 1998-2, Eurocode 8-Part 2: Bridges, May 2002.
- [9] Michaltsos GT. Dynamical Problems of Steel Bridges. (in Greek) Symeon Publ Co, Athens, 2005.
- [10] <http://www.ngdc.noaa.gov/seg/hazard/earthqk.shtml>
- [11] Wylie CR. Advanced Engineering Mathematics. McGraw-Hill Kogakusha Ltd, Tokyo 1975.
- [12] Abrahamson NA, Schneider JF, Stepp JC. Empirical spatial coherency functions for application to soil-structures interaction analyses, Earthquake Spectra, 1991;7(1):25-32.
- [13] Bogdanoff JL, Goldberg JE, Schiff AJ. The effect of ground transmission time on the response of long structures. Bull seismological Soc of America, 1965;55: 627-640.



## **SHEAR DESIGN OF BRIDGE PIERS WITH RECTANGULAR AND CIRCULAR CROSS-SECTION**

Ioannis A. Tegos<sup>1</sup>, Sevasti D. Tegou<sup>2</sup> and Vasileios G. Pilitsis<sup>3</sup>

<sup>1,2,3</sup> Aristotle University of Thessaloniki, Dept. of Civil Engineering, Greece  
e-mail: itegos@civil.auth.gr, stegou@civil.auth.gr, vpilitsi@civil.auth.gr

**ABSTRACT:** This study is analytical and presents the investigation on the resistance of circular and rectangular section bridge piers under shear and axial loading. Design diagrams taking into account the angle  $\theta$  between the concrete compression strut and the member's angle perpendicular to the shear action are proposed. The effect of the compressive axial loading is taken into account for the determination of the aforementioned angle  $\theta$ . Both Codes and bibliography give the incorrect impression that the angle  $\theta$  is independent from the compressive axial loading. Consequently, the shear design is not rational and, more importantly, in most cases its result is not on the safe side. Furthermore the codes neglect the effect of the axial loading on the determination of the lever arm of the internal forces.

**KEY WORDS:** Bridge; Pier; Shear; Axial loading.

### **1 INTRODUCTION**

The last years, more and more codes emphasize to the seismic safety of structures and as a result the seismic criteria predominate to the design methods of structures. The aforementioned remark strongly affects checks concerning loading combinations without earthquake. There are many issues on the design of concrete structures which until today have not received the same attention and the current treatment is not adequate. These issues are mainly related to the shear and punching shear design of concrete members. The differences observed on the aforementioned design issues between design codes ensure the statement about insufficient attention on important design issues.

Geometry of the concrete members is an important parameter which affects shear design. A typical example is the case of the analysis and design of short members for which the Bernoulli beam theory can't be applied, as well as the case of particular members of hollow circular or rectangular cross-sections. The hollow circular or rectangular sections are used at columns, bridge piers, tubes, refrigeration towers, chimneys, water-towers etc. It is known that if the diameter of a circular cross-section is greater than 2.5m, it is desirable to use a hollow rather than a solid cross-section [1]. Solid pier cross-sections with a

diameter greater than 2.5m must be avoided, because the heat diffusion has negative influence on the concrete strength. On the other hand the critical point of hollow sections is the sensitivity of the compression zone under seismic loading especially in the case that two layers hoop reinforcement are used. In these cases it is necessary to tie the inner longitudinal reinforcements with transverse ties. Current Codes use rectangular cross-section as the base for the dimensioning of the rest types of sections [2], [3].

The aim of this study is to present an investigation on the dimensioning of solid circular and rectangular sections. The dimensioning of the members with the aforementioned cross-sections for the ultimate limit states is the bending with axial loading design, shear design, torsion and buckling. As far as serviceability limit states, current codes include only indicative provisions about the determination of the crack width as well as the deflection, while methodologies for the determination of the neutral axis of the section can be found in the bibliography [4], [5]. It is also noted that, in the case of bridge piers, serviceability and ultimate limit states are the main concerns for seismic design.

## **2 PROPOSED METHODOLOGY**

### **2.1 Rectangular solid cross-sections**

In general, there are two methods for the determination of the shear capacity of a section. Both methods adopted a truss model for determining the capacity of a section with shear reinforcement. In the standard method, the concrete compression struts are assumed to act at  $45^\circ$  to the horizontal and the shear capacity of the concrete section is added to the capacity of the shear reinforcement to determine the total capacity of the cross-section.

In the variable strut inclination method, the designer is free, within certain limits, to choose the angle of the concrete compression strut. The area of the shear reinforcement required to maintain equilibrium can then be calculated. In this method the shear capacity of the concrete is not added to the shear capacity of the truss [6].

Variable strut inclination method is used by Current Codes and consequently by the most reliable software like Sofistik and Static for the calculation of the shear resistance of concrete members with shear reinforcement.

An accurate calculation of the shear resistance  $V_{Rd,s}$  of members with vertical shear reinforcement is necessary in the case of solid circular and rectangular cross-section of bridge piers. The seismic shear action is usually critical for the dimensioning of the bridge piers. The critical cross-sections are the positions of the maximum moment and never the positions where the moment is zero as it usually happens at beams [7].

The calculation of the shear resistance depends on the accurate estimation of the inner lever arm  $z$ . The indicative angle  $\theta$  of the compression strut usually is

determined by an upper and a lower limit. For example DIN 1045-1 assigns the limits given in Equation (1) for the determination of angle  $\theta$  [8]:

$$0.58 \leq \cot \theta \leq \frac{1.2 - 1.4 \sigma_{cd} / f_{cd}}{1 - V_{Rd,c} / V_{Ed}} \quad (1)$$

Equation 1 is developed by the study in order to propose a new design method for the calculation of the shear reinforcement of solid circular and rectangular cross-sections. Fig.1 summarizes the proposed methodology. The  $\rho_v$  and  $\cot \theta$  curves are referred to the coordinate system whose y-coordinate is  $v$  and x-coordinate is  $v_E / \zeta$ . The following equations were used for the derivation of the  $\rho_v$  curves.

$$v_E = \frac{V_E}{b \cdot h \cdot f_{cd}} \quad (2)$$

$$z = \zeta \cdot h \quad (3)$$

$$\frac{A_{sv}}{s \cdot b} = \rho_v \quad (4)$$

$$\begin{aligned} V_E = V_{Rd,sv} &= \frac{A_{sv}}{s} \cdot f_{yv} \cdot z \cdot \cot \theta \Rightarrow \\ \Rightarrow v_E \cdot b \cdot h \cdot f_{cd} &= \rho_v \cdot b \cdot f_{yv} \cdot \zeta \cdot h \cdot \cot \theta \Rightarrow \\ \Rightarrow \frac{v_E}{\zeta} &= \rho_v \cdot \cot \theta \cdot \frac{f_{yv}}{f_{cd}} \end{aligned} \quad (5)$$

$$\cot \theta = \frac{1.2 - 1.4 \frac{\sigma_{cd}}{f_{cd}}}{1 - \frac{V_{Rd,c}}{V_E}} \quad (6)$$

$$v = \frac{\sigma_{cd}}{f_{cd}} \quad (7)$$

$$f_{ck}^{1/3} \cong 3.0 \quad (8)$$

$$\begin{aligned}
V_{Rd,c} &= \beta_{ct} \cdot 0.10 \cdot f_{ck}^{1/3} \cdot (1 + 1.2 \cdot \frac{\sigma_{cd}}{f_{cd}}) \cdot b \cdot z = \\
&= 2.4 \cdot 0.10 \cdot 3.0 \cdot (1 + 1.2 \cdot v) \cdot b \cdot z \Rightarrow \\
\Rightarrow V_{Rd,c} &= 0.72 \cdot (1 + 1.2 \cdot v) \cdot b \cdot z
\end{aligned} \tag{9}$$

From Eq.(5), Eq.(6) and Eq.(9) derives:

$$\begin{aligned}
\cot \theta &= \frac{1.2 - 1.4 \cdot \frac{\sigma_{cd}}{f_{cd}}}{1 - \frac{V_{Rd,c}}{V_E}} = \frac{1.2 - 1.4 \cdot v}{1 - \frac{0.72 \cdot (1 + 1.2 \cdot v) \cdot b \cdot z}{V_E}} = \\
&= \frac{1.2 - 1.4 \cdot v}{1 - \frac{0.72 \cdot (1 + 1.2 \cdot v) \cdot \zeta}{\frac{V_E \cdot f_{cd}}{b \cdot h \cdot f_{cd}}}} = \frac{1.2 - 1.4 \cdot v}{1 - \frac{0.72 \cdot (1 + 1.2 \cdot v)}{\frac{v_E}{\zeta} \cdot f_{cd}}} \Rightarrow \\
\Rightarrow \cot \theta &= \frac{1.2 - 1.4 \cdot v}{1 - \frac{0.04 \cdot (1 + 1.2 \cdot v)}{\frac{v_E}{\zeta}}}
\end{aligned} \tag{10}$$

The value of  $z$  for elements of rectangular cross-sections under concurrent action of moment and axial compressive force can be expressed as a function of the normalized axial force. The resultant stress in tensile zone is always equal to the sum of stresses in compression zone and the axial compressive force.

$$F_c = A_{s1} \cdot f_{yd} + N_d = A_{s2} \cdot f_{yd} + N_d \tag{11}$$

The moment of the two actions in the compression zone relative to the center of gravity of tensile reinforcement is:

$$x = \frac{\varepsilon_c}{\varepsilon_c + \varepsilon_s} \cdot d = \frac{3.5}{3.5 + \varepsilon_s} \cdot d \tag{12}$$

Regarding the previous equations it is possible to say that in the this problem yielding of reinforcement in compression always precedes yielding of reinforcement in tension, so at the ultimate limit state yielding of compression reinforcement is always present while the deformation of reinforcement in tension is not known and must be calculated from the specific interaction diagrams of literature.

Following the above mentioned, regarding the lever arm of internal forces, the following apply:

$$z = \frac{A_{s2} \cdot f_{yd} \cdot (h - d') + N_d \cdot (d - k_y \cdot x)}{A_{s2} \cdot f_{yd} + N_d} \Rightarrow$$

$$\frac{z}{h} = \frac{\frac{0.5 \cdot A_{st} \cdot f_{yd}}{b \cdot h \cdot f_{cd}} \cdot 0.9 + 0.95 \cdot \frac{N_d}{b \cdot h \cdot f_{cd}} \cdot (1 - 0.416 \cdot \frac{\varepsilon_c}{\varepsilon_c + \varepsilon_s})}{\frac{0.5 \cdot A_{st} \cdot f_{yd}}{b \cdot h \cdot f_{cd}} + \frac{N_d}{b \cdot h \cdot f_{cd}}} \Rightarrow$$

$$\frac{z}{h} = \frac{0.45 \cdot \omega \cdot 0.9 + 0.95 \cdot (1 - 0.416 \cdot \frac{\varepsilon_c}{\varepsilon_c + \varepsilon_s}) \cdot \nu}{0.5 \cdot \omega + \nu} \quad (13)$$

And therefore:

$$\frac{z}{h} = \frac{0.45 \cdot \omega + (0.95 + 0.395 \cdot \frac{3.5}{3.5 + \varepsilon_s}) \cdot \nu}{0.5 \cdot \omega + \nu} \quad (14)$$

Where:  $\frac{d_1}{h} = \frac{d_2}{h} = 0.05$

By using the corresponding interaction diagram, from which the corresponding  $\varepsilon_s$  values for  $\omega$  and  $\nu$  are obtained, follows the diagram of Fig.1. With the aid of this diagram the value of  $z$  accrues, based on the two values of the parameters  $\nu$ ,  $\mu$  or  $\omega$ .

## 2.2 Circular solid cross-sections

Working in an analogous way for circular solid cross-sections the diagram of Fig.2 accrues.

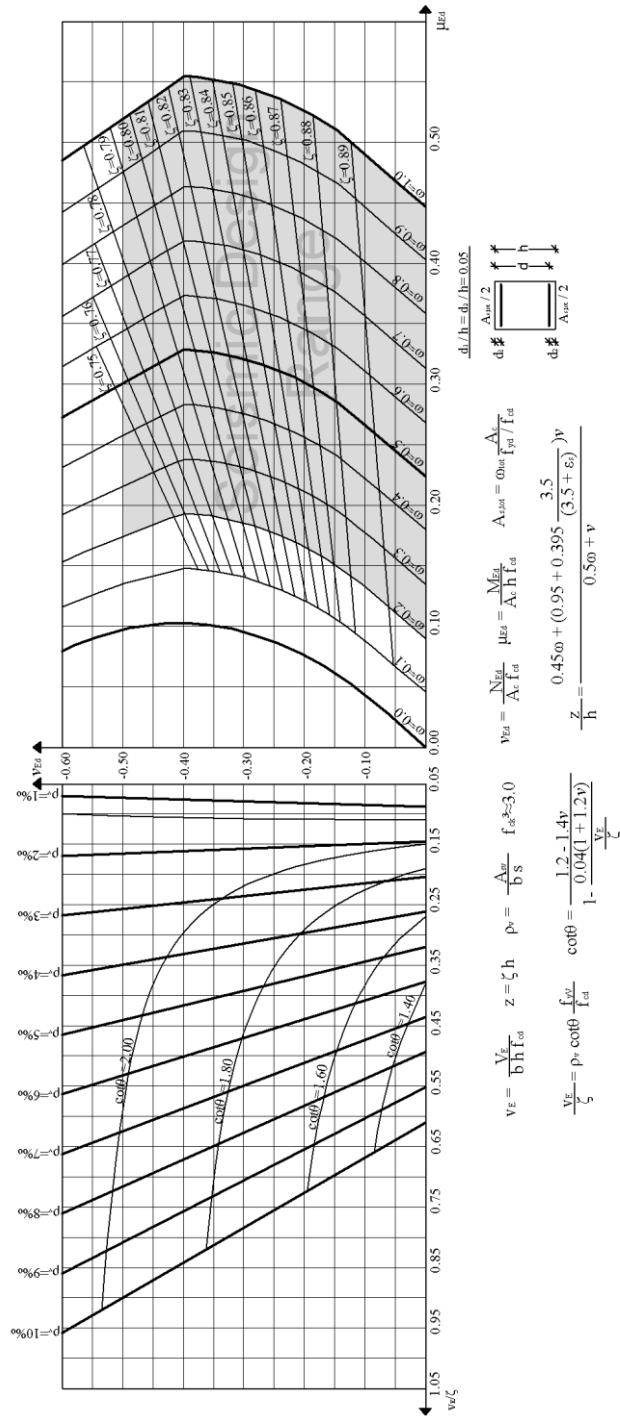


Figure 1.  $v - \mu - v$  diagram for rectangular solid cross-sections

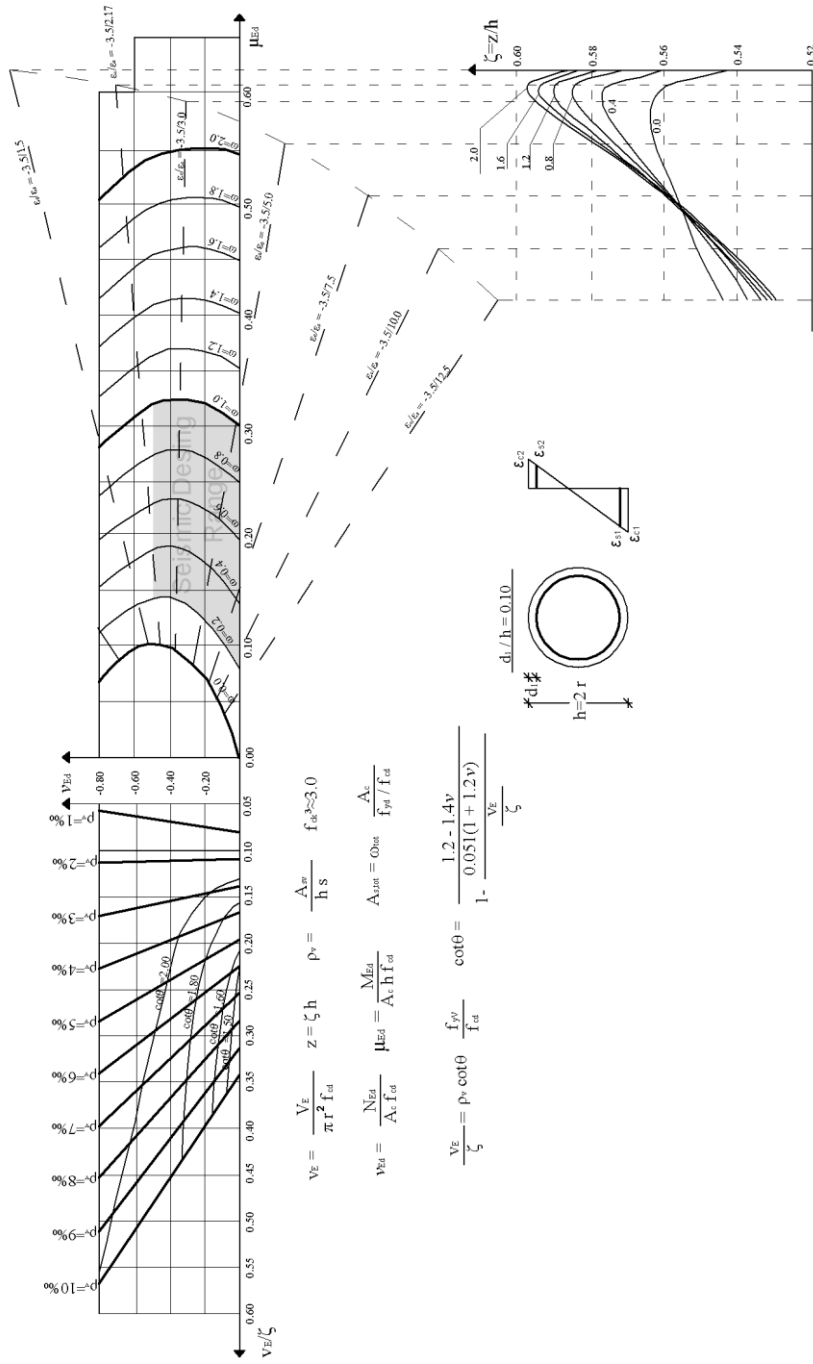


Figure 2.  $v - \mu - v$  diagram for circular solid cross-sections

### 3 CONCLUSIONS

The present study aims at a rational shear design management, with the concurrent action of axial force and bending moment, in piers of bridges, as the contained in EC2 methodology underestimates the concurrent presence of these three actions. The main findings of the study can be summarized in the following:

1. The transverse reinforcement cannot be calculated without taking into account the influence of the normalized axial force due to the strong influence of the value of lever arm  $z$  of internal forces in the result.
2. The slope of the diagonal struts  $\theta$ , on which depend both the ratio of shear reinforcement and also its strength, cannot be elected based on criteria that ignore the presence of the axial compressive force.
3. The proposed methodology is illustrated in the present work for the case of rectangular and circular cross-sections at appropriate interaction diagrams among the three involved cross-section forces.

### REFERENCES

- [1] Priestley, M J N, "Seismic Design Issues of Hollow Bridge Piers", Report No 98/01,8/1998, 1998
- [2] CEN [Comité Européen de Normalisation], *EN 1992-1: Eurocode 2: Design of Concrete Structures - Part 1-1: General Rules and Rules for Buildings*, 2004.
- [3] CEN [Comité Européen de Normalisation], *EN 1992-2: Eurocode 2: Design of Concrete Structures - Part 2: Concrete Bridges – Design and Detailing Rules*, 2004.
- [4] Rusch, H, "Researches toward a General Flexural Theory for Structural Concrete", ACI Materials Journal, title no. 57(7), 1-28,1960.
- [5] Hognestad, E, "Study of Combined Bending and Axial Load in Reinforced Concrete Members", University of Illinois, Engineering Experimental Station, bulletin no.399, vol.49-52, 1951.
- [6] Rabbat, B G, Collins, M P, "A Variable Angle Space Truss Model for Structural Concrete Members Subjected to Complex Loading", American Concrete Institute, Farmington Hills, SP 55-22, 1978.
- [7] Priestley, M J N, Seible, F, Calvi, G M, "Seismic Design and Retrofit of Bridges", John Wiley & Sons, New York, USA, 1996
- [8] Deutsches Institut Fur Normung E.V., DIN 1045-1: Plain, Reinforced and Prestressed Concrete Structures – Part 1: Design and Construction, 2008.



## EFFECTIVENESS OF CLASSICAL PENDULUM BEARINGS

Ioannis G. Raftoyiannis<sup>1</sup>, Theodore G. Konstantakopoulos<sup>2</sup>  
and George T. Michaltsos<sup>3</sup>

<sup>1,2,3</sup> National Technical University of Athens, Dept. of Civil Engineering, Greece  
e-mail: rafto@central.ntua.gr, theokons@teemail.gr, michalts@central.ntua.gr

**ABSTRACT:** During the last decades, Friction Pendulum Bearings (FPB) with one or more concave sliding surfaces are dominating bridge structures. For bridges with relative small lengths, the use of classical pendulum bearings maybe a more simple and economical solution. In this paper, an attempt to investigate the dynamical behavior of such system is presented. Special emphasis is given on its behavior due to seismic excitation.

**KEYWORDS:** Bridge Dynamics; Pendulum bearings; Seismic excitation

### 1 INTRODUCTION

Although considerable progress has been made in earthquake engineering towards the end of last century, catastrophic bridge failure examples are found wherever large-scale earthquakes occur. Damage of the bridge structures occurs primarily in the piers, which may in turn result in collapse of the bridge spans. The effort on protection of bridges against earthquakes should therefore be focused on minimizing the forces to be carried by the piers, and particularly the shear forces. Isolation systems are basically categorized into rubber bearings and sliding bearings, while the old classical pendulum rolling bearings are practically abandoned.

This paper attempts to investigate the effectiveness of pendulum systems, and especially its behavior in the case of seismic excitation.

### 2 INTRODUCTORY CONCEPTS

#### 2.1 The Classical Pendulum Rolling Bearings (CPRB)

Let us consider a CPRB isolator with one concave rolling such as the one shown in Fig. 1. For angles  $\varphi$  up to  $15^\circ$  (0.2618 rad), which is an extreme limit-value of the maximum displacement of a friction isolators, we have  $\tan\varphi - \sin\varphi = 0.009 \ll 1$ . Therefore we may assume that:

$$\tan\varphi \cong \sin\varphi, \quad \cos\varphi \cong 1 \quad (1)$$

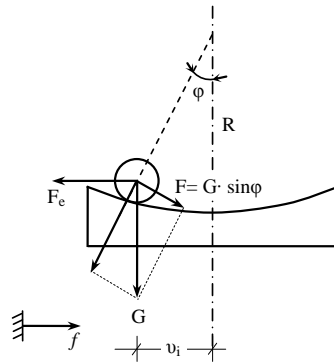


Figure 1. CPRB-type bearing

Analyzing the weight  $G$  into the force components  $F$  and  $V$ , we see that they are related as follows  $F=G \sin\varphi$ , or according to Fig.1:

$$F = G \cdot \frac{v_i}{R} \quad (2)$$

This mechanism acts as damper through the forces  $F$  (Fig. 1) that are developed because of the weight  $G$ . The friction forces due to rolling friction can be neglected, given that the rolling friction coefficient takes values up to 0.02.

It is obvious that the usefulness of such bearings is limited because of their limited strength and therefore, they can be applied on bridges with length up to 30 or 40 meters.

## 2.2 The bridge

Let us consider now a bridge without traffic loads but under the action of earthquake forces. The lateral displacement of an arbitrary point  $A(x)$  of the bridge resting on an FPB isolator is given by the relation (see Fig.2):

$$v(x, t) = f(t) + v_i(t) + v_o(x, t) \quad (3)$$

where  $f(t)$  is the ground displacement due to earthquake,  $v_i(t)$  is the displacement of the bridge support from the isolator's axis and  $v_o(x,t)$  is the elastic deformation of the bridge at point  $A(x)$ .

Considering for example that each end of the bridge is based on four supports (see Fig. 3) and assuming that the cross-section of the deck is non-deformable, the total acting forces are:

$$\left. \begin{aligned} H = \int_0^{\ell} m \cdot \ddot{u} \, dx, \quad V = m \cdot g \cdot \ell \end{aligned} \right\} \quad (4a,b)$$

Thus, on each support  $V_1$  it will be  $V_i = \frac{mg \ell}{8}$ , and because it is  $V_1=3V_2$  and  $V_1+V_2b/3=H \cdot e/2$ , we finally have  $V_1 = \frac{He}{2b(1+1/9)}$ .

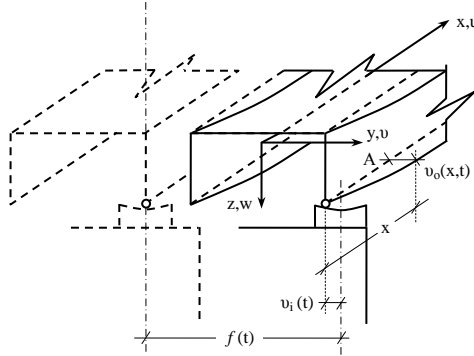


Figure 2. Displacement of arbitrary point A.

Therefore, the forces acting on the support 1 will be:

$$\left. \begin{aligned} H_1 &= \frac{1}{8} \cdot \int_0^\ell m \ddot{u} dx, & V_1 &= \frac{mg \ell}{8} + \frac{e}{b(1+1/9)} \cdot \int_0^\ell m \ddot{u} dx \end{aligned} \right\} \quad (5a,b)$$

where  $e$  is the distance of weight center from the isolator.

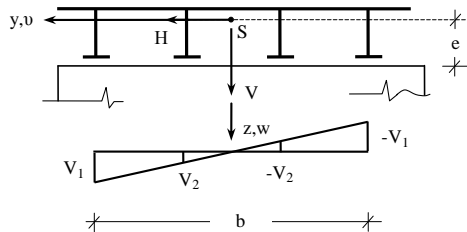


Figure 3. Forces on supports

Similarly, for a bridge based on two isolators at each end will be:

$$\left. \begin{aligned} H_1 &= \frac{1}{4} \cdot \int_0^\ell m \ddot{u} dx, & V_1 &= \frac{mg \ell}{4} + \frac{e}{2b} \cdot \int_0^\ell m \ddot{u} dx \end{aligned} \right\} \quad (6a,b)$$

### 3 THE EQUATIONS OF THE PROBLEM

The divergence forces (i.e. the inertia forces caused by earthquake) are produced by the total displacement of the bridge and thus, they will be equal to:

$$F_e = \int_0^{\ell} m \ddot{v} dx = \int_0^{\ell} m(\ddot{f} + \ddot{v}_i + \ddot{v}_o) dx \quad (7)$$

The above must be equilibrated by the restoring forces  $Gv_i/R$ , while for  $\varphi < 15^\circ$  the following equation is valid:

$$\int_0^{\ell} m \ddot{v} dx + G \frac{v_i}{R} = 0 \quad (8a)$$

On the other hand, the equation of the bridge's motion is valid, i.e.  $EI_z v'''' + c\dot{v} + m\ddot{v} = 0$ , which because of equation (3) becomes:

$$EI_z v'''' + c\dot{v}_o + m\ddot{v}_o = -c\dot{f} - m\ddot{f} - c\dot{v}_i - m\ddot{v}_i \quad (8b)$$

The above system of eqs. (8a) and (8b) gives the unknowns  $v_o(x,t)$  and  $v_i(t)$ . It is known that  $v_o(x,t)$ , can be expressed as follows:

$$v_o(x,t) = \sum_{\rho} \Psi_{\rho}(x) \Phi_{\rho}(t) \quad (9)$$

where  $\Psi_{\rho}(x)$  are the shape functions of the bridge for lateral displacements and  $\Phi_{\rho}(t)$  are time functions, under determination. Introducing eq.(9) into (8a) and (8b), and taking into account that  $\Psi_{\rho}(x)$  satisfies the equation of free motion, we obtain the following system after some manipulations:

$$\left. \begin{aligned} \sum_{\rho} \ddot{\Phi}_{\rho}(t) \int_0^{\ell} \Psi_{\rho}(x) dx + \frac{g\ell}{R} v_i(t) + \ell \ddot{v}_i(t) + \ell \ddot{f}(t) &= 0 \\ \ddot{\Phi}_{\rho} + \frac{c}{m} \dot{\Phi}_{\rho} + \omega_{\rho}^2 \Phi_{\rho} &= \frac{\int_0^{\ell} \Psi_{\rho} dx}{\int_0^{\ell} \Psi_{\rho}^2 dx} \cdot \left( -\frac{c}{m} \dot{f} - \ddot{f} - \frac{c}{m} \dot{v}_i - \ddot{v}_i \right), \quad \rho = 1, \dots, n \end{aligned} \right\} \quad (10a,b)$$

From the above system of eqs (10a) and (10b), one can determine the unknowns  $v_i(t)$  and  $\Phi_{\rho}(t)$ .

### 4 SOLUTION OF THE SYSTEM

In order for us to solve the above system, we use the Laplace transformation. Thus, we set:

$$L\Phi_{\rho}(t) = \varphi_{\rho}(p), \quad Lv_i(t) = U_i(p), \quad Lf(t) = F(p) \quad (11a,b,c)$$

with initial conditions:

$$\Phi_\rho(0) = v_i(0) = f(0) = 0 \quad (12a,b,c)$$

and hence, eqs (10a,b) become:

$$\left. \begin{aligned} \sum_\rho p^2 \varphi_\rho \int_0^\ell \Psi_\rho(x) dx + \frac{g\ell}{R} U_i + \ell p^2 U_i + \ell p^2 F = 0 \\ \left( p^2 + \frac{c}{m} p + \omega_\rho^2 \right) \varphi_\rho + \frac{\int_0^\ell \Psi_\rho dx}{\int_0^\ell \Psi_\rho^2 dx} \cdot \left( \frac{c}{m} p F + p^2 F + \frac{c}{m} p U_i + p^2 U_i \right) = 0 \end{aligned} \right\} \quad (13a,b)$$

with:  $\rho = 1$  to  $n$

The solution of the above system eqs (13), gives  $U_i(p)$  and  $\varphi_\rho(p)$ .

Therefore, it will be:

$$\left. \Phi_\rho(t) = L^{-1} \varphi_\rho(p), \quad v_i(t) = L^{-1} U_i(p) \right\} \quad (14a,b)$$

## 5 NUMERICAL EXAMPLES AND DISCUSSION

### 5.1 The isolator

Let us consider the CPRB of Fig. 1, which effectiveness we are going to study, with the following geometrical characteristics and limitations:

1. The diameter of the sphere must be:  $d > h = R(1 - \cos\varphi)$ , which for  $\varphi < 15^\circ$  gives:

$$d > 0.034 R \quad (15a)$$

2. The maximum displacement  $v_i$  must be:  $v_i < R \sin\varphi$  or

$$v_i < 0.2618 R \quad (15b)$$

3. Because of its strength limitations, the maximum load that such a mechanism can undertake is lower than 200 kN. For this reason, such a mechanism may have the form shown in Figs 5a, b, c etc.

### 5.2 The bridge

Let us consider a bridge with the following data:  $L=70\text{m}$ ,  $m=1500\text{kg/m}$ ,  $I_z=2\text{m}^2$ . The bridge, has cross-section like the one shown in Fig.3, with  $b=7.5$  and  $e=1.2\text{m}$ .

The first three eigenfrequencies are:  $\omega_1=10.66$ ,  $\omega_2=95.92$ ,  $\omega_3=266.45 \text{ sec}^{-1}$ . According to eq(5b) we find:  $V_1=1500 \text{ kN}$ ,  $V_2=1350 \text{ kN}$ , that means a similar distress of the supports.

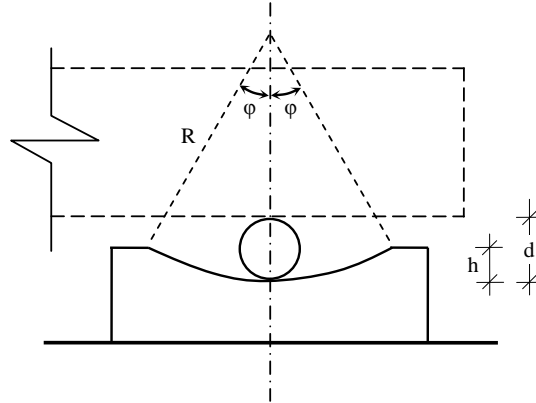


Figure 4. A typical CPRB

**5.3 The isolator’s and bridge’s behavior**

The ground motion considered, is given by the expression  $f = k \cdot e^{-\beta t} \sin \Omega t$ , with  $k=0.05$ ,  $\beta=0.20$ , and  $\Omega=8\text{sec}^{-1}$  ( $\gamma \cong 3\text{m/sec}^2$ ),  $\Omega=10\text{sec}^{-1}$  ( $\gamma \cong 4.9\text{m/sec}^2$ ),  $\Omega=12 \text{sec}^{-1}$  ( $\gamma \cong 6.98\text{m/sec}^2$ ).

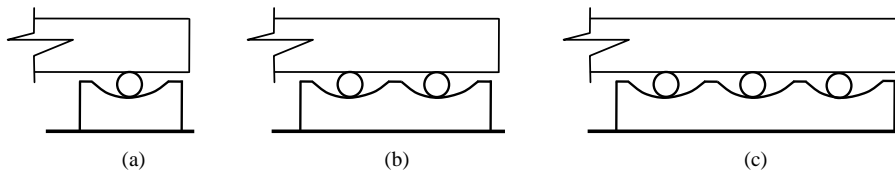


Figure 5. The use of a CPRB

This last solution of a rolling ball bearing with two concaves is first described, then patented and, finally, used by Jules Touaillon in 1870.

*5.3.1 Motion in parallel with ox-axis*

In this case, we have  $v_0=0$  and the system (10a,b) simplifies to the equation:

$$\ddot{v}_i(t) + (g/R) \cdot v_i(t) + \ddot{f}(t) = 0 \tag{16}$$

In the plots of Fig 6, 7, and 8, the displacements  $v_i$  are drawn for different values of  $\Omega$  and  $R=0.6$ ,  $R=0.8$  and  $R=1.2$ , respectively. Finally, in Fig. 9 the displacements  $v_i$  are drawn for  $\Omega=10$  and different values of  $R$ .

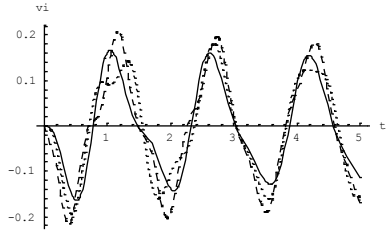


Figure 6.  $\text{--- } \Omega=8, \text{---} \Omega=10, \text{---} \Omega=12$

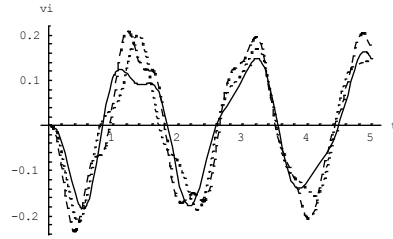


Figure 7.  $\text{--- } \Omega=8, \text{---} \Omega=10, \text{---} \Omega=12$

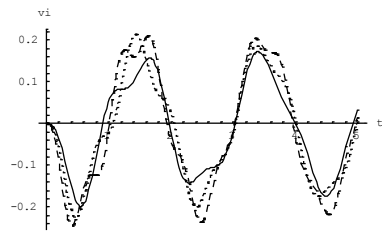


Figure 8.  $\text{--- } \Omega=8, \text{---} \Omega=10, \text{---} \Omega=12$

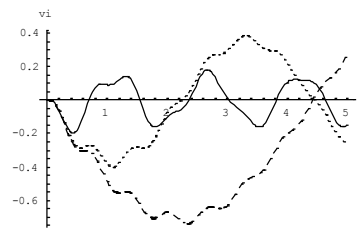


Figure 9.  $\text{--- } R=0.6, \text{---} R=5, \text{---} R=20$

### 5.3.2 Motion in parallel with Oy-axis

The plots of Fig. 10, 11, 12 and 13 show the same curves as in the figures of the previous paragraph but for motion in parallel with Oy-axis.

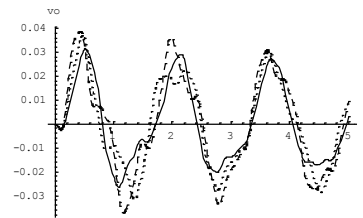
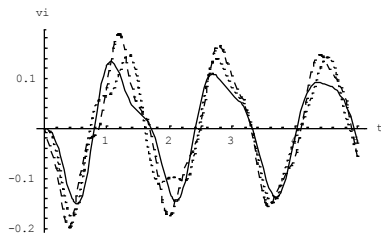


Figure 10. The displacements  $v_i$  and  $v_o$  for  $R=0.6$

## 6 CONCLUSIONS

From the results of the bridge – CFPB bearings model considered, we may draw the following conclusions:

1. The systems of CPRB are effective for a wide range of earthquakes.

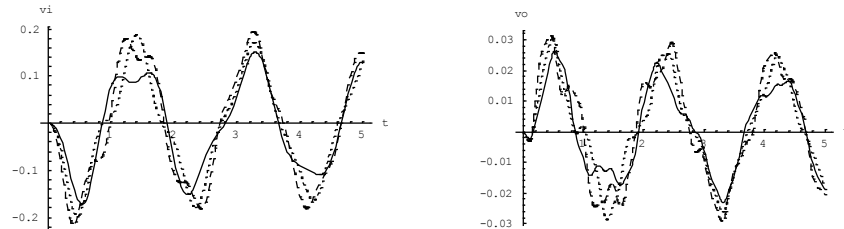


Figure 11. The displacements  $v_i$  and  $v_o$  for  $R=0.8$

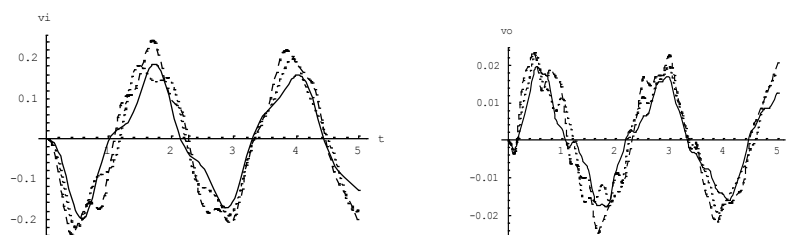


Figure 12. The displacements  $v_i$  and  $v_o$  for  $R=1.2$

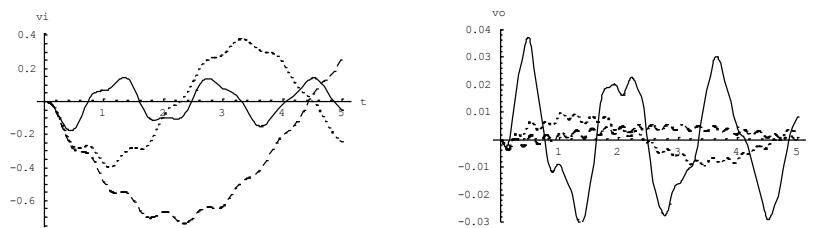


Figure 13. The displacements  $v_i$  and  $v_o$  for  $\_ \_ R=0.6$ ,  $--- R=5$ ,  $.. R=20$  and  $\Omega=10$

2. For motions acting in parallel with  $Ox$  or  $Oy$  axes, the isolator's movements are in the range from 0.15 to 0.31 rad. These extreme values occur for seismic accelerations greater than  $6.9 \text{ m/sec}^2$ .
3. The decrease of the bridge's oscillations is 90%. For  $\gamma=6\text{m/sec}^2$  it is:  $v_o=0.038 \text{ m}$  with CPRB, while without CPRB it is  $v_o=0.32\text{m}$ .
4. As the radius  $R$  increases, deflection  $v_o$  decreases and  $v_i$  increases. The last reaches unacceptable values for  $R>2\text{m}$ .

## REFERENCES

- [1] Touaillon J. Improvement in Buildings. U.S. Patent Office, Letters Patent No.99973, 1870.



IBSBI 2014, October 16-18, 2014, Athens, Greece

## **DEPENDENCE MODELLING FOR BRIDGE STRUCTURAL COMPONENTS UNDER ASYNCHRONOUS SEISMIC EXCITATION**

Panagiotis Spyridis<sup>1</sup>, Alexios Tamparopoulos<sup>2</sup>, Konrad Bergmeister<sup>2</sup>  
and Angelos Liolios<sup>3</sup>

<sup>1</sup>Polytropos Engineering Ltd., UK

<sup>2</sup>Univ. of Natural Resources and Applied Life Sciences (BOKU), Vienna, Austria

<sup>3</sup>Democritus University of Thrace, Dept. of Civil Engineering, Xanthi, Greece

e-mail: pspyridis@polytropos.eu.com, alexios.tamparopoulos@boku.ac.at,  
konrad.bergmeister@boku.ac.at, aliolios@civil.duth.gr

**ABSTRACT:** The assessment of a bridge's resistance and performance is directly linked with reliability aspects of both the resistance and the loading characteristics. Long bridges may be strongly affected by the ground spatial variability which affects both the resistance characteristics (foundation design), and the loading characteristics, especially under seismic excitation. The uncertainties pertaining to multivariate idiosyncrasy are discussed, and a generalized dependence paradigm is suggested in the framework of bridge analysis under asynchronous seismic excitation.

**KEYWORDS:** Structural reliability, uncertainty, copula functions, multivariate modelling, earthquake engineering, asynchronous excitation.

### **1 INTRODUCTION**

The assessment of a structure's resistance and performance, particularly in a performance based design framework, is directly linked with reliability aspects of both the resistance and the loading characteristics. Besides geometry and material parameters – related to resistance characteristics – large structures as bridges may be strongly affected by the ground spatial variability which affects both the resistance characteristics (foundation design), and the loading characteristics especially under seismic excitation.

The assessment of bridges can be enhanced by the use of probabilistic models, invoked by the random nature of load and resistance effects. Moreover, intrinsic properties of such models should relate to the commonly encountered dependencies among the input random variables. A currently standard approach, i.e. the use of correlation coefficients may prove to be efficient, but case may be that this approach overlooks, or even induces considerable

uncertainties, and it may lead to false results at a very low failure probability regime. Therefore, models which acknowledge and estimate this uncertainty type can serve the requirements for high reliability and robust decision-making. The uncertainties pertaining to multivariate idiosyncrasy are discussed, and a generalized dependence paradigm is suggested in the framework of bridge analysis under asynchronous seismic excitation.

This contribution presents advanced models of correlation for dependent variables in the framework of bridge analysis under geotechnical and structural uncertainty, i.e. by use of stochastic models [1]. The application is oriented to large structures and bridges whereby significant likelihoods of variance appear in (a) their resistance (e.g. geometry and material) properties, and (b) the loading characteristics, commonly associated with geotechnical properties (e.g. asynchronous excitation [14],[10] and varying foundation response). It has been evident in studies that we have performed to date [17], [18] that the implemented correlation model can significantly influence the results of a stochastic analysis. This effect is pronounced when the estimation of a small failure probability comes to focus as the cases are indicatively for bridge Fragility Curves [9], or other aspects of performance based design [6]. The presented case study may be perceived as a simplified analytical/numerical model with correlated input variables which have been developed on the basis of information in the literature [3], [13].

## **2 UNCERTAINTY AND DEPENDENCE IN RELIABILITY ENGINEERING**

### **2.1 General**

In the presence of uncertainty, one mainly has to distinguish between randomness and knowledge-related uncertainty or, in other terms, aleatory and epistemic [2]. Aleatory uncertainty stands for inherent randomness and cannot be reduced and handled otherwise than statistically. Epistemic uncertainty encompasses incomplete knowledge or lack thereof regarding the parameters of interest, and can be reduced e.g. through an advance in relevant information and study methods.

The main characteristic of the probabilistic approach is that input parameters, consequently resistance and load effects, are elaborated as random variables, i.e. they are represented by their probability distribution. Main requirement for the design of a structural system is that resistance is greater than load effect, hence the subtraction of the probability distributions for a load case from the system's resistance can deliver the probability of failure,  $p_f$ .

An exhausting treatment of the individual variable uncertainty is by no means enough: uncertainty is also confined to the magnitude and the type of variable interrelation. Measuring and propagating this dependence can be a

challenging task and its influence on the calculated probability of failure quite significant. The typical approach suggests the use of a scalar measure to express dependence; within this framework, Pearson's linear correlation coefficient has been widely used as a simple measure of variable association, coupled with methods that allow for inserting correlation values into the probabilistic models. While this strategy has lent itself to the construction of tractable and quite effective models for numerous problems, there are some common pitfalls in this approach while its limited usefulness has been criticized [5], [8].

## 2.2 Advanced multivariate modelling – copula functions

Copula functions provide a way to model the dependence structure separated from the marginal distributions, as well as a generic framework to construct multivariate models. Copulas, unlike scalar coefficients, contain all available dependence information. Definitions, basic theorems and examples can be found e.g. in the monograph of [11]. A two-dimensional copula can be viewed as the joint cumulative distribution function of a random pair with standard uniform marginal distributions; extension to arbitrary dimensions can also be built. The connection between copula functions, marginal distributions and the multivariate model is established thanks to Sklar's Theorem (see [11]).

When only a scalar dependence measure is available, there exist infinitely many feasible joint distributions. This means that extracting the correlation coefficient from observed data results to a loss of information and induces a dependence-type uncertainty to the model. Assuming different copulas, all having the same correlation coefficient and marginal distributions, allows for exploring the magnitude of this uncertainty. On the basis of these mathematical formulations, spatial variability can also be modelled, as the case is often for large ground areas or large structures with substantially varying material parameters throughout the investigated geometry.

## 2.3 Performance based design approach

The requirement for the design of a structure or structural component is that resistance is greater than the load effect. In the context of this paper, the performance based design is developed as the subtraction of the probability distributions for various load cases from the system's resistance, providing the safety margins and the reliability of the load bearing element.

A formal expression of this requirement, defined as the limit state is described as  $G = g(X) = R - S$ , with  $X$  being a set of input random variables,  $g(X)$  the limit state function (with  $g(X) < 0$  being the failure state),  $R$  the resistance of the structure, and  $S$  the action. When the distribution function  $F_G$  of the limit state function  $G$  is known, the failure probability  $p_f$  can be generally

calculated as  $p_f = P(g \leq 0)$

### **3 STOCHASTIC MODELLING FOR STRUCTURES AND SOIL – STRUCTURE INTERACTIONS**

#### **3.1 Structural and geotechnical variability for large structures**

The theories discussed above may be used for the stochastic modeling of large structures such as bridges (as well as e.g. tunnels, dams and defence structures, and generally buildings with large footprint) with certain soil structure interaction effects. In the case of bridges under seismic excitation, the soil characteristics can affect both the action side (seismic action characteristics) and/or the resistance (foundation response).

In case of concrete structures, various locations of the structure constructed with the different concrete batches may exhibit variance in their structural characteristics (E-modulus) due to variances in production or due to different curing histories. However, although the abovementioned properties can vary, they are typically ruled by some type of correlation. Both the material properties and their interconnection for different locations of the soil-structure model in focus can be described with the familiar tools of probabilistic analyses, i.e. probability distribution modelling, Monte Carlo Sampling methods, multivariate dependence modelling etc.

#### **3.2 Asynchronous seismic excitation**

A significant aspect of bridge analysis and design that is associated with large structure material variability is asynchronous excitation at different found points, which may be the result of the seismic wave's transfer delay from one location to another and its alteration through the traveling medium, as well as the difference in foundation response due to spatial geotechnical variability.

The design impacts of asynchronous excitation may prove decisive in several cases [4],[13] while the estimated failure probabilities may differ even by an order of magnitude for calculations with or without account of asynchronous movements [10]. [13] provides an overview on the effects of correlation in time-histories and geotechnical conditions in practical bridge design, indentifying a variance in the range of 20-25% for deck displacements and pier bending moments compared to a synchronised seismic action. Furthermore, it has been shown that variance of geotechnical conditions across bridge foundations induce crucial differences in the expected design actions of maximum displacements and bending moments.

## 4 INDICATIVE CASE STUDY

### 4.1 System description

A simplified structural system is presented herein only for demonstration of the proposed dependence modelling features and some indicative comparison of the results from various model assumptions. The system comprises a frame bridge structure on two piers of equal height. The piers are simulated as spring supported cantilevers, with a transverse point load. The system is depicted in Figure 1. The point load is calculated as  $F_E = a \cdot S$ , where  $a$  represents the seismic excitation acceleration magnitude (random variable) and  $S$  represents deterministic agents of the seismic load (e.g. foundation type, structure's response).

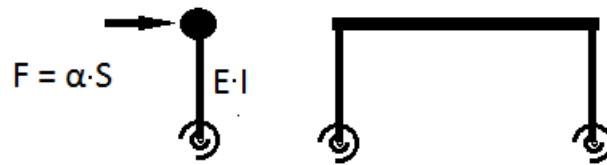


Figure 1. Sketch of the theoretical frame model used in the case study: A two-dimensional bridge structure with equally tall piers.

The single pier's end deformation may be calculated as  $\delta = K^{-1} \cdot F$ , where  $K$  represents the stiffness agents of the pier (e.g. material properties, geometry, and foundation response). The limit state function in the scope of this demonstration may be assumed in the spirit of Eurocode 8 [6] as  $\Delta\delta_{crit} - \Delta\delta \geq 0$ , where  $\Delta\delta$  is the differential end displacement of the piers, ( $\Delta\delta = \delta_1 - \delta_2$ ), and  $\Delta\delta_{crit}$  is a design value for this differential end displacement.

### 4.2 Random variables and dependence modelling

As discussed above the values  $a$  for each pier are probabilistically elaborated. For simplicity, they are both modelled with a normal distribution, allowed to vary between positive and negative values with a mean of zero and a standard deviation of 1/3, thus ranging from -1 to +1. The  $a$  values for the loads on each pier are correlated with a correlation coefficient of 0.5 which is implied to account for the excitation variance associated to the wave propagation, and the geotechnical conditions.

Under the assumptions above, there exist infinitely many bivariate models with equivalent validity, in the sense that they possess exactly the same probability distributions and correlation coefficient. In order to demonstrate the significance of the underlying dependence structure, different bivariate models

relying on the same numerical assumptions are implemented. These models are built by use of the Normal, and the t–student copula families. Figure 2 presents the scatter graph of the constructed bivariate distributions (namely the dependence structure between  $\alpha_1$  and  $\alpha_2$  for the two piers), while Figure 3 depicts the probability densities of the resulting system’s limit state function for the assumed models.

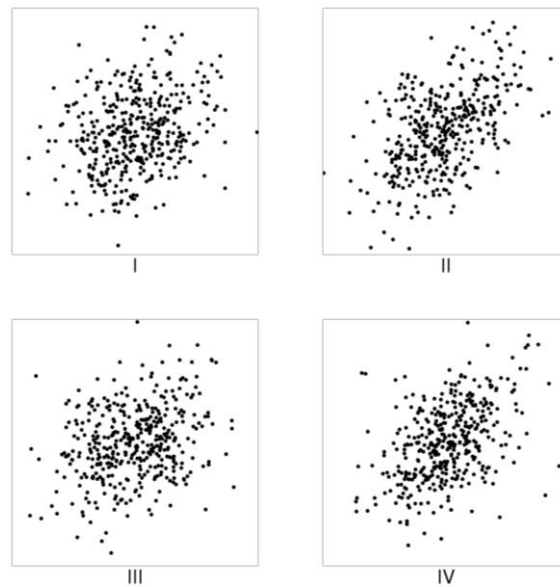


Figure 2. Scatter graphs of the four constructed bivariate models for the random variables  $\alpha_1$  and  $\alpha_2$ ; I: Normal copula ( $\rho = 0.25$ ), II: Normal copula ( $\rho = 0.50$ ), III: t-student copula ( $\rho = 0.25$ ), IV: t-student copula ( $\rho = 0.50$ ).

### 4.3 Results

The system’s failure probability for each of the assumed models was calculated by use of a Monte Carlo technique. The simulation involved a large number of iterations in order to ensure precision. The resulting probabilities were  $7.2 \cdot 10^{-4}$  for uncorrelated  $\alpha_1$  and  $\alpha_2$  ( $\rho = 0$ ),  $1.2 \cdot 10^{-4}$  for the Normal copula with  $\rho = 0.25$ ,  $3.1 \cdot 10^{-6}$  for the Normal copula with  $\rho = 0.50$ ,  $8.4 \cdot 10^{-4}$  for the t-student copula with  $\rho = 0.25$ , and  $2.5 \cdot 10^{-4}$  for the t-student copula with  $\rho = 0.50$ . Thus, the deviations exceed even orders of magnitude, posing a question concerning the predictive ability of the dependence models that are being used.

It should be remarked that these deviations can increase if additional multivariate dependence structures in more complex problems involving a greater number of associated variables be considered. It is worth noticing that, the deviations persist even if the resistance models rely upon exactly the same

marginal distributions and the same linear correlation coefficient, as they yield different density shapes, tail behaviour and low failure probability estimations.

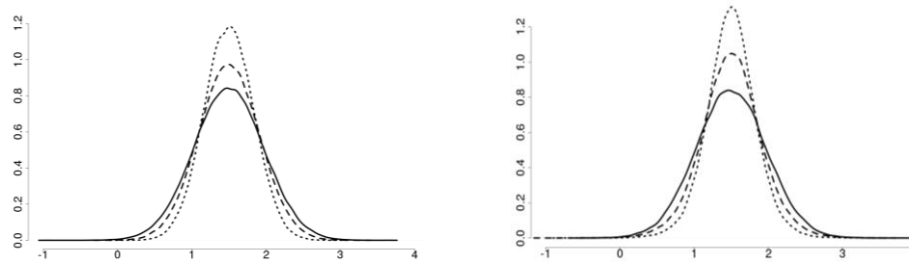


Figure 3. Probability density of the system's limit state function for the various assumed bivariate models; left: Normal Copula, right t- student copula; from upper to lower curve: correlation coefficient of 0.50, 0.25, 0 (uncorrelated).

## 5 CONCLUSIONS

In the present paper, the uncertainty pertaining to the particular dependence structure of two correlated parameters in an asynchronous bridge pier excitation is investigated. Through the examination of a simple structural system, represented as a model with two covariates, it is shown that the predicted failure probability may contain significant uncertainty. Therefore, the failure probability of similar systems can be calculated, at best, as an order of magnitude. Moreover, linear correlation coefficients may fail to describe dependence if the estimation of low target probabilities be desired. The results suggest that attention should be drawn to proper multivariate modelling in order to deal with high reliability requirements. To that end, modern sophisticated techniques can play an important role.

## REFERENCES

- [1] Adachi, T. and Ellingwood, B. R. (2009), Serviceability Assessment of a Municipal Water System Under Spatially Correlated Seismic Intensities. *Computer-Aided Civil and Infrastructure Engineering*, 24: 237–248. doi: 10.1111/j.1467-8667.2008.00583.x
- [2] Ang A.H-S.: On Risk and Reliability - Contributions to Engineering and Future Challenges. Proc. of ICOSSAR2009, 10th International Conference on Structural Safety and Reliability, Osaka 2009.
- [3] Bergmeister, K., Novak, D., Pukl, R., & Červenka, V. (2009). Structural assessment and reliability analysis for existing engineering structures, theoretical background. *Structure and infrastructure engineering*, 5(4), 267-275.
- [4] Carnevale, L., S. Imperatore, D. Lavorato, C. Nuti, G. Leoni, and G. Tropeano. "Assessment of Seismic Behavior of RC Bridges under Asynchronous Motion and Comparison with Simplified Approaches." In *15th World Conference on Earthquake Engineering*. 2012.
- [5] Embrechts P., McNeil A., Straumann D.: Correlation and dependence in risk management: properties and pitfalls, *Risk Management: Value at Risk and Beyond*. pp.176-223,

- Cambridge University Press 2002
- [6] European Committee for Standardization. Brussels. "Eurocode 8: Design of structures for earthquake resistance." (2003).
  - [7] Fardis, M. N. (2013). Performance and displacement based seismic design and assessment of concrete structures in fib Model Code 2010. *Structural Concrete*, 14(3), 215-229
  - [8] Ferson S., Nelsen R., Hajagos J., Berelant D., Zhang J., Tucker T.W., Ginzburg L.R., Oberkampf W.L.: Dependence in probabilistic modeling, Dempster-Shafer theory, and probability bounds analysis. Sandia National Laboratories 2004
  - [9] Panetsos, P., A. Liolios, K. Liolios, N. Theodoulidis, and P. Spyridis. "Maintenance life-cycle costs for bridges of Egnatia Motorway, Northern Greece, considering their seismic risk assessment." In *Life-Cycle and Sustainability of Civil Infrastructure Systems: Proceedings of the Third International Symposium on Life-Cycle Civil Engineering (IALCCE'12), Vienna, Austria, October 3-6, 2012*, p. 102. CRC Press, 2012.
  - [10] Lupoi, A., P. Franchin, P. E. Pinto, and G. Monti. "Seismic design of bridges accounting for spatial variability of ground motion." *Earthquake engineering & structural dynamics* 34, no. 4-5 (2005): 327-348
  - [11] Nelsen R.B.: An Introduction to Copulas. Springer Verlag 2006.
  - [12] Pukl, R., M. Jansta, J. Cervenka, M. Vorechovsky, D. Novák, and R. Rusina. "Spatial variability of material properties in nonlinear computer simulation." *Computational Modelling of Concrete Structures* (2006): 891-896.
  - [13] Sextos, A.G. and Kappos A.J. Asynchronous seismic excitation practice, In: G. Gazetas (Ed.), 3<sup>rd</sup> Panhellenic Conference on Anitseismic Mechanics and Technical Seismology, Athens, 2008
  - [14] Sextos, A.G. Kappos A.J. and Mergos P., Effect of Soil-Structure Interaction and Spatial Variability of Ground Motion on Irregular Bridges: The Case of the Krystallopigi Bridge, 13th World Conference on Earthquake Engineering, Vancouver, Canada, 2004
  - [15] Strauss A. 2003. Stochastische Modellierung und Zuverlässig-keitsanalyse von Betonkonstruktionen (Stochastic modeling and reliability of concrete structures—in German). Dissertation, University of Natural Resources and Life Sciences, Vienna, Austria
  - [16] Strauss A. , Bergmeister K. (2009). Integrative reliability assessment of structures, 7<sup>th</sup> International Probabilistic Workshop, Delft, 2009
  - [17] Tampakopoulos, A. E., P. Spyridis, and K. Bergmeister. "Uncertainty in multivariate modelling: Main concepts and an application on fracture mechanics." In *Proceedings of the Third International Symposium on Life-Cycle Civil Engineering (IALCCE'12), Vienna, Austria*, p. 460. CRC Press, 2012.
  - [18] Tampakopoulos, A. E., P. Spyridis, and K. Bergmeister. Small failure probabilities and copula functions: preliminary studies on structural reliability analysis. In: Berenguer, C., Grall, A., & Soares, C. G. (Eds.). (2011). *Advances in Safety, Reliability and Risk Management: ESREL 2011*. CRC Press.



IBSBI 2014, October 16-18, 2014, Athens, Greece

## **THE INFLUENCE OF THE VERTICAL INERTIA FORCES ON THE BEHAVIOR OF FPB ISOLATORS**

Ioannis G. Raftoyiannis<sup>1</sup> and George T. Michaltsos<sup>2</sup>

<sup>1,2</sup> National Technical University of Athens, Dept. of Civil Engineering, Greece  
e-mail: rafto@central.ntua.gr, michalts@central.ntua.gr

**ABSTRACT:** A procedure for determining the governing equations that provide the isolator's displacement due to strong ground motion is applied to bridges isolated with Friction Pendulum Bearing (FPB) systems. The resulting equations, which contain the vertical inertia forces, are studied in order to estimate the influence of the last forces on the isolator's behavior. The gathered non-linear equations are solved through the technique of successive approximations.

**KEY WORDS:** bridge dynamics, friction pendulum bearings, vertical inertia

### **1 INTRODUCTION**

Among the structures, bridges are vulnerable when subjected to severe earthquakes. Damage of the bridge structure occurs primarily at the piers, which may in turn result to the collapse of the bridge spans. Although the ductility design concept has been widely accepted for seismic design of structures in engineering practice, this may not be appropriate for bridges due to their lack of structural redundancy by nature. Moreover, ultimate strength design does not seem to work for bridge structures as often the piers are found to fail in shear rather than flexure. Design effort on protection of bridges against earthquakes should therefore be focused on minimizing the forces to be carried by the piers, in particular the shear forces. Although rubber bearings have been extensively used as base isolation systems, sliding bearings are becoming in recent years more popular in bridge applications for economical reasons. Dynamics of sliding structures is a highly non-linear problem due to friction mechanism. Analytical solutions are complicated and restricted to harmonic motions for systems with no more than two degrees of freedom, under idealized conditions. More realistic transient responses to isolating sliding systems can be obtained only numerically. Many numerical tests on a rigid frame model conducted by Mosqueda, Whittaker and Fenves, showed that the effect of the vertical shaking on the force and displacement report is negligible. In 2009, Khoshnoudian and Hagdoust showed that the stiffness interaction between the two horizontal

directions reduces structural shear, and that the vertical component of an earthquake considerably affects the lateral response.

In this paper, we attempt to estimate the influence of the vertical inertia forces on the isolator's behavior. The non-linear equations were solved through the technique of successive approximations. The results obtained showed that the influence of the vertical inertia forces is negligible for the case of a long distant ground motion and become considerable for a near-source ground motion.

## 2 INTRODUCTORY CONCEPTS

### 2.1 The earthquake

Let us consider the bridge B shown in Fig. 1, that is subjected to an earthquake with focus A and epicenter A'. The horizontal distance between the bridge and the epicenter is L and the focal depth is H. An earthquake has either the character of a shock, or the character of a normal dynamic excitation. For the first case [1] the time function of the ground motion can be approximated by the following expression:

$$f_o(t) = k e^{-\beta t} \sin \Omega t \tag{1}$$

while for the second one, the following expression can be used:

$$f_o(t) = k t e^{-\beta t} \sin \Omega t \tag{2}$$

where  $k$  is a constant that depends on the soil characteristics,  $\beta$  is the damping ratio and  $\Omega$  is the frequency of the ground motions. The two components of the earthquake's characteristics at focus A in  $t=0$ , are:

$$\left. \begin{aligned} f_{ho} &= f_o \cdot \frac{L}{R}, & v_{ho} &= v_o \cdot \frac{L}{R}, & \gamma_{ho} &= \gamma \cdot \frac{L}{R} \\ f_{vo} &= f_o \cdot \frac{H}{R}, & v_{vo} &= v_o \cdot \frac{H}{R}, & \gamma_{vo} &= \gamma \cdot \frac{H}{R} \end{aligned} \right\} \tag{3}$$

The above equations (1), (2), and (3) are valid in an area close to focus A, while they decrease as we move from the focus.

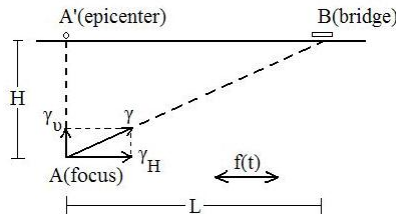


Figure 1. Earthquake's epicenter focus and bridge locations

This decrease is due to geometrical reasons and to damping. Because of the geometrical reasons the horizontal components of the above characteristics decrease according to the following formula [1,2]:

$$(f_h, v_h, \gamma_h) = (f_{ho}, v_{ho}, \gamma_{ho}) \cdot K_1 \cdot K_2 \tag{4}$$

$$K_1 = \frac{\Omega}{\Omega_o} \cdot \sqrt{\frac{F_d \cdot F_\ell}{F_d \cdot F_\ell + \pi \cdot R \cdot F_d + F_\ell \cdot R \cdot \text{ArcSin}(H/R) + \pi \cdot R \cdot (R+H)}} \tag{5}$$

Where:

$$K_2 = e^{-\zeta_1 \cdot \Omega \cdot L / V}, \quad \text{with: } \Omega = \frac{2\pi \Omega_o}{2\pi + 0.003 \Omega_o L}$$

$$\zeta_1 = 0.001 \quad \text{for granite and } \zeta_1 = 0.05 \quad \text{for schist}$$

Where  $F_\ell$  is the length and  $F_d$  the height of the fault that causes the earthquake, and  $V$  the speed of the transmission of the earth’s motion. On the other hand it is proved that the vertical components are practically nullified for  $L \geq H$ . Given that there is no broadly known and acceptable formula, we propose and we will use in this paper the following empirical relation:

$$(f_v, v_v, \gamma_v) = (f_{vo}, v_{vo}, \gamma_{vo}) \cdot K_3 \quad \text{with } K_3 = e^{-\zeta_2 L - \zeta_3 H}$$

$$\text{and } \zeta_2 = 0.05, \quad \zeta_3 = 0.004 \quad \text{for granite}$$

$$\zeta_2 = 0.08, \quad \zeta_3 = 0.015 \quad \text{for schist} \tag{6}$$

**2.2 The FPB isolators**

Let us consider the FPB isolator with one concave sliding, as shown in Fig. 2.

For small  $\varphi$  it is generally accepted that:

$$\tan \varphi \cong \sin \varphi, \quad \cos \varphi \cong 1 \tag{7}$$

The forces  $H$  and  $V$  are related as follows:  $H=V \tan\varphi$ , or:

$$H = V \cdot v / R \tag{8}$$

The friction forces, acting along the sliding are depended on the friction coefficient  $\mu$ . This coefficient can be either a constant (Coulomb’s model) or depended on the sliding velocity and the bearing pressure, (Mokha and Constantinou).

$$\mu = \mu_{max} - (\mu_{max} - \mu_{min}) \cdot e^{-\alpha |v_i|} \tag{9}$$

where  $\mu_{max}$  and  $\mu_{min}$  are the maximum and minimum values of the coefficient of friction, respectively, and  $\alpha$  is coefficient to be determined from the bearing pressure. As it is expected and also shown by Wang et al [3] both hypotheses do not present remarkable differences.

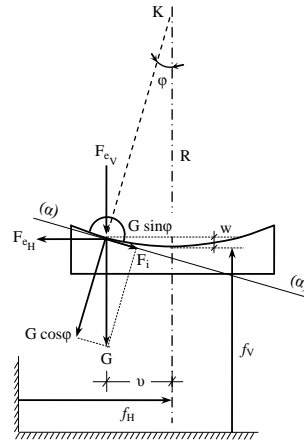


Figure 2. F.P.R. of one concave

### 3 THE EQUATIONS OF THE PROBLEM

The system studied is a rigid mass  $m$ , supported by a single F.P. isolator, where the weight  $G$  of the system rests on a slider, which slides on the spherical surface because of horizontal dynamic forces (Fig. 2).

Projecting the forces of Fig. 2 on the  $a$ - $a$  axis, we get the following equation:

$$F_{eH} \cos \varphi - F_{eV} \sin \varphi = G \sin \varphi + F_f \tag{10}$$

where:  $F_{eH}$ ,  $F_{eV}$ ,  $G$ , and  $F_f$ , are shown in Fig.2. We know that:

$$\left. \begin{aligned} F_{eH} &= m(\ddot{f}_H - \ddot{u}), & F_{eV} &= m(\ddot{f}_V - \ddot{w}), & F_f &= \mu G Z \end{aligned} \right\} \tag{11a}$$

where  $f_H$ ,  $f_V$ ,  $u$ ,  $w$ , are shown in Fig. 2, while  $\mu$  is the Coulomb friction coefficient and  $Z$  is a coefficient independent of  $u$  and  $w$  given by the relation:

$$Z = \text{Sign}[\dot{u}] \tag{11b}$$

By setting  $\cos \varphi \cong 1$  and  $\sin \varphi \cong \tan \varphi = u/R$ , eq(10) becomes:

$$\ddot{u} + \frac{g}{R} \cdot u = \ddot{f}_H - \mu \cdot g \cdot Z - \frac{1}{R} \cdot \ddot{f}_V \cdot u - \frac{\ddot{w}}{R} \cdot u \tag{12}$$

#### 3.1 No vertical inertia forces are considered

Neglecting the vertical inertia forces, we get the following equation:

$$\ddot{u} + \frac{g}{R} \cdot u = \ddot{f}_H - \mu \cdot g \cdot Z \tag{13a}$$

The solution of the above is given by the Duhamel integral as follows:

$$\left. \begin{aligned} v_1(t) &= A \cdot \sin \omega(t-t_0) + B \cdot \cos \omega(t-t_0) + \frac{1}{\omega} \int_{t_0}^t [\ddot{f}_H(\tau) - \mu g Z] \sin \omega(t-\tau) d\tau \\ \text{where: } \omega &= \sqrt{\frac{g}{R}} \quad \text{and} \quad t \geq t_0 \end{aligned} \right\} \quad (13b)$$

From the time conditions  $v(t_0) = v_0$  and  $\dot{v}(t_0) = v_0$ , we determine A and B:

$$\left. \begin{aligned} A &= \frac{v_0}{\omega}, \quad B = v_0 \end{aligned} \right\} \quad (13c)$$

### 3.2 The influence of the vertical inertia forces

In this case, we the governing equation of motion is eq(12). From the geometry considerations of Fig. 2 we get:  $w = R(1 - \cos \varphi) = R(1 - \sqrt{1 - \sin^2 \varphi})$ .

Expanding the above in series and neglecting the higher order terms, we get:

$$\left. \begin{aligned} w &= \frac{v^2}{2R} \quad \text{and therefore} \quad \dot{w} = \frac{v\dot{v}}{R}, \quad \ddot{w} = \frac{v\ddot{v} + \dot{v}^2}{R} \end{aligned} \right\} \quad (14)$$

Introducing eq(14) into eq(12), we find:

$$\ddot{v} + \frac{g}{R} \cdot v = \ddot{f}_H - \mu \cdot g \cdot Z - \Phi_2, \quad \text{with: } \Phi_2 = \frac{1}{R} \cdot \ddot{f}_V \cdot v + \frac{v^2 \ddot{v} + v \dot{v}^2}{R^2} \quad (15a)$$

For the solution of the first of eq(15a), we use the method of successive approximations [4]. As first approximation function we use the solution  $v_1(t)$ , given by eq(13b) and thus, we have:

$$\ddot{v} + \frac{g}{R} v = \ddot{f}_H - \mu \cdot g \cdot Z - \frac{1}{R} \cdot \ddot{f}_V \cdot v_1 - \frac{v_1^2 \ddot{v}_1 + v_1 \dot{v}_1^2}{R^2} \quad (15b)$$

The solution of the above equation, with time conditions  $v(t_0) = \dot{v}(t_0) = 0$ , is given by the Duhamel's integral:

$$v_2(t) = \frac{1}{\omega} \cdot \int_{t_0}^t \left[ \ddot{f}_H(\tau) - \mu g Z - \frac{1}{R} \cdot \ddot{f}_V(\tau) \cdot v_1(\tau) - \frac{v_1^2(\tau) \cdot \ddot{v}_1(\tau) + v_1(\tau) \cdot \dot{v}_1^2(\tau)}{R^2} \right] \cdot \sin \omega(t-\tau) d\tau \quad (15c)$$

Usually, a second approximation step is not necessary. In a different case, one can use the above  $v_2(t)$  and follow the same procedure.

## 4 NUMERICAL EXAMPLES AND DISCUSSION

### 4.1 The FPB isolators

We study an isolator with one concave sliding, like the one shown in Fig. 2, with friction coefficient  $\mu=0.10$ , and radii  $R=0.50, 1.00, 1.50$  and  $2.00$  m.

## 4.2 The Earthquake

We consider a fault with  $F_l=300\text{km}$  and  $F_d=50\text{km}$ , which produces a ground motion at the focus given by eq(1) with  $k=0.06$ ,  $\beta=0.30$ , and  $\Omega=12$  :

The resulting earthquake gives an acceleration at the focus  $\gamma = 8.32\text{m/sec}^2$ , (at  $t=0.125$  sec). We will study a shallow earthquake with focal depth  $H=3$  km, two intermediate ones with  $H=15$  and  $H=30$  km, and finally a deep earthquake with  $H=80$  km. The soil consider is granite with characteristics  $V=5.5$ ,  $\zeta_1=0.001$ ,  $\zeta_2=0.05$  and  $\zeta_3=0.004$ .

The diagrams of Figs 4 and 5, show the variation of the two acceleration's components  $\gamma_H$ , and  $\gamma_V$ , along the length  $L$  (distance from the epicenter).

## 4.3 The influence of vertical inertia forces

Applying the equations of §3.3 and with the data of §4.2, we obtain the following plots of Figs 6, 7, 8 and 9, showing the influence of the vertical inertia forces (as percentage of the deformation  $v$ ) in relation to the distance  $L$  from the epicenter and for different radius  $R$ . From the plots of Fig. 6, we see that for shallow earthquakes, the vertical inertia forces strongly affect the value of the displacement  $v$ , mainly near the epicenter (16% for small values of  $R$ ), while this effect becomes negligible for  $L>2H$ . In addition (Figs 9 to 11), we observe a disturbance, which is very clear for shallow earthquakes, becomes smaller for middle depth earthquakes and indistinct for deep earthquakes. Summarizing, we see that for shallow earthquakes and  $L<2H$ :

$\Delta$  varies from 16 to 1,8% for  $R=0.5\text{m}$ , from 8 to 1.2% for  $R=1.0\text{m}$ , from 5 to 1.0% for  $R=1.5\text{m}$ , and from 3.5 to 0.5% for  $R=2.0\text{m}$ .

For intermediate earthquakes and  $L<1.4H$ :

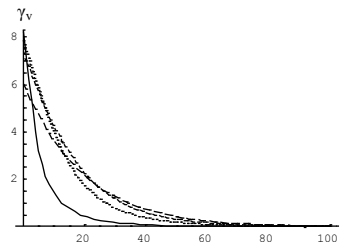
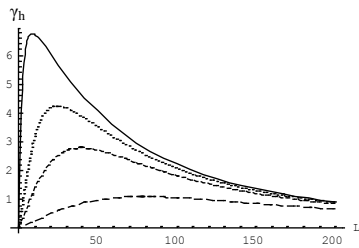


Figure 4. Acceleration  $\gamma_H$  for  $H=3\text{km}$  (\_\_\_),  $H=15\text{km}$  (....),  $H=30\text{km}$  (- - -),  $H=80\text{km}$  (- \_ -)      Figure 5. Acceleration  $\gamma_V$  for  $H=3\text{km}$  (\_\_\_),  $H=15\text{km}$  (....),  $H=30\text{km}$  (- - -),  $H=80\text{km}$  (- \_ -)

$\Delta$  varies from 8 to 1,8% for  $R=0.5\text{m}$ , from 3.5 to 1.2% for  $R=1.0\text{m}$ , from 2.5 to 0.8% for  $R=1.5\text{m}$ , and from 1.8 to 0.5% for  $R=2.0\text{m}$ .

Finally, for deep earthquakes and  $L<H$ :

$\Delta$  varies from 5.5 to 0.2% for  $R=0.5\text{m}$ , from 2.8 to 0.15% for  $R=1.0\text{m}$ , from 1.8 to 0.10% for  $R=1.5\text{m}$ , and from 1.5 to 0.03% for  $R=2.0\text{m}$ .

### 5 CONCLUSIONS

From the results of the models considered, one can draw the following conclusions:

1. Using the widely used mathematical model for FBP isolators, the equation of motion including the vertical inertia forces is derived and solved through the method of successive approximations.
2. The influence of vertical inertia forces on the value of the horizontal displacement  $v$  is very significant for small  $R$  and for every kind of earthquakes. This influence is significant for intermediate  $R$  and for both shallow and middle depth of earthquakes, while it becomes negligible for big  $R$ .

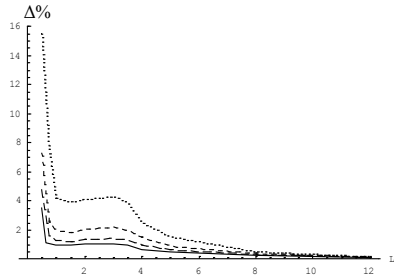


Figure 6. The influence of vertical inertia forces for  $H=3$  km and  $R=0.5m$  ( .... ),  $R=1.0m$  ( - - - ),  $R=1.5m$  ( \_ \_ ),  $R=2.0m$  ( \_\_\_ )

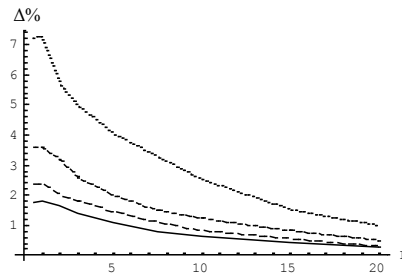


Figure 7. The influence of vertical inertia forces for  $H=15$  km and  $R=0.5m$  ( .... ),  $R=1.0m$  ( - - - ),  $R=1.5m$  ( \_ \_ ),  $R=2.0m$  ( \_\_\_ )

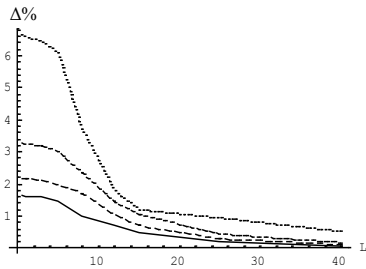


Figure 8. The influence of vertical inertia forces for  $H=30$  km and  $R=0.5m$  ( .... ),  $R=1.0m$  ( - - - ),  $R=1.5m$  ( \_ \_ ),  $R=2.0m$  ( \_\_\_ )

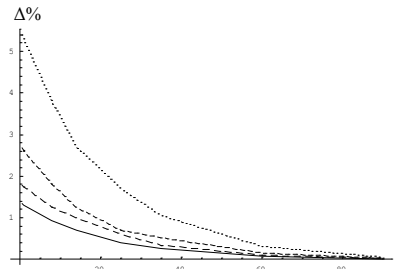


Figure 9. The influence of vertical inertia forces for  $H=80$  km and  $R=0.5m$  ( .... ),  $R=1.0m$  ( - - - ),  $R=1.5m$  ( \_ \_ ),  $R=2.0m$  ( \_\_\_ )

**REFERENCES**

- [1] N.A. Abrahamson, J.F. Schneider and J.C. Stepp, "Empirical spatial coherency functions for application to soil-structures interaction analyses", *Earthquake Spectra*, 1991, 7(1), 25-32.
- [2] G.T. Michaltsos and I.G. Raftoyiannis, "A mathematical model for the rocking, overturning and shift problems in bridges", *Engineering Structures*, 30, 2008, 3587-3594.
- [3] Yen-Po Wang, Lap-loi Chung, and Wei-Hsin Liao, "Seismic response analysis of bridges isolated with friction pendulum bearings", *Earthquake Eng. and Struct. Dynamics*, 27, 1998, 1069-1093.
- [4] A.N. Kounadis, "An efficient and simple approximate technique for solving non-linear initial and boundary-value problems", *Comp. Mechanics*, 9, 1992, 221-231.



## OPTIMAL LOCATION OF ARCH BRACINGS IN ARCH BRIDGES FOR MAXIMUM BUCKLING LOAD

Jin Cheng<sup>1</sup>, Jian Ni<sup>2</sup>, Lijun Jia<sup>3</sup>, Rucheng Xiao<sup>4</sup>

Department of Bridge Engineering, Tongji University, Shanghai, 200092, China  
email: chengjin@tsinghua.org.cn, 1332846@tongji.edu.cn, jialj@tongji.edu.cn,  
xiaorc@tongji.edu.cn

**ABSTRACT:** To overcome the drawbacks of existing design methods for location of arch bracings in arch bridges, a systematic topology optimization based approach for identifying the optimum location of arch bracings is proposed in this paper. The accuracy and efficiency of the proposed method is demonstrated through a numerical example.

**KEY WORDS:** Arch bridge; Buckling; Location of arch bracings; Optimization.

### 1 INTRODUCTION

Arch bridges are one of the oldest types of bridges and have great natural strength. However, they can be subjected to a loss of stability under combined loadings. One common and cost-effective approach to increasing the buckling loads of arch bridges is the addition of arch bracing, which supplements the rigidity of base structures by increasing their moment of inertia of cross-sections. The design of arch bracings involves the determination of the location of the added arch bracings. To obtain the maximum advantage from the added arch bracings, the location of the added arch bracings should be placed optimally.

Traditionally an initial feasible location of arch bracings is efficiently designed by following some heuristic design rules. However, there exist some design situations, with special loading conditions or structural singularities for which these simple design rules cannot be applied. Moreover, the design procedure does not seem to be optimal. The location of arch bracings obtained was often improved by the designer in a later stage of the process of obtaining the final design. In these cases it is necessary to use a more direct approach in order to automatically identify the optimal location of arch bracings with minimum designer intervention.

The parametric analysis-based design method has been proposed by Ney et al. [1] as a rational tool for identifying the optimal location of arch bracings. Unfortunately, extensive computational effort may be required to obtain the

optimal location of arch bracings if the parametric analysis is repeated for every change in location of arch bracings.

To overcome these difficulties and to increase efficiency in identifying the optimal location of arch bracings, the application of the topology optimization procedure, which has received considerable attention in recent years, has been introduced as an alternative approach. Topology optimization is a tool that can be used to find optimal layout of the structural elements in a given design domain. The application of the topology optimization to shell/plate structures has been studied by a considerable number of investigators including Diaz and Kikuchi [2], Ma and Kikuchi [3], Yang and Chahande [4] and Lam and Santhikumar [5]. However, to the authors' knowledge, its application to an optimal location problem of arch bracings in an arch bridge has not been reported.

The objective of this paper is to propose a systematic topology optimization method to deal with the problem of optimizing location of arch bracings in an arch bridge to maximize buckling load. The optimum location problem is formulated as a nonlinear mathematical programming problem because the objective function in general is a nonlinear function of the design variables representing the location of arch bracing. A numerical example is given to show the efficiency and accuracy of the present method. It is found that the proposed method can be an alternative useful tool for engineering applications.

## 1 PROBLEM STATEMENT OF OPTIMAL LOCATION OF ARCH BRACINGS

The optimal location problem is to find a design variable vector representing location of arch bracings to maximize the buckling load of arch bridges subjected to the design constraints that are imposed as inequality constraints on design variables. The optimal location problem may be correspondingly stated as follows:

$$\text{Maximize } P_i(V), i = 1, \dots, k \quad (1)$$

$$\text{Subjected to } L_j \leq V_j \leq U_j, j = 1, \dots, n \quad (2)$$

where  $P_i(V)$  is the  $i$  th buckling load of arch bridges. Here we assume that  $P_i$  is in ascending order, i.e.,  $P_1 \leq P_2 \leq P_3 \dots$ . General speaking, in application the lowest buckling load  $P_1$  receive the most interest, whereas the higher buckling loads only have a theoretical interest, hence are not important from the designer's point of view;  $V$  is the design variable vector representing location of arch bracings;  $V_j$  is the nodal coordinates of the finite element model specifying the location of the  $j$  th arch bracing;  $L_j$  and  $U_j$  are the lower and upper bounds of the location of arch bracing, respectively.  $k$  and  $n$  are the total number of

buckling modes to extract and the total numbers of arch bracings in arch bridges, respectively.

Not that the above optimization problem can be transformed into the following form:

$$\text{Minimize } R_i(V), \quad i = 1, \dots, k \quad (3)$$

$$\text{Subjected to } L_j \leq V_j \leq U_j, \quad j = 1, \dots, n \quad (4)$$

where  $R_i(V) = \frac{1}{P_i(V)}$ . This is a standard minimization problem with bound constraints, which can be solved by the proposed method discussed next.

## 2 THE PROPOSED SOLUTION METHOD FOR OPTIMAL LOCATION PROBLEM OF ARCH BRACINGS

### 2.1 Principle

The proposed method is a hybrid method, consisting of penalty function method (PFM), finite element method (FEM) and the first-order method (FOM). The method is based on three key concepts: (1) transformation of the constrained location problem defined in Eq. (3) to an unconstrained location problem by PFM; (2) actual finite element representation of the constrained location problem defined in Eq. (3) by FEM; and (3) solution of the constrained location problem defined in Eq. (3) by FOM.

The determination of location of arch bracing is a problem in constrained optimization. For the constrained optimization, finding points that satisfy all the constraints is often the difficult problem. One approach is to use the PFM for the constrained optimization. In this approach, a constrained problem is transformed into an unconstrained problem by using penalty functions. Two types of penalty functions are commonly used: interior and exterior penalty functions. In this paper, we use the exterior penalty function, which is considered to be the easiest to incorporate into the optimization process. The idea behind this algorithm is to penalize the objective function when it is not satisfying the constraints. By using the exterior penalty function, we transform the constrained problem defined in Eq. (3) into an unconstrained problem:

$$\text{Minimize } \phi(V, r_p) = R(V) + r_p Q(V) \quad (5)$$

where  $Q(V)$  is an imposed penalty function;  $r_p$  is a multiplier which determines the magnitude of the penalty. A detailed description of the exterior penalty function can be found in [6].

Because the objective function in Eq. (5) is an implicit function of the design variables, the use of the proposed method may involve in evaluation of the

implicit objective function. FEM is considered to be the most popular/reliable evaluation method. In this paper, the primary purpose of applying FEM is to compute the value of the implicit objective function. The detailed description of the method can be found in [7]. However, for the sake of completeness, a brief description is given below.

The objective function in Eq. (5) represents the elastic buckling problem of an arch bridge. In FEM the elastic buckling problem is expressed as the following eigenvalue problem:

$$([K_e] - P_{cr}[K_\sigma])\{\phi\} = \{0\} \quad (6)$$

where  $[K_e]$  is the linear elastic stiffness matrix;  $K_\sigma$  is the geometric stiffness matrix [7];  $P_{cr}$  is the buckling load; and  $\phi$  is the buckling mode shape. In this paper, the method of subspace iterations is used to compute the values of  $P_{cr}$  and  $\phi$ .

Once the above-mentioned constrained optimization problem is successfully transformed into an unconstrained problem, we can easily use any unconstrained optimization methods such as zero-order method and first-order method to solve the constrained optimization problem. In this study, we use the first-order method for solving the unconstrained problem defined in Eq. (5). This first-order method is based on the Fletcher-Reeves variant of the conjugate gradient method, see Ref. [6]. The key aspect of this method is finding a stepping direction, within the design space, and updating the vector  $V$  of design variable vector representing location of arch bracings according to

$$V^{n+1} = V^n + \lambda s^n \quad (7)$$

where  $\lambda$  is the parameter obtained by means of a unidirectional minimization. Finally the vector  $s$  represents the stepping direction, see Ref. [6].

## 2.2 Procedure for the proposed method

The procedure of the proposed method is:

- a) Define the optimization problem including the objective function,  $P(V)$  and design variables  $V$ .
- b) Define the initial location of arch bracing in terms of a set of design variables.
- c) Transform the constrained problem defined in Eq. (3) into an unconstrained problem using exterior penalty function
- d) Calculate the value of objective functions using FEM and evaluate the sensitivity of the objective functions of current design with respect to the design variables.
- e) Using the sensitivity information and a suitable unconstrained optimization algorithm, such as FOM, generate a new location of arch bracing (usually of

higher buckling load than the previous design) which satisfies the constraints.

- f) If the new location of arch bracing is not optimum, go to step 2; otherwise stop.

### 3 NUMERICAL EXAMPLE

A numerical example is presented for demonstrating how the proposed method can be used for finding the optimum location of arch bracings in an arch bridge structure. The problem selected for this purpose is of relatively small size consisting of only five I-type arch bracings, but the results and conclusions obtained from this example were the same as obtained from several other small and large problems. A larger problem is not being presented in this paper because of the huge amount of associated data.

#### 3.1 Description of the example bridge

The example bridge studied here is a through arch bridge having a span length of 66m. The bridge consists of twin parallel arches with a 66m span and 13.2m clear width. The shape of the arch bridge is parabolic and the rise to span ratio of arch bridge is 1:4. The arch rib is made from concrete filled steel circular section. The arch bridge deck system consists of two horizontal tied girder, end cross girder, middle cross girder and concrete deck slab. The horizontal tied girder bears not only the horizontal thrust generated by arch ribs but also vertical loads brought over by the transverse beams. In order to increase the lateral stability of the arch bridge, five I-type arch bracings are located symmetrically between two parallel arch ribs. Symmetric requirements for the location of these arch bracings are kept unchanged during location optimization of these arch bracings. The deck is suspended from the two arches by means of 24 suspenders.

#### 3.2 Formulation of optimal location problem of arch bracings in the example bridge

The process of formulating this optimal location problem involves identifying the design variables, the objective function and the corresponding constraints, which are presented below.

Design variables are independent quantities that are varied in order to achieve the optimum design. For the arch bracing, the design variables must identify the exact location. The location of each arch bracing is defined by a set of control points. Each of these points is defined by three cartesian coordinates ( $X$ ,  $Y$  and  $Z$ ). To reduce the number of design variables, only five boundary points are taken as control points in this work. Namely, one arch bracing is represented by one boundary point. Thus, the location of the arch bracings is determined by three cartesian coordinates  $X$ ,  $Y$  and  $Z$  of these control points. The location of

the arch bracings in the example arch bridge with I-type arch bracings is identified by the one cartesian coordinate  $X$  of these control points. As shown in Fig.1, the arch bridge model has five I-type arch bracings, and therefore, there are 5 design variables. Due to the symmetry and the simplicity of the problem, only 2 cartesian coordinates of the control points 1 and 2 are defined as independent design variables, the other 2 cartesian coordinates of control points 4 and 5 are symmetric with respect to the independent design variables and the last one cartesian coordinate of control point 3 are kept fixed. If  $X_i$  is the one cartesian coordinate of  $i$  th control point, the Eq. (8) represents the vector of design variables.

$$V = (X_1, X_2) \quad (8)$$

Two cases are considered in the following optimization procedures: Case I: only one design variable of  $X_1$  are used; Case II: all two design variables of  $(X_1, X_2)$  are used. The initial value of design variables for Cases I and II is shown in Table 1.

Objective function is the dependent variable that must be maximized. One of the most advantageous reasons for using the arch bracings in an arch bridge is their ability to increase buckling stability of the arch bridge. At the present work the elastic buckling load of the arch bridge is selected as an objective function.

Constraints are dependent variables and functions of the design variables that constrain the design. The coordinates of control points representing location of arch bracings are limited in the arch bracing and must be considered as constraints. The location constraint is a bound constraint to ensure that no location violation occurs when design variables are updated. For example, when design variables of coordinates  $X_1$  are considered, their value of coordinates can not exceed the value of coordinates  $X_2$ . Table 2 presents the lower and upper bounds imposed on design variables.

*Table 1. Initial value of design variables*

Design variable	Initial value (m)
$X_1$	13.000
$X_2$	23.000

*Table 2. Lower and upper bounds imposed on design variables*

Design variable	Lower bound (m)	Upper bound (m)
$X_1$	0	22.9
$X_2$	0	32.9

### 3.3 Optimization results and discussion

The initial and optimal designs for Cases I and II are given in Table 3. From Table 3, it can be seen that: (1) arch bracings have moved towards the ends of arch ribs to increase the buckling load of arch bridges. The final buckling loads for Cases I and II are increased from 6.926 to 7.016 and from 6.926 to 7.138, respectively. Even though these increments are not much, the main feature is to observe where to place arch bracings to increase or maintain the largest buckling load; (2) the buckling loads of the optimal designs for Cases I and II obtained by using the proposed method are higher than those of the initial designs. This result shows that the proposed method can be employed for finding optimal arch bracing locations in arch bridge structures; (3) the Case I optimum design is worse than the Case II optimum design in this example. This is due to the fact of having more design variables for Case 2, which means more choices in the optimal design space. The noteworthy difference indicates that the number of design variables can considerably affect the design processes.

Table 3. The initial and optimal designs for Cases I and II

Different design	Case I		Case II		
	$X_1$	$P_1$	$X_1$	$X_2$	$P_1$
Initial design	13.000	6.926	13.000	23.000	6.926
Optimal design	11.850	7.016	9.95	19.25	7.138

In order to ensure that the optimization process converged to the global optimum point, the location of arch bracings was optimized using several start points. Table 4 shows the first selected start point and three different start points with their corresponding coordinates and buckling load after optimization. It can be seen that the maximum difference between the obtained coordinates is about 0.4 m or 3.12% and between the buckling loads is about 0.008 or 0.11%. Therefore, there is confidence that the convergence to the global optimum point is achieved.

Table 4. Location of arch bracing and buckling load obtained from different start points

Start point	Case I		Case II		
	$X_1$	$P_1$	$X_1$	$X_2$	$P_1$
I	11.850	7.016	9.95	19.25	7.138
II	11.850	7.016	10.0	19.45	7.136
III	11.850	7.016	10.15	20.20	7.131
IV	11.850	7.016	9.95	19.15	7.139

#### 4 CONCLUSIONS

The location design of arch bracings in an arch bridge structure has been treated as a constrained optimization problem in which the elastic buckling load has been used to construct the objective function of the optimization problem. An efficient, accurate, and robust algorithm is developed to solve the optimization problem and identify the location of arch bracings by maximizing the objective function. The proposed algorithm integrates the concepts of the penalty function method, finite element method and the first-order method. Penalty function method is used to transform the constrained optimization problem to an unconstrained optimization problem. Finite element method is adopted to compute values of implicit objective functions. First-order method is used to solve the unconstrained optimization problem. An example is presented to demonstrate the practical application of the proposed method. The optimal location results obtained by using several different start points demonstrate the robustness of the proposed method.

#### ACKNOWLEDGMENTS

This work presented herein has been supported by the National Natural Science Foundation of China under grant number 51178334 and the National Basic Research Program of China (973 Program) under grant number 2013CB036303 and a research grant from the Program for the New Century Excellent Talents in University (Project No.NCET-11-0380) and a research grant from Shaanxi highway bridge and tunnel laboratory (Project No.2013G1502026). These supports are gratefully acknowledged.

#### REFERENCES

- [1] Ney, L, Degoyet, VD, Maquoi, R. "Optimum bracing of the arches of tied-arch bridges", *Journal of Constructional Steel Research*, Vol. 18, No. 3, pp. 239-249, 1991.
- [2] Diaz, AR, Kikuchi, N. "Solutions to shape and topology eigenvalue optimization problems using a homogenization method". *International Journal for Numerical Method in Engineering*, Vol. 35, pp. 1487-1502, 1992.
- [3] Ma, ZD, Kikuchi, N, Hagiwara, I. "Structural topology and shape optimization for a frequency response problem", *Computational Mechanics*, Vol. 13, pp. 157-174, 1993.
- [4] Yang, RJ, Chahande, AI. "Automotive application of topology optimization", *Structural Optimization*, Vol. 9, pp. 245-249, 1995.
- [5] Lam, YC and Santhikumar, S. "Automated rib location and optimization for plate structures", *Structural Multidisciplinary Optimization*, Vol. 25, pp. 35-45, 2003.
- [6] Vanderplaats, GN. *Numerical optimization techniques for engineering design: with applications*. New York: McGraw-Hill Publishers, 1984.
- [7] Cook, RD, Malkus, DS, and Plesha, M.E. *Concepts and applications of finite element analysis*, 3rd Ed., Wiley, New York, 1989.



## **TOPIC 4**

### Long Span Bridges



IBSBI 2014, October 16-18, 2014, Athens, Greece

## **CABLES WITH DAMPERS FOR FLOW-INDUCED VIBRATION**

Theodore G. Konstantakopoulos<sup>1</sup> and George T. Michaltsos<sup>2</sup>

<sup>1,2</sup> National Technical University of Athens, Dept. of Civil Engineering, Greece  
e-mail: michalts@central.ntua.gr, theokons@teemail.gr

**ABSTRACT:** Rain-wind induced stay cable vibrations may occur at different cable eigenfrequencies. Therefore, external transverse dampers are applied for decreasing the amplitude of these vibrations. For the analytical study of cables with dampers or movable anchorages, it is generally employed a finite series of sinusoidal form. This paper studies the effect of such a system through the use of the exact eigenshapes of the cable, taking into account sagging, inclination and axial flexibility of the cable model.

**KEY WORDS:** Stay-Cables, Cables with dampers, Flow-Induced vibrations

### **1 INTRODUCTION**

A significant problem which arises from the praxis is the cables' rain-wind induced vibrations. Large amplitude Rain-Wind-Induced-Vibrations (RWIV) of stay cables is a challenging problem in the design of cable-stayed bridges. Such phenomena were first observed on the Meikonishi bridge in Nagoya, Japan [1] and also later on other bridges. It was found that the cables, which were stable under wind action only, were oscillating under a combined influence of rain and wind, leading to large amplitude motions, even for light-to-moderate simultaneous rain and wind action. The frequency of the observed vibrations was much lower than the critical one of the vortex-induced vibrations, while it was also perceived that the cable oscillations took place in the vertical plane mostly in single mode; for increasing cable length however, higher modes (up to the 4<sup>th</sup>) appeared. Most importantly, during the oscillations a water rivulet appeared on the lower surface of the cable, which was characterized by a leeward shift and vibrated in circumferential directions [1, 2, 3]. The produced vibrations in this way can cause reduced life of the cable and connections due to fatigue or rapid progress of the corrosion.

Several methods, including aerodynamic or structural means, have been investigated in order to control the vibrations of bridge's stay cables. Aerodynamic methods, just as change of the cables' roughness were effective only for certain classes of vibration. Another method is the coupling of the stays with secondary wires, in order to reduce their effective length and thereby

to avoid resonance. This method changes the bridge’s aesthetics. Another widely applied method is this of external dampers attached transverse to the stay-cables or a system of movable anchorage by using a Friction Pendulum Bearing or an Elastomeric bearing to replace the conventional fixed support of stay cables.

This paper studies the effect of a system with external damper, through the use of the exact eigenshapes of the cable, taking into account sag, inclination and axial flexibility to the cable model.

**2 BASIC ASSUMPTIONS**

- a. The studied cable has, under the dead and live loads, the catenary shaped elastic line, with displacements  $w_0$  and tensile forces  $T_0$  (see fig.1). Because of its shallow form, the above line can be replaced by a parabola of second order. The equation of a parabola passing from the points (0,0), (L,0) and having  $w''_0 = -\bar{m}g/H_0$ , is given by the following formula:

$$w_0(x) = \frac{\bar{m}g}{2H_0}x(L-x) \tag{1a}$$

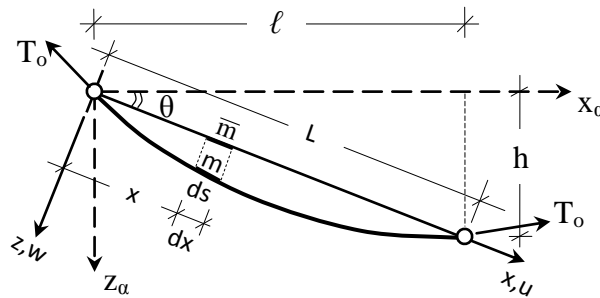


Figure 1. Cables and reference axes

- b. Under the action of the dynamic loads  $p_y(x,t)$  and  $p_z(x,t)$ , the cable takes the shape of figure 2, with additional displacements  $u_d$ ,  $v_d$ ,  $w_d$  and tensile forces  $T_d$ .
- c. The static and dynamic tensile forces are connected with the following relations:  $T(t) = T_0 + T_d(t)$ ,  $H(t) = H_0 + H_d(t)$  } (2a,b)  
where  $H$ , is the projection of  $T$  on  $x$ -axis.
- d. The  $\bar{m}(x)$  and  $m(s)$  of figure 1, are connected through the relation

$$\bar{m}(x) = m(s)ds/dx \tag{3}$$

- e. We neglect the flexural rigidity of the cables, (as it is proved in [4]).
- f. The studied cables are referred to the inclined axis system 0-xyz of fig.2.

### 3 THE EQUATIONS OF MOTION

#### 3.1 Projection on xoz-plane

For a shallow form of the cable, the following relations are valid:

$$\left. \begin{aligned} \cos \rho_z &= dx/ds \cong 1, & \sin \rho_z &= dw/ds, & \sin d\rho_z &\cong 0 \end{aligned} \right\} \quad (4.1a,b,c)$$

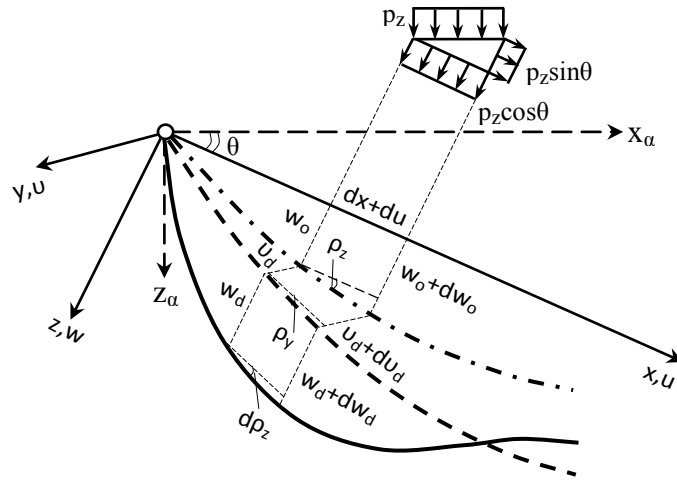


Figure 2. Deformation of the cable

Projecting the on xoz and xoy-planes and from the equilibrium of horizontal and vertical forces, we finally obtain:

$$\frac{\partial H}{\partial s} - c\dot{u} - m\ddot{u} = -p_x(x,t) \quad (4.2)$$

$$T_o \frac{\partial^2 w_d}{\partial x^2} + T_d \left( \frac{\partial^2 w_o}{\partial x^2} + \frac{\partial^2 w_d}{\partial x^2} \right) - c\dot{w}_d - m\ddot{w}_d = -p_z(x,t) \quad (4.3)$$

$$T_o \frac{\partial^2 v_d}{\partial x^2} + T_d \frac{\partial^2 v_d}{\partial x^2} - c\dot{v}_d - m\ddot{v}_d = -p_y(x,t), \quad \text{with } \bar{m} \text{ from (2)} \quad (4.4)$$

### 4 THE VERTICALLY FREE VIBRATING CABLE

In order to determine the eigenfrequencies and shape functions, we have to find the tensile  $T_d$ . The following relations are valid:

$$\left. \begin{aligned} ds^2 &= dx^2 + dw_o^2 \\ (ds + \Delta ds)^2 &= (dx + \Delta dx)^2 + (\Delta dv)^2 + (dw_o + \Delta dw_o)^2 \end{aligned} \right\} \quad (5.1)$$

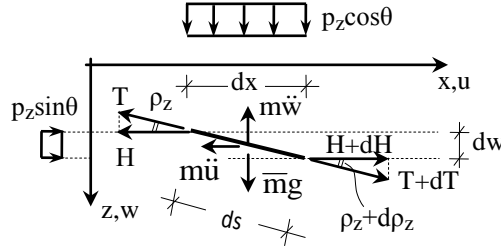


Figure 3. Projection on xoz-plane

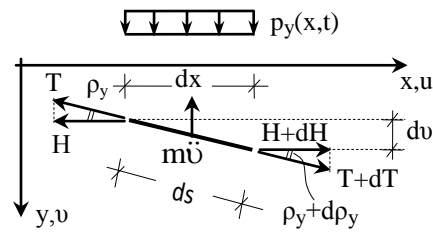


Figure 4. Projection on xoy-plane

Taking into account that  $\epsilon = \sigma/E = T_d/EA$  and using the condition

$$\int_0^L \Delta dx = 0, \text{ we finally find: } T_d = -\frac{w_o'''}{L_o} \int_0^L w_d dx, \text{ with: } L_o = \int_0^L \frac{dx}{EA \cos^3 \rho_z} \quad \left. \vphantom{\int_0^L} \right\} \quad (5.2 \text{ a,b})$$

From equations (4.3), (5.2 a) and since it is  $w_d \ll w_o$ , we get:

$$T_o w_d'' - c \dot{w}_d - m \ddot{w}_d - \frac{w_o''^2}{L_o} \int_0^L w_d dx = 0 \quad (5.3)$$

We are searching for a solution of separate variables under the form:

$$w_d(x, t) = W(x) \cdot \Phi(t) \quad (5.4)$$

Therefore, equation (5.3) gives the following uncoupled equations:

$$W'' + \frac{m \omega_w^2}{T_o} W = \frac{w_o''^2}{T_o L_o} \int_0^L W dx, \quad \ddot{\Phi} + \frac{c}{m} \dot{\Phi} + \omega_w^2 \Phi = 0 \quad \left. \vphantom{\int_0^L} \right\} \quad (5.5a,b)$$

Equation (5.5a) has the solution:

$$W(x) = c_1 \sin \lambda_w x + c_2 \cos \lambda_w x + \frac{w_o''^2}{T_o L_o} \int_0^L W dx, \quad \text{with: } \lambda_w^2 = \frac{m \omega_w^2}{T_o} \quad \left. \vphantom{\int_0^L} \right\} \quad (5.6a,b)$$

Equation (5.6a) has the solution:

$$W(x) = c_1 [\sin \lambda_w x + G(1 - \cos \lambda_w L)] + c_2 [\cos \lambda_w x + G \sin \lambda_w L] \quad \left. \vphantom{\int_0^L} \right\} \quad (5.7a,b)$$

where :  $G = \frac{w_o''^2}{\lambda_w (\lambda_w^2 T_o L_o - w_o''^2 \cdot L)}$

The boundary conditions are:

$$W(0) = W(L) = 0 \quad (5.8a,b)$$

Introducing equation (5.7a) into the above equations we get:

$$\left. \begin{aligned} G(1 - \cos \lambda_w L) \cdot c_1 + (1 + G \sin \lambda_w L) \cdot c_2 &= 0 \\ [\sin \lambda_w L + G(1 - \cos \lambda_w L)] \cdot c_1 + [\cos \lambda_w L + G \sin \lambda_w L] \cdot c_2 &= 0 \end{aligned} \right\} \quad (5.9a,b)$$

In order for the above system to have a non-trivial solution, the determinant of the coefficients of the unknowns must be zero. This condition gives:

$$2G \cos \lambda_w L - \sin \lambda_w L - 2G = 0 \quad (5.10)$$

Finally, from equs. (5.11), (5.12) and (5.9a), one can determine the following form of the shape functions:

$$W_n(x) = c_1 \cdot \left[ \sin \lambda_{wn} x - \frac{G_n(1 - \cos \lambda_{wn} L)}{1 + G_n \sin \lambda_{wn} L} \cdot \cos \lambda_{wn} x + \frac{G_n(1 - \cos \lambda_{wn} L)}{1 + G_n \sin \lambda_{wn} L} \right] \quad (5.11)$$

## 5 THE VERTICALLY FORCED VIBRATING CABLE

According to the acceptances of §1, the equations of vertical motion of a cable subjected to external dynamic loadings and supported by a damper system, can be written as follows:

$$\left. \begin{aligned} T_o w_d'' + T_d w_o'' - c \dot{w}_d - m \ddot{w}_d &= -p_z(x)f(t) - c_d \dot{w}_d \delta(x - a_d) \\ T_d &= -\frac{w_o''}{L_o} \int_0^L w_d dx \end{aligned} \right\} \quad (6.1a,b)$$

Where  $c_d$  is the damper's coefficient,  $a_d$  its position and  $\delta(x)$  the Dirac's delta function (see figure 5). We are searching for a solution of the form:

$$w_d(x,t) = \sum_n W_n(x) \Phi_n(t) \quad (6.2)$$

where  $W_n(x)$  from equ.(5.13) and  $\Phi_n(t)$  unknown functions under determination.

Introducing (6.2) into (6.1a) we get:

$$\begin{aligned} H_o \sum_n W_n'' \Phi_n - \frac{w_o''^2}{L_o} \int_0^L \sum_n W_n \Phi_n dx - c \sum_n W_n \dot{\Phi}_n - m \sum_n W_n \ddot{\Phi}_n = \\ - p_z(x)f(t) + c_d \sum_n W_n \dot{\Phi}_n \delta(x - a_d) \end{aligned}$$

Substituting expression (6.2) into (6.1a) we get:

$$\left. \begin{aligned} H_o \sum_n W_n'' \Phi_n - \frac{w_o''^2}{L_o} \int_0^L \sum_n W_n \Phi_n dx - c \sum_n W_n \dot{\Phi}_n - m \sum_n W_n \ddot{\Phi}_n = \\ - p_z(x)f(t) + c_d \sum_n W_n \dot{\Phi}_n \delta(x - a_d) \end{aligned} \right\} \quad (6.3a)$$

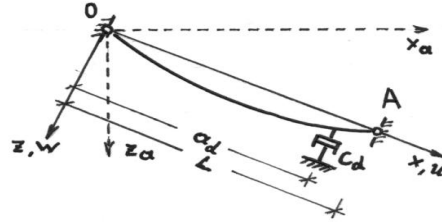


Figure 5. Cable with damper

Since  $W_n$  satisfies equation (5.7a), the above becomes:

$$m \sum_n \omega_n^2 W_n \Phi_n + c \sum_n W_n \dot{\Phi}_n + m \sum_n W_n \ddot{\Phi}_n = p_z(x) f(t) - c_d \sum_n W_n \dot{\Phi}_n \delta(x - a_d) \quad (6.3b)$$

Multiplying by  $W_k$ , integrating the out come from 0 to L, we finally obtain:

$$\left. \begin{aligned} \ddot{\Phi}_k + \frac{c}{m} \dot{\Phi}_k + \omega_k^2 \Phi_k + \frac{c_d W_k(a_d)}{m \int_0^L W_k^2 dx} \sum_n W_n(a_d) \dot{\Phi}_n &= \frac{\int_0^L p_z(x) W_k dx}{m \int_0^L W_k^2 dx} \cdot f(t) \\ \text{for : } k &= 1 \text{ to } n \end{aligned} \right\} \quad (6.3c)$$

In order to solve the above differential system, we use the Lagrange transformation. Therefore, we set:

$$L\Phi_k(t) = \varphi_k(s) \quad , \quad Lf(t) = F(s) \quad \} \quad (7.1a,b)$$

with initial conditions:  $\Phi_k(0) = \dot{\Phi}_k(0) = 0 \quad (7.2)$

The system (6.3b) becomes:

$$\left. \begin{aligned} \alpha_{k1}\varphi_1 + \alpha_{k2}\varphi_2 + \dots + \alpha_{kn}\varphi_n &= \beta_k \quad , \quad \text{where :} \\ \alpha_{k\rho} &= \frac{c_d W_k(a_d)}{m \int_0^L W_k^2 dx} \cdot W_\rho(a_d) \cdot s \quad , \quad \alpha_{kk} = s^2 + \left( \frac{c}{m} + \frac{c_d W_k^2(a_d)}{m \int_0^L W_k^2 dx} \right) \cdot s + \omega_k^2 \\ \beta_k &= \frac{\int_0^L p_z(x) W_k dx}{m \int_0^L W_k^2 dx} \cdot F(s) \quad , \\ k &= 1 \text{ to } n, \quad \rho = 1 \text{ to } n \end{aligned} \right\} \quad (7.3a,b,c,d)$$

Solving the system of eqs (7.3a), we get  $\varphi_k(s)$  and therefore:

$$\Phi_k(t) = L^{-1} \varphi_k(s) \quad (7.4)$$



## 6 NUMERICAL EXAMPLE AND DISCUSSION

### 6.1 The cable

We consider a c-s-bridge with dense distribution of cables. We separate a cable with the following characteristics:  $T_0=300000\text{dN/cable}$ ,  $D=0.130\text{m}$ ,  $m=7\text{kg/m}$ ,  $A=7.5\cdot 10^{-3}\text{m}^2$ , and  $L=150, 250, \text{ and } 350\text{m}$ . According to (5.10) we get the following table 1 with the first three eigenfrequencies.

TABLE 1

	L=150m	L=250m	L=350m
$\omega_1$	4.4697	2.8186	2.1507
$\omega_2$	8.6716	5.2029	3.7164
$\omega_3$	13.0125	7.8130	5.5868

### 6.2 The load

It has been observed that the rain-wind applied excitation usually occurs in a frequency range from  $0.5$  to  $4\text{ sec}^{-1}$ . For the restricted length of a conference paper we choose  $p=p(x) f(t)=20\cdot\sin 3t$ .

### 6.3 The damper

We study two kind of dampers with:  $c_d=0.01, 0.10, \text{ and } 0.5\text{ dNsec/mm}$ , applied at  $a_d=0.99L, \text{ and } 0.97L$ .

Applying the above exposed method we obtain the following diagrams of figures 6, 7 and 8.

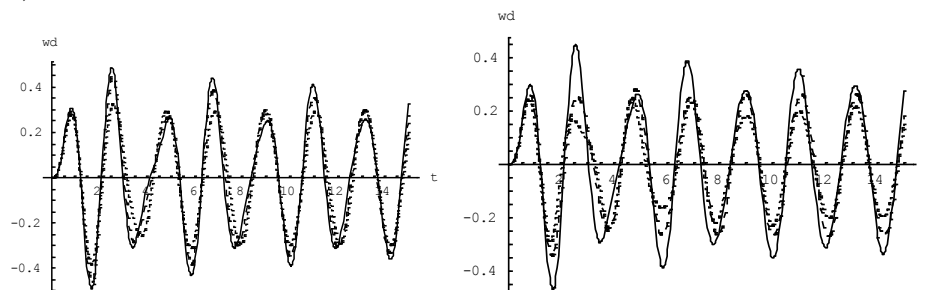


Figure 6. Cables  $L=150\text{m}$ , with dampers  
 —  $c_d=0.01$ , - -  $c_d=0.1$ , - - -  $c_d=0.5\text{ dN sec/mm}$

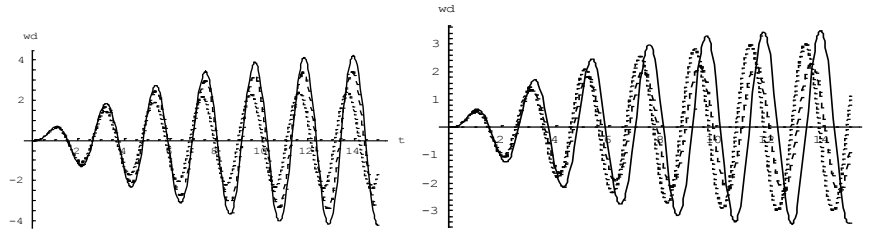


Figure 7. Cables  $L=250\text{m}$ , with dampers

—  $cd=0.01$ , - -  $cd=0.1$ , - - -  $cd=0.5$  dN sec/mm

Noting that the studied loading  $p=p*\sin 3t$ , produces very large oscillations because the  $\omega=3$  approaches the first eigenfrequency of the cable  $\omega_1 = 2.81 \text{ sec}^{-1}$

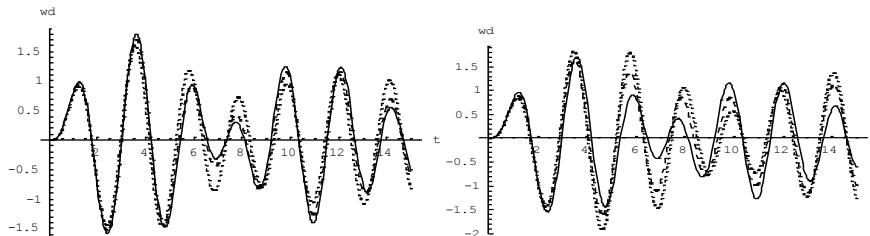


Figure 8. Cables  $L=350\text{m}$ , with dampers

—  $cd=0.01$ , - -  $cd=0.1$ , - - -  $cd=0.5$  dN sec/mm

## 7 CONCLUSIONS

Based on the preceding results, the following conclusions can be drawn:

1. A mathematical model is proposed, based on the use of the real shape functions of the cable.
2. From the studied data, we see that the effective point to apply a damper is, as possible, far from the joint of the cable.
3. Even for the case of an external excitation with frequency near of an eigenfrequency of the cable, the damping system decreases the amplitude of the oscillations.

## REFERENCES

- [1] Hikami, Y., Shiraishi, N., "Rain-wind-induced vibrations of cables in cable stayed bridges", Journal of Wind Engineering and Industrial Aerodynamics, Vol. 29, Nos. 1-3, pp. 409-418, 1988.
- [2] Wilde, K, Witkowski, W, "Simple model of rain-wind-induced vibrations of stayed cables", Journal of Wind Engineering and Industrial Aerodynamics, Vol. 91, No. 7, pp. 873-891, 2003.
- [3] Ibrahim, RA, "Nonlinear vibrations of suspended cables – Part III: Random excitation and interaction with fluid flow", Applied Mechanics Reviews, Vol. 57, No. 6, pp. 515-549, 2004.
- [4] Kollbruner C.F., Hajdin N. and Stipanic B., "Contribution to the analysis of cable-stayed Bridges", (1980), Inst. For Engineering Research Editions, Schulthess Verlag Zürich, N.48

## **CABLES WITH MOVABLE ANCHORAGES FOR FLOW-INDUCED VIBRATION**

Ioannis Raftoyiannis<sup>1</sup>, Georgina Papastergiou<sup>2</sup> and George Michaltsos<sup>3</sup>

<sup>1,2,3</sup>National Technical University of Athens

e-mail: rafto@central.ntua.gr, papastergiou.georgina@gmail.com, michalts@central.ntua.gr

**ABSTRACT:** Rain-wind induced stay cable vibrations may occur at different cable eigenfrequencies. Therefore, external transverse dampers are applied for decreasing these vibrations. For the analytical study of cables with dampers or movable anchorages are generally used finite series of sinus form. This paper studies the effect of such a system through the use of the exact eigenshapes of the cable, taking into account inclination and several other parameters.

**KEY WORDS:** Stay-Cables, Cables with movable anchorages, Flow-Induced vibrations

### **1 INTRODUCTION**

A significant problem, which arose from the praxis, is the cables' rain-wind induced vibrations. Such phenomena were first observed on the Meikonishi bridge in Nagoya, Japan [1] and also later on other bridges. It was found that the cables, which were stable under wind action only, were oscillating under a combined influence of rain and wind, leading to large amplitude motions. The frequency of the observed vibrations was much lower than the critical one of the vortex-induced vibrations, while it was also perceived that the cable oscillations took place in the vertical plane mostly in single mode; for increasing cable length however, higher modes (up to the 4<sup>th</sup>) appeared. It is important the appearance of water rivulet on the lower surface of the cable [1, 2, 3]. The produced in this way vibrations can cause reduced life of the cable due to fatigue or rapid progress of the corrosion. Several methods, including aerodynamic or structural means, have been investigated in order to control the vibrations of bridge's stay cables. Aerodynamic methods, just as change of the cables' roughness were effective only for certain classes of vibration. Another method is the coupling of the stays with secondary wires, in order to reduce their effective length and thereby to avoid resonance. This method changes the bridge's aesthetics. Another widely applied method is this of external dampers attached transverse to the stay-cables or a system of movable anchorage by using a Friction Pendulum Bearing or an Elastomeric bearing to replace the conventional fixed support of stay cables. This paper studies the effect of a

system with movable anchorages, through the use of the exact eigenshapes of the cable, taking into account sag, inclination and axial flexibility to the cable model.

**2 ACCEPTANCES**

- a. The studied cable has, under the dead and live loads, the catenary shape elastic line, with displacements  $w_0$  and tensile forces  $T_0$  (see fig.1). Because of its shallow form, the above line can be replaced by a parabola of second order. The equation of a parabola passing from the points (0,0), (L,0) and having  $w''_0 = -\bar{m}g/H_0$ , is given by the following formula:

$$w_0(x) = \frac{\bar{m}g}{2H_0}x(L-x) \tag{1a}$$

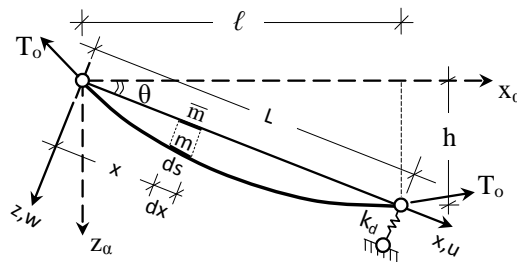


Figure 1. Cables and reference axes

- b. Under the action of dynamic loads, the cable takes the shape of figure 2, with additional displacements  $u_d, v_d, w_d$  and tensile forces  $T_d$ .
- c. The static and dynamic tensile forces are connected with the following relations:  $T(t) = T_0 + T_d(t), H(t) = H_0 + H_d(t)$  } (2a,b) where H, is the projection of T on x-axis.
- d. The  $\bar{m}(x)$  and  $m(s)$  of figure 1, are connected through the relation  $\bar{m}(x) = m(s)ds/dx$  (3)
- e. We neglect the flexural rigidity of the cables, (as it is proved in [4]).
- f. The studied cables are referred to the inclined axis system 0-xyz of figure 2.

**3 THE EQUATIONS OF MOTION**

**3.1 Projection on xoz-plane**

For a shallow form of the cable, the following relations are valid:

$$\cos \rho_z = dx/ds \cong 1, \quad \sin \rho_z = dw/ds, \quad \sin d\rho_z \cong 0 \quad \} \tag{4.1a,b,c}$$

Projecting the on xoz and xoy-planes and from the equilibrium of horizontal and vertical forces, we finally obtain:

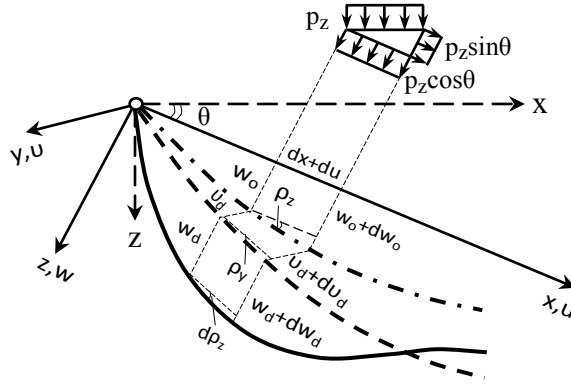


Figure 2. Deformation of the cable

$$\frac{\partial H}{\partial s} - c\dot{u} - m\ddot{u} = -p_x(x, t) \tag{4.2}$$

$$T_o \frac{\partial^2 w_d}{\partial x^2} + T_d \left( \frac{\partial^2 w_o}{\partial x^2} + \frac{\partial^2 w_d}{\partial x^2} \right) - c\dot{w}_d - m\ddot{w}_d = -p_z(x, t) \tag{4.3}$$

$$T_o \frac{\partial^2 v_d}{\partial x^2} + T_d \frac{\partial^2 v_d}{\partial x^2} - c\dot{v}_d - m\ddot{v}_d = -p_y(x, t), \quad \text{with } \bar{m} \text{ from (2)} \tag{4.4}$$

#### 4 THE VERTICALLY FREE VIBRATING CABLE

In order to determine the eigenfrequencies and shape functions, we have to find the tensile  $T_d$ . The following relations are valid:

$$\left. \begin{aligned} ds^2 &= dx^2 + dw_o^2 \\ (ds + \Delta ds)^2 &= (dx + \Delta dx)^2 + (\Delta dv)^2 + (dw_o + \Delta dw_o)^2 \end{aligned} \right\} \tag{5.1}$$

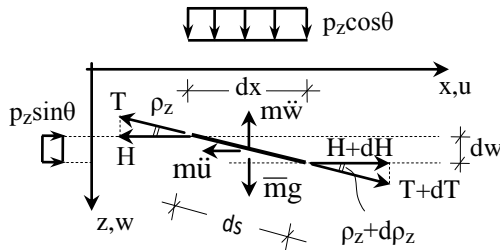


Figure 3. Projection on xoz-plane

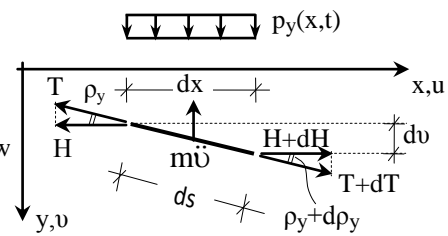


Figure 4. Projection on xoy-plane

Remembering that  $\varepsilon = \sigma/E = T_d/EA$  and using the condition  $\int_0^L \Delta dx = 0$ , we

finally find: 
$$\frac{T_d}{EA} \int_0^L \frac{dx}{\cos^3 \rho_z} - \int_0^L \frac{dw_d}{dx} \cdot \frac{dw_o}{dx} \cdot dx = 0.$$
 From this last, after

integration by members and with boundary condition  $w_d(0) = 0$  we obtain:

$$T_d = \frac{1}{L_o} \left( w'_o(L)w_d(L) - w''_o \int_0^L w_d dx \right), \quad \text{with : } L_o = \int_0^L \frac{dx}{EA \cos^3 \rho_z} \quad \left. \vphantom{\frac{1}{L_o}} \right\} \quad (5.2a,b)$$

From equations (4.3), (5.2a) and taking into account that  $w_d \ll w_o$ , we get:

$$T_o w''_d - c \dot{w}_d - m \ddot{w}_d = - \frac{w''_o \cdot w'_o(L)}{L_o} \cdot w_d(L) + \frac{w''_o{}^2}{L_o} \int_0^L w_d dx = 0 \quad (5.3)$$

We are searching for a solution of the form:

$$w_d(x, t) = W(x)\Phi(t) \quad (5.4)$$

Therefore, equation (5.3) gives the following uncoupled equations:

$$W'' + \frac{m\omega_w^2}{T_o} W = \frac{\bar{m} g L w''_o}{2H_o L_o T_o} W(L) + \frac{w''_o{}^2}{T_o L_o} \int_0^L W dx, \quad \ddot{\Phi} + \frac{c}{m} \dot{\Phi} + \omega_w^2 \Phi = 0 \quad \left. \vphantom{\frac{m\omega_w^2}{T_o}} \right\} \quad (5.5a,b)$$

The solution of equation (5.5a) is:

$$W(x) = c_1 \sin \lambda_w x + c_2 \cos \lambda_w x + \frac{\bar{m} g L w''_o}{2H_o L_o T_o \lambda_w^2} W(L) + \frac{w''_o{}^2}{T_o L_o \lambda_w^2} \int_0^L W dx, \quad \lambda_w^2 = \frac{m\omega_w^2}{T_o} \quad \left. \vphantom{\frac{\bar{m} g L w''_o}{2H_o L_o T_o \lambda_w^2}} \right\} \quad (5.6a,b)$$

Equation (5.6a) has the solution:

$$\left. \begin{aligned} W(x) &= c_1 (\sin \lambda_w x + D_1) + c_2 (\cos \lambda_w x + D_2) \\ \text{where : } D_1 &= G_1 \sin \lambda_w L + \frac{G_2 + G_3}{1 - (G_2 + G_3)} \left( \frac{1 - \cos \lambda_w L}{\lambda_w} + G_1 L \sin \lambda_w L \right) \\ D_2 &= G_1 \cos \lambda_w L + \frac{G_2 + G_3}{1 - (G_2 + G_3)} \left( \frac{\sin \lambda_w L}{\lambda_w} + G_1 L \cos \lambda_w L \right) \end{aligned} \right\} \quad (5.7a,b,c)$$

The boundary conditions are:

$$W(0) = 0, \quad T_o W'(L) + k_s W(L) = 0 \quad (5.8a,b)$$

Introducing equation (5.7a) into the above conditions we obtain:

$$\left. \begin{aligned} c_1 D_1 + c_2 (1 + D_2) &= 0 \\ c_1 [\lambda_w T_o \cos \lambda_w L + k_s (\sin \lambda_w L + D_1)] + c_2 [-\lambda_w T_o \sin \lambda_w L + k_s (\cos \lambda_w L + D_2)] &= 0 \end{aligned} \right\} \quad (5.9a,b)$$

In order for the above system to have a non-trivial solution, the determinant of the coefficients of the unknowns must be zero. This condition gives:

$$D_2 [D_1 - (1 + D_2) k_s] + [D_1 k_s - (1 + D_2) T_o \lambda_w] \cos \lambda_w L - [(1 + D_2) k_s + D_1 T_o \lambda_w] \sin \lambda_w L = 0 \quad (5.10)$$

Finally from equations (5.11), (5.12) and (5.9a), one can determine the following form of the shape functions:

$$W_n(x) = c_1 \left[ (\sin \lambda_w x + D_1) + \frac{\lambda_w T_o \cos \lambda_w L + k_s (\sin \lambda_w L + D_2)}{\lambda_w T_o \sin \lambda_w L - k_s (\cos \lambda_w L + D_2)} \cdot (\cos \lambda_w x + D_2) \right] \quad (5.11)$$

## 5 THE VERTICALLY FORCED VIBRATING CABLE

According to the acceptances of §1, the equations of vertical motion of a cable subjected to external dynamic loadings and supported by a damper system, can be written as follows (see fig.5):

$$\left. \begin{aligned} T_o w_d'' + T_d w_o'' - c \dot{w}_d - m \ddot{w}_d &= -p_z(x) f(t) - (k_d w_d + c_d \dot{w}_d) \delta(x - L) \\ T_d &= \frac{1}{L_o} \left( w_o'(L) w_d(L) - w_o'' \int_0^L w_d dx \right) \end{aligned} \right\} \quad (6.1a,b)$$

where  $c_d$  is the damper's coefficient,  $a_d$  its position and  $\delta(x)$  the Dirac's delta function (see figure 5). We are searching for a solution of the form:

$$w_d(x, t) = \sum_n W_n(x) \Phi_n(t) \quad (6.2)$$

where  $W_n(x)$  from equ.(5.11) and  $\Phi_n(t)$  unknown functions under determination. Introducing (6.2) into (6.1a) we get:

$$\left. \begin{aligned} - \sum_n W_n'' \Phi_n + \frac{m' g L}{2 H_o T_o} \sum_n W_n(L) \Phi_n + \frac{w_o''^2}{L_o} \int_0^L \sum_n W_n \Phi_n dx + \frac{c}{T_o} \sum_n W_n \dot{\Phi}_n + \frac{m}{T_o} \sum_n W_n \ddot{\Phi}_n &= \\ = \frac{p_z(x) f(t)}{T_o} - \left( \frac{k_d}{T_o} \sum_n W_n \Phi_n + \frac{c_d}{T_o} \sum_n W_n \dot{\Phi}_n \right) \delta(x - L) \end{aligned} \right\} \quad (6.3a)$$

Remembering that  $W_n$  satisfies equation (5.5a), the above becomes:

$$\left. \begin{aligned} \sum_n \omega_n^2 W_n \Phi_n + \frac{c}{m} \sum_n W_n \dot{\Phi}_n + \sum_n W_n \ddot{\Phi}_n &= \\ &= \frac{p_z(x)f(t)}{m} - \left( \frac{k_d}{m} \sum_n W_n \Phi_n + \frac{c_d}{m} \sum_n W_n \dot{\Phi}_n \right) \delta(x-L) \end{aligned} \right\} \quad (6.3b)$$

Multiplying by  $W_k$ , integrating the outcome from 0 to L, we finally obtain:

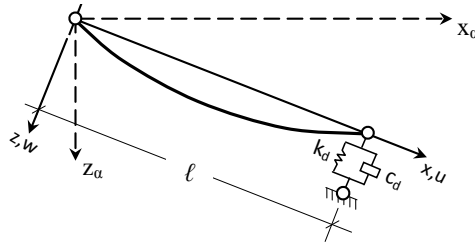


Figure 5. Cable with damper

$$\left. \begin{aligned} \ddot{\Phi}_k + \frac{c}{m} \dot{\Phi}_k + \omega_k^2 \Phi_k &= \frac{f(t) \int_0^L p_z(x) W_k dx}{m \int_0^L W_k^2 dx} - \frac{\left( k_d W_k(L) \sum_n W_n(L) \Phi_n + c_d W_k(L) \sum_n W_n(L) \dot{\Phi}_n \right)}{m \int_0^L W_k^2 dx} \end{aligned} \right\} \quad (6.3c)$$

for :  $k = 1$  to  $n$

In order to solve the above differential system, we use the Lagrange transformation. Therefore we put:

$$L\Phi_k(t) = \varphi_k(s) \quad , \quad Lf(t) = F(s) \quad \} \quad (7.1a,b)$$

with initial condition:  $\Phi_k(0) = \dot{\Phi}_k(0) = 0$  (7.2)

We conclude to the following system:

$$\left. \begin{aligned} \alpha_{k1}\varphi_1 + \alpha_{k2}\varphi_2 + \dots + \alpha_{kn}\varphi_n &= \beta_k \quad , \quad \text{where :} \\ \alpha_{kp} &= \frac{k_d W_k(L) W_p(L) + c_d W_k(L) W_p(L) \cdot s}{m \int_0^L W_k^2 dx} \\ \alpha_{kk} &= s^2 + \frac{c}{m} \cdot s + \omega_k^2 + \frac{(k_d + c_d \cdot s)}{m \int_0^L W_k^2 dx} \cdot W_k^2(L) \quad , \quad \beta_k = \frac{\int_0^L p_z(x) W_k dx}{m \int_0^L W_k^2 dx} \cdot F(s) \end{aligned} \right\} \quad (7.3a,b,c,d)$$

$k = 1$  to  $n$ ,  $\rho = 1$  to  $n$

and finally:  $\Phi_k(t) = L^{-1}\varphi_k(s)$  (7.4)



## 6 NUMERICAL EXAMPLE AND DISCUSSION

### 6.1 The cable

We consider a cable with the following characteristics:  $T_0=300000\text{dN/cable}$ ,  $D=0.130\text{m}$ ,  $m=7\text{kg/m}$ ,  $A=7.5\cdot 10^{-3}\text{m}^2$ , and  $L=150, 250, \text{ and } 350\text{m}$ . According to (5.10) and for  $k_s=5000\text{ dN/m}$ , we get the following Table 1 giving the eigenfrequencies of the cables.

TABLE 1

	L=150m	L=250m	L=350m
$\omega_1$	3.3989	2.3108	1.8079
$\omega_2$	7.1529	4.4900	3.3223
$\omega_3$	11.2465	6.8850	5.0020

### 6.2 The load

It has been observed that the rain-wind applied excitation usually occurs in a frequency range from  $0.5$  to  $4\text{ sec}^{-1}$ . For the restricted length of a conference paper we choose  $p=p(x) f(t)=20\cdot\sin 3t$ .

### 6.3 The damping system

We study a damping system consisted by a spring of constant  $k_d=5000\text{ dN/m}$  and a damper of constant  $c_d=7500\text{ dNsec/m}$ .

Applying the above exposed method we obtain the following diagrams of figures 6, 7 and 8, which show the oscillations of the middle of the cables and of the anchor points.

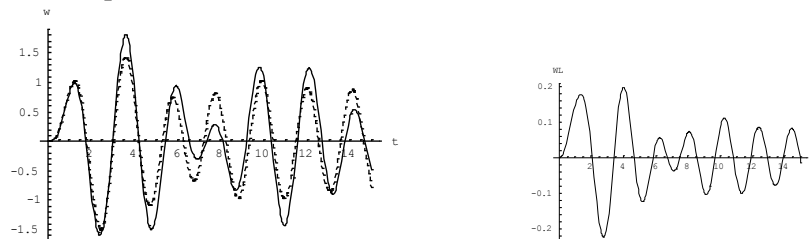


Figure 6. Cables  $L=350\text{m}$ , with dampers  $k_d=5000, c_d=7500$   
 \_\_\_ without movable anchorage, \_\_ with movable anchorage

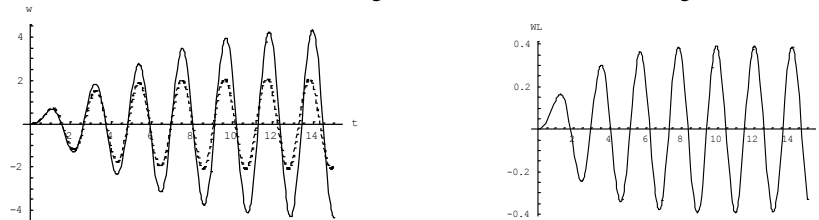


Figure 7. Cables  $L=250\text{m}$ , with dampers  $k_d=5000, c_d=7500$   
 \_\_\_ without movable anchorage, \_\_ with movable anchorage

From the above diagrams we see that the selected system is effective even for the case where the frequency of the external loading coincides with the first eigenfrequency of the cable. We see also that this system is ineffective for the cable of  $L=150\text{m}$ . Applying another system with  $k_d=3000$  and  $c_d=9000$ , we get an effective one (fig. 9).

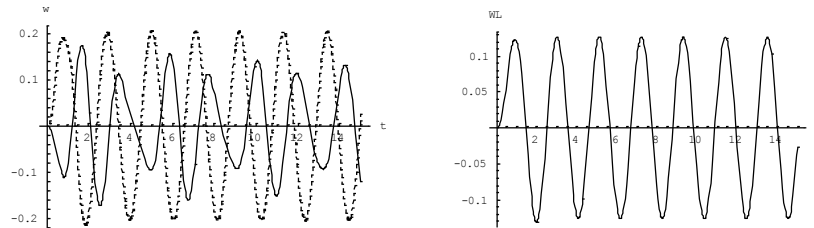


Figure 8. Cables  $L=150\text{m}$ , with dampers  $k_d=5000$ ,  $c_d=7500$   
 — without movable anchorage, - - with movable anchorage

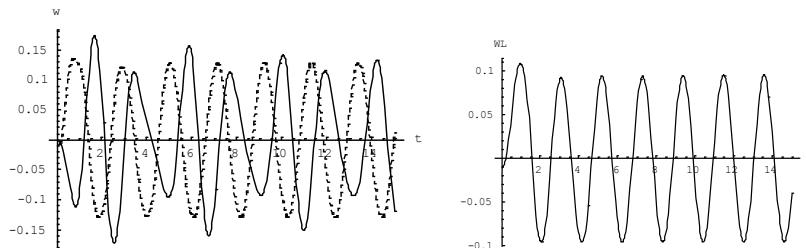


Figure 9. Cables  $L=150\text{m}$ , with dampers  $k_d=3000$ ,  $c_d=9000$   
 — without movable anchorage, - - with movable anchorage

## 7 CONCLUSIONS

1. A mathematical model is proposed, based on the use of the real shape functions of the cable.
2. From the studied data, we ascertain that we must, each time, to search the effective combination of spring and damper.
3. Even for the case of an external excitation with frequency near of an eigenfrequency of the cable, the damping system decreases the amplitude of the oscillations.

## REFERENCES

- [1] Hikami, Y., Shiraishi, N., "Rain-wind-induced vibrations of cables in cable stayed bridges", Journal of Wind Engineering and Industrial Aerodynamics, Vol. 29, Nos. 1-3, pp. 409-418, 1988.
- [2] Wilde, K, Witkowski, W, "Simple model of rain-wind-induced vibrations of stayed cables", Journal of Wind Engineering and Industrial Aerodynamics, Vol. 91, No. 7, pp. 873-891, 2003.
- [3] Ibrahim, RA, "Nonlinear vibrations of suspended cables – Part III: Random excitation and interaction with fluid flow", Applied Mechanics Reviews, Vol. 57, No. 6, pp. 515-549, 2004.
- [4] Kollbruner C.F., Hajdin N. and Stipanac B., "Contribution to the analysis of cable-stayed Bridges", (1980), Inst. For Engineering Research Editions, Schulthess Verlag Zürich, N.48

IBSBI 2014, October 16-18, 2014, Athens, Greece

## **OPTIMUM DESIGN ANALYSIS OF CABLE SUPPORTED BRIDGES**

Domenico Bruno, Fabrizio Greco and Paolo Lonetti

University of Calabria, Dept. of Civil Engineering, Italy  
e-mail: d.bruno@unical.it, f.greco@unical.it, lonetti@unical.it

**ABSTRACT:** A design methodology to predict optimum post-tensioning forces and dimensioning of the cable system for cable supported bridges is proposed. The formulation is quite general to include several bridge schemes of cable supported bridges, such as cable-stayed, suspension, hybrid cable-stayed suspension typologies. The governing equations introduce a nonlinear constrained optimization problem, which is solved by means an iterative methodology based on the SNOPT algorithm. Results are proposed in terms of comparisons with existing formulations to validate the proposed methodology.

**KEY WORDS:** Hybrid Cable-Stayed Suspension Bridges, structural optimization, finite element, nonlinear analysis, design.

### **1 INTRODUCTION**

Cable supported bridges are employed to overcome medium or long spans because of their structural, economical and aesthetic properties and typically can assume a cable-stayed or a suspension configurations [1]. Moreover, hybrid configuration, obtained by the coexistence of pure suspension and cable-stayed systems, can be adopted leading to a combined system characterized by better structural and economical performances. The use of hybrid cable-stayed suspension bridges is quite limited in practice and it still remains in the design proposal phase. Cable supported bridge design requires to correctly identify the cable dimensioning and the post-tensioning forces of the initial configuration. Most of existing cable supported bridges are designed by using traditional techniques, based on simple design rules obtained by the designer's experience and expertise were utilized. During the last decades, many research efforts are carried out with the aim to propose proper procedures to calculate the initial configuration of the bridge [2-3]. In such context, direct methods as zero displacement methods (ZDMs) and force equilibrium methods (FQMs) represent numerical procedures whose the main objective is to evaluate the initial post tensioning cable forces under dead loading [4]. Alternatively to direct methods, structural optimization (SO) techniques was developed [5]. From the minimization of the objective function, such methods are able to

calculate the optimum set of post-tensioning forces, which achieves minimum deflections under the effect of dead loading. However, these kind of methods, especially in the cases of long span bridges, due to the presence of a large number of variables are affected by convergence problems in the solving procedure, which may lead to a local minimum of the objective function and unpractical results in the bridge definition. Furthermore, most of the structural optimization model was concerned to investigate only cable-stayed bridges. In the proposed formulation, a generalized approach based on two-step algorithm is developed, which evaluates post-tensioning cable forces in the DL configuration and optimum steel quantity involved in the cable system on the basis of LL results. It is worth noting that most of the models presented above are concerned to investigate cable-stayed and, only in rare cases, hybrid cable-stayed suspension bridges; in particular, none of those is involved in the description of hybrid cable-stayed suspension bridges. Therefore, in the present study, an hybrid model based on two different steps is proposed in which the analysis is developed on the basis of the results obtained by dead and live load configurations.

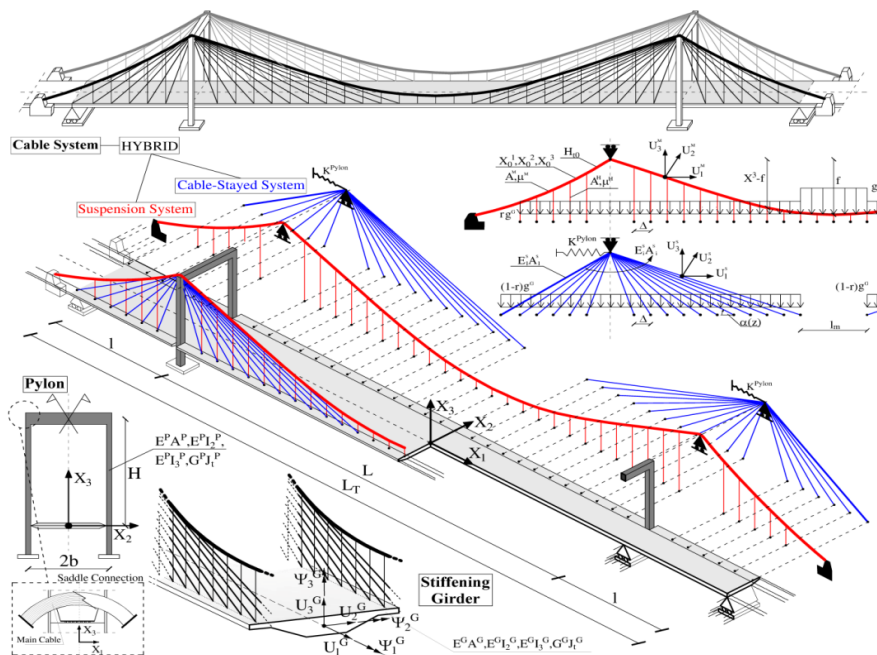


Figure 1. Structural scheme of the hybrid cable-stayed suspension (HCS) bridge

## 2 FORMULATION OF THE DESIGN METHOD

The bridge scheme, reported in Fig.1, is consistent with an hybrid cable-stayed suspension bridge typology, in which suspension and cable-stayed systems are

based on earth and self-anchored schemes. The main aim of the proposed model is to evaluate optimum set of post-tensioning forces and cable cross-sections to satisfy structural and design requirements in either dead and live configurations. In particular, under the action of dead loads (DL), the post-tensioning forces of the cables are calculated in such a way that the bridge should have reduced displacements of the girder and pylons (STEP1). Moreover, the cross-sections of the cable system elements should be designed in such a way that under the worst live load LL combinations, the maximum absolute or incremental applied stresses is equal to the corresponding allowable strength values (STEP2). In the proposed formulation, such task is developed by means of an iterative procedure defined by a two-step algorithm, based on the results arising from both DL and LL configurations. The design variables are represented by the cross-sections  $(A_i^S, A_i^H, A^M)$  and the post-tensioning forces of the cable system  $(S_i^S, S_i^H, S^M)$ , which are designed by means of the following relationships:

$$\underline{S}_C = \{S_1^S, \dots, S_{2N^S}^S, S_1^H, \dots, S_{N^H}^H, S^M\}, \quad \underline{A} = \{A_1^S, \dots, A_{2N^S}^S, A_1^H, \dots, A_{N^H}^H, A^M\} \quad (1)$$

where  $N^S$  is the number of stays of the left or right pylons,  $N^H$  is the number of hangers and the superscripts  $S$ ,  $H$  and  $M$  refer to the stays, hangers and main cable, respectively. The unknown quantities, reported in Eq.(1), are derived in the DL configuration by solving a set of constraint equations, which enforce the bridge to remain in the undeformed configuration. The constraint operators are defined through the following hypotheses, namely H.1 and H.2:

- the displacements of girder and pylons must be zero, under the action of dead loads (H.1);
- the internal stresses of the  $i$ -th stay,  $j$ -th hanger (with  $i=1..N^S$  and  $j=1..N^H$ ) and main cable should be equal to the corresponding initial design values, which are identified as  $S_{gi}^S$ ,  $S_{gj}^H$  and  $S_g^M$  are determined on the basis of the results obtained in the subsequent steps, i.e. STEP2, based on the live load analysis (H.2).

The constraint equations, which enforce hypothesis H.1, are expressed in terms of the incremental values of the internal cable tensions, i.e.  $\Delta S_i$ , measured from the converged ones obtained from the previous step, i.e.  $\bar{S}_{i-1}$  or in the case of the first iteration by initial trial values:

$$\begin{aligned} \underline{L}_S \left[ (\bar{S}_1^S + \Delta S_1^S, \dots, \bar{S}_{2N^S}^S + \Delta S_{2N^S}^S), \underline{U}^S \right] &= 0 \\ \underline{L}_H \left[ (\bar{S}_1^H + \Delta S_1^H, \dots, \bar{S}_{N^H}^H + \Delta S_{N^H}^H), \underline{U}^H \right] &= 0, \\ \underline{L}_M \left[ (\bar{S}^M + \Delta S^M), \underline{U}^M \right] &= 0 \end{aligned} \quad (2)$$

where  $\underline{L}_S$ ,  $\underline{L}_H$  and  $\underline{L}_M$  are multifreedom constraint operators referred to the stays, hangers and main cable variables, respectively, whereas

$\underline{U}^{S(T)} = [U_1^S, U_2^S, \dots, U_{N^S}^S, V_{N^S+1}^S, \dots, V_{N^S}^S]$ ,  $\underline{U}^{H(T)} = [V_1^H, V_2^H, \dots, V_{N^H}^H]$  are vectors which element are horizontal displacements of the pylons and vertical displacements of stays and hangers at the girder connections,  $U^M$  is the vertical displacement of the main cable at the midspan cross section. Similarly, additional equations are introduced to verify prescription provided by hypotheses H.2. In particular, the cross-sections of the stays, hangers and main cable elements are changed from their previous estimated values, introducing additive incremental variables as a function of explicit constraint equations, which enforce the stresses in the cables to be equal to the design quantity:

$$\begin{aligned} C_S \left[ (\bar{A}_i^S + \Delta A_i^S), S_i^S - S_{gi}^S \right] &= 0, & i = 1, \dots, 2N^S, \\ C_H \left[ (\bar{A}_i^H + \Delta A_i^H), S_i^H - S_{gi}^H \right] &= 0, & j = 1, \dots, N^H, \\ C_M \left[ (\bar{A}^M + \Delta A^M), S^M - S_g^M \right] &= 0, \end{aligned} \quad (3)$$

where  $C_S, C_H$  and  $C_M$  are the constrain operators, which ensures that the stress variables of the cable elements, i.e.  $(S_i^S, S_j^H$  and  $S^M)$ , are equal to the prescribed values  $(S_{gi}^S, S_{gi}^H$  and  $S_g^M)$ . In this framework, the analysis is developed with the purpose to verify the bridge behavior under live loads taking into account ultimate, fatigue and serviceability limit states, i.e. ULS, FLS and SLS. In particular, the following conditions, concerning maximum and relative stresses and maximum absolute displacements should be verified:

$$\max [S_i^{S,H,M}]_{ULS} \leq S_A, \quad \max [\Delta S_i^{S,H,M}]_{FLS} \leq \Delta S_A \quad (4)$$

$$\max [U_3^G]_{SLS} \leq \delta_A^G, \quad \max [U_1^P]_{SLS} \leq \delta_A^P \quad (5)$$

where  $S_A$  and  $\Delta S_A$  are the maximum or incremental allowable stress values of the cables,  $\delta_A^G$  and  $\delta_A^P$  are the maximum allowable displacements of the girder (vertical) and pylons (horizontal), respectively. The initial stresses of the cable elements  $(S_g^S, S_g^H, S_g^M)$  are evaluated as a function of two sets of factors defined for each cable element, namely  $\Phi_i$  and  $\Omega_i$ , which are introduced to verify code prescriptions reported in Eq.s (4)-(5) and designed in such a way to modify, on the basis of the LL results, the stiffness of the cable system. According to a secant approach, at the generic iteration step, the initial stresses are defined from the previously converged value by the following relationships:

$$(S_{gi}^S)^k = [\Phi^S \Omega^S]_i^k (S_g^S)^{k-1}, \quad (S_{gi}^H)^k = [\Phi^H \Omega^H]_i^k (S_g^H)^{k-1}, \quad (S_g^M)^k = [\Phi^M \Omega^M]_i^k (S_g^M)^{k-1} \quad (6)$$

where the superscript  $k$  or  $k-1$  refer to the current or the previous iteration step and the subscript  $i$  refers to the generic  $i$ -th cable element. In particular, the

factors  $\Phi_i$  concerning the stresses for the  $i$ -th stay, hanger or the main cable are derived by the ratios between the allowable stress and the maximum value observed in the LL combinations:

$$(\Phi^S)_i^k = \frac{S_A}{\max_{LL} (S_{LL}^S)_i^k}, \quad (\Phi^H)_i^k = \frac{S_A}{\max_{LL} (S_{LL}^H)_i^k}, \quad (\Phi^M)_i^k = \frac{S_A}{\max_{LL} (S_{LL}^M)_i^k}, \quad (7)$$

where  $S_{LL}$  is the value of the stress observed during the LL combinations. Moreover, the definition of the factors  $\Omega_i$  is strictly connected to the following limit functions, which indicate the distance from the limit allowable values of the current displacement and stress quantities:

$$g_{U_{1i}^k}^P = \frac{\delta_{1A}^P}{\max(|U_{1LL}^P|)_i^k} - 1, \quad g_{U_{3i}^k}^G = \frac{\delta_{3A}^G}{\max(|U_{3LL}^G|)_i^k} - 1, \quad g_{S_{Ai}^k} = \frac{(S_A)_i^{k-1}}{S_A} - 1, \quad j = S, H, M \quad (8)$$

The definition of the  $\Omega_i$  for a generic element is based on the following piecewise functions:

$$(\Omega)_i^k = \begin{cases} \frac{|\Delta_{\max}|}{\max_{LL} [ (|\Delta|)_i^k ]} \frac{(S_A)_i^{k-1}}{S_A} & \text{if } g_{\Delta} \leq 0 \\ \frac{|\Delta_{\max}|}{\max_{LL} [ (|\Delta|)_i^k ]} \frac{(S_A)_i^{k-1}}{S_A} & \text{if } g_{S_{Ai}^k} < 0 \text{ and } g_{\Delta} > 0 \\ 1 & \text{if } g_{S_{Ai}^k} \geq 0 \text{ and } g_{\Delta} > 0 \end{cases} \quad (9)$$

Where  $\Delta_{\max}$  and  $\Delta$  are the allowable and maximum LL displacements, respectively, and  $g_{\Delta}$  the displacement limit function. It is worth noting that Eq.(9).1 is essentially utilized when the displacements are larger than the allowable quantity and thus an increment of stiffness is required; when  $g_{\Delta} > 0$  and  $g_{S_{Ai}^k} < 0$ , namely in the case of Eq.(9).2, prescriptions on displacements are satisfied and thus the current allowable stress level of cable can be increased to enforce the equality with strength value ( $S_A$ ). The design analysis defined by the previous steps is based on an iterative procedure, in which the initial stresses of the cable elements, namely  $(S_g^S, S_g^H, S_g^C)$ , are modified during the iterations.

### 3 NUMERICAL IMPLEMENTATION

The numerical algorithm was implemented by using an external subroutine, which interacts with the three-dimensional FE modeling created in Comsol Multiphysics (Comsol, 2012) [6] to calculate the optimum configuration. The

subroutine utilized to calculate the optimum solution, is based on the following different steps, which are executed iteratively:

- STEP 1: generation of the finite element model, evaluation of the initial post-tensioning forces and the cable cross-sections in the cable system by means of the optimization procedure;
- STEP 2: calculation of the maximum stresses and displacements under live loads and prediction of the new set of the initial stress quantities on the basis of the performance factors.

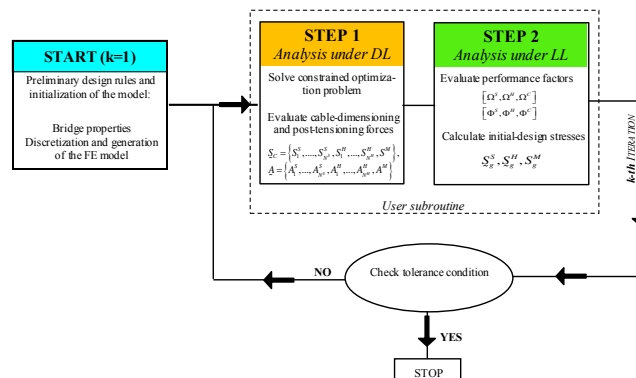


Figure 2. Flowchart of the optimization procedure

The evaluation of the post-tensioning forces and the optimum cable cross-sections is developed by solving the governing equations concerning equilibrium (EQ) and constrain equations, (CE) defined according to Eqs.(2)-(3). Once the configuration under dead loads is evaluated, the analysis is developed to determine maximum effects on the bridge components produced by the live loads in terms of stresses and displacements. Such procedure can be handled by using an external subroutine whose flowchart is reported synoptically in Fig.2.

#### 4 RESULTS AND CONCLUSIONS

Comparisons with existing optimization techniques on cable-stayed bridges are performed to validate the proposed modeling. The structural scheme, reported in [5] refers to a geometry similar to that of the Quincy Bayview Bridge, located in Illinois (USA). More details concerning the data can be recovered in [7]. At first, results in terms of distribution of optimized cable cross-sections are presented in Fig.3-a, in which comparisons between the data predicted by proposed model and those obtained in [5] are analyzed. Moreover, in the same figure, the evolution of the total steel quantity as a function of the percentage number of iterations is also reported. The analyses show that the distribution of cable cross-sections determined by the proposed formulation is always below the cross-section values obtained in [5]. Furthermore, the proposed formulation



appears to be quite stable in reaching the optimum configuration. Additional analyses, reported in Fig.3-b, are developed with the purpose to investigate the stress distribution observed in the cable system produced by the application of LL. The envelope of maximum internal stresses for each element of the cable system is reported as function of the position of the cable along girder profile. Finally, in Fig.4a-b, comparisons with results developed in [5] are proposed in terms of envelope of vertical and horizontal displacements of girder and pylons, respectively. The analyses show how prescriptions on maximum deflections for both girder and pylons are below the permissible values.

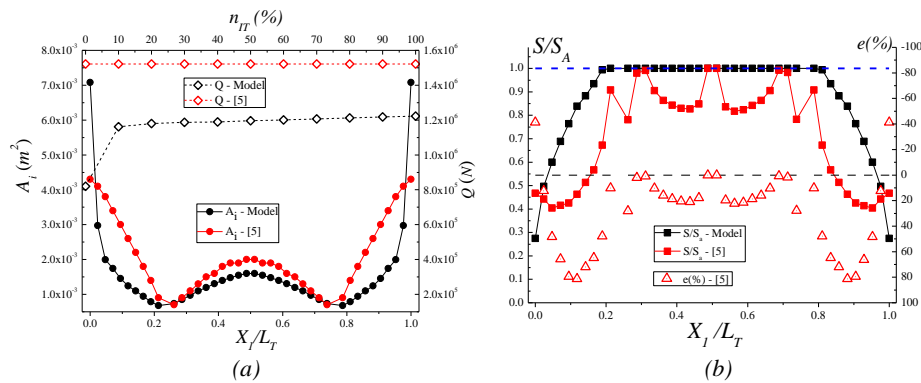


Figure 3. (a) Comparisons in terms of cross-section distribution of the cables ( $A_i$ ), total steel quantity ( $Q$ ) as a function of the number of iterations with results obtained in [5]; (b) Comparisons in terms of maximum stresses produced by live loads and percentage error ( $e$ ) with the value determined in [5]

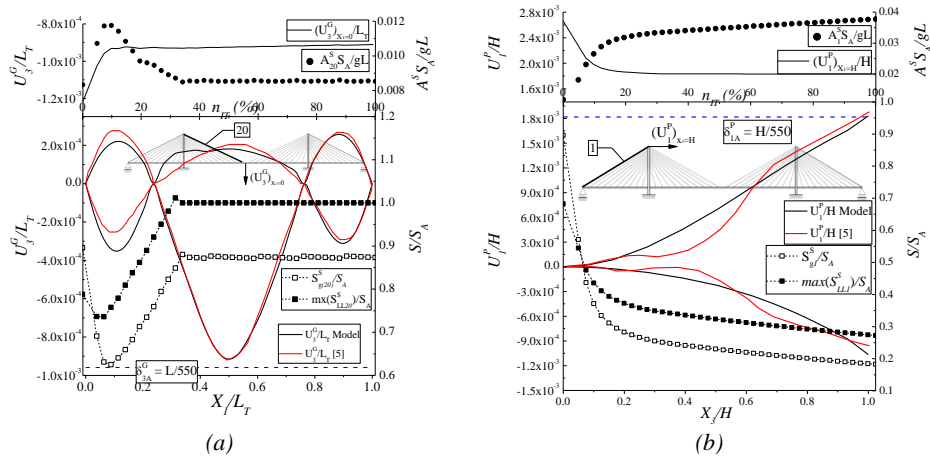


Figure 4. Comparisons in terms of girder displacements (a) and top pylon displacement (b) produced by live loads with values determined in [5], convergence behavior of the cross-sections, maximum and initial post-tensioning stresses as a function of the percentage value of the iteration steps ( $n_{IT}$ ).

In order to prove the effectiveness and the applicability of the design procedure for more complex structures involving several configurations of the cable system and a large number of variables, results in the framework of HCS bridges are proposed. In particular, the analysis is extended to more complex structure based on HCS configurations whose the data utilized for the simulations are refers to a long span bridge scheme. Results concerning the variability of the cross-sections of the cable system elements and their stress ranges observed under dead and live loads are reported in Fig.5a. Moreover, results concerning bridge deformability Fig.5b denote that from the initial configuration, girder displacements and maximum stresses in the cable system present a convergent behavior toward the final solution.

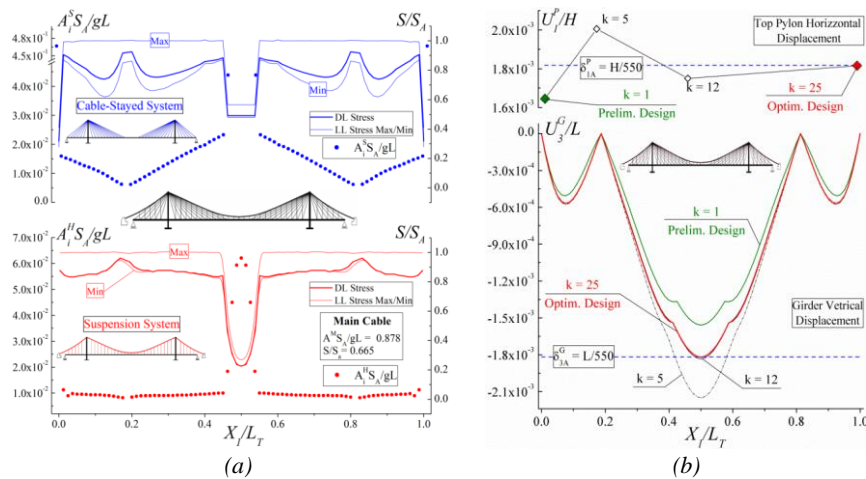


Figure 5. (a) Distribution of the cable cross-sections and envelope of the stresses in the cable-system for the stays, hangers and main cable; (b) Convergence behavior of the girder and pylon displacements in the cable systems as a function of the iteration steps.

## REFERENCES

- [1] Gimsing NJ, Georgakis CT. Cable Supported Bridges Concept and Design. 3rd Ed. New York: John Wiley & Sons, Ltd, 2012.
- [2] Bruno D, Greco F., Lonetti P. A parametric study on the dynamic behaviour of combined cable-stayed and suspension bridges under moving loads. International Journal for Computational Methods in Engineering Science & Mechanics 2009; 10: 243-258.
- [3] Konstantakopoulos TG, Michaltsos GT. A Mathematical Model for a Combined Cable System of Bridges. Engineering Structures 2010; 32: 2717–2728.
- [4] Wang PH, Tseng TC, Yang CG. Initial Shape of Cable-Stayed Bridges. Computers and Structure 1993; 46:1095–1106.
- [5] Hassan MM. Optimization of Stay Cables in Cable-Stayed Bridges using Finite Element Genetic Algorithm and B-spline Combined Technique, Engineering Structures 2013; 49:643–654.
- [6] Comsol (2012). Reference Manual. Stockholm: Comsol
- [7] Lonetti P, Pascuzzo A., Optimum design analysis of hybrid cable-stayed suspension bridges, Advances in Engineering Software, 73, 53-66, 2014

## **A MATHEMATICAL RESEARCH ON CABLES WITH FIXED OR MOVABLE ANCHORAGES**

Theodore G. Konstantakopoulos<sup>1</sup> and George T. Michaltsos<sup>2</sup>

<sup>1,2</sup> National Technical University of Athens, Dept. of Civil Engineering, Greece  
e-mail: theokons@teemail.gr, michalts@central.ntua.gr

**ABSTRACT:** For the analytical study of cables, finite series of sinusoidal form are usually employed. This paper aims to determine the eigenfrequencies and shape functions of cables with various end conditions, so that application of the modal superposition method will be more accurate.

**KEY WORDS:** Stay-cables, Shape functions, Eigenfrequencies

### **1 INTRODUCTION**

A significant problem which arises from the praxis is the cables' rain-wind induced vibrations. Large amplitude Rain-Wind-Induced-Vibrations (RWIV) of stay cables are a challenging problem in the design of cable-stayed bridges. Such phenomena were first observed on the Meikonishi bridge in Nagoya, Japan [1] and also later on other such bridges, as for instance on the fully steel Erasmus bridge in Rotterdam, the Netherlands (1996) and the Second Severn Crossing, connecting England and Wales [2]. During the oscillations a water rivulet appeared on the lower surface of the cable, which was characterized by a leeward shift and vibrated in circumferential directions [1,3,4]. Several methods have been investigated in order to control the vibrations of bridge's stay cables. A widely applied method is this of external dampers attached transverse to the stay-cables. Many researchers have proposed passive control of cables using viscous dampers. The last method consist in a system of movable anchorage by using a Friction Pendulum Bearing or an Elastomeric bearing to replace the conventional fixed support of stay cables. For the analytical study of the two last methods are usually used finite series of sinus form.

This paper aims to determine the eigenfrequencies and shape functions of stay-cables with end conditions like the ones of the cables showed in figure 1, in order to be more accurate the application of the modal superposition method.

### **2 BASIC ASSUMPTIONS**

- a. The studied cable has, the catenary shape elastic line, with displacements  $w_0$  and tensile forces  $T_0$  (fig.2), which is replaced by a parabola of second order.

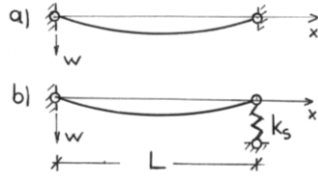


Figure 1. (a) Cable with fixed ends (b) Cable with movable end

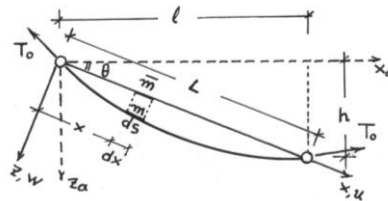


Figure 2. Cables and reference axes

- b. Under the action of the dynamic loads the cable takes the shape of figure 3, with additional displacements  $u_d, v_d, w_d$  and tensile forces  $T_d$ .
- c. The  $\bar{m}(x)$  and  $m(s)$  of figure 2, are connected through the relation

$$\bar{m}(x) = m(s) \frac{ds}{dx} \tag{1}$$

### 3 THE EQUATIONS OF MOTION

#### 3.1 Projection on xoz-plane

For a shallow form of the cable, the following relations are valid:

$$\left. \begin{aligned} \cos \rho_z = dx/ds \cong 1, \quad \sin \rho_z = dw/ds, \quad \sin d\rho_z \cong 0 \end{aligned} \right\} \tag{2.1a,b,c}$$

##### 3.1.1 Equilibrium of horizontal forces

Projecting the on xoz-plane and taking the equilibrium of horizontal forces we obtain:

$$\frac{\partial H}{\partial s} - c\dot{u} - m\ddot{u} = -p_x(x, t) \tag{3.1}$$

##### 3.1.2 Equilibrium of vertical forces

Projecting the on xoz-plane and taking the equilibrium of vertical forces we obtain:

$$-T \frac{\partial w}{\partial s} + T \frac{\partial w}{\partial s} + \partial \left( T \frac{\partial w}{\partial s} \right) + \bar{m}g ds + p_z ds - c\dot{w} ds - m\ddot{w} ds = 0 \tag{3.2a}$$

Remembering that the equation of the static equilibrium is valid, that means

$$\frac{\partial}{\partial s} (T_0 \frac{\partial w_0}{\partial s}) = -\bar{m}g, \quad \text{and that are valid: } w = w_0 + w_d \text{ and } \frac{\partial w_0(x)}{\partial t} = 0$$

equation (2.3a) becomes:

$$T_0 \frac{\partial^2 w_d}{\partial x^2} + T_d \left( \frac{\partial^2 w_0}{\partial x^2} + \frac{\partial^2 w_d}{\partial x^2} \right) - c\dot{w}_d - m\ddot{w}_d = -p_z(x, t) \tag{3.3}$$

**3.2 Projection on xoy-plane**

Projecting the on xoy-plane, taking the equilibrium of vertical forces and through a similar process like the one of §3.1.2 we obtain:

$$T_o \frac{\partial^2 v_d}{\partial x^2} + T_d \frac{\partial^2 v_d}{\partial x^2} - c\dot{v}_d - m\ddot{v}_d = -p_y(x, t) \tag{3.4}$$

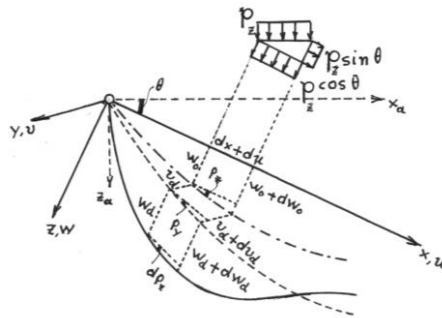


Figure 3. Deformation of the cable

**4 THE PARABOLA APPROACH**

The equation of a parabola passing from the points (0,0), (L,0) and with  $w''_0 = -\frac{\bar{m}g}{H_0}$ , is the following:

$$w_0(x) = \frac{\bar{m}g}{2H_0} x(L-x) \tag{4}$$

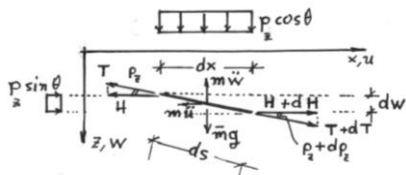


Figure 4. Projection on xoz-plane

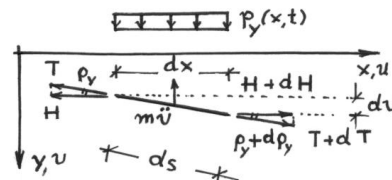


Figure 5. Projection on xoy-plane

**5 CABLES WITH FIXED ENDS**

In order to determine the eigenfrequencies and shape functions, we have to find the tensile  $T_d$ . The following relations are valid:

$$ds^2 = dx^2 + dw_0^2, \quad (ds + \Delta ds)^2 = (dx + \Delta dx)^2 + (\Delta dv)^2 + (dw_0 + \Delta dw_0)^2 \tag{5.1}$$

From this last, neglecting the higher order terms, remembering that  $\Delta dw_0 = dw_d$ ,

$$\epsilon = \frac{\sigma}{E} = \frac{T_d}{EA} \text{ and using the condition } \int_0^L \Delta dx = 0, \text{ we get:}$$

$$\frac{T_d}{EA} \int_0^L \frac{dx}{\cos^3 \rho_z} - \int_0^L \frac{dw_d}{dx} \cdot \frac{dw_o}{dx} \cdot dx = 0 \quad (5.2)$$

The above, after integration by members and with boundary conditions  $w_d(0) = w_d(L) = 0$  gives:

$$T_d = -\frac{w_o''}{L_o} \int_0^L w_d dx, \quad \text{with: } L_o = \int_0^L \frac{dx}{EA \cos^3 \rho_z} \quad (5.3a,b)$$

Therefore the equations of free motion can be written as follows:

$$\left. \begin{aligned} T_o w_d'' + T_d w_o'' &= c \dot{w}_d + m \ddot{w}_d, \quad T_o v_d'' = c \dot{v}_d + m \ddot{v}_d, \\ \text{with } T_d &= -\frac{w_o''}{L_o} \int_0^L w_d dx, \quad \text{and: } L_o = \int_0^L \frac{dx}{EA \cos^3 \rho_z} \end{aligned} \right\} (5.4a,b,c,d)$$

### 5.1 The vertical motion

Equation (5.4a) because of (5.4c) is written:

$$T_o w_d'' - c \dot{w}_d - m \ddot{w}_d - \frac{w_o''^2}{L_o} \int_0^L w_d dx = 0 \quad (5.5)$$

We are searching for a solution under the form:  $w_d(x,t) = W(x) \cdot \Phi(t)$

Therefore, equation (5.5) gives the following uncoupled equations:

$$W'' + \frac{m \omega_w^2}{T_o} W = \frac{w_o''^2}{T_o L_o} \int_0^L W dx, \quad \ddot{\Phi} + \frac{c}{m} \dot{\Phi} + \omega_w^2 \Phi = 0 \quad (5.6a,b)$$

$$\left. \begin{aligned} W(x) &= c_1 [\sin \lambda_w x + G(1 - \cos \lambda_w L)] + c_2 [\cos \lambda_w x + G \sin \lambda_w L] \\ \text{where: } G &= \frac{w_o''^2}{\lambda_w (\lambda_w^2 T_o L_o - w_o''^2 \cdot L)}, \quad \lambda_w^2 = \frac{m \omega_w^2}{T_o} \end{aligned} \right\} (5.7a,b)$$

The boundary conditions are:  $W(0) = W(L) = 0$

Introducing equation (5.8a) into the above conditions we get:

$$\left. \begin{aligned} G(1 - \cos \lambda_w L) \cdot c_1 + (1 + G \sin \lambda_w L) \cdot c_2 &= 0 \\ [\sin \lambda_w L + G(1 - \cos \lambda_w L)] \cdot c_1 + [\cos \lambda_w L + G \sin \lambda_w L] \cdot c_2 &= 0 \end{aligned} \right\} (5.8a,b)$$

From this eigenvalue problem we get the following eigenfrequencies equation:

$$2G \cos \lambda_w L - \sin \lambda_w L - 2G = 0 \quad (5.9)$$

Finally, from eqs. (5.5), (5.9) and (5.7), one can determine the following form of the shape functions:

$$W_n(x) = c_1 \cdot \left[ \sin \lambda_{wn} x - \frac{G_n(1 - \cos \lambda_{wn} L)}{1 + G_n \sin \lambda_{wn} L} \cdot \cos \lambda_{wn} x + \frac{G_n(1 - \cos \lambda_{wn} L)}{1 + G_n \sin \lambda_{wn} L} \right] \quad (5.10)$$

## 5.2 The lateral motion

Following the previous procedure, we conclude to the following expressions:

$$V_n(x) = d_1 \sin \frac{n\pi x}{L}, \quad \text{and:} \quad \omega_{\text{on}}^2 = \frac{n^2 \pi^2 T_0}{mL^2} \quad \left. \vphantom{\omega_{\text{on}}^2} \right\} \quad (5.11a,b)$$

## 6 CABLES WITH MOVABLE END

In order to determine the tensile  $T_d$  we are starting from equation (5.3b), from this last, after integration by members and with boundary condition  $w_d(0) = 0$  we obtain:

$$T_d = \frac{1}{L_0} \left( w'_0(L)w_d(L) - w''_0 \int_0^L w_d dx \right), \quad \text{with:} \quad L_0 = \int_0^L \frac{dx}{EA \cos^3 \rho_z} \quad \left. \vphantom{L_0} \right\} \quad (6.1a,b)$$

And thus:

$$\left. \begin{aligned} T_0 w''_d + T_d w''_0 &= c\dot{w}_d + m\ddot{w}_d, \quad T_0 v''_d = c\dot{v}_d + m\ddot{v}_d \\ T_d &= \frac{1}{L_0} \left( w'_0(L)w_d(L) - w''_0 \int_0^L w_d dx \right), \quad \text{with:} \quad L_0 = \int_0^L \frac{dx}{EA \cos^3 \rho_z} \end{aligned} \right\} \quad (6.2a,b,c)$$

### 6.1 The vertical motion

Equation (6.2a), because of (6.3c) gives:

$$T_0 w''_d - c\dot{w}_d - m\ddot{w}_d = - \frac{w''_0 \cdot w'_0(L)}{L_0} \cdot w_d(L) + \frac{w''_0{}^2}{L_0} \int_0^L w_d dx = 0 \quad (6.3)$$

The above, solved as equ.(5.5) gives:

$$\left. \begin{aligned} W(x) &= c_1(\sin \lambda_w x + G_1 \sin \lambda_w L) + c_2(\cos \lambda_w x + G_1 \cos \lambda_w L) + (G_2 + G_3) + \int_0^L W dx \\ \text{where: } G_1 &= \frac{\bar{m}g L w''_0}{2H_0 L_0 T_0 \lambda_w^2 - \bar{m}g L w''_0}, \quad G_2 = \frac{w''_0{}^2}{L_0 T_0 \lambda_w^2}, \quad G_3 = G_1 \cdot G_2 \end{aligned} \right\} \quad (6.4)$$

Following the procedure of §5.1, we finally obtain:

$$\left. \begin{aligned} W(x) &= c_1(\sin \lambda_w x + D_1) + c_2(\cos \lambda_w x + D_2) \\ \text{where: } D_1 &= G_1 \sin \lambda_w L + \frac{G_2 + G_3}{1 - (G_2 + G_3)} \left( \frac{1 - \cos \lambda_w L}{\lambda_w} + G_1 L \sin \lambda_w L \right) \\ D_2 &= G_1 \cos \lambda_w L + \frac{G_2 + G_3}{1 - (G_2 + G_3)} \left( \frac{\sin \lambda_w L}{\lambda_w} + G_1 L \cos \lambda_w L \right) \end{aligned} \right\} \quad (6.5a,b,c)$$

With boundary conditions:  $W(0)=0$ ,  $T_0W'(L)+k_sW(L)=0$  we conclude to the following eigenvalue problem:

$$\left. \begin{aligned} c_1D_1 + c_2(1+D_2) &= 0 \\ c_1[\lambda_w T_0 \cos\lambda_w L + k_s(\sin\lambda_w L + D_1)] + c_2[-\lambda_w T_0 \sin\lambda_w L + k_s(\cos\lambda_w L + D_2)] &= 0 \end{aligned} \right\}$$

which gives the eigenfrequencies equation:

$$D_2[D_1 - (1+D_2)k_s] + [D_1k_s - (1+D_2)T_0\lambda_w]\cos\lambda_w L - [(1+D_2)k_s + D_1T_0\lambda_w]\sin\lambda_w L = 0 \quad (6.6)$$

and the shape functions:

$$W_n(x) = c_1 \left[ (\sin\lambda_w x + D_1) + \frac{\lambda_w T_0 \cos\lambda_w L + k_s(\sin\lambda_w L + D_2)}{\lambda_w T_0 \sin\lambda_w L - k_s(\cos\lambda_w L + D_2)} \cdot (\cos\lambda_w x + D_2) \right] \quad (6.7)$$

## 6.2 The lateral motion

From equ.(6.2b,c), with boundary conditions  $V(0)=0$ ,  $T_0V'(L)+k_sV(L)=0$  and following the previous procedure we conclude to the following equations of eigenfrequencies and shape functions:

$$\left. \begin{aligned} T_0\lambda_v \cos\lambda_v L + k_s \sin\lambda_v L = 0, \quad V_n(x) = d_1 \sin\lambda_v x, \quad \lambda_v^2 = \frac{m\omega_v^2}{T_0} \end{aligned} \right\} \quad (6.8a,b,c)$$

## 7 NUMERICAL RESULTS AND DISCUSSION

Let us consider now a cable with the following characteristics:  
 $L=250$  m,  $m=7$  kg/m,  $T_0=300000$ dN,  $E_c=2.08 \cdot 10^{10}$  dN/m<sup>2</sup>.

### 7.1 Cables with fixed ends

Applying equ. (5.9) of §5.1, we determine the following eigenfrequencies:

$$\omega_1 = 2.8186 \quad \omega_2 = 5.2030 \quad \omega_3 = 7.8130 \quad \omega_4 = 10.4059 \quad \omega_5 = 13.0093 \quad \omega_6 = 15.6089 \text{sec}^{-1},$$

while using equation (5.11) we obtain the shape functions of figure 6.

### 7.2 Cables with movable end

#### 7.2.1 The vertical motion

According to the formula (6.6) of §6.1, and for different values of  $k_s$ , we determine the following Table 1 of the first three eigenfrequencies.

Using equation (6.7) of §6.1, and for different values of  $k_s$ , we determine the following plots of figures 7 to 9, showing the first three eigenshapes in relation to  $k_s$ .

#### 7.2.2 The lateral motion

According to the formula (6.8a) of §6.2 and for different values of  $k_s$ , we determine the following Table 2 of the first three eigenfrequencies.



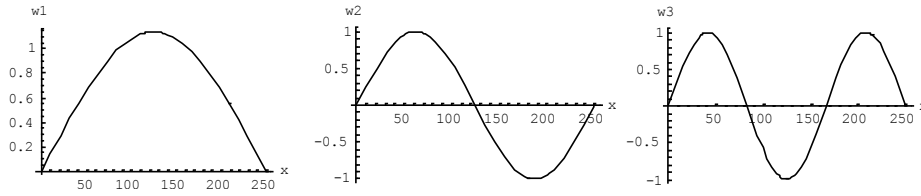


Figure 6. The first three shape functions

TABLE 1 (vertical motion)

$k_s$	$\omega_1$	$\omega_2$	$\omega_3$
5000	2.3108	4.4900	6.8850
50000	2.7104	5.1082	7.6368
100000	2.7390	5.1658	7.7257
	2.8186	5.2030	7.8130

TABLE 2 (lateral motion)

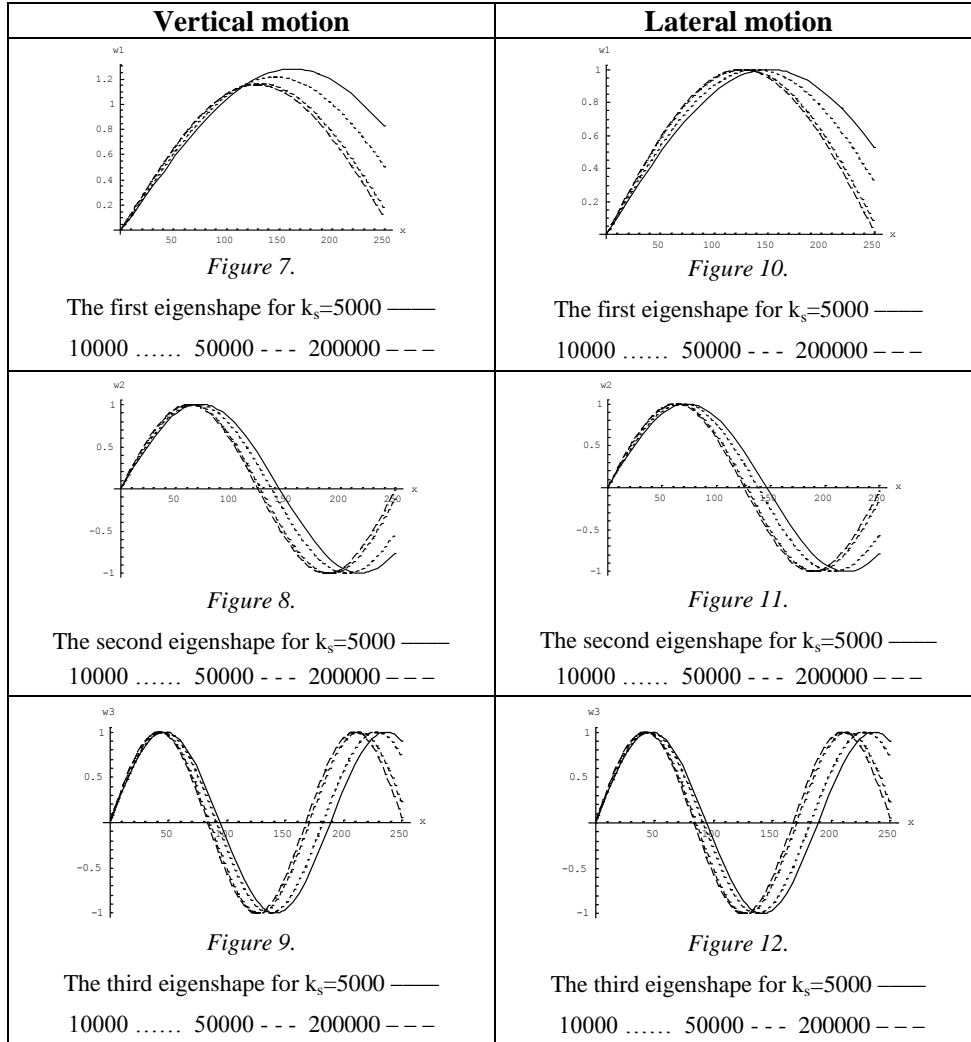
$k_s$	$\omega_1$	$\omega_2$	$\omega_3$
5000	2.1415	4.4485	6.8882
50000	2.5406	5.0819	7.6244
100000	2.5706	5.1414	7.7130
$\infty$	2.6015	5.2030	7.8045

Finally using equation (6.8b) of §6.2, and for different values of  $k_s$ , we determine the following plots of figures 10 to 12, showing the first three eigenshapes in relation to  $k_s$ .

## 8 CONCLUSIONS

On the basis of the chosen cable models, we may draw the following conclusions:

1. A mathematical model for determining and studying the eigenfrequencies and eigenshapes of a cable fixed at both ends or fixed at the one and elastically joined at the other end has been presented. Using the classic equations of a cable and determining the related equations for a cable with moving and we conclude to an integral-differential equation, which is finally solved.
2. For the vertical motion, we see that the eigenfrequencies are affected, and compared to the eigenfrequencies of the corresponding cable with fixed ends, we ascertain that the differences amount from 18% for soft springs to 2.3% for hard ones.
3. For  $k_s > 100000 \text{dN/m}$ , we observe that the cable behaves rather as a cable with fixed ends while the eigenshapes are strongly affected for soft springs and lightly for springs with  $k_s > 100000 \text{dN/m}$ .



**REFERENCES**

[1] Hikami, Y., Shiraishi, N., “Rain-wind-induced vibrations of cables in cable stayed bridges”, *Journal of Wind Engineering and Industrial Aerodynamics*, Vol. 29, Nos. 1-3, pp. 409-418, 1988.

[2] Macdonald, JHG, Dagless, EL, Thomas, BT, Taylor, CA, “Dynamic measurements of the Second Severn Crossing”, *Proceedings of the Institution of Civil Engineers – Transport*, Vol. 123, No. 4, pp. 241-248, 1997.

[3] Wilde, K, Witkowski, W, “Simple model of rain-wind-induced vibrations of stayed cables”, *Journal of Wind Engineering and Industrial Aerodynamics*, Vol. 91, No. 7, pp. 873-891, 2003.

[4] Ibrahim, RA, “Nonlinear vibrations of suspended cables – Part III: Random excitation and interaction with fluid flow”, *Applied Mechanics Reviews*, Vol. 57, No. 6, pp. 515-549, 2004.

## **TOPIC 5**

Fabrication

Construction

Experimental



## **FOUNDATION OF A LIGHTWEIGHT STEEL ROAD BRIDGE ON PEAT**

Chrysanthos Maraveas<sup>1</sup>, Konstantinos Miamis<sup>2</sup> and Konstantina Tasiouli<sup>3</sup>

<sup>1,2,3</sup>C. Maraveas Partnership, Consulting Engineers, Greece

<sup>1</sup>University of Manchester, School of Mechanical, Aerospace & Civil Engineering, UK  
e-mail: c.maraveas@maraveas.gr, steelstru@maraveas.gr, structures@maraveas.gr

**ABSTRACT:** This paper presents the foundation study of the new road bridge in the valley of “Tenagi”, Kavala, Greece. Selection of a lightweight superstructure was mandated by the region’s poor foundation conditions (peat). Soil improvement techniques, such as deep soil mixing as well as construction of vertical sand drains and preloading embankments were also proposed.

**KEY WORDS:** Peat; Sand Drains; Soil Deep Mixing; Soil Improvement; Through-Truss Steel Bridge.

### **1 INTRODUCTION**

Foundation of bridges on weak soils has always proven to be a great challenge for civil engineers, especially when the superstructure transfers heavy loads to the foundation system. In certain occasions, the geotechnical conditions determine the selection of the load-carrying system. This is the case for the new lightweight steel road bridge near Kavala, Greece, which will replace an old reinforced concrete one that is no longer in service due to failure (excessive rotation) of the foundation of the pier. Besides minimizing the weight of the bridge, techniques to improve the existing soil (peat with very poor geotechnical characteristics) were necessary to complete the foundation design.

### **2 DESCRIPTION OF THE BRIDGE**

#### **2.1 General Information**

The studied steel road bridge is located in the valley of “Tenagi”, Kavala (northern Greece) and will serve as an overpass for a 40m wide aqueduct canal. The 67m long, 4.75m wide single-span bridge is considered of vital importance for the region, as it will facilitate the crossing of agricultural vehicles and will dramatically decrease transportation times among the local farmlands.

#### **2.2 Description of the superstructure**

The poor foundation conditions, which are discussed below, mandated the selection of a lightweight structural system for the bridge. After considering

different alternatives, it was concluded that a through-truss steel bridge would be the most efficient solution. Its final configuration follows that of a Pratt truss and is shown in *Fig. 1*. More specifically, the bridge consists of two such trusses placed in the longitudinal direction. Their height varies from 2m (edges) to 5.5m (middle). In contrast to the straight bottom chord, the top chord consists of inclined straight members that follow a parabolic curve shape. The spacing of the vertical truss members is 5m, with the exception of the edges (3.5m). In the transverse direction, the trusses, which will be spaced at 3.75m to form the traffic lane corridor, are connected at the bottom chord via cross girders (at the location of the vertical members) and diagonal bracing. Top lateral bracing is only provided at the central portion of the bridge due to height restrictions. The bridge will be supported, via elastomeric bearings, on two spread footings (one on each side of the canal). The 16mm steel deck will have closed section stiffeners attached to its bottom and will be overlain by a 40mm asphalt layer.

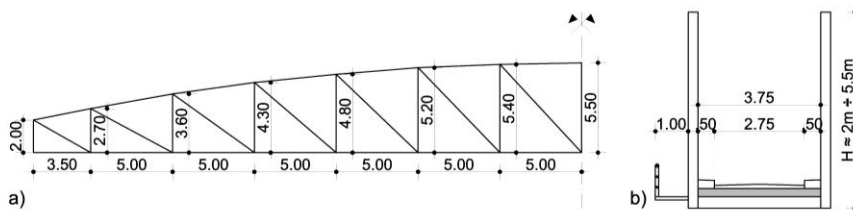


Figure 1. a) Side view of the superstructure of the bridge and b) Cross-section of the bridge

### 3 EXISTING FOUNDATION CONDITIONS

#### 3.1 Site Investigation

A thorough geotechnical investigation was conducted to determine the soil profile in the foundation region of the bridge. Two boreholes were drilled (one on each side of the canal) to a depth of 23m and Standard Penetration Tests (SPTs) were carried out every 2m. The blow count in most cases was very low, ranging from 0 to 5. Samples taken from the field were subjected to laboratory testing. Additionally, four cone-penetrometer tests (CPTs) were carried out to depths ranging approximately from 26 to 33m. In all cases the measured resistance  $q_c$  at the tip of the cone was less than 0.5MPa.

#### 3.2 Soil Profile

Based on the conducted geotechnical investigation, the soil in the foundation region of the bridge was identified as peat with poor geotechnical characteristics. The estimated characteristic values of the soil parameters, namely the unit weight  $\gamma$ , the undrained shear strength  $S_u$ , the effective cohesion  $c'$  and internal friction angle  $\phi'$  as well as the constrained elastic modulus  $E_s$ , are summarized in Table 1.

*Table 1.* Estimated geotechnical parameters for the existing soil profile

Depth	$\gamma$ (kN/m <sup>3</sup> )	$S_u$ (kPa)	$c'$ (kPa)	$\phi'$ (°)	$E_s$ (MPa)
0-10m	11	4	0.5	10	0.25
>10m	11	10	2.5	10	2.0

## 4 PROPOSED SOIL IMPROVEMENT TECHNIQUES

### 4.1 Necessity for improvement of the soil

Due to the extremely poor foundation conditions discussed in the previous section, a lightweight superstructure (through-truss steel bridge with a steel deck) was selected to minimize the loads transferred to the foundation system. Despite this, results from the preliminary foundation study showed that a shallow foundation on the existing soil was not applicable, due to low bearing capacity issues and excessive settlement, which would evolve slowly due to the low permeability of the soil. The deep foundation solution (piles) was not effective either, because the weak soil stratum extends to a great depth (more than 200m according to geological data for the region). For this reason, various techniques of soil improvement were proposed in conjunction with the shallow foundation solution. These are described below.

### 4.2 Vibratory soil replacement

The construction of vertical sand drains in the foundation region of the bridge was deemed necessary for the following reasons:

- a) Increase of the bearing capacity of the soil by increasing the effective internal friction angle  $\phi'$  and the unit weight  $\gamma$
- b) Increase of the constrained elastic modulus  $E_s$  that will result in a decrease of the expected settlement
- c) Reduction of the consolidation settlement time after application of the preloading embankment

To cover the needs of the specific project, the construction of two sand drain grids (one for each footing region) was proposed. Each grid will be constructed in two phases. Initially (1<sup>st</sup> phase), 20m long stone columns with a diameter of  $\Phi=80\text{cm}$ , will be constructed according to a triangular pattern at an axial spacing of 1.40m (*Fig. 2*). Each grid will extend to a rectangular area with dimensions (plan view) of 20.60m x 20.40m. Moreover, less compacted gravel infill will be placed at the bottom of each sand drain (forming 5m long piles with a diameter of 0.8m), to prevent possible collapse of their tip. A total of 247 stone columns will be constructed during this phase for each footing region. Afterwards (2<sup>nd</sup> phase), 475 shorter sand drains (3.5m long) of the same diameter will be constructed at the regions between the initial stone columns as shown in *Fig. 2*. The purpose of the shorter stone columns is essentially to

create a strong top layer that will further increase the bearing capacity of the soil to meet the demand from the superstructure.

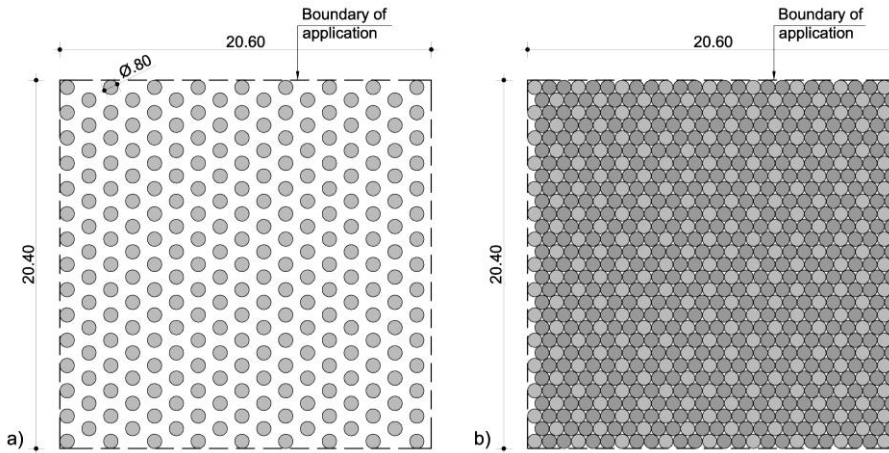


Figure 2. Arrangement of sand drains during construction of the a) 1<sup>st</sup> phase b) 2<sup>nd</sup> phase

It should be noted that the filling material for the sand drains will be well graded (with size ranging from 6mm to 38mm according to the Greek Technical Specification 1501-11-03-03-00:2009 [1]) angular gravels obtained from tough rock materials. The produced gravel infill will have a minimum effective internal friction angle  $\phi' = 40^\circ$ , unit weight of  $\gamma = 20 \text{ kN/m}^3$  and constrained elastic modulus of  $E_s = 20 \text{ MPa}$ . After the construction of the stone columns, the improved soil parameters (Table 2) were calculated as the weighted average properties of the initial soil profile (peat) and the sand drain infill material. It should be noted that the already low cohesion of peat was further reduced by the addition of gravel. Consequently, cohesion was neglected for the improved soil.

Table 2. Improved soil parameters after the construction of sand drains

Depth	$\gamma$ (kN/m <sup>3</sup> )	$c'$ (kPa)	$\phi'$ (°)	$E_s$ (MPa)
< 3.5m	19.0	0	36.5	17
3.5-20m	13.5	0	19	6.0

The construction procedure will follow the Greek Technical Specification 1501-11-03-03-00:2009 [1] pertaining to vibratory soil replacement. The “driven closed tube” method will be used because of the weak nature of the soil, which might otherwise lead to the collapse of the holes drilled for the stone columns. Following the same specification [1], a trial sand drain grid (plan dimensions of 4.3m x 4.45m) with the same stone column arrangement will be constructed in



the vicinity of the project prior to the application of this technique.

### 4.3 Soil deep mixing

Besides the construction of sand drains, the deep soil mixing technique is also necessary for the materialization of the project, as it will improve the mechanical properties of the soil and, more importantly, increase the shear strength in the regions surrounding the stone columns. This will prevent possible slope stability failures arising from the proximity of the foundation to the canal.

The soil deep mixing technique will be applied to a depth of 30m and will result in the construction of intersecting cement columns with a diameter of  $\Phi=80\text{cm}$ , spaced at a distance of 0.60m. These will be arranged symmetrically in four, 3.20m wide regions (buttresses) to surround the sand drains (*Fig. 3*).

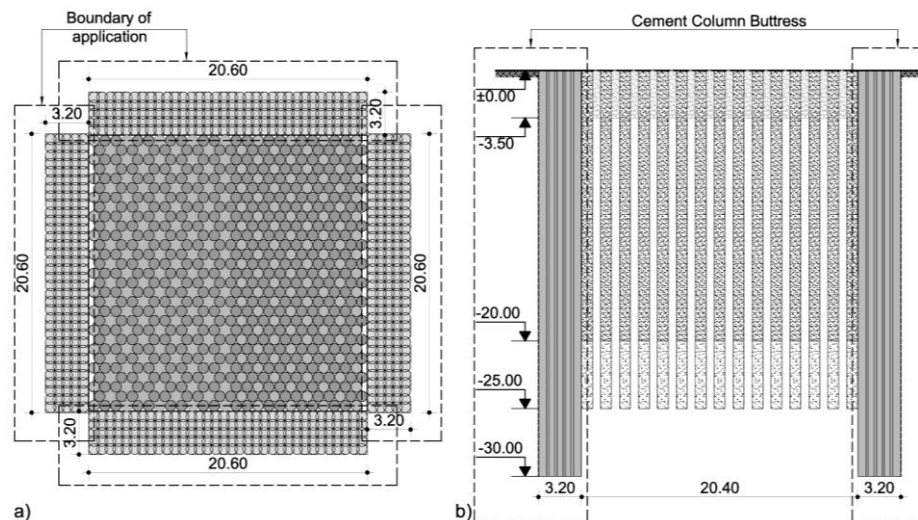


*Figure 3.* Arrangement and application of the soil deep mixing technique: a) plan view and b) vertical section

The cement columns will be constructed according to the methodology of the relevant Greek Technical Specification 1501-11-03-04-00:2009 [2], which also mandates the construction of a trial field (with plan dimensions of 3.20m x 3.20m) before applying the soil deep mixing technique. From this field, which will be constructed in close proximity to the foundation region of the bridge, samples will be taken for testing and verification of the improved strength of the soil. The type of binder was selected according to information on relevant experimental results given in the “Design Guide: Soft Soil Stabilization” [3]. Based on this, the use of cement was deemed the most appropriate for the needs of the project. Furthermore, according to recommendations from the same

source [3], the binder quantity that will result in the greatest soil strength increase is  $300\text{kg/m}^3$ . This quantity will be used to ensure the effectiveness of the soil deep mixing technique. It should also be mentioned that the resulting shear strength (according to the experimental results) for the improved soil should be at least  $150\text{kPa}$ .

#### 4.4 Preloading embankments

Despite the aforementioned soil improvement techniques, calculations showed that the expected settlement ( $\approx 7.0\text{cm}$ ) is more than that permissible for bridges according to relevant specifications [4]. Therefore, to eliminate settlement during the working life of the bridge, the construction of two preloading embankments (one for each footing of the bridge) was proposed. Each embankment will have a total height of  $2.20\text{m}$  at its top flat surface (rectangular with plan dimensions of  $10\text{m} \times 3.5\text{m}$ ) and a slope inclination of  $2/3$ . It will consist of a bottom sand layer ( $0.8\text{m}$  thick) for drainage purposes and a compacted top clay layer. The specified minimum dry unit weight for both materials is  $20\text{kN/m}^3$ . The resulting load from the embankment is greater than the serviceability loads to be imposed during the working life of the bridge and, therefore, settlement will occur only during the preloading period. The temporary embankments will be removed after a period of six months. To calculate settlement time, the existence of sand drains was taken into account following a widely recognized methodology encountered in the literature [5].

### 5 DESIGN OF THE FOOTINGS AND CALCULATIONS

The bridge will be founded on two spread footings with plan dimensions  $10\text{m} \times 3.5\text{m}$ . The foundation depth is specified at  $-2.0\text{m}$  from the ground level. The subgrade modulus is estimated at approximately  $2000\text{ kN/m}^3$ . Table 3 summarizes the safety factors pertaining to bearing, sliding and overturning calculated according to the regulations of EN 1997-1:2004 [6].

Table 3. Safety factors for the bridge footings

	Bearing	Sliding	Overturning
Safety Factor	1.40	1.85	2.25

Besides these checks, possible slope stability failures of the nearby region due to the proximity to the aqueduct canal were investigated. To this end, the specialized geotechnical engineering software LARIX-5 [7] was used. It should be noted that failure was investigated for both the preloading embankment phase as well as the operational stage of the bridge and the minimum calculated factor of safety was approximately 1.2. The critical sliding surface is depicted in Fig. 4.

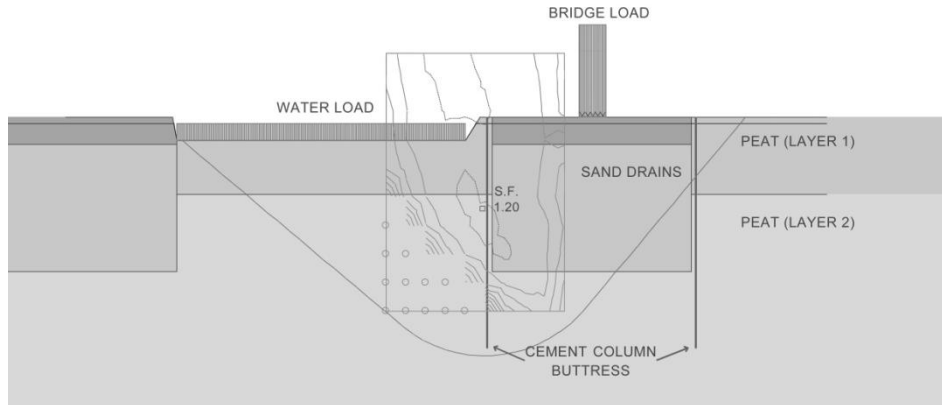


Figure 4. Critical sliding surface for slope stability failure of the foundation region

## 6 CONSTRUCTION STAGES OF THE PROJECT

The sequence of the construction stages for the project (Fig. 5) is listed below:

- a) Creation of access zones for vehicles and site works, followed by construction of the sand drains in two stages
- b) Application of the deep soil mixing technique
- c) Construction of the preloading embankments and removal after six months
- d) Excavation and construction of the spread footings

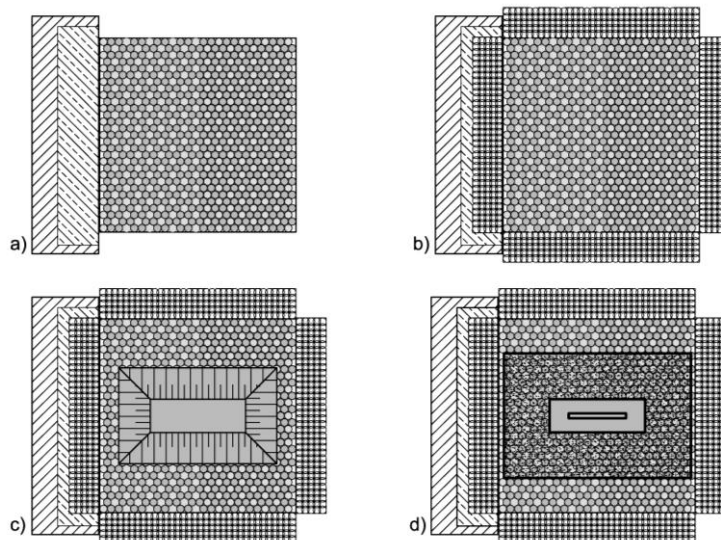


Figure 5. Sequence of the construction stages for the project: a) sand drains b) deep soil mixing c) temporary preloading embankments d) spread footings

## 7 CONCLUSIONS

This article presented the foundation study of the new bridge near Kavala, Greece. The design posed several design challenges because of the poor geotechnical conditions encountered in the region (the soil is peat with weak characteristics). For this reason, besides selecting a lightweight superstructure, several state-of-the-art soil improvement techniques were implemented. Construction of vertical sand drains placed in a triangular pattern was proposed to improve the bearing capacity of the soil, reduce consolidation settlement and accelerate its evolution. Slope stability issues arising from the proximity to the canal were resolved by deep soil mixing. Construction of two temporary preloading embankments was proposed to eliminate settlements.

## REFERENCES

- [1] Greek Organization for Standardization, "Vibratory soil replacement (stone column construction)", Hellenic Technical Specification 1501-11-03-03-00, Athens, Greece, 2009.
- [2] Greek Organization for Standardization, "Soil piles using jet grouting", Hellenic Technical Specification 1501-11-03-04-00, Athens, Greece, 2009.
- [3] BRE, *Design Guide: Soft Soil Stabilization. EuroSoilStab: Development of Design and Construction Methods to Stabilize Soft Organic Soils*, First Edition, IHS BRE Press, Watford, UK, 2010.
- [4] German Institution for Standardization, "Road and foot bridges; design loads", German National Standard DIN 1072, Berlin, Germany, 1985.
- [5] Craig, RF, *Craig's Soil Mechanics*, Seventh Edition, E&FN SPON, Chapman & Hall, London, UK, 2004.
- [6] European Committee for Standardization, "Eurocode 7: Geotechnical design - Part 1: General rules", European Standard EN 1997-1, Brussels, Belgium, 2004.
- [7] Cubus Hellas, Ltd., LARIX-5 Geotechnical Engineering Software, 2005.

## **A PROPOSAL FOR THE CONSTRUCTION OF CAST IN-SITU BRIDGES WITH TALL PIERS**

Ioannis A. Tegos<sup>1</sup>, Sevasti D. Tegou<sup>2</sup>, Ioannis Thomaidis<sup>3</sup> and  
Ioannis-Prodrornos Thomaidis<sup>4</sup>

<sup>1,2,3,4</sup> Aristotle University of Thessaloniki, Dept. of Civil Engineering, Greece  
e-mail: itegos@civil.auth.gr, stegou@civil.auth.gr

**ABSTRACT:** This study presents a new type of form traveler used for the construction of cast in-situ bridges with tall piers. Many details concerning support, cross-sections and weight of the proposed form traveler are presented. The applicability and the cost-effectiveness of the proposed construction method is examined to a real precast I-beam bridge of P.A.TH.E. Motorway in Greece. The investigation showed that the proposed method has advantages concerning not only constructability, but also serviceability performance, earthquake resistance and structural cost of the bridge.

**KEY WORDS:** Bridge; Form traveler; Steel; Prestress.

### **1 INTRODUCTION**

In conventional construction bridge deck typically consists of simply supported spans separated by expansion joints and is supported on the abutments and piers by bearings. The main disadvantage of these bridge systems concerns the installation and maintenance of the expansion joints and bearings [1]. Failed expansion joints by fatigue, leaked expansion joints and corroded bearings are representative phenomena. These problems increase the initial and long-term cost of the structure while a more extensively effort is required for the maintenance of the bridge.

On the other hand, Integral Abutment and Jointless Bridges (IAJB) has become an increasingly popular alternative to conventional bridge design in recent years. A recent survey indicates that there are over 13 000 integral abutment bridges in service in the United States [2]. Although European experience in this field is significantly less [3], the trend is towards making integral bridges a larger percentage of all newly constructed bridges.

In integral construction the superstructure and the vertical supports, piers and abutments, form a continuous, monolithic structure [4]. The increased popularity of the integral bridges is due to their advantages concerning the cost-effectiveness and durability of these structures [5][6]. Furthermore, integral

bridges are the preferred structures in more seismically regions, due to their increased capacity during seismic events.

The main parameter which determines the applicability of the cast in situ construction method is the distance between the bridge deck and the ground. The aforementioned distance must be less than 10m in order to ensure the safe removal of the formwork. As a result, the selection of the precast construction method constitutes the advisable construction method in cases of bridges with piers of height is greater than 10m.

In this study a construction process for integral bridges whose height exceed 10m is proposed. According to the proposed method, form travelers supported on bridge piers are used in the first stage of the deck construction. Many details of the proposed form traveler as far as concerns support, cross-sections and weight are presented in this study. The applicability and the cost-effectiveness of the proposed construction method is examined to a real precast I-beam bridge of P.A.T.H.E. Motorway in Greece. The proposed method has advantages concerning not only constructability, but also serviceability performance, earthquake resistance and structural cost of the bridge.

## **2 DESCRIPTION OF THE PROPOSED FORM TRAVELLER**

This study briefly presents the investigation on the use of a new type of form travelers which constitute part of the gradually constructed bridge deck. The aforementioned form travelers are used for the construction of the bridge deck at any distance from the ground.

There are two main construction methods of conventional concrete bridges which constitute a percentage greater than 99.9 % of bridge construction. Cast in-situ construction method is the first one which supposes the small distance between bridge deck and ground for the safe and economic support of the forms on the ground. The maximum allowable distance is 10m.

Precast is the indicative construction method in cases that the distance between bridge deck and ground is greater than 10m. This constitute one of the many advantages of precast construction method. However, on the other hand, the many disadvantages of the precast construction method are also known, the most important of which is the low aesthetic of the structure. The need of the use of elastomeric bearings for the support of the deck constitute also a disadvantage of the precast construction method. These members have reduced lifetime, are replaced many times during the life of the bridge and as a result, their replacement cost is of the same order with the initial construction cost. Their high construction and replacement cost constitute a big part of the total cost of the bridge per m<sup>2</sup>, which, either-way, is greater than the corresponding one of the cast in-situ concrete bridges. Precast concrete bridges, are considered non-ductile structures and as a result a behavior factor equal to one is used for the seismic design. On the other hand, cast in-situ bridges, as ductile structures

are designed for a behavior factor  $q > 1$ . Of course, the use of elastomeric bearings for the support of the bridge deck on the piers increases the fundamental period of the structure and as a result, the resultant seismic action is reduced.

According to the proposed construction method, the total bridge's length is divided into parts whose length is between 30m and 40m. Two balanced cantilevers are casted on both sides of the elevated piers. Each cantilever has a length equal to the 1/3 of the corresponding span length of the bridge. The tendons used for the prestressing of the deck are straight. Formworks supported on the ends of the cantilevers are used for the in-situ casting of the parts of the deck between the cantilevers.

In this study, two types, of form travelers are proposed, as described in the following paragraphs:

The first type consists of steel bars (hollow cross-sections and double T cross-sections) which compose with the pier of the bridge that has already been constructed, a Y-shaped member, Fig. 1. This member has the ability to carry the weight of the symmetrical constructed cantilevers of the deck whose length is about 12m. The prestressing of the aforementioned cantilevers follows the hardening of the concrete. The prestressing force is mainly determined by the magnitude of the final maximum moment action at the support due to the sum of the loadings.

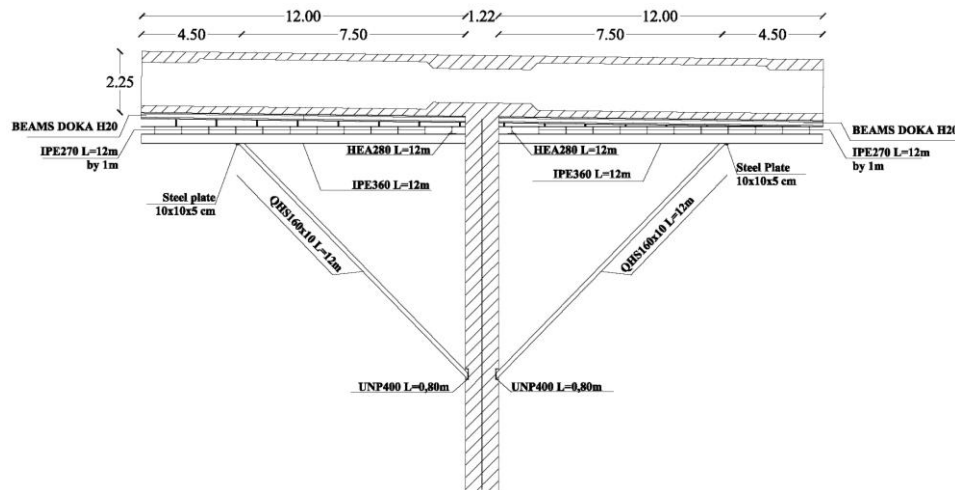


Figure 1. The first type of the form traveler consisting of steel bars which composes with the pier a Y-shaped member

After the construction and the prestressing of the bilateral cantilevers at each pier the second stage is following, which includes the following steps:

Two reticulate steel beams are hanged through high strength steel bars

(Dywidag) at the ends of the cantilevers, Fig. 2. The aforementioned beams, whose length is 12m, are used as a support for transverse steel beams of double T cross-section. The transverse steel beams are also used for the support of the form used for the casting of the bottom flange of the bridge deck between the two cantilevers.

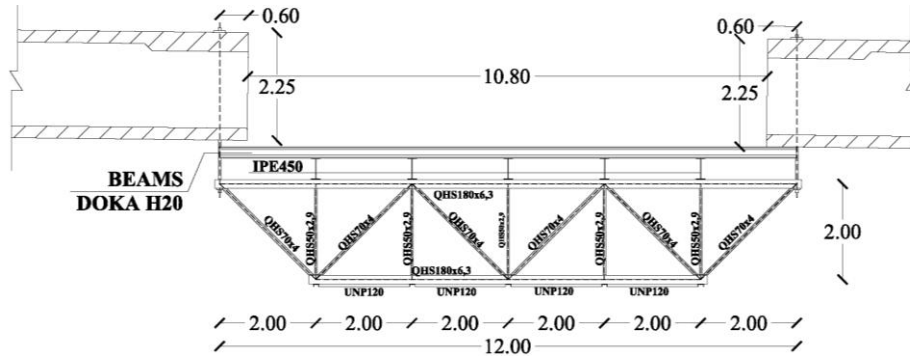


Figure 2. The second type of the form traveler consisting of a steel lattice structure

### 3 REDESIGN OF A PRECAST I-BEAM BRIDGE AS A MONOLITHIC BRIDGE SYSTEM

#### 3.1 Description of the “reference” precast I-beam bridge

A precast I-beam bridge of the P.A.T.H.E. Motorway in Greece, named T8 which is located on the right part of the Agia Marina- Raches route, Fig. 3, was used as the reference case of the investigation.

The bridge is straight in plan. The end spans are 34.75m long and the intermediate three are 36.00m long, Fig 3(a). Hence the length of the bridge which has 5 spans in total, is 177.50m. The superstructure in the transverse direction consists of six precast and prestressed I-beams, precast deck slabs and a cast in-situ part of the slab, Fig 3(b). The beams have a height of 2.00m, their distance is 2.50 m from each other and the deck slab is 300mm thick. Hence the total height of the deck is 2.30 m. The total deck width is 14.20m. The deck is supported on both abutments and piers by low damping rubber bearings. The bearings, used for supporting the deck on the abutments and the piers, have circular cross-sections with diameters of 500mm and 450mm respectively, while the total thickness of the elastomeric rubber is 110mm and 99mm accordingly. The piers, Fig. 3(c), have a hollow circular section with an external diameter of 3.0m and a web thickness of 0.5m. They are founded on 3x3 pile groups. The piles are circular with a diameter equal to 1.0m and a length of 7.0m for piers P1, P2 and P3 and of 13.0m for pier P4. The pile-caps of the foundations have dimensions 7.5x7.5m and cross-sections heights equal to 2.0m, Fig. 3(d).



According to the Greek Seismic Design Code [7], the bridge is founded on a ground type B. It should be noted that the corner periods of the spectrum used are 0.15s and 0.60s for ground type B, and this corresponds to a ground type between B and C according to Eurocode 8 [8]. The design ground acceleration is equal to 0.24g. The importance factor adopted is equal to  $\gamma_I=1.0$ , while the behavior factors are equal to 1.0 for both horizontal directions and also 1.0 for vertical seismic action.

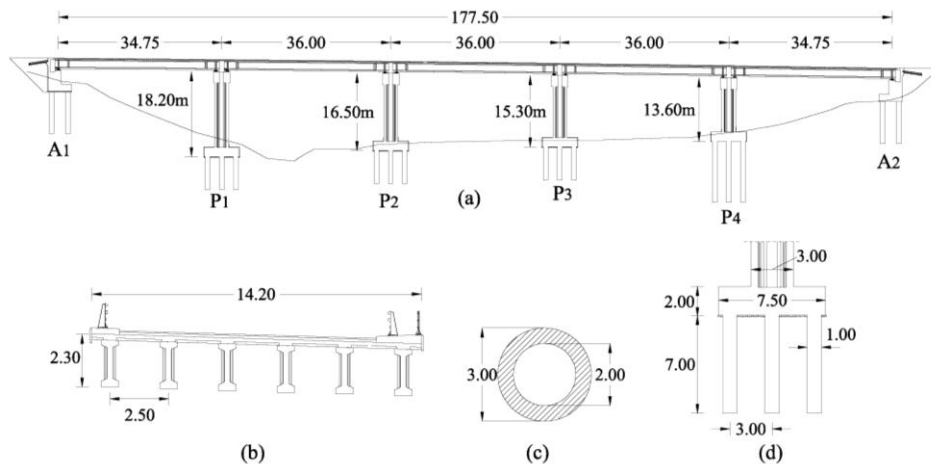


Figure 3. Longitudinal section of the “reference” precast I-beam bridge, (b) The cross-section of the deck at the mid-span and (c) The cross section of the pier and (d) longitudinal section of the deep foundation

### 3.2 Description of the monolithic bridge

The bridge described in the previous section is redesigned as a monolithic bridge system whose deck is rigidly connected to the piers while PTFE bearings are used for the support of the deck on the abutments. This bridge has the same length with the reference one. The prestressed deck has a hollow T-beam-like section, whose dimensions differs between the support and the mid-span, Fig. 4.

The rigid connection of the piers with the deck restrains the expansion and contraction of the deck due to the serviceability requirements of the bridge, which require a system as flexible as possible and that makes necessary the modification of the piers' cross-section. A reasonable solution is the selection of wall-like columns whose weak axis is longitudinally oriented. Considering that the piers' height is fixed, the selection of their width is based on the demand limitation of their in-service loading under the inevitable constraint-type movements of the deck. The in-service constraint movements are maximized at the bridge's ends and minimized at the middle of the deck. As a result, piers  $P_3$  and  $P_4$  are the ones which suffer more distress due to the in-service loading of the bridge. A parametric investigation was performed in order to optimize the

piers' thickness according to [9]. In order to increase the longitudinal stiffness of the bridge, each pier of the initial bridge system is replaced by two wall-like columns whose thickness is equal to 0.60m. Consequently, the piers of the new integral bridge system have a total thickness equal to 1.22m.

This bridge is redesigned according to the current Code's provisions [10][11]. Fig. 5 shows a detail of the high strength reinforcement (Dywidag) used for the suspension of the lattice structure while Fig. 6 shows the reinforcement detailing of the piers' cross-sections.

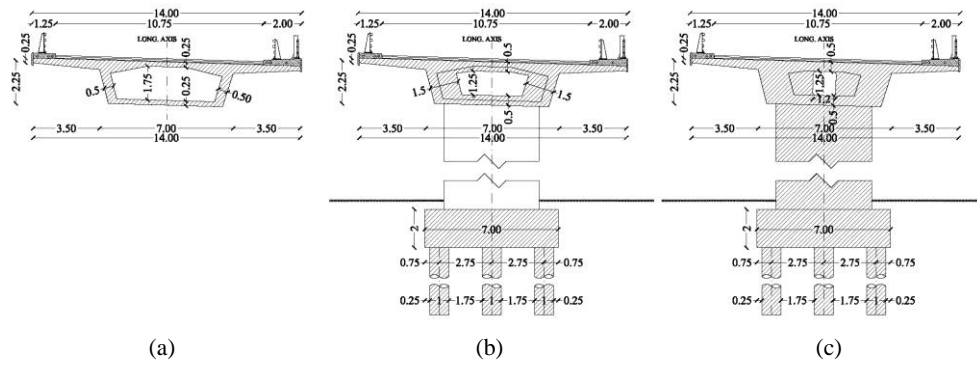


Figure 4. Cross-section of the deck of the integral bridge (a) at the mid-span, (b) near the pier and (c) at the pier

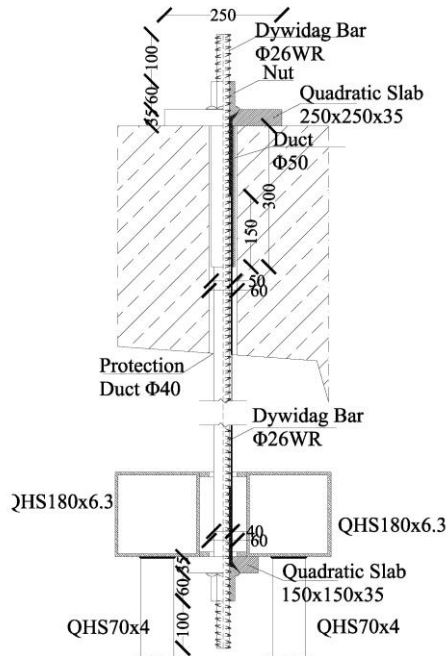


Figure 5. Detail of the high strength reinforcement Dywidag

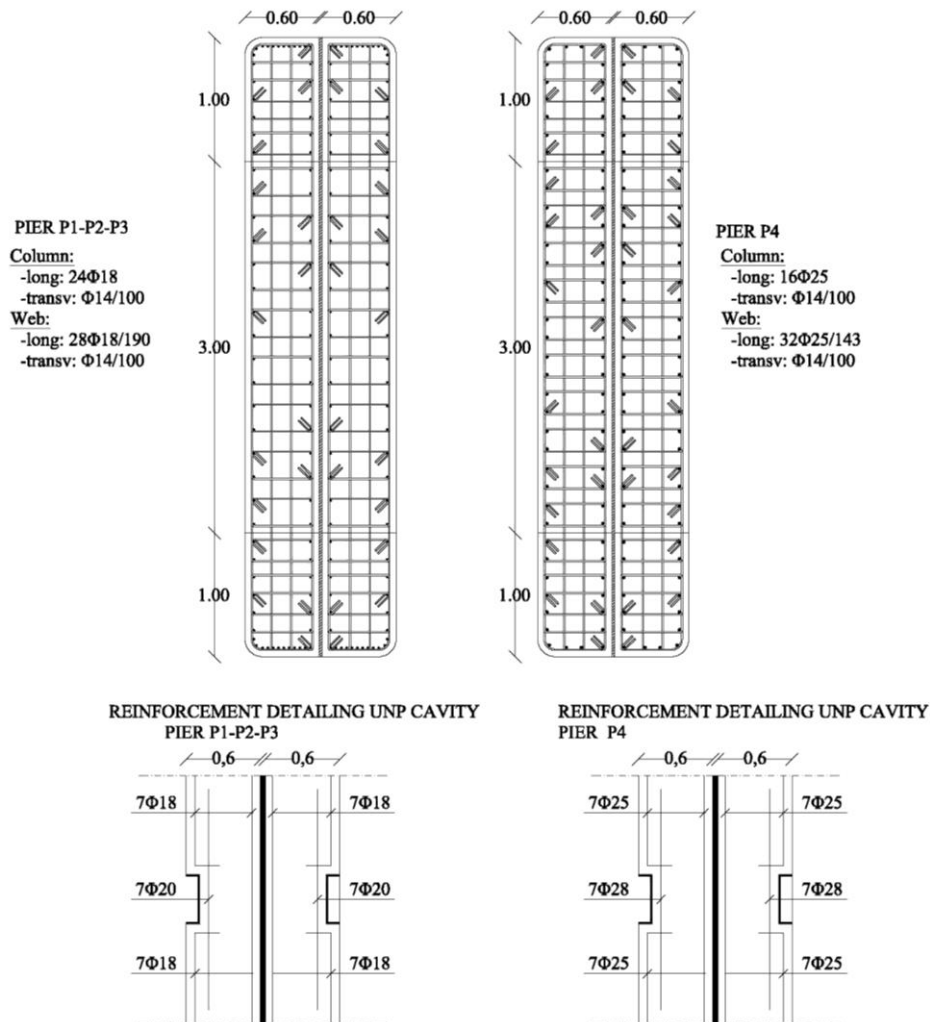


Figure 6. Reinforcement detailing of the bridge piers

#### 4 CONCLUSIONS

In this study a construction process for integral bridges whose height exceed 10m is proposed. According to the proposed method, form travelers supported on bridge piers are used at the first stage of the deck construction. Many details of the proposed form traveler as far as concerns support, cross-sections and weight are presented in this study. The main conclusions of the study are summarized at the following:

- The construction cost is low, due to the low weight of the steel members used for the construction of the proposed form travelers. The total weight of the steels used for the construction of the “Y-shaped member” is of the order

of 15 t while the corresponding weight of the steel lattice structure is 10 t.

- Considering that the maintenance cost of the monolithic bridge system is quite low, the construction cost of the form traveler is negligible in comparison to the maintenance cost of the precast bridges.
- The rest desirable properties of the structure such as safety, aesthetics and serviceability are also enhanced. Monolithic bridges have increased capacity under seismic events, while aesthetics are also improved, as both piers and deck have smaller cross-sections.

## REFERENCES

- [1] CEB-FIB, *fib bulletin 29: Precast concrete bridges State of the art report*, Task Group 6.4, Switzerland, 2004.
- [2] Maruri, RF, Petro, SH, “Integral abutments and jointless bridges (IAJB), 2004 survey summary”, in *FHWA Integral Abutment and Jointless Bridges Conference*, pp. 12 – 29, 2005.
- [3] White, H. et al. "Integral Abutment Bridges: The European Way." *Practice Periodical on Structural Design and Construction*, 15: 201, 2010.
- [4] Mistry, VC, “Integral abutment bridges”, *Conference of High Performance Steel Bridge Others*, Nov 30-Dec 1, Baltimore Maryland, 2000.
- [5] Burke, MP, *Integral and semi-integral bridges*, Wiley- Blackwell Pub., 2009.
- [6] Hassiotis, S, Roman EK, “A survey of current issues on the use of integral abutment bridges”, *Bridge Structures* 1(2): 81 – 101, 2005.
- [7] Ministry of Environment, Physical Planning and Public Works, *Greek Seismic Code—EAK 2000*, Athens, 2000 (amended 2003, in Greek).
- [8] CEN, *Eurocode 8: Design of structures for earthquake resistance, Part 1: General rules, seismic actions and rules for buildings*, 2003.
- [9] Tegou, SD, Tegos, IA, “Segmentation of piers and abutments into vertical layers with expanded polystyrene insertions”, *International Conference IBSBI 2011- Innovations on Bridges and Soil- Bridge Interaction, 13-15 October 2011*, Athens, Greece, 2011.
- [10] CEN, *Eurocode 2: Design of concrete structures-Part 1: General rules and rules for buildings*, 2004.
- [11] CEN, *Eurocode 8: Design of structures for earthquake resistance, Part 2: Bridges*, 2003.

## **REALIZATION OF NEW SAVA RIVER CROSSING IN BELGRADE (SERBIA)**

Bratislav Stipanic<sup>1</sup> and Nikola Hajdin<sup>2</sup>

<sup>1</sup> University of Belgrade, Faculty of Civil Engineering, Serbia

<sup>2</sup> Serbian Academy of Sciences and Arts, Serbia

e-mail: stipanic.bratislav@gmail.com, nikola.hajdin@sanu.ac.rs

**ABSTRACT:** The paper deals with the realization of Sava River Crossing with its approach bridges as first section of Belgrade Inner City Semi-Ring Road (ICSRR). The Sava River Crossing, as the first section of the ICSSR Project (with overall length of 17,5 km), consists of the main bridge across Sava River and so-called South Approach Roads (SAR) and North Approach Roads (NAR). The Ada Bridge carries 6 lanes of vehicular traffic, 2 rail tracks for LRT (future Belgrade metro BGM) and 2 lanes of pedestrian/cycle-way. The bridge has total length of 967 m and 43500 m<sup>2</sup> bridge deck area. SAR contains altogether 22 bridges (viaducts and ramps) with overall length of 3350 m and 36700 m<sup>2</sup> bridge deck area. NAR contains altogether 19 bridges (viaducts and ramps) with overall length of 2830 m and 36300 m<sup>2</sup> bridge deck area. The new Sava River Crossing with its approach bridges is a major infrastructure project realized in Belgrade last years that significantly effects to the reduction of traffic jams of vehicular traffic in the city. Sava River crossing with its approach bridges was completed for roadway traffic by start 2014.

**KEY WORDS:** Bridge design; Bridge construction; Roadway bridges.

### **1 INTRODUCTION**

In order to reduce traffic congestion in Belgrade city and increase the capacity of the network, it was constructed Sava River Crossing with its approach bridges. The Sava River Crossing, as the first section of the Project named Belgrade Inner City Semi-Ring Road (with overall length of 17,5 km), consists of the main bridge across Sava River (Ada Bridge) and so-called South Approach Roads (SAR) and North Approach Roads (NAR). As a part of the planned Inner City Semi-Ring Road (ICSRR), the Sava River Crossing serves for the distribution of traffic flows between diametric peripheral city zones, and operationally connected to the city highway, it shall allow diversions of highway flows to the Inner City Semi-Ring Road and vice versa. The new Sava River Crossing significantly improves the link from the “old” Belgrade City (on the right bank) to New Belgrade (on the left bank). The new Sava River

Crossing with its Approach Bridges is a major infrastructure project realized in Belgrade last years that significantly effects to the reduction of traffic jams of vehicular traffic in the city. The Sava River crossing with its approach bridges was completed for roadway traffic by start 2014. The LRT traffic will be firstly introduced by tramway, that it is planned for the next year, and later by BGM. The works according to rest NAR Lot 1 is planned for 2015. The whole Project was financed by EBRD & EIB loans and partly by the client - City of Belgrade.

## 2 PROJECT OF INNER CITY SEMI-RING ROAD (ICSRR)

The new Sava Bridge and approach roads will form the first stage of the first section of the Inner City Semi-Ring Road (ICSRR). Inside the continuously built Belgrade City area, according to General Plan of Belgrade until 2021, it is planned to form ICSRR around the wide central city zone that includes: old Belgrade centre, New Belgrade and centre of Zemun.

ICSRR, with overall length of 16 km, is divided in five sectors - from sector I to sector V (Fig. 1). ICSSR starts from west traffic artery T6, passing around the wide central city zone across Sava Bridge (in sector II/1) and 3 tunnels (in sectors II/2, IV and V), leading to Pancevo Bridge across the Danube on the north-east. The overall planned route of ICSRR contains 26 junctions – 10 on the left and 16 on the right bank of Sava River.

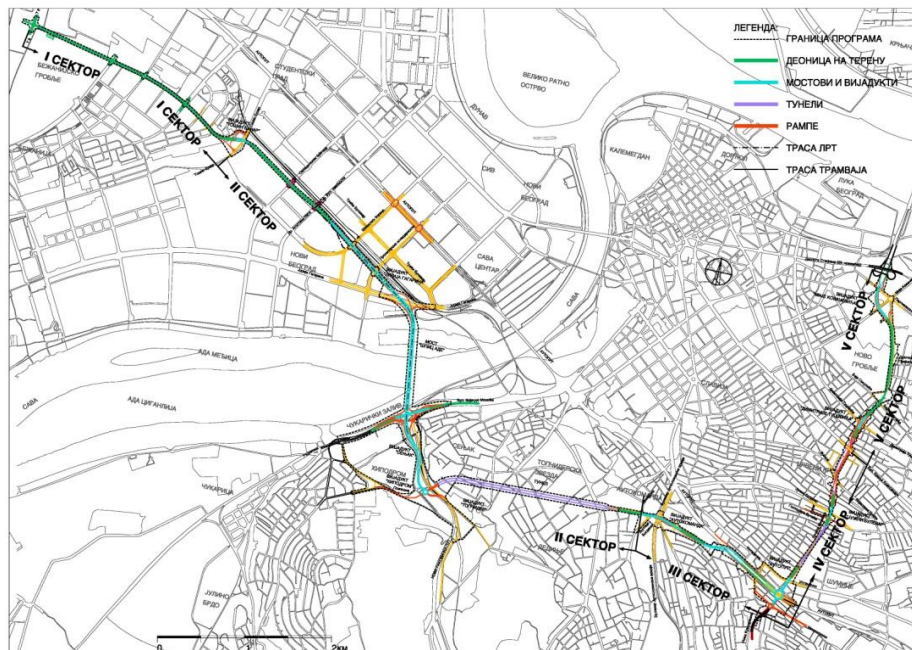
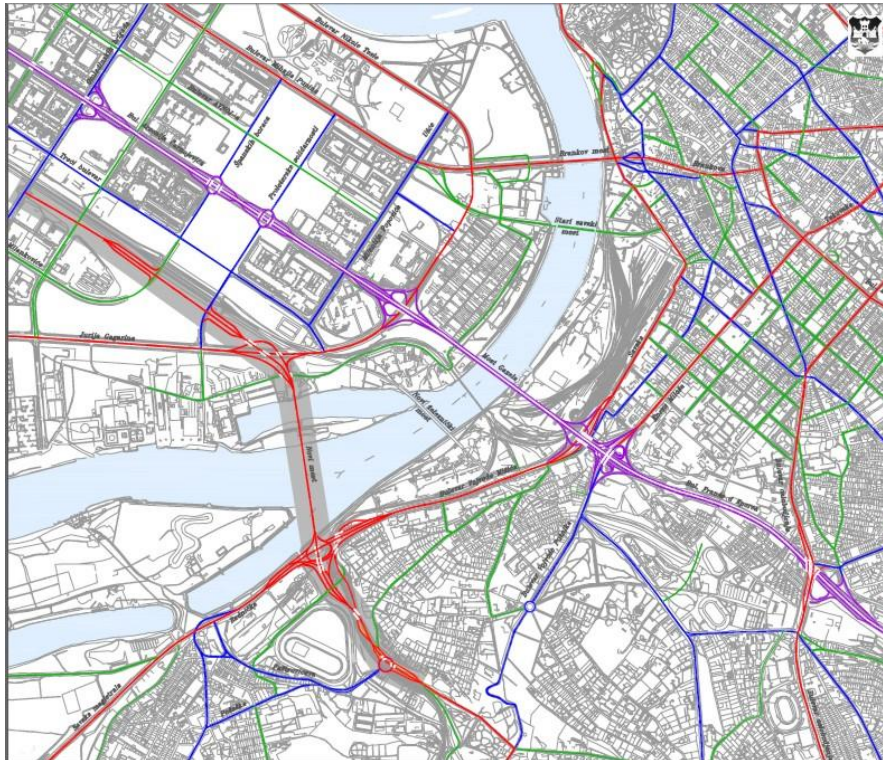


Figure 1. Project of ICSRR – Division in sectors

It is studied the transport and economic effectiveness and justification, of the construction of the first stage of ICSRR. It comprises the section defined as sector II/1 of ICSRR, which includes new Sava Bridge Crossing with both-sided approach roads (SAR & NAR). The resulted traffic flow analysis is presented in *Fig. 2*.



*Figure 2.* Traffic flow with first stage of ICSRR

Based on the detailed traffic and economic analyses, the following conclusions were established:

- 1) Without finalization of the first stage of ICSRR there would come to a complete traffic collapse on the previous city network. Therefore, the first stage of ICSRR was urgent necessity.
- 2) First stage of ICSRR discharges main city bridge around 30% and it brings large traffic savings.
- 3) The evaluation showed a positive net present value.
- 4) First stage of ICSRR, as regards traffic, can act well for about ten years. In the meantime it will be necessary to continue constructions of the next stages of ICSRR.

The first stage of ICSRR is traffic and economically justified. The next stages are necessary as well.

### 3 PROJECT REALIZATION OF SAVA BRIDGE-ADA BRIDGE

The Sava Bridge is located in wide central zone of Belgrade, passing over the lower tip of Ada Ciganlija Island – popular recreation area. Thus Sava Bridge is popularly named the Bridge on Ada (or shortly Ada Bridge). The bridge route from New Belgrade side overpasses the “winter storage” bay (130 m), left bank area (170 m), Sava River (350 m), the lower tip of Ada Ciganlija Island (50 m) and Cukarica Bay (180 m).

The design office Ponting Maribor (with DDC Ljubljana & CPV Novi Sad), as it was awarded for concept design proposal, finalized the preliminary design in 2006. The Louis Berger Group Inc. (with local partner Euro Gardi Group Novi Sad), as the awarded Project Manager – Engineer, started in 2007. The consortium POOR-SCT-DSD, as the awarded design-build Contractor, started the works by middle 2008 and the final completion of all finishing works was by middle 2012. The final design is prepared by LAP Stuttgart (with DCF Vienna engaged for foundation design). The project is co-financed mainly by the EBRD loan and partly by the City of Belgrade’s own funds. The client is the City of Belgrade - Belgrade Development Land and Public Agency.



Photo 1. Ada Bridge (by night)



Photo 2. Ada Bridge (by day)

The main bridge across Sava River over Ada Island (Ada Bridge) was constructed in the period 2008 – 2011. The Ada Bridge carries 6 lanes of



vehicular traffic, 2 rail tracks for LRT (future Belgrade metro BGM) and 2 lanes of pedestrian/cycle-way. The bridge deck has a constant depth (4,75 m). The bridge has total length of 967 m, deck width of 45m, that makes 43500 m<sup>2</sup> bridge deck area. The main bridge part is an asymmetric cable-stayed structure (steel main span of 376 m and concrete back span of 200 m), with a single concrete 200 m high pylon. The bridge deck (45 m width) as a three-cell box (14,5 m width), having an orthotropic steel deck (main span) or concrete deck (back span & side spans), with cantilever parts supported by outer steel struts.

The bridge erection consisted of: both-sided deck launchings (back span 20000 t and side spans 30000t) over temporary piers and one-sided cantilever erection of main span simultaneously with the installation of pair stays anchored in the pylon. The steel erection units (16m length, 45 m width, 330 t weight) were lifted by derrick crane from barges, after preassembling at site from steel segments delivered by ship transport from CRSBG factory (China). All assembling and preassembling splices were welded at site.

The Ada Bridge (*Photos 1 & 2*), with the direct accessing bridges – ramps, was open for vehicular & cycle/pedestrian traffic by 1<sup>st</sup> January 2012.

#### **4 PROJECT REALIZATION OF NORTH APPROACH ROADS**

The so-called Project of North approach roads (NAR-Lot2), on the left bank of Sava River, was contracted according to FIDIC red book, where the final design was enabled by the Client – City of Belgrade. The construction works were carried out mainly by the Contractor Porr (Austria), after withdraw of two non-solvent contractor firms from Slovenia (SCT and Primorje). The Engineer was Louis Berger Group with Euro Gardi Group as local partner. The construction works started in 2011, when by the end of year 3 direct access ramps to Ada Bridge were completed. The rest of NAR (Lot 2) structures were finalized in December 2013 and completely open for traffic by start 2014 (*Photo 3*).



*Photo 3.* NAR – Viaducts with ramps

NAR project (Lot2) contains:

- Two parallel roadway viaducts ICSRR, carrying 2x3 traffic lanes, having length 980m each;
- Five access ramps to ICSRR, having total length 506m;
- One double-track railway viaduct, firstly for tram traffic and later for light metro (BGM), having length 906m;
- One embankment of reinforced soil for incorporation of tram/BGM line into the existing network, including the tram/BGM station.

NAR contains 19 bridge structures, with overall length of 2830 m and 36300 m<sup>2</sup> bridge deck area.



Photo 4. NAR – Viaducts over J. Gagarina street

Both 980m long ICSRR viaducts are divided in six independent bridge structures with 3-8 spans, varying from 24,0m till 42.5m, dictated by the existing obstacles needed to be over passed (streets or non-displaceable installations). The most significant bridge structures is pair of 281m long deck over J.Gagarina street (*Photo 4*), with main span of 42,5m and variable depth of 1,6-2,6m. The all other viaduct superstructures (*Photo 5*) have a depth of 1,4 m (3-6 spans of 24-34m).

Although the construction of NAR was contracted according to FIDIC red book, i.e. with the final design enabled by the Client, the Contractor made the design modifications with reference to the point “Value engineering” of FIDIC contract conditions. Consequently, the design was modified with respect to contractor’s technology of works and the positions of piers were adopted to the exact installation locations, that made cost savings for the Client. Furthermore the modifications in design resulted in more favourable architecture look of viaducts and lower maintenance costs because the classical concrete hinges are changed by fixed link and ICSSR viaducts were constructed as semi-integral type of bridge structures (deck: slab-type with 2 girders, deep foundation on bored piles).



Photo 5. NAR – viaducts

Taking into account the site configuration, the construction works of superstructure were carried out by relatively simple scaffoldings – tube type scaffold mainly and heavy scaffold for the street flyovers. The special building challenge were foundation works in leafy underground communal installations and construction works under frequent city traffic with minimum traffic closures.

The rest works according to next Lot 1, in the frame of North approach roads, are planned for 2015.

## 5 PROJECT REALIZATION OF SOUTH APPROACH ROADS

The so-called South approach roads (SAR), on the right bank of Sava River, link the Ada Bridge with: Radnicka interchange, Hippodrome interchange and the existing tram network (*Fig. 3*).

The construction works were carried out by the Contractor Porr (Austria) according to yellow FIDIC contract conditions. The Engineer was Louis Berger Group with Euro Gardi Group as local partner. The works started in 2011, partly finished in 2012-2013 and they were finalized in autumn 2013, when SAR completely open for traffic.

The Radnicka interchange (*Photo 6*) contains:

- Two parallel roadway viaducts ICSRR, carrying 2x2 traffic lanes, having length 380 m each;
- One viaduct for 2-track LRT, firstly for tram later for light metro (BGM), having length 906m;
- The elevated ring for circle traffic flow, carrying 2 traffic lanes, having length 251m;
- Two overpasses (flyovers) in Radnicka street, carrying 2x3 traffic lanes over 5 rail tracks railways and Topcider River, having length 385m each;

- Eight access ramps to ICSRR, having total length 1012m.
- SAR contains altogether 22 bridges (viaducts and ramps) with overall length of 3350 m and 36700 m<sup>2</sup> bridge deck area.

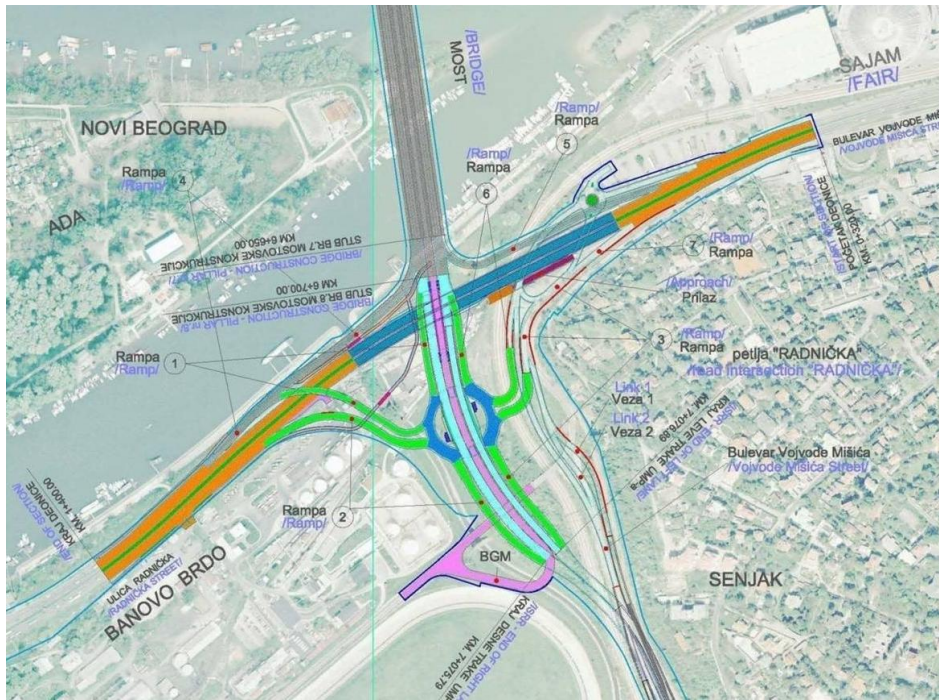


Figure 3. SAR – Plan view

Project realization of South approach roads (SAR) was more complex than NAR project, not only because of the complexity of bridge structures to be constructed but also due to the other contract conditions.

- The building works were contracted according to FIDIC yellow book – design & built contract. The preliminary – tender design was enabled by the Client.
- The building site was very limited by: Hippodrome area, Jugopetrol oil tanks complex and a distinguish Senjak residential area.
- In the building site area they were present: 4-tracks railway line, 1-track industrial railway line, 2-track tramway line and Topcider River.
- The interchange was built at the crossing place of crowded Radnicka street and 5-tracks railway line, where the existing 2-track railway overpass and roadway underpass to be changed into 2 flyovers, carrying 3 traffic lanes each, with minimal disturbance of roadway traffic flow and non-closure of railway traffic.



Photo 6. NAR – Viaducts with ramps

Both 980m long ICSRR viaducts are divided in three independent semi-integral type bridge structures with 4-5 spans (27,7 - 31.5m), with constant depth 1,6m (slab-type deck of pre-stressed concrete).

The 502m long LRT viaduct is divided in three independent semi-integral type bridge structures with 6 -7 spans (29,8 - 32,0m), with constant depth 1,6m (slab-type deck of pre-stressed concrete). The 251m elevated ring is circle continuous beam-type bridge structure over 16 spans of 15,7m each, 13,1m wide, with constant depth 1,45m. (slab-type deck of pre-stressed concrete).

The access ramps to ICSSR are semi-integral type bridge structures over 3-6 spans (28,8 – 33,5m), with constant depth 1,45m (slab-type deck of pre-stressed concrete). The most significant bridge structures is pair of about 385m long flyover along Radnicka street, with main span of about 46m, with constant depth 1,6/1,7m (slab-type deck of pre-stressed concrete).

During the execution of the works the different building technologies were applied, as well as scaffolding systems: tube scaffolds, heavy scaffolds and movable scaffolds.

The most complex building operation was the construction of pair of viaducts in Radnicka street across 5-tracks railway line, carried out to change the existing one-direction roadway overpass and underpass. Because of limited height over the railway line the special scaffolding system was applied that enabled to construct the deck in main span in several steps (*Photos 7-10*), as follows.

- Erection of special scaffold to carry the suspended formwork for deck concreting 1,5m over the designed alignment.
- Lifting of scaffold mounted on the ground, reinforcing and cable works, concreting and pre-stressing.
- Dismounting of scaffold – concrete deck structure is carried by 16 strong tendon bars anchored in concrete deck.
- Devolvement of concrete deck structure to the designed alignment.



Photo 7-10. NAR – Main construction stages of viaduct in Radnicka street

## 6 CONCLUSIONS

It should be pointed out that the whole Project of Sava River crossing with its approaches (Ada Bridge project, NAR project & SAR project), was successfully realized due to exceptional engagement of all participants: Client (City of Belgrade - Belgrade Development Land and Public Agency), Investors (EBRD, EIB & City of Belgrade), Contractor (mainly PORR Austria, DSD Germany, SCT Slovenija, with its subcontractors) and Engineer (Louis Berger Group, with local partner Euro Gardi Group).

The realization of Project significantly reduced traffic jams in the city.

IBSBI 2014, October 16-18, 2014, Athens, Greece

**EXPERIMENTAL STUDY ON A COSTLESS  
MOVEMENT RESTRAINING SYSTEM**  
**Application of struts - ties in seismically designed bridges**

Olga Markogiannaki<sup>1</sup>, Ioannis Tegos<sup>2</sup>

<sup>1,2</sup> Aristotle University of Thessaloniki, Dept. of Civil Engineering, Greece  
e-mail: omarkogiannaki@civil.auth.gr, itegos@civil.auth.gr

**ABSTRACT:** The key objective of the present paper is to present the experimental results of the mechanical response of steel bar bundles inside plastic ducts under compression. The steel bundles are part of a restraining system that has been proposed by the authors for the seismic protection of bridges against longitudinal earthquake movements.

**KEY WORDS:** Concrete Bridge, Restrainer, Experiment, Compression

## **1 INTRODUCTION**

Bridges in earthquake prone areas are designed for lateral forces induced by seismic excitations. Several design practices that enhance the seismic response of bridges have been developed. The most widely used is seismic isolation which involves devices, such as bearings (i.e. elastomeric, lead) or dampers (i.e. hydraulic, viscous), that are installed on bridges. Another common design practice is the design of bridges as ductile structures that aim on the contribution of the post-elastic behavior of the structural components of the bridge, i.e. more often the piers. Except from the contribution of piers, international seismic design codes, i.e. Eurocode [1] and researchers suggest the participation of other structural members of bridges such as the abutments that can participate in the seismic resistance of bridges. The ongoing research has shown that except the traditional seismic links that transfer forces to the abutments there are further effective systems that can activate their participation. Such examples include the design of the approach slab for the connection of bridges with the abutments [2], the design of integral abutments with transversely directed R/C walls [3] and the design of sidewalks connected with the abutments as restrainers [4]. Furthermore, steel or cables restrainers [5] can be used for limiting the longitudinal displacements between the abutments and the deck of the bridge. Recently, shape memory alloys [6] were introduced as a more effective restrainer system for bridges than steel restrainers for limiting longitudinal drifts, as well. Systems like steel cable restrainers, [7], and

seismic isolation systems are applicable for design and retrofit purposes, as well.

The authors have presented in previous research work, [8] [9], a restraining system with steel bundles that can be installed on R/C bridges and can increase the contribution of the abutments to the seismic resistance of bridges and limits longitudinal bridge movements. The key part of the behavior of the steel bundles is that they act as a struts-ties system. It is noted that the restraining system of struts-ties can be applied with some modifications, regarding its installation, in the superstructure of the bridge for the seismic retrofit of concrete bridges, as well [10]. The aim of this paper is to present the experimental results for the tests that were performed for the response of the steel bundles under compression loading. The steel bundles are placed inside ducts that prevent the transverse deformation of the steel bundles that could be developed due to buckling. The density, level of filling of the duct with steel bundles, is considered as the main parameter of the experimental investigation. The specimens tested in the experiment included duct cross sections that had variable densities, filling levels.

## 2 LONGITUDINAL STRUTS-TIES SYSTEM

### 2.1 Description of the struts-ties system

The restraining system can be described as a mechanism that reduces bridge seismic displacements through the activation of its components that act in tension and compression, (struts-ties), as well. The mechanism can be applied in different bridge classes. A schematic representation is shown in *Fig. 1*. The restraining system involves the installation of four bundles of steel bars in the cross section of the deck of the bridge.

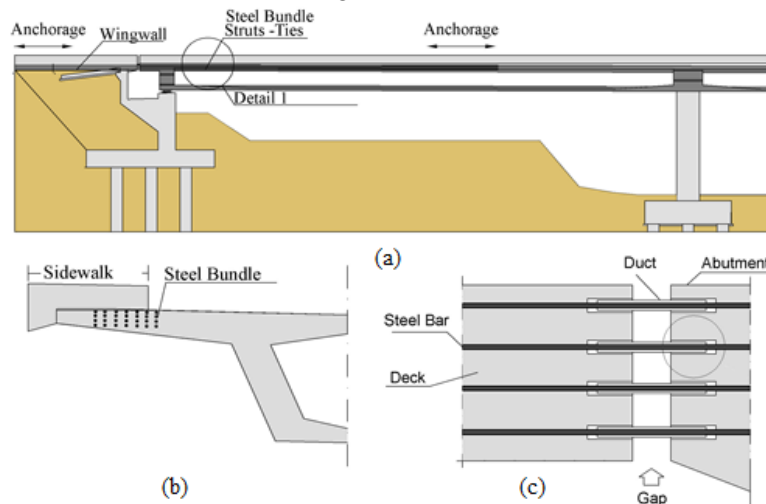


*Figure 1.* Restraining System. a. Longitudinal view of the bridge, b. Detail 1: cross section of the deck of the bridge, c. Detail at the Expansion Joint between Deck and Abutment



The bundles are installed along the longitudinal direction of the bridge and each two bundles are placed in the outer spans of the bridge extending through the abutments' wing walls. The bars are placed in ducts in order to avoid bonding between the steel bars and the concrete of the bridge. The steel bars are only bonded with the concrete at their ends to ensure sufficient anchorages. Each of the four bundles consists of groups of steel bars that are anchored at different points so that the anchorage forces are not developed in the same positions. The bundles of the steel bars are not only activated as tension members but also as members that receive compression, since the installation of the steel bars inside the deck protects them from buckling issues. The area of the outer joint is the most sensitive regarding the response of the steel bars under compression because of the gap between the decks and abutments concrete. Both mechanical responses inside the deck and at the expansion joint were investigated in the experimental procedure.

**2.2 Case study - Numerical Analysis**

A case study presentation that shows the response of a bridge with the restraining system was considered necessary. A typical six span concrete box girder bridge as demonstrated in Fig. 2 was used. The total length of the bridge is 240m and the deck is monolithically connected to the piers, while sliding bearings on the abutments support the two outer spans of the deck. The bridge components are modeled with frame elements taking into consideration material nonlinearities. The section analysis for the assignment of concentrated plasticity at the top and bottom of piers was performed with Bomber Biaxial v3.8.2,[11].. For the passive resistance of the abutments, the stiffness values from Caltrans, [12], and the procedure demonstrated by Nielson, [13], were used.

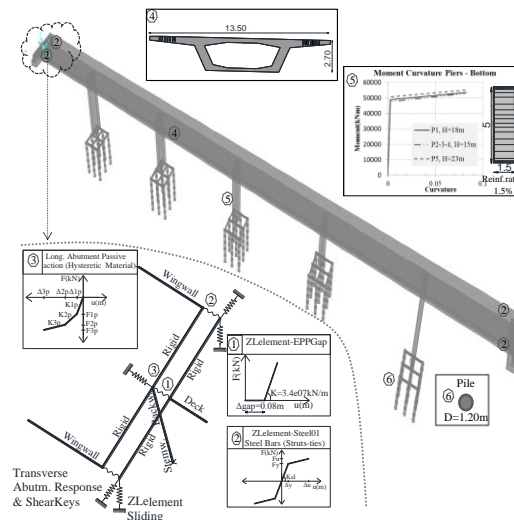


Figure 2. 3D Bridge Model

The steel bars (in 4 bundles) were modeled as nonlinear springs, as shown in Fig. 2 and Table 1 (AsBars refers to the Steel area of each of the four bundles and lbar to the length of each steel bar without accounting for the anchorage length). Time-history nonlinear dynamic analyses were carried out with 7 independent recorded events, selected with REXEL 3.5 Beta [14] and compatible, their average spectra, to Eurocode design spectra for 0.16g, 0.24g and 0.36g and for soil B. The analyses results indicate remarkable reduction in the longitudinal bridge movements for all seismic design levels especially for large steel bundle cross sections, Fig 3. The efficiency of the mechanism is reduced when the length of the steel bundles is increased. However, the length increase may be a preferable choice for achieving less stresses on the steel bars.

Table 1. Steel bundle properties /wingwall

Steel Bundle Properties			
$f_y$	AsBars x $\sigma_y$ (500MPa)	$f_u$	AsBars x $\sigma_u$ (600MPa)
$\Delta y$	$e_{sy}(0.0027) \times lbar$	$\Delta u$	$e_{su} \times lbar$
Kel	E x Area of Bars / lbar	Kinel	0.8% x Kel

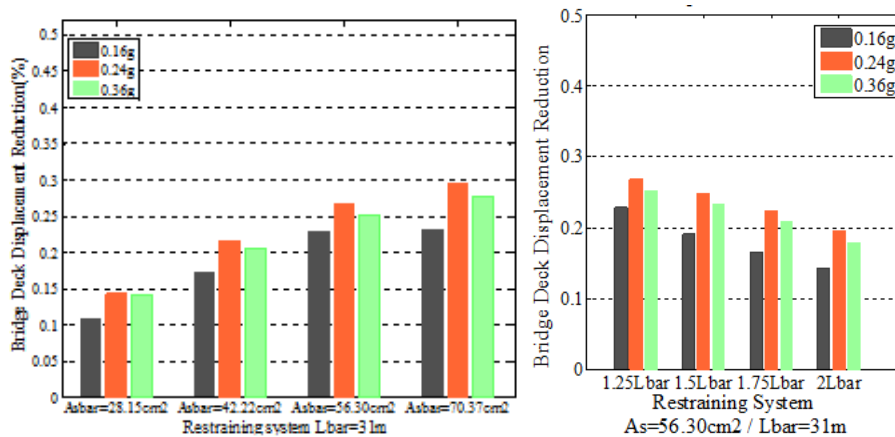


Figure 3. Longitudinal Movement Reductions

### 3 EXPERIMENTAL RESEARCH

#### 3.1 Aim of the study

The target of the experimental investigation is to study the mechanical behaviour of the steel bundles under compression loading. For this purpose several steel bundle specimens were tested. By evaluating the experimental results the aim is to indicate whether the use of the steel bundles in plastic ducts as struts; if the reception of compression loading without buckling, is feasible.

### 3.2 Parameters

The steel bundles are placed inside ducts that prevent the transverse deformation of the steel bundles that could be developed due to buckling. One main parameter is the presence of concrete around the steel bundles or not which corresponds to the position of the steel bundles inside the decks concrete or the area of the expansion joint where the steel bundles are exposed to the environment. Another significant parameter of the experimental investigation is the level of filling of the duct with steel bundles. The specimens tested in the experiment included duct cross sections that had variable filling levels.

### 3.3 Specimens

Table 2 presents the specimens used in the experimental tests and the filling level for each specimen. Common steel rebars were used for the research with a diameter of 8mm. The filling level of 76% is the highest feasible for the available diameters. The two large classes of specimens are steel bundles that are inside concrete and bare steel ducts. The ducts used were steel type, 30cm log and had 30mm inner diameter. High strength concrete (emaco) with spiral 4mm transverse reinforcement was used in order to simulate the presence of the massive deck's concrete. A square steel plate with a steel dowel welded on it was used for all specimens for accommodating the requirement for a smooth surface to transfer the compression loading to the steel bars inside the ducts uniformly. The two arrangements are shown in Fig. 4 and Photo 1.

Table 2. Specimen Properties

Concrete			No Concrete		
Name	Characteristics	Density (%)	Name	Characteristics	Density (%)
S-C-1	4D8mm	38%	S-NC-1	4D8mm	38%
S-C-2	5D8mm	47%	S-NC-2	5D8mm	47%
S-C-3	6D8mm	57%	S-NC-3	6D8mm	57%
S-C-4	7D8mm	66%	S-NC-4	7D8mm	66%
S-C-5	8D8mm	76%	S-NC-5	8D8mm	76%

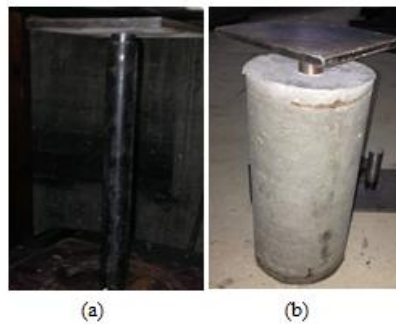
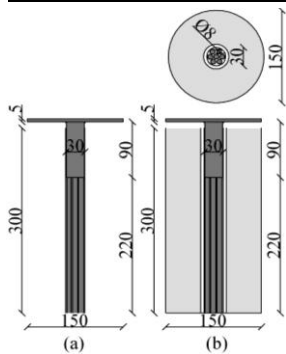


Figure 4. a) Specimen S-NC b) Specim. S-C Photo 1. a) Specimen S-NC b) Specimen S-C

### 3.4 Test Set-up and Results

To conduct the experiment, the compression machine of the Laboratory of Experimental Strength of Materials and Structures in Aristotle University of Thessaloniki was used. The specimens were centred on the table of the machine and the steel smooth plates were placed at the top of the specimens so that the loading part of the machine could rest on them. The target of the process was to induce clear compression loading to the steel bars without any bending or lateral additional forces. Fig. 5 shows the test set up for the compression of the specimens. The deformation of the specimens was measured during the experiments, as well. The machine used for these tests had a capacity of 20 tonnes in the vertical direction and only static loading could be applied.



Figure 5. Test set-up

Table 2. Specimen Properties

Specimen Name		$P_{euler}$ [kN]	$\sigma_{euler}$ [MPa]
S-C-1	S-NC-1	65.6	326.26
S-C-2	S-NC-2	82.	326.26
S-C-3	S-NC-3	98.4	326.26
S-C-4	S-NC-4	114.8	326.26
S-C-5	S-NC-5	131.2	326.26

The compression tests were performed until the failure of the steel bars. The force-displacement and stress-strain curves are shown in Fig. 6 and 7 respectively. It is noted that as presented in Table 2, the critical stress due to Euler buckling is predicted to be lower than the yielding stress value. Therefore, in the cases where buckling occurs, it precedes yielding. Characteristic examples of such failures are specimens S-NC-1 and S-NC-2. From the experimental results, it can be concluded that the sparse (<50%) application of steel bars in a duct has negative effects on their response under compression loading. In the case of high densities the performance is gradually improved and is similar to that of a tension loading behavior. Especially, in the case of the

highest filling level the walls of the steel duct were engaged in the response of the steel bundle resulting in higher forces than the failure of the steel bars but at the same time in the early damage of the steel duct that is not a preferable response for the system.

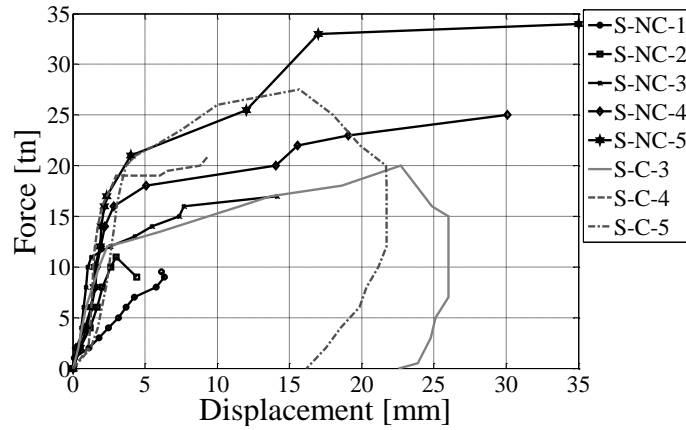


Figure 6. Force Displacement Curves

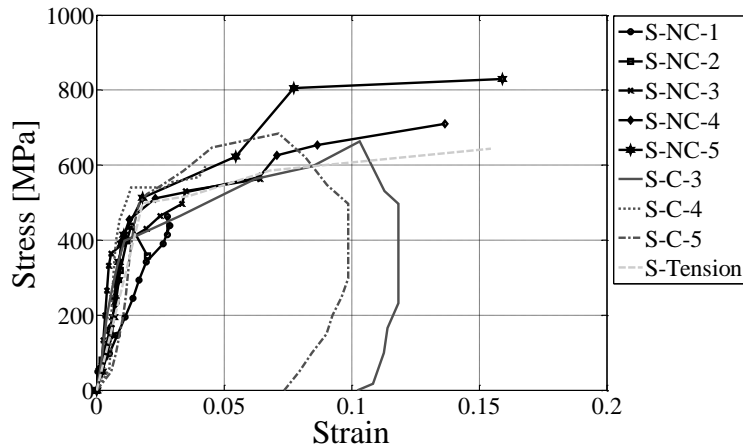


Figure 7. Stress- Strain Curves

#### 4 CONCLUSIONS

The experimental results have shown that the cross section of the steel bundles shall be in accordance with the cross section of the steel duct used. The figures presented in the paper aimed on determining the proper density of filling the cross section of the steel duct. An extremely sparse installation of steel bars in the steel duct indicated that it will cause side effects on the response of the bars as struts, under compression loading. Extreme high filling level of the steel ducts can develop side effects as well. It has to be noted that as tension

members, ties, the steel bars are not affected by the more or less density of the filling level of the steel bars in the steel duct.

The side effects developed for the highest density achieved are related to the fact that friction forces are developed and activated which increase the efficiency of the struts. However, wear phenomena of the walls of the steel ducts and premature degradation arise that are not acceptable for the use of the ducts as part of the restraining system.

## ACKNOWLEDGMENTS

The authors would like to acknowledge the assistance of the Laboratory of Experimental Strength of Materials and Structures.

## REFERENCES

- [1] CEN[Comité Européen de Normalisation], *Eurocode 8: Design of structures for earthquake resistance - Part 2: Bridges*. 2003.
- [2] Mitoulis, SA, Tegos, IA, "Connection of Bridges with Neighborhooding Tunnels," *Journal of Earthquake Engineering*, Vol. 14, No. 3, pp. 331–350, 2010.
- [3] Tegou, SD, Mitoulis, S a., Tegos, I a., "An unconventional earthquake resistant abutment with transversely directed R/C walls," *Engineering Structures*, Vol. 32, No. 11, pp. 3801–3816, 2010.
- [4] Tegos, IA, Tsitotas, MA, Tegou, SD, Mitoulis, SA, "Reduction in seismic actions of bridges by utilizing the sidewalks as restrainers."
- [5] DesRoches, R, Fenves, GL, "Simplified Restrainer Design Procedure for Multiple-Frame Bridges," *Earthquake Spectra*, Vol. 17, No. 4, pp. 551–567, 2001.
- [6] DesRoches, R, Delemont, M, "Seismic retrofit of simply supported bridges using shape memory alloys," *Engineering Structures*, Vol. 24, No. 3, pp. 325–332, 2002.
- [7] Choi, E, Park, J, Yoon, S-J, Choi, D-H, Park, C, "Comparison of Seismic Performance of Three Restrainers for Multiple-Span Bridges Using Fragility Analysis," *Nonlinear Dynamics*, Vol. 61, No. 1–2, pp. 83–99, 2009.
- [8] Tegos, I, Markogiannaki, O, "A Seismic Restraining System for Bridges Analytical Study of a Strut-Ties Mechanism," *IBSBI*, Athens, Greece, 2011.
- [9] Markogiannaki, O, Tegos, I, "A smart and costless solution for upgrading the seismic resistance of bridges Description of the proposed struts-ties system," *IABSE Conference*, Sharm el Sheikh, Egypt, 2012.
- [10] Markogiannaki, O, Tegos, I, "Seismic retrofit of bridges through the external installation of a new type restraining system," *15WCEE*, Lisbon, 2012.
- [11] Papanikolaou, VK, "Analysis of arbitrary composite sections in biaxial bending and axial load," *Computers & Structures*, Vol. 98–99, pp. 33–54, 2012.
- [12] Caltrans, "SEISMIC DESIGN CRITERIA VERSION 1 . 6," No. November, 2010.
- [13] Nielson, BG, "Analytical Fragility Curves for Highway Bridges in Moderate Seismic Zones Analytical Fragility Curves for Highway Bridges in Moderate Seismic Zones," No. December, 2005.
- [14] Iervolino, I, Galasso, C, Cosenza, E, "REXEL: Computer Aided Record Selection for Code-Based Seismic Structural Analysis," *Bulletin of Earthquake Engineering*, Vol. 8, No. 2, pp. 339–362, 2009.

## **EXPERIMENTAL INVESTIGATION ON THE SHEAR TRANSFER BETWEEN CONCRETE INTERFACES**

### **Case Study: The Problem of Designing Bridge Seismic Stoppers**

Sevasti D. Tegou<sup>1</sup>, Ioannis A. Tegos<sup>2</sup>

<sup>1,2</sup> Aristotle University of Thessaloniki, Dept. of Civil Engineering, Greece  
e-mail: stegou@civil.auth.gr, itegos@civil.auth.gr

**ABSTRACT:** This study presents the investigation on the effect of the shear span as resistance parameter, on the design of concrete interfaces. In the first part of the study the shear transfer between concrete interfaces, in which the value of the shear span is equal to zero is investigated. The experimental investigation is extended to include values of the shear span greater than zero. These values are usually observed at bridge seismic stoppers. The experimental results presented in this study are used to derive an analytical expression of the resistance of bridge seismic stoppers.

**KEY WORDS:** Bridge; Stopper; Shear Resistance; Interface.

## **1 INTRODUCTION**

Shear failure is one of the failure modes of R/C structures which mechanism is much different from the flexural one, as this type follows a formation of diagonal cracks. In general, it is a brittle failure compared with the flexural tension one. Shear failure is related to the shear span, which constitutes an important design parameter of concrete members. As it is known if the shear span-effective depth ratio ( $a/d$ ) is large, diagonal tension failure occurs, but when it is small, shear compression failure occurs. For the case of so-called deep beam the aforementioned ratio  $a/d$  is very small ( $a/d < 1$ ) the tied-arched shear resisting mechanism is formed as a compression strut joining the loading and the support points.

The behavior of structural members of low slenderness subjected to antisymmetrical flexural distress and shear with or without axial force is characterized by two distinguished limits. The upper limit coincides with the case of the bending with axial force while the lower limit is the case of the interface shear transfer.

Concrete corbels are also a typical example of structural members of low slenderness. In this case the ratio of shear to span depths is often less than 1.0 [1]. The analysis and design of these corbels and other non-flexural members, like deep beams and pile caps becomes difficult with ordinary flexure theory.

Different empirical approaches have been used for the design of such non-flexural members [2].

Bridge seismic stoppers [3] constitute a typical example of short corbels. These structural members are typically reinforced concrete blocks provided at the head of the piers and are used to protect bearing vulnerability mainly in the transverse direction of the bridge. However, current Codes [3] allow the use of the aforementioned seismic stoppers also in the longitudinal direction in order to reduce the seismic displacements of the deck and to prevent the unseating of the deck's beams. Bridge stoppers have usually small dimensions and usually receive the impact seismic forces of the adjacent beams.

Longitudinal seismic stoppers usually remain inactive during design earthquake [3] [4]. However in cases that they are used in combination with elastomeric bearings that have been designed according to the capacity design procedure, they should be designed by using the capacity design strengths of the pier. The aforementioned design procedure leads to large strength demands and disproportional stoppers' dimensions. The proper reinforcement of the stopper is the indicated method to maximize the strength of the stopper as the increase of the stoppers' dimensions is restricted. The dimensioning of these members usually follows the codes' provisions about short corbels in which the shear distance is between 1 and 0.5. However seismic stoppers fall in the category of ultra short corbels in which the value of the previous ratio is lower than 0.5 and for this reason the improvement of the reinforcement of these members is necessary. The aim of this study is to propose proper reinforcement arrangements which maximize the resistance of the stoppers and are simultaneously characterized by construction simplicity.

## **2 SHEAR SPAN EQUAL TO ZERO**

In the first part of the study the shear transfer between concrete interfaces in which the value of the shear span is equal to zero is investigated. The effect of the following parameters on the shear resistance of the interface is investigated: (1) Reinforcement ratio (7.5%, 2.5%, 0.5%, 0.0%), (2) roughness of the interface (smooth, rough and monolithic connection). Three groups of specimens had been constructed according to the roughness of the interface. The specimens are cubic (200mm x 200mm x 200mm), Figure 1.

The construction of the specimens includes two stages in order to achieve the creation of the construction joint. The first stage includes the construction of the middle 1/3 part of each specimen. Punched metallic plates of thickness less than 1mm were used for the hold of the reinforcement bars at the predefined position and the division of the form into three parts. A part of expanded polystyrene of thickness of 5mm was placed in the middle 1/3 of the specimen before the construction in order to achieve the construction of the "legs" of the specimen. After the hardening of the middle part of the specimen the metallic



plates were removed and the construction of the other two parts of the specimens followed. Between the two construction stages the careful treatment of the interfaces (e.g. use of hammer and chisel in the case of the rough interfaces) have been interposed.

The machine of uni-axial loading of the Laboratory of the Experimental Strength of Materials and Structures of the Aristotle University of Thessaloniki was used for the loading of the specimens, Photo 1. A metallic plate of thickness 1cm was placed at the middle part of each specimen for the accomplishment of the uniform distribution. Each interface receives the half loading of the machine. All specimens were subjected to cycling loading. The value of the step of the loading was variable.

During the loading measurements of the width of crack as well as the relevant displacement of the interfaces were taken, Figure 1. These measurements were taken at the middle of the construction joint. Figures 2,3,4 present the experimental results for the specimens whose reinforcement ratio is 2.5%. These specimens are considered the most representative of the investigation. The analytical strengths of the specimens calculated according to the codes provisions [5-8] are also marked at the diagrams.

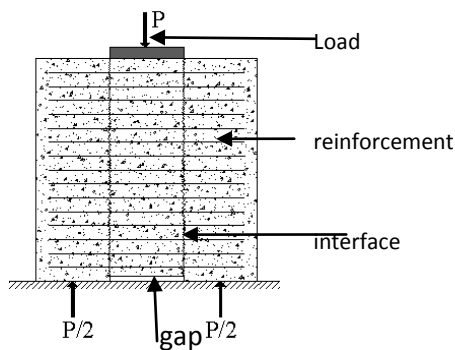


Figure 1. Loading setup



Photo 1. Loading Setup

### 3 SHEAR SPAN <0.5

The experimental investigation was extended to include values of the shear span less than one. In this part of the study reinforcement layouts for bridge seismic stoppers is proposed. The proposed reinforcement layout consists of opened stirrups uniformly arranged in plan. This reinforcement has the advantage of the full activation in contrary to the conventional single bars.

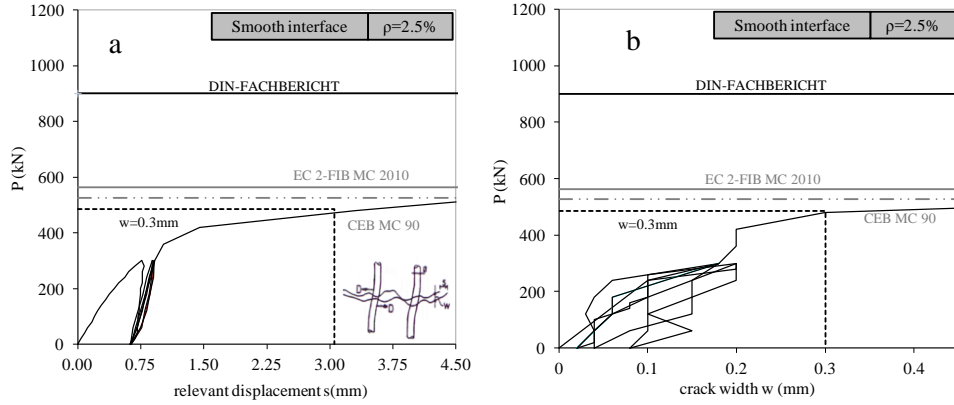


Figure 2. (a) Loading-Relevant displacement diagram, (b) Loading-crack width diagram (smooth interface,  $\rho=2.5\%$ )

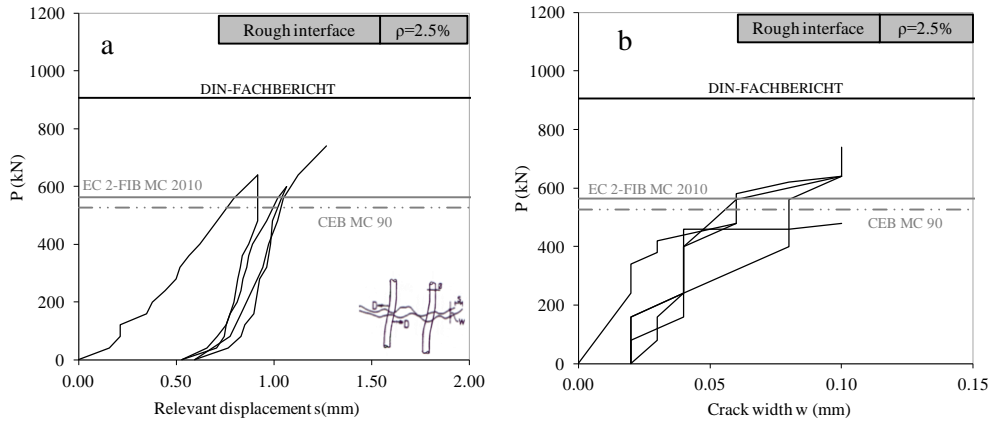


Figure 3. (a) Loading-Relevant displacement diagram, (b) Loading-crack width diagram (rough interface,  $\rho=2.5\%$ )

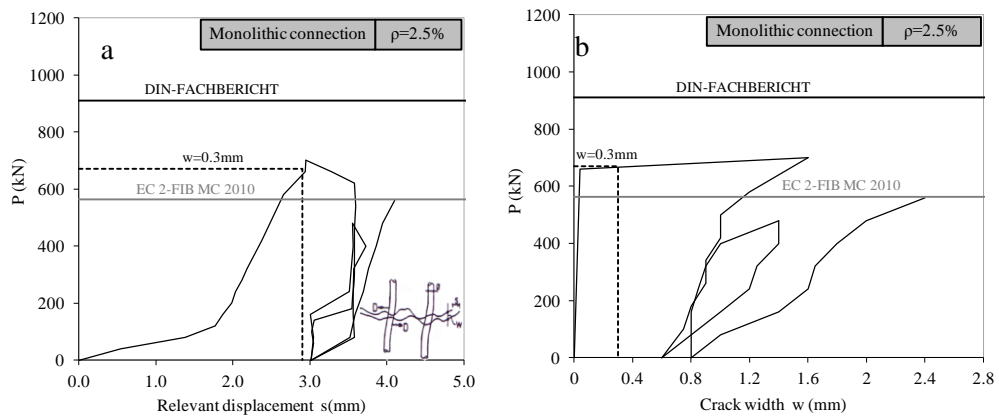


Figure 4. (a) Loading-Relevant displacement diagram, (b) Loading-crack width diagram (monolithic connection,  $\rho=2.5\%$ )

In order to maximize the specimens' resistance the use of thick reinforcement bars is necessary. The bend radius of the bars in these cases should be about 15D. The need of increase of the number of the legs of the stirrups leads to the second reinforcement arrangement, Figure 5(b). The third complex reinforcement arrangement consists of inclined bars, Figure 5(c), and is most proper for the case of cyclic loading. The aforementioned reinforcement arrangements are analytically and experimentally investigated.

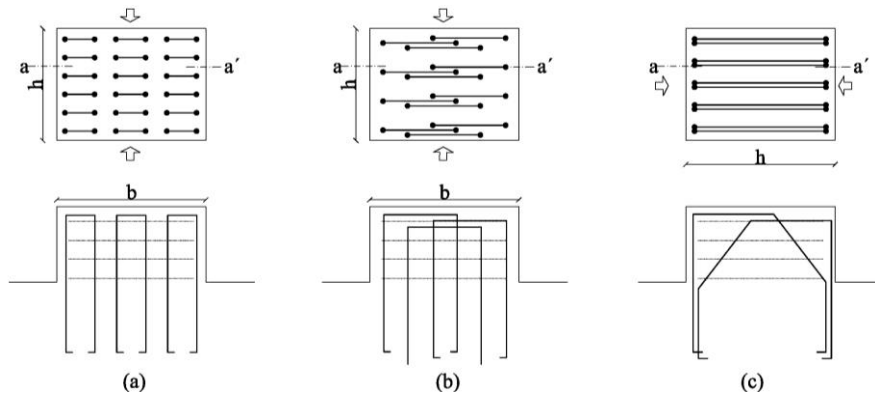


Figure 5. Proposed reinforcement layouts

### 3.1 Analytical investigation

The seismic stopper illustrated at Figure 6 is used as the reference case of the investigation.

The loading is applied across the short direction of the specimen. In this direction, the reinforcements are divided in two groups. The first group is referred to the distance  $h_1$  and the second one to the distance  $h_2$ . The reinforcements of the first group are activated when the angle  $\theta$  of the compression strut takes the maximum value. The angle  $\theta$  corresponding to the second group of reinforcements is smaller than the previous one. According to Eurocode 2 the cotangent of the angle  $\theta$  of the compression strut must be greater than 1 but smaller than 2.5 ( $22^\circ < \theta < 45^\circ$ ). A conservative value of the angle  $\theta=45^\circ$  is considered in this study.

As a result, the shear resistance of the reinforcements consists of two parts, according to Figure 6.

$$V_1 = \frac{b}{x} \cdot \frac{h_1}{y} \cdot a_s \cdot f_{yd} \cdot \tan \theta \quad (1)$$

$$V_2 = 0.5 \cdot \frac{b}{x} \cdot \frac{h_2}{y} \cdot a_s \cdot f_{yd} \cdot \tan \theta \quad (2)$$

The sum of  $V_1$  and  $V_2$  gives the total shear resistance of the stoppers' reinforcements.

$$V_{tot} = V_1 + V_2 = A_s \cdot f_{yd} \cdot (1 - 0.5 \cdot \frac{a_v}{h} \cdot \tan \theta) \tag{3}$$

In the previous equation,  $A_s$  is the total reinforcement area of the stopper.

The shear resistance of an ultra sort member with inclined reinforcement bars is calculated according Equation (4), Figure 7. In this equation  $\theta_1$  is the angle between the inclined bar and the longitudinal axis of the member. Furthermore  $\tan \theta_2 = 0.5h/a_v$ .

$$V_{tot} = f_{yd} \cdot (\tan \theta_1 \cdot \sum a_{s1} + 2 \cdot \sin \theta_2 \cdot \sum a_{s2}) \tag{4}$$

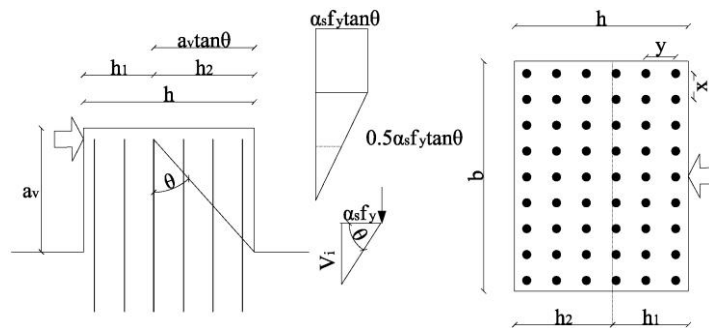


Figure 6. Corbel's characteristics and arrangement of reinforcement in plan

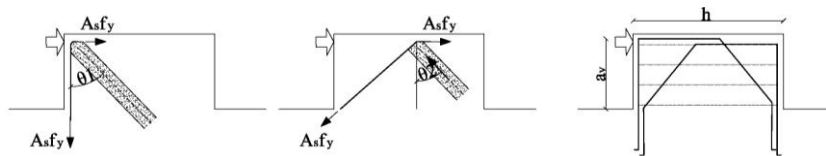


Figure 7. Features of short corbels with an arrangement of inclined reinforcement bars

The previous equations are used for the dimensioning of the active seismic stoppers of a precast I-beam bridge. Due to the lack of space in this paper, the characteristics of the analyzed bridge is omitted. More details about the analyzed bridge system can be found at the reference [4]. This bridge has three piers and active longitudinal stoppers are considered at the head of the two of the three piers. The capacity design effects used as design action effects and a overstrength factor equal to 1.35 is used in order to determine the design shear action. The capacity design shear action is equal to 401,7 kN. Supposing that the reinforcement ratio  $\rho$  of the stopper is equal to 1.0% and by applying Equation (3) is derived that the required cross-section of the stopper is 0.185 m<sup>2</sup>. Considering that the dimension of the stopper along the longitudinal direction of the bridge is  $h=1.00\text{m}$ , the required width is smaller than the available one which is equal to the width of the flange of the beam (0.63m).

### 3.2 Experimental investigation

The aim of the experimental investigation is the determination of the strengths of the specimens which have been dimensioned according to the proposal of this study. The geometry of the specimens and the concrete class (C25/30) is the same for all of the specimens. The main parameters examined in this study is (a) the reinforcement ratio  $\rho$ , i.e. the total area of the bars to the area of the cross-section of the specimen, (b) The diameter of the bars (D4mm and D8mm), (c) the morphology of the bars (inclined or vertical legs). Figure 9 illustrates a typical section of the specimens as well as the loading setup. Table 1 presents the main characteristics of the constructed specimens. Figure 8 presents indicative results of the investigation, while Figure 9 presents the comparison between theoretical and experimental results.

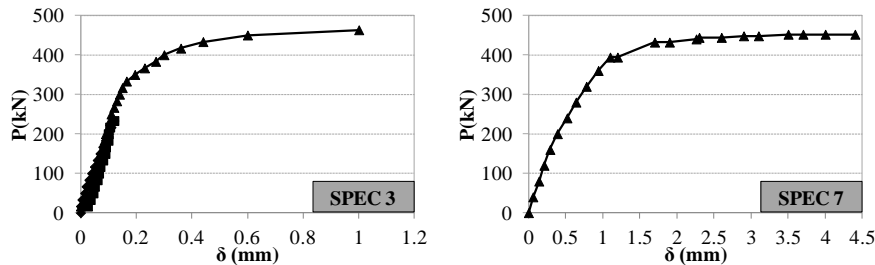


Figure 8. Loading – displacement diagram for two specimens of the investigation (SPEC 3 and SPEC 7)

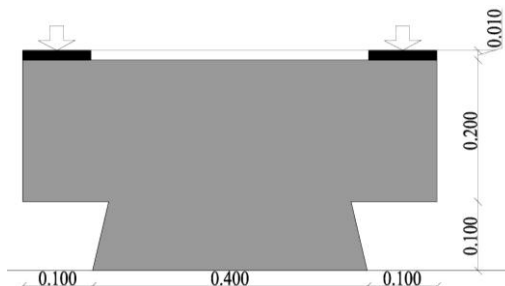


Figure 9. Loading setup

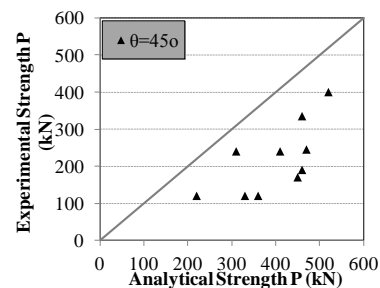


Figure 10. Comparison of experimental and analytical strengths of the specimens

## 4 CONCLUSIONS

The experimental investigation on the effect of the shear span as resistance parameter was presented in this study. The main conclusions of the study are summarized in the following:

Shear span equal to 0:

- The investigation showed that the experimental shear resistance is, in general, greater than the one calculated according to Eurocode 2 provisions, due to the upper limit of the compression of the concrete. Din Fachbericht overestimates

Table 1. Characteristics of the specimens

Specimen	Reinforcement	Layout (according to Figure 5)
SPEC 1	Unreinforced	-
SPEC 2	12D4	a
SPEC 3	24 D4	a
SPEC 4	12D4	b
SPEC 5	18D8	b
SPEC 6	12D8	a
SPEC 7	12D4+2D8(INCLINED)	a, c
SPEC 8	12D8+4D8(INCLINED)	a, c
SPEC 9	6D8	c
SPEC 10	10D8	c
SPEC 11	12D4	a

the shear resistance due to the absence of the previous upper limit.

- The experimental investigation proved the necessity of the presence of the upper limit of the resistance, as the strength of specimens with multiple reinforcement ratio was similar to the strength of specimens with lower reinforcement ratio.

Shear span <0.5:

- The reinforcement layout consisting of vertical bars uniformly arranged in the cross-section of the specimen was proved to be very effective.
- The reinforcement layout consisting of inclined bars has the advantage of the construction simplicity and is more effective for members subjected to cycling loading.
- The analytical strengths calculated according to the expressions proposed in this study are quite close to the experimentally calculated strengths.
- The angle  $\theta$  of the compression strut is suggested to be considered equal to  $45^\circ$ .

## REFERENCES

- [1] Mattock, AH, Chen, KC, and Soongswang, K., "The Behavior of Reinforced Concrete Corbels", *Journal of Pre-Stressed Concrete International*, Vol. 2, Issue 12, pp. 52–77, 1976.
- [2] Ahmad, S, Shah, A, "Evaluation of shear strength of High Strength Concrete Disturbed Regions using Strut & Tie Model (STM)" *Arabian Journal for Science & Engineering*, Vol. 34 Issue 1B, p27, 2009
- [3] EN 1998-2. *Eurocode 8: Design of structures for earthquake resistance, Part 2: Bridges.*, 2005.
- [4] Tegou, SD, Tegos, IA, "A proposal for cost-effective design of precast I-beam bridges", *International Conference IBSBI 2011- Innovations on Bridges and Soil- Bridge Interaction, 13-15 October 2011, Athens, Greece*, 2011.
- [5] *Eurocode 2: Design of concrete structures-Part 1: General rules and rules for buildings*, 2004.
- [6] DIN Deutsches Institut für Normung, *DIN-Fachbericht 102 - Betonbrücken*. Berlin: Beuth Verlag GmbH, 2003.
- [7] CEB-FIB, *Design of Concrete Structures, CEB-FIP Model Code 1990, Vol. Final Draft, CEB Bulletin No 204*. Thomas Telford, 1993.
- [8] Federation Internationale du Beton (fib) , *Model Code 2010 First complete draft* , Vol. 2., fib Bulletin No. 56, pp. 288, 2010.

## **CALIBRATION OF FINITE ELEMENT MODELS OF METSOVO BRIDGE USING AMBIENT VIBRATION MEASUREMENTS**

Costas Argyris<sup>1</sup>, Dimitra-Christina Papadioti<sup>1</sup>, Panagiotis Panetsos<sup>2</sup>  
and Costas Papadimitriou<sup>1</sup>

<sup>1</sup> University of Thessaly, Department of Mechanical Engineering, Volos 38334, Greece

<sup>2</sup> Egnatia Odos S.A, Capital Maintenance Department, Thermi 57001, Greece

e-mail: koargiri@uth.gr, dxpapadioti@uth.gr, ppane@egnatia.gr, costasp@uth.gr

**ABSTRACT:** A Bayesian inference method for structural model updating is used to develop high fidelity finite element (FE) models of the Metsovo bridge-foundation-soil system using modal characteristics identified from ambient vibration measurements. These models are representative of the initial structural condition of the bridge and can be further used for structural health monitoring purposes.

**KEY WORDS:** Structural dynamics, Modal estimation, Bayesian inference, Model calibration, Soil-Bridge Interaction.

### **1 INTRODUCTION**

In Northern Greece the largest and most challenging Greek project of design, supervision, construction, operation, maintenance and exploitation of 680 km of the motorway, linking Europe with Turkish borders, has been constructed. This is the Egnatia Motorway project, carried out by Egnatia Odos S.A.

The evaluation of the actual dynamic characteristics and the development of high-fidelity finite element models of some major bridges over steep and deep ravines, in the west sector of the Egnatia Motorway, crossing particularly difficult geological terrain and obstacles, like the Metsovo bridge, has been attracting an increasing research effort.

Recent developments in Bayesian methodologies [1] based on ambient vibration measurements are used for estimating the modal frequencies and mode shapes of the bridge and their uncertainties. Due to the large size of the bridge, the mode shapes of the structure are assembled from a number of sensor configurations. The modal properties and their uncertainties are then integrated within Bayesian model updating formulations to calibrate the parameters of FE model as well as the associated uncertainty. These formulations require a moderate to very large number of repeated FE model analyses to be performed and can increase substantially the computational effort to excessive levels. Fast

and accurate component mode synthesis (CMS) techniques, consistent with the finite element (FE) model parameterization, are integrated with Bayesian techniques to reduce efficiently and drastically the computational effort [2]. Further computational savings are achieved by adopting parallel computing algorithms such as the Transitional MCMC to efficiently distribute the computations in available multi-core CPUs [3].

In the context of this work, high performance computing and model reduction techniques are integrated within Bayesian tools that are used to calibrate the uncertainty in FE models of Metsovo Bridge within very reasonable computational time, despite the very large number of DOFs of the models.

## 2 BAYESIAN INVERSE MODELLING

### 2.1 Bayesian Model Calibration

Bayesian techniques are used for calibrating uncertainty models in structural dynamics based on vibration measurements. Let  $\hat{\omega}_r$  be the estimated modal frequencies and  $\hat{\phi}_r \in \mathbb{R}^{N_0, r}$  the modeshape components at  $N_0$  measured DOFs, where  $m$  is the number of observed modes. In this work, the modal properties are estimated from output only vibration measurements using the Bayesian modal parameter estimation method proposed in [1]. The Bayesian approach to model calibration deals with updating the values of the parameter set  $\underline{\theta}$  associated with the structural model parameters and the prediction error parameters. Following the Bayes theorem, the uncertainty in the parameters given the measured data  $D$  is quantified by the posterior distribution as

$$p(\underline{\theta} | D) = \frac{p(D | \underline{\theta}) \pi(\underline{\theta})}{p(D)} \quad (1)$$

where  $p(D | \underline{\theta})$  is the likelihood,  $\pi(\underline{\theta})$  is the prior distribution of the uncertain parameters and  $p(D)$  is the evidence of the finite element model. Assuming that the prediction errors for the modal frequencies and mode shapes are independent Gaussian zero-mean random variables with variance  $\sigma_\omega^2$  and  $\sigma_\phi^2$ , the likelihood is readily obtained by the following form

$$p(D | \underline{\theta}) \propto \frac{1}{\sigma_\omega^m \sigma_\phi^M} \exp \left[ -\frac{1}{2\sigma_\omega^2} J_\omega(\underline{\theta}) - \frac{1}{2\sigma_\phi^2} J_\phi(\underline{\theta}) \right] \quad (2)$$

where  $J_\omega(\underline{\theta})$  and  $J_\phi(\underline{\theta})$  represent the measure of fit between the experimentally obtained modal data and the modal data predicted by the FE model. Moreover,



the model prediction error parameters  $\sigma_\omega$  and  $\sigma_\phi$  are considered to be unknown and are incorporated in the unknown parameter set  $\underline{\theta}$ .

Using the vector  $\underline{a}_r(\underline{\theta}) = [\Phi_r^T(\underline{\theta})\Phi_r(\underline{\theta})]^{-1}\Phi_r^T(\underline{\theta})\hat{\phi}_r$  to guarantee that the modal mode shapes  $\underline{\phi}_r(\underline{\theta})$   $r=1, \dots, m$  predicted from a particular value of the parameter set  $\underline{\theta}$  are closest to experimentally obtained  $\hat{\phi}_r$  and given that  $\Lambda(\underline{\theta}) = \text{diag}[\omega_r^2(\underline{\theta})]$ , the functions  $J_\omega(\underline{\theta})$  and  $J_\phi(\underline{\theta})$  are given by

$$J_\omega(\underline{\theta}) = \sum_{r=1}^m \frac{\underline{a}_r^T(\underline{\theta})\Lambda(\underline{\theta})\underline{a}_r(\underline{\theta}) - \hat{\omega}_r^2 \underline{a}_r^T(\underline{\theta})\underline{a}_r(\underline{\theta})}{\hat{\omega}_r^2 \underline{a}_r^T(\underline{\theta})\underline{a}_r(\underline{\theta})}, \quad J_\phi(\underline{\theta}) = \sum_{r=1}^m \frac{\|\Phi_r(\underline{\theta})\underline{a}_r(\underline{\theta}) - \hat{\phi}_r\|^2}{\|\hat{\phi}_r\|^2} \quad (3)$$

## 2.2 Bayesian Computing Tools

The Bayesian tools for identifying FE models as well as performing robust prediction analyses are Laplace methods of asymptotic approximation and stochastic simulation algorithms. In this work the Transitional MCMC (TMCMC) stochastic simulation algorithm [5] is employed. High performance computing techniques are integrated within the TMCMC tool and fast and accurate component mode synthesis techniques [2] are used, consistent with the FE model parameterization, to efficiently handle large number of DOF in FE models. Further computational savings are achieved by adopting parallel computing algorithms to efficiently distribute the computations in available multi-core CPUs [3].

## 3 METSOVO BRIDGE

### 3.1 Description

The ravine bridge of Metsovo is the highest bridge of Egnatia Motorway, with the height of the taller pier M2 equal to 110m. The total length of the bridge is 537 m. The key of the central span is not in midspan due to the different heights of the superstructure at its supports to the adjacent piers (13,0m in pier M2 and 11,50 in pier M3) for redistributing mass and load in favor of the short pier M3 and thus relaxing strong structural abnormality.

The bridge has 4 spans, of length 44,78m /117,87m /235,00m/140,00m and three piers of which M1, 45m high, supports the boxbeam superstructure through pot bearings, while M2, M3 piers connect monolithically to the superstructure. The total width of the deck is 13,95m, for each carriageway. The superstructure is limited prestressed of single boxbeam section, of height varying from 4,00 m to 13,5m. Piers M2, M3 are founded on huge circular Ø12,0m rock sockets in a depth of 25m and 15m, respectively.

### 3.2 Finite Element Modelling

Detailed FE models are created using 3-dimensional tetrahedral quadratic Lagrange FEs to model the whole bridge. An extra coarse mesh is chosen to predict the lowest 10 modal frequencies and mode shapes of the bridge. The model has 97,636 FEs and 563,586 DOFs. In order to examine the contribution of soil conditions on the dynamic response of the bridge, two different classes of finite element models of the bridge are developed to predict the dynamic behavior of the bridge, a fixed base model and one that models the soil stiffness with translational springs attached in the two horizontal and the vertical directions at each base of the three piers and the two abutments.

The lowest ten modal frequencies of the left branch of Metsovo Bridge predicted by the fixed base model are presented in Table I and are compared to those predicted by the flexibly supported model. It can be seen from the results in Table I that soil contribution varies from 0.35% (1<sup>st</sup> Mode) to 2.47% (10<sup>th</sup> Mode). It is obvious that the effect of soil-structure interaction on dynamic response of Metsovo Bridge cannot be ignored. Finally, it is obvious that modal frequencies predicted by the bridge model including the contribution of soil are, as expected, lower than the ones for the fixed base bridge model.

Table 1. Modal Frequencies in Hz of left branch of Metsovo Bridge

No	Identified Mode	Fixed Base FEM	FEM With Soil	% Difference
1	1 <sup>st</sup> Transverse	0.3179	0.3168	0.35
2	2 <sup>nd</sup> Transverse	0.6219	0.6190	0.47
3	1 <sup>st</sup> Bending	0.6462	0.6406	0.57
4	3 <sup>rd</sup> Transverse	0.9897	0.9837	0.61
5	2 <sup>nd</sup> Bending	1.1121	1.1045	0.68
6	4 <sup>th</sup> Transverse	1.1734	1.1643	0.78
7	3 <sup>rd</sup> Bending	1.5164	1.4988	1.16
8	5 <sup>th</sup> Transverse	1.7117	1.7021	0.56
9	4 <sup>th</sup> Bending	1.9341	1.9233	0.56
10	6 <sup>th</sup> Transverse	2.3187	2.2615	2.47

## 4 MODAL IDENTIFICATION

### 4.1 Bridge Instrumentation

The acceleration time histories recorded by 5 triaxial and 3 uniaxial accelerometers paired with a 24-bit data logging system and an internal SD flash-card for data storage, shown in Fig.1, are used to identify the modal properties of the bridge under normal operating conditions. The recorded responses are mainly due to road traffic, which ranged from light vehicles to heavy trucks, and environmental excitation such as wind loading which classifies this case as ambient modal identification.



Figure 1. Instrumentation

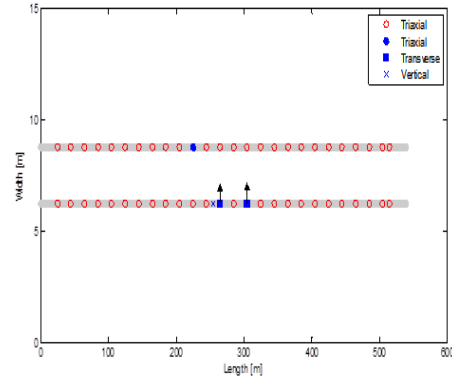


Figure 2. Sensor Configuration

An important aspect of this measurement system is the fact that it is wireless, since this allowed for multiple sets of repeated measurements that had to be performed for accurate mode shape identification, given the limited number of sensors and the large length of the deck. Specifically, the entire length of the deck was covered in 13 sensor configurations, shown in Fig.2, with each configuration recording for 20 minutes with a sampling rate of 100 Hz. One tri-axial and three uniaxial sensors (one vertical and two horizontal), one at each side of the bridge, remained at the same position, in order to provide common measurement points along different configurations so as to enable the procedure of mode shape assembling [4].

#### 4.2 Modal Identification Software

For the estimation of modal properties from the ambient acceleration data, software developed by the System Dynamics Laboratory of University of Thessaly was used. The software for Ambient (Output-only) Modal Identification has four distinct modules, namely Data insertion, Pre-processing, Modal Identification and Post processing.

The *Data insertion module* is used to load the experimentally measured acceleration time histories, even of multiple sets, into the program. The data insertion module imports any number of sensor configurations, each one represented by a MATLAB file.

In the *Pre-processing module* the user can visually inspect the Power Spectral Density (PSD) in Fig. 3 and the Singular Value Spectrum (SVS) in Fig. 4 of the acceleration time histories in order to obtain a rough estimate of the natural frequencies of the structure and define the frequency bands that are utilized by the Modal Identification module.

The *Modal Identification module* uses the recently proposed Bayesian methodology [1] in order to estimate the modal frequencies, mode shapes, and

damping ratios. The method is based on the Fast Fourier Transform (FFT) of the acceleration signals in specific bands of interest and also provides the uncertainty in the estimates of the modal properties.

In the *Post processing module* the user can insert the geometry, define the measured degrees of freedom, assemble the full mode shapes, and perform other auxiliary actions such as animate the mode shapes in *Fig. 5*.

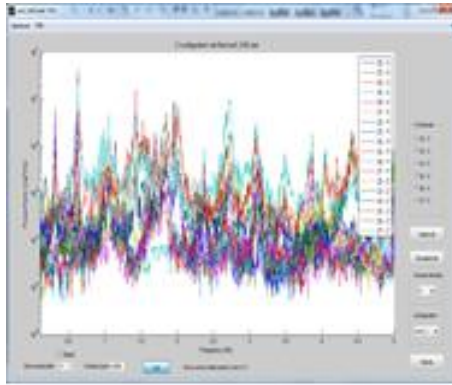


Figure 3. PSD Plot

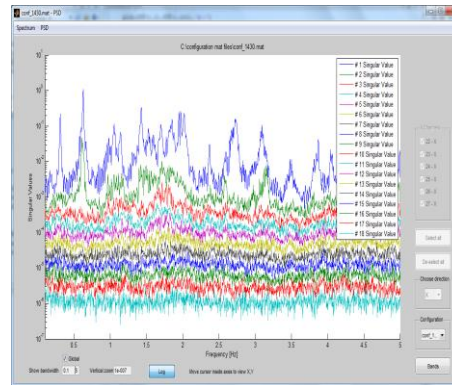


Figure 4. SVS Plot

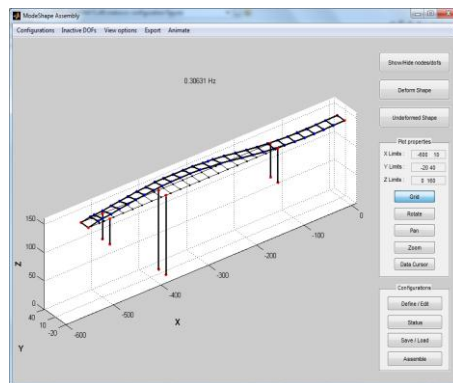


Figure 5. Identified Mode Shape Plot

### 4.3 Modal Identification Results

Using the software incorporating the Bayesian Methodology and the mode shape assembling algorithm, the natural frequencies and damping ratios of the structure were estimated. For comparison purposes, Table 2 presents the mean and the standard deviation (STD) of the experimentally identified modal frequencies for the lowest 10 modes of the Metsovo bridge. The experimental values should be compared to the FE model predictions in Table 1. It can be

seen that the bridge is less stiff than the fixed-base FE model predicts which suggests that the FE model with soil is more appropriate to model the bridge.

*Table 2.* Experimental and model predicted natural frequencies

No	Type of Mode	Modal Frequencies in Hz				Damping Ratios (%)	
		Experimental		Calibrated Model		Experimental	
		Mean	STD	Mean	STD	Mean	STD
1	Transverse	0.3063	0.0007	0.3064	0.0042	1.1	0.25
2	Transverse	0.6034	0.0014	0.5993	0.0058	1.8	0.24
3	Bending	0.6227	0.0008	0.6242	0.0069	0.85	0.24
4	Transverse	0.9646	0.0084	0.9330	0.0233	1.4	1.1
5	Bending	1.0468	0.0066	1.1107	0.0092	1.9	1.1
6	Transverse	1.1389	0.0049	1.1427	0.0099	1.1	0.43
7	Bending	1.4280	0.0042	1.4678	0.0140	1.4	0.64
8	Transverse	1.6967	0.0112	1.6549	0.0147	1.6	1.6
9	Bending	2.0053	0.0054	1.8389	0.0175	1.1	0.41
10	Transverse	2.3666	0.0025	2.2978	0.0252	0.85	0.16

## 5 CALIBRATION OF METSOVO FE MODEL

The flexibly supported FE model of Metsovo Bridge is parameterized using five parameters associated with the modulus of elasticity of one or more structural components, shown in *Fig. 6*. The model parameters scale the nominal values of the properties that they model. In order to reduce the computational effort, a parameterization-consistent component mode synthesis (CMS) technique is applied [2] resulting in a reduced model of 588 generalized coordinates, with errors in the estimates for the lowest 20 modal frequencies to be less than 0.02%. Thus, the time to solution for one run of the reduced model is of the order of a few seconds which should be compared to the 2 minutes required for solving the unreduced FE model. Also, in order to further reduce the time to solution, the computations were performed in parallel using 8 cores available from a 4-core double threaded computer.

The calibration is done using the lowest 10 modal frequencies and mode shapes identified for the structure in Table 2. The TMCMC is used to generate samples from the posterior PDF of the structural model and prediction error parameters and then the uncertainty is propagated to estimate the uncertainty in the modal frequencies of the bridge. The mean and the standard deviation of the uncertainty in the first 10 modal frequencies are presented in Table 2. It can be seen that predictions of the uncertainty for the first 10 modal frequencies are overall closer to the experimental data than the ones predicted from the nominal

model in Table 1. The overall fit between the experimental and the model predicted modal frequencies is shown in Fig. 7.

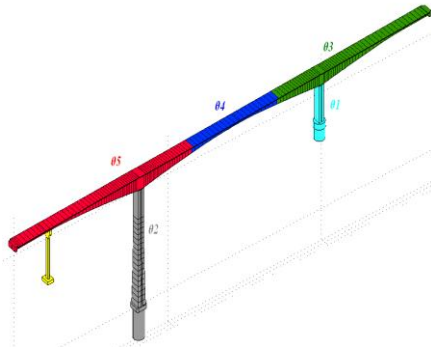


Figure 6. Model Parameterization

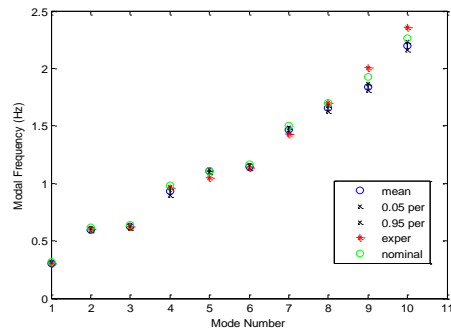


Figure 7. Modal Frequency Fit

## 6 CONCLUSIONS

The application of the proposed Bayesian methodology for model calibration to Metsovo Bridge demonstrated its computational efficiency and accuracy. The proposed CMS method and parallel implementation strategies allowed for two to three orders of magnitude reduction of computational time. The calibrated FE models of the Metsovo bridge predict modal frequencies and mode shapes that are very close to those identified from ambient vibration measurements.

## ACKNOWLEDGMENTS

This research has been implemented under the “ARISTEIA” Action of the “Operational Programme Education and Lifelong Learning” and was co-funded by the European Social Fund (ESF) and Greek National Resources.

## REFERENCES

- [1] S. K. Au. Fast Bayesian ambient modal identification in the frequency domain, Part II: Posterior uncertainty. *Mechanical Systems and Signal Processing*, Vol. 26, pp. 76-90, 2012.
- [2] C. Papadimitriou, D.C. Papadioti. Component mode synthesis techniques for finite element model updating. *Computers and Structures*, Vol. 126, pp. 15-28, 2013
- [3] P. Angelikopoulos, C. Papadimitriou, P. Koumoutsakos. Bayesian uncertainty quantification and propagation in molecular dynamics simulations: A high performance computing framework. *The Journal of Chemical Physics*, Vol. 137, No. 14. 2012. DOI: 10.1063/1.4757266.
- [4] S. K. Au. Assembling mode shapes by least squares. *Mechanical Systems and Signal Processing*, Vol. 25, pp. 163-179, 2010.
- [5] J. Ching, Y. C. Chen. Transitional Markov Chain Monte Carlo method for Bayesian updating, model class selection, and model averaging. *ASCE Journal of Engineering Mechanics*, 133, 816-832, 2007.

## **DYNAMIC CHARACTERISTICS OF BRIDGE- FOUNDATION-SOIL SYSTEMS BASED ON LABORATORY AND ON-SITE MEASUREMENTS**

Periklis Faraonis<sup>1</sup>, Anastasios Sextos<sup>2</sup>, Volkmar Zabel<sup>3</sup>, Frank Wuttke<sup>4</sup>

<sup>1,2</sup> Aristotel University of Thessaloniki, Dept. of Civil Engineering, Greece

<sup>3</sup> Bauhaus University of Weimar, Dept. of Civil Engineering, Germany

<sup>4</sup> Christian-Albrechts University of Kiel, Dept. of Geosciences, Germany

e-mail: pfaraonis@civil.auth.gr, asextos@civil.auth.gr, volkmar.zabel@uni-weimar.de,  
fw@gpi.uni-kiel.de

**ABSTRACT:** The natural frequencies of the Metsovo bridge during construction are identified both in actual scale and in 1:100 scale. Finite element models of increasing modeling complexity are developed in order to investigate their efficiency in representing the measured dynamic stiffness of the bridge-foundation-soil system. The results highlight the importance of accurately simulating boundary conditions in Structural Health Monitoring applications.

**KEY WORDS:** Bridges; caissons; finite elements; soil-structure interaction.

### **1 INTRODUCTION**

The dynamic characteristics of structures can be either identified through System Identification (SI) methods or predicted by modal analysis of numerical finite element (FE) models. System Identification methods can identify the modal properties of structures by measuring their response to a known excitation (input-output methods, [1], [2]) or to an unknown excitation (output-only methods, [3], [4]). The modeling assumptions of the FE models can be evaluated by comparing the identified with the predicted modal characteristics. A wide variety of studies ([5], [6] and [7]) present the influence of soil stiffness to the SI results and the importance of taking into account soil compliance in FE models, in order to minimize the discrepancies between identified and numerically predicted dynamic characteristics.

One option to account for soil compliance is by numerically modeling the entire structure-foundation-soil system as a whole [8]. Due to the fact that this method is quite expensive from a computational standpoint and is not easily implemented in engineering practice, alternative methods have also been developed. In these methods the structure-foundation-soil interaction is decoupled to kinematic and inertial component. As far as the shallow embedded foundations are concerned, it is common to replace the foundation-soil system

with six degrees-of-freedom (DOF) springs, the stiffness of which is calculated according to Elsabee et al. [9]. Alternatively, the subsoil may be replaced by 6-DOF springs concentrated at the base of the foundation (defined according to Kausel [10]) as well as additional springs attached on the foundation [11]. Experimental and numerical evaluation of the efficiency of the aforementioned methods in representing the dynamic stiffness of various foundation-soil systems is presented by Varun et al. [11].

In this framework, the scope of this paper is to experimentally verify the influence of soil compliance on the predictions of System Identification and to investigate the efficiency of existing numerical methods in simulating the soil stiffness.

## 2 PROTOTYPE STRUCTURE

The Metsovo ravine bridge was constructed in 2008 in Greece along the Egnatia Highway and consists of two structurally independent branches (one for each carriageway). The bridge was constructed by the balanced cantilever construction method, which made feasible the modal identification of structurally independent bridge components during construction. The modal characteristics of the M3 (cantilever) pier (*Figure 1, left*) were identified prior to the construction of the key connecting segments to the M2 pier, the latter also temporary acting as a balanced cantilever [12]. The modal identification of the M3 cantilever was based on ambient vibration measurements triggered by wind and induced operational loads. Detailed information regarding the measurements and the applied identification methodology can be found in [12].



*Figure 1.* Metsovo Bridge segments during the construction stage (left) and its equivalent scaled structure tested at the laboratory (right).



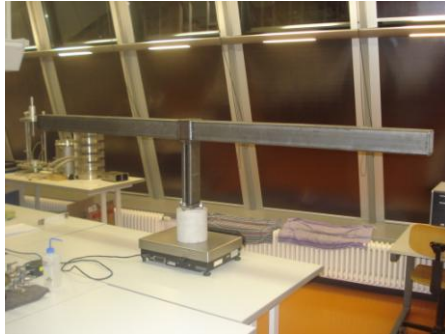


Figure 2. Scaled structure on concrete caisson before placement within the stabilized soil.

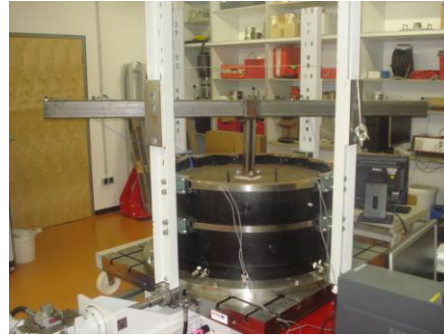


Figure 3. Scaled structure on stabilized soil.

### 3 SCALED STRUCTURE WITH ALTERNATIVE BOUNDARY CONDITIONS

A scaled model structure of the prototype M3 pier cantilever of Metsovo Bridge was constructed in the laboratory of Soil Mechanics at the Bauhaus University Weimar. Apart from the stiff foundation soil corresponding to the actual conditions of the prototype structure, alternative boundary conditions were also examined in the form of gradually stabilized soil to investigate the influence of soil compliance on the prediction of modal characteristics.

#### 3.1 Scaled structure fixed

The construction of a scaled structure dictates the determination of the scaling laws relating the prototype geometry to that of the scaled structure. The scaling laws can be determined either by dimensional analysis or the analysis of the system's characteristic equation. Based on dimensional analysis and by neglecting the gravity distortion effects that arise during scaling, the scaling factor that relates the natural frequencies of a scaled structure with its prototype is given in Eq. (1) [13]:

$$\lambda_f = \frac{1}{\lambda_l} \cdot \sqrt{\frac{\lambda_E}{\lambda_\rho}} \quad (1)$$

where:  $\lambda_f$  is the prototype to the model frequency ratio,  
 $\lambda_l$  is the prototype to the model dimension ratio,  
 $\lambda_E$  is prototype to the model young modulus of Elasticity ratio,  
 $\lambda_\rho$  is prototype to the model density ratio.

Herein, the scale set to 1:100, to accommodate the fact that the deck length of the prototype structure is 215m (Figure 1). It is noted that as the exact section of the concrete deck could not be reproduced at a 1:100 scale (i.e., the

resulting web and flanges would be as thin as 22 mm and 3 mm) an equivalent steel structure with the same dynamic characteristics was formed in the laboratory based on parametric modal analysis. Several standard steel sections were considered until matching with the modal characteristics of the concrete scaled structure was achieved. The equivalent, steel balanced cantilever was finally formed by the following commercially available sections:

- a 90X90X3 HSS steel hollow section of 215cm length corresponding to an 1:100 replication of the prototype deck,
- a 100X100X5 HSS steel hollow section of 6,15cm length corresponding to the prototype central deck-segment, and
- a 80X20X3 HSS steel hollow section of 32cm length corresponding to 1:100 replication of the prototype M3 pier.

### 3.2 Scaled structure on stabilized soil

Next, the scaled structure was fixed on a circular concrete foundation (15cm diameter and height) *Figure 2*. The structure was then placed within a 95cm diameter laboratory box that was filled with stabilized soil (*Figure 3*). The stabilized soil consisted of clay (CL), with 24% water and 4% lime. The latter was added in order to increase the stiffness of the soil and its percentage was determined according to DIN EN 459-1 [14]. The total height of the stabilized soil in the box was 30cm and the dry density was determined as  $\rho_s=1.86t/m^3$ . Sensors were placed inside the box in order to measure the shear wave velocity of the stabilized soil.

## 4 FINITE ELEMENT MODELS

### 4.1 Fixed conditions

A refined finite element (FE) model using three-dimensional solid elements was developed to simulate the fixed scaled structure as shown in *Figure 1 (right)*. The resulted FE model consisted of approximately 19,000 triangular elements corresponding to 88620 degrees of freedom. The measured mass of the physical model was 20.46kg with a density of  $\rho=7.46t/m^3$ . The modulus of elasticity of the stainless steel was taken equal to 210GPa.

### 4.2 Soil compliant conditions

Several FE models were developed for the scaled structure fixed on a concrete foundation (*Figure 2*) and then embedded within the stabilized soil (*Figure 3*).

#### 4.2.1 Holistic method

A three-dimensional finite element model of approximately 200,000 degrees of freedom was further developed for the entire pier-foundation-subsoil system. Stainless steel ( $E=210GPa$ ,  $\nu=0.3$ ) was once more assigned to the superstructure, whereas C30/37 concrete properties ( $E=32GPa$ ,  $\nu=0.3$ ) were

assigned to the caisson. The mass of the foundation was measured 7.56kg corresponding to a density  $\rho=2.71\text{t/m}^3$ . The shear modulus of the stabilized soil was taken equal to  $G=186\text{MPa}$  based on the shear wave velocity  $V_s=316\text{m/s}$  and density  $\rho_s=1.86\text{t/m}^3$  values that were measured in the laboratory.

#### 4.2.2 Inertial and kinematic interaction




##### 4.2.2.1 Large diameter caisson model

Soil was modeled through 6-DOF springs at the base of the foundation and by 6-DOF springs at the middle of the foundation height. The stiffness of the former springs was obtained from the theory of rigid circular foundations on a stratum over rigid base suggested by Kausel [10] while the stiffness of the latter springs was calculated by the solution of Varun et al [11] for cylindrically shaped large diameter caisson foundations. In these formulas the soil shear modulus  $G$  was again estimated based on the measured  $V_s$  of the stabilized soil.

##### 4.2.2.2 Shallow embedded cylindrical foundation model

Both the foundation and the soil were replaced by 6-DOF Winkler type springs. Their values were obtained from the theory of rigid embedded cylindrical foundations welded into a homogenous soil stratum over bedrock, proposed by Elsabee et al. [9]. Again the  $G$  shear modulus was also estimated based on the measured  $V_s$  of the stabilized soil.

Table 1. Identified and numerically predicted natural frequencies for the case that the scaled structure was fixed at its base.

Modes	M3 cantilever Prototype on Rock [12]	Ideal 1:100 scaled structure	Equivalent scaled (steel) structure Fixed	FE model of the equivalent scaled (steel) structure Fixed
		<i>Theoretical (not constructed)</i>		
	(Hz)	(Hz)	(Hz)	(Hz)
Rotational	0.159	15.90	15.96	16.01
1 <sup>st</sup> Longitudinal	0.305	30.50	23.67	23.13
Transverse	0.623	62.30	65.56	68.23
2 <sup>nd</sup> Longitudinal	0.686	68.60	67.68	69.71
Bending (deck)	0.908	90.80	88.65	89.45
Average $\Delta f$ (%)			<b>6.34%</b>	<b>2.12%</b>





## 5 RESULTS

### 5.1 Prototype structure vs. equivalent scaled structure

The first five identified natural frequencies of the M3 cantilever prototype structure range between 0.159-0.908Hz and are presented in Table 1. The corresponding natural frequencies that are theoretically anticipated for an 1:100 scaled structure, ideally comprising of the same material, are also presented in Table 1 and vary between 15.90Hz and 90.80Hz. These expected natural frequencies are used to validate the equivalence of the constructed scaled (steel) structure with the prototype.

The equivalent scaled (steel) structure was subjected to hammer impulses in order to simulate a broad band excitation, similar to ambient excitations applied to the actual M3 cantilever. The natural frequencies were identified by the stochastic subspace identification method [4] with the use of MACEC, which is a Matlab toolbox for operational modal identification. The first five identified natural frequencies given in Table 1 range between 15.96-88.65Hz. It has been observed that the natural frequencies of the equivalent scaled structure present a 6.34% average deviation compared to those expected from the prototype's ideal 1:100 scaled structure, indicating good agreement between the equivalent (steel) and the prototype (concrete) bridge pier.

*Table 2.* Identified and numerically predicted natural frequencies for the case that the foundation of the scaled structure was embedded in stabilized soil.

Modes	Scaled structure on stabilized soil	FE model on stabilized soil <i>Holistic method</i> $G=186MPa$	FE model on stabilized soil <i>6+6 DOFs springs</i> <i>Kausel [10]</i> <i>Varun et al. [11]</i> $G=186MPa$	FE model on stabilized soil <i>6 DOFs springs</i> <i>Elsabee et al. [9]</i> $G=186MPa$
				
	(Hz)	(Hz)	(Hz)	(Hz)
Rotational	14.88	15.63	15.64	15.82
1 <sup>st</sup> Longitudinal	19.15	21.74	21.69	21.98
Transverse	46.52	57.42	56.77	60.6
2 <sup>nd</sup> Longitudinal	56.87	63.80	63.34	66.59
Bending (deck)	85.25	88.77	88.72	88.76
Average $\Delta f$ (%)		<b>11.66%</b>	<b>11.16%</b>	<b>14.51%</b>

## 5.2 Identified and numerically predicted natural frequencies

### 5.2.1 Fixed boundary conditions

Next, it is verified that the first five natural frequencies predicted by the fixed FE model and range between 16.01-89.45Hz are in very good agreement with those of the tested equivalent structure showing only a 2.12% average error as are summarized in Table 1.

### 5.2.2 Stabilized soil as foundation soil

A hammer impulse excitation was also applied to identify the natural frequencies of the scaled structure when the latter was placed within the stabilized soil. The first five identified natural frequencies are presented in Table 2, and range between 14.88-85.25Hz. In Table 2 it is also observed that the average deviation between the identified and the numerical predicted frequencies range is of the order of 11-14%. Given that the experimentally and numerically predicted natural frequencies of the fixed system were almost identical, it is evident that this difference is clearly attributed to the method used to represent soil stiffness using equivalent springs, as well as to the determination of the actual soil stiffness at the laboratory. It is interesting to notice that even though the hammer excitations were of low intensity and the induced soil shear strain subsequently small, the value of soil stiffness that was introduced in the numerical model was overestimated.

## 6 CONCLUSIONS

This paper presents an effort to comparatively assess the efficiency of numerical models to capture the effect of soil compliance on the predicted dynamic characteristics of bridge-foundation-soil systems. The study focuses on the case of the Metsovo bridge during the construction stage where measurements were made available and compared to the results of equivalent scaled systems tested in the laboratory. Due to the difficulties in constructing an actual concrete deck at a scale 1:100, an equivalent steel scaled structure was constructed in the laboratory presenting minimum deviation (as low as 6%) in terms of dynamic characteristics. The respective finite element model also successfully predicted the natural frequencies of the fixed scaled structure presenting a 2.12% average error. When the scaled structure was embedded in stabilized soil, a decrease was observed both experimentally and numerically for all considered modes. Three methods were adopted to simulate the soil compliance of the stabilized soil, namely: (a) a holistic method with 3D solid finite elements, (b) a 6+6 DOF springs method suggested by Kausel [10] and Varun et al [11] and (c) a 6-DOF spring method introduced by Elsabee et al. [9]. The average deviation between the identified and the numerically predicted natural frequencies range at all three methods between 11.3-14.5%, indicating that the stabilized soil's measured shear modulus was probably overestimated. Despite this, the

influence of soil compliance was demonstrated by all numerical and experimental data thus highlighting the necessity of carefully considering soil compliance in the framework of structural health monitoring.

### ACKNOWLEDGMENTS

The material herein presented is based on work supported by a research grant from the DAAD organization. The authors would also like to thank Dr. Panagiotis Panetsos (Egnatia Highway S.A.) and Professor Konstantinos Papadimitriou (University of Thessaly) for making available the measurements of the prototype structure and providing valuable comments as well as Professor George Manolis (Aristotle University of Thessaloniki) for his scientific input.

### REFERENCES

- [1] Werner, SD, Beck JL, Levine, MB, "Seismic response evaluations of Meloland road overpass using 1979 Imperial Valley earthquake records", *Earthquake Engineering Structural Dynamics*, Vol. 15, pp.249–274, 1987.
- [2] Chaudhary, MTA, Abe, M, Fujino, Y, "System identification of two base-isolated buildings using seismic records", *Journal of Structural Engineering*, Vol. 126 (10), pp. 1187–1195, 2000
- [3] Basseville, M, Benveniste, A, Goursat, M, Hermans, L, Mevel, L, Van der Auweraer, H, "Output-only subspace-based structural identification: from theory to industrial testing practice", *Journal of Dynamic Systems Measurement Control*, Vol. 123 (4), pp. 668-676, 2001.
- [4] Peeters, B, De Roeck, G, "Stochastic system identification for operational modal analysis: a review", *Journal of Dynamic Systems Measurement Control*, Vol. 123 (4), pp. 659-667, 2001.
- [5] Crouse, C, Hushmand, B, Martin, G, "Dynamic soil-structure interaction of single-span bridge", *Earthquake Engineering and Soil Dynamics*, Vol. 15, pp. 711–729, 1987.
- [6] Chaudhary, M, Abe, M, Fujino, Y, "Identification of soil-structure interaction effects in base isolated bridges from earthquake records", *Soil Dynamics and Earthquake Engineering*, Vol. 21, pp. 713–725, 2001.
- [7] Morassi, A, Tonon, S, "Dynamic testing for structural identification of a bridge", *Journal of Bridge Engineering*, Vol. 13 (6), pp. 573-585, 2008.
- [8] Wolf, JP, "Soil-structure interaction analysis in time domain", *Journal of Nuclear Engineering and Design*, Vol. 11 (3), pp. 381-393, 1989.
- [9] Elsabee, F, Morray, JP, "Dynamic behaviour of embedded foundations", R77-33, MIT, 1977.
- [10] Kausel, E, "Soil-forced vibrations of circular foundations on layered media", Research Report, R74-11, MIT, 1974.
- [11] Varun, Assimaki, D, Gazetas, G, "A simplified model for lateral response of large diameter caisson foundations - Linear elastic formulation" *Soil Dynamics Earthquake Engineering*, Vol. 29 (2), pp. 268-291, 2009.
- [12] Panetsos, P, Ntotsios, E, Liokos, N, Papadimitriou, C, "Identification of dynamic models of Metsovo (Greece) Bridge using ambient vibration measurements", *ECCOMAS Thematic Conference on Computational Methods in Structural Dynamics and Earthquake Engineering (COMPDYN '09)*, Rhodes, 2009.
- [13] Bridgman, PW, "Dimensional Analysis", 2<sup>nd</sup> Edition, Yale University Press, New Haven, 1931.
- [14] DIN EN 459-1:2010-12, Building lime - Part 1: Definitions, specifications and conformity criteria.

## **TOPIC 6**

Soil-Structure Interaction  
Geotechnical Problems





## SOIL-STRUCTURE INTERACTION OF SEISMIC ISOLATED BRIDGES

Panos Tsopelas<sup>1</sup>, Spyridoula M. Papathanasiou<sup>2</sup>, Alper Ucak<sup>3</sup>,  
Evgenia Prapa<sup>4</sup>

<sup>1</sup> University of Thessaly, Volos, Dept. of Civil Engineering, Greece

<sup>2</sup> National Technical University of Athens, Dept. of Civil Engineering, Greece

<sup>3</sup> Catholic University of America, Dept. of Civil Engineering, Washington DC, USA

<sup>4</sup> University of Patras, Dept. of Civil Engineering, Greece

e-mail: tsopelas@uth.gr, sm.papathanasiou@gmail.com, 48ucak@cardinalmail.cua.edu,  
evprapa@gmail.com

**ABSTRACT:** The impact of the Soil-Structure Interaction (SSI) on seismic isolated bridges is investigated. Two stick models for the two seismic isolated bridges of interest are considered and equivalent models of the frequency-dependent impedance functions of the soil and foundation are introduced, with the new elements known as "gyromasses" being involved. Their importance is discussed.

**KEY WORDS:** Bridges; Earthquakes; Gyromass; Isolation; SSI effects

### 1 INTRODUCTION

Many design codes state that the SSI effects may be safely ignored during the design process of heavy structures. The myth of the SSI effects being safely neglected stems from the perception that the phenomenon makes the structural system more flexible when subjected to an earthquake and hence it reduces the overall seismic loading. The aforementioned statements have been examined before by many researchers, after considering quite representative models for soil, foundations and superstructures. Spyrakos[1] used simple linear elastic models and concluded that the soil-structure interaction effects make structures more flexible and less seismically affected. In another study, Mylonakis and Gazetas [2] used another simplified elastoplastic model for a bridge and its foundation, which was subjected to a set of actual acceleration time histories recorded on soft soil. Though the lengthening of the period made the structure more flexible, the SSI phenomenon played detrimental role on the seismic performance of the bridge. In fact, damage in structures associated with SSI effects has been proven or suspected in many cases in the past. For instance, the Mexico City earthquake of 1985 was particularly destructive to 10 to 12-story buildings (founded on soft clay) whose period increased from about 1.0 sec (for

the fixed-base structure) to nearly 2.0 seconds due to SSI [3]. Other evidence for a detrimental role of SSI has been presented by Meymand [4] and Celebi [5].

## 2 SOIL- FOUNDATION-BRIDGE SYSTEM MODELING

### 2.1 Bridge Systems

In this study the role of the soil-structure interaction is investigated on seismic isolated bridges. Two bridge structures are considered: the first (Bridge I) is representative of a typical highway overcrossing with a stiff short pier, while the second one (Bridge II) could be part of a long multispan bridge with flexible tall piers. Figure 1 depicts the geometric characteristics of each bridge. The dynamic impedances of the 5x5 pile groups for both bridges are presented later. The superstructures were chosen to be modeled with the help of the so-called “stick model”, as simple and approximate solutions are desired.

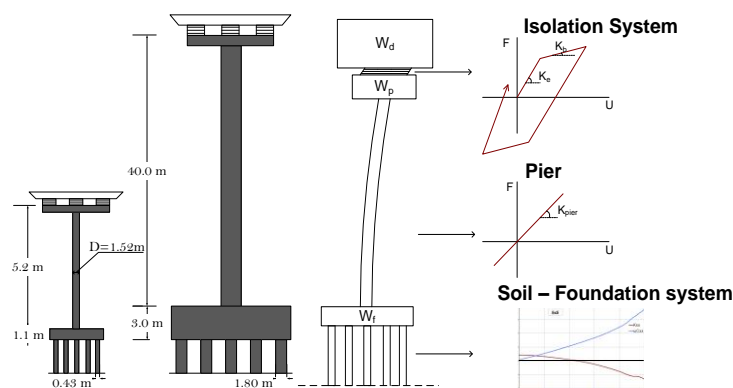


Figure 1. Geometrical representation of Bridge I and Bridge II.

The bridge models consist of a single linear pier (no yield considered), at the top of which the bilinear isolation system carries the deck's weight. At the bottom, the pier is monolithically connected to the pile group cap. The mass of the deck, the pier and the foundation are considered concentrated.

The isolation system is located between the deck and the pier and considered to behave as a bilinear hysteretic spring with smooth elastic to post yielding transition. Such a behavior could be representative of typical lead rubber bearings, as well as of sliding bearings with restoring force capability. Its nonlinear hysteretic behavior was modeled using Ozdemir's model [6]. The variables controlling the systems behavior are the yield strength ( $F_y$ ), the elastic stiffness ( $K_e$ ) and the post-yielding stiffness ( $K_b$ ). There are design philosophies which call for large  $K_b$  stiffness, in order to limit the displacement response and minimize potential permanent displacements, while others call for low so as to protect the bridge piers from large shear forces. The values used in this study

are presented in Table 1.

Table 1. Properties of the bridge models considered.

Bridge model	Bridge I	Bridge II
Deck seismic weight, $m_d$ ( Mg )	265	1440
Isolation system period, $T_b$ ( sec )	2	4.5
Isolation strength ratio ( $F_y / W_d$ )	0.12	0.04
Pier seismic weight, $m_p$ ( Mg )	38.5	620
Pier weight/ Deck weight	0.15	0.43
Pier height, $h$ ( m )	5.2	40
Pier elastic stiffness, $k_p$ ( kN/m )	1.24E5	1.09E5
Pier damping ratio, $\xi$	5%	5%
Foundation seismic weight, $m_f$ ( Mg )	84	4248
Foundation moment of inertia, $I_f$ ( Mg m <sup>2</sup> )	173	126200
Pile cup height, $H_f$ ( m )	1.1	3

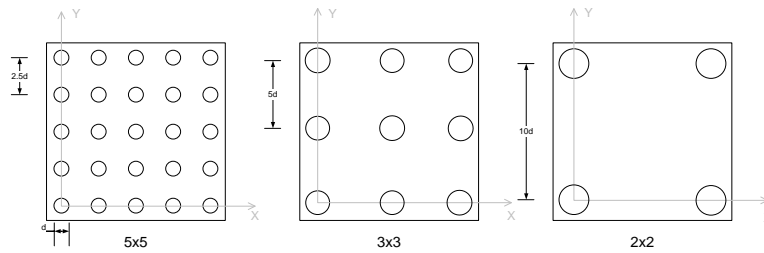


Figure 2. Geometry of 5x5 and equivalent 3x3 and 2x2 pile groups (for both bridges).

Table 2. Properties of the 3 equivalent pile groups of study.

Pile Group Label	Bridge I			Bridge II		
	5x5	3x3	2x2	5x5	3x3	2x2
Number of piles, $N$	25	9	4	25	9	4
Diameter, $d$ ( m )	0.43	0.7	1	1.8	3	4.5
Length, $L$ ( m )	21.5	21.5	21.5	21.5	21.5	21.5
Distance, $S$ , from pile to pile ( m )	1.08	3.5	10	4.5	9	18
Mass Density, $\rho_p$ ( kg/m <sup>3</sup> )	2500	2500	2500	2500	2500	2500
Modulus of Elasticity, $E_p$ ( GPa )	18.5	18.5	18.5	18.5	18.5	18.5
$L/d$	50	31	21	12	7	5

The pile caps are supported by a 5x5 pile group, with pile spacing ( $S$ ) 2.5 times the pile diameter ( $d$ ) (see Figure 2). The pile diameters were considered different for the two bridges, due to the different dimensions of the

superstructures ( $d_1 = 0.43$  m,  $d_2 = 1.80$  m). The models are also analyzed with the equivalent 2x2 and 3x3 pile groups, with the diameter of each pile in the groups to be adjusted in such a way as the total area of the pile groups ( $m^2$ ) to be the same in all three cases.

## 2.2 Dynamic impedances of pile groups

Under lateral loading, the impedances of the foundation are related to: bending ( $K_{xx}$ ), rocking ( $K_{rr}$ ) and coupled bending-rocking effects ( $K_{xr}$ ). It is preferable to express impedances as:

$$K_{xx} = K_{xx} + i\omega C_{xx} \quad (1)$$

where,  $K_{xx}$  is the “spring” coefficient modeling the soil and the foundation,  $C_{xx}$  is the “dashpot” coefficient,  $\omega$  is the frequency of the harmonic input (rad/sec) and  $i = (-1)^{1/2}$ . In this study, for the estimation of the dynamic impedances of pile groups, the boundary element program **PILES** [7] was utilized. This software uses the elastodynamic method which is based on a frequency domain solution of the closed-form Green’s function for both the soil and the piles. The soil used in this study is assumed to be a linear, homogeneous half-space, with mass density  $\rho_s = 1800$  kg/m<sup>3</sup>, shear wave velocity  $V_s = 110$  m/sec, damping ratio  $\xi = 10\%$  and Poisson’s ratio  $\nu = 0.40$  ( $E_p/E_s = 300$ ). The considered value for the shear wave velocity is rather low for typical elastic soil properties. However, it is chosen here in to represent inelastic the soil properties during strong soil motion.

Figure 3 presents the pile group dynamic stiffnesses  $K_{xx}$  for lateral and rocking motions as a function of dimensionless wave parameter  $a_0 = \omega d/V_s$ . For a range of excitation’s periods  $T = 0.25$ -2 secs and a mean value of shear wave velocity  $V_s = 100$  m/sec and diameter  $d = 1$  m, the  $a_0$  parameter takes the values between 0 and 0.25. This study focuses to values up to 1, which is considered as an upper bound for the values of interest. Same results are obtained for rocking impedance and for Bridge II.

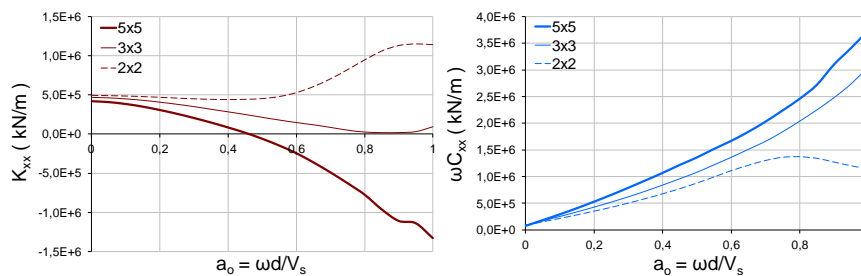


Figure 3. Comparison of the stiffnesses,  $K_{xx}(\omega)$  and dampings,  $\omega C_{xx}(\omega)$ , of 5x5, 3x3 and 2x2 pile groups, Bridge I.

The inherent nonlinear behavior of the isolation system, does not allow the use

of frequency domain analysis techniques to treat the bridge-foundation-soil system. In order to overcome this incompatibility, it is customary to introduce an approximation omitting the frequency dependency of the soil-foundation system considering that the springs and dashpots have constant, frequency-independent, values corresponding to the values that the impedances take for  $a_0=0$ . The simple **Voigt model**, consisting of a spring and a dashpot, connected to the foundation mass, is a simple option for modeling the impedance functions, under the aforementioned simplifications. For the capturing the frequency dependent behavior of the soil-foundation system, Saitoh [8] presented a new model consisting of a system of basic mechanical elements (springs and dashpots) together with an element named “gyromass” capable of representing frequency dependent impedance functions while eliminating the shortcomings of the models introduced by De Barros and Luco [9] and Wolf and Somani [10].

The **gyromass** is a mechanical element which has the same dimensions as mass. It is defined as a frequency-independent unit generating a reaction force due to the relative acceleration of the nodes between which the gyromass is placed (Figure 4), but adding no inertial forces. The model introduced by Saitoh containing springs, dashpots, and gyromasses to achieve better fitting of the dynamic impedances in the frequency domain is the **Type II model** (Figure 4). It consists of one *base system*, where the spring-dashpot unit and the gyromass are connected in parallel and two *core systems* where the spring-dashpot unit and the gyromass are connected in series.

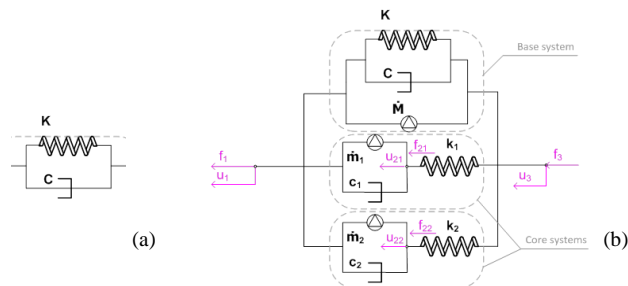


Figure 4. a) Voigt model and b) Saitoh's Type II model.

With the help of the equilibrium equation of Type II system and the mathematical method of Levenberg Marquadt for achieving an accurate curve fitting, the dynamic impedances are calibrated for each case of soil and foundation and both lateral and rocking components. The values  $K$ ,  $C$ ,  $\hat{M}$ ,  $\hat{m}_1$ ,  $c_1$ ,  $k_1$ ,  $\hat{m}_2$ ,  $c_2$  and  $k_2$  are now known and the most important, frequency-independent. The time history analysis is performed with 40 appropriate seismic excitations, categorized in two groups: the near fault set of motions [11] and the far field set of motions [12], [13].

### 3 ANALYSES RESULTS AND DISCUSSION

Non-linear time history analyses of the two bridge models (Bridge I and Bridge II) with different foundations (2x2, 3x3, and 5x5 pile groups) utilizing two different soil-structure interactions models (Voigt, Type II for translation and rotation) subjected to both Far Field (FF) and Near Fault (NF) sets of seismic excitations are performed. In the present study the results of the parametric analyses are presented in terms of ratios as isolation drift ratio (IDR) and pier shear ratio (PSR). Thus IDR and PSR are defined as follows:

$$\text{IDR} = \frac{\text{Isolation drift}_{\text{TYPE II}}}{\text{Isolation drift}_{\text{VOIGT}}} \quad (2)$$

$$\text{PSR} = \frac{\text{Pier shear}_{\text{TYPE II}}}{\text{Pier shear}_{\text{VOIGT}}} \quad (3)$$

Figure 5 summarizes the results of the largest discrepancies between the Voigt and Type II models, which correspond to Bridge II excited by the far field set of motions. The differences in the isolation drift range between -10% and +10% (-2% on the average over all motions). The PSR shows larger differences than IDR: -16% maximum and -10% on the average over all seismic motions. This indicates that using a more accurate SSI model (Type II) than the simple Voigt the shear forces in the pier are on the average 10% smaller over this FF motion set. PSR is sensitive to the pile groups with differences between them ranging from 2% (motion #3) to 10% (motion #9).

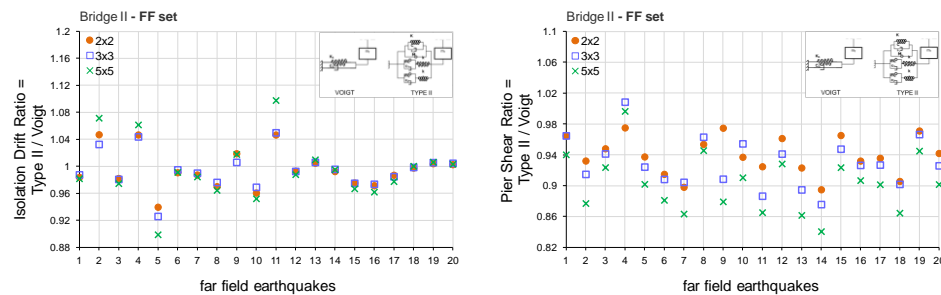


Figure 5. IDR and PSR for Bridge II,  $E_p/E_s=300$  (FF set).

#### 3.1 Effect of $E_p/E_s$

Considering the results presented in the previous figures, another case of analysis is introduced. The model of Bridge II, founded on a 2x2 pile group with pile diameter  $d=1.8$  m and  $S/d=10$ , resting on a much softer soil, so as the value of  $E_p/E_s$  to be 1000. The soil of interest now is a linear, homogeneous halfspace, with mass density  $\rho_s=1800$  kg/m<sup>3</sup>, shear wave velocity  $V_s=63$  m/sec, damping ratio  $\xi=10\%$  and Poisson's ratio  $\nu=0.40$ . This low value of the shear

wave velocity  $V_s$  represents the case of soil behaving well into the inelastic range where strong softening behavior in the soil is predominant.

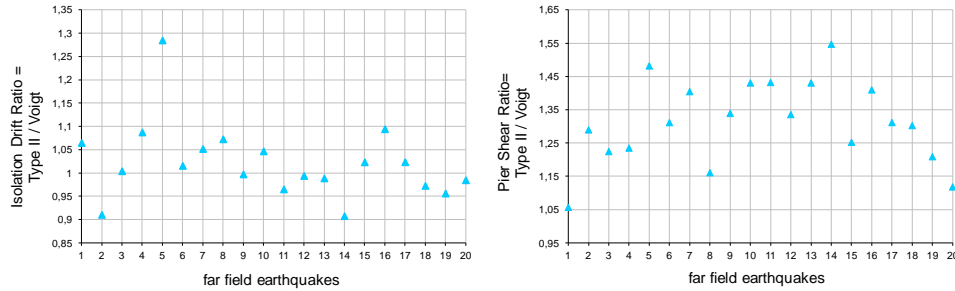


Figure 6. IDR and PSR for Bridge II,  $E_p/E_s=1000$  (FF set).

In Figure 6 the ISR and PSR appear to be much more sensitive to the model used for the SSI effects. There is one excitation where the isolation system reaches 28% larger displacements for Type II (motion #5), while for the rest of the motions the differences on the isolation drift are between +10% and -10%. There are also motions that develop up to 45% larger pier shear forces when Type II model is utilized.

#### 4 CONCLUSIONS

The most important conclusions of this study are:

- Generally, in cases of stiff foundation resting on linear homogeneous soil based on halfspace, the SSI can be satisfactorily modeled with simple Voigt systems. The discrepancies between the Type II (gyromasses) and Voigt models are up to 10-20% for both isolation displacements and pier shear forces.
- A system, with flexible pile group resting on a very soft soil can lead to great loss of accuracy in case Voigt models are used. The differences observed are up to 50% for both isolation displacements and pier shear forces, with the Type II model outweighing the Voigt. This case of such a small value of shear wave velocity could be a simplified approach of the nonlinear behavior of the soil, which is the actual one.

#### ACKNOWLEDGMENTS

The authors wish to extend their sincere thanks to Dr. A. Kaynia of the NGI for providing the software PILES used obtain the soil-foundation impedances of the pile groups considered in this study.

#### REFERENCES

- [1] Spyrakos, C. C., "Seismic Behavior of Bridge Piers Including Soil-Structure Interaction" in

- Journal of Computational Structures, 43(2), pp 373-384, 1992.
- [2] Mylonakis, G. G. Gazetas, A. Nikolaou and O. Michaelides, "The Role of Soil on the Collapse of 18 Piers of the Hanshin Expressway in the Kobe Earthquake" in 12WCEE, 2000.
  - [3] Resendiz, D. and Roesset J.M., "Soil-Structure Interaction in Mexico City During the 1985 Earthquake", The Mexico Earthquakes -1985, ASCE special publication, 1987.
  - [4] Meymand, P.J, "Shaking Table Scale Model Tests of Nonlinear Soil-Pile-Superstructure Interaction in Soft Clay", Ph.D. Dissertation, University of California, Berkeley, 1998.
  - [5] Celebi, M. (1998). "Turkish Earthquakes: Two Reports. Lessons from the Adana-Ceyhan Quake and the Dinar Aftershock" in EERI Newsletter, Vol. 32, No. 9, 8 pages.
  - [6] Ozdemir, H., "Nonlinear Transient Dynamic Analysis of Yielding Structures", PhD dissertation, University of California, Berkeley, 1976.
  - [7] Kaynia, A. and E. Kausel, "Dynamic Stiffness and Seismic Response of Pile Groups", Research Report, Publication Number: R82-03, Department of Civil Engineering, MIT, Cambridge, January 1982.
  - [8] Saitoh, M., "Simple Model of Frequency-Dependent Impedance Functions in Soil-Structure Interaction Using Frequency-Independent Elements" in Journal of Engineering Mechanics, ASCE, pp. 1101-1114, October 2007.
  - [9] De Barros, F.C. P., and Luco, J.E., "Discrete Models for Vertical Vibrations of Surface and Embedded Foundations" in Earthquake Engineering and Structural Dynamics Journal, 19 (2), pp.289-303, 1990.
  - [10] Wolf, J.P., and Somani, D.R., "Approximate Dynamic Model of Embedded Foundation in Time Domain" in Earthquake Engineering and Structural Dynamics Journal, 14 (5), pp.683-703, 1986.
  - [11] Somerville, P., Smith, N., Punyamurthula, S., and Sun, J., "Development of Ground Motion Time Histories for Phase 2 of the FEMA/SAC Steel Project", Rep. No. SAC/BD-97/04, SAC Joint Venture, Sacramento, Calif, 1997.
  - [12] Whittaker, A., Constantinou, M. C., and Tsopelas, P., "Displacement Estimates for Performance-Based Seismic Design" in Journal of Structural Engineering, 124(8), pp 905-912, 1998.
  - [13] Constantinou, M. C., and Quarshie, J. K., "Response Modification Factors for Seismically Isolated Bridges", Rep. No. MCEER-98-0014, Multidisciplinary Center for Earthquake Engineering Research, Buffalo, N.Y., 1998.



## PERFORMANCE-BASED DESIGN OF BRIDGE FOUNDATION ON PARTIALLY IMPROVED LIQUEFIABLE SOIL

Dimitris Karamitros<sup>1</sup>, George Bouckovalas<sup>2</sup>  
and Konstantinos Andrianopoulos<sup>3</sup>

<sup>1</sup> University of Bristol, Dept. of Civil Engineering, U.K.

<sup>2,3</sup> National Technical University of Athens, Dept. of Civil Engineering, Greece  
e-mail: d.karamitros@bristol.ac.uk, gbouck@central.ntua.gr, kandrian@tee.gr

**ABSTRACT:** This paper employs a sophisticated numerical methodology, in order to investigate whether a typical highway bridge pier may be founded on liquefiable soil, through a shallow footing, instead of the conventional pile foundations, through the application of ground improvement measures only in a small zone, in the upper part of the liquefiable layer.

**KEY WORDS:** Ground improvement; Liquefaction; Numerical analyses; Settlements; Shallow foundation.

### 1 INTRODUCTION

According to currently applicable seismic codes, the foundation of a typical highway bridge pier on liquefiable soil would require the use of a pile group, in order to transfer the loads to underlying layers not susceptible to liquefaction, as well as ground improvement measures, in order to mitigate liquefaction-induced large bending moments and shear forces in the piles. Still, recent studies (e.g. [1,2,3]) have indicated that the presence of a sufficiently thick and shear resistant non-liquefiable clay crust between the foundation and the liquefiable subsoil, could potentially ensure a viable performance-based design. In this case, it is of cornerstone importance to be able to estimate:

- the post-shaking bearing capacity of the foundation, as well as the relevant degraded static factor of safety  $FS_{deg}$ , and
  - the accumulating dynamic settlements  $\rho_{dyn}$ ,
- and to ensure that they both remain within the allowable limits.

Following a similar logic, it is examined, herein, whether the above performance-based design principles may also be applied to cases where a natural clay crust does not exist, but it is artificially formed, as a zone of improved soil. A typical highway bridge foundation is analyzed for this purpose, resting on top of a relatively thick liquefiable sand layer. The beneficial role of the clay crust is played by an artificially created non-

liquefiable zone, formed by the application of gravel piles-drains within the upper part of the liquefiable sand layer. A sophisticated numerical methodology is utilized for the simulation of the combined foundation-soil response and parametric analyses are performed, in order to determine the required plan size and depth of the zone where the liquefaction mitigation measures should be applied.

## 2 OUTLINE OF CASE STUDY

The soil profile and the characteristics of the foundation considered herein, correspond to a typical bridge pier foundation of the Egnatia Highway, in northern Greece. As shown in Figure 1, the examined foundation supports the self-weight of a 12.5m high pier, as well as the self-weight and applied loads of two simply supported bridge decks, each featuring a length of 45m. The corresponding vertical loads are presented in Figure 1, together with the applied horizontal force and overturning moment, which were computed through a conventional pseudo-static analysis of the superstructure, for a maximum acceleration of  $a_{\max}=0.36g$ .

The soil profile characteristics are also shown in Figure 1, in terms of soil classification, SPT number  $N_{\text{SPT}}$ , and factor of safety against liquefaction  $F_{\text{SL}}$ , computed according to Youd et al [4]. Observe that the foundation subsoil mainly consists of loose silty sands, down to a depth of 30m, where the bedrock is encountered. In the upper 18m of the silty sand layer,  $F_{\text{SL}}$  remains well below unity, indicating high liquefaction susceptibility. Note that the bridge pier is located within a river basin where the water table is above the ground surface.

The actual foundation for the above bridge and soil profile was conventionally designed, according to the currently available seismic codes, and consisted of a combination of a group of bored piles, as well as ground improvement of the entire liquefiable sand layer through stone columns. In case that no ground improvement measures were applied, subsoil liquefaction would result in a significant degradation of the piles shaft resistance, while excessive bending moments and shear forces would also develop. Therefore, foundation safety requirements would result in larger pile diameters, pile lengths and reinforcement, considerably increasing the overall cost of the foundation.

The stone-columns used with the conventional design to mitigate liquefaction, featured a diameter of 0.80m and they were placed on a rectangular grid, at axial distances of 2.00m, as shown in Figure 2. The replacement ratio of  $a_s=0.125$  and the distance ratio of  $D/S=0.8/(2.0/1.77)$  were selected by taking into account both the compaction of the foundation subsoil and the associated increase of the SPT resistance, as well as the beneficial effect of drainage [5]. The proposed ground improvement measures successfully increase the factor of safety against liquefaction to  $F_{\text{SL}}>1$ , while it was estimated that the corresponding excess pore pressure ratios are expected to

remain below  $r_u=0.4$ .

Taking into account the high costs of the conventional construction, the above case-study is re-examined, herein, in order to evaluate the feasibility of a performance-based design of the pier foundation using the concept of partial with depth improvement of the liquefiable subsoil. Hence, a shallow footing was designed for the bridge pier, as shown in Figure 2. More specifically, a  $9\text{m}\times 17\text{m}$  footing, resting on top of a 1m thick gravel layer, was found sufficient to undertake the applied vertical, horizontal forces and overturning moments, considering a friction angle of  $\phi=38^\circ$  for the foundation subsoil. This is the friction angle corresponding to the improved soil, estimated by taking into account the initial soil properties, the effects of sand densification during the construction of the stone columns, as well as the gravel properties and the soil replacement ratio ( $a_s=0.125$ ). It is important to note that the design loads that were considered conservatively ignore the acceleration de-amplification that is expected to occur at the ground surface, due to the shear strength degradation of the liquefied subsoil.

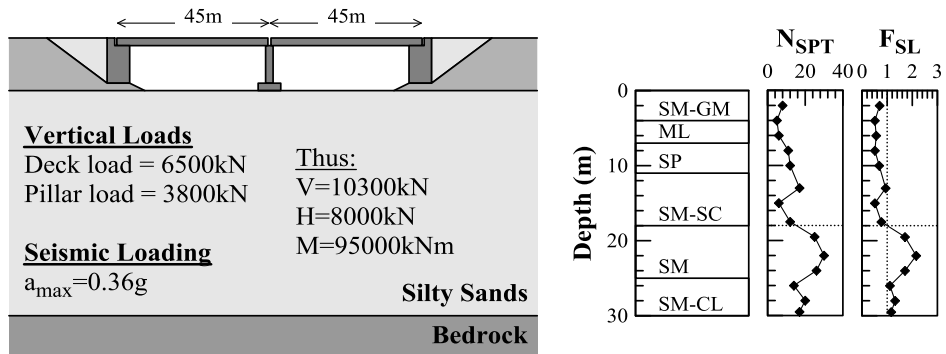


Figure 1. Schematic of the examined highway bridge foundation and soil profile characteristics.

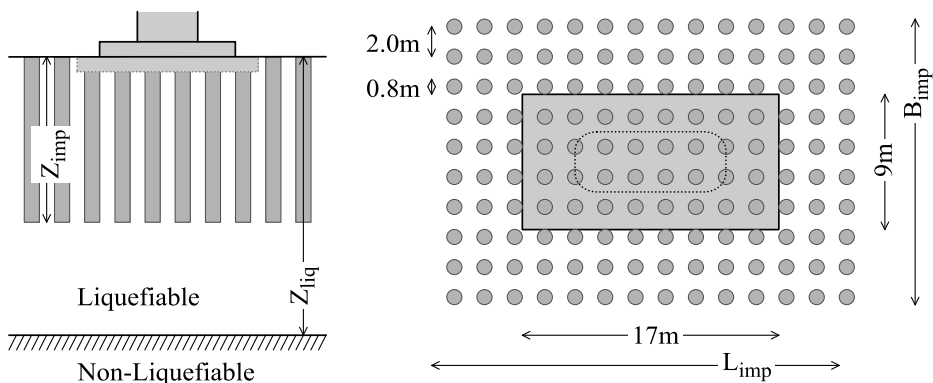


Figure 2. Cross section and plan view of the examined foundation and the proposed grid of stone columns, used for liquefaction mitigation.

### 3 NUMERICAL SIMULATION

#### 3.1 Numerical Methodology

The liquefaction performance of the examined foundation was investigated through 3-d fully-coupled effective-stress dynamic analyses, using the numerical methodology developed by Andrianopoulos [6,7]. This methodology is based on the implementation of the NTUA-SAND bounding-surface critical-state constitutive model, into the commercial finite difference code FLAC3d, and its accuracy has been verified against the results of various centrifuge experiments, including the tests performed by Liu & Dobry [8], which refer to the problem examined herein.

The above described algorithm was applied to perform twelve (12) parametric analyses, considering different thicknesses  $Z_{imp}$  and widths  $B_{imp}$  of the improved zone underneath the foundation (see Figure 2). In each case, the length  $L_{imp}$  of the improved zone was taken as equal to  $L_{imp} = L + (B_{imp} - B)$  with  $L$  being the length of the foundation.

The model configuration considered for the analyses is presented in Figure 3a. Note that only the upper 18m of the sand layer were modeled, as the lower part was not found susceptible to liquefaction and is therefore expected to have a significantly higher shear wave velocity, essentially behaving as the seismic bedrock. The NTUA-SAND model was used to model the behavior of the liquefiable soil, while the Mohr-Coulomb model was used for the improved ground, considering a friction angle of  $\phi_{imp}=38^\circ$ . The water table was assumed to be located at 1m above the ground surface, while the simulated footing was rigid and massless, with an average bearing pressure of 115kPa.

Each numerical analysis was performed in three (3) steps:

- Initial, pre-seismic, static loading, under drained conditions (part a-b of the load-settlement curve of Figure 3b).
- Dynamic loading (part b-c of the load-settlement curve), consisting of  $N=7$  sinusoidal cycles, of amplitude  $a_{eff}=0.24g$  and a period equal to  $T=0.25sec$ , applied at the model's base. The dynamic analysis was fully-coupled, thus accounting for drainage through the stone columns.
- Post-seismic static loading to failure under drained conditions (part c-d of the load-settlement curve), with the effective stresses and excess pore pressures attained at the end of shaking.

#### 3.2 Typical Results

Aiming to highlight the basic characteristics of the foundation's liquefaction performance, Figure 4 presents typical results from the performed numerical analyses, in terms of the acceleration time-histories at the base of the model and at the soil surface, the foundation settlements  $\rho$ , as well as the excess pore pressure ratios  $r_u$ , developing at different depths below the footing's axis.

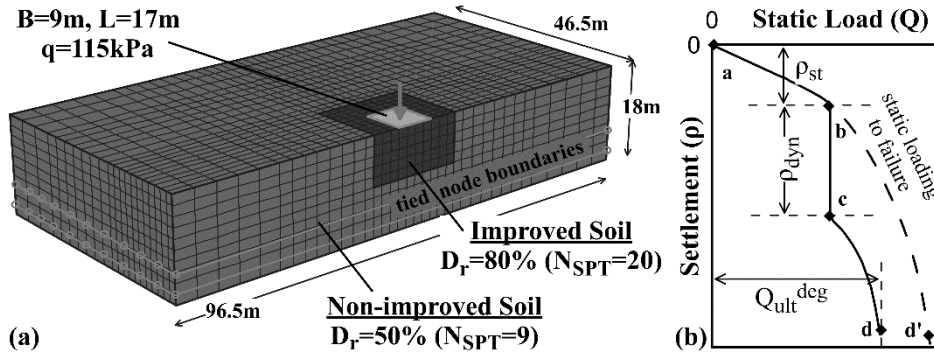


Figure 3. (a) Numerical model used for the parametric analyses and (b) load-settlement curve.

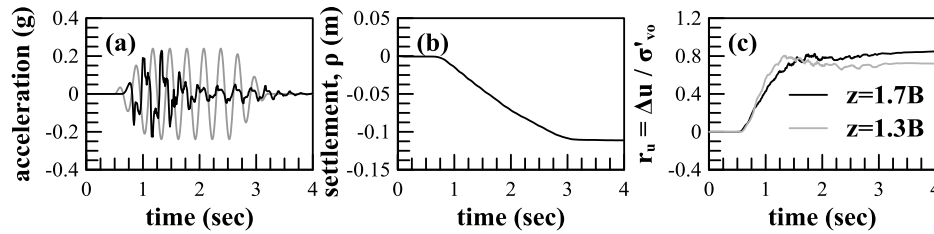


Figure 4. Typical results from the numerical analyses: Time-histories of (a) acceleration at the base of the model and at the soil surface, (b) dynamic settlements of the foundation and (c) excess pore pressure ratios at depths  $Z=1.3B$  and  $1.7B$  underneath the footing's axis.

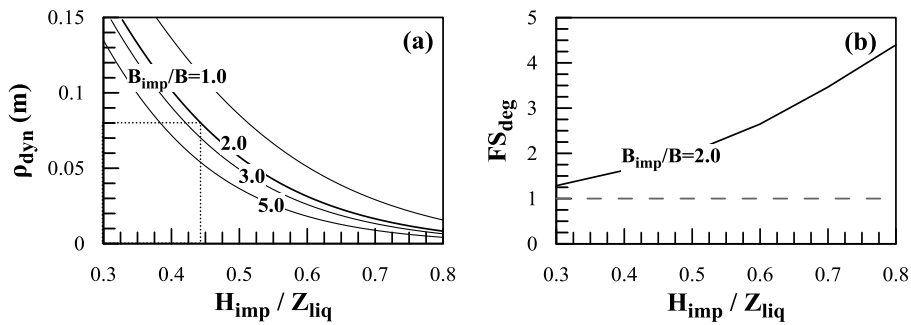


Figure 5. Variation of (a) the dynamic settlements  $\rho_{dyn}$  and (b) the post-shaking degraded factor of safety  $FS_{deg}$  of the foundation, with the increasing normalized thickness  $Z_{imp}/Z_{liq}$  of the improved zone.

First of all, it may be observed that, in accordance with numerical and experimental evidence (e.g. [1,8,9,10]), foundation settlements mostly develop during shaking, with only a small portion developing due to the post-shaking excess-pore pressure dissipation. It may be therefore confirmed that they are mainly associated to inertia-induced failure of the foundation subsoil and not to volume densification. This implies that increasing the size of the improved zone

would reduce the shear stresses applied by the foundation to the liquefiable subsoil, thus decreasing the earthquake-induced foundation settlements.

Furthermore, excess pore pressures in the region below the foundation do not exceed a maximum value of  $r_u=0.8$ , thus remaining lower than the ones developing in the free-field, where complete liquefaction occurs ( $r_u=1$ ). This acts as a natural restraining mechanism to foundation settlement accumulation and bearing capacity degradation, thus allowing performance-based design criteria to be fulfilled without the need to apply soil improvement measures over the whole liquefiable foundation subsoil.

Finally, Figure 4 indicates that the accelerations at the ground surface are significantly de-amplified, as compared to the excitation applied at the model's base. This effect is attributed to the failure of the foundation subsoil, as well as to the liquefaction-induced soil softening and the associated increase of the soil column's eigen-period. Therefore, it becomes evident that allowing excess pore pressures to develop in a region underneath the foundation may create a zone of "natural seismic isolation", which acts beneficially for the dynamic performance of the superstructure.

#### 4 RESULTS OF PARAMETRIC ANALYSES

The results of the parametric analyses that were performed in this study are summarized in Figure 5, in terms of the variation, with the normalized thickness of the improved zone  $Z_{imp}/Z_{liq}$ , of the dynamic settlements  $\rho_{dyn}$  of the foundation, as well as of the post-shaking degraded factor of safety  $FS_{deg}$ , for the various examined normalized widths  $B_{imp}/B$  of the improved zone.

It may be readily observed that, using  $B_{imp}/B=2.0$ , the post-shaking degraded factor of safety  $FS_{deg}$  remains larger than 1.25 for the whole range of examined thicknesses of the improved zone. Note that this factor of safety refers to a rather short-living threat, which will no longer exist when earthquake-induced excess pore pressures have dissipated. Therefore, its design value may be well below the conventional values for static loads, and close to unity. As a result,  $FS_{deg}$  is not the key performance-based design criterion, in the case examined herein. Nevertheless, this conclusion should not be readily generalized, since, for weaker applied excitations, dynamic settlements are expected to be lower than in the present case-study, thus the foundation safety may be primarily controlled by its post-shaking degraded bearing capacity.

Focusing on the accumulating dynamic settlements, they are drastically decreased by increasing the thickness of the improved non-liquefiable zone. Nevertheless, an allowable value should be defined, in order to proceed to the selection of the minimum required thickness of the non-liquefiable zone. Numerous performance-based design criteria have been proposed and may be found in the literature, for this purpose (e.g. [11,12,13,14,15]). Taking into account that subsoil liquefaction is an extreme loading case, the criterion of

$\rho < 10\text{cm}$  proposed by Grover [11], Bozozuk [12] and Walhs [13] is conservatively adopted herein. According to this criterion, damage will occur on the superstructure, though it will remain within tolerable levels, resulting in minor driving disturbance along the bridge.

According to the initial static design of the foundation, pre-shaking settlements are expected to remain below  $\rho_{st}=2\text{cm}$ . Therefore, an additional allowable dynamic settlement of  $\rho_{dyn}=8\text{cm}$  is considered, herein, resulting in a required normalized thickness of the improved zone, equal to  $Z_{imp}/Z_{liq}=0.45$  (i.e. absolute thickness of the improved zone  $Z_{imp}=8\text{m}$ ).

## 5 CONCLUDING REMARKS

The conventional design practice for geotechnical structures in a liquefaction regime may result in highly overpriced foundation systems, which may include ground improvement measures, drainage and use of pile foundations. A similar case-study of a typical highway bridge pier was examined herein, where a combination of all three of the above techniques was used in the actual construction site. Aiming to provide an alternative, cost-effective solution, a sophisticated numerical methodology was utilized and the performance-based design feasibility of a surface footing resting on partially (with depth) improved foundation subsoil was examined.

The numerical analyses indicated that the application of liquefaction mitigation measures at an area wider than  $B_{imp} > 2.0B$  has only minor effects to the liquefaction performance of the foundation, while, focusing on the case where  $B_{imp}/B=2.0$ , it was shown that increasing the thickness of the improved zone results in a significant reduction of the expected dynamic settlements, while also increasing the post-shaking degraded bearing capacity. As a result, a feasible solution was eventually obtained, that may ensure foundation safety and minimize operational disturbance, at a fraction of the initial cost of the conventionally designed foundation.

Finally, it is stressed that allowing excess pore pressures to develop in a region underneath the foundation essentially creates a zone of natural seismic isolation, which significantly de-amplifies the accelerations reaching the ground surface, and may thus prove beneficial for the dynamic performance of the superstructure, as compared to the case where liquefaction mitigation measures are applied to the whole thickness of the liquefiable layer.

## ACKNOWLEDGEMENTS

This research has been co-financed by the European Union (European Social Fund – ESF) and Greek national funds through the Operational Program "Education and Lifelong Learning" of the National Strategic Reference Framework (NSRF) – Research Funding Program: THALES. Investing in knowledge society through the European Social Fund.

## REFERENCES

- [1] Karamitros D.K., Bouckovalas G.D. & Chaloulos Y.K. (2013a): "Insight into the Seismic Liquefaction Performance of Shallow Foundations", *ASCE Journal of Geotechnical and Geoenvironmental Engineering*, vol. 139(4), pp. 599-607.
- [2] Karamitros D.K., Bouckovalas G.D., Chaloulos Y.K. & Andrianopoulos K.I. (2013b): "Numerical analysis of liquefaction-induced bearing capacity degradation of shallow foundations on a two-layered soil profile", *Soil Dynamics and Earthquake Engineering*, vol. 44, pp. 99-101.
- [3] Karamitros D.K., Bouckovalas G.D. & Chaloulos Y.K. (2013c): "Seismic settlements of shallow foundations on liquefiable soil with a clay crust", *Soil Dynamics and Earthquake Engineering*, vol. 46, pp. 64-76.
- [4] Youd, T.L., Idriss, I.M. et al (2001): "Liquefaction resistance of soils: Summary report from the 1996 NCEER and 1998 NCEER/NSF workshops on evaluation of liquefaction resistance of soils", *Journal of Geotechnical and Geoenvironmental Engineering*, 127 (10), pp. 817-833.
- [5] Seed, H.B. & Booker, J.R. (1977): "Stabilization of potentially liquefiable sand deposits", *ASCE Journal of the Geotechnical Engineering Division*, 103 (7), pp. 757-768.
- [6] Andrianopoulos K.I., Papadimitriou A. G., Bouckovalas G. D. (2010a): "Bounding surface plasticity model for the seismic liquefaction analysis of geostructures", *Soil Dynamics and Earthquake Engineering*. 30(10): 895-911.
- [7] Andrianopoulos K. I., Papadimitriou A. G., Bouckovalas G.D. (2010b): "Explicit integration of bounding surface model for the analysis of earthquake soil liquefaction", *International Journal for Numerical and Analytical Methods in Geomechanics*, 34(15), pp. 1541-1650.
- [8] Liu, L., Dobry, R. (1997): "Seismic response of shallow foundation on liquefiable sand", *Journal of Geotechnical and Geoenvironmental Engineering*, 123 (6), pp. 557-566.
- [9] Adalier, K., Elgamal, A., Meneses, J., Baez, J.I. (2003): "Stone columns as liquefaction countermeasure in non-plastic silty soils", *Soil Dynamics and Earthquake Engineering*, 23 (7), pp. 571-584.
- [10] Coelho, P.A.L.F., Haigh, S.K., Madabhushi, S.P.G. (2004): "Centrifuge modelling of the effects of earthquake-induced liquefaction on bridge foundations", *Proc. of the 11th ICSDEE, University of California, Berkeley*.
- [11] Grover, R.A. (1978): "Movements of bridge abutments and settlements of approach pavements in Ohio", *Transportation Research Record*, 678, pp. 12-17.
- [12] Bozozuk, M. (1978): "Bridge foundations move", *Transportation Research Record*, 678, pp. 17-21.
- [13] Walkinshaw (1978): "Survey of bridge movements in the Western United States", *Transportation Research Record*, 678, pp. 6-11.
- [14] Wahls, H.E. (1986): "ISSMFE Technical subcommittee on allowable deformations of buildings and damages", *General report*, 14 pp, 4 tables & 7 figs.
- [15] Moulton, L.K. (1986): "Tolerable movement criteria for highway bridges", 86 pp. Report No. FHWA-TS-85-228, Federal Highway Administration, Washington D.C.



IBSBI 2014, October 16-18, 2014, Athens, Greece

## **DEVELOPMENT OF FOUNDATION SPRINGS AND SOIL STRUCTURE INTERACTION EVALUATION FOR THE THIRD BOSPHORUS BRIDGE**

Wei-Yu Chen<sup>1</sup>, Amalia Giannakou<sup>2</sup> and Jacob Chacko<sup>3</sup>

<sup>1</sup> Fugro Consultants, Oakland, California, USA

<sup>2,3</sup> Fugro Sial, Istanbul, Turkey

e-mail: wychen@fugro.com, agiannakou@fugro.com, jchacko@fugro.com

**ABSTRACT:** The Third Bosphorus Bridge (about 1.4 km) will cross the Bosphorus straight. Considering the significant change in topography, 2-D site response analyses and 3-D SSI evaluations were conducted to develop input motions. Foundation springs were developed by 3-D numerical models as input for dynamic bridge evaluations.

**KEY WORDS:** Bridge; Kinematic Motion; Site Response; Soil-Structure Interaction.

### **INTRODUCTION**

The proposed Third Bosphorus Bridge will cross the Bosphorus straight connecting the European and Asian Continents. The bridge is designed as a single span suspension bridge, oriented roughly northwest-southeast, and spans a distance of about 1.4 kilometers. As shown on Figure 1, the main span will be supported by two land-founded towers on the European and Asian sides. The backspans are about 375 meters long with the anchorages located at the top of the shoreline cliff.

Fugro is retained to provide services to geological, seismological, and geotechnical evaluations. Integrated site investigations are conducted to provide data for site characterization and foundation design. Considering the active tectonic environment of the project, soil structure interaction (SSI) analyses are performed to evaluate the dynamic performance of the bridge. Foundation stiffness parameters (i.e. foundation springs) and kinematic motions are developed by Fugro using 2-D and 3-D numerical models.

This paper presents a general overview for the development of the bridge foundation springs and kinematic motions which are used in subsequent global structural dynamic analyses. Different bridge foundations (i.e., tower, approach and anchorage), rock/foundation interface and subsurface rock properties are

explicitly modeled such that no “simplification” is considered. The methodologies to develop foundation springs and kinematic motions are similar at both Asian and European sides, therefore only Asian side foundations are presented in this paper.

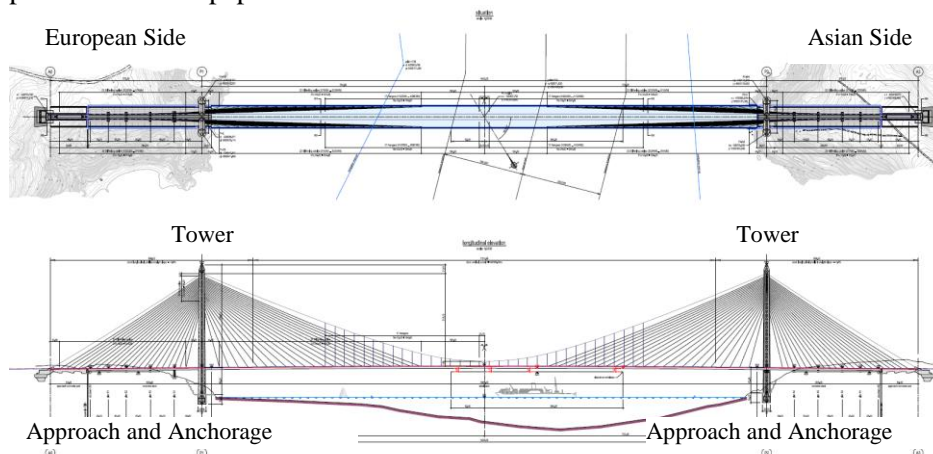


Figure 1. Third Bosphorus Bridge Alignment and Foundation Plan.

### PROJECT SITE CONDITION (ASIAN SIDE)

At the Asian side a northwest facing steep slope is present at the Tower location that rises from water to a maximum elevation of about 80 meters with an average inclination of approximately 25 degrees. Bathymetry data collected in the nearshore area indicate that the slope continues to dip into water but with a smaller dip angle than on the onshore part.

Excavations are conducted to create platforms for the Towers. Behind the Towers, the approaches are excavated directly into rock followed by the anchorages which are also excavated into rock (Figure 1). The Tower location on the Asian side is covered by Agglomerate which is moderately strong to strong, and generally slightly weathered to fresh. The Approach Part and Anchorage are underlain by the Agglomerate/weathered unit which is typically extremely weak to weak, and completely to moderately weathered. Beneath the Agglomerate/weathered unit, the underlying rocks appear to primarily consist of Agglomerate. A shear zone with maximum apparent thickness of 8.4m is observed around Anchorage location and modeled in subsequent analyses.

### 2-D SITE RESPONSE ANALYSES

It has been recognized that topography can significantly affect the amplitude and frequency characteristics of ground motion during seismic events. Observations from recent earthquakes (San Fernando, USA 1971; Friuli, Italy 1976; Irpinia, Italy 1980; Athens, Greece 1999; and Bingöl, Turkey 2003)

indicated that structures located at the tops of hills, ridges and canyons tend to suffer more intensive damage than those located at the base. Studies on topography effects on ground motions verify the macroseismic observations by predicting systematic amplification of seismic motion over convex topographies such as hills and ridges, de-amplification over concave topographic features such as canyons and hill toe, and complex amplification and deamplification patterns on hill slopes (Assimaki et al, 2005[1]).

### Finite Difference Models

Two-dimensional (2-D) finite difference analyses were performed to evaluate the topographic effects on the horizontal ground motions. Due to the presence of good quality rock across the site, elastic analyses were performed to evaluate the diffraction potential of the slope geometry and the frequency-dependence of topographic amplifications. 2-D site response analyses were performed using the finite difference program FLAC (Itasca, 2011[2]). FLAC is an explicit finite difference program for engineering mechanics computations, which operates in the time domain. The finite difference model for the site response analyses is illustrated on Figure 2.

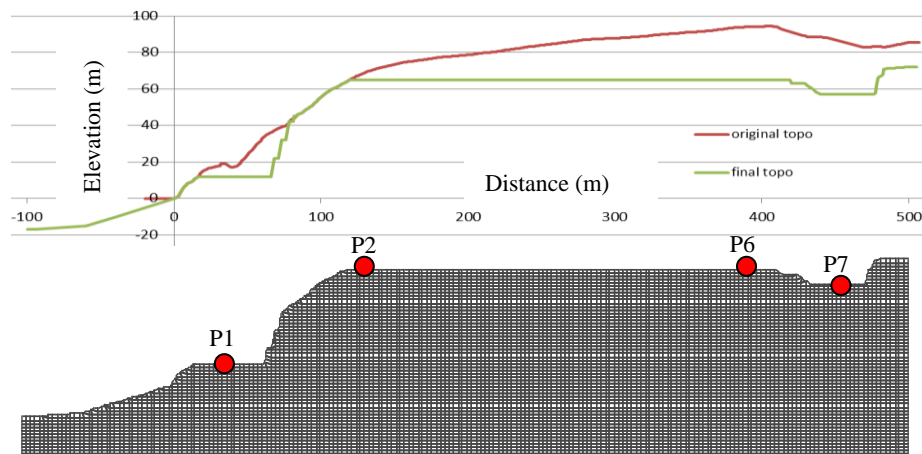


Figure 2. Modeled Geometry and Finite Difference Mesh - Asian Side

### Results

Site response evaluations were conducted for two project design return periods (i.e., 475- and 2,475-year) with seven sets of ground motions for each return period. Acceleration time histories were obtained at selected locations as shown on Figure 2: the tower (P1), the first pier (P2), the approach part (P6) and the anchorage (P7). Figure 3 presents the horizontal acceleration response spectra for the 2,475-year event at the Tower, Pier 1, Approach Part and Anchorage locations at the Asian side. Superimposed on these figures is the

response spectrum of the outcrop motion from the PSHA analyses. As shown on these figures, the presence of the steep slope amplifies the design ground motion in the high frequency range (i.e., up to 0.4 seconds) at the foundations located near the slope crest. At the Tower foundation which is located at the base of the slope the design motions are de-amplified up to structural periods of about 0.6 second. Similar trends are also observed for the 475-year event.

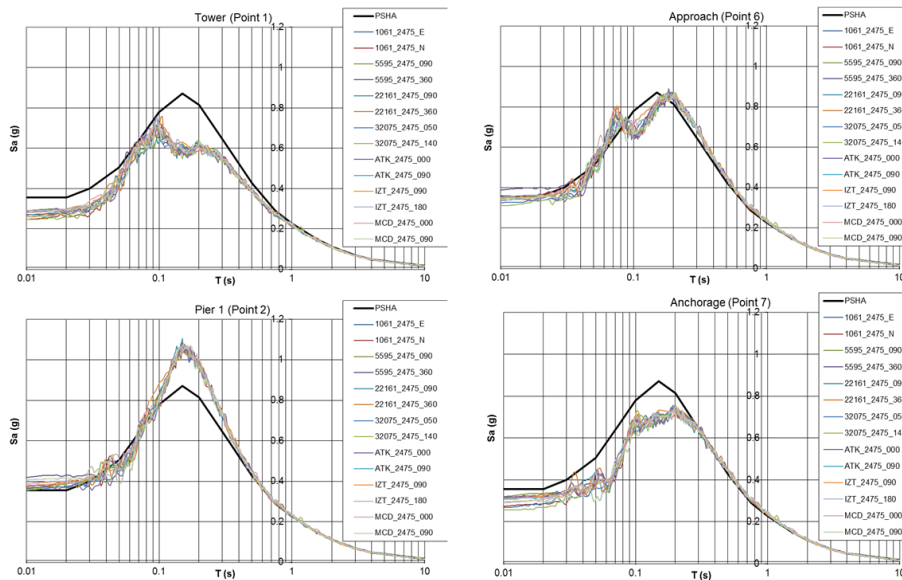


Figure 3. Topography effects in 5% damped horizontal acceleration Response spectra at different foundation locations (Asian Side, 2,475-year event)

### 3-D DYNAMIC SOIL-STRUCTURE INTERACTION

The presence of the foundation tends to “resist” and, hence, modify soil deformations generated by the passage of propagating seismic waves. As a result the motion at the foundation (also called kinematic motion) differs from the free-field ground motion presented in the previous section. This effect is mainly observed in cases where the stiffness contrast between foundation and surrounding soil is large, and especially in the case of embedded foundations.

Three-dimensional (3-D) finite difference models were developed at the Tower, Approach Part and Anchorage locations including the foundation and the surrounding rock. Superstructures (i.e., bridge towers) were not included in these analyses. The ground motions recorded at the top of the foundations were compared with the ground motions developed from 2-D site response analyses in order to evaluate the effects of the 3-D topography and the presence of the foundation.

### 3-D Finite Difference Models

The 3-D dynamic Soil-Structure Interaction (SSI) evaluations were performed using the computer program FLAC3D (Itasca 2011[3]). Rock was modeled as elastic due to the small strains induced by the wave propagation. Rock properties similar to what was used in the 2-D site response analyses were also used in 3-D analyses. The foundation was also modeled as elastic with typical reinforced concrete properties.

The boundary conditions at the edges of the model were modeled as “free field” to allow for transmitting of scattering motions generated by the foundation. The target motions (i.e. the PSHA compatible ground motions) were used as “outcrop” input motion at the base of the model. Figure 4 presents the 3-D models of the Tower, Approach Part and Anchorage for Asian side bridge foundations.

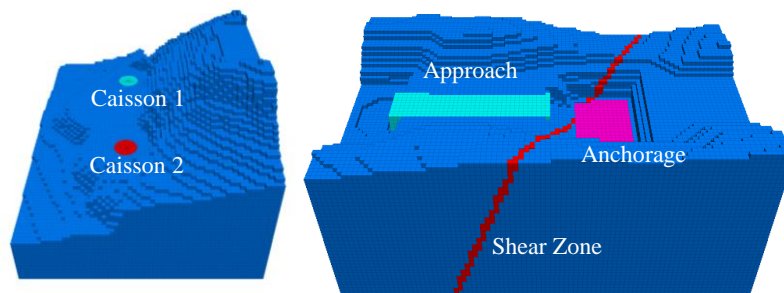


Figure 4. FLAC3D Finite Difference Models of Tower, Approach Part and Anchorage Foundations (Asian Side)

### Results

Figure 5 presents the horizontal acceleration response spectra in the longitudinal bridge direction recorded at the Tower, Approach and Anchorage foundations from 3-D SSI analyses. The results from 2-D site response analyses are also plotted. It is observed that effects of the full 3-D topography and the presence of the foundation in the 3-D analyses result in a de-amplification of spectral accelerations in the high frequency range (i.e., for periods less than 0.3 seconds).

Given that the response of the bridge structures is controlled primarily by spectral accelerations at longer periods (i.e., greater than 0.5 to 1 second), it was concluded that ground motions developed with 2-D site response analyses can be used and will result a reasonable and conservative design.

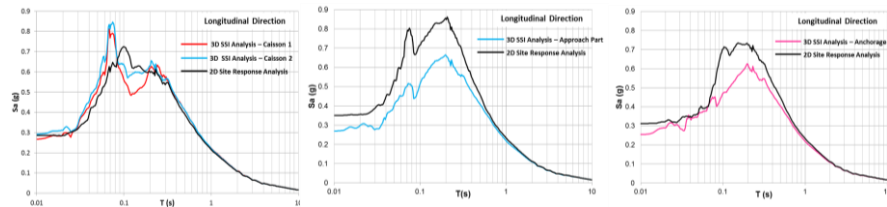


Figure 5. Comparison of Ground Motions Developed by 2-D Site Response and 3-D SSI Analyses (Asian Side)

## DEVELOPMENT OF FOUNDATION SPRINGS

Foundation springs are developed for two 20-meter-deep caissons at the Tower location (Figure 6a), a concrete block with shear keys where the deck cables are anchored (approach part) and a concrete block where the main suspension cable is anchored (anchorage). Also shown on Figure 6 are the locations of force/moment application to develop springs.

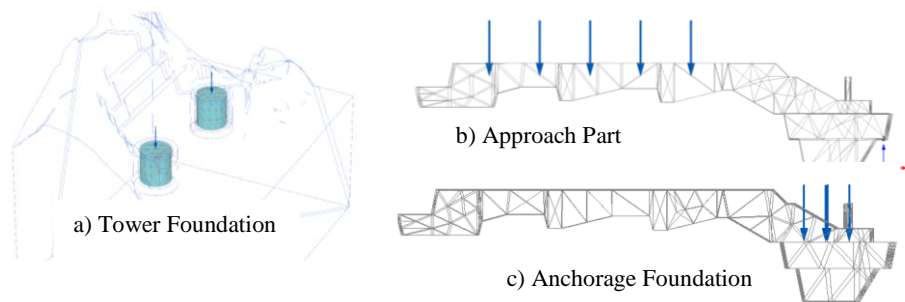


Figure 6. Illustration of Bridge Foundation and Locations of Force/Moment Applications: a) Tower; b) Approach Part; c) Anchorage.

For this project, foundation springs are obtained from 3-D finite element analyses using the computer program Plaxis3D (PLAXIS 2011 [4]). The springs are developed by applying loads and moments at the foundation in all six directions and evaluating the foundation deformation due to the applied loads/moments. The analyses performed modeled the nonlinear behavior of the rock mass, the interface between concrete and rock as well as the presence of shear zones at the Asian Side Anchorage.

Consideration is given to the potential influence of radiation damping and kinematic soil structure interaction effects. The radiation damping is not expected to be significant since the site period is significantly smaller than the period of the bridge structure due to the presence of rock. Additionally, frequency independent dashpots generally de-amplify the structural system's response, therefore it is not uncommon to neglect radiation damping altogether (Makris et al. 1995 [5]; Jeremic et al. 2004 [6]; Ciampoli and Pinto 1995 [7];

Bielak et al. 2003 [8]). For the final foundation springs, no dashpots are used to represent the foundation-soil behavior in the structural dynamic analyses of the bridge.

The deformation patterns of the anchorage foundation and the force/displacement relationships subjected to vertical forces (i.e., downward and upward) are illustrated on Figures 7. Translational springs in the horizontal directions (i.e., parallel and perpendicular with respect to the bridge axis) as well as rotational springs are developed with the same methodology.

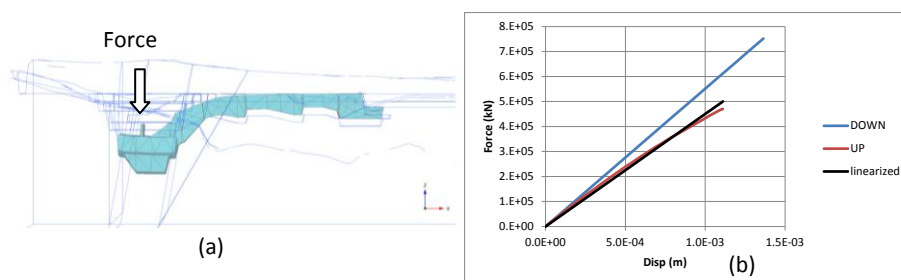


Figure 7. Example Anchorage Spring Development – (a) Foundation Deformed Shape (Exaggerated) under Vertical Loads; (b) Vertical Foundation Spring.

## CONCLUSIONS

The Third Bosphorus Bridge which spans a distance of about 1.4 kilometers will cross the Bosphorus straight near the mouth of the Black Sea. The bridge is designed with a single span suspended between two land-founded towers located on both the European and Asian side of the Bosphorus straight. Kinematic motions and foundation springs are developed as input for the global dynamic structural analyses. For the kinematic motions, 2-D and 3-D finite difference analyses are conducted. It is found that both topography (i.e., natural slope and excavation) as well as the presence of embedded bridge foundations affect the ground motions. Results from 2-D site response analyses which do not consider the bridge foundation are typically higher than 3-D results and are used in dynamic structural analyses.

Foundation springs are developed by 3-D numerical models using PLAXIS3D. Forces and moments are applied at the point of load application of bridge foundation parts: 1) Tower, 2) Approach and 3) Anchorage to develop the springs. Rock mass is modeled using the Hoek-Brown failure criterion (Hoek et al. (2002) [9]). Interface surrounding the foundations is also modeled to allow for slipping and gapping of the foundation with respect to the rock. Shear zones mapped in the site investigation are also considered in the development of the springs.

The flexibility of the concrete foundation is considered in the spring development. The developed springs showed only moderate nonlinearity due to

the high stiffness of the rock mass. It is concluded that springs can be approximated with linear constants and will provide reasonable response. Radiation damping and hysteresis material damping are not included due to the close-to-linear behavior of the springs.

Springs and kinematic motions developed per the procedures described in this paper are provided to structural engineers to conduct the global dynamic structural analyses for the bridge. The global structural model involved detail structural elements to model the dynamic bridge behavior during earthquakes, while the dynamic input at the foundation level are provided by Fugro with procedures described in this paper.

### ACKNOWLEDGMENTS

The Joint Venture of IC İçtaş İnşaat Sanayi ve Ticaret A.Ş. & Astaldi S.p.A. is designing, building and operating a road transportation system that crosses the Bosphorus Straits using a suspension bridge. İçtaş-Astaldi has retained the services of Fugro to assist them with geological, seismological, and geotechnical evaluations for the bridge crossing. As part of the above program, Fugro performed developed estimates of foundation dynamic stiffness, and conducted soil structure interaction analyses to provide support for the bridge foundation design. We appreciate the opportunity to work on this challenging project.

### REFERENCES

- [1] Assimaki D., Kausel E. and Gazetas G. (2005) "Wave Propagation and Soil-Structure Interaction on a Cliff Crest during the 1999 Athens Earthquake," *Soil Dynamics and Earthquake Engineering*, 25, 513-527.
- [2] Itasca (2011) "FLAC Manual".
- [3] Itasca (2011) "FLAC3D Manual".
- [4] Plaxis3D (2011) "User's Manual".
- [5] Makris N., Badoni D., Delis E., and Gazetas G. (1995). Prediction of observed bridge response with soil-pile-structure interaction. *ASCE J. of Structural Engineering*, 120(10):2992-3011.
- [6] Jeremic B. Kunnath S., Xiong F. (2004) Influence of Soil-Foundation-Structure Interaction on Seismic Response of the I-880 Viaduct, *International Journal for Engineering Structures*, Vol. 26, Issue 3, pp. 391-402.
- [7] Ciampoli M. and Pinto P.E. (1995). Effects of soil-structure interaction on inelastic seismic response of bridge piers. *ASCE J. of Structural Engineering*, 121(5):806-814.
- [8] Bielak J., Loukakis K., Hisada Y., and Yoshimura C.. Domain reduction method for three-dimensional earthquake modeling in localized regions. part I: Theory. *Bulletin of the Seismological Society of America*, 93(2):817-824, 2003.
- [9] Hoek, E., Carranza-Torres, C.T., and Corkum, B. (2002), Hoek-Brown failure criterion – 2002 edition. *Proc. North American Rock Mechanics Society meeting in Toronto in July 2002*.



## ASPECTS OF THE SOIL-STRUCTURE INTERACTION

### The dynamic response of bridge piers on caisson foundations

Roberto Cairo<sup>1</sup>, Giovanni Dente<sup>1</sup>

<sup>1</sup> University of Calabria, Dept. of Civil Engineering, Italy  
e-mail: rcairo@unical.it, giovanni.dente@unical.it

**ABSTRACT:** Site conditions and soil flexibility play an important role in determining the seismic response of bridges. In particular, the motion imposed at the foundation can differ from that in the free-field and relevant rocking component may be induced. Using simple analytical methods, the dynamic response of a bridge-soil system excited by harmonic S-waves is investigated.

**KEY WORDS:** Kinematic interaction; Inertial interaction; Caisson foundation.

## 1 INTRODUCTION

Under strong earthquake, several highway structures such as viaducts, bridge piers and abutments exhibited damage in the past owing to excessive displacements and deflections, in general. Most part of these lateral movements were induced by soil liquefaction even if lateral spreadings generated by non-liquefied crust were also detected.

As summarized by Sextos et al. [1], other important features that showed their influence in the seismic behavior of extended structures such as bridges are: 1) the spatial and temporal variations of seismic motion at the support points; 2) the local site conditions which can strongly modify the surface motion; 3) the deformability of the soil that may lead to erroneous evaluation of structural displacements. In particular, the key role of the dynamic soil-structure interaction (SSI) on the design of structures with massive or deep foundation is well documented and recognized in the literature [2].

A first kinematic consequence of the interaction between soil and foundation derives from the propagation of the seismic waves which makes the soil motion at any given instant generally different from point to point. A relatively stiff foundation produces an averaging effect in which the overall motion at the foundation interface,  $u_{ko}$ , is less than the maximum displacement,  $u_{ffo}$ , that would have occurred in the free-field soil, i.e. in the absence of the structure. Moreover, the distribution of soil displacements along depth is incompatible with the rigid lateral movement of the side-walls of the foundation, so that a rotation (rocking) component,  $\theta_{ko}$ , develops.

Both base-slab averaging and embedment effects cause foundation motion

(usually called *foundation input motion*, or FIM) to deviate from free-field motion in a manner that is independent of the superstructure. These occurrences are strongly frequency-dependent as they are influenced by the wavelength of seismic waves compared to the dimension of the foundation elements. This type of interaction is known as *kinematic interaction*. In the case of a shallow foundation, the kinematic components  $u_{k_0}$  and  $\theta_{k_0}$  are usually negligible respect to the motion ( $u_o$  and  $\theta_o$ ) which is in turn generated at the foundation level by the oscillation of the superstructure. This latter phenomenon is called *inertial interaction*. Kinematic interaction should be in principle more relevant for drilled shafts and caissons, owing to the foundation size and embedment.

Although earthquake response of bridges should be evaluated with a direct analysis capable of modeling the entire system composed of the superstructure, foundation and the supporting soil, to date the state of practice is usually restricted to a multistep approach, which makes use of the superposition theorem. It consists of: (a) evaluating the free-field response of the site; (b) solving the kinematic interaction, i.e. the response to incident seismic waves of the soil-foundation system with the mass of the superstructure set equal to zero; (c) determining the inertial interaction, that is the response of the overall soil-foundation-superstructure system to forces associated with accelerations arising from the kinematic interaction.

As a further simplification, kinematic interaction can be reduced to the evaluation of the foundation input motion, disregarding the presence of the superstructure. The FIM is subsequently applied at the base of the superstructure (Fig. 1). In the inertial interaction, the soil-foundation system is conveniently modeled with springs and dashpots (dynamic impedances) associated with each mode of vibrations. The response of the structure is thus determined.

In this paper, some aspects of the dynamic behavior of a bridge pier founded on caisson subjected to harmonic shear waves are analysed. The bridge is idealized as a single-degree-of-freedom (SDOF) structure and the foundation is represented by a rigid block connected to the surrounding soil by a series of springs and dashpots according to the Winkler-type model developed by Gerolymos and Gazetas [3].

## **2 OUTLINES OF THE METHOD USED**

Although the seismic analysis of bridge structures has received considerable attention in recent years, some aspects concerning the effects of soil-structure interaction are not yet completely investigated and clarified. Bridge piers, together with the abutments, constitute one of the most critical elements in securing the safety of bridges during earthquakes. They are widely supported by drilled shafts and caissons embedded in soft soil or founded directly on a firm stratum.

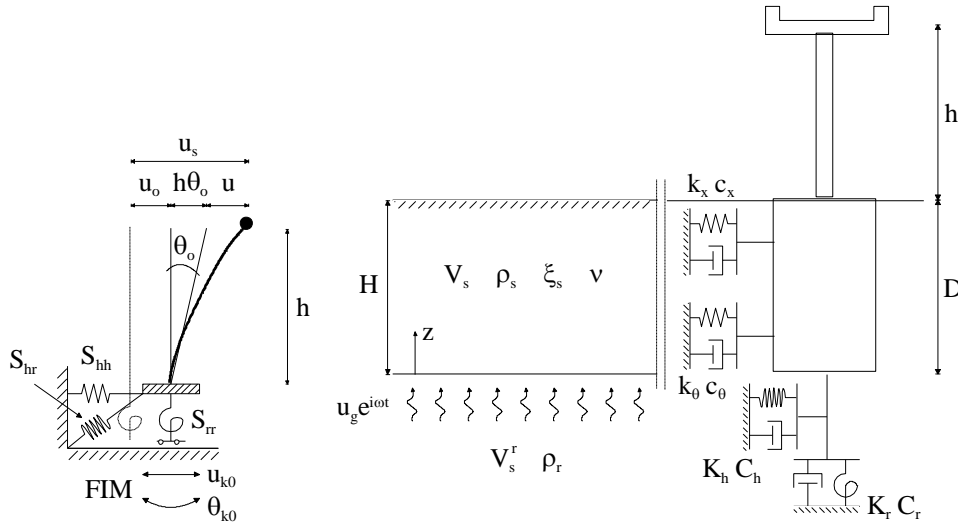


Figure 1. Idealized model studied      Figure 2. Soil deposit and bridge-pier on Winkler foundation.

A Winkler-type model for the dynamic response of rigid caisson foundations has been developed by Gerolymos and Gazetas [3]. It consists of four types of linear springs and dashpots (impedances): two distributed translational and rotational impedances on the shaft of the caisson, two concentrated translational and rotational impedances, indicated with capital letter, at the base (Fig. 2). The spring coefficient  $k$  ( $K$ ) takes into account the stiffness and inertia of the supporting soil and is therefore termed dynamic stiffness;  $c$  ( $C$ ) is the dashpot coefficient which reflects the radiation and material damping generated in the system. As known, in the frequency domain each dynamic impedance component can be written in complex notation as

$$\bar{k} = k + ia_0c \tag{1}$$

where  $i = -1^{0.5}$ ;  $a_0 = \omega B / V_s$  is the dimensionless frequency being  $\omega$  the circular frequency of the harmonic excitation,  $B$  the diameter or width of the caisson,  $V_s$  the shear wave velocity of the soil. Both  $k$  and  $c$  are functions of  $\omega$ .

The impedance matrix of the soil-foundation model, referred to the base of the caisson, takes the following form [3]

$$[S] = \begin{bmatrix} \bar{K}_h + \bar{k}_x D & \bar{k}_x D^2 / 2 \\ \bar{k}_x D^2 / 2 & \bar{K}_r + \bar{k}_\theta D + \bar{k}_x D^3 / 3 \end{bmatrix} \tag{2}$$

In general, the dynamic impedances of rigid caissons come indirectly from studies of the dynamic response of embedded footings [3,4]. According to Tsigginos et al. [4], the impedances of the base of the caisson can be selected as

the springs,  $K$ , and dashpots,  $C$ , coefficients of a surface foundation on halfspace or on a soil stratum underlain by a homogeneous halfspace. The lateral springs,  $k$ , and dashpots,  $c$ , of the equivalent Winkler model can be derived by equating the translational and rocking components of the impedance matrix in Eq. (2) with the aforementioned elastodynamic solution [3,4] or by curve-fitting with 3D finite element simulations [2]. In this study, the simple relations of the dynamic spring and dashpot coefficients furnished by Varun et al. [2] are used.

### 3 BRIDGE-SOIL SYSTEM STUDIED

In this section the dynamic response of a bridge pier founded on rigid caisson is studied (Fig. 2). The superstructure is idealized as a SDOF system with lumped mass  $m=450$  Mg, height  $h=10$  m, elastic stiffness  $k=5.9 \times 10^4$  kN/m and damping ratio  $\xi=5\%$ . For fixed-base response, the structure has undamped natural frequency  $\omega_s=(k/m)^{0.5}=11.45$  rad/s that corresponds to 1.8 Hz. The base is assumed to be a square prismatic block of height  $D=8$  m, width  $B=4$  m, mass  $m_o=320$  Mg, embedded in a uniform elastic soil stratum overlying a homogeneous halfspace. The system is subjected to vertically propagating harmonic S-waves. The soil-foundation interaction is solved by the aforementioned Winkler-type model for both kinematic and inertial interaction.

#### 3.1 Kinematic interaction

The first step of the kinematic analysis is to evaluate the free-field response of the soil deposit. To this end, a soil layer resting on bedrock is considered (Fig. 2). The soil has thickness  $H=8$  m, shear wave velocity  $V_s=100$  m/s, damping ratio  $\xi_s=0.10$ , mass density  $\rho_s=2$  Mg/m<sup>3</sup> and Poisson's ratio  $\nu=0.4$ . The bedrock is represented by a homogeneous halfspace with shear wave velocity  $V_s^r$  and mass density  $\rho_r$ . Assuming a harmonic motion with circular frequency  $\omega$  and amplitude  $u_g$  at the bedrock level, the displacement of the soil with the depth  $z$  can be evaluated [3].

This wave pattern imposes forces and moments at the supports of the distributed springs and dashpots along the caisson height and at the concentrated impedances of the base. By solving the dynamic equilibrium of the caisson in the absence of the superstructure, the horizontal displacement  $u_{ko}$  and the rotation  $\theta_{ko}$  (foundation input motion) of the caisson are calculated.

Figure 3 plots the components of the FIM as a function of the ratio of the excitation frequency  $\omega$  to the fixed-base natural frequency  $\omega_s$  of the superstructure. Two cases are examined: one in which the caisson is embedded in a homogeneous halfspace ( $V_s^r = V_s$ ), the other, termed layered, with the caisson embedded in a soft soil overlying a firm stratum ( $V_s^r = 4V_s$ ). The amplitudes (absolute values) of the input motion are normalized by the amplitude of the

surface free-field motion (*kinematic factors*). The solutions obtained with the mass of the caisson  $m_o$  set equal to zero are also shown.

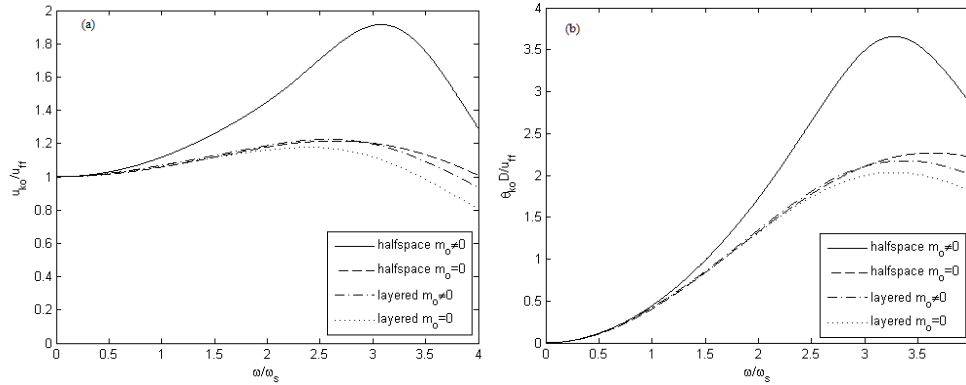


Figure 3. Kinematic response of the foundation as a function of frequency ratio

As can be noticed, for a frequency ratio  $\omega/\omega_s < 3$  the kinematic response of the caisson  $u_{ko}$  is greater than the surface free-field displacement (Fig. 3a). This is caused by the rapid development of the rocking component  $\theta_{ko}$  in the same frequency range (Fig. 3b). At higher frequencies,  $u_{ko}$  tends to attenuate rapidly and becomes minor than the movement of the ground, although significant values of the rocking motion remain. The more pronounced kinematic effects are found when the foundation is embedded in a homogenous halfspace. In this case, the mass of the caisson determines an increase of the kinematic factors. When the caisson is founded directly on the bedrock, the kinematic response reduces and the influence of mass  $m_o$  is practically negligible.

### 3.2 Inertial interaction

In the inertial interaction, the soil-foundation system is modeled through the dynamic impedances computed at the top of the caisson (Fig. 1), obtained by means of coordinate transformation of the impedance matrix of Eq. (2) [3].

The response of the bridge pier to the foundation input motion with amplitude  $u_{ko}$  and  $\theta_{ko}$  is thus evaluated solving the dynamic equilibrium of the idealized structural system sketched in Fig. 1. The foundation has two degrees of freedom consisting of the horizontal displacement with amplitude  $u_o$  and rocking with amplitude  $\theta_o$ . The elastic horizontal displacement of the top mass relative to the base mass has amplitude  $u$ . The latter is representative of the shear force  $Q_o$  and overturning moment  $M_o$  at the base. The total displacement amplitude of the superstructure results  $u_s = u_o + h\theta_o + u$ .

Formulating dynamic equilibrium of the mass of the superstructure and the translational and rotational equilibrium of the entire system yields

$$\begin{bmatrix} -1 + \frac{1+2i\xi}{(\omega/\omega_s)^2} & -1 & -1 \\ -1 & \frac{S_{hh}}{\omega^2 m} - (1+\bar{m}) & \frac{S_{hr}}{\omega^2 mh} - 1 \\ -1 & \frac{S_{hr}}{\omega^2 mh} - 1 & \frac{S_{rr}}{\omega^2 mh^2} - \left(1 + \frac{I_t}{mh^2}\right) \end{bmatrix} \begin{Bmatrix} u \\ u_0 \\ h\theta_0 \end{Bmatrix} = \begin{Bmatrix} 1 \\ 1+\bar{m} \\ 1 \end{Bmatrix} u_{k0} + \begin{Bmatrix} 1 \\ 1 \\ 1 + \frac{I_t}{mh^2} \end{Bmatrix} h\theta_{k0} \quad (3)$$

being  $\bar{m} = m_0 / m$  and  $I_t$  the total centroidal moment of inertia of the masses.

The total displacement amplitude of the structure normalized by the amplitude of the surface free-field displacement is presented in Figs. 4-5. The solution disregarding the soil, i.e. for fixed-base structure, is also presented. This corresponds to the well-known frequency response curve with the peak of  $1/2\xi$  occurring at  $\omega/\omega_s=1$ .

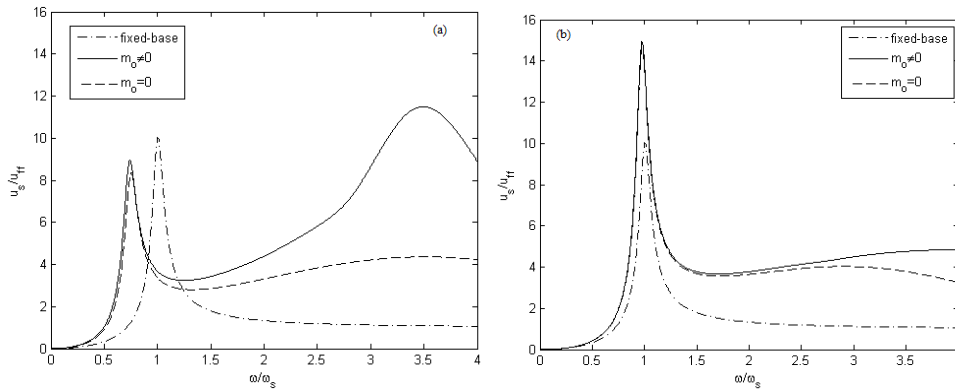


Figure 4. Frequency response curve of the structure: homogeneous (a) and layered (b) soil

When the soil is assimilated to a homogeneous halfspace (Fig. 4a), the peak response of the coupled soil-structure system results smaller than that of the same structure on a rigid base and occurs at a lower frequency, corresponding to a more flexible system. This curve is also broader, indicating that the damping is larger due to radiation in the surrounding soil. A different behavior is exhibited when the caisson is based on the bedrock ( $V_s' = 4V_s$ ), as shown in Fig. 4b. The peak response occurs nearly at the fixed-base natural frequency, but it is considerably greater than the displacement of the structure when the presence of the soil is neglected. In this case, the movement of the caisson is restricted by the presence of the bedrock in such a way that the fundamental natural frequency of the system is not affected by the flexibility of the soil. However, the displacement of the structure tends to be larger because the amplitude of the motion imposed at the foundation is higher than that of the free-field (Fig. 3a). Furthermore, radiation damping reduces because of the presence of the bedrock.

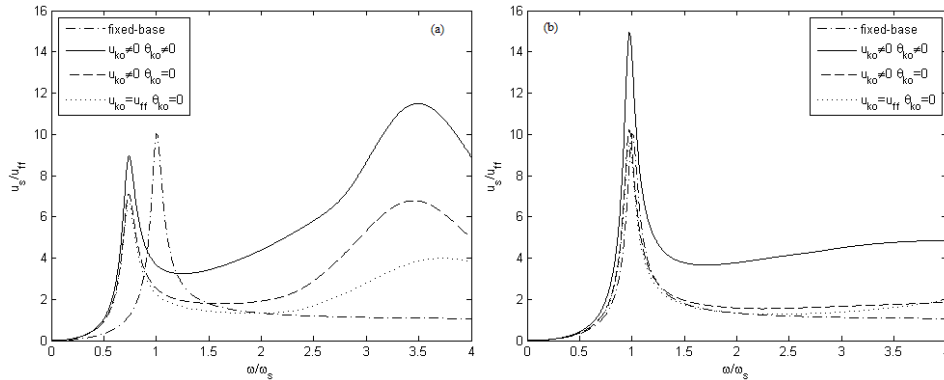


Figure 5. Frequency response curve of the structure for different foundation motion

In the high frequency range, the foundation compliance influences significantly the response of the bridge (Fig. 4). This interaction effect can be correlated to the large values of the rocking component of the FIM, especially when the foundation is embedded in homogeneous halfspace (Fig. 4a). In Fig. 5 the importance of kinematic interaction on the frequency response curves is depicted. As can be seen, large amplitudes of  $u_s$  at high frequencies are essentially due to the presence of the rocking component  $\theta_{ko}$  of the foundation input motion (Fig. 5a). This effect is evident when the base of the caisson rests on the bedrock (Fig. 5b). Moreover, it is worth noting that the assumption of the foundation input motion does not modify the natural frequency of the soil-structure system.

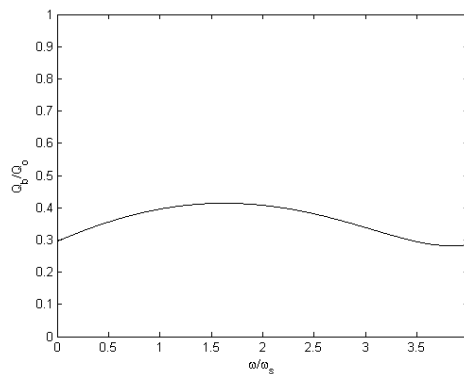


Figure 6. Shear forces acting on the caisson as a function of frequency

Finally, the ratio of the shear force at the base of the caisson  $Q_b$  to that at the top  $Q_0$  as a function of the frequency ratio is displayed in Fig. 6 in the case of layered soil. It can be observed that a small part of the force induced by the oscillation of the bridge and generated by the mass of the caisson is transmitted

at the foundation as a consequence of soil-foundation interaction. The overturning moment at the base  $M_b$  is set equal to zero since the corresponding rocking spring  $K_r$  and dashpot  $C_r$  coefficients have been ignored for the aspect ratio  $D/B$  considered [2]. More accurate analyses have shown that  $M_b$  is almost negligible compared with the overturning moment  $M_o$  induced at the top (<10%) in the whole frequency range [5].

#### 4 CONCLUSIONS

From the presented results, the following remarks can be drawn:

- a) the kinematic interaction for caisson foundations is characterized by a significant rotational component, which leads to a lateral displacement greater than the surface free-field motion in a wide frequency range;
- b) the soil profile can play an important role both in kinematic and inertial interaction: in the case of a homogeneous soil, the fundamental natural frequency of the soil-structure system is reduced with respect to that calculated ignoring SSI and the peak response becomes smaller, owing to radiation damping; when the base of the caisson is embedded in a soil layer underlain by a stiffer halfspace, the peak response occurs at the fixed-base natural frequency, but may be considerably greater than the displacement of the structure determined neglecting the soil. Similar amplification of structural response is attained in the high frequency range, owing to the large values of the rocking component of the foundation input motion;
- c) the overturning moment induced at the base of the caisson is negligible respect to that acting at the top.

Although the used approaches are based on some approximate assumptions, the conclusions drawn in the present study can be of help in predicting the seismic response of bridges on deep foundations, or in interpreting the results of more rigorous numerical studies.

#### REFERENCES

- [1] Sextos, AG, Pitilakis, KD, Kappos, AJ, "Inelastic dynamic analysis of RC bridges accounting for spatial variability of ground motion, site effects and soil-structure interaction phenomena. Part 1: Methodology and analytical tools", *Earth. Eng. and Struct. Dyn.*, Vol. 32, pp. 607-627, 2003.
- [2] Varun, Assimaki, D, Gazetas, G, "A simplified model for lateral response of large diameter caisson foundations – Linear elastic formulation", *Soil Dyn. and Earth. Eng.*, Vol. 29, pp. 268-291, 2009.
- [3] Gerolymos, N, Gazetas, G, "Winkler model for lateral response of rigid caisson foundations in linear soil" *Soil Dyn. and Earthq. Eng.*, Vol. 26, No. 5, pp. 347–361, 2006.
- [4] Tsigginos, C, Gerolymos, N, Assimaki, D, Gazetas, G, "Seismic response of bridge pier on rigid caisson foundation in soil stratum", *Earthq. Eng. and Eng. Vib.*, Vol. 7, No. 1, pp. 33-44, 2008.
- [5] Cairo, R, Conte, E, "L'interazione terreno-struttura nella risposta sismica di ponti con fondazioni profonde", *Proc. Convegno Nazionale di Geotecnica*, 2014 (in Italian).



## **SIMPLIFIED METHOD FOR SEISMIC ANALYSIS OF MOTORWAY BRIDGES**

Athanasios Agalianos<sup>1</sup>, Lampros Sakellariadis<sup>2</sup>  
Ioannis Anastasopoulos<sup>3</sup> and George Gazetas<sup>4</sup>

<sup>1,2</sup> University of Dundee, UK (formerly NTUA)

<sup>3</sup> University of Dundee, UK

<sup>4</sup> National Technical University of Athens, Greece

e-mail: ath\_agali@hotmail.com , sakil90@windowslive.com , i.anastasopoulos@dundee.ac.uk ,  
gazetas@central.ntua.gr

**ABSTRACT:** The paper develops a simplified method to analyse the seismic performance of motorway bridges. An actual bridge is used as an illustrative example. Detailed 3D model of a typical overpass bridge is developed and used to assess the effectiveness of the simplified method. Both longitudinal and transverse shaking is considered. The contribution of key structural components and the effect of soil structure interaction (SSI) are properly taken into account. The simplified models compare well with the full 3D model of the bridge–abutment–foundation–soil system, and are therefore proposed as a reasonable approximation.

**KEY WORDS:** Seismic vulnerability; bridge pier; nonlinear analysis; soil-structure interaction; Attiki Odos highway.

### **1 INTRODUCTION**

Bridges tend to be most vulnerable during strong seismic shaking. The large number and complexity of bridges encountered along motorways in operation worldwide, present a particular challenge to engineers. The development of detailed 3D models of the bridge–foundation–abutment–soil system is the most comprehensive way to simulate their seismic performance. However, in order to cover a wide range of strong motion characteristics, a large number of seismic excitations are necessary. Conducting such analysis with full 3D models of the bridge–foundation–abutment–soil system would require quite a substantial computational effort, rendering the use of simplified models a practical necessity. To this end, a simplified method for seismic vulnerability assessment of typical motorway bridges is introduced herein using as an illustrative example a characteristic bridge of Attiki Odos, in the Athens metropolitan area.

## 2 PROBLEM DEFINITION, ANALYSIS METHODOLOGY

### 2.1 Case study

A typical overpass bridge (A01-TE20) of the Attiki Odos Motorway has been selected. Besides its simplicity, the selected bridge system is representative of about 30% of the bridges of the specific motorway, and is also considered quite common for other metropolitan motorways in the world. As shown in Fig. 1a, the selected system is a symmetric 3-span bridge with a continuous pre-stressed concrete box-girder deck, supported on two reinforced concrete (RC) cylindrical piers of diameter  $d = 2$  m and height  $h = 8.8$  m.

The piers are monolithically connected to the deck, which is supported by 4 elastomeric bearings at each abutment. Each bearing is 0.3 m x 0.5 m (longitudinal x transverse) in plan and has an elastomer height  $t_b = 63$  mm. The piers are founded on  $B = 8$  m square footings, while the abutments consist of retaining walls of 9 m height and 1.5 m thickness. The latter are connected to two side walls of 0.6 m thickness and founded on a rectangular 7 m x 10.4 m rectangular footing.

### 2.2 Finite element modelling

The seismic performance of the bridge is analysed employing the FE method. The deck and the piers are modeled with elastic and inelastic beam elements, respectively. The reinforcement of the  $d = 2$  m RC piers has been computed according to the provisions of the Greek Code for Reinforced Concrete (ΕΚΩΣ, 2000) for columns with large ductility demands. The inelastic behavior of the piers is simulated with a nonlinear model, calibrated against the results of RC section analysis using the USC-RC software [2001]. The result of such a calibration is shown in Fig. 1b. Linear elastic springs and dashpots are used to model the compression ( $K_{c,b}$ ) and shear stiffness ( $K_{s,b}$ ) and damping ( $C_{c,b}$ ,  $C_{s,b}$ ) of the bearings (Fig. 1b).

The footings and the abutments are modelled with elastic hexahedral continuum elements, assuming the properties of RC ( $E = 30$  GPa). An idealised 20 m deep substratum of homogeneous stiff clay is considered, having an undrained shear strength  $S_u = 150$  kPa (Fig. 1c). The latter is also modeled with hexahedral continuum elements. Nonlinear soil behaviour is modelled with a kinematic hardening model, having a Von Mises failure criterion and an associated flow rule [Anastasopoulos et al., 2011].

Appropriate “free-field” boundaries are used at the lateral boundaries of the model, while dashpots are installed at the base of the model to simulate the half-space underneath the 20 m of the soil that is included in the 3D model. Special contact elements are introduced at the soil-footing interfaces to model possible separation (uplifting) and sliding. A friction coefficient  $\mu = 0.7$  is assumed, which is considered realistic for the soil conditions investigated herein. The same applies to the interfaces between the abutment and the embankment soil.

A reinforced soil embankment is considered, which is quite common in such motorway bridges (due to space limitations). The latter is modeled in a simple manner, by “installing” appropriate kinematic constraints in the transverse direction.

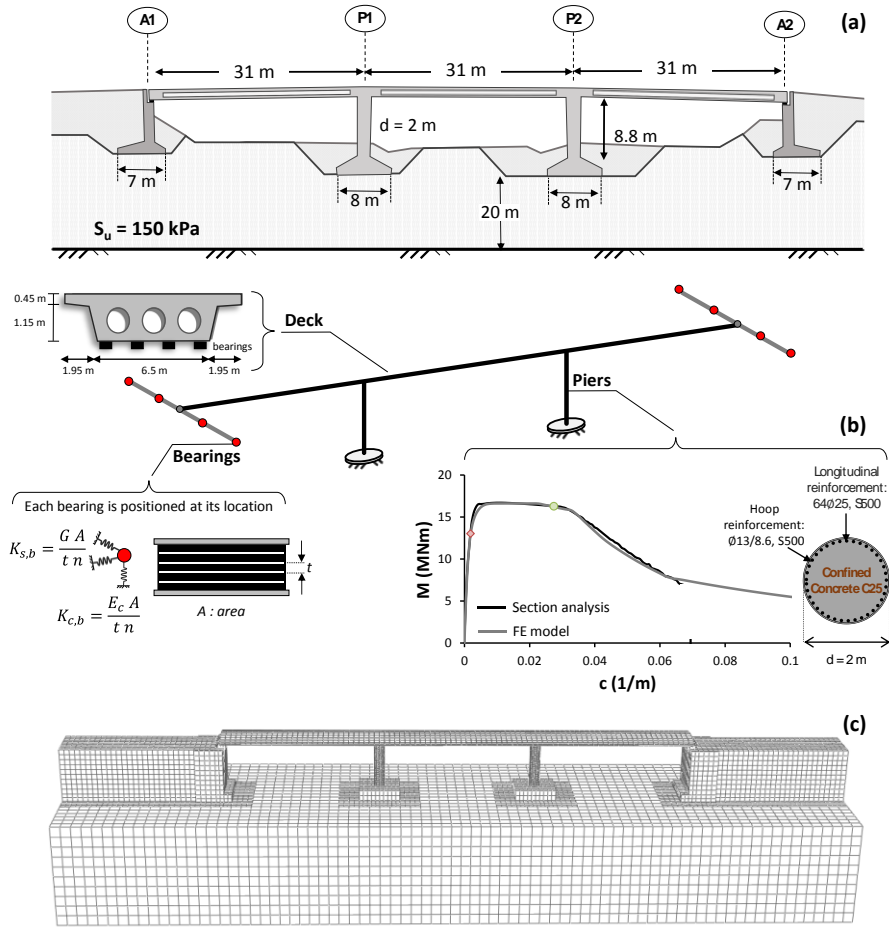


Figure 1. (a) Typical overpass bridge (A01-TE20) of the Attiki Odos motorway used as an example for the analyses (b) key attributes of the bridge and (c) full 3D model of the bridge, including the foundations, the abutments, and the subsoil.

### 3 SIMPLIFIED METHOD

#### 3.1 Development of models

A simplified model is developed for the selected bridge. The simplified model is composed of a SDOF system of a pier with lateral and rotational springs and dashpots connected at the top, representing the deck and the abutment bearings. Its definition requires section analysis of the pier, and computation of spring and dashpot coefficients using simple formulas. The nonlinear soil–structure interaction is also considered replacing the soil–foundation system with horizontal, vertical, and rotational springs and dashpots. While the horizontal and vertical springs and dashpots are assumed elastic, the nonlinear rotational spring is defined on the basis of non–dimensional moment–rotation relations. The proposed models in both directions are presented in Fig. 2.

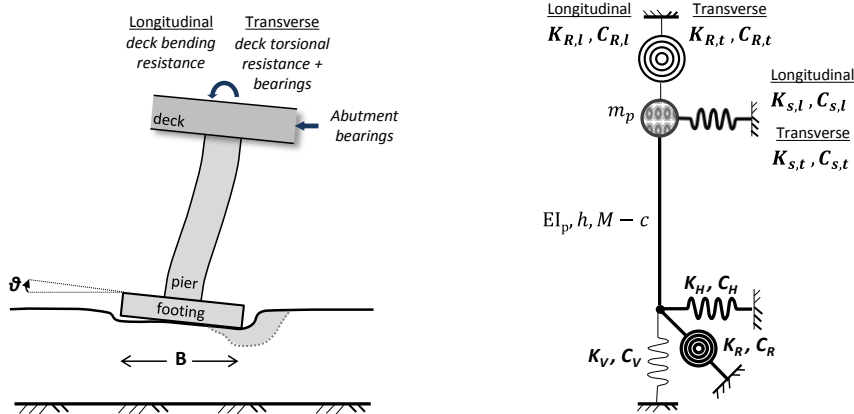


Figure 2. Proposed simplified models in longitudinal and transverse direction accounting for the contribution of the key structural components and SSI.

#### 3.2 Efficiency of the proposed method

The performance of the simplified models in both directions is assessed using as a benchmark the detailed 3D model of the bridge–abutment–foundation–soil system. The latter requires substantial computational effort, calling for careful selection of the seismic excitations. Hence, three characteristic records are selected: (a) Aegion, which is considered representative of moderate intensity shaking; (b) Lefkada-2003, which contains multiple strong motion cycles and can be considered representative of medium intensity shaking; and (c) the notorious Rinaldi-228 record (Northridge 1994), containing a very strong forward rupture directivity pulse, and being representative of very strong seismic shaking. The comparison is performed in terms of time histories of deck drift  $\delta$  and moment–curvature ( $M$ – $c$ ) response of pier P1 (left column).

As depicted in Figs. 3, 4 indicatively for the Aegion record the simplified model compares well with the full 3D model in both directions of seismic loading and therefore can be considered a reasonable approximation of the seismic response of the bridge.

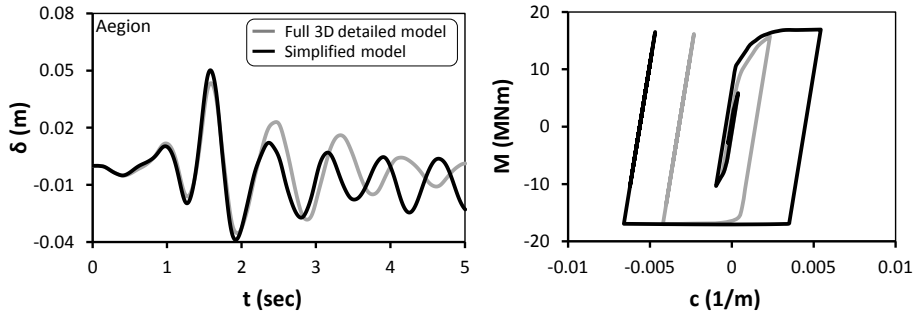


Figure 3. Comparison of the simplified model to the full 3D detailed model in the transverse direction. Time histories of deck drift  $\delta$  (left column) and moment–curvature response of pier P1 (right column), using as seismic excitation the Aegion record.

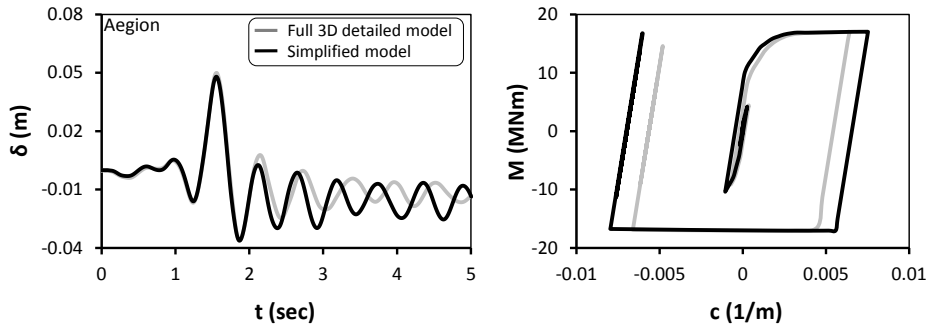


Figure 4. Comparison of the simplified model to the full 3D detailed model in the longitudinal direction. Time histories of deck drift  $\delta$  (left column) and moment–curvature response of pier P1 (right column), using as seismic excitation the Aegion record.

#### 4 CONCLUSIONS

Conducting dynamic analyses using detailed 3D models of bridge–abutment–foundation–soil systems requires substantial computational effort, rendering the use of simplified models indispensable. The present study introduced such a simplified method for seismic analysis of typical motorway bridges, accounting for the key structural components and the nonlinear soil–structure interaction (SSI).

For this purpose a typical overpass bridge of the Attiki Odos Motorway in Athens (Greece) is used as an illustrative example. A detailed 3D model of the

bridge is developed to assess the effectiveness of the simplified method. The proposed model comprises an equivalent SDOF system of a single bridge pier, with lateral and rotational springs and dashpots connected at the top, representing the deck and the abutment bearings. The definition of the model requires cross-sectional analysis of the most vulnerable pier, and computation of spring and dashpot coefficients using simple formulas. The simplified models also account for nonlinear SSI.

Although the proposed models are based on a number of simplifying approximations, they have been found reasonably accurate, as was highlighted in the paper. Despite our focusing on a representative but specific bridge system, the results could perhaps be of more general validity.

### ACKNOWLEDGMENTS

The financial support for this paper has been provided by the research project “SYNERGY 2011” (Development of Earthquake Rapid Response System for Metropolitan Motorways) of GGET–EYDE–ETAK, implemented under the “EPAN II Competitiveness & Entrepreneurship”, co-funded by the European Social Fund (ESF) and national resources.

### REFERENCES

- [1] ABAQUS 6.11. (2011). Standard user's manual. Dassault Systèmes Simulia Corp., Providence, RI, USA.
- [2] Agalianos A., Sakellariadis L., (2013), “*A simplified method to estimate seismic vulnerability of bridges considering soil-structure interaction*”, Diploma Thesis, National Technical University of Athens, Greece
- [3] Anastasopoulos I., Kontoroupi Th. (2014), “Simplified approximate method for analysis of rocking systems accounting for soil inelasticity and foundation uplifting”, *Soil Dynamics and Earthquake Engineering*, Vol. 56, pp. 28-43.
- [4] EAK (2000) “Greek Seismic Code”, Organization of Seismic Planning and Protection, Athens (in Greek).
- [5] ΕΚΩΣ (2000) “Greek code for reinforced concrete”, Organization of Seismic Planning and Protection, Athens (in Greek).
- [6] Gazetas G., Anastasopoulos I., Adamidis O., Kontoroupi Th. (2013). “Nonlinear Rocking Stiffness of Foundations”, *Soil Dynamics & Earthquake Engineering*, Vol. 47, pp.83-91, 2013
- [7] Gazetas G. (1983), “Analysis of machine foundation vibrations: state of the art”, *Soil Dynamics and Earthquake Engineering*, Vol 2, pp. 2–42.
- [8] Karim, K.R., Yamazaki, F. (2001). “Effect of earthquake ground motions on fragility curves of highway bridge piers based on numerical simulation”. *Earthquake Engineering and Structural dynamics* 30, 1839-1856.
- [9] Nielson B. & DesRoches R. (2007). “Analytical Seismic Fragility Curves for Typical Bridges in the Central and Southeastern United States”, *Earthquake Spectra*, Volume 23, No. 3, pages 615–633
- [10] USC-RC, “Moment-Curvature, Force-Deflection, and Axial Force-Bending Moment Interaction Analysis of Reinforced Concrete Members”. University of South California, 2001

## AUTHOR INDEX

Afantenou, A. 211  
Agalianos, A. 437  
Alexakis, H. 201  
Alogdianakis, F. 161  
Anastasopoulos, D. 245  
Anastasopoulos, I. 437  
Andrianopoulos, K. 413  
Argyris, C. 387  
Augustesen, A.H. 69  
Avraam, T. 229

Balafas, I. 161  
Bergmeister, K. 285  
Bouckovalas, G. 413  
Bruno, D. 3, 327

Cairo, R. 429  
Chacko, J. 421  
Charmpis, D.C. 161  
Chen, W.-Y. 421  
Cheng, J. 301  
Chorafa, E. 111  
Chrysanidis, T. 119

Dente, G. 429

Faraonis, P. 395  
Flamand, O. 33  
Foged, B. 69

Gazetas, G. 19, 437  
Giannakou, A. 421  
Gikas, V. 185  
Greco, F. 3, 327

Hajdin, N. 361  
Hatzigeorgiou, G. 103

Jia, L. 301

- Kalkinis, D. 103  
Kapogiannis, I. 211  
Karamitros, D. 413  
Karani, I. 111  
Karatzas, V. 221  
Karatzas Roussou, E. 221  
Karydakis, P. 185  
Karydis, G. 221  
Kavianipour, F. 57  
Konstantakopoulos, T.G. 221, 277, 311, 335  
Kopelia, Z. 245
- Liolios, Ast. 103  
Liolios, Ang. 103, 285  
Liontos, K. 253  
Lonetti, P. 3, 327
- Makris, N. 143, 201  
Maraveas, C. 345  
Markogiannaki, O. 87, 135, 371  
Miamis, K. 345  
Michaltsos, G.T. 229, 261, 277, 293, 311, 319, 335  
Moschas, F. 177  
Mouroukis, D. 253  
Mpimis, T. 185
- Nakashoji, B. 57  
Ni, J. 301
- Panagiotopoulos, T. 169  
Panagakis, A. 185  
Panagis, A. 33  
Panetsos, P. 103, 387  
Papadimitriou, F. 185  
Papadimitriou, C. 387  
Papadioti, D.-C. 387  
Papanikolas, P. 33  
Papastergiou, G. 319  
Papathanasiou, S.M. 405  
Papavasileiou, V.D. 193  
Pecker, A. 43  
Pilitsis, V. 95, 119, 151, 245, 269  
Piniotis, G. 185  
Pitilakis, K. 111  
Prapa, E. 405  
Psimoulis, P. 177



- Rovithis, E. 111  
Raftoyiannis, I.G. 193, 261, 277, 293, 319
- Saiidi, S.M. 57  
Sakellariadis, L. 437  
Sextos, A. 395  
Spiliopoulos, K. 211  
Spyridis, P. 285  
Stathopoulos-Vlamiis, A. 33  
Stavridis, L. 211  
Steenfelt, J.S. 69  
Stipanic, B. 361  
Stiros, S. 177  
Sun, B. 237
- Tamparopoulos, A. 285  
Tasiouli, K. 345  
Tazarv, M. 57  
Tegos, I.A. 87, 95, 119, 127, 135, 151, 245, 269, 353, 371, 379  
Tegou, S.D. 127, 269, 353, 379  
Thomaidis, I. 353  
Thomaidis, I.-P. 353  
Tsopelas, P. 405
- Ucak, A. 405
- Varela, S. 57  
Vasileiou, S. 87, 135  
Vassiliou, M.F. 143  
Veros, P. 253  
Vlachoulis, T. 111
- Wuttke, F. 395
- Xiao, R. 237, 301  
Xue, E. 237
- Yuan, S. 237
- Zabel, V. 395  
Zacharopoulos, D. 169  
Zarogiani, E. 111  
Zhuang, D. 237

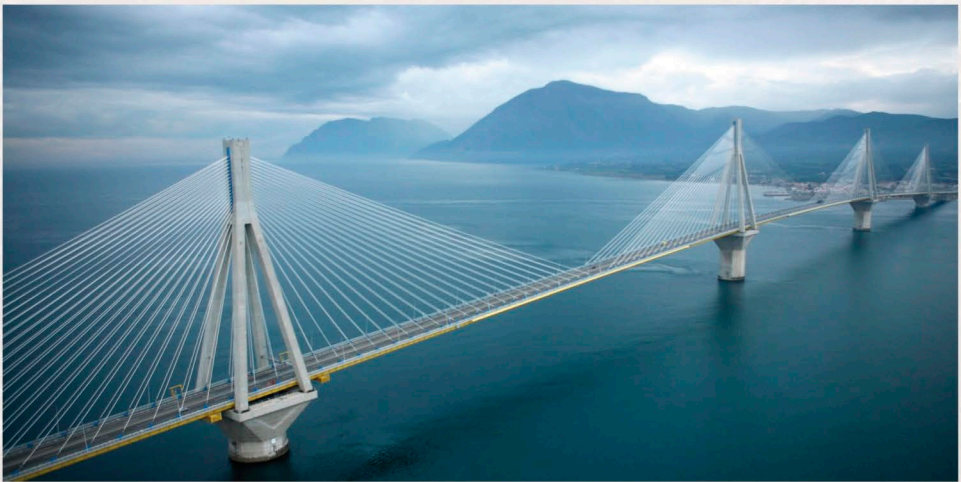




HELLENIC SOCIETY OF BRIDGES STUDY

Proceedings of the  
**INTERNATIONAL CONFERENCE IBSBI 2014**  
**“Innovations on Bridges and Soil-Bridge Interaction”**

October 16-18, 2014  
Athens, Greece



Editors

**George T. Michaltsos**  
**Konstantinos V. Spiliopoulos**  
**Ioannis G. Raftoyiannis**



TSOTRAS  
PUBLICATIONS

Proceedings of the  
**INTERNATIONAL CONFERENCE**  
**IBSBI 2014**





HELLENIC SOCIETY OF BRIDGES STUDY

Proceedings of the  
**INTERNATIONAL CONFERENCE IBSBI 2014**  
“Innovations on Bridges and Soil-Bridge Interaction”

16-18 October 2014  
Athens, Greece

Editors

**George T. Michaltsos**  
**Konstantinos V. Spiliopoulos**  
**Ioannis G. Raftoyiannis**



## SPONSORS



EUGENIDES FOUNDATION  
Gold Medal Award of the Athens Academy



National Technical  
University of Athens

IBSBI 2014  
“Innovations on Bridges and Soil-Bridge Interaction”  
Proceedings of the Conference

© Copyright 2014 “Hellenic Society of Bridges Study”  
Published by Tsotras Publications

ISBN 978-618-5066-23-9

All rights reserved. No part of this book may be produced in any form or by any means,  
without written permission.

Cover photo:  
*The Rion-Antirion Bridge “Charilaos Trikoupis”*

## **FOREWORD**

The Second International Conference on “Innovations on Bridges and Soil-Bridge Interaction” (IBSBI 2014) is held 16-18 October 2014 in Athens, Greece.

IBSBI 2014 conference aims to bring in contact engineers and researchers with interest in the area of Bridge Design and Construction and in Soil-Bridge Interaction in order to promote the exchange of ideas and experiences among participants for consolidation of recent developments in this important area.

IBSBI 2014 Conference covers a broad spectrum of 6 topics related to Bridge Design and Construction and Soil Bridge Interaction, with 7 keynote lectures and is presented in 10 technical sessions by experts from many countries around the world during the three days of Conference.

A number of selected high quality Conference papers will be published after invitation in the journal “International Journal of Bridge Engineering”.

The “Hellenic Society of Bridges Study” (HSBS) who organized this International Conference is a non-profit scientific association with members from all around Greece, while its purpose is the promotion of the theoretical and applied research on the design and construction of Bridge Structures and Soil-Bridge Interaction. This International Conference is already established as a permanent institution, which takes place every three years.

The financial support provided by the “Eugenides Foundation” is gratefully acknowledged, especially in this difficult economic period for Greece.

We would like also to acknowledge the National Technical University of Athens for its kind sponsoring.

Finally, we would like to extend our appreciation to the members of the Local Organizing Committee, and the International Scientific Committee for their time and also the Conference Secretariat for their hard work in preparing the Conference.

Athens October 2014

George T. Michaltsos  
Konstantinos V. Spiliopoulos  
Ioannis G. Raftoyiannis



#### ORGANIZING COMMITTEE

Avraam Tassos  
Konstantakopoulos Theodore  
Michaltsos George  
Raftoyiannis Ioannis  
Spiliopoulos Konstantinos  
Voudiklaris Theodore

#### HONORARY COMMITTEE

Golias Ioannis  
Hajdin Nikola  
Kounadis Anthony  
Simopoulos Simos

#### STEERING COMMITTEE

Bruno Domenico  
Gazetas George  
Hajdin Nikola  
Michaltsos George  
Papanikolas Panayiotis  
Pecker Alain  
Saiidi Saiid M.  
Spiliopoulos Konstantinos

#### KEYNOTE SPEAKERS

Bruno Domenico  
Gazetas George  
Papanikolas Panayiotis  
Pecker Alain  
Saiidi Saiid M.  
Steenfelt Jørgen S.  
Stipanac Bratislav

#### SCIENTIFIC COMMITTEE

Michaltsos George, Chairman

Avraam Tassos  
Baniotopoulos Charalampos  
Beskos Dimitrios  
Bousias Efstathios  
Bruno Domenico  
Constantinou Michael  
Hajdin Nikola  
Kawashima Kazuhiko  
Kotsovos Michalis  
Liolios Asterios  
Makris Nikolaos  
Malakatas Nikolaos  
Marinos Pavlos  
Papanikolas Panayiotis  
Pecker Alain  
Priestley Nigel  
Raftoyiannis Ioannis  
Saiidi Saiid M.  
Sophianopoulos Dimitrios  
Spiliopoulos Konstantinos  
Stavridis Leonidas  
Steenfelt Jørgen S.  
Stipanac Bratislav  
Tsiknias Telemachos  
Tsopelas Panagiotis

## CONTENTS

Foreword.....	v
The Mycenaean bridges in Argolis. A dedication to the milestone of Kazarma Bridge.....	xiii

### KEYNOTE LECTURES

Nonlinear static response of self-anchored cable supported bridges <i>D. Bruno, F. Greco, P. Lonetti</i> .....	3
Some new trends in seismic design of bridge–pier foundations..... <i>G. Gazetas</i>	19
Monitoring data processing for fatigue verification under particular deck vibration of “Charilaos Trikoupis” Bridge .....	33
<i>P. Papanikolas, A. Stathopoulos-Vlavis, A. Panagis, O. Flamand</i>	
Kinematic soil structure interaction for bridge piled foundations..... <i>A. Pecker</i>	43
Resilient and sustainable bridges of the future..... <i>M. S. Saiidi, M. Tazarv, B. Nakashoji, S. Varela, F. Kaviani-pour</i>	57
Izmit Bay Bridge. Geotechnical challenges and innovative solutions..... <i>J.S. Steinfelt, B. Foged, A.H. Augustesen</i>	69

### TOPIC 1

Longitudinal and transverse seismic retrofit of bridges..... <i>O. Markogiannaki, I. Tegos, S. Vasileiou</i>	87
A proposal for improving regularity of integral concrete bridges..... <i>V. Pilitsis, I. Tegos</i>	95
Vulnerability functions to estimate the seismic damage response for the Krystallopigi bridge of Egnatia motorway, Northern Greece.....	103
<i>Ast. Liolios, P. Panetsos, Ang. Liolios, G. Hatzigeorgiou, D. Kalkinis</i>	

“De bosset” monumental stone bridge in Cephalonia: strengthening measures and seismic response under the earthquakes of 26/01/2014 and 03/02/2014.....	111
<i>E. Rovithis, K. Pitilakis, T. Vlachoulis, I. Karani, E. Chorafa, E. Zarogiani</i>	
A proposal for the use of a new type of pier connections with deck and pile cap with in-service and seismic advantages.....	119
<i>I. Tegos, V. Pilitsis, T. Chrysanidis</i>	
A proposal for the improvement of the earthquake resistance of multi-span precast I-beam bridges.....	127
<i>I.A. Tegos, S.D. Tegou</i>	
The use of unbonded tendons on bridges in seismic regions.....	135
<i>O. Markogiannaki, I. Tegos, S. Vasileiou</i>	
The dynamics of a vertically restrained rocking bridge.....	143
<i>N. Makris, M.F. Vassiliou</i>	
The use of piers of high flexibility for the degradation of seismic inertial forces on integral bridges.....	151
<i>I. Tegos, V. Pilitsis</i>	

## TOPIC 2

Environmental effects on bridges. Statistical durability study based on existing inspection data.....	161
<i>F. Alogdianakis, I. Balafas, D.C. Charmpis</i>	
Evaluation of the remaining strength of Rion-Antirion cables-stayed bridge using the multiscaling fracture mechanics approach.....	169
<i>D. Zacharopoulos, T. Panagiotopoulos</i>	
Identification of soil-structure interaction effects based on geodetic monitoring of a railway bridge.....	177
<i>P. Psimoulis, S. Stiros, F. Moschas</i>	
Design and implementation of a multi-sensor monitoring system for structural integrity assessment. The case of Attiki Odos, Pallini cable-stayed bridge.....	185
<i>V. Gikas, P. Karydakis, G. Piniotis, T. Mpimis, F. Papadimitriou, A. Panagakis</i>	
Strengthening and maintenance measures of a bailey-type road bridge.....	193
<i>V.D. Papavasileiou, I.G. Raftoyiannis</i>	
The effect of stereotomy on the shape of the thrust-line and the minimum thickness of masonry arches.....	201
<i>N. Makris, H. Alexakis</i>	

### TOPIC 3

Appraisal of simplified methods for the analysis of box-girder bridges.....	211
<i>L. Stavridis, K. Spiliopoulos, A. Afantenou, I. Kapogiannis</i>	
Investigation on stability problems of piers with practically infinite bending stiffness.....	221
<i>E. Karatzas Roussou, V. Karatzas, G. Karydis, T. Konstantakopoulos</i>	
Inclined bridge under free moving load. A special problem.....	229
<i>T. Avraam, G.T. Michaltsos</i>	
Practical method for completed dead load state determination in cable-stayed bridges with earth anchors.....	237
<i>B. Sun, R. Xiao, D. Zhuang, S. Yuan, E. Xue</i>	
Conventional and alternative design of highway bridge in Egnatia motorway including many innovative solutions.....	245
<i>D. Anastasopoulos, Z. Kopelia, V. Pilitsis, I. Tegos</i>	
The design of a network arch bridge crossing over Arachthos river in Arta, Greece.....	253
<i>D. Mouroukis, P. Veros, K. Lontos</i>	
Rocking and overturning problems in bridges.....	261
<i>G.T. Michaltsos, I.G. Raftoyiannis</i>	
Shear design of bridge piers with rectangular and circular cross-section.....	269
<i>I.A. Tegos, S.D. Tegou, V.G. Pilitsis</i>	
Effectiveness of classical pendulum bearings.....	277
<i>I.G. Raftoyiannis, T.G. Konstantakopoulos, G.T. Michaltsos</i>	
Dependence modelling for bridge structural components under asynchronous seismic excitation.....	285
<i>P. Spyridis, A. Tamparopoulos, K. Bergmeister, Ang. Liolios</i>	
The influence of the vertical inertia forces on the behavior of FPB isolators.....	293
<i>I.G. Raftoyiannis, G.T. Michaltsos</i>	
Optimal location of arch bracings in arch bridges for maximum buckling load.....	301
<i>J. Cheng, J. Ni, L. Jia, R. Xiao</i>	

#### TOPIC 4

Cables with dampers for flow-induced vibration.....	311
<i>T.G. Konstantakopoulos, G.T. Michaltsos</i>	
Cables with movable anchorages for flow-induced vibration.....	319
<i>I. Raftoyiannis, G. Papastergiou, G. Michaltsos</i>	
Optimum design analysis of cable supported bridges.....	327
<i>D. Bruno, F. Greco, P. Lonetti</i>	
A mathematical research on cables with fixed or movable anchorages.....	335
<i>T.G. Konstantakopoulos, G.T. Michaltsos</i>	

#### TOPIC 5

Foundation of a lightweight steel road bridge on peat.....	345
<i>C. Maraveas, K. Miamis, K. Tasiouli</i>	
A proposal for the construction of cast in-situ bridges with tall piers.....	353
<i>I.A. Tegos, S.D. Tegou, I. Thomaidis, I.-P. Thomaidis</i>	
Realization of new Sava river crossing in Belgrade (Serbia).....	361
<i>B. Stipanic, N. Hajdin</i>	
Experimental study on a costless movement restraining system Application of struts-ties in seismically designed bridges.....	371
<i>O. Markogiannaki, I. Tegos</i>	
Experimental investigation on the shear transfer between concrete interfaces Case Study: The Problem of Designing Bridge Seismic Stoppers.....	379
<i>S.D. Tegou, I.A. Tegos</i>	
Calibration of finite element models of Metsovo bridge using ambient vibration measurements.....	387
<i>C. Argyris, D.-C. Papadioti, P. Panetsos, C. Papadimitriou</i>	
Dynamic characteristics of bridge-foundation-soil systems based on laboratory and on-site measurements.....	395
<i>P. Faraonis, A. Sextos, V. Zabel, F. Wuttke</i>	

## TOPIC 6

Soil-structure interaction of seismic isolated bridges.....	405
<i>P. Tsopelas, S.M. Papathanasiou, A. Ucak, E. Prapa</i>	
Performance-based design of bridge foundation on partially improved liquefiable soil.....	413
<i>D. Karamitros, G. Bouckovalas, K. Andrianopoulos</i>	
Development of foundation springs and soil structure interaction evaluation for the third Bosphorus Bridge.....	421
<i>W.-Y. Chen, A. Giannakou, J. Chacko</i>	
Aspects of the soil-structure interaction. The dynamic response of bridge piers on caisson foundations.....	429
<i>R. Cairo, G. Dente</i>	
Simplified method for seismic analysis of motorway bridges.....	437
<i>A. Agalianos, L. Sakellariadis, I. Anastasopoulos, G. Gazetas</i>	
<b>AUTHOR INDEX</b> .....	443



## **THE MYCENAEAN BRIDGES IN ARGOLIS**

### **A dedication to the milestone of Kazarma Bridge**

Today, from the saved ruins we guess that the first bridges were constructed in Assyria, in Egypt and in Minoan Crete, although no historical reference regarding the above has been found anywhere.

The introduction and use of plate-covered drains and domes in buildings in Assyria and Minoan Crete is very old.

The oldest known existing bridges in the form of bridge-drain of small span (from 1 to 2.5m) are dated in the Minoan period in which we have the first significant morphological and static evolution.



*Photo 1.* The ancient bridge of Draconera over water flow

From the primitive plate-covered drain in Draconera of Argolis, Photo 1 (about 1,400 B.C.), until the most known “bridge of Kazarma”, Photo 2, on the side of the highway of Nafplion-Epidavros (about in 1,300 B.C.) one can see the progress in the span increase through the use of the corbel construction system, and finally the use of the functional keystone. According to the above corbel system, spans from 2.5 to 6 m were achieved.





*Photo 2.* The ancient bridge of Kazarma in Epidavros

The invention of keystone (or crown) led to the primitive evolution of the simple arch and later of the three-hinged one.

Therefore, one can recognize the significance of the Kazarma bridge not only because it is the oldest known bridge in Europe but also because it is the first time where the “crown” or “keystone” was used.

Near the village of Arcadikon, on the local road that links Nafplion city to Epidaurus lies the Mycenaean bridge of "Kazarma", the most ancient bridge in Europe. This imposing bridge that constitutes an excellent creation of Mycenaean era was manufactured around 1300 B.C. with bulky crude limestones following closely the characteristic Mycenaean way of construction without connecting materials.

It has a length of 22m, width 5,6m and height of 4m. As the still visible remains of the ancient car road prove, it served as the connection between Mycenae, Ancient Tiryntha and Epidaurus. At the same time it constituted also a dam for impetuous waters of the local river. **Its particular characteristic is the sidelong wedge that retained the walls of the triangular opening in place.**



*Photo 3.* Another view of the ancient bridge of Kazarma in Epidavros

Nowadays, the single-arch bridge that is still in use by the residents of the region as well as four nearby villages, come to remind us that in this region the famous Mycenaean culture was developed.



*Photo 4.* Detail of the arch of the ancient bridge of Kazarma in Epidavros

The Arkadiko Bridge is one of only four known Mycenaean corbel arch bridges near Arkadiko, all belonging to the same Bronze Age highway between the two cities, and all of similar design and age. One of them is the Petrogephyri bridge, which crosses the same stream 1 km to the west of the Arkadiko bridge. Otherwise similar in size and appearance, the structure has a larger span and a little higher vault. It, too, is still used as a local track.

A fifth, well-preserved Mycenaean bridge is located in the wider region at Lykotroupi, where it was part of another Mycenaean main road. Its measurements are close to the Arkadiko Bridge: 5.20 metres wide at the bottom, 2.40 metres at the top and with a corbelled arch span of a little more than a metre. The road still features curbs for guiding fast-moving chariots.



*Photo 5. The megalithic bridge of Lykotroupi*

## **KEYNOTE LECTURES**



IBSBI 2014, October 16-18, 2014, Athens, Greece

## **NONLINEAR STATIC RESPONSE OF SELF-ANCHORED CABLE SUPPORTED BRIDGES**

Domenico Bruno, Fabrizio Greco and Paolo Lonetti

Department of Civil Engineering, University of Calabria, Cosenza, Italy.  
e-mail: d.bruno@unical.it; f.greco@unical.it; paolo.lonetti@unical.it

**ABSTRACT:** A parametric analysis of the nonlinear static behaviour of self-anchored long-span bridges is here carried out by using a 3D nonlinear finite element model of the bridge. Both cable-stayed bridges with a fan-shaped arrangement of stays and combined cable-stayed-suspension bridges are considered in the numerical investigations. The importance of an accurate description of geometrically nonlinear effects, arising from the cables nonlinear behavior in coupling with the instability effect of axial compression in girder and pylons, is pointed out by means of comparisons with results obtained by using different cable models. Numerical simulations are devoted to analyze the influence of the main physical characteristics of the bridge, on the maximum load-carrying capacity and related collapse mechanisms. A nonlinear procedure for finding the initial geometry of the bridge and prestress distribution under dead load is incorporated in the model. The strong role of nonlinear cables response, in coupling with the notable influence of the relative girder stiffness on the stability bridge behavior is analyzed. For the self-anchored combined cable-stayed-suspension bridges the influence of the dead load distribution factor on the limit load evaluation is also accounted.

**KEYWORDS:** Nonlinear cable behavior, Finite element model, Stability.

### **1 INTRODUCTION**

Due to their ability to overcome long spans, during last decades cable supported bridges received notable attention. Several applications are proposed in the framework of both suspension and cable stayed bridge typologies. The erection procedures for a typical cable stayed bridge, due to the free cantilever arms growing to the half length of the main span, produce dangerous conditions because large displacements and rotations are observed [1]. Contrarily, the construction processes in the suspension bridges, are very safe, because the main cable guarantees stability during girder erection procedure also for long spans [1]. Moreover, the cable-stayed bridges with respect to the suspension systems denote, under live loads, enhanced stiffness properties. Consequently,

the combination of the two systems seems able to provide notable advantages especially in the context of long span bridges, providing stable and safe erection processes due to the suspension cable system and reduced deformability of the girder due to the stiffening effect of additional stay elements.

In general, self-anchored long-span bridges exhibit a remarkable nonlinear behavior. Nonlinear effects in cable supported bridges may arise from different sources, including the nonlinear behavior of a single cable due to the sag effect induced by self-weight, changes in geometrical configurations due to large deflections effects (usually large rotations but small strains) in both towers and girder due to their slenderness, the geometrical instability effect of the axial compression induced in the towers and girder, as well as the interactions between cables, deck and pylons nonlinearities [2, 3].

Other nonlinear effects may be related to the constitutive behavior of materials [4-5] or to the coupling between torsion and bending of the girder. Considerable attention has been devoted in the literature to the nonlinear structural behavior problem of cable supported bridges [2-5, 6,7]. In order to reduce the complexity of the highly non-linear problem, most studies available in the literature have introduced some reasonable assumptions in their formulations including one or more of sources of nonlinearities. For instance, pylons nonlinearities arising from beam-column effect are often neglected assuming a high flexural stiffness in pylons. An in-plane analysis is typically carried out excluding out-of-plane and torsional deformation modes and their interaction [2, 5], which can be usually not important in absence of eccentric load also when a three-dimensional bridge model is developed [3]. Moreover, in the framework of the stability analysis of the long span cable supported bridges, the prebuckling behavior is often assumed to evolve linearly with the load parameter, thus leading to a linear eigenvalue problem for the critical load [3, 6]. Although most nonlinear analyses have focused on geometrical nonlinear effects some analyses have involved both geometric and material nonlinearities and analyzed the ultimate behavior and load capacity of a cable-stayed bridge [4, 5, 7].

Due to its inherently nonlinear behavior a conventional analysis of the cable supported bridge, based on linear assumptions is often not applicable especially for long span bridge for which the main girder has the tendency to become more slender and lighter. Existing models which do not take into account appropriately for the softening stay behavior, such as those based on the equivalent tangent modulus of elasticity or those assuming that the cable resists only tensile axial force increment with no stiffness against axial compression increment may lead to a notable underestimation of the maximum load carrying capacity of the bridge for specific loading conditions. Moreover, the actual prebuckling behavior of the bridge may notably deviate from the linear assumptions and a nonlinear limit point analysis should be carried out in place of a linear stability analysis [5]. As a consequence, a more realistic nonlinear

structural analysis accounting for the most important geometrically nonlinear effects should be adopted in conjunction with a nonlinear stability one. To this aim this contribution proposes a numerical investigation on the nonlinear static behavior of long span cable supported bridges (both fan-shaped cable-stayed bridges and combined cable-stayed-suspension bridges are analyzed), by considering the nonlinear behavior of cables in coupling with the instability effect of the axial compression in both girder and pylons. The study is carried out by introducing a general nonlinear model for both the analyzed cable-stayed and combined bridges, after an introductory analysis illustrating the general features of the buckling and post-buckling behavior of the cable supported bridges. Therefore a nonlinear three-dimensional finite element model of the bridge is formulated to accurately determine the influence of nonlinear effects on the structural bridge behavior and on its maximum load carrying capacity. The cable system is modeled according to the multi element cable system approach, where each cable is discretized using multiple truss element and large deformations are accounted by using Green-Lagrange strains. The bridge is modeled by means of a 3D assembly of beam elements and the connections between cables and girder have been obtained by using constraint equations. A nonlinear procedure for finding the bridge initial shape is incorporated in the analysis in order to determine properly the initial geometry and pre-stress distribution under dead load.

## 2 OVERVIEW OF NONLINEAR BRIDGE BEHAVIOR

Cable behavior is one of the most relevant sources of nonlinear elastic behavior of cable supported bridges. In particular, for cable-stayed systems the axial stiffness of stays must be accurately evaluated in order to avoid inappropriate predictions of the actual load carrying capacity. To this end, it must be observed that for large stress increments the secant modulus of the stress-strain relationship should be adopted instead of the tangent one.

The stress increment  $\Delta\sigma$  in the stay may be written in the form:

$$\Delta\sigma = E_s^*(\sigma_0, \Delta\varepsilon)\Delta\varepsilon, \quad (1)$$

where  $E_s^*$  is the secant modulus of the stay which is a nonlinear function of the axial strain increment  $\Delta\varepsilon$ , measured along the stay chord, and of the initial tension  $\sigma_0$ .

If a parabolic shape of the stay deformed configuration is assumed, the well-known Dischinger theory can be employed to model the secant and the tangent elastic moduli  $E_s^*$  and  $E_t^*$ , respectively:

$$E_s^* = \frac{\Delta\sigma}{\Delta\varepsilon} = \frac{E}{1 + \frac{\gamma^2 l_0^2 E}{12\sigma_0^3} \frac{1 + \beta}{2\beta^2}}, \quad \beta = 1 + \frac{\Delta\sigma}{\sigma_0}, \quad E_t^* = \lim_{\beta \rightarrow 1} E_s^* = \frac{E}{1 + \frac{\gamma^2 l_0^2 E}{12\sigma_0^3}} \quad (2)$$



where  $E$  is the Young modulus of the material cable,  $\gamma$  the cable weight per unit volume,  $l_o$  the horizontal projection of the stay length, and  $\sigma_0$  the initial stress in the stay. It must be observed that the tangent modulus is related to small stress increments from the initial configuration (i.e.  $\beta \rightarrow 1$ ). In this case, the cable equivalent modulus can be considered constant during load increment and the nonlinear cable response can be approximated by the tangent linearized one. Assuming that when shortening occurs the cable stiffness vanishes leads to the tension only approximation of stay behavior (see for instance [2,6]):

$$\Delta\sigma / \Delta\varepsilon = E_t^* \quad \text{if } \Delta\varepsilon \geq 0; \quad \Delta\sigma / \Delta\varepsilon = 0 \quad \text{if } \Delta\varepsilon \leq 0. \quad (3)$$

The effects of the above assumptions on the nonlinear cable behavior, can be analyzed qualitatively by considering a complete fan shaped and self-anchored cable-stayed bridge scheme with the girder not horizontally constrained and the load uniformly applied on the central span. Generally speaking, assuming a linear prebuckling behavior, the girder compression produces an equilibrium bifurcation when the load reaches the critical value.

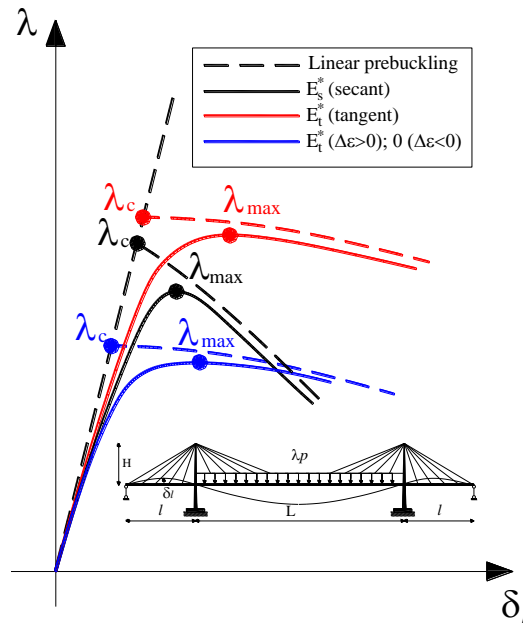


Figure 1. Nonlinear bridge behavior: load parameter versus lateral midspan deflection.

The postbuckling behavior strictly depends on the shape of the buckling mode and may show a decreasing behavior due to the softening cable response in compression (see the dashed line curve in Fig. 1). The actual bridge behavior taking into account the nonlinear prebuckling effects, doesn't exhibit an equilibrium bifurcation and is qualitatively shown by means of a continuous line in Fig. 1. In particular, when the secant modulus is adopted for the cable response a strong snap buckling behavior is expected with the maximum load parameter  $\lambda_{max}$  significantly below the critical load  $\lambda_c$  and post-buckling behavior of asymmetric unstable type.

This behavior is mainly attributed to the softening behavior of stays under shortening. On the other hand, when the stay behavior is modeled by means of the tangent modulus a non conservative prediction can be obtained since the limit load is larger than that based on the secant modulus formulation and a mild snap buckling occurs as in a symmetric unstable bifurcation. The

magnitude of the critical load, depending exclusively on the tangent modulus distribution along the stays, changes slightly with respect to the secant modulus formulation. For instance, the critical load should remain unchanged provided that for each stay the stress at bifurcation is adopted as initial stress in the tangent modulus formula. Note that when buckling occurs at high load level, as in the case of uniform loading on the entire bridge, a value near to  $E$  can be assumed for the tangent modulus. A similar behavior occurs when the tension only truss model is adopted but the maximum load may be notably lower than the more accurate prediction obtained using the secant modulus model, thus leading to a conservative prediction of the maximum load-carrying capacity.

It results that bridge stability is mainly a consequence of two competing nonlinear effects in the tangent stiffness expression: the instability of axial compression in both girder and pylons and the stabilizing one due to the tangent stiffness of stays attached to the left and right pylons. The former generally increases with the load parameter  $\lambda$ , the latter may increase or decrease depending on the actual deformed configuration of the bridge due to the softening cable behavior under shortening.

### 3 BASIC ASPECTS OF BRIDGE MODELS

#### 3.1 Cable-stayed bridge

Here a cable stayed bridge scheme with a fan-shaped arrangement of stays is analyzed, based on a diffused stays arrangement ( $\Delta/L \ll 1$ ). The bridge model is able to predict the static behavior of cable stayed bridges taking into account the nonlinear behavior of stays, adopting the Dischinger's fictitious modulus and taking into account the instability effect due to the axial compression in the girder [8].

The analyzed bridge scheme is illustrated in the Fig. 2. The girder is supported by stays joining at the tower tops. The two lateral couple of stays, called anchor stays, assure the bridge equilibrium and are anchored by means of two vertical supports; the girder is not constrained in the longitudinal direction.

It is assumed that the erection method is such that the deck final configuration is practically straight and free from bending moments. The bridge static response when the live load  $\lambda p$  increasing with the parameter  $\lambda$  is applied, is now considered starting from the straight equilibrium configuration of the bridge deck corresponding to the application of the dead load  $g$  and cables pre-stress. As a matter of fact, the horizontal equilibrium of the bridge requires shear forces to be the same at the pylon top sections and this ensures that displacements of the pylon tops will always be equal and opposite. Similarly due to rotational equilibrium considerations about the y-axis, the pylon tops torsional rotations will always be equal and opposite.

The vertical, horizontal and torsional equilibrium equations for the girder respectively are:

$$\begin{aligned}
EIv^{IV} + \left[ (N^g + \Delta N(w))v' \right]' - q_v &= \lambda p \\
EAw'' + q_h &= 0 \\
C_t \theta'' &= -m_t - \lambda p e
\end{aligned} \tag{4}$$

where  $EI$  is the girder flexural stiffness,  $N^g$  is the axial force in the girder due to the dead load  $g$ .  $\Delta N(w) = EA w'$  indicates the axial force increment in the girder due to live loads  $p$ ;  $E$ ,  $A$  and  $C_t$  are respectively the Young modulus, the cross section area and the torsional stiffness of the girder. Moreover  $q_v$  and  $q_h$  are the vertical and the horizontal components of the stays-girder interaction, respectively, whereas  $m_t$  denotes the stays-girder torsional couple interaction.

The two components of the stays-girder interaction depend on  $E_{SL}^*$  and  $E_{SR}^*$ , representing the Dischinger's secant modulus for the cables, respectively applied on the left (L) and on the right (R) stays with respect to the  $y$ - $z$  plane (see the right of Fig.2). Note that  $E_{SL}^*$  and  $E_{SR}^*$  depend on the additional axial strain  $\Delta \varepsilon$  in the cables produced by the additional displacements  $v$ ,  $w$ ,  $u$ ,  $\theta$  and  $\psi$  and that the initial stress of eqn (2) here represents the stress in the cables under the dead loads  $g$ .

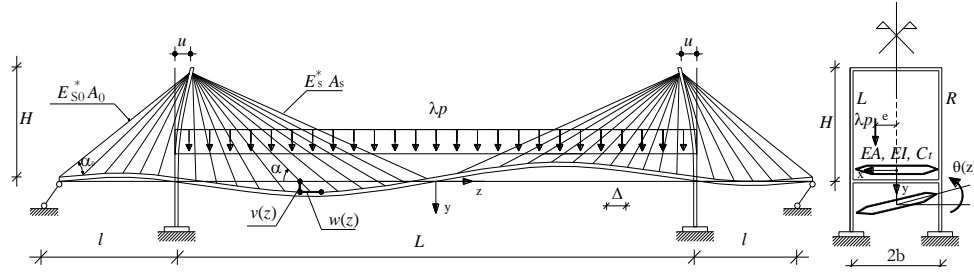


Figure 2. The long-span cable stayed bridge structural scheme.

Usually the stays cross section area  $A_s$  of the left or right curtains of stays is designed so as dead loads produce constant tension in all stays and this leads to  $A_s = g\Delta / (2\sigma_g \sin \alpha)$  in which  $\sigma_g$  is defined as a function of the allowable stress  $\sigma_a$  as  $\sigma_g = g\sigma_a / (p+g)$  assuming that the stress increment in the stays are proportional to the design live load  $p$ . For the anchor stays the cross sectional area  $A_0$  is designed in such a way that the allowable stress  $\sigma_a$  is obtained for live loads  $p$  applied to the central span only, leading to:

$$A_0 = \frac{gl}{4\sigma_{g0}} \left[ 1 + (l/H)^2 \right]^{1/2} \left[ (L/(2l))^2 - 1 \right], \quad \sigma_{g0} = \sigma_a \left[ 1 + \frac{p}{g} \frac{(L/(2l))^2}{(L/(2l))^2 - 1} \right]^{-1} \tag{5}$$

where  $\sigma_{g0}$  is the initial tension in the anchor stays under dead load  $g$ .

The horizontal and torsional equilibrium equations of the pylons, involving the effects of the stays-girder interaction, lead to integral equations [9]. If the left pylon equilibrium is considered, the following equation is obtained:

$$\int_{-(l+L/2)}^0 q_h dz + Ku + S_L^0 + S_R^0 = 0, \quad \int_{-(l+L/2)}^0 m_f dz + Kb^2 \psi + (S_L^0 - S_R^0)b = 0, \quad (6)$$

where  $K$  and  $m_f$  are the pylon tops flexural stiffness and the horizontal flexural couple per unit length acting on the left side of the bridge ( $z < 0$ ), respectively. Moreover, in equations (6)  $S_L^0$  and  $S_R^0$  are the horizontal components of the anchor stays axial forces, for the left and right curtains of stays with respect to the vertical  $yz$  plane, respectively, and  $\psi$  is the torsional rotation of the tower top. A similar equation is obtained for the right pylon.

In order to analyze the main parameters governing the bridge behavior, the following dimensionless quantities are introduced:

$$a = \frac{\gamma^2 EH^2}{12\sigma_g^3}, \quad \varepsilon = \sqrt[4]{\frac{4I\sigma_g}{H^3g}}, \quad \varepsilon_A = \frac{A\sigma_g}{Hg}, \quad \tau = \sqrt{\frac{C_t\sigma_g}{Eb^2Hg}}. \quad (7)$$

The parameters  $\varepsilon$ ,  $\varepsilon_A$  and  $\tau$ , respectively represent a measure of the relative bending, axial and torsional stiffness between the girder and stays, whereas  $a$  is related to the stay deformability accounting for the cable sag effect. Additional details on the continuum bridge formulation can be found in [8]. It is worth noting that the above formulation does not take into account for buckling in the horizontal plane (out-of-plane buckling) and is strictly valid for the H- shape pylons. These restrictions will be removed in the discrete bridge model.

### 3.2 Combined cable-stayed suspension bridge

The structural model of the combined bridge, as shown in Fig.3, is based both on stayed and suspension cable systems, arranged in a self-anchored scheme, where the connection between suspension main cable and pylon is assumed to be a frictionless saddle system. Moreover, the bridge scheme is consistent with a fan-shaped system, in which the stays are perfectly constrained to the pylons and simply supported constraints are considered at girder pylon connections and at the left and right girder cross section ends. The bridge model is founded on the assumption of a uniform distribution of stays along the deck. In particular, the stay spacing  $\Delta$  is small in comparison to the bridge central span  $L$ . As a result, the self-weight loads produce negligible bending moments on the girder with respect to that raised by the live loads.

A proper erection procedure is supposed to guarantee that the girder position under self-weight is practically coincident with the undeformed configuration and, consequently, free from bending moments. In particular, the initial stress distribution produces tension in the cable systems and compression in both

girder and pylons. The overall geometrical parameters of the combined cable system are governed by the self-weight loading condition (Fig.3). In particular, the stay and hanger cross sections are designed in such a way that the self-weight loads produce constant tension over all distributed elements and equal to a fixed value, namely  $\sigma_g$ .

The hanger elements follow a linear elastic behavior and are characterized by negligible weight in comparison to that involved by the main cable or the girder. These assumptions are defined consistently with some formulations recoverable from the literature [1]. In particular, it is supposed that the hanger elements remain always in tension, due to fact that a proper pre-stress system applied during the erection procedure is able to prevent compression state. Moreover, a proper erection procedure is assumed to distribute the girder self-weight load with a rate  $r$  ( $0 < r < 1$ ), namely dead load distribution factor. This hypothesis is in agreement with the main theory on combined supported bridges, which considers the dead load distribution subdivided into equivalent loads depending on the amount required of the cable steel quantity involved in the cable system [1].

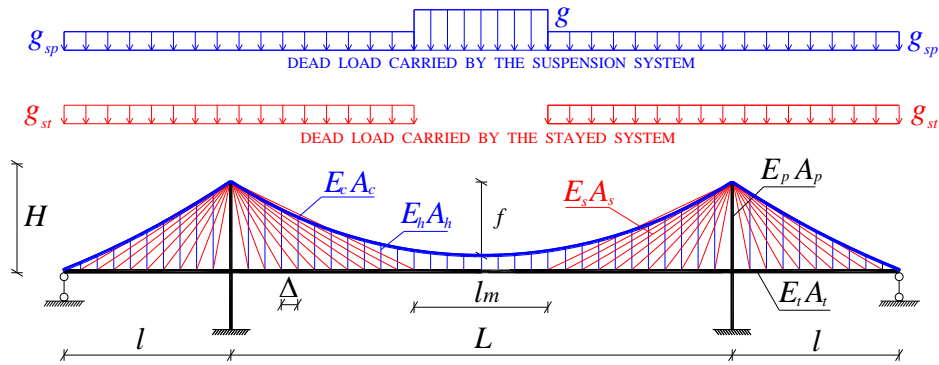


Figure 3. The long-span combined cable-stayed-suspension bridge structural scheme.

From an analytical point of view  $r$  corresponds to a dead loads distribution factor, equal to the fraction of the total girder dead load taken by the suspension system in the regions where both suspension and cable stayed systems are present. Therefore, the girder self-weight amounts applied to the cable stayed (st) and the suspension (sp) systems,  $g_{st}$  and  $g_{sp}$  respectively, are defined by the following expressions:

$$g_{st} = (1-r)g, \quad g_{sp} = rg, \quad (8)$$

where  $g$  represents the girder self-weight loads per unit length. The cross section area of a generic stay or hanger, and of the the anchor stays are dimensioned by means of the following equations:

$$A_s = \frac{g_{st}\Delta}{\sigma_g \sin \alpha}, \quad A_h = \frac{g_{sp}\Delta}{\sigma_g}, \quad A_0 = \frac{g_{st}l}{2\sigma_{g0}} \left[ 1 + (l/H)^2 \right]^{1/2} \left[ (L/2l)^2 - 1 \right] \quad (9)$$

where  $\sigma_g$  and  $\sigma_{g0}$  are the self-weight design tension before defined for the cable-stayed bridge scheme,  $\Delta$  is the stay and hangers spacing step,  $\alpha$  is the stay orientation angle with respect to the horizontal direction. Similarly for the anchor stays, the geometric area is determined in such a way that the corresponding allowable stress, i.e.  $\sigma_a$ , is reached in the static case, for live loads applied on the central span only.

From a practical point of view, the design parameter  $r$  is an indicator of the ratio between the suspension system steel quantity and that involved in the combined bridges. As an example, assuming that  $r$  is equal to 0 or 1, the combined bridge tends to a perfect cable stayed or suspension bridge scheme, respectively. The cable stayed system, especially for long spans, is affected by high stiffness reduction due to Dischinger effects. As a consequence, the stays are supposed to be distributed on a reduced portion of the main span, namely  $2l+L-lm$  (Fig.3), which can be estimated, approximately, by the following relationship [1]:

$$l_m = L - L \left[ 1 + \left( (g_{sp} + g_c) / (g + g_c) \right)^{1/2} \right]^{-1} \quad (10)$$

where  $g_c$  is the self-weight main cable suspension distributed loads. In the framework of long span bridges, the ratio between sag and horizontal main cable projection length is usually small. Therefore, the initial main cable configuration  $y$  and the corresponding horizontal axial force  $H_g$  can be determined, utilizing a parabolic approximation of the cable profile, as:

$$y(z) = -M(z)/H_g, \quad H_g = \left[ (g_c + rg)L^2/8 + g_{st}l_m(L-l_m/2)/4 \right] / f \quad (11)$$

where  $M(z)$  is a fictitious bending moment due to distributed self-weight loads taken by the suspension system calculated as for a simply supported beam and  $f$  is the main cable sag. The cross sectional area of the main cable is given by [1]:

$$A_c = H_{g+pl} / (\sigma_a \cos \phi), \quad (12)$$

where  $\phi$  is the orientation angle formed by the main cable tangent at pylon intersection and the vertical direction and  $H_{g+pl}$  is the horizontal main cable force related to live loads applied to the whole central span. The main cable position as well as the corresponding axial force horizontal projection, i.e.  $(\bar{y}_c, H_t)$ , are supposed to be expressed as the sum of contributions related to self-weight loading  $(y, H_g)$  defined by eqn (11), and corresponding ones produced by the live loads application, i.e.  $(v_c, h)$ :

$$\bar{y}_c(z) = y(z) + v_c(z), \quad H_t(z) = H_g + h(z) \quad (13)$$

According to a continuum approach, the interaction forces  $q_s$  between main cable and girder, are expressed, analytically, for small hanger spacing, by means of a continuous function depending on the bridge kinematic, the main cable configuration and the hanger stiffness properties, as:

$$q_s = -EA_h(v - v_c) / (H - y)\Delta \quad (14)$$

in which  $v$  and  $v_c$  are the vertical displacements for the girder and the main cable, respectively. Consistently with a flat-sag based cable formulation, which admits a parabolic approximation of the main cable profile, the equilibrium equation along vertical direction is a function of the hangers interaction forces and can be expressed in terms of incremental quantities measured starting from the undeformed configuration:

$$\left[ H_t v_c' \right]' = q_s. \quad (15)$$

The vertical equilibrium equation for the girder is in this case:

$$EIv^{IV} + \left[ (N^g + \Delta N(w))v' \right]' - q_v - q_s = \lambda p, \quad (16)$$

where  $q_v$  is the vertical component of the stays-girder interaction. Horizontal and torsional equilibrium equations for both girder and pylons can be expressed like in the case of cable-stayed bridges keeping in mind that here the torsional couple  $m_t$  includes both the stay-girder torsional interaction and the hanger-girder torsional interaction.

#### 4 3D-DISCRETE MODEL

In this section a 3D discrete FE bridge model is examined for both the case of cable-stayed and combined cable-stayed suspension bridges, taking into account the geometric nonlinear effects for the cable system under general loading conditions, in order to obtain accurate results. In particular, the actual stays (and hangers for combined bridges) spacing is considered in the model. This discrete model has been analyzed by means of a displacement-type finite element (FE) approximation, implemented in the commercial software COMSOL MULTIPHYSICS™ [10]. A three dimensional finite element model has been developed by using beam elements for the girder and the pylons and nonlinear truss elements for the cable system. Specifically, the bridge deck is replaced by a longitudinal spline with equivalent sectional and material properties and the pylons are composed by two columns connected at their top and at the level of the bridge deck by two horizontal beam elements. Moreover, the instabilizing effects produced in both girder and pylons by the axial compression force  $N$  has been accounted by adding the following weak contributions for pylons and girder, respectively, to the virtual work principle formulation:

$$\begin{aligned}
& - \left( \int_{L_e} N \theta_x \delta \theta_x dL + \int_{L_e} N \theta_z \delta \theta_z dL \right)_{Pylons} \\
& - \left( \int_{L_e} N \theta_y \delta \theta_y dL + \int_{L_e} N \theta_x \delta \theta_x dL \right)_{Girder}
\end{aligned} \tag{17}$$

where  $N$  is the axial force,  $\theta_x$ ,  $\theta_y$  and  $\theta_z$  the denote rotations about the  $x$ ,  $y$ , and  $z$  axes, and  $L_e$  is the element length.

The cable system is modeled according to the Multi Element Cable System (MECS) approach, where each cable is discretized using multiple truss element. The stiffness reduction caused by sagging is accounted for by allowing the cable to deform under applied loads. Large deformations are accounted by using Green Lagrange strains and the axial strain is calculated by expressing the global strains in tangential derivatives and projecting the global strains on the cable edge. Additional details about the approach here adopted to model nonlinear cable behavior can be found in [10]. It is worth noting that different approaches have been proposed in the literature to model the nonlinear cable behavior ranging from the simple equivalent modulus approach, according to which each cable is replaced by one bar element characterized by an equivalent tangent modulus [4,7] often with a tension only behavior [2, 5, 6], to more accurate techniques based on the elastic catenary results.

In the case of the simplified cable behavior simulated by using the tangent modulus for the cable-stayed bridges, a single truss element is adopted for each stay and the geometrical nonlinearities are deactivated. The constitutive behavior is simulated by introducing the expression shown in eqn (2) for the truss element constitutive modulus, with the initial stress derived from results obtained through the initial shape analysis formulated in the sequel.

The tension only behavior (always for the cable-stayed bridges) is modeled similarly except that a nonlinear constitutive behavior according to eqn (3) is incorporated in the constitutive relationship of the truss element representing the single stay. To this end the longitudinal modulus of the truss element is multiplied by a step function depending on the axial strain increment with respect to the initial configuration of the bridge under dead loading, in order to exclude any stiffness contribution of the cable under shortening. Therefore, the constitutive behavior of the truss element is (see [8] for additional details):

$$\Delta \sigma = E_t^* \text{step}(\Delta \varepsilon) \Delta \varepsilon, \text{step}(\Delta \varepsilon) = 1 \text{ if } \Delta \varepsilon \geq 0; \text{step}(\Delta \varepsilon) = 0 \text{ if } \Delta \varepsilon < 0 \tag{18}$$

The constraint condition between the girder and the stays (and the hangers for combined bridges) is modeled with offset rigid links to accommodate cable anchor points, by means of the extrusion coupling variable methodology (see [10] for additional details). The buckling and post-buckling behaviors have been investigated by using nonlinear analyses taking into account large deformation but small strains with linear stress-strain relationship and a solution strategy



based on the damped Newton method has been adopted. A suitable modeling technique in this case, where the relationship between applied loads and displacements is highly nonlinear, is to use an algebraic equation that controls the applied live loads  $\lambda p$  so that the generalized deflection of a control point reaches the prescribed values. In order to capture the typical snapping behavior of the load-displacement curve, a generalized deflection increasing monotonically with the evolution of the loading process is adopted, so that no snap-back are detected when the load-displacement curve is plotted in terms of the assumed control parameter. In the case of loading on the central span of the bridge, an appropriate choice to capture the snapping behavior is the lateral midspan deflection  $\delta_l$  or the girder end in-plane rotation  $\theta$ , although in some cases relevant to the TO model the central midspan deflection  $\delta_c$  has been adopted. An initial shape analysis must be carried out to find the geometric configuration together with the associated pre-stress force distribution in cables satisfying both equilibrium and the design requirements of a straight initial bridge configuration. All geometric nonlinearities are taken into consideration in the initial shape analysis, namely geometric effects of axial compression in both girder and towers and cable sag nonlinearities induced by cable dead load.

## 5 NUMERICAL RESULTS

### 5.1 Cable-stayed bridge

Here numerical results for the cable-stayed bridge model are presented to examine the instabilizing effect produced by the axial force in the girder for increasing live loads  $\lambda p$ . In particular two types of loadings are considered: a uniform load distributed on the whole bridge length and a uniform load applied on the central span only. The following dimensionless parameters are used in the numerical analyses:

$$L/2H=2.5, \quad l/H=5/3, \quad b/H=0.1, \quad \Delta/L=1/105, \quad \sigma_d/E=7200/2.1 \times 10^6, \quad K/g=50$$

whereas the material properties assume the values that concern the usual case of steel girders and towers. The value of the dead load  $g$  is equal to 300,000 N/m, typical of a steel deck, whereas the cable unit volume weight has been assumed equal to  $\gamma=77.01$  kN/m<sup>3</sup>. The other parameters  $\varepsilon$ ,  $\tau$ ,  $\varepsilon_A$  and  $a$  are used to define the bridge geometrical parameters according to eqn (7).

A parametric analysis is carried out by adopting the following values:  $\varepsilon = 0.2$  or  $0.3$ ,  $a = 0.10$  or  $0.20$  and  $p/g = 0.5$  or  $1$ , whereas  $\varepsilon_A$  has been assumed equal to 54.5. As far as the analysis carried out with the discrete model is concerned, the following additional parameters are needed:

$$\varepsilon_h = \sqrt[4]{4I_{yy}\sigma_g/b^3g}, \quad I_r = I_{pxx}/I$$

defining respectively the relative girder to stay stiffness for bending in the horizontal plane and the tower to girder bending stiffness ratio for bending in

the vertical plane. The former parameter gives the bending stiffness  $EI_{yy}$ , whereas the latter the pylon bending stiffness  $EI_{pxx}$ . The towers stiffness  $I_{pzz}$  for out-of-plane bending has been assumed equal to  $EI_{pxx}$  and the ratio between the height of the pylon from pier bottom to bridge deck  $H_l$  and  $H$  has been assumed equal to 0.25. The axial, bending and torsional stiffnesses of the beams connecting the two towers of the pylons have been assumed equal to the corresponding ones adopted for the towers. Moreover, the cross section area and the torsional stiffness of the towers have been assumed equal to those of the girder. These parameters allow to define the bridge characteristics for the 3D discrete model. On the other hand the following parameters have been assumed for the remaining parameters:  $\tau=0.1$ ,  $\varepsilon_h=5$ ,  $t=0.1$ . The influence of the different stays response approaches introduced in section 2, on the bridge nonlinear behavior by using the more general 3D discrete model is here investigated. To this end the response of a single stay has been modeled by using the multiple truss element nonlinear formulation, which will be denoted as NLM, the tangent modulus linear model (denoted as LM in the sequel) and the tension only approximation (denoted as TO in the sequel).

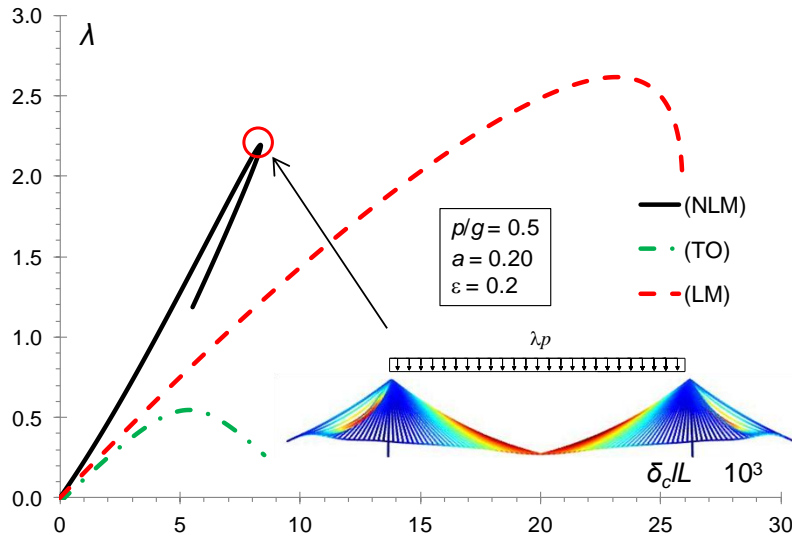


Figure 4. Cable stayed bridge: load parameter  $\lambda$  versus central midspan deflection  $\delta_c$ .

Figure 4 shows for  $\varepsilon=0.2$ ,  $a=0.2$  and  $p/g=0.5$  the typical snapping for low values of  $\lambda$  due to the coupling between the instability effect of the axial compression in the girder and the softening behavior of stays response in the lateral span, occurring in the case of the central loading condition and the H pylon shape. As the load parameter increases while in the central span the instability effect of the axial compression is balanced by the stiffening stays in the lateral spans stays show a large stress reduction produced by the lateral

spans deflection and an instability condition is rapidly reached producing a bound in the applied load. The load-displacement curves are represented in term of the central midspan deflection  $\delta_c$  in order to better appreciate the differences between the three considered models, although the nonlinear analyses have been driven always by the lateral midspan deflection. In figure 4 the results obtained by using the linear tangent model (LM) and the tension only model (TO), are also shown in order to appreciate the influence of the nonlinear cable response modeling on the global bridge behavior.

## 5.2 Combined cable-stayed-suspension bridge

Here numerical results for the self-anchored combined cable-stayed suspension bridge model are presented. It's well known that for the combined bridges a distribution of the girder self-weight load with a rate  $r$  ( $0 < r < 1$ ), namely dead load distribution factor, is assumed. This hypothesis is in agreement with the main theory on combined bridges, which considers the dead load distribution subdivided into equivalent loads depending on the amount required of the cable steel quantity involved in the cable system. In particular,  $r$  corresponds to a dead load distribution factor, equal to the fraction of the total girder dead load taken by the suspension system in the regions where both suspension and cable stayed systems are present. From a practical point of view, assuming that  $r$  is equal to 0 or 1, the combined bridge tends to a perfect cable stayed or suspension bridge scheme, respectively. In the numerical simulations three different values for  $r$  are considered, namely  $r=0$  (cable stayed bridge),  $r=1$  (suspended bridge) and  $r=0.5$  (combined bridge).

In this section the influence of the coupling stayed-suspension parameter  $r$  on the maximum load parameter for the self-anchored combined cable-stayed suspension bridge is analyzed. The load condition corresponding to a uniform load applied on the central span only is considered in the analysis.

The geometrical configuration is characterized by  $L=1500$  m,  $l=500$  m and  $f=214$  m. The value of the dead load  $g$  is equal to 300,000 N/m, typical of a steel deck. The stays and hangers spacing  $\Delta$  is assumed equal to  $L/30$ , whereas two different value for  $p/g$  are considered ( $p/g=0.25$  and  $0.50$ ). For the combined bridges the multiple truss element nonlinear formulation is used to model the single cable response (main cable and stays). For the hangers a single linear truss element is employed. Figure 5 shows for the analyzed geometrical configuration ( $L=1500$  m,  $l=500$  m,  $f=214$  m) and  $p/g=0,25$ ;  $0.50$  the load-displacement curves for the three bridge schemes corresponding to the distribution dead load factor  $r$  ( $r=0, 0.5, 1$ ). In particular, the typical snapping behavior for relatively low values of  $\lambda$  occurring in the case of the central loading condition can be observed. The load-displacement curves are represented in term of the lateral midspan deflection  $\delta_l$  (used like control parameter to drive the nonlinear analyses) and show the differences between the

three considered bridge schemes. The diagrams evidence the conservative prediction of the limit load in the case of suspension bridge ( $r=1$ ) with respect to the cable-stayed system ( $r=0$ ). Moreover, it's possible to observe how combination of the two systems provides stabilizing effect in terms of maximum load parameter ( $0 < r < 1$ ).

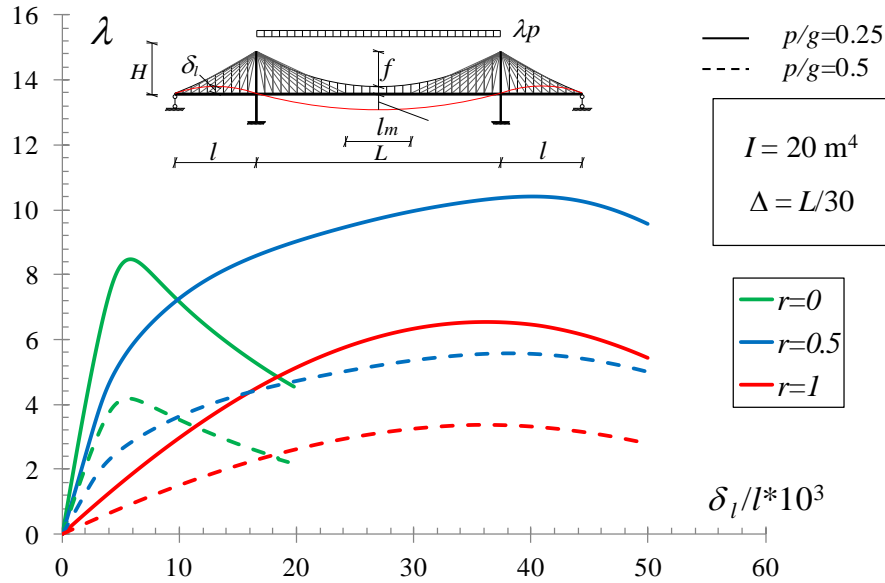


Figure 5. Combined bridge: load parameter  $\lambda$  versus lateral midspan deflection  $\delta_l$ .

## 6 CONCLUDING REMARKS

A numerical investigation on the geometrically nonlinear static behavior of self-anchored long span cable supported bridges is carried out by adopting a tridimensional finite element model for the bridge. Both long span cable-stayed bridges, with a fan-shaped arrangement of stays and self-anchored combined cable-stayed-suspension bridges are considered in the numerical computations. For the first bridge model analyzed numerical investigations are devoted to study the influence of three different stays response approaches on the bridge nonlinear behavior by using a more general discrete approach. In particular, the mechanical response of a single stay has been modeled by using the multiple truss element nonlinear formulation (denoted as NLM), the tangent modulus linear model (denoted as LM) with the initial stress derived from the initial shape analysis and the tension only approximation (denoted as TO) according to which cable assumes a vanishing stiffness under shortening.

Numerical results show the typical snapping behavior for high values of the load parameter  $\lambda$  due to the coupling between the instability effect of the axial

compression in the girder and the softening behavior of stays response in the lateral span, occurring in the case of the central loading condition. Moreover, from numerical investigations it was found that in the case of uniform loading on the whole bridge length, contrarily to that found for central loading condition, as the load parameter increases the effect of softening in stays tangent stiffness is negligible occurring for a very small group of cables and for larger load level. For this loading condition it is possible to appreciate the conservative behavior of the LM and TO models with respect to the NLM, in terms of the maximum load parameter  $\lambda_{max}$ . In the case of the self-anchored combined cable-stayed-suspension bridges the influence of the coupling stayed-suspension parameter  $r$  on the maximum load for the bridge is analyzed. Results evidence the conservative prediction of the limit load in the case of suspension bridge ( $r=1$ ) with respect to the cable-stayed system ( $r=0$ ). Moreover, numerical investigation show that combination of the two cable systems provides stabilizing effect in terms of maximum load parameter.

## REFERENCES

- [1] N.J. Gimsing, *Cable supported bridges: concepts and design*. John Wiley & Sons, NJ (1997).
- [2] Pao-Hsii Wang, Hung-Ta Lin, Tzu-Yang Tang, "Study on nonlinear analysis of a highly redundant cable-stayed bridge". *Computers and Structures*, 80, 165-182 (2002).
- [3] C.C. Tang, H. S. Shu, Y.C. Wang, "Stability analysis of steel cable-stayed bridges". *Structural Engineering and Mechanics*, 11, 35-48 (2001).
- [4] H. Adeli, J. Zhang, "Fully nonlinear analysis of composite girder cable-stayed bridges". *Comput Struct*, 54(2), 267-77 (1995).
- [5] Weon-Keun Song, Seung-Eock Kim, "Analysis of the overall collapse mechanism of cable-stayed bridges with different cable layouts". *Engineering Structures*, 29, 2133-2142 (2007).
- [6] Y.C. Wang, "Number of cable effects on buckling analysis of cable-stayed bridges". *Journal of bridge Engineering*, 4(4), November (1999).
- [7] X. Ying, J.S. Kuang, "Ultimate load capacity of cable-stayed bridges". *Journal of Bridge Engineering*, 4(1) (1999).
- [8] D. Bruno, F. Greco, P. Nevone Blasi, E. Bianchi, "A 3D nonlinear static analysis of long-span cable stayed bridges". *Annals of Solid and Structural Mechanics*, DOI 10.1007/s12356-013-0033-8, (2013).
- [9] D. Bruno, F. Greco, P. Lonetti, "A parametric study on the dynamic behavior of combined cable-stayed and suspension bridges under moving loads". *International Journal for Computational Methods in Engineering Science and Mechanics*, 10(4), 243-258 (2009).
- [10] COMSOL AB, *Structural Mechanics Module User's Guide*, (September 2008).

IBSBI 2014, October 16-18, 2014, Athens, Greece

## **SOME NEW TRENDS IN SEISMIC DESIGN OF BRIDGE–PIER FOUNDATIONS**

George Gazetas

National Technical University of Athens, Greece  
e-mail: gazetas@central.ntua.gr

**ABSTRACT:** Numerical and experimental research is outlined on the idea of rocking-isolation of bridge pier through a non-conservative design of the foundations. Shallow foundations are studied in detail, but piled foundations and embedded caissons are also discussed.

**KEY WORDS:** Footings; Piles; Caissons; Capacity Design; Uplifting; Bearing Capacity; Earthquake Engineering

### **1 INTRODUCTION**

Inspired by post-seismic field observations and engineering concerns in actual bridge projects, in the last 10-15 years significant theoretical and experimental research aimed at challenging one of cornerstones in earthquake engineering: “capacity design”. One of the motives of such design was to control seismic damage by strategically directing inelastic deformation to structural components that could be inspected and repaired after a damaging event. For bridge piers this meant ensuring that “plastic hinging” will occur in the column rather than the foundation. Hence, current design leads to strong unyielding foundation-soil systems. Overstrength factors are invoked to increase the maximum moment that can be (nominally) transmitted by the pier column, and foundation design is performed with this increased moment, and (in addition) conservatively. As a result, in regions of high seismicity piled foundations or rigid caissons or oversized footings are often required even in excellent ground conditions. Evidence from numerous earthquakes shows that such unyielding foundations (“nailing” the structure to the ground) have not prevented heavy damage and even catastrophic collapse in case of a strong seismic excitation. In response, a number of studies have explored the possibilities and constraints of an alternative design concept: allowing the development of plastic hinging in the soil or at the soil–foundation interface, so as to reduce the possibility of damage to the structure.

Focusing on surface foundations, where nonlinearity manifests itself through uplifting and/or soil yielding, a “reversal” of the current capacity design principle is proposed: the foundation is intentionally underdesigned compared

with the supported pier/column to promote rocking response and accumulation of plastic deformation at the soil–foundation interface. Supporting evidence for this new approach has been provided as follows:

- Several theoretical and numerical studies on the rocking response of rigid blocks and elastic single-degree-of-freedom (SDOF) oscillators provide compelling evidence that uplifting drastically reduces the inertial load transmitted into the oscillating structure.
- Because of the transient and kinematic nature of seismic loading, rocking response does not lead to overturning even in the case of very slender structures except in rather extreme cases of little practical concern.
- Referred to as rocking isolation, allowing for foundation uplift has been proposed, and in a few exceptional cases employed in practice, as a means of seismic isolation (Rion-Antirrion bridge, Greece; Rangitikei Railway Bridge, N. Zealand).
- Even in the case of relatively heavily loaded footings or footings on soft soils, when rocking is accompanied with yielding of the supporting soil (and possibly momentary mobilizing bearing capacity failure mechanisms), substantial energy is dissipated in the foundation providing increased safety margins against overturning owing to the inherently self-centering characteristics and the ductile nature of rocking on compliant soil.
- Most importantly, a number of studies have recently investigated the scheme of rocking isolation, with emphasis on its effects on structures, which consistently point to a beneficial role of nonlinear foundation behavior for the overall system performance.
- A variety of modern numerical tools have been developed enabling comprehensive modeling of non-linear rocking response alleviating to some degree the skepticism regarding the uncertainties traditionally associated with prediction of the performance of rocking foundations for use in design.

## **2 SEISMIC RESPONSE OF BRIDGE-PIER ON SHALLOW FOUNDATION: THE “ROCKING–ISOLATION” CONCEPT**

### **2.1 Theoretical Studies**

The concept of “Rocking Isolation” is illustrated in Fig. 1 by examining the response of a 12 m tall bridge pier carrying a deck of four lanes of traffic for a span of about 35 m — typical of elevated highways around the world.

The bridge chosen for analysis is similar to the Hanshin Expressway Fukae bridge, which collapsed spectacularly in the Kobe 1995 earthquake. The example bridge is designed in accordance to EC8-2000 for an effective acceleration  $A = 0.30$  g, considering a (ductility-based) behavior factor  $q = 2$ . With an elastic (fixed-base) vibration period  $T = 0.48$  sec the resulting design bending moment  $M_{COL} \approx 45$  MN m.

The pier is founded through a square foundation of width  $B$  on an idealized homogeneous 25 m deep stiff clay layer, of undrained shear strength  $s_u = 150$  kPa (representative soil conditions for which a surface foundation would be a realistic solution). Two different foundation widths are considered to represent the two alternative design approaches. A large square foundation,  $B = 11$  m, is designed in compliance with conventional capacity design, applying an overstrength factor  $\psi_{Rd} = 1.4$  to ensure that the plastic “hinge” will develop in the superstructure (base of pier). Taking account of maximum allowable uplift (eccentricity  $e = M / N < B/3$ , where  $N$  is the vertical load), the resulting safety factors for static and seismic loading are  $F_S = 5.6$  and  $F_E = 2.0$ , respectively. A smaller, under-designed,  $B = 7$  m foundation is considered in the spirit of the new design philosophy. Its static safety factor  $F_S = 2.8$ , but it is designed applying an “*under-strength*” factor equal to  $1/1.4 \approx 0.7$  for seismic loading. Thus, the resulting safety factor for seismic loading is lower than 1.0 ( $F_E \approx 0.7$ ).

The seismic performance of the two alternatives is investigated through nonlinear FE dynamic time history analysis. An ensemble of 29 real accelerograms is used as seismic excitation of the soil–foundation–structure system. In all cases, the seismic excitation is applied at the bedrock level. Details about the numerical models and the requisite constitutive relations can be seen in Anastasopoulos et al [4, 5].

Results are shown here only for a severe seismic shaking, exceeding the design limits: the Takatori accelerogram of the 1995  $M_{JMA} 7.2$  Kobe earthquake. With a direct economic loss of more than \$100 billion, the Kobe earthquake needs no introduction. Constituting the greatest earthquake disaster in Japan since the 1923  $M_s = 8$  Kanto earthquake, it is simply considered as one of the most devastating earthquakes of modern times. Of special interest is the damage inflicted to the bridges of Hanshin Expressway, which ranged from collapse to severe damage. The aforementioned bridge chosen for our analysis is very similar to the Fukae section of Hanshin Expressway, 630 m of which collapsed during the earthquake of 1995. It is therefore logical to consider this as a reasonably realistic example of an “*above the limits*” earthquake. In particular, the Takatori record constitutes one of the worst seismic motions ever recorded :  $PGA = 0.70$  g,  $PGV = 169$  cm/s, bearing the “mark” of both forward rupture directivity *and* soil amplification.

Fig. 1 compares the response of the two alternatives, in terms of deformed mesh at the end of shaking with superimposed the plastic strains. In the conventionally designed system there is very little inelastic action in the soil; the red regions of large plastic deformation are seen only under the severely “battered” edges of the rocking foundation — but without extending below the foundation. “Plastic hinging” forms at the base of the pier, leading to a rather intense accumulation of curvature (deformation scale factor = 2). The  $P$ – $\delta$  effect



of the mass will further aggravate the plastic deformation of the column, leading to collapse.

In stark contrast, with the new design scheme the “plastic hinge” takes the form of mobilization of the bearing capacity failure mechanisms in the underlying soil, leaving the superstructure totally intact. Notice that the red regions of large plastic shearing are of great extent, covering both half-widths of the foundation and indicating alternating mobilization of the bearing capacity failure mechanisms, left and right.

The above observations are further confirmed by the time history of deck drift shown in Fig. 1(c). The two components of drift, are shown, one due to footing rotation in blue and one due to structural distortion in green. Their sum is shown in red. Evidently, the conventional design experiences essentially only structural distortion which leads to uncontrollable drifting — collapse. In marked contrast, the system designed according to the new philosophy easily survives. It experiences substantial *maximum* deck drift (about 40 cm), almost exclusively due to foundation rotation. Nevertheless, the *residual* foundation rotation leads to a tolerable 7 cm deck horizontal displacement at the end of shaking.

Fig. 1(d) further elucidates the action of the foundation-soil system. The  $M-\theta$  relationship shows for the 11 x 11 m<sup>2</sup> foundation a nearly linear viscoelastic response, well below its ultimate capacity and apparently with no uplifting. On the contrary, the 7 x 7 m<sup>2</sup> (under-designed) foundation responds well past its ultimate moment capacity, reaching a maximum  $\theta \approx 30$  mrad, generating hysteretic energy dissipation, but returning almost to its original position, i.e. with a negligible residual rotation.

However, energy dissipation is attained at a cost: increased foundation settlement. While the practically elastic response of the conventional (*over-designed*) foundation leads to a minor 4 cm settlement, the *under-designed* foundation experiences an increased accumulated 15 cm settlement. Although such settlement is certainly not negligible, it can be considered as a small price to pay to avoid collapse under such a severe ground shaking.

Perhaps not entirely fortuitously, the residual rotation in this particular case turned out to be insignificant. The recentering capability of the design certainly played some role in it, as will be discussed in the sequel.

## 2.2 Experimental Studies

Numerous experimental investigations have been conducted by Kutter and coworkers in the large centrifuge of the University of California Davis. Here we summarize two other studies, one conducted in small-scale 1-g shaking tests in the Laboratory of NTUA, and one conducted in the centrifuge of the University of Dundee. The small-scale (1:20) tests refer to the system of Fig. 2

The Gilroy record from the 1989Ms 7.1 Loma Prieta earthquake is utilized as an example of relatively strong seismic shaking, slightly exceeding the design. As in the previous case, the response of the two design alternatives is comparatively assessed in Figs. 3-5 in terms of deck acceleration time histories, foundation  $M-\theta$  and  $w-\theta$  response, and time histories of deck drift. Time histories of deck acceleration of the two systems are compared in Fig. 3. The increase of seismic demand has a marked effect on the response of both systems, which now clearly mobilize their ultimate moment capacity as evidenced by the acceleration cut-off at 0.40 g for the conventionally designed foundation (Fig. 3a), and at 0.19 g for the rocking-isolation alternative (Fig. 3b). Both values are in very good agreement with the previously discussed  $\alpha_c$  estimates (on the basis of monotonic and cyclic pushover tests).

These observations are confirmed by the  $M-\theta$  loops of Fig. 4. The larger conventionally designed foundation reaches its ultimate moment capacity, but without exhibiting substantial nonlinearity (Fig. 4a). In stark contrast, the smaller foundation of the rocking-isolated system experiences strongly nonlinear response, as evidenced by its oval-shaped  $M-\theta$  loops. As a result (and as it would be expected), the conventional system experiences substantially lower rotation compared to the rocking-isolated system. As evidenced by the  $w-\theta$  curves, the larger foundation demonstrates uplifting-dominated response (observe the very steep edges of the corresponding loops) resulting in minor residual settlement of merely 1.1 cm.

On the contrary, the smaller foundation of the rocking-isolated system moves downwards upon each cycle of rotation, accumulating about three times larger settlement (3.2 cm). However, the superior performance of the larger foundation (with respect to permanent displacements) is unavoidably associated with the development of larger inertia forces. While for the rocking-isolated system the bending moment that develops at the base of the pier is bounded by the inferior moment capacity of the footing ( $M_u \approx 30$  MNm), in the case of the conventionally designed foundation a moment of roughly 60 MNm is allowed to develop, substantially exceeding the capacity of the RC pier ( $M_{uP} \approx 46$  MNm). In reality, this would be associated with flexural cracking at the base of the pier, and its survival (or collapse) would be a function of the ratio of ductility demand to ductility capacity. The larger rotation of the smaller foundation is also reflected in the time histories of deck drift (Fig. 5).

The rocking-isolated system experiences substantially larger maximum deck drift  $\delta \approx 10$  cm, as opposed to roughly 6 cm of the conventional system. Interestingly, thanks to the inherent self-centering mechanism of rocking, the residual deck drift is limited to 2.4 cm (instead of 1.9 cm of the conventional system) — a value that can easily be considered tolerable. In reality, however, the system on conventionally designed foundation would be subjected to bending failure, unavoidably experiencing additional permanent drift due to plastic flexural distortion. Although the extent of such additional deformation

cannot be quantified, on the basis of numerical analysis results it is almost certain that the comparison would be largely in favor of the rocking-isolated alternative had the inelastic response of the RC pier been taken into account.

### **3 SEISMIC RESPONSE OF BRIDGE-PIER ON UNDER-DESIGNED DEEP FOUNDATIONS.**

#### **3.1 Unconnected Piles**

Along similar lines, the idea of unconnected piles has been explored in recent years and has been applied in a number of actual projects. In some cases the piles are treated as simply inclusions, aimed at improving the bearing characteristics of the soil. Example: The foundations of the four piers of the Rion-Antirion Bridge.

But the idea of piles not connected to the base of their cap can be extended to earthquake design: as sketched in Fig. 6 using such piles with an interposed stiff sand-and-gravel layer offers a number of advantages for structural performance (e.g. reduced accelerations) while saving the pile heads from large shear forces that result from the inertial loading of the bridge deck.

On the other hand, it was found that the disconnection of the piles from the cap does not lead to any appreciable reduction of the vertical bearing capacity of the foundation, provided that the interposed soil layer (between the raft and pile heads) is adequately stiff.

#### **3.2 Under-designed Embedded Caissons**

In several recent studies it was shown that embedded caissons are currently designed very conservatively, and that despite this fact they do not improve the seismic safety of the whole bridge pier. Ignoring or even reversing the “capacity” design and the conservative rules regarding uplifting of the foundation, leads to reduced size of the caisson and mobilises nonlinearities in the interfaces between caisson and soil and inelastic action in the soil. Increased capacity for energy dissipation and perhaps limited level of transmitted acceleration contribute to better seismic performance.

### **4 CONCLUSIONS**

(a) Current seismic design practice leads most often to very conservative foundation solutions. Not only are such foundations un-economical but are sometimes difficult to implement. Most significantly: they are agents of transmitting relatively large accelerations up to the superstructure. The ensuing large inertial forces send back in “return” large overturning moments (and shear forces) onto the foundation — a vicious circle.

(b) On the contrary, seriously under-designed foundation dimensions limit the transmitted accelerations to levels proportional to their (small) ultimate moment

capacity. This is one of the reasons of achieving much safer superstructures. In earthquake engineering terminology the plastic “hinging” moves from the columns to the foundation-soil system, preventing dangerous structural damage.

(c) For tall-slender systems that respond seismically mainly in rocking, under-designing the footings “invites” strong uplifting and mobilization of bearing capacity failure mechanisms. It turns out that the statically determined ultimate overturning moment capacity is retained without degradation during cyclic loading, at least for the few numbers of cycles of most events — hence the geotechnical reliability in such a design. Moreover, the cyclic response of such foundations reveals that the amount of damping (due to soil inelasticity and uplifting–retouching impacts) is appreciable, if not large, while the system has a fair re-centering capability. These are some of the secrets of their excellent performance.

(d) The key variable in controlling the magnitude of uplifting versus the extent of bearing–capacity yielding is the static factor of safety  $F_S$  against vertical bearing–capacity failure. The designer may for example, choose to intervene in the subsoil to increase  $F_S$  and hence enhance uplifting over soil inelasticity. Such intervention need only be of small vertical extent, thanks to the shallow dynamic “pressure bulb” of a rocking foundation.

(e) In classical geotechnical engineering, avoiding bearing capacity failure at any cost is an unquestionably prudent goal. Seismic “loading” is different — it is not even loading, but an imposed displacement. Sliding mechanisms develop under the footing only momentarily and hence alternately, and may at worst lead to (increased) settlement. It would be the task of the engineer to “accommodate” such settlements with proper design.

## **ACKNOWLEDGMENTS**

The financial support for this paper has been provided by the research project “FORENSEIS” (Investigating Seismic Case Histories and Failures of Geotechnical Systems), implemented under the “ARISTEIA” Action of the “Operational Programme Education and Lifelong Learning ” and is co-funded by the European Social Fund (ESF) and national resources.

The help of Marianna Loli in preparing the paper is kindly acknowledge.

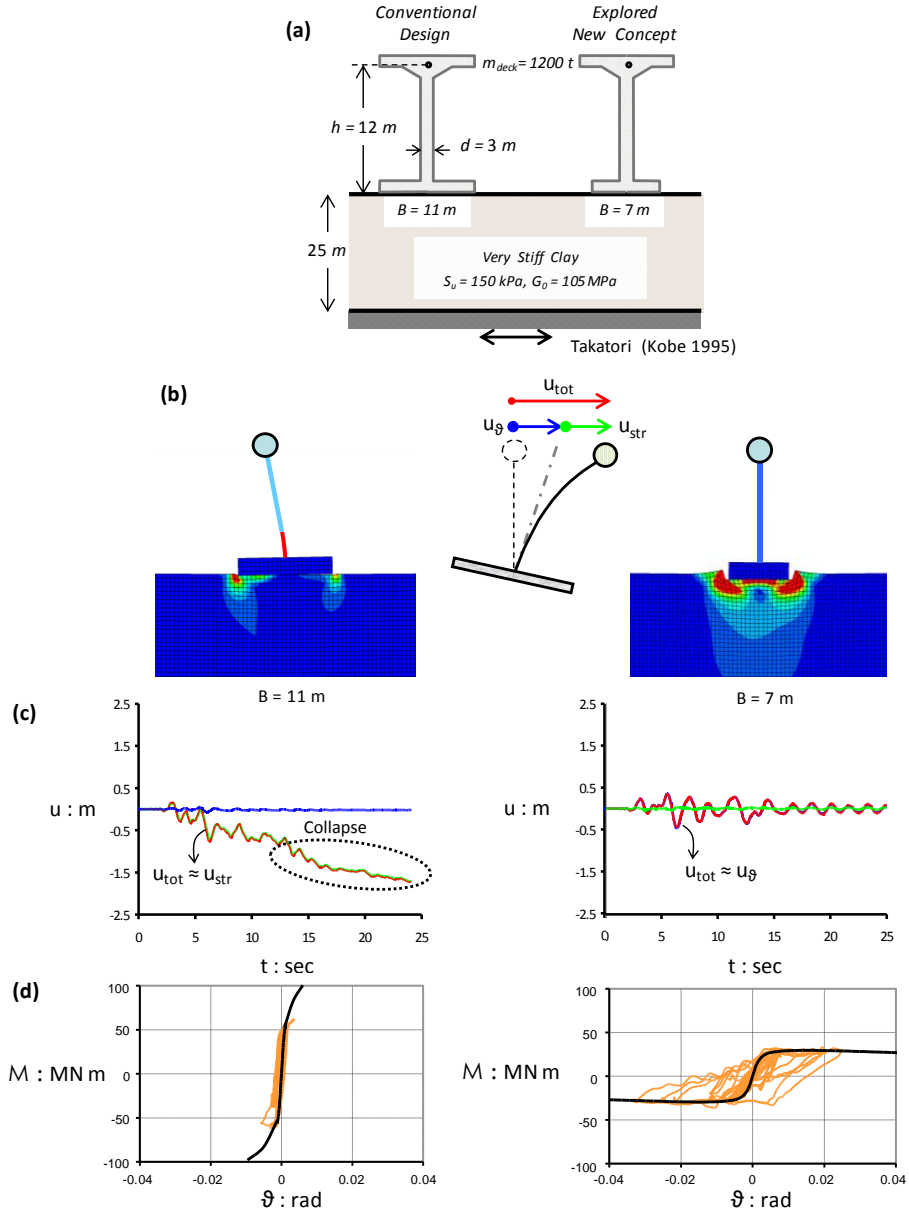


Figure 1. (a) Two bridge piers on two alternative foundations subjected to a large intensity shaking, exceeding the design limits; (b) deformed mesh with superimposed plastic strain, showing the location of “plastic hinging” at ultimate state; (c) time histories of deck drift; (d) overturning moment–rotation ( $M$ – $\theta$ ) response of the two foundations.

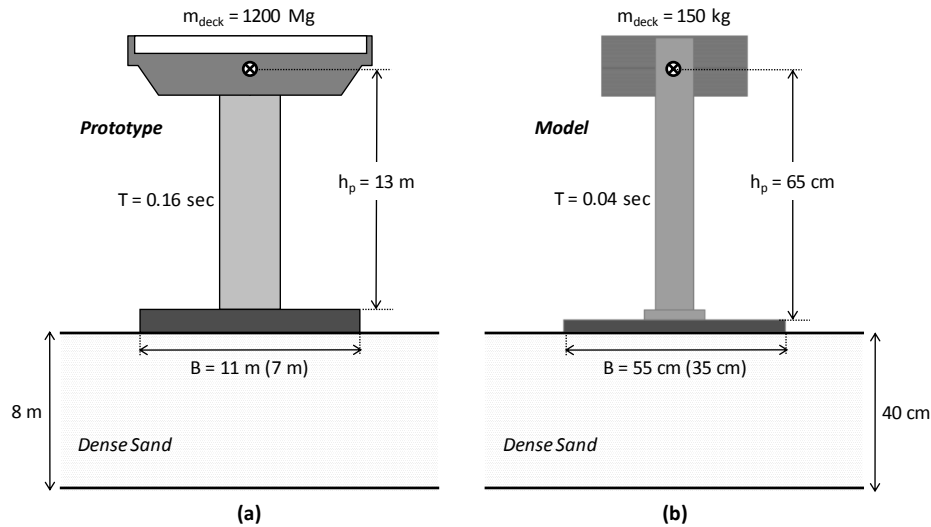


Figure 2. The 1-g experiment : (a) prototype; (b) model (scale = 1:20).

## REFERENCES

- [1] Adamidis O., Gazetas G., Anastasopoulos I., 2014. Equivalent-linear stiffness and damping in rocking of circular and strip foundations, *Bulletin of Earthquake Engineering*, 12(3), 1177-1200.
- [2] Allotey N., El Naggar M.H., 2003. Analytical moment-rotation curves for rigid foundations based on a Winkler model. *Soil Dynamics and Earthquake Engineering*, 23, 367-381.
- [3] Anastasopoulos I., Loli M., Georgarakos T., and Drosos V. (2013). "Shaking Table Testing of Rocking-isolated Bridge Piers", *Journal of Earthquake Engineering*, Vol.17(1), pp. 1-32.
- [4] Anastasopoulos I., Gazetas G., Loli M., Apostolou M, Gerolymos N., 2010. Soil failure can be used for seismic protection of structures. *Bulletin of Earthquake Engineering*, 8, 309-326.
- [5] Anastasopoulos I., Gelagoti F., Kourkoulis R., Gazetas G., 2011. Simplified constitutive model for simulation of cyclic response of shallow foundations: Validation against Laboratory Tests. *Journal of Geotechnical and Geoenvironmental Engineering*, 137, 1154-1168.
- [6] Apostolou M., Gazetas G., Garini E., 2007. Seismic response of slender rigid structures with foundation uplifting, *Soil Dynamics and Earthquake Engineering*, 27, 642-654.
- [7] Bartlett P. E., 1976. *Foundation Rocking on a Clay Soil*. ME thesis, Report No. 154, School of Engineering, University of Auckland, New Zealand.
- [8] Budek AM., Priestley MJN, Benzoni G., 2000. Inelastic seismic response of bridge drilled-shaft RC pile/columns. *Journal of Geotechnical and Geoenvironmental Engineering*, ASCE, 126, 510-517.
- [9] Chatzigogos CT, Figini R., Pecker A. Salençon J., 2010. A macroelement formulation for shallow foundations on cohesive and frictional soils. *International Journal of Numerical and Analytical Methods in Geomechanics*.
- [10] Chatzigogos C.T., Pecker A., Salençon J., 2009. Macroelement modeling of shallow foundations. *Soil Dynamics and Earthquake Engineering*, 29(5), 765-781.
- [11] Chen X.C., Lai Y.M., 2003. Seismic response of bridge piers on elastic-plastic Winkler foundation allowed to uplift. *Journal of Sound and Vibration* , 266, 957-965.

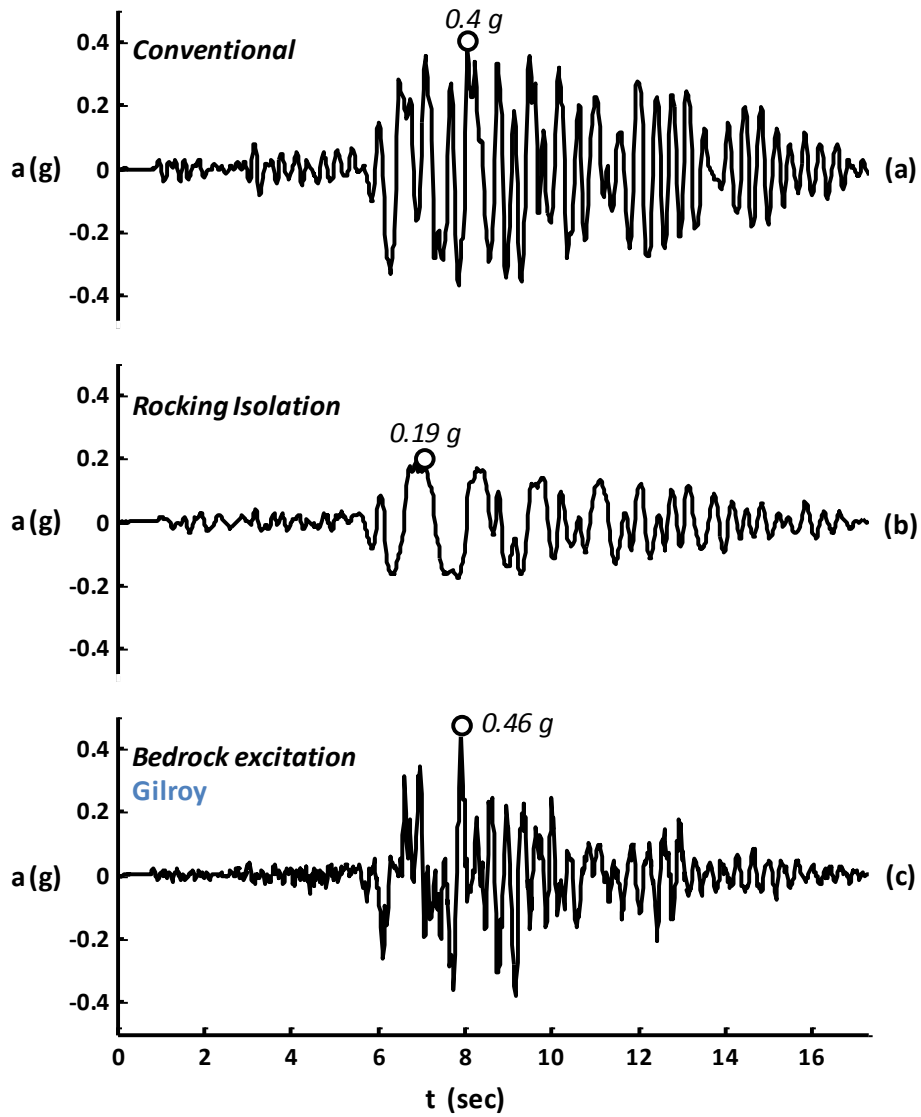


Figure 3. Deck acceleration time histories for strong seismic shaking (Gilroy): (a) conventional system with over-designed  $B = 11$  m foundation, compared to (b) rocking isolated alternative with under-designed (to promote uplifting)  $B = 7$  m foundation ; (c) bedrock excitation

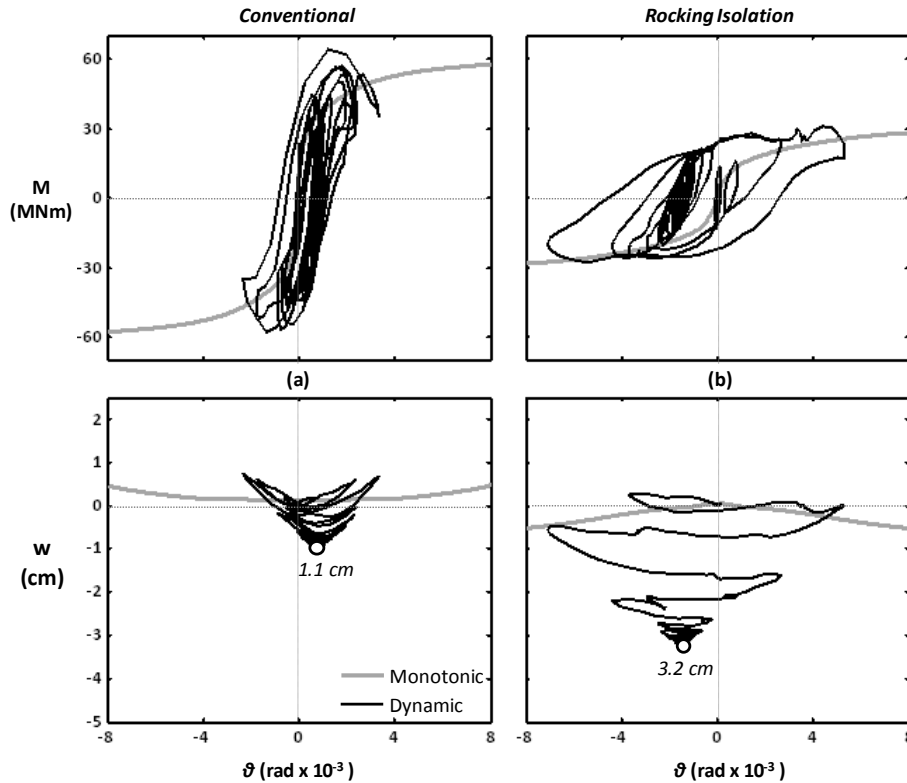


Figure 4. Foundation performance for *strong* seismic shaking (Gilroy). Moment–rotation ( $M-\theta$ ) and settlement–rotation ( $w-\theta$ ) response for : (a) conventional system with over-designed  $B = 11$  m foundation, compared to (b) rocking isolated alternative with under-designed  $B = 7$  m foundation.

- [12] Drosos V., Georgarakos P., Loli M., Zarzouras O., Anastasopoulos I., Gazetas G. 2012. Soil–foundation–structure interaction with mobilization of bearing capacity: An experimental study of sand. *Journal of Geotechnical and Geoenvironmental Engineering, ASCE*, 138, 1369-1386.
- [13] Faccioli E., Paolucci R., Vanini M., 1998. *3D Site Effects and Soil-Foundation Interaction in Earthquake and Vibration Risk Evaluation*. Final report of the European research project TRISEE, European Commission, Brussels.
- [14] Faccioli E., Paolucci R., Vivero G., 2001. Investigation of seismic soil-footing interaction by large scale cyclic tests and analytical models. *Proceedings of the 4th International Conference on Recent Advances in Geotechnical Earthquake Engineering and Soil Dynamics*, CD-ROM, S. Prakash Foundation publisher, Univ. of Missouri-Rolla.
- [15] Fardis M. N. (ed.), 2010. *Advances in Performance-Based Earthquake Engineering*. Springer, University of Patras, Greece, pp. 485.
- [16] FEMA-356, 2000. *Prestandard and Commentary for the Seismic Rehabilitation of Buildings*, Federal Emergency Management Agency, Washington, D.C.
- [17] Gajan S, Phalen JD, Kutter BL, Hutchinson TC, Martin G. 2005. Centrifuge modeling of load-deformation behavior of rocking shallow foundations. *Soil Dynamics & Earthquake Engineering*, 25, 773-783.



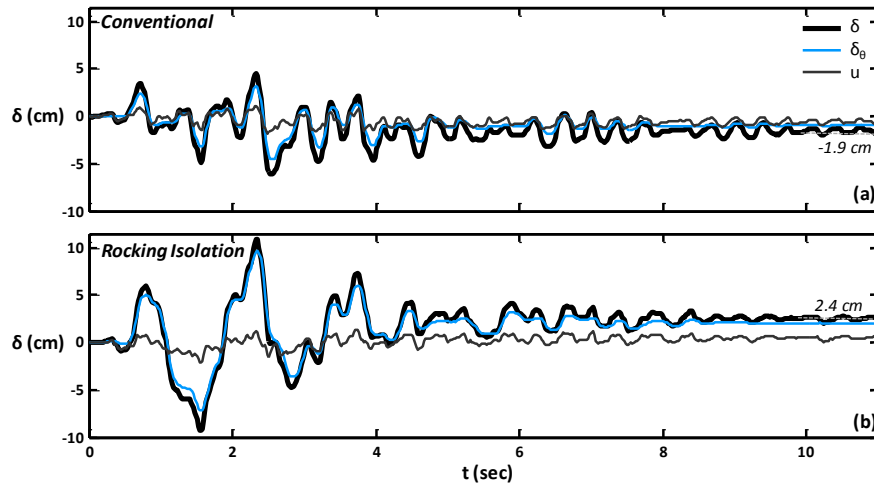


Figure 5. Time histories of deck drift  $\delta$ , due to foundation rotation  $\delta_\theta$  and swaying displacement  $u$ , for strong seismic shaking (Gilroy): (a) conventional system with over-designed  $B = 11$  m foundation, compared to (b) rocking isolated alternative with under-designed  $B = 7$  m foundation

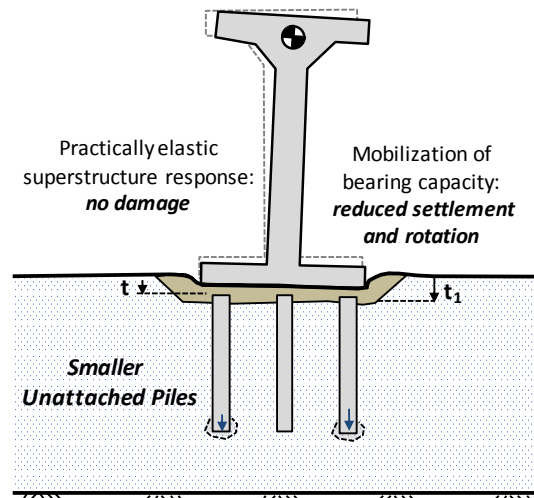


Figure 6. Bridge Pier on unconnected piles with interposed stiff soil layer

- [18] Gajan S, Kutter BL., 2008. Capacity, settlement and energy dissipation of shallow footings subjected to rocking, *Journal of Geotechnical and Geoenvironmental Engineering*, 134, 1129-1141.
- [19] Gajan S., Kutter B. L., 2009b. Effects of moment-to-shear ratio on combined cyclic load-displacement behavior of shallow foundations from centrifuge experiments. *Journal of Geotechnical and Geoenvironmental Engineering, ASCE*, 135, 1044-1055.
- [20] Garini E., Gazetas G., Anastasopoulos I., 2011. Asymmetric 'Newmark' sliding caused by motions containing severe 'Directivity' and 'Fling' pulses. *Géotechnique*, 61, 753-756.

- [21] Gazetas G., Anastasopoulos I., Garini E., 2014. Geotechnical design with apparent seismic safety factors well-below 1. *Soil Dynamics and Earthquake Engineering*, 57, 37-45.
- [22] Gazetas G., Anastasopoulos I., Adamidis O., Kontoroupi Th., 2013. Nonlinear rocking stiffness of foundations. *Soil Dynamics & Earthquake Engineering*, 47, 83-91.
- [23] Gazetas G., & Mylonakis G., 1998. Seismic Soil-Structure Interaction : New Evidence and Emerging Issues. *Soil Dynamics III*, ASCE, Specialty Geotechnical Conference, 2, 1119-1174.
- [24] Gazetas G., Garini E., Anastasopoulos I., Georgarakos P., 2009. Effects of near-fault ground shaking on sliding systems. *Journal of Geotechnical and Geoenvironmental Engineering*, 135, 1906-1921.
- [25] Gerolymos N., Apostolou M., Gazetas G., 2005. Neural network analysis of overturning response under near-fault type excitation. *Earthquake Engineering and Engineering Vibration*, 4, 213-228.
- [26] Gerolymos N., Gazetas G., 2006. Development of Winkler Model for Static and Dynamic Response of Caisson Foundations with Soil and Interface Nonlinearities. *Soil Dynamics & Earthquake Engineering*, 26, 363-376.
- [27] Gerolymos N., Drosos V., Gazetas G., 2009. Seismic response of single-column bent on pile:evidence of beneficial role of pile and soil inelasticity. *Bulletin of Earthquake Engineering*, 7, 547-573.
- [28] Housner G. W., 1963. The behavior of inverted pendulum structures during earthquakes, *Bulletin of the Seismological Society of America*, 53, 403-417.
- [29] Huckelbridge A.A., Clough R., 1978. Seismic response of uplifting building frame. *Journal of Structural Engineering*, 104, 1211-1229.
- [30] Ishiyama Y., 1982. Motions of rigid bodies and criteria for overturning by earthquake excitations. *Earthquake Engineering Structural Dynamics* 10, 635-650.
- [31] Kawashima K., Nagai T., Sakellarakis D., 2007. Rocking seismic isolation of bridges supported by spread foundations. *Proceedings of 2nd Japan-Greece Workshop on Seismic Design, Observation, and Retrofit of Foundations*, Japanese Society of Civil Engineers, Tokyo, 254-265.
- [32] Kirkpatrick P., 1927. Seismic measurements by the overthrow of columns. *Bulletin of the Seismological Society of America* , 17, 95-109.
- [33] Koh A.S., Spanos P., Roesset J.M., 1986. Harmonic rocking of rigid block on flexible foundation. *Journal of Engineering Mechanics*, 112, 1165-1180.
- [34] Kutter B.L., Wilson D.L., 2006. Physical Modeling of Dynamic Behavior of Soil-foundation-superstructure Systems. *International Journal of Physical Modelling in Geotechnics*, 6(1), 1-12.
- [35] Loli M., Knappett J.M., Brown M.J., Anastasopoulos I., & Gazetas G. (2014). "Centrifuge Modeling of Rocking-Isolated Inelastic RC Bridge Piers", *Earthquake Engineering & Structural Dynamics*, DOI : 10.1002/eqe.2451
- [36] Makris N., Roussos, Y., 2000. Rocking response of rigid blocks under near source ground motions. *Géotechnique*, 50, 243-262.
- [37] Martin G.R., Lam I.P., 2000. Earthquake resistant design of foundations: Retrofit of existing foundations. *Geoengineering 2000 Conference (GeoEng2000)*, 19-24 November 2000, Melbourne, Australia.
- [38] Meek J., 1975. Effect of foundation tipping on dynamic response, *Journal of Structural Division*, 101, 1297-1311.
- [39] Mergos P.E., Kawashima K., 2005. Rocking isolation of a typical bridge pier on spread foundation. *Journal of Earthquake Engineering*, 9, 395-414.
- [40] Negro P., Paolucci R., Pedrett S., Faccioli E., 2000. Large-scale soil-structure interaction experiments on sand under cyclic loading, *12<sup>th</sup> World Conference on Earthquake Engineering*, Auckland, New Zealand, Paper No. 1191

- [41] Panagiotidou A.I., Gazetas G., Gerolymos N., 2012. Pushover and seismic response of foundations on stiff clay: analysis with P- $\delta$  effects, *Earthquake Spectra*, 28, 1589-1618.
- [42] Panagiotidou A.I., 2010. *2D and 3D inelastic seismic response analysis of foundation with uplifting and P- $\delta$  effects*. Diploma thesis, National Technical University, Athens, Greece.
- [43] Paolucci R., 1997. Simplified evaluation of earthquake induced permanent displacements of shallow foundations. *Journal of Earthquake Engineering*, 1, 563-579.
- [44] Paolucci R. Shirato M., Yilmaz MT., 2008. Seismic behavior of shallow foundations: shaking table experiments vs. numerical modeling. *Earthquake Engineering & Structural Dynamics*, 37, 577-595.
- [45] Paolucci R., Pecker A., 1997. Seismic bearing capacity of shallow strip foundations on dry soils. *Soils and Foundations*, 37, 95–105.
- [46] Paolucci R., Figini R., Petrini L., 2013. Introducing dynamic nonlinear soil-foundation-structure interaction effects in displacement based seismic design. *Earthquake Spectra*, 29, 475-496.
- [47] Paulay T., Priestley M.J.N., 1992. *Seismic design of reinforced concrete and masonry buildings*. John Wiley & Sons, New York.
- [48] Pecker A., 2003. A seismic foundation design process, lessons learned from two major projects : the Vasco de Gama and the Rion Antirion bridges. *ACI International Conference on Seismic Bridge Design and Retrofit*, University of California at San Diego.
- [49] Pecker A., 1998. Capacity design principles for shallow foundations in seismic areas. Keynote lecture. *11<sup>th</sup> European Conference Earthquake Engineering* (P. Bisch, P. Labbe, and A. Pecker, eds.) A. A. Balkema, Rotterdam, Netherlands, 303–315.
- [50] Pender M.J., 2007. Seismic design and performance of surface foundations. Chapter 10 in *Earthquake Geotechnical Engineering*, (K. Pitilakis, ed.) Springer, 216-225.
- [51] Pender M.J., 2010. *Seismic assessment and improvement of building foundations*. Supplement to “assessment and improvement of structural performance of buildings in earthquake. University of Auckland, N. Zealand.
- [52] Priestley M.J.N., 1993. Myths and fallacies in earthquake Engineering—Conflicts between design and Reality. *Bulletin, New Zealand Society for Earthquake Engineering*, 26, 329–341.
- [53] Priestley M.J.N., 2003. Myths and fallacies in earthquake engineering, revisited. *Ninth Mallet-Milne Lecture*, Rose School, IUSS Press, Instituto Universitario di Studi Superiori, Pavia, Italy.
- [54] Shi B., Anoooshehpour A., Zeng Y., Brune J., 1996. Rocking and overturning of precariously balanced rocks by earthquake. *Bulletin of the Seismological Society of America*, 86, 1364–1371.
- [55] Shirato M., Kouno T., Nakatani S., Paolucci R., 2007. Large-scale model tests of shallow foundations subjected to earthquake loads, in *Proceedings of the 2<sup>nd</sup> Japan-Greece Workshop on Seismic Design, Observation, and Retrofit of Foundations*, Japanese Society of Civil Engineers, Tokyo, 275–299.
- [56] Shirato M., Kuono T., Asai R., Fukui J., Paolucci R., 2008. Large scale experiments on nonlinear behavior of shallow foundations subjected to strong earthquakes. *Soils and Foundations*, 48, 673–692.
- [57] Tassios T.P., 1983. Assessment of concrete structures and design procedures for upgrading. *CEB bull.* 162.
- [58] Wotherspoon L.M., Pender J.J., 2010. Effect of shallow foundation modeling on seismic response of moment frame structures. *Soil–Foundation–Structure Interaction*, Orense R.P., Chouw N., Pender M.J. (editors), CRC Press, Taylor & Francis Group: New York, pp. 117-124.
- [59] Zhang J., Makris N., 2001. Rocking response of free-standing blocks under cycloidal pulses. *Journal of Engineering Mechanics*, 127(5), 473–483
- [60] Zafeirakos A. (2014). *Inelastic static and seismic response of deeply embedded foundations*. Doctoral Dissertation, School of Civil Engineering, National Technical University of Athens.

IBSBI 2014, October 16-18, 2014, Athens, Greece

## **MONITORING DATA PROCESSING FOR FATIGUE VERIFICATION UNDER PARTICULAR DECK VIBRATION OF “CHARILAOS TRIKOUPIIS” BRIDGE**

Panayiotis Papanikolas<sup>1</sup>, Aris Stathopoulos-Vlami<sup>2</sup>, Akis Panagis<sup>3</sup>  
and Olivier Flamand<sup>4</sup>

<sup>1,2,3</sup> GEFYRA S.A. – Concession Company for the Rion-Antirion Bridge, Greece

<sup>4</sup> Centre Scientifique et Technique du Batiment (CSTB), France

e-mail: ppapanikolas@gefyra.gr, aris.stathopoulos@gefyra.gr, akis.panagis@gefyra.gr,  
olivier.flamand@cstb.fr

**ABSTRACT:** Structural monitoring systems produce an enormous volume of data, the storage and processing of which is both costly and difficult. To tackle this problem a different approach can be applied using sparse data. The exploration of such data assisted in acquiring all vortex shedding deck excitation events, in order to rebuild vibration history and evaluate fatigue risk.

**KEY WORDS:** Bridge; Fatigue; Monitoring; Vortex-shedding; Sparse data.

### **1 INTRODUCTION**

The “Charilaos Trikoupiis Bridge, in Greece, is equipped with a very complete monitoring system including accelerometers on the deck, piers and pylons and cables along the five spans as well as anemometers. This system records continuously sparse data. One single value, 0.5 sec average, of each sensor is recorded every 30 seconds, real dynamic data are recorded either every two hours with one continuous record of at least 60 seconds or during threshold overpassing.

During operation period, the bridge exhibited occasionally limited amplitude vibration of deck due to vortex shedding excitation. CSTB was asked to extend and improve the processing of five years monitoring data in order to assist the designer on estimating fatigue risk for crucial structural elements and to propose mitigation measures if required.

### **2 CHARACTERISTICS OF THE VORTEX SHEDDING PHENOMENON ON LARGE BRIDGES**

Civil engineering structures like slender bridges are prone, in many occasions, to deformation under service loads. Traffic, temperature, earth movement and

wind apply loads on such a bridge, the structure of which comes back to its stable state after the load ceased, with various typical times, i.e. various frequencies. For this reason vibrations are not exceptional on a bridge, they are just part of its casual behaviour, they only need to be observed and analysed to check that they don't go over security thresholds. Vibrations induced by wind draw special attention because their origin could be considered negligible when their consequences can be much visible.

Vortex shedding is one of these phenomena that produce anxiety mainly because it gives way to detectable amplitude movements of the structure when the origin, a moderate wind, does not appear basically as yielding risk. This movement usually corresponds to small amplitude of deformation but on such a long line like structure this gives way to large amplitude of displacement at low frequency, observable by a user.

Vortex shedding, also known as Karman vortex excitation, is a moderate energy instability occurring when the frequency at which vortices are formed in the wake of a bluff body, like a bridge deck, corresponds to a modal frequency of vertical vibration of this deck. The shedding frequency depends on the wind speed. When the wind speed increases, the shedding frequency increases at the same rate. The so called Strouhal number  $St$ , introduced by Vincent Strouhal a Czech physician of the 19th century, gives the basic relation between frequency of shedding,  $f$ , wind speed  $U$  and the lateral to wind dimension of the body,  $B$ .

$$f = St \cdot \frac{U}{B} \quad (1)$$

Because natural wind varies in time and in space, the shedding frequency is not maintained for a long time in usual meteorological conditions, which is the reason why bridges are not prone to everyday excitation. But for unusually stable and long lasting wind conditions, vortex shedding can lead to an excitation of bridge deck in vertical direction, the duration of which ranges between some minutes and some hours with amplitude up to decimeters.

Vortex shedding excitation on a bridge deck concern users' comfort till the acceleration becomes noticeable to them and the risk of fatigue on the most critical structural elements.

### **3 VORTEX SHEDDING EVENTS ON THE RION ANTIRRION BRIDGE**

#### **3.1 Monitoring system**

One of design considerations of the monitoring system of the Rion-Antirion Bridge was the follow up of the deck vibration in flexural bending and torsion as well as vibrations of stays, including measurement of wind speed on deck level. Due to proper follow up and maintenance of the monitoring system, the monthly serviceability rate equals to 100% most of time and never less than

90% during the period of current study.

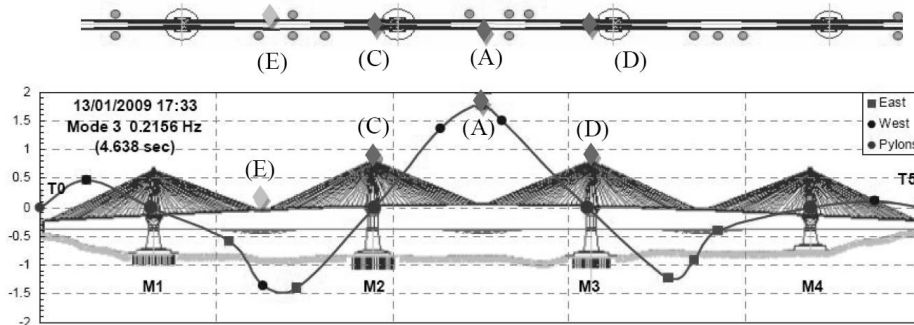


Figure 1. Critical sensors locations and 3<sup>rd</sup> vertical mode shape of the RION ANTIRION Bridge.

The monitoring system output, apart from alert “over threshold” events consisting of high sampling rate records with minimum duration of 60 sec, initiates regularly (every 2 hours) continuous records of low frequency data (sampling rate every 30 sec). These records were mined over five years in order to extract the vortex shedding occurrences which usually lead to vibration level lower than alert thresholds.

Processing the high sampling rate records, hereinafter named "Dynamic files", a number of vortex shedding events corresponding to excitation of the 3<sup>rd</sup> flexural bending mode (0,216Hz) were revealed, but due to the large record interval (2 hours) compared with the expected event duration, some events were assumed to be undetected. Additionally, even though the maximum amplitude could be reasonably estimated, the total duration of event could not be deduced in order to estimate the number of vibration cycles.

In excess to the analysis of Dynamic files, the peculiar work described in this paper concerns a method developed for processing the low sampling data taken every 30 seconds, corresponding only to the “Instant value” given by sensors, as sentries of vortex shedding event. This work proves it is possible to count the vibration events over a long period using a reduced set of recorded data.

### 3.2 Relationship between wind characteristics and the occurrence of vortex shedding

As wind data were available as well as some of the vortex shedding events captured by the every 2 hours Dynamic files, it was investigated whether the wind force, direction and turbulence were main parameters of alternate eddies excitation or not, over a two years period including 2009 and 2010.

Wind was most of the time normal to bridge axis and stronger from East than from West (Fig 2 and 3)

It was first observed that west wind turbulence was lower than east wind turbulence for 2009 and 2010. The wind appears very smooth compared to usual Eurocode specifications. The Eurocode turbulence intensity for sea wind at 57m above the sea (height of bridge deck) is over 10%. This reference was used for the design process, yielding to consider  $I_u=12\%$  for the wind model. Full scale data show a turbulence level of 5% or less occurring more than 50% of the time for western winds. This is of particular importance because the vortex shedding excitation strength depends on the turbulence intensity of the wind, the lower the turbulence, the stronger the excitation.

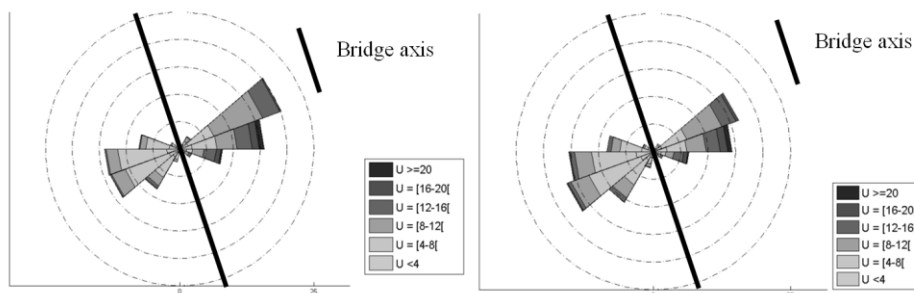


Figure 2. Rose of wind mean speed, M1M2 anemometer, year 2009 & 2010

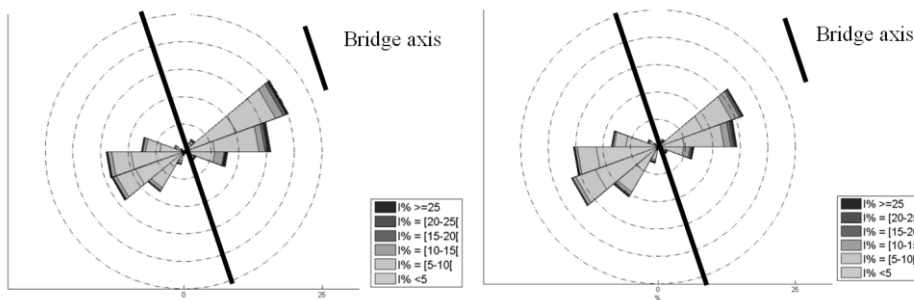


Figure 3. Rose of wind turbulence intensity, M1M2 anemometer, year 2009 & 2010

Figure 4 graphs present respectively the standard deviation (STD) of the acceleration of the deck in the vertical direction, measured at mid span (Deckaccelerometer 17E M2M3E E17E-Z, sensor A of figure 1) versus mean wind speed and versus wind direction (sensor E) for all 2009 monitoring records. Red points on the graphs were identified as 2009 vortex shedding events, due to single mode vibration at a narrow wind range.

These 15 vortex shedding events, denoted by large STD acceleration amplitude at moderate wind speed, occurred mainly on west wind direction ( $\sim 255^\circ$ ). The average mean wind speed was 8.4 m/s while the average turbulence level was 2% (0.1-1 Hz bandwidth). This turbulence level is surprisingly low.

Same process applied to data from the 2010 monitoring which gave very similar results with 28 vortex shedding events occurring mainly on west wind direction ( $\sim 255^\circ$ ). The average mean wind speed was 8.5 m/s while the average turbulence level was 2.5 % (0.1-1 Hz bandwidth).

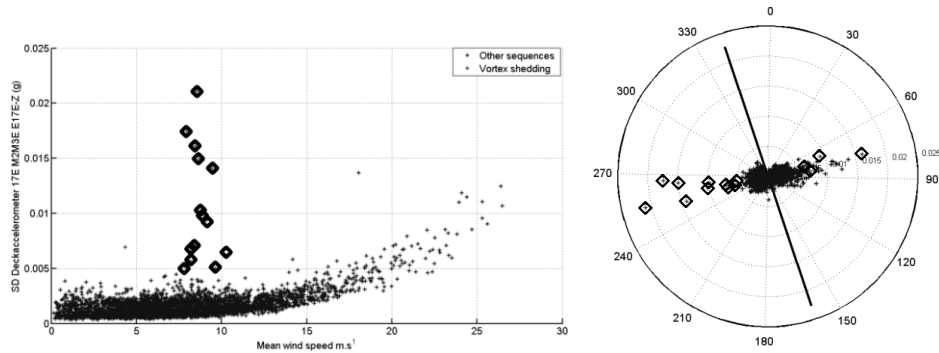


Figure 4. STD Deckaccelerometer 17E M2M3E E17E-Z vs mean wind speed & direction (2009,M2 PXI)

It must be underlined that this limited value of turbulence intensity was calculated from short records (60s) that could not express the low frequency wind fluctuations giving way to turbulence. For this reason turbulence intensity calculated from Dynamic file records underestimates the actual variability of wind speed by comparison with turbulence issued from standard 10 minutes records.

The number of vortex shedding events in 2010, characterized by large amplitude at reduced wind speed and a quasi-sinusoidal movement, was twice the one of 2009. Figure 5 illustrates a typical example of record of vortex shedding event, where various accelerometers on the deck show sinusoidal signal in phase while pylons on both sides of the deck show opposite sign sinusoidal signal, which is consistent with the modal shape (3rd mode of deck) excited during vortex shedding event.

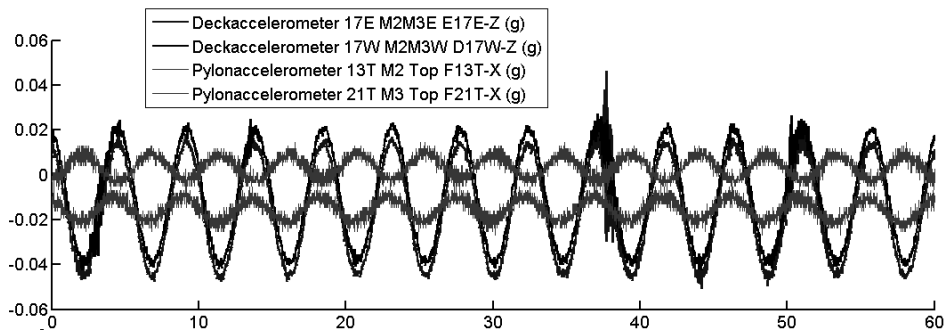


Figure 5. Typical vortex shedding records (m2Dynamic record – 070609 22h00m.txt)



## 4 RECONSTRUCTION OF VORTEX SHEDDING EVENTS FROM INSTANT RECORDS

### 4.1 Validating the method

As explained previously, the processing of the Dynamic files revealed only 15 events in 2009 and 28 events in 2010 due to records interval. Figure 6 illustrates a “missed” event from Dynamic records. However, these few events can serve as reference for a signal processing analysis using the low sampling (every 30 sec) records titled "Day history" files with the aim to detect and characterize every vortex shedding events (number, duration, maximum displacement). It is reminded that Day history files consist of averaged data over 0.5 sec and one value is recorded every 30 sec (sampling frequency 0.0333 Hz) for all sensors.

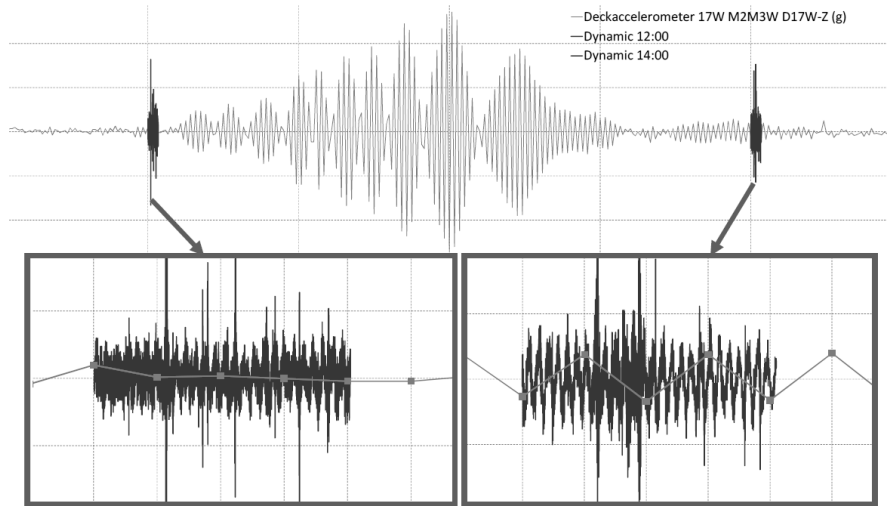


Figure 6. Vortex shedding event occurred between 60sec “Dynamic files” (2hours interval)

These particular features affect the properties of the recorded signal and they should be investigated in order to interpret the records. The main consequences are:

- Averaging the signal over 0.5s yield to low pass filtering
- Low sampling rate at 0.033 Hz yields to aliasing

For the filtering effect, the amplification and the phase information are presented in figure 7 (for  $dt=0.5$  sec averaging), comparing the raw signal  $V(t)$  and the averaged (filtered) one  $V_A(t)$  regarding amplitude and phase :

$$V_A(t) = \int_{t-dt}^t V(\tau) \cdot \frac{d\tau}{dt} \quad V(t) = A \sin(2\pi ft + \theta) \quad (2)$$

Averaging over 0.5s does not significantly filter any of the modes participating

in deck vibration. Especially for the 3rd deck mode (0.216 Hz), the amplification factor is 0.981, and the delay is 0.25 sec. Consequently the vibration of the deck calculated from the day history files and from the instant files will almost have the same amplitude.

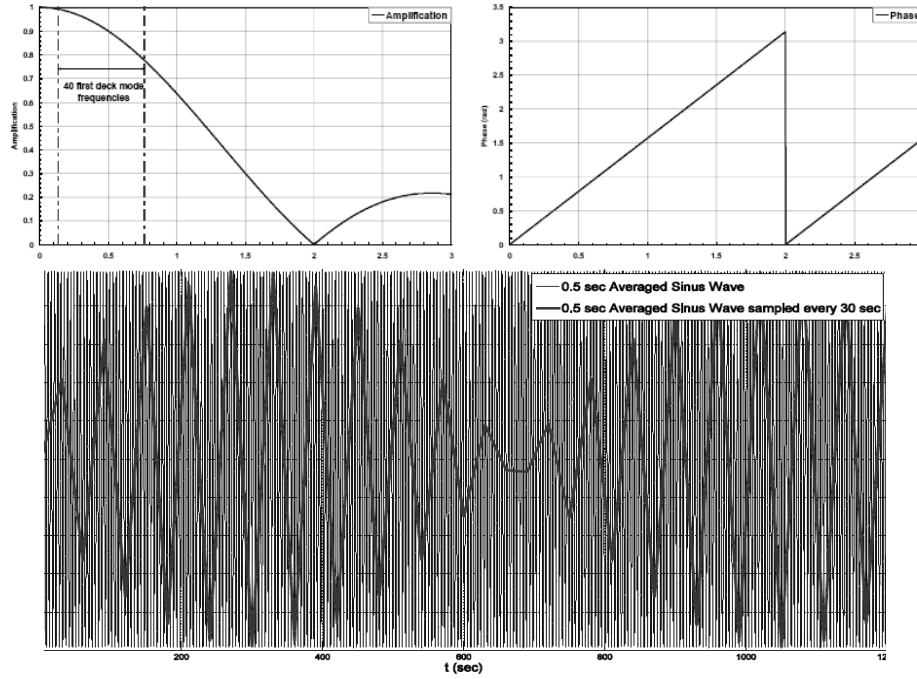


Figure 7. Filtering effect of averaging on amplification and phase shift & Aliasing effect.

Low sampling rate ( $f_s=0.033$  Hz) forces every vibration event with frequency  $f_n$  more than ( $f_s/2=0.0166$  Hz) to be represented in an aliased frequency  $f_a$ .

Aliasing effect is illustrated in figure 7, where a sinus wave (amplitude 1 and frequency 0.216 Hz) contaminated with white noise (noise/signal=0.05) and sampled at 100 Hz is subjected to 0.5 sec averaging and resampled to 30 sec.

The amplitude variation of the aliased signal (red) is due to the fact that the aliased frequency (from 0.216 Hz to 0.016 Hz) is close to the Nyquist frequency ( $f_s/2$ ). If the aliased frequency  $f_a$  can be rewritten as  $f_a=f_s/2-df$ , the samples  $S_i$  expressed as

$$S_i = A \cdot \sin\left(2\pi \frac{f_a}{f_s} i\right), \quad (3)$$

can be modified to

$$S_i = -A \cdot \cos\left(2\pi \frac{f_s}{2 \cdot f_s} i\right) \cdot \sin\left(2\pi \frac{df}{f_s} i\right) \quad (4)$$

as a multiplication of a constant amplitude wave with frequency  $f_s/2$  with a very slow wave with frequency  $f_d$ . In this case the slow wave has a frequency  $1/60-0.016=0.00066$  Hz (1500 sec period).

For each value of original "History" record with sampling frequency  $f_{acq}$ , 2 different type of subsamples (time window) were selected, a centered one, and a backward shifted with  $N$  values duration (size of time window). For each subsample, the Standard deviation was calculated as an index of vibration amplitude. The standard deviation of a subsample is defined by:

$$STD_{ssamp}(t) = \sqrt{\frac{1}{N-1} \sum_{i=1}^N (x_i - \bar{x}_N)^2} \quad (5)$$

For a subsample  $x_N$  the calculation window could be centred or shifted backward:

$$x_N(t) = \left\{ \begin{array}{l} x(t - \frac{N}{2 \cdot f_{acq}}), \dots, x(t + \frac{N}{2 \cdot f_{acq}}) \text{ (centered)} \\ x(t), \dots, x(t + \frac{N}{f_{acq}}) \text{ (shifted backward)} \end{array} \right\} \quad (6)$$

Both methods were compared for occurrences when Dynamic files have been recorded and can serve as "reference". Figure 8 shows that the centred method induced less time shift in the time localization of the maximum of amplitude than the backward method. Therefore the centred method was preferred even if the determination of amplitude was not so accurate.

The size of the calculation window was optimized too by comparing the value of RMS of a Dynamic file with STD of "History" records. As shown on figure 8 a 5-minute window was found best fitting the results from Dynamic files with a correlation between STD calculated by the two methods of 90% to 95%. This optimization is a balance between a reduced number of data (5-minute window means STD is calculated only upon 11 values) and the duration of the phenomenon lying on natural wind steady state (less constant over a 10 minutes period than over a 5 minutes one).

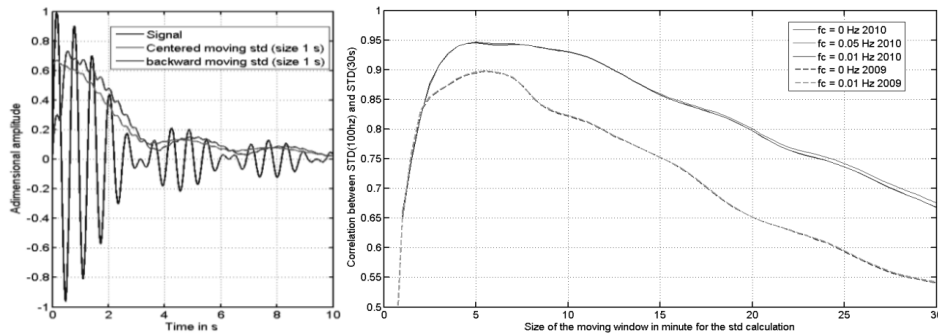


Figure 8. Comparison of centred and backward subsamples and time window optimization.

After optimizing STD calculation parameters on the “History” records, a final correction factor, occurred from the correlation with the RMS values of each “Dynamic” record that captures a vortex shedding event. This correction factor took a value of 0.893 in this case.

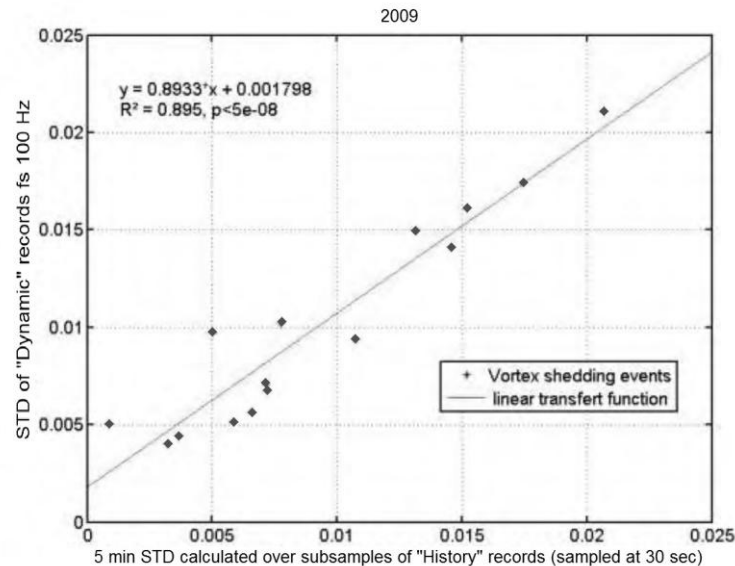


Figure 9. Correlation between STD calculated from “Dynamic” records and STD calculated from a time window of “History” records.

For application of current methodology to different structure with different properties, the whole process, first the optimized window length for calculation of STD, and then to the correction factor between the “real” STD value and the one issued from the low sampled records should be repeated.

#### 4.2 Applying the method over 5 year data files

Finally, occurrences of vortex shedding events were reconstructed over years 2006 to 2010 (5 years) and showed that many short duration events had not been detected by the standard monitoring process. For instance for year 2010 the number of vortex shedding events detected by the processing of the Day history files is 144, when only 28 events had been evidenced when processing the Dynamic files.

For each occurrence of an excitation due to vortex shedding, both the duration of the event and the max amplitude reached have been computed.

For the calculation of fatigue of the structural elements it was conservatively considered that the maximum amplitude was applied in a number of cycles deduced from the event duration multiplied by the frequency of the 3rd flexural mode. A table of loads has been filled for each stay with the summation of all

cycles related to all event of the same year. The five years load tables are combined in one unique table and multiplied the figures in boxes of this load table by 24, a load table for a period of 120 years (bridge service life) was obtained that was used for checking the risk of fatigue on each cable's anchorage. This process finally ended to the conclusion that there was no risk of fatigue due to the accumulated effect of loads induced by the vortex shedding excitations of the deck.

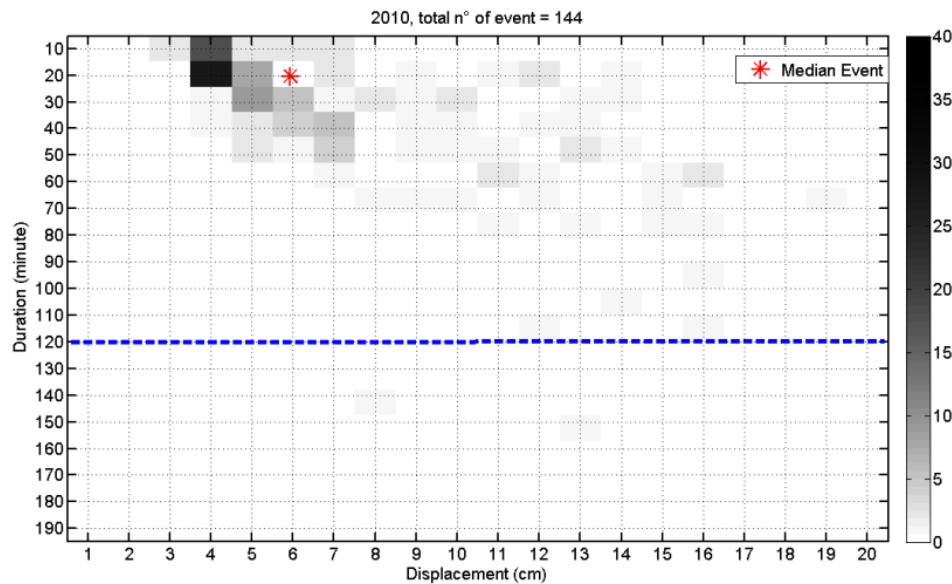


Figure 10. Table of reconstructed vortex shedding events for the year 2010

## 5 CONCLUSIONS

Current analysis indicates the possibility to obtain crucial and complete information of particular structural response, such as deck excitation due to vortex shedding, without requiring an enormous database of high frequency records.

## REFERENCES

- [1] FLORI J.P., "Frequency of strong winds on the site of Rion-Antirion Bridge", CSTB Report, EN-AEC 99.25 C, 1999.
- [2] O'CONNOR C. and SHAW P.A., "Bridge Loads", SPON PRESS, 2002.
- [3] O. FLAMAND, F. De OLIVEIRA and A. STATHOPOULOS-VLAMIS, P. PAPANIKOLAS, "Conditions for occurrence of vortex shedding on a large cable stayed bridge. Full scale data from monitoring system", *6th European and African Conference on Wind Engineering*, Nottingham UK, 2013

IBSBI 2014, October 16-18, 2014, Athens, Greece

## **KINEMATIC SOIL STRUCTURE INTERACTION FOR BRIDGE PILED FOUNDATIONS**

Alain Pecker

Géodynamique et Structure, Bagnaux, France  
Ecole Nationale des Ponts ParisTech, France  
e-mail: alain.pecker@geodynamique.com

**ABSTRACT:** Kinematic interaction is well recognized as being the cause of the development of significant internal forces in the piles under seismic loading. Another aspect of kinematic interaction which is often overlooked is the modification of the effective foundation input motion. Both aspects are illustrated on a real project.

**KEY WORDS:** Soil structure interaction; piled foundations; kinematic interaction.

### **1 INTRODUCTION**

Kinematic interaction is well recognized as being the cause of the development of significant internal forces in the piles under seismic loading. These internal forces are developed as the consequence of the ground displacement induced by the passage of the seismic waves. These displacements are imposed to the piles which may, or may not, follow the soil displacements depending on the bending stiffness of the piles relative to the soil shear stiffness (e.g. [1]). For flexible piles, the internal forces, i.e. pile bending moments and shear forces, can be computed by simply imposing the soil displacements to the pile; for stiff piles a soil structure analysis shall be conducted with proper modelling of the soil-pile interaction. Obviously, kinematic effects are more pronounced when the piles are stiff relative to the surrounding soil and when they cross consecutive layers of sharply different stiffnesses because the soil curvature is very large at such interfaces. This aspect of kinematic interaction is well understood and correctly accounted for in seismic design of piled foundations; for instance the European Seismic code ([2]) requires that kinematic bending moments be computed whenever the two following conditions occur simultaneously:

- The ground profile has an average shear wave velocity smaller than 180m/s (ground type D) and contains consecutive layers of sharply differing stiffness; consecutive layers of sharply differing stiffness are defined as layers with a ratio for the shear moduli greater than 6.

- The zone is of moderate or high seismicity, i.e. presents a ground surface acceleration larger than 0.1g, and the category of importance of the structure is higher than normal (importance category III or IV).

There is another aspect of kinematic interaction often overlooked, even in seismic building codes, which is the modification of the effective foundation input motion. For example the European Seismic code ([2]) does not mention it, nor does the ASCE 41-13 standard ([3]) which however dedicates several pages to the effect of kinematic interaction for shallow or embedded foundations.

This issue might be critical when substructuring is used and the global soil-structure-interaction problem is solved in several steps. However, when a global model including both the soil and the superstructure is implemented, kinematic interaction is accounted for in the analysis, provided the global model correctly reflects the physical character of the problem. These aspects are illustrated below on a real bridge project.

## **2 SOIL STRUCTURE INTERACTION MODELLING**

As opposed to spread footings, for which a single method of analysis to determine the forces transmitted by the foundation emerges in practice (based on a substructuring approach and the definition of the foundation stiffness matrix and damping), several modeling techniques are used to model piled foundations for seismic response studies; the most common methods are the simplified beam on Winkler foundation model and the coupled foundation stiffness matrix (substructuring). These two modeling techniques are illustrated in Figure 1 for the global model and in Figure 2 for the substructure model ([4]).

### **2.1 Global SSI model for piled foundations**

In the global model, piles are represented by beam elements supported by linear or nonlinear, depth-varying, Winkler springs. In the case of earthquake excitation, ground motion would impart different loading at each soil spring and these motions need to be calculated from a separate analysis (site response analysis). Kinematic interaction is therefore correctly accounted for. However, the main drawback of this modeling technique is the large number of degrees of freedom needed to formulate the complete system.

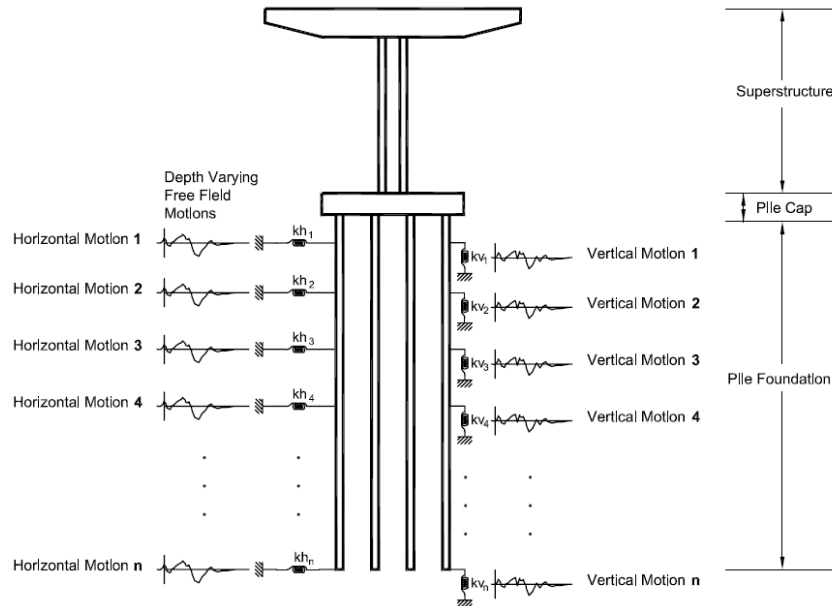


Figure 1. Global pile-structure model

The p-y relation, representing the nonlinear spring stiffness, is generally developed on the basis of a semi-empirical curve, which reflects the nonlinear resistance of the local soil surrounding the pile at specified depth. A number of p-y models have been proposed by different authors for different soil conditions. The two most commonly used p-y models are those proposed by Matlock ([6]) for soft clay and by Reese *et al* ([7]) for sand. These models are essentially semi-empirical and have been developed on the basis of a limited number of full-scale lateral load tests on piles of smaller diameters ranging from 0.30 to 0.40 m. To extrapolate the p-y criteria to conditions that are different from the one from which the p-y models were developed requires some judgment and consideration. For instance in Slovenia, values of the spring stiffnesses are derived from the static values, increased by 30%. Based on some field test results, there are indications that stiffness and ultimate lateral load carrying capacity of a large diameter drilled shaft are larger than the values estimated using the conventional p-y criteria. Pender ([8]) suggests that the subgrade modulus used in p-y formulation would increase linearly with pile diameter.

Studies have shown that Matlock and Reese p-y criteria give reasonable pile design solutions. However, the p-y criteria were originally conceived for design against storm wave loading conditions based on observation of monotonic static and cyclic pile load test data. Therefore, Matlock and Reese's static p-y curves



can serve to represent the initial monotonic loading path for typical small diameter driven isolated piles. If a complete total system of a bridge is modeled for seismic response study, individual piles and p-y curves can be included in the analytical model.

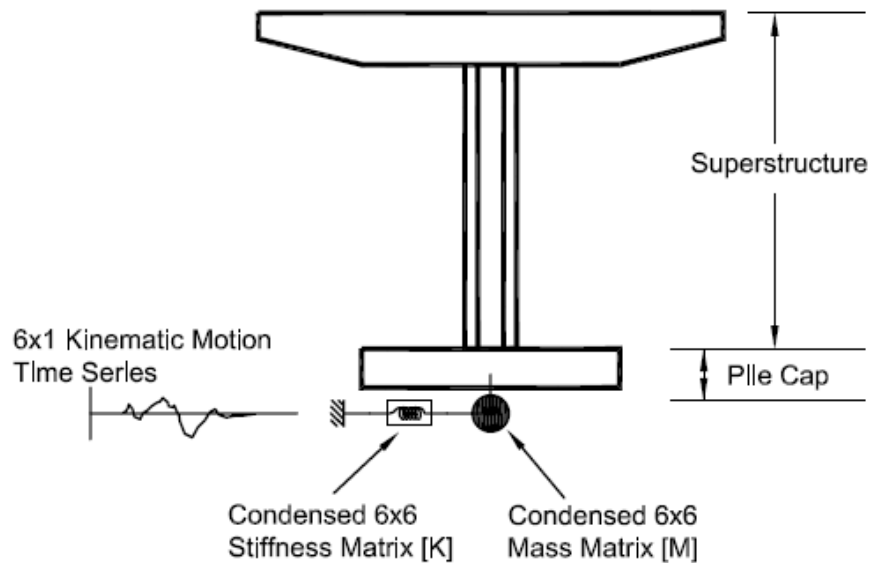


Figure 2. Substructure model

However, for a large pile group, group effects become important. An example is given in Figure 3 which presents the results of horizontal impedance calculations of the group of piles of half the foundation (22 piles) of one of the pylon of the Vasco da Gama bridge in Lisbon ([9]); the group efficiency, computed from elastodynamic theory, is of the order of  $1/6$  at low frequencies and decreases with frequency due to the constructive interference of diffracted waves from adjacent piles. Typically, for large pile groups it is not uncommon to calculate group efficiency in the range  $1/3$  to  $1/6$ .

Although group effect has been a popular research topic within the geotechnical community, currently there is no common consensus on the design approach to incorporate group effects. Full scale and model tests by a number of authors show that in general, the lateral capacity of a pile in a pile group is less than that of a single isolated pile due to so-called group efficiency. The reduction is more pronounced as the pile spacing is reduced. Other important factors that affect the efficiency and lateral stiffness of the pile are the type and strength of soil, number of piles, type and level of loading. In the past, analyses of group effects were based mostly on elastic halfspace theory due to the

absence of costly full-scale pile experiments. In addition to group effect, gapping and potential cyclic degradation have been considered in the recent studies. It has been shown that a concept based on p-multiplier applied on the standard static loading p-y curves works reasonably well to account for pile group and cyclic degradation effects ([10]). The p-multiplier is a reduction factor that is applied to the p-term in the p-y curve for a single pile to simulate the behavior of piles in the group.

For instance, the values proposed in [10] are given in Table 1. Clearly, p-multipliers are dependent on site conditions, soil types and details of stratification and displacement amplitudes ([11]).

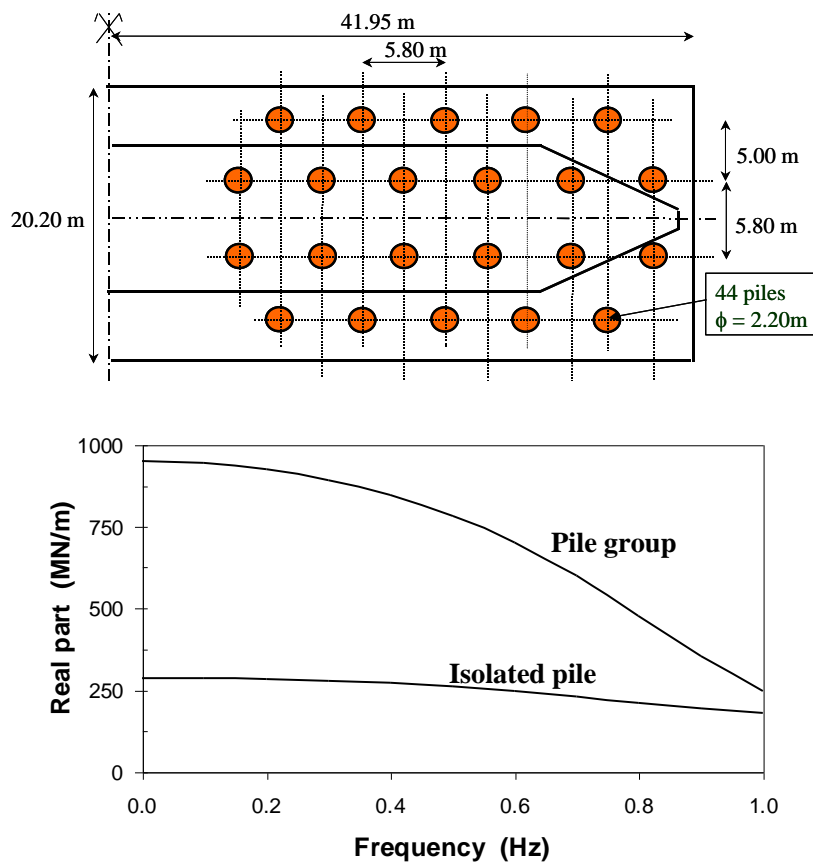


Figure 3. Horizontal pile group impedance for the Vasco da Gama bridge ([9])

*Table 1: p-multipliers for pile group design ([10])*

Row spacing	Front row	Second row	Third and more rows
3D	0.80	0.45	0.35
4D	0.90	0.65	0.55
5D	1.00	0.85	0.75

It must be recognized that the current practice in the world is mainly based on the use of p-y curves despite all the difficulties and limitations associated with this method ([12]).

## **2.2 Substructure model for piled foundations**

A direct (or global) interaction analysis in which both the soil and the structure are modelled with finite elements is very time demanding and not well suited for design, especially in 3D. The alternative approach employing a substructure system in which the foundation element is modeled by a condensed foundation stiffness matrix and mass matrix along with equivalent forcing function represented by the kinematic motion, may be more attractive; in addition, it more clearly separates the role of the geotechnical engineer and of the structural engineer.

The substructuring approach is based on a linear superposition principle and therefore linear soil behavior is more appropriate. In that case, the condensed stiffness matrix may be obtained either from the beam on Winkler springs model or from continuum impedance solutions ([5]). When nonlinear soil behavior is considered, the condensed stiffness matrix is generally evaluated by a pushover analysis of the pile group and linearization at the anticipated displacement amplitude of the pile head.

Substructuring reduces the problem to more amenable stages and does not necessarily require that the whole solution be repeated again if modifications occur in the superstructure. It is of great mathematical convenience and rigor which stem, in linear systems, from the superposition theorem ([13]). This theorem states that the seismic response of the complete system can be computed in two stages (Figure 4):

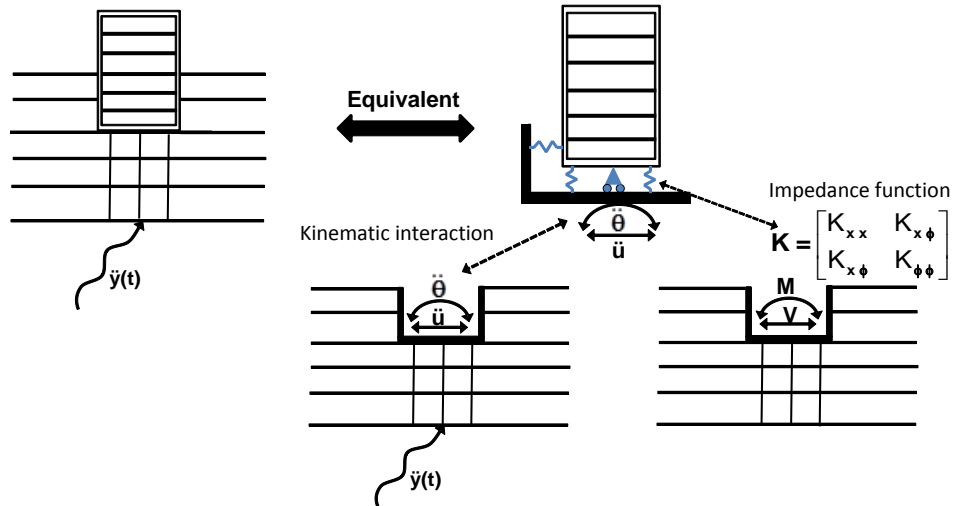


Figure 4. Substructuring approach for soil structure interaction

- Determination of the kinematic interaction motion, involving the response to base acceleration of a system which differs from the actual system in that the mass of the superstructure is equal to zero;
- Calculation of the inertial interaction effects, referring to the response of the complete soil-structure system to forces associated with base accelerations equal to the accelerations arising from the kinematic interaction.

The second step is further divided into two subtasks:

- computation of the dynamic impedances at the foundation level; the dynamic impedance of a foundation represents the reaction forces acting under the foundation when it is directly loaded by harmonic forces;
- analysis of the dynamic response of the superstructure supported on the dynamic impedances and subjected to the kinematic motion, also called effective foundation input motion.

Although the substructure approach described above is rigorous for the treatment of linear SSI, its practical implementation is subject to several simplifications:

- full linear behavior of the system is assumed; it is well recognized that this assumption is a strong one since nonlinearities occur in the soil and at the soil pile interface. Soil nonlinearities can be partly accounted for, as recommended in Eurocode 8 - Part 5, by choosing for the calculation of the impedance matrix reduced soil properties that reflect the soil

nonlinear behavior in the free field. This implicitly assumes that additional nonlinearities taking place at the soil pile interface, along the pile shaft, do not contribute significantly to the overall seismic response.

- kinematic interaction is usually not considered. Very often flexural piles are flexible with respect to the surrounding soil and the soil displacement is not altered by the presence of the pile group. In that case, provided the foundation embedment can be neglected, step 1 is straightforward: the kinematic interaction motion, or foundation effective input motion, is simply the freefield motion. No additional burden is imposed to the analyst since the freefield motion is a given input data.

### **3 KINEMATIC INTERACTION**

In the remaining of the paper we will focus on the first step of the substructure analysis described above with illustration of two foundations responses of the same bridge. Two aspects are illustrated: the internal forces induced in the piles by kinematic interaction and the modification of freefield motion due to kinematic interaction.

#### **3.1 Description of foundations**

Foundation 1 is composed of 18 concrete piles, 1800mm in diameter, 20m long, penetrating a 2.50m thick layer of a residual soil with a shear wave velocity 300m/s, overlying a 10m thick weathered layer of the rock formation with a shear wave velocity of 580m/s; the rock formation is found at 12.50m below the ground surface.

Foundation 2 of the same bridge is composed of 35 large diameter concrete piles (2.5m), 49m long, crossing a very soft mud layer, 11m thick, with a shear wave velocity of the order of 100m/s; the piles go through a residual soil ( $V_S = 250$  to 400m/s) and reach the competent rock formation at 25m depth (Figure 6).

#### **3.2 Foundation input motions**

Site response analyses were carried out with the software SHAKE (linear equivalent viscoelastic model) and for 7 time histories spectrally matched to the design spectrum; these time histories were input at an outcrop of the rock formation. The foundation response was modeled with the software SASSI-2010; the models include the 18, respectively 35, piles, a massless pile cap and the soil layers; the strain compatible properties retrieved from the SHAKE analyses are used for each soil layer and the input motion is represented by the 7 ground surface time histories computed in the SHAKE analyses. Figure 5 compares for foundation 1 the freefield ground surface spectrum to the foundation response spectra calculated at the same elevation. Note that because

of the asymmetric pile layout the motion in the X-direction is different from the motion in the Y-direction. As expected since the soil profile is stiffer than the piles in flexure, both the freefield motion and the foundation motions are very close to each other. For that configuration, using the freefield motion for the effective foundation input motion would not be a source of error.

Freefield and foundation response spectra are compared in Figure 7 for foundation 2. The free-field ground response spectrum determined from the site specific response analysis has a smooth shape; the kinematic interaction motion, i.e. the motion of the piled foundation, exhibits a marked peak at 0.5s and a significant deamplification with respect to the free-field motion between 0.8s and 3.0s. This phenomenon is due to the inability of the piled foundation to follow the ground motion because of the piles stiffnesses.

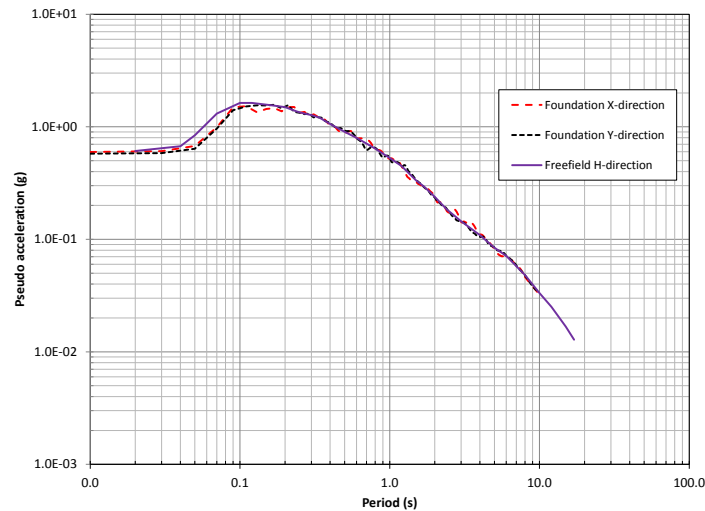


Figure 5. Kinematic interaction motion for "flexible" piled foundation 1

Obviously, in that case, using the freefield motion for the foundation input motion would be strongly misleading and may produce an unconservative design.

These two examples, drawn from a real project clearly illustrate the need for a careful examination of the relative foundation-soil profile stiffness before deciding whether or not there is a chance that the freefield motion be modified by the foundation. When faced to that latter situation, it is mandatory to correctly evaluate the effective foundation input motion to obtain meaningful results.

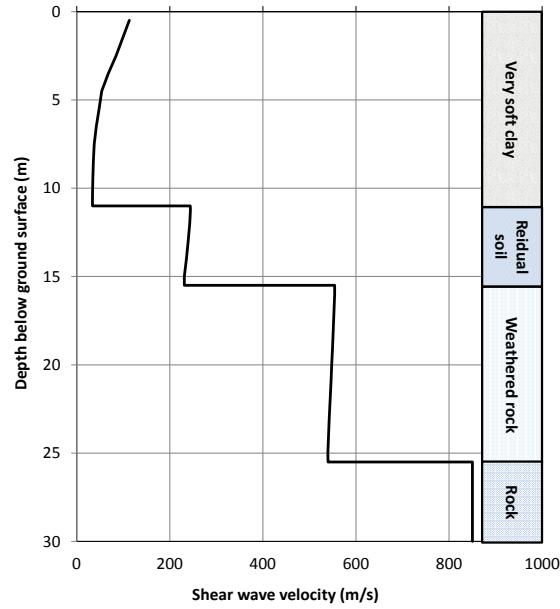


Figure 6. Soil profile at location of foundation 2

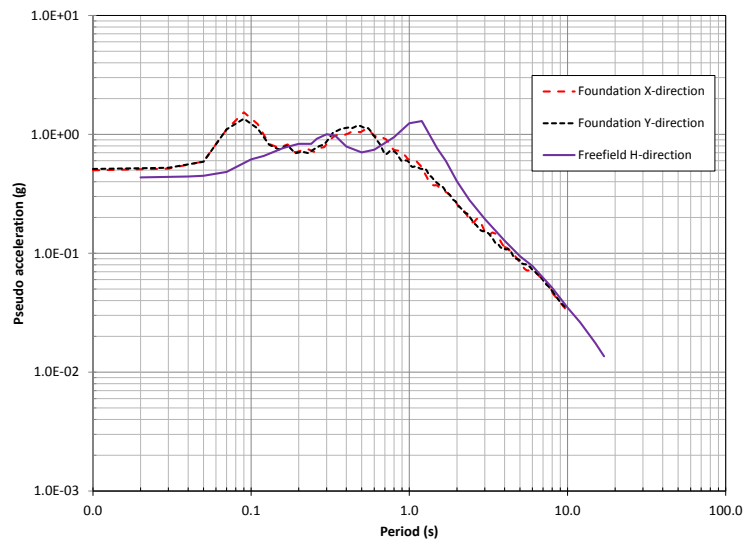


Figure 7. Kinematic interaction motion for "stiff" piled foundation 1

### 3.3 Kinematic forces in the piles

An additional adverse effect of kinematic interaction is the development of internal forces in the piles due to the imposed soil displacements. As noted in

paragraph 1, the effect is well recognized in seismic building codes and shall be considered for soft deposits. In the example considered in this paper, it is expected that internal forces (bending moments and shear forces) should be larger for Foundation 2 with larger piles diameters and softer ground conditions. The kinematic interaction forces were computed with the same models used for the determination of the foundation input motions. Results are presented in Figure 8 for the bending moments and in Figure 9 for the shear forces.

As expected the internal forces developed in the piles of Foundation 2 are an order of magnitude larger than the forces developed in Foundation 1.

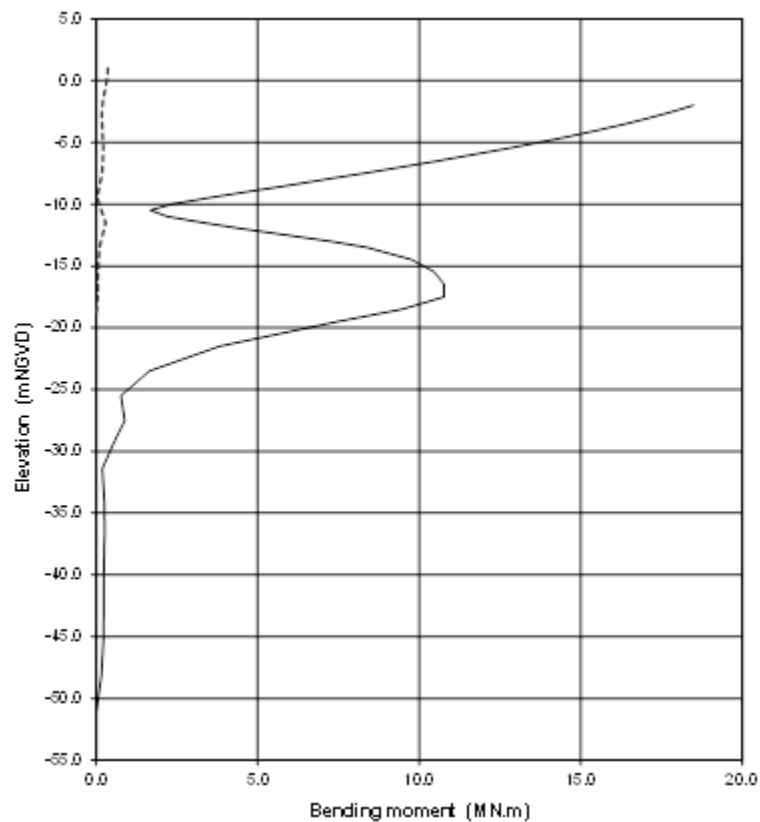


Figure 8. Kinematic bending moment in the piles for Foundation 1 (dotted line) and Foundation 2 (solid line)



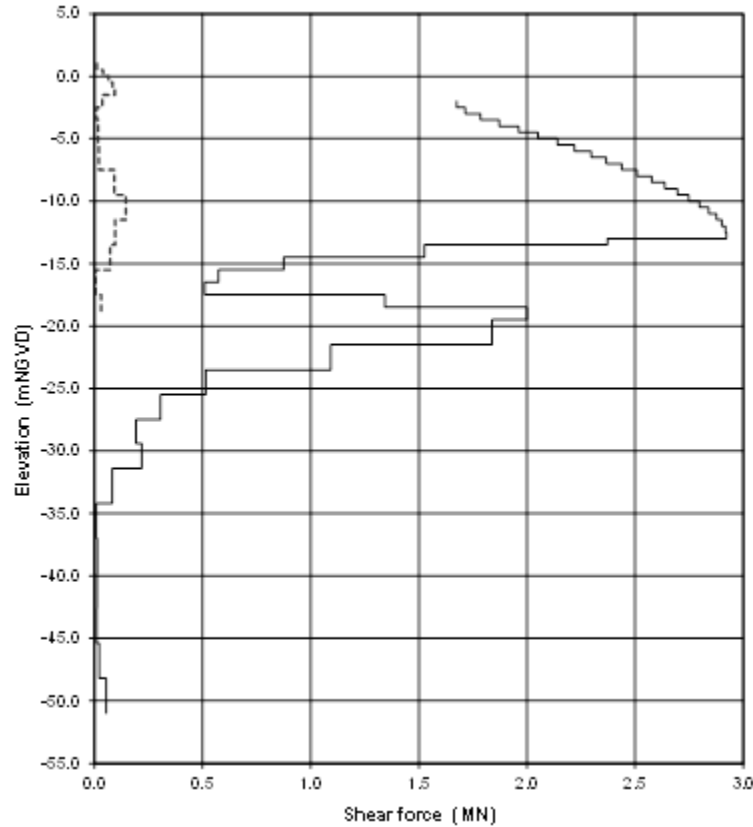


Figure 9. Kinematic shear forces in the piles for Foundation 1 (dotted line) and Foundation 2 (solid line)

Note that the forces plotted in both figures are maximum values occurring in the piles regardless of the time at which they occur. Despite the large pile diameters that offer larger capacity, Foundation 2 is much more demanding than Foundation 1 in terms of cross section reinforcement.

#### 4 CONCLUSIONS

Experience gained from several projects involving piled foundation in a seismic environment shows that the most amenable and versatile approach to soil structure interaction is the substructuring technique. It presents several advantages like a correct treatment of the pile group effect, which is not the case with a global model where the piles are modelled as beams on Winkler foundations, the need for calculating the foundation input motions and foundation impedances only once as long as the foundation is not modified, the reduced size of the structural model, especially for extended structures like

bridges, etc...The main drawback of this approach lies in its restriction to linear, or moderately nonlinear, systems. Since it is attractive, the method is often used with approximations in its implementation and the designer must be fully aware of those shortcuts. In this paper, one such approximation, which consists in taking the freefield motion for the effective foundation input motion, has been illustrated on a real project. It has been shown that significant differences may take place between both motions when the piled foundation cannot be considered flexible with respect to the soil profile. If this situation is faced, rigorous treatment of soil-structure interaction requires that the effective foundation input motion be calculated, an additional step in the design.

## REFERENCES

- [1] Kavvadas, M, Gazetas, G, "Kinematic seismic response and bending of free head piles in layered soils", *Geotechnique*, Vol 43, No. 2, pp. 207-222, 1993.
- [2] CEN. European Standard EN 1998-5: 2004 Eurocode 8: "Design of structures for earthquake resistance. Part 5: Foundations, retaining structures, geotechnical aspects". Comité Européen de Normalisation. Brussels, 2004.
- [3] ASCE/SEI 41-13 "Seismic evaluation and retrofit of existing buildings, Chp. 8, Foundations and Geologic site Hazards, 2014.
- [4] Lam, P.I, Law, H, "Soil Structure Interaction of Bridges for Seismic Analysis". Technical Report MCEER-00-008, 2000.
- [5] Gazetas, G, *Foundation Vibrations*, in *Foundation Engineering Handbook*, 2nd edition, Hsai Yang Fang Eds, Van Nostrand Rheinhold, 1991.
- [6] Matlock, H, "Correlation for Design of Laterally Loaded Piles in Soft Clay," *2nd Annual Offshore Technology Conference*, Paper No 1204, 1970.
- [7] Reese, L, Cox, W, Koop, R, "Analysis of Laterally Load Piles in Sand," *6th Annual Offshore Technology Conference*, Paper No. 2080, 1974.
- [8] Pender, MJ, "Aseismic Pile Foundation Design and Analysis", *Bulletin of the New Zealand National Society for Earthquake Engineering*, Vol 26, No. 1, 49-160, 1993.
- [9] Pecker, A, "Aseismic foundation design process - lessons learned from two major projects : the Vasco da Gama and the Rion-Antirion bridges", *Proceedings 5th ACI International Conference on Seismic Bridge Design and Retrofit for Earthquake Resistance*, La Jolla, California, 2003.
- [10] Brown, DA, Bollman, HT, "Lateral Load Behavior of Pile Group in Sand," *Journal of Geotechnical Engineering*, ASCE, Vol. 114, No. 11, pp1261-1276, 1996.
- [11] Finn, WDL, "A Study of Piles during Earthquakes: Issues of Design and Analysis". The Tenth Mallet Milne Lecture, *Bulletin of Earthquake Engineering*, Vol. 3, n°2, pp141-234, 2005.
- [12] *Seismic Bridge Design and Retrofit – Structural Solutions. FIB bulletin 39*, 2006.
- [13] Kausel, E, Roesset, JM, *Soil Structure Interaction for Nuclear Containment Structures. Proc. ASCE, Power Division Specialty Conference*, Boulder, Colorado, 1974.
- [14] Idriss, IM, Sun, JI, "SHAKE 91: A computer program for conducting equivalent linear seismic response analyses of horizontally layered soil deposits. Program modified based on the original SHAKE program published in December 1972 by Schnabel, Lysmer and Seed", *Center of Geotechnical Modeling, Department of Civil Engineering, University of California, Davis, California*, 1992.
- [15] Ostadan, F, Nan, D, *SASSI 2010 - A system for analysis of soil-structure interaction. Geotechnical Engineering Division, Civil Engineering Department, University of California, Berkeley*, 2012



## **RESILIENT AND SUSTAINABLE BRIDGES OF THE FUTURE**

M. Saiid Saiidi<sup>1</sup>, Mostafa Tazarv<sup>2</sup>, Brian Nakashoji<sup>3</sup>, Sebastian Varela<sup>4</sup>,  
and Fatemeh Kavianipour<sup>5</sup>

<sup>1-5</sup> University of Nevada, Reno, Dept. of Civil and Environmental Engineering, USA  
e-mail: saiidi@unr.edu, mostafa.tazarv@gmail.com, bnakashoji@gmail.com,  
sebastianvarela@gmail.com, fatemeh.kavianipour@gmail.com

**ABSTRACT:** Highlights of several investigations on seismic performance of new generation of bridges are presented. Low-damage materials such as shape memory alloy, engineered cementitious composite, fiber reinforced polymer, and elastomeric rubber pad were incorporated in bridge columns to facilitate construction, enhance performance, minimize damage, reduce permanent deformations, and reduce or totally eliminate the post-earthquake repair costs.

**KEY WORDS:** Bridge; Low-damage materials, SMA, ECC, FRP, Rubber pad

### **1 INTRODUCTION**

Conventional bridge construction (CBC) in which bridge components are cast in-place has a history of more than a century in the United States. Several months of construction are typically required using CBC techniques to fully build a bridge. Accelerated bridge construction (ABC), in contrast, utilizes advanced technologies and improved planning to facilitate construction and minimize interruption to highway network. Precast components are the essence of ABC. Even though ABC offers many advantages over CBC, precast component connections present a challenge in the moderate and high seismic areas. Low-damage high-performance materials may be used to improve ABC connection performance and to enhance the overall seismic behavior of bridges even under severe earthquakes. This article presents the highlights of several studies in which novel materials and details were explored to develop earthquake-resistant connections and elements. The article also includes a study on design for deconstruction of bridge columns.

### **2 ADVANCED MATERIALS**

#### **2.1 Shape memory alloy (SMA)**

SMA is a class of metallic materials with superior properties, which makes it a viable alternative to reinforcing steel. Large strains induced to SMA can be fully recovered by heating (shape memory effect) or unloading (superelastic

effect) [1]. Superelastic SMAs has gained more attention for structural engineering applications since they exhibit minimal residual deformations without applying external heat or electrical current. Among many alloys of SMA, Nickel-Titanium (NiTi or Nitinol) alloy is more common because of its high superelastic range, high energy dissipation capacity, low- and high-cycle fatigue properties, and excellent corrosion resistance [2].

Tazarv and Saiidi [3] defined mechanical properties of reinforcing superelastic SMA for structural applications and proposed a method to extract the properties from a ASTM standard test. A simple flag-shape material model (Fig. 1) was proposed and a design specification for reinforcing NiTi superelastic SMA bars was presented. Statistical analyses on a pool of tensile tests showed that reinforcing SMA has 10-20% lower yield strength, 80% lower modulus of elasticity, and slightly higher ultimate stress and strain capacities compared to reinforcing steel.

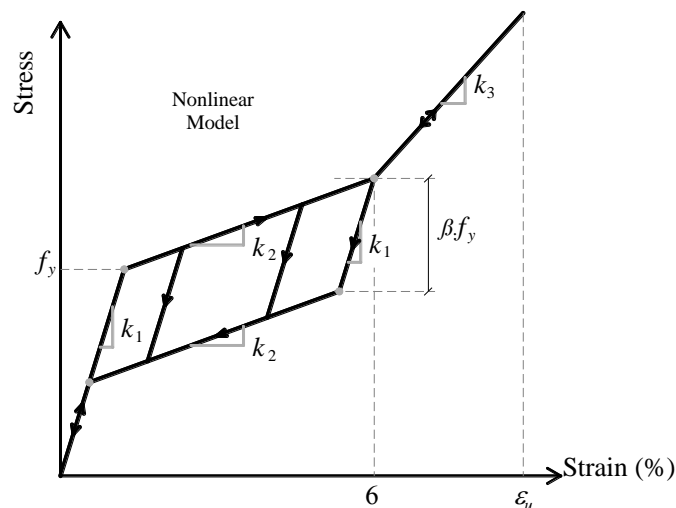


Figure 1. Nonlinear model for reinforcing NiTi superelastic SMA [3]

## 2.2 Engineered cementitious composite (ECC)

ECC is a class of high-performance fiber reinforced concrete with 4% or more tensile strain capacity. Polyvinyl alcohol (PVA) with 2% volumetric ratio is the most common type of fiber used in ECC mix. Seismic performance of ECC structural components have been studied by several researchers [4, 5, 6, and 7]. A minimal damage of elements incorporating ECC plastic hinge was observed in these studies, and the damage was mainly limited to minor cover ECC spalling.

### **2.3 Fiber reinforced polymer (FRP)**

Even though FRP is linear-elastic and brittle material, satisfactory performance can be achieved when FRP be incorporated as either reinforcement or external jacket in concrete structures. Seismic performance of FRP tubes filled with concrete has been investigated in several studies. A state-of-the-art review on the topic was presented in Bakis et al. [8].

### **2.4 Elastomeric rubber plastic hinge**

Rubber has been widely used in bridge industry for bearings and seismic isolators. Since rubber has a significantly lower stiffness than steel and concrete, it softens the behavior of a structure in an isolator configuration resulting in higher vibration periods thus lower seismic forces. A new application for rubber as an elastomeric rubber plastic hinge for ABC bridge columns was investigated by Motaref et al. [9]. The rubber pad was reinforced with steel shims to reduce bulging of the rubber and prevent buckling of the column longitudinal steel bars (Fig. 2). A high drift ratio capacity with no rubber plastic hinge damage was observed in shake table testing of the column.

## **3 LOW-DAMAGE PLASTIC HINGES FOR CONVENTIONAL BRIDGE CONSTRUCTION (CBC)**

Two 1/3-scale, SMA/ECC bridge columns were tested under slow reversed cyclic loading to failure. ECC was used in entire length of columns but NiTi superelastic SMA bars were used only in plastic hinges (Fig. 3). The test variable in the two columns was the length of SMA bars with 18-in. (475-mm) bars in one column and 13.5-in. (343-mm) bars in the other. #4 (Ø13 mm) SMA bars were connected at both ends to #5 (Ø16 mm) steel bars using mechanical headed bar splices. These column models were cast in-place.

The test results showed that even under 12% drift ratio, the plastic hinge damage of SMA/ECC columns was minor (Fig. 4). Flag-shape hysteretic behavior with negligible residual displacements was observed in both columns (Fig. 5). It was found that displacement capacity of SMA/ECC column with a SMA bar length equal to one column side dimension is 85% higher than a steel-reinforced concrete column and 30% higher than the SMA/ECC column with shorter SMA bars. The drift capacity of the column with long-SMA was 11% versus 6% for the RC column and 8% for the column with shorter SMA bars.



Figure 2. Elastomeric Rubber Hinge [9]



Figure 3. Reinforcing SMA bars used in plastic hinge



Figure 4. SMA/ECC column plastic hinge damage after 12% drift cycles

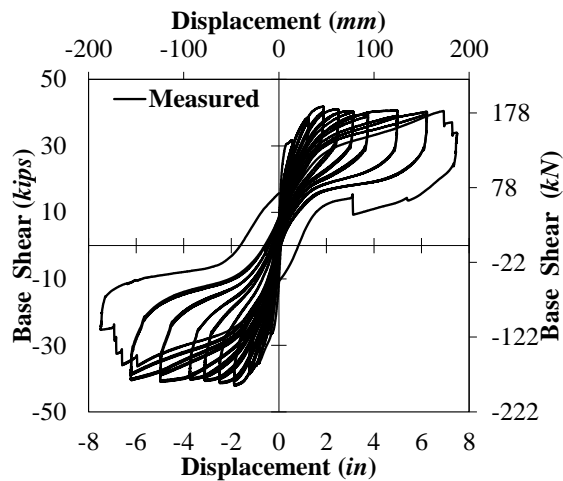


Figure 5. Measured force-displacement hysteresis for SMA/ECC column with long SMA bars

#### 4 LOW-DAMAGE MATERIALS FOR ACCELERATED BRIDGE CONSTRUCTION (ABC)

Low-damage materials may be used in precast bridge columns. Tazarv and Saiidi [10] developed a new ABC connection for precast columns in high seismic zones. Ultra-high performance concrete (UHPC), which is another class of low-damage materials with five times higher tensile and compressive strength compared to conventional concrete, was used to fill the ducts that were

installed in adjoining members. Precast member longitudinal bars were secured in ducts before casting UHPC.

A half-scale precast reinforced concrete column was built incorporating eight different materials: conventional concrete, reinforcing steel, reinforcing NiTi superelastic SMA, headed bar couplers, corrugated galvanized metal ducts, UHPC, self-consolidating concrete (SCC), and ECC. The column was connected to the footing by inserting protruded precast column bars in UHPC-filled ducts. #10 ( $\text{Ø}32 \text{ mm}$ ) SMA bars were connected to #11 ( $\text{Ø}36 \text{ mm}$ ) steel bars using headed bar couplers. ECC was used only in the plastic hinge of the column with a depth of 1.5 column diameter. The precast column was hollow-core to facilitate the transportation but it was filled with SCC after installing the shell.

The column was tested under slow cyclic loads. The plastic hinge damage of the SMA/ECC column and a reference cast-in-place (CIP) steel-reinforced column after 12% drift cycles is shown in Fig. 6. The damage in SMA/ECC column was limited to only cover concrete while the core concrete was crushed in the CIP column. The UHPC-filled duct connection exhibited no damage.

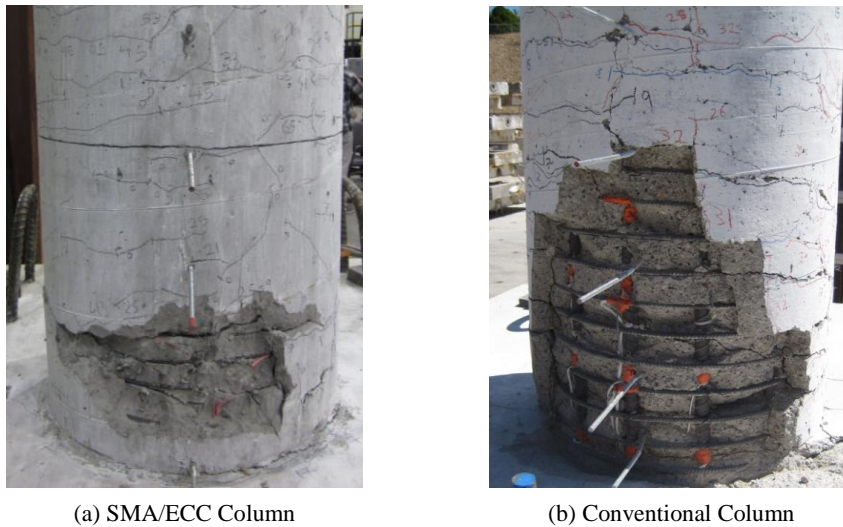


Figure 6. Plastic hinge damage of SMA/ECC and conventional columns after 12% drift cycles

Figure 7 shows the measured lateral force-drift hysteresis of the SMA/ECC and reference columns. A flag-shape behavior with residual displacements that were on average 70% lower than the reference column was observed. It can be seen that low-damage materials incorporated in the precast column improved the seismic performance.



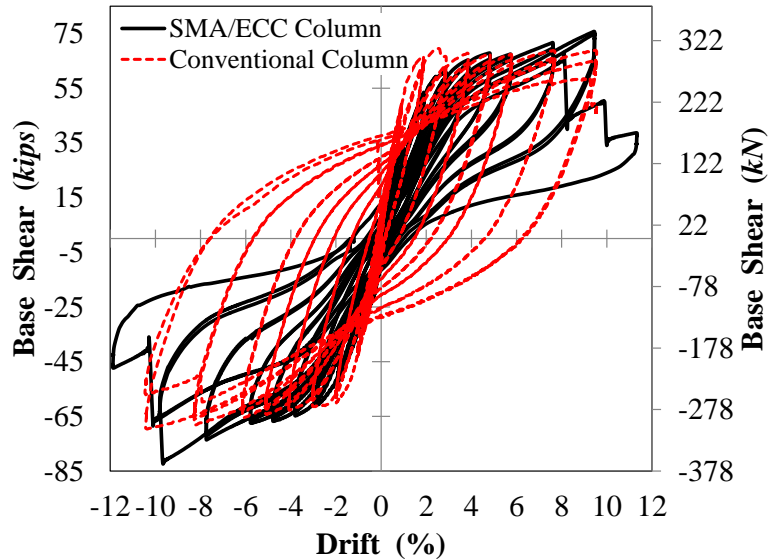


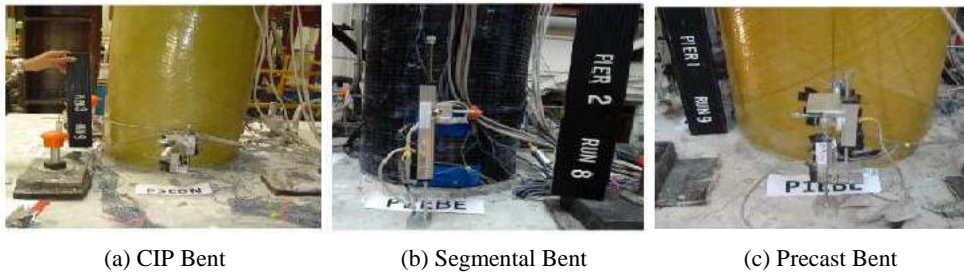
Figure 7. Measured force-drift hysteresis for SMA/ECC and conventional columns

A quarter-scale, four-span bridge model incorporating concrete-filled FRP-tube (CFFT) bents was studied by testing on shake tables (Fig. 8). The total length and the width of the bridge model were 107 ft (32.6 m) and 7.5 ft (2.3 m), respectively. The bridge had three two-column bents, each built with different FRP jackets or different ABC techniques. One bent consisted of cast-in-place CFFT columns. The second bent consisted of post-tensioned segmental FRP wrapped columns. The third bent was similar to the first but consisted of precast CFFT columns connected to a precast footing and cap beam using a member pocket and pipe-pine connections, respectively.

The performance of the columns was satisfactory. The bridge withstood a 9.3% drift ratio with minor apparent damage only to the cap beams and the footings (Fig. 9). The seismic performance of all three bents were approximately the same and FRP remained intact with concrete in all columns. All columns showed less than 1% residual displacements but residual displacements of the segmental bent were even smaller than the other bents since posttensioning tendons remained elastic under seismic loads and increased the self-centering tendency of the bent. The ABC connections used in this bridge model successfully transferred the column loads to the footings and maintained the integrity of the bent.



Figure 8. Quarter-scale bridge model on shake Tables



(a) CIP Bent

(b) Segmental Bent

(c) Precast Bent

Figure 9. Concrete-filled FRP-tube plastic hinge damage after run 9 (under 9% drift ratio)

## 5 LOW-DAMAGE MATERIALS FOR FUTURE BRIDGES

The form of bridges of the future is imagined by some visionary designers. One example is the bridge by Chetwood, who designed a futuristic bridge (Fig. 10) [11], which is a residential green bridge powered by solar energy. Equally important is the construction techniques that will be used in the future and the performance of bridges of the future under severe events.

Three objectives are sought in the present study for bridges of the future: (1) construct a full bridge in a relatively short time than that the time conventional construction takes, (2) minimize or completely eliminate bridge damage under destructive loads, and (3) totally disassemble the bridge after its lifetime and recycle the components.

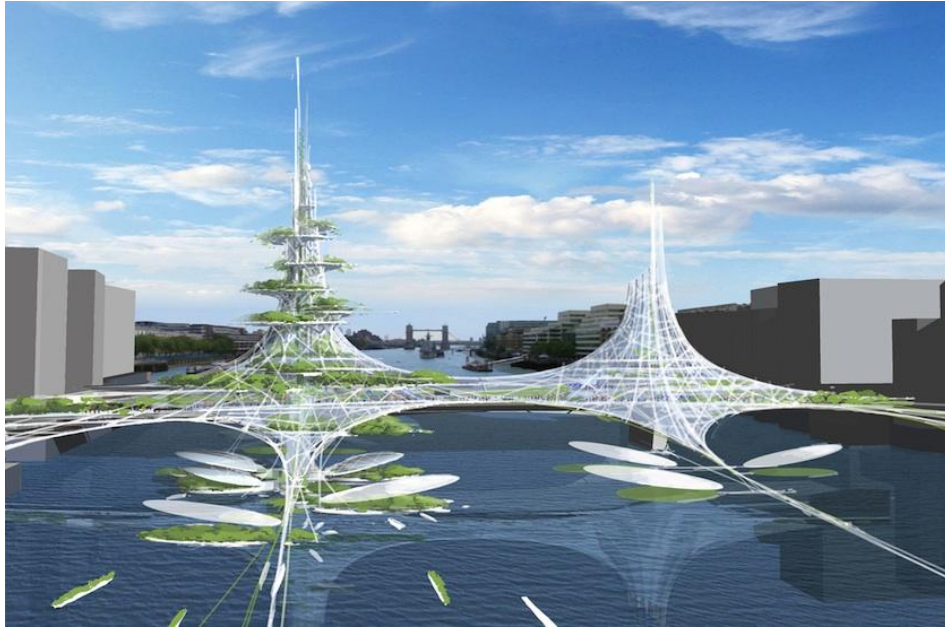
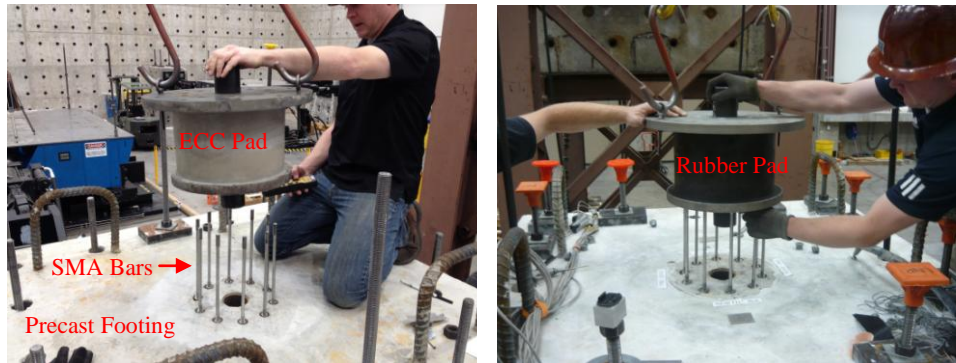


Figure 10. A conceptual bridge of the future [11]

Feasibility of the first two objectives was investigated in the experimental studies presented in previous sections in which satisfactory performance was achieved. In order to study the feasibility of the third objective, seismic behavior of three quarter-scale modular bridge columns using innovative materials and precast segments was investigated.

Each modular column consisted of three segments (Fig. 11): precast footing, pre-fabricated plastic hinge element, and precast column. ECC or elastomeric rubber were used in different plastic hinge elements. Two types of SMA alloy bars, NiTi and an emerging CuAlMn alloy, were passed through plastic hinges to connect the footing to the precast segment of the column, which was built with a concrete-filled FRP tube. Combination of ECC/rubber pad with NiTi/CuAlMn SMA bars resulted in three modular column models. The CFRT segment was designed to remain elastic during ground excitations. Therefore, all nonlinearities were expected to occur only in plastic hinges. Connection of all segments was provided by threaded couplers so the segment could be disassembled after the tests. Each modular column was tested twice by going through these steps: (1) assemble a column model, (2) test the column model on a shake table, (3) totally disassemble the column model including removing of the plastic hinge bars, and (4) retest it under similar loading protocol as step (2).



(a) Installing precast ECC Pad

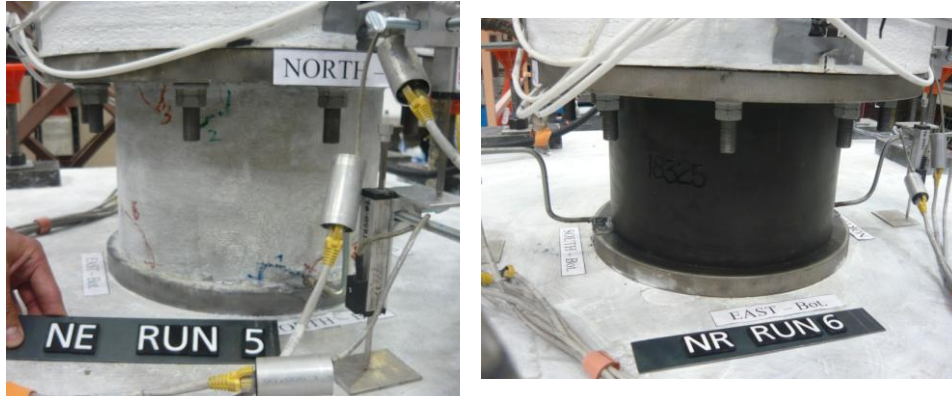
(b) Installing prefabricated rubber pad



(c) Installing precast concrete-filled FRP tube segment

Figure 11. Deconstructible bridge columns incorporating low-damage materials

The tests showed promising results with minimal damage in plastic hinges and no damage elsewhere. ECC plastic hinges reinforced with SMA bars suffered only minor concrete spalling under a motion simulating twice the design earthquake (Fig. 12a). The column with SMA bars and elastomeric rubber plastic hinge exhibited no damage even under 250% design earthquake (Fig. 12b). Since SMA bars were used in all modular columns, negligible residual displacements were observed in testing and retesting stages.



(a) SMA/ECC Plastic Hinge

(b) SMA/Rubber Plastic Hinge

Figure 12. Damage of detachable bridge column plastic hinges under 200-250% design earthquake

The columns were disassembled, assembled, and retested. A similar seismic performance with minimal damage was observed in all column models. Fig. 13 shows the SMA/rubber column initial and retested force-displacement curves under 250% of design earthquake. It can be seen that column performance was not affected by disassembling the column into its segments, which confirms the feasibility of the third objective sought for the bridges of the future.

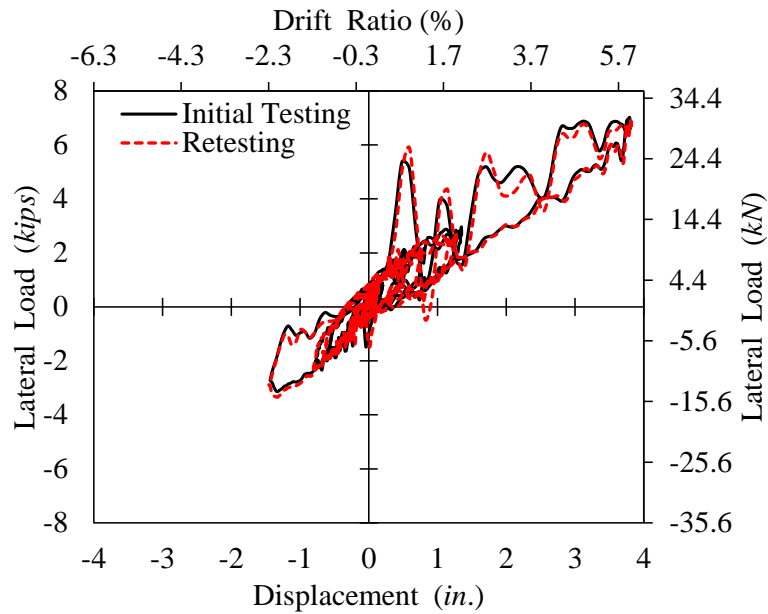


Figure 13. Lateral force-displacement relationships of SMA/Rubber column under 250% design earthquake before and after disassembly

## 6 CONCLUSIONS

Low-damage materials such as shape memory alloy (SMA), engineered cementitious composite (ECC), fiber reinforced polymer (FRP), and elastomeric rubber were incorporated in large-scale bridge component or complete bridge system test models to accelerate bridge construction and reduce or totally eliminate bridge damage after an earthquake. The summary of experimental investigations were presented. It was found that SMA can substantially reduce bridge column residual displacements and provide equal or improved displacement capacity compared to conventional bridges. ECC can reduce the column damage significantly, and when combined with reinforcing SMA, a superior seismic performance can be achieved. Concrete filled FRP tube columns showed no damage even under large drift demands. The low-damage materials were also exhibited an excellent performance when used in precast bridge components. Three characteristics for the bridges of the future were sought: being fast in construction, being damage-free, and being totally detachable into segments for recycling as bridge components. Feasibility of all three properties was experimentally confirmed in the present paper.

## ACKNOWLEDGMENTS

The studies presented in this article were funded by various grants from the California Department of Transportation, National Science Foundation, Federal Highway Administration, and Washington Department of Transportation.

## REFERENCES

- [1] Otsuka, K, and Wayman, CM, *Mechanism of Shape Memory Effect and Superplasticity*, Cambridge University Press, Cambridge, U.K., pp. 27–48, 1998.
- [2] Alam, MS, Nehdi, M and Youssef, MA, “Seismic Performance of Concrete Frame Structures Reinforced with Superelastic Shape Memory Alloys”, *Smart Structures and Systems*, Vol. 5, No. 5, 565-585, 2009.
- [3] Tazarv, M, and Saïdi, MS, “Reinforcing NiTi Superelastic SMA for Concrete Structures”, Submitted to *Journal of Structural Engineering*, ASCE , Vol. xx, No. xx, pp. xx-xx, 201x.
- [4] Li, VC, *Engineered Cementitious Composites (ECC): Material, Structural, and Durability Performance*, in *Concrete Construction Engineering Handbook*, Chapter 24, Ed. E. Nawy: published by CRC Press, 2008.
- [5] Saïdi, MS, and Wang H, “Exploratory Study of Seismic Response of Concrete Columns with Shape Memory Alloys Reinforcement”, *ACI Structural Journal*, Vol. 103, No. 3, pp. 436-443, 2006.
- [6] Saïdi, MS, O'Brien, M and Sadrossadat-Zadeh, M, “Cyclic Response of Concrete Bridge Columns Using Superelastic Nitinol and Bendable Concrete”, *ACI Structural Journal*, Vol. 106, No. 1, pp. 69-77, 2009.
- [7] Cruz Noguez, CA, and Saïdi, MS, “Shake Table Studies of a 4-Span Bridge Model with Advanced Materials”, *Journal of Structural Engineering*, ASCE , Vol. 138, No. 2, pp. 183-192, 2012.
- [8] Bakis, CE, Bank, LC, Brown, VL, Cosenza, E, Davalos, JF, Lesko, JJ, Machida, A, Rizkalla, SH, and Triantafyllou, TC, “Fiber-Reinforced Polymer Composites for Construction: State-of-the-Art Review”, *Journal of Composites for Construction*, ASCE, Vol. 6, No. 2, pp. 73-

- 87, 2002.
- [9] Motaref, S, Saiidi, MS, and Sanders, D, “Seismic Response of Precast Bridge Columns with Energy Dissipating Joints”, Center for Civil Engineering Earthquake Research, Department of Civil and Environmental Engineering, University of Nevada, Reno, Report No. CCEER-11-01, 2011.
- [10] Tazarv, M and Saiidi, MS, “UHPC-Filled Duct Connections for Accelerated Bridge Construction of RC Columns in High Seismic Zones”, Submitted to ACI Structural Journal, Vol. xx, No. x, pp. xx-xx, 201x.
- [11] Chetwoods Architects, <http://chetwoods.com>.

IBSBI 2014, October 16-18, 2014, Athens, Greece

## IZMIT BAY BRIDGE

### Geotechnical challenges and innovative solutions

Jørgen S. Steenfelt<sup>1</sup>, Brian Foged<sup>2</sup> and Anders H. Augustesen<sup>3</sup>

<sup>1,2,3</sup>COWI, Kongens Lyngby, Denmark

e-mail: jos@cowi.com, bfo@cowi.com, ahau@cowi.com

**ABSTRACT:** The Izmit Bay Suspension Bridge, app. 50 km east of Istanbul, crosses the Sea of Samara with a main span of 1550 m. The foundation of the bridge poses interesting challenges in that the bridge site is in a highly seismic region. Moreover the ground profile ranges from Dolomitic Limestone to a thick sandwich of silty sand and clay layers overlying the bedrock.

**KEY WORDS:** Earthquake; Foundations; Pile inclusions; Suspension bridge.

## 1 INTRODUCTION

The Izmit Bay Bridge will feature the world's 4<sup>th</sup> longest suspension bridge, main span of 1550 m, by the slated time of inauguration in 2016 (see *Figure 1*). It is part of a major BOT infrastructure project in Turkey, the 420 km long Gebze-Izmir highway, with an approximate construction cost of \$1.2 billion out of the total cost of \$11 billion.

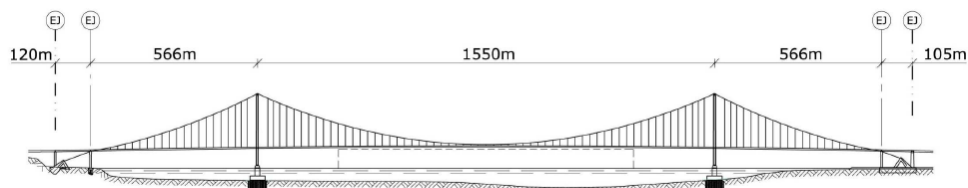


*Figure 1.* General layout of Izmit Bay Bridge (North to south = left to right)

The Owner is NÖMAYG / Nurol-Özaltın-Makyol-Astaldi-Yüksel-Göçay and the Contractor is IHI Infrastructure Systems CO., Ltd with COWI as bridge designer.



The bridge site is located app. 50 km east of Istanbul and crosses the Sea of Samara. This is a highly seismic region in close proximity to the North Anatolian fault which caused the 1999 earthquake. Moreover, the ground profile ranges from Dolomitic Limestone at ground level on the northern side to kilometre thick sandwich of silty sand and clay layers overlying the bedrock. The top of the soil deposits are very loose/soft and susceptible to liquefaction. The foundation structures are therefore different when moving from North to South.

The North anchor block is a gravity type foundation taking advantage of the Limestone rock but at the same time addressing the effects from inherent bedding planes and joints. The tower foundations are precast concrete caissons. As the subsoil exhibits inferior strength and deformation properties the subsoil is improved by 35 m long Ø2 m driven steel pile inclusions. To allow energy dissipation during seismic events a gravel fuse is separating the concrete bottom of the caisson and the piles. The South anchor block is placed within an artificial island where dense sand at relatively shallow depth allows for a direct foundation. The South anchor block is also verified for a potential secondary fault passing through the anchor site.

The paper focusses on the geotechnical and soil-structure interaction aspects of the design and construction. It describes the design process allowing the foundation challenges to be met by innovative solutions.

The project has been under preparation from the early 1990'ties but after a new tender submission in Sep. 2010 IHI was awarded the contract with COWI as designer. After contract negotiations the detailed design started in September 2011 with preparatory site works in September 2012 and permanent site works in January 2013.

## **2 GEOLOGICAL SETTING & GROUND INVESTIGATIONS**

The Izmit Bay is the eastern continuation of the Sea of Marmara and is primarily shaped by the tectonic movement along the North Anatolian Fault. This is some 1600 km long and extends from Karliova in eastern Turkey to the Aegean. A major right lateral strike slip fault forms the tectonic boundary between the Eurasian plate and the Anatolian block of the African plate. The northern strand of the Anatolian Fault zone occupies the Izmit Bay and projects across the project alignment, presenting the greatest seismogenic hazard source within the area. However, no active faults were recognized in the bridge alignment.

Two investigation campaigns were carried out. The Phase I campaign in 2009/2010 aimed at identifying regional faults, stratigraphy and ground conditions along the proposed bridge alignment and at site specific locations for the bridge foundation. The investigations comprised geophysical surveys offshore and onshore, CPTU tests (100) and geotechnical boreholes (30 vertical and 3 inclined, with depths from 36 to 200 m below ground level) with

sampling and in situ testing (ranging from SPT to down-hole CPTU and suspension logging). Samples of soil and rock were tested to provide classification, strength, deformation and hydraulic parameters. The tests ranged from normal classification testing to advanced laboratory testing comprising anisotropically consolidated triaxial compression and extension test, CRS and incremental loading oedometer tests, static direct shear tests, resonant column/torsional shear tests, strain and stress-controlled cyclic direct simple shear tests.

The Hazard Zonation map forming the basis for the tender showed that the South anchor block location was well within a “Non-fault” area. However, during the detailed design the zone with possible secondary (inactive) faults were extended to the South anchor block location. Furthermore, it was concluded that the location for the North anchor block on the “beach area” in front of the rock outcrop (see Figure 2) was an area of relatively homogeneous Paleozoic limestone without major faults, shear zones or adverse geologic structures.

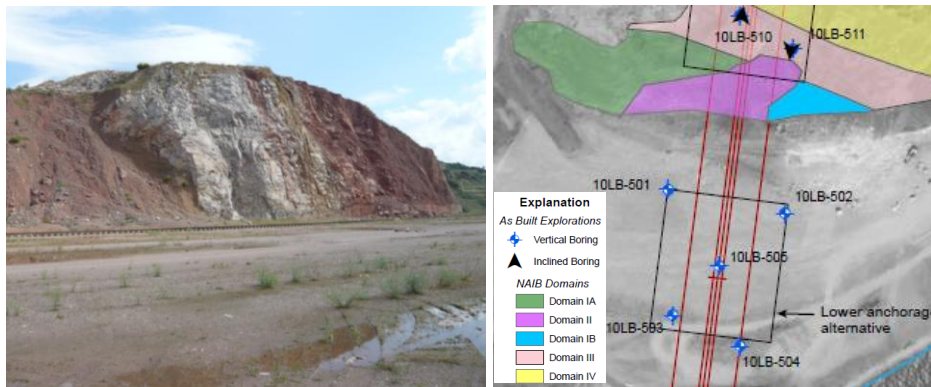


Figure 2. (a) “Beach” in front of rock outcrop at North anchor block site 2010-06-10; (b) initial interpretation of rock domains (area in grey is the “beach”)

After award supplementary investigations (Phase II) were carried out in 2011/2012. These aimed specifically to identify areas of no-faulting for the South anchor block location area and to gain insight into possible multi-rock-domains rather than one single competent limestone domain at the North anchor block area. This is discussed in more detail in Sec. 4.2.

Furthermore, supplementary geotechnical boreholes and CPTU probing were carried out in the final tower foundation positions as the re-positioning of the South anchor block 160 m to the north necessitated re-location of both of the towers by 80 m to the north.

Based on the ground investigations and with due respect to interpolation between investigation points at foundation locations far apart it was possible to

derive idealized geological models in the Geotechnical Interpretative Report prepared by COWI. The design profiles for the different foundation locations are seen in Figure 3 and Figure 4 for anchor blocks and towers, respectively.

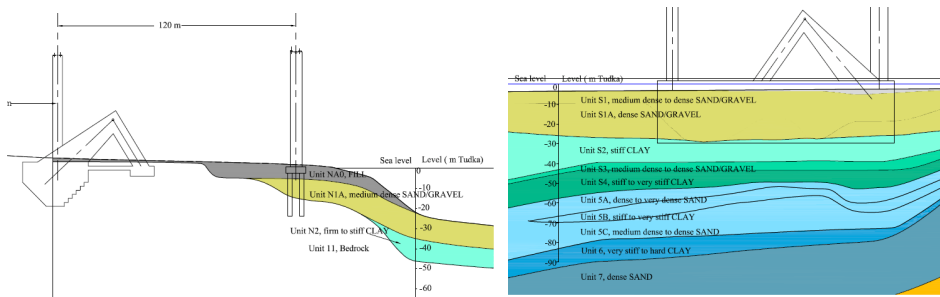


Figure 3. Design profiles; (a) North anchor block; (b) South anchor block

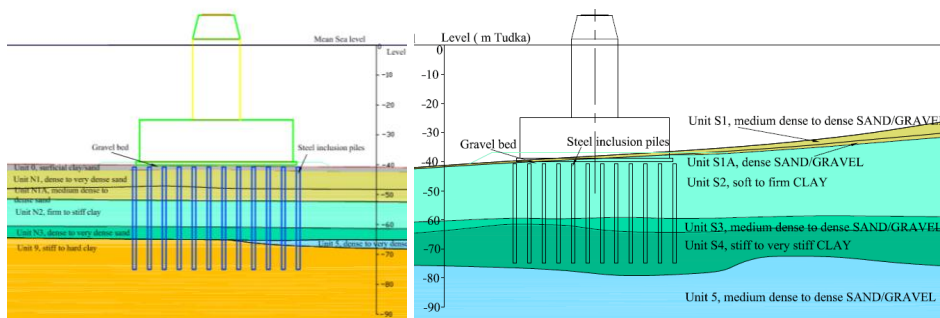


Figure 4. Design profiles; (a) North tower; (b) South tower

Note that the “foundation outline” for the South anchor block corresponds to the original concept with a piled foundation.

It is apparent that the rock (shown non-shaded on Figure 3a) dips rather steeply from the onshore outcrop area behind the North anchor block towards south. Bedrock was met at level -186.7 m at the North tower but was not met in the southern part of the alignment (assumed kilometre depth).

Ten different soil units were distinguished along the alignment although not all of them were found at all locations. In broad terms the soil stratification is a sandwich of sand and clay at the tower locations and the South anchor block.

At the North anchor block location the “beach area” is partly quarried and partly reclaimed with sand/gravel and limestone blocks as seen from vintage Google earth maps in Figure 5 and as indicated in Figure 3.



Figure 5. North anchor block area changes from Google Earth photos; (a) 2004-11-19; (b) 2007-12-31; (c) 2009-04-11; (d) 2013-04-13

### 3 REQUIREMENTS

The bridge is designed according to Eurocodes with the UK National Annex with the exception that ship impact forces are calculated according to AASHTO. The structural design life requirement is 100 years.

The minimum navigational clearance envelope is 64 m by 1000 m, where the vertical clearance is measured relative to 0.3 m above mean sea level.

For the severe seismic loading three seismic events are considered with rock outcrop PGAs of 0.25, 0.65 and 0.87 g, respectively:

- FEE - Functional Evaluation Earthquake; return period 150 years (equivalent to the 1999 earthquake). Demand: immediate access and no damage
- SEE - Safety evaluation earthquake; return period 1000 years. Demand: Limited access and repairable damage
- NCE - Non collapse earthquake; return period 2475 years. Demand: No collapse and no casualties.

The seismic load response spectra at bedrock level were used for the initial analyses but all foundations were verified by the load output from seven sets of earthquake time histories. As this involved four foundation structures, three return periods and each comprising three components a total of 252 analyses were carried out using COWI's in-house Integrated Bridge Analysis and Design Software (IBDAS), described in [1]. For information on the IBDAS modelling and the substructure structural design see [2] and [3].

As the bedrock was hundreds of metres below seabed for the major part of the alignment PSHA analyses on competent soils, developing 5% damped target

response spectra at depths of 126, 89 and 100 m (with input shear wave velocities of 1000, 490 and 490 m/s), were carried out for North tower, South tower and South anchor block, respectively.

Despite relocation of the South anchor block it was not possible to rule out completely the possible occurrence of a secondary fault within the anchor block foot print (see Figure 6). It was recommended to take this into account by assuming a fault plane at level -100 m with horizontal and vertical slip movements of 0.70 m and 0.25 m for SEE and 1.00 m and 0.50 m for NCE.

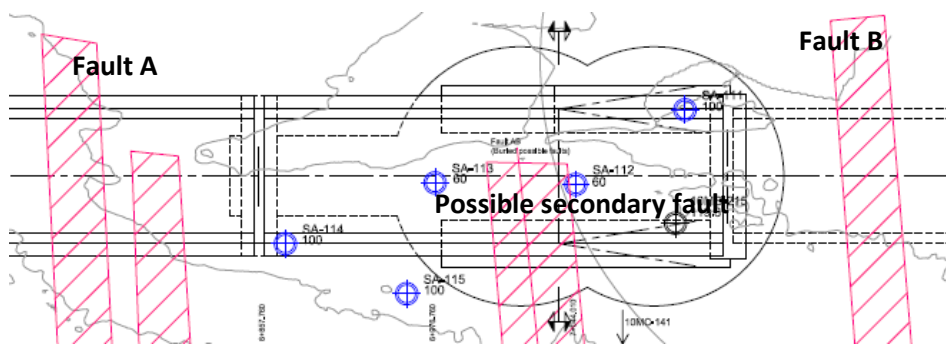


Figure 6. Interpretation of (inactive) faults at the South anchor block location

## 4 FOUNDATION SOLUTIONS & CHALLENGES

### 4.1 General

The foundation solutions adopted for the Izmit Bay Bridge are shown schematically in Figure 7 with gravity structures for the anchor blocks and a hybrid gravity/pile inclusion solution for the two towers.

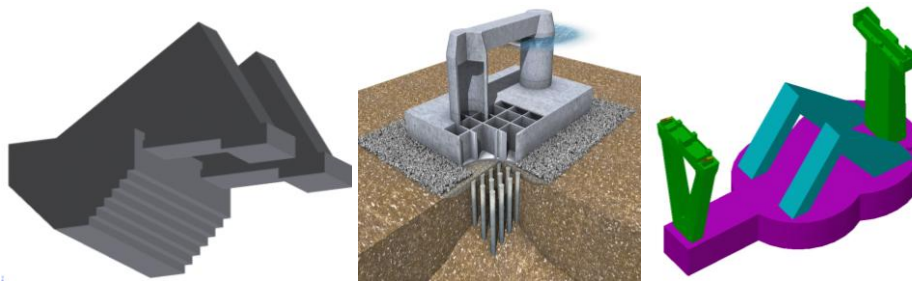


Figure 7. Foundation concepts; (a) North anchor block; (b) Tower foundations; (c) South anchor block

The very high ship impact loads, 246 MN from the 160,000 DWT design ship and particularly the seismic load cases with horizontal forces typically of the order 400 MN, posed very significant challenges for the pylon foundations. Direct foundation was obviously not an option and traditional piled foundations would be very hard to verify for the seismic NCE event.

Fortunately the ground conditions and the magnitude of loading were similar to the conditions for the Rion-Antirion Bridge in Greece (see f.inst. [5]). The characteristics in both cases are: deep water (40-65 m), deep soil strata, weak alluvial deposits, soil strength increasing with depth and strong seismic activity with large tectonic movement. Despite being a cable stayed bridge the design displacement in between pylons was 2 m for Rion-Antirion where the innovative concept of ground improvement by steel pile inclusions and a gravel bed “fuse” between the piles and the concrete foundation base had been tried out in practice. As that bridge had survived an earthquake and the concept had been successfully modelled by physical modelling (centrifuge testing) and by 2D and 3D FEM calculations it proved possible to transfer this foundation solution to the tower foundations for the Izmit Bay Bridge as shown in Figure 7.

#### **4.2 North anchor block**

At the outset it was agreed by the design team that the North anchor block was by far the simplest and most straight forward of the foundation structures. It was considered to use the cavern anchorage concept but due to anticipated problems with a very deep cavern below the ground water table it was decided to use a traditional type gravity structure.

It is constructed as a large concrete gravity massif embedded in dolomitic limestone and two counter reacting front pads. The front pads are rigidly connected to the concrete rear massif by 2m high and 11.7m wide concrete beams. Tension load is transferred to the large concrete massif through the cables running through the splay chamber and the counter reacting compression load is transferred to both front pads via two saddle legs. The entire anchor block works as a monolith and is considered a rigid structure for foundation design and analysis purposes.

The rear concrete massif is 22m deep with basic plan dimensions: 33m in width along bridge alignment by 50m in length perpendicular to bridge alignment. At 10m depth the width of the rear concrete massif is reduced at a 45 degree angle. The south face of the massif is stair stepped by six 2m tall and 2m wide steps. The width at the base of the rear concrete massif is 9m. The main resistance to uplift of the North anchor block is provided by gravity of the large concrete mass and by friction developed along the stair stepped face of the massif.

The front pads are also embedded into dolomitic limestone. With the basic plan dimensions: 12m in width along bridge alignment and 14.96m in length

perpendicular to bridge alignment. Each concrete footing is 5m high with minimum 4.5m embedment into Dolomitic Limestone.

Since the North anchor block was assumed to be located in a competent Limestone, referred to as Domain 1, a wedge failure where different joints and bedding link up in front of the anchor block is possible. Such discontinuities that would link up are relatively discontinuous and would require breaking of intact rock bridges between existing discontinuities. The rock mass shear strength along the inferred wedge failure plane(s) should consider the rock mass “Global Strength” derived from the in situ rock mass using the Hoek-Brown failure criterion. Thus, very ample capacity of the anchor block could be easily demonstrated.

However, the North anchor block turned out to produce by far the most comments from the Independent Design Checker and proved to be very challenging in terms of both design and execution.

During the detailed design a specialist review of the ground conditions was carried out. This review revealed a number of uncertainties with possible impact on the design of the permanent structure:

- Clay layers could be present, but have not been identified.
- Marl layers have been described in two of the boreholes within the footprint of the anchorage, but their overall distribution is not well defined. They are likely to be present in other boreholes, but may not have been logged due to reduced effects of weathering or core loss.
- The thickness of possible marl layers is poorly defined.
- Strength of marl layers has not been determined due to the negligible amount recovered in boreholes.
- The fault zone at the southern edge of the anchorage has not been adequately investigated and its nature is currently poorly defined.

In the design a bedding plane (strike as observed on site) was included to provide the most onerous sliding plane in a wedge failure as shown in Figure 8a. It was envisaged that any such plane would be “undulating and discontinuous as confirmed in subsequent investigations

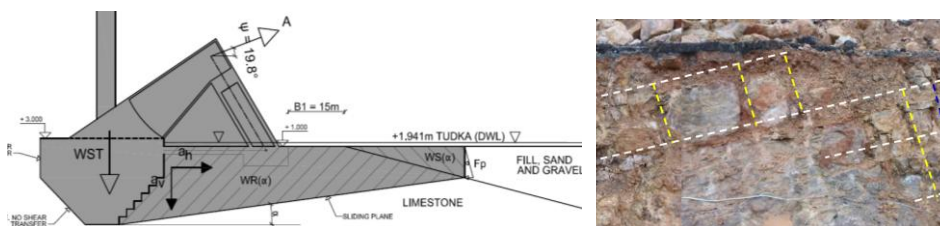


Figure 8. (a) Failure mechanism assumed for North anchor block; (b) Photo of interpreted bedding discontinuity planes in trial excavation wall (white broken lines)

However, to manage the perceived residual risks a programme of additional investigations was initiated. These included one vertical and four inclined boreholes and two major trial trench excavations for identifying the location and nature of the geologic domains and the shear zone(s) boundary, material and strike and to provide samples from the zone (see Figure 9a, b).

Furthermore, samples from the existing cores with and without apparent fissures and beddings were tested in direct shear at a specialized laboratory.

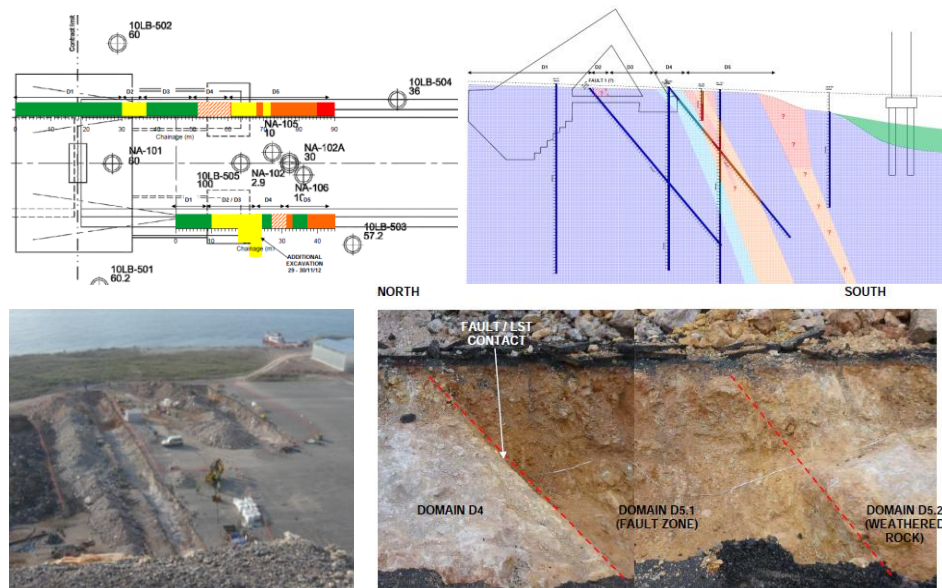


Figure 9. (a) Plan of trial excavations; (b) Cross section showing boreholes and updated geological model; (c) Initial excavation with backhoe; (d) Fault boundary

A site visit where the existing cores and the rock outcrop behind the anchor block were inspected together with the initial trenching brought some comfort as it was concluded that

- There are no clay layers in relation to bedding surfaces
- Marl was not identified in the boreholes
- The presence of a fault zone indicated in one of the boreholes was confirmed but no evidence of larger scale karsts was found
- To err on the safe side a wedge type failure defined by thinly laminated zones at an angle of  $15^\circ$  to the horizontal should be considered
- The design can be progressed with an agreed lower bound angle of friction of  $40^\circ$  for the kinematic failure mechanism

The reporting from the trench excavations and the results from the laboratory testing did (fortunately) confirm that the cautious estimates of strength proper-



ties, bedding plane orientation and geologic zonation were justified and the design could be approved.

The resulting geological model is seen on Figure 9b. During the excavation for the anchor block site inspection and mapping confirmed the updated geological model. Minor karstic features were seen during excavation but without impact on stability as all of them were above the global failure mechanism. However, some of them led to water ingress into the excavation possibly assisted by the major blasting operations with dynamite for every 3-5 m depth of excavation of the rear pad (away from the stepped front of the rear pad) necessary to break the sound limestone. Before blasting the excavation was partly filled with water to reduce impact on the surroundings and after drawdown of the water the debris could be broken down by chisel and taken away (ref. Figure 10a, b). Some major inflows were observed before perimeter grouting for the whole anchor block foot print was effectively completed as seen in Figure 10c.



*Figure 10.* Excavation for North anchor block, (a) Blasting from a safe distance; (b) Debris after blasting; (c) Major water ingress in north wall after blasting

The progress of the excavation is seen in Figure 11. In order to provide safety during construction the walls were secured by rock bolts and shotcrete as deemed necessary and water inflows from fissures were stopped by polyurethane injection or steel plates for the main water inflow locations on the north wall. For the front of the rear pad, the stepped face and the front pads concreting against intact rock was ensured.



*Figure 11.* North anchor block excavation and casting of front pads and base

The kinematic approach necessitated for the SEE and NCE load cases, with  $FOS < 1$ , led to maximum displacements of 50 and 110 mm, respectively.

### 4.3 North and South towers

The tower foundation is a hybrid solution with steel pile inclusions for soil improvement and a gravel bed acting as a horizontal load fuse between the caisson base and the free-standing piles. This also has the advantage to allow the same foundation level for the prefabricated caissons at level -40 m for both towers. The caissons are 67 m by 54 m rectangular cell structures (to level -25 m) with steel/concrete composite shafts with top at level +10.15 m for easy and fast erection of the low weight prefabricated steel tower units (total height of 241.85 m). The caissons were built in a purpose-built dry dock at the peninsula on the south side close to the South anchor block and subsequently floated out to a wet dock to allow sufficient depth for completion.

Figure 12 shows a section through the caisson and tower and the float out of the first caisson.

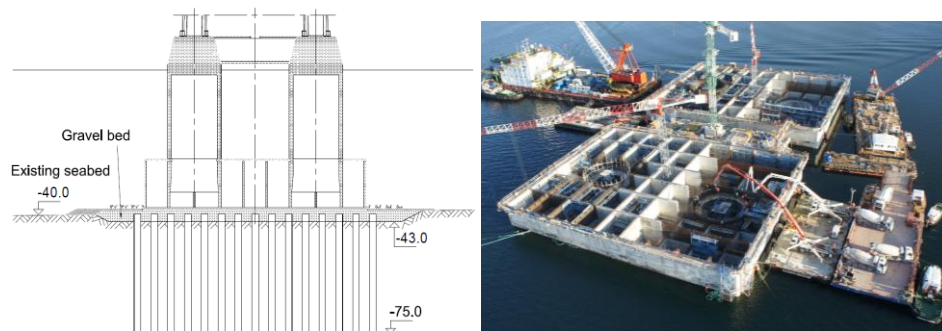


Figure 12. (a) Section through tower foundation; (b) float out from dry to wet dock of caisson

The soil is improved by 195  $\text{Ø}2.0$  m tubular steel piles with wall thickness of 20 mm placed in a 13 by 15 grid with centre to centre distance of 5 m with the top of piles 0.75 m below the top of the 3 m thick gravel bed. The steel piles are provided with external shear keys in the gravel bed to provide transfer of the requisite vertical and horizontal forces from the gravel bed. The hybrid foundation system allows for verification of horizontal and vertical bearing capacity and acceptable settlements.

After initial dredging at the tower positions the inclusion piles were driven and the gravel bed placed by tremie pipe from floating equipment. A purpose-built sub-sea levelling unit (Figure 13a) was used to achieve a level and uniform top of the gravel bed to allow positioning of the precast concrete caisson. To verify the stiffness of the produced gravel bed, gravel was tremied under site conditions (to 3 m thickness) into a large container, where plate loading tests were subsequently performed on land (see Figure 13b).

This allowed for an update of the initial settlements in the gravel bed. This was important as short and long term settlements needed to be compensated for before tower erection in order to meet the clearance requirements.



Figure 13. (a) Demonstration of sub-sea levelling unit; (b) Plate loading test on “retrieved” gravel

The most challenging part of the tower foundation design was the verification for the seismic events. This is described in details in [4] applying the base isolation concept which was previously used for the Rion-Antirion Bridge (see e.g. [5], [6] and [7]).

In order to generate stresses acting on the caisson bottom directly the modelling applied distributed springs at the 13 by 15 grid of the inclusion piles which provided sufficient resolution and accuracy. The springs were linear in the vertical direction but non-linear in the horizontal direction and included hysteretic behaviour. A very comprehensive calibration exercise was carried out in order to provide a match between the global IBDAS model and 2D plane strain Plaxis finite element modelling (vertical load) and ABAQUS 3D finite element modelling to determine the load-displacement behaviour of the gravel bed springs. The latter was achieved by applying different vertical loads to the caisson bottom slab and “pushing” it in the horizontal direction.

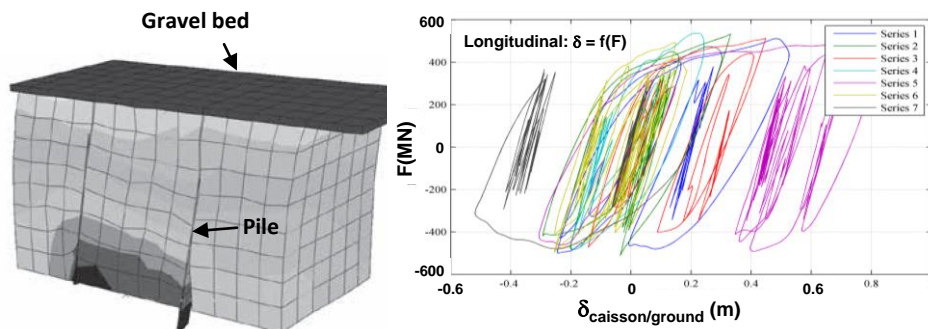


Figure 14. (a) Abaqus model for determining gravel bed springs; (b) Relative displacement at gravel bed/caisson base for NCE time histories for the North tower in the longitudinal direction

The relative displacement of the North tower in the longitudinal direction between gravel bed and caisson slab for the NCE time histories are seen in Figure 14 together with the Abaqus model for determining the gravel bed springs.

The application of an advanced non-linear model with distributed springs allowed implementation in a practical manner of a displacement based verification for high magnitude earthquakes with dissipation of seismic energy by rocking as well as a controlled and limited sliding.

The serviceability limit state verification involved calculations by an axisymmetric Plaxis finite element model to represent a pile inclusion in an infinitely large pile group. From the pile toe level and downwards the calculated settlements are manually modified to consider a load spread of 1:2 together with calculation of the contribution from creep in the clay layers. The resulting estimated settlements are seen for the North tower in Figure 15a.

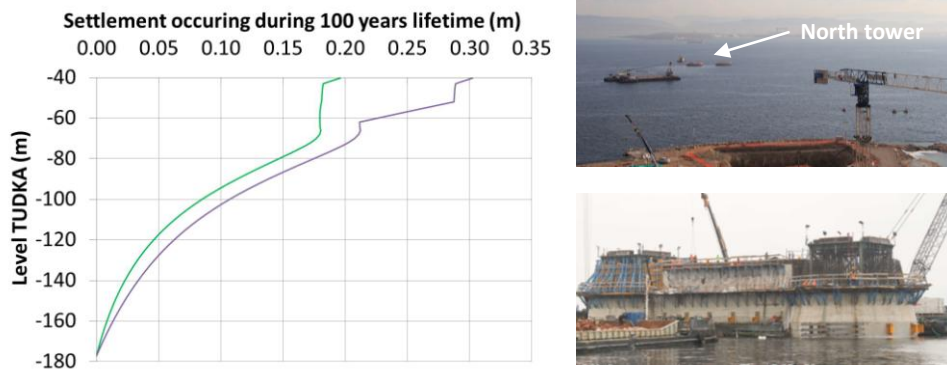


Figure 15. (a) Settlements estimated for the North tower during the 100 years lifetime; (b) Caisson on gravel bed (view from North side span pier); (c) Work for transition to steel tower erection

Intensive settlement monitoring is in place for the tower foundations. The initial settlements, recorded when the caisson was transferred from the wet dock and lowered on the gravel bed and the following weeks, indicated that the short term settlement prediction was accurate enough to allow erection of the steel tower without further compensations. The first steel segment was mounted in early July 2014.

#### 4.4 South anchor block

In the Tender Design the layout of the South anchor block was in line with the North anchor block using two front pads and a rear pad. However, as the shallow ground conditions were relatively soft alluvial deposits the pads needed to be founded on piles to provide sufficient bearing capacity and acceptable settlements. The modelling of this layout and the choice of piles (bored piles versus barrettes in both cases inside an anchored diaphragm wall) to resist the

earthquake were causes for concern. The particular problem of providing non-collapsible transition between the piles and the anchor block pads called for very intricate plastic hinge design. Any consideration of deep direct foundation was futile, as the ratio of horizontal to vertical load,  $H/V$ , was well above unity. The construction and the schematic layout of the South anchor block from the tender stage are shown in Figure 16a.

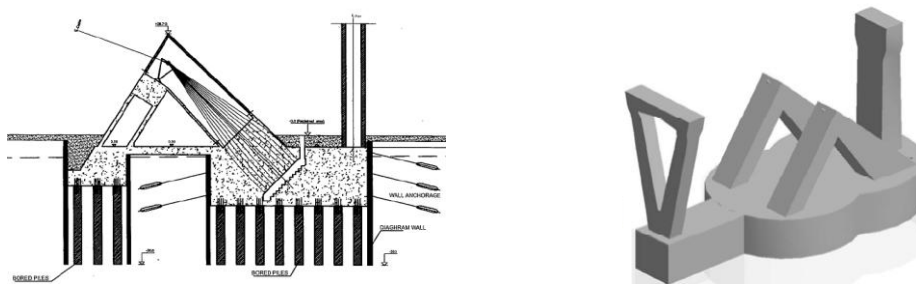


Figure 16. (a) Conceptual design of Tender design for South anchor block; (b) Alternative plan

As the detailed design progressed the loads changed (in part due to the relocation of the anchor block) and in view of the conceived risk of possible secondary faults, it proved beneficial to include the South side span pier in the anchor block structure. Thus, very late in the design process it became clear that due to the composite changes and more accurate modelling of loads in IBDAS that  $H/V$  was now considerably lower than unity.

Thus, as competent sand was found at a reasonable depth the concept was “overnight” changed to direct foundation at level -15 m. However, due to the poor ground conditions at shallow depth, the high ground water table and the risk of liquefaction in the top sand layers the challenge was how to establish the excavation for casting the gravity structure.

A new solution was arrived at where the side span pier would be an integral part of the structure and where ground anchors could be avoided. The latter was almost a must due to program problems resulting from multiple anchor levels and space constraints in the excavation. To resist the earth pressures a “banjo-type” solution with two overlapping circular walls ( $\text{Ø } 58 \text{ m}$ ) of secant piles with a capping beam as internal ring support allow space for the splay chamber as shown schematically in Figure 16b. The length of the anchor block is 124 m.

The rectangular front of the anchor block (37.5 m by 18 m) the secant pile walls are supported by internal strutting. The secant piles served two purposes, to allow water cut off and to retain the earth pressure. The supplementary investigation hence also aimed at finding the depth to the continuous clay layer serving as a cut off and to allow sufficient soil plug weight inside the walls to eliminate the need for dewatering.

Figure 17 shows the South anchor block in its position at the reclaimed area. At the intersection of the two circles an internal temporary support is established by consecutive concrete slabs supported by steel piles.



Figure 17. South anchor block after completion of excavation and initial concreting at the base

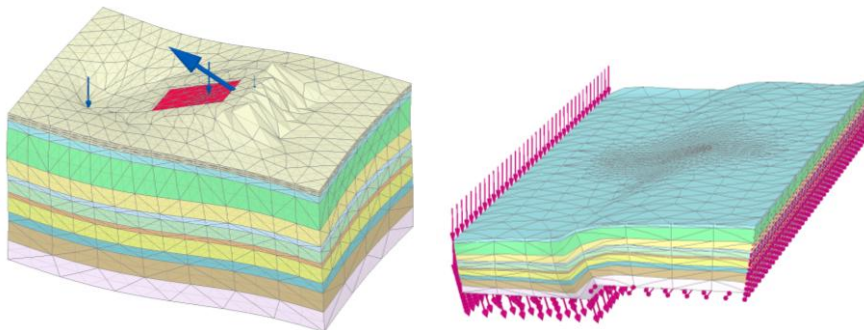


Figure 18. Exaggerated displacements for 1.0 m horizontal and 0.5 m vertical slip at 100 m depth

The very robust design of the anchor block as one big gravity structure had the added advantage that it could be verified even when subjected to severe oblique-slip fault movement, cf. [6]. The verification entailed very sophisticated 3D finite element modelling with an innovative cushion material as horizontal boundary as described in [8].

An example of the graphical output is shown in Figure 18. Furthermore, the geo-technical verification of the South anchor block involving detailed model-

ling of the geometry in 3D finite element and the impact of liquefaction is presented in [9].

## 5 CONCLUSIONS

This extremely interesting project posed a multitude of geotechnical challenges. The project re-emphasized that in geotechnics you must expect the unexpected. By dedicated cooperation between geotechnical and structural engineers and very fruitful cooperation with the Contractor IHI it was possible to overcome the challenges using innovative solutions and readiness to adapt to changing conditions brought about by the ground conditions, the construction programme and economy.

## ACKNOWLEDGEMENTS

The authors gratefully acknowledge the permission by Owner NÖMAYG / Nurul-Özaltın-Makyol-Astaldi-Yüksel-Göçay and the Contractor IHI Infrastructure Systems CO., Ltd to publish this paper.

## REFERENCES

- [1] Sørensen, KA, Jakobsen, PF, Andersen, GB., "IBDAS, an integrated bridge design and analysis system, *3rd Int. Conf. on Short and Medium Span Bridges*, 105-116, Toronto, 1990.
- [2] Christensen, SC, "Izmit Bay Suspension Bridge – Global Analyses incorporating Local Sub Models for Foundations in the Global Finite Element Model", *Proc. 36<sup>th</sup> IABSE Symposium 'Long Span Bridges and Roofs – Development, Design and Implementation', Kolkata, India, September 24-27, 2013*.
- [3] Assad, J, Löhning, T, Ullner, R, "Izmit Bay Suspension Bridge – Substructure Design", *Proc. 36<sup>th</sup> IABSE Symposium 'Long Span Bridges and Roofs – Development, Design and Implementation', Kolkata, India, September 24-27, 2013*.
- [4] Lyngs, JH, Kasper, T, Bertelsen, KS, "Modelling of soil-structure interaction for seismic analyses of the Izmit Bay Bridge, *Proc. 18<sup>th</sup> Int. Conf. Soil Mech. Geotec. Eng.*, 763-768, Paris, 2013.
- [5] Pecker, A, Teyssandier, J.-P, "Seismic design for the foundations of the RionAntirion Bridge", *Proc. Instn Civil Engrs Geotech. Engng*, Vol. 131: 4-11, 1998.
- [6] Fédération internationale du béton (FIB), "Seismic bridge design and retrofit – structural solutions", *State-of-the-art report*, Bulletin 39, Sprint-Digital-Druck, Stuttgart, 2001.
- [7] Yang, D, Dobry, R., Peck, RB, "Foundation inclusion interaction modelling for Rion-Antirion Bridge seismic analysis", *4<sup>th</sup> Int. Conf. on Recent Advances in Geotechnical Earthquake Engineering and Soil Dynamics*, San Diego, 2001.
- [8] Avar, BB, Augustesen, AH, Kasper, T, Steenfelt, JS, "3D Numerical Analysis of a Suspension Bridge Anchor Block to Oblique-Slip Fault Movement", *Proc. 18<sup>th</sup> Int. Conf. Soil Mech. Geotec. Eng.*, 1427-1430, Paris, 2013.
- [9] Avar, BB, Augustesen, AH, Kasper, T, Steenfelt, JS, Foged, B, "Geotechnical Verification of the South Anchor Block of the Izmit Bay Suspension Bridge", submitted for *Proc. 15<sup>th</sup> Eur. Conf. Soil Mech. Geotec. Eng.*, Edinburgh, 2015.